PROCEEDINGS OF THE 37TH ANNUAL HIGHWAY GEOLOGY SYMPOSIUM

GEOTECHNICAL ASPECTS OF CONSTRUCTION IN MOUNTAINOUS TERRAIN

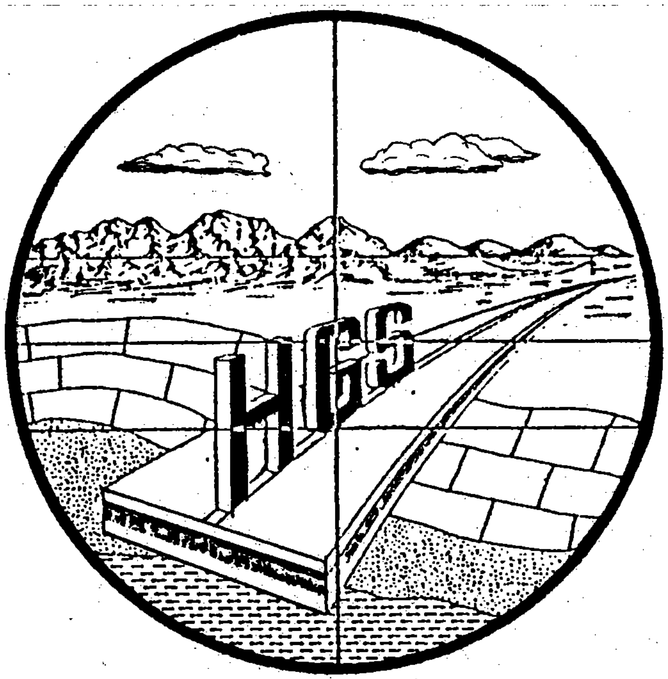

HELENA, MONTANA
AUGUST 20-22, 1986

CO-SPONSORED BY

Montana Department of Highways
and
Montana Division - Federal Highway Administration

PROCEEDINGS OF THE 37TH ANNUAL HIGHWAY GEOLOGY SYMPOSIUM

Geotechnical Aspects of Construction in Mountainous Terrain

August 20-22, 1986
Helena, Montana

Co-Sponsored by

Montana Department of Highways
and
Montana Division, Federal Highway Administration

Co-Chairman: Joseph E. Armstrong - Montana Department of Highways
and
Mark Zitzka - Federal Highway Administration

Cost $15.00

"Geotechnical Aspects of
Construction In Mountainous Terrain"

37TH ANNUAL HIGHWAY GEOLOGY SYMPOSIUM AND FIELD TRIP

August 20-21, 1986 - Helena, Montana

Co-Sponsored By

MONTANA DEPARTMENT OF HIGHWAYS

AND

MONTANA DIVISION - FEDERAL HIGHWAY ADMINISTRATION

Welcome Pardners. The planning committee for the 37th Annual Highway Geology Symposium would like to extend to you a very warm greeting from Montana. We want you to enjoy our state and particularly your stay in the Helena area. We have planned this years technical program and field trip to provide you with valuable information concerning engineering geology/ geotechnical engineering associated with road construction in mountainous conditions. It is our intent that the symposium will offer you new information to use on future projects and also support your present practices.

As always the sessions have been planned to rekindle old friendships with many the opportunity to make new friends and to share our experiences.

We hope your plans will enable you to take advantage of our state, its scenic beauty and historical sites which are one of a kind. Thanks for joining us and once more welcome to Montana and Helena.

JOSEPH E. ARMSTRONG
MARK ZITZKA
SYMPOSIUM CO-CHAIRMEN

HIGHWAY GEOLOGY SYMPOSIUM

History, Organization, and Function

Established to foster a better understanding and closer cooperation between geologists and civil engineers in the highway industry, the Highway Geology Symposium was organized and held its first meeting on February 16, 1950, in Richmond, Virginia. Since then, 37 consecutive annual meetings have been held in 24 different states. Between 1950 and 1962, the meetings were held east of the Mississippi River, with Virginia, Ohio, West Virginia, Maryland, North Carolina, Pennsylvania, Georgia, Florida, and Tennessee serving as the host states.

In 1962, the Symposium moved west for the first time to Phoenix, Arizona. Since then, it has rotated, for the most part, back and forth from east to west. Following meetings in Texas and Missouri in 1963 and 1964, the Symposium moved to Lexington, Kentucky in 1965, Ames, Iowa in 1966, Lafayette, Indiana in 1967, back to West Virginia at Morgantown in 1968, and then to Urbana, Illinois in 1969. Lawrence, Kansas was the site of the 1970 meeting, Norman, Oklahoma in 1971, and Old Point Comfort, Virginia the site in 1972.

The Wyoming Highway Department hosted the 1973 meeting in Sheridan. From there it moved to Raleigh, North Carolina in 1974, back west to Coeur d'Alene, Idaho in 1975, Orlando, Florida in 1976, Rapid City, South Dakota in 1977, and then back to Maryland in 1978; this time in Annapolis. Portland, Oregon was the site of the 1979 meeting, Austin, Texas in 1980, and Gatlinburg, Tennessee in 1981. The 1982 meeting was held in Vail, Colorado, and in Stone Mountain, Georgia in 1983. The 35th meeting in 1984 was held in San Jose, California and the 36th HGS was in Clarksville, Indiana. This year's meeting, the 37th, was held in Helena, Montana, the capital of the Big Sky Country.

Unlike most groups and organizations that meet on a regular basis, the Highway Geology Symposium has no central headquarters, no annual dues, and no formal membership requirements. The governing body of the Symposium is a steering committee composed of approximately 20 engineering geologists and geotechnical engineers from state and federal agencies, colleges and universities, as well as private service companies and consulting firms throughout the country. Steering committee members are elected for three-year terms, with their elections and re-elections being determined principally by their interests and participation in and contributions to the symposium. The officers include a chairman, vice chairman, secretary, and treasurer, all of whom are elected for a two-year term. Officers except for the treasurer may only succeed themselves for one additional term.

A number of three-member standing committees conduct the affairs of the organization. Some of these committees are: By-Laws, Public Relations, Awards Selection, and Publications. The lack of rigid requirements, routing, and the relatively relaxed overall functioning of the organization is what attracts many of the participants.

Meeting sites are chosen two or four years in advance and are selected by the Steering Committee following presentations made by representatives of potential host states. These presentations are usually made at the steering committee meeting which is held during the Annual Symposium. Upon selection, the state representative becomes the state chairman and a member protem of the Steering Committee. Depending on interest and degree of participation, the temporary member may gain full membership to the Steering Committee.

The symposia are generally for two and one-half days, with a day-and-a half for technical papers and a full-day for the field trip. The symposium usually begins on Wednesday morning. The field trip is usually Thursday, followed by the annual banquet that evening. The final technical session generally ends by noon on Friday.

The field trip is the focus of the meeting. In most cases, the trips cover approximately from 150 to 200 miles, provide for six to eight scheduled stops, and require about eight hours. Occasionally cultural stops are scheduled around geological and geotechnical points of interest. In Wyoming, the group viewed landslides in the Big Horn Mountains; Florida's trip included a tour of Cape Canaveral and the NASA space installation; the Idaho and South Dakota trips dealt principally with mining activities; North Carolina provided stops at a quarry site, a dam construction site, and a nuclear generating site; in Maryland the group visited the Chesapeake Bay hydraulic model and the Goddard Space Center; the Oregon trip include visits to the Columbia River Gorge and Mount Hood; the Central Mineral Region was visited in Texas; and the Tennessee trip provided Stops at several repaired landslides in Appalachia. The Colorado field trip consisted of stops at geological and geotechnical problem areas along Interstate 70 in Vail Pass and Glenwood Canyon, while the Georgia trip in 1983 concentrated on highway design and construction problems in the Atlanta urban environment. The 1984 field trip had stops in the San Francisco Bay area which illustrated the interaction of fault activity, urban landslides, and coastal erosion with the planning, construction and maintenance of transportation systems. In 1985 the one day trip illustrated new highway construction procedures in the greater Louisville area. The 1986 field trip was through the Rockies of recent interstate construction in the Boulder Batholith. The trip highlight was a stop at the Berkley Pit in Butte, Montana, an open pit copper mine.

At the technical sessions, case histories and state-of-the-art papers are most common with highly theoretical papers the exception. The papers presented at the technical sessions are published in the annual proceedings. Some of these proceedings are out of print, but copies of most of the last sixteen proceedings may be obtained from the Treasurer of the Symposium, David Bingham, of the North Carolina Department of Transportation in Raleigh 27611. Costs generally range from #5.00 to $15.00, plus postage.

JEA:sk:5gg

Highway Geology Symposium

MEDALLION AWARD WINNERS

Hugh Chase	1970
Tom Parrott	1970
Paul Price	1970
K. B. Woods	1971
R. J. Edmonson	1972
C. S. Mullin	1974
A. C. Dodson	1975
Burrell Whitlow	1978
Bill Sherman	1980
Virgil Burgat	1981
Henry Mathis	1982
David Royster	1982
Terry West	1983
Dave Bingham	1984
Vernon Bump	1986

In 1969, the Symposium instituted an awards program, and with the support of Mobile Drilling Company of Indianapolis, Indiana designed a plaque to be presented to individuals who have made significant contributions to the Highway Geology Symposium over a period of years. The award, a 3.5" medallion mounted on a walnut shield and appropriately inscribed, is presented during the banquet at the Annual Symposium.

Highway Geology Symposium

STEERING COMMITTEE MEMBERS

	TERM EXPIRES
Mr. Joseph A. Gutierrez Mgr. Mine Planning and Development Mideast Division Vulcan Materials Company P. O. Box 4195 Winston-Salem, NC 27105 Phone - (919) 767-4600	1988
Mr. Henry Mathis - Chairman Manager, Geotechnical Branch Division of Materials Kentucky Department of Highways Frankfort, KY 40622 Phone - (502) 564-3160	1989*
Mr. Vernon L. Bump - Vice-Chariman Foundation Engineer Department of Transportation Division of Engineering Pierre, SD 57501 Phone - (605) 773-3401	1987*
Mr. Willard McCasland - Secretary Materials Division Oklahoma Department of Transportation 200 N. E. 21st Street Oklahoma City, OK 73105 Phone - (405) 521-2677	1988*
Mr. W. D. Bingham - Treasurer State Highway Geologist Department of Transportation Division of Highways Raleigh, NC 27611 Phone - (919) 733-6911	1987*

NOTE: Officer's terms expire at conclusion of 1987 Symposium.

STEERING COMMITTEE MEMBERS - Continued...

	TERM EXPIRES
Mr. Joe E. Armstrong Chief Geologist Montana Department of Highways 2701 Prospect Avenue Helena, MT 59620 Phone - (406) 444-6280	1989
Mr. John B. Gilmore Colorado Highway Department 4340 East Louisiana Denver, CO 80222 Phone - (303) 757-9275	1989
Mr. Jeffrey L. Hynes Colorado Geological Survey 1313 Sherman Street, Room 715 Denver, CO 80203 Phone - (303) 866-3520	1988
Mr. C. William Lovell Professor of Civil Engineering Purdue University Grissom Hall West Lafayette, IN 47907 Phone - (317) 494-5034	1988
Mr. Harry Ludowise Federal Highway Administration 610 East Fifty Street Vancouver, WA 98661 Phone - (206) 696-7738	1989
Mr. Marvin McCauley California Department of Transportation 5900 Folsom Boulevard Sacramento, CA 95819 Phone - (916) 739-2480	1988

STEERING COMMITTEE MEMBERS - Continued...

	TERM EXPIRES
Mr. David Mitchell Chief, Geotechnical Bureau Georgia Department of Transportation Forest Park, GA 30050 Phone - (404) 363-7546	1987
Mr. Harry Moore Geological Engineering Supervisor I Tennessee Department of Transportation Geotechnical Section P. O. Box 58 Knoxville, TN 37901 Phone - (615) 673-6219 Work - (615) 933-6776	1988
Mr. William F. Sherman Chief Geologist Wyoming Highway Department P. O. Box 1708 Cheyenne, WY 82002-9019 Phone - (307) 777-7450	1989
Mr. Mitchell D. Smith, Engineer Research and Development Division Oklahoma Department of Transportation 200 N. E. 21st Street Oklahoma City, OK 73105 Phone - (405) 521-2671	1989
Mr. Berke Thompson, Assistant Director Materials Control, Soil & Testing Division West Virginia Department of Highways 312 Michigan Avenue Charleston, WV 25311 Phone - (304) 348-3664	1988
Dr. Terry West, Associate Professor Department of Geosciences & Civil Engineering Purdue University West Lafayette, IN 47907 Phone - (317) 494-3296	1988

STEERING COMMITTEE MEMBERS - Continued...

	TERM EXPIRES
Mr. W. A. Wisner, Geologist Florida Department of Transportation Office of Materials and Research P. O. Box 1029 Gainesville, FL 32602 Phone - (904) 372-5304	1987
Mr. Burrell S. Whitlow, President Geotechnics, Inc. 321 Walnut Avenue (P.O. Box 217) Vinton, VA 24179 Phone - (703) 344-4569; 344-0198	1989
Mr. T. Leslie Youd 368 Clyde Building Brigham Young University Orem, Utah 84057 Phone - (801) 378-6327	1989
Mr. Ed J. Zeigler, Associate Rummel, Klepper, and Kahl 1035 N. Calvert Street Baltimore, MD 21202 Phone - (301) 247-2260 and 685-3105	1989

EMERITUS MEMBERS

R. F. Baker

Virgil E. Burgat

Robert G. Charboneau

Hugh Chase

A. C. Dodson

Walter F. Fredericksen

John Lemish

George S. Meadors, Jr.

W. T. Parrot

Paul Price

David L. Royster

Highway Geology Symposium

STANDING COMMITTEES

Medallion Selection Committee

Bill Sherman, Chairman
Mitch Smith
Burrell Whitlow

Public Relations Committee

Bill Lovell, Chairman
Dave Bingham (Eastern States)
Bill Sherman (Western States)

By Laws Committee

Burrell Whitlow, Chairman
Henry Mathis
Bill Wisner

Publications and Proceedings Committee

Dave Bingham, Chairman
Joe Gutierrez
Jeff Hynes

Emeritus Members Committee

Terry West, Chairman
Dave Mitchell

Committee on Guidelines for Appointments to National Steering Committee

Bill Wisner, Chairman
Harry Ludowise
Willard McCasland

Historian/Reporter

Jeff Hynes

Mailing List Committee

Willard McCasland, Chairman
Berke Thompson
Bill Wisner

Certificate of Appreciation Committee

Vernon Bump, Chairman
John Gilmore
Harry Moore

Highway Geology Symposium

CHAIRMAN OF LOCAL ARRANGEMENTS
FOR UPCOMING SYMPOSIUMS

Mr. Charles T. Janik *1987*
Soils Engineer
Pennsylvania Department of Transportation
1118 State Street
Harrisburg, PA 17120
Phone - (717) 787-4209

Mr. T. Leslie Youd *1988*
368 Clyde Building
Brigham Young University
Orem, Utah 84057
Phone - (801) 378-6327

Mr. Larry Lockett *1989*
Assistant Materials and Test Engineer
Alabama Highway Department
1409 Coliseum Boulevard
Montgomery, AL 36130
Phone - (205) 261-5788

Mr. Kenneth R. White, Director *1990*
Engineering Research Center
New Mexico State University
Box 3449
Las Cruces, NM 88003
Phone - (505) 646-3421

Page

WELCOME AND OPENING REMARKS
Gary J. Wicks, Director, Montana Department of Highways......... 1

GEOLOGY OF MONTANA
Richard S. Berg, Montana Bureau of Mines and Geology 2

GEOTECHNICAL DESIGN CONSIDERATIONS FOR ROAD CONSTRUCTION OF AN ACTIVE TALUS SLOPE
Walter V. Jones and Alan Stilley, Northern Engineering and Testing, Inc. 11

STATISTICAL ANALYSES OF FACTORS RELATED TO ROCK SLOPE STABILITY IN EASTERN TENNESSEE
C. Allen Torbett and Patrick T. Ryan, University of Tennessee .. 27

STABILITY PROBLEMS OF ROCK CUTS, U.S. 23 IN EASTERN KENTUCKY
Earl M. Wright, Kentucky Department of Highways, and Michael Bukovansky, Golder Associates. 42

ANALYSIS AND REHABILITATION OF AGING ROCK SLOPES
Lee W. Abramson and William F. Daly, Parsons Brinckerhoff Quade and Douglas, Inc. 56

A TIME-BASED MODEL TO HELP EVALUATE FUTURE STABILITY OF CUT SLOPES
Stanley M. Miller, University of Idaho 87

WIRE NETTING FOR ROCKFALL PROTECTION
Massimo Ciarla, Terra Aqua Inc. 100

ROCKFALL MITIGATION AS A FUNCTION OF COST BENEFIT AND PROBABILITY ASSESSMENT
Robert J. Watters, University of Nevada & Lyn Karwaki, ... 119
University of California, Berkeley

STATEWIDE INVENTORY AND HAZARD ASSESSMENT OF DEEP SEATED LANDSLIDES IN MONTANA
Edith M. Wilde and Mervin J. Bartholomew, Montana Bureau of Mines and Geology 132

THE CONSTRUCTION OF A SHOT-IN-PLACE ROCK BUTTRESS FOR LANDSLIDE STABILIZATION
Harry L. Moore, Tennessee Department of Transportation 137

APPLICATION OF PERSONAL COMPUTER MODELS FOR THE STABILITY ANALYSIS OF THREE LAND SLIDES NEAR VAIL, COLORADO
A. Keith Turner, Colorado School of Mines 158

GENERAL METHOD FOR THREE DIMENSIONAL SLOPE STABILITY FEATURING RANDOM GENERATION OF THREE DIMENSIONAL SURFACES
J.E. Thomaz and C. W. Lovell, Purdue University 177

POLYMER GEOGRID REINFORCED SOIL SLOPES REPLACE RETAINING WALLS
Michael J. Cowell, Ron Anderson, and Bob Anderson, The Tensar Corporation 198

DESIGN AND SPECIFICATION OF TIED BACK WALLS
R. Bruce Reeves, Lang Tendons, Inc............................. 212

PERFORMANCE OF INTERNALLY REINFORCED SOIL RETAINING SYSTEM
A. Kullathu Aiyer, New Mexico State University 250

ROADWAY STABILIZATION USING A TIEBACK WALL
John A. Franceski, Schnabel Foundation Company 261

RESILIENT MODULUS - WHAT IS IT?
Sam I. Thornton and Robert P. Elliott, University of Arkansas .. 267

RESILIENT MODULUS - WHAT DOES IT MEAN?
Sam I. Thornton and Robert P. Elliott, University of Arkansas .. 283

DYNAMIC PILE MONITORING AND PILE LOAD TESTS IN UNCONSOLIDATED SANDS AND GRAVELS, WYOMING
Michael P. Schulte, Wyoming Highway Department 302

SURVEY OF NON-DESTRUCTIVE WAVE PROPAGATION TESTING METHODS FOR THE CONSTRUCTION INDUSTRY
Larry D. Olson, and Edward O. Church, Olson-Church, Inc. ... 311

EVALUATION OF NONLINEAR STABILIZED ROTATIONAL STIFFNESS OF PILE GROUPS
Gary Norris, University of Nevada 331

REFRACTION SEISMIC STUDY TO EXPLORE A BORROW SOURCE IN A REMOTE AREA
Harry Ludowise, Federal Highway Administration 387

USE OF COMPUTER SPREAD SHEETS IN GEOTECHNICAL DESIGN AND REVIEW
Michael D. Remboldt, USDA Forest Service 399

WELCOME AND OPENING REMARKS

by GARY J. WICKS
Director, Montana Department of Highways
Helena, Montana

Mr. Wicks welcomed the symposium on behalf of the Montana Department of Highways. He commented on the challenge we all share in the transfer of technical information and innovation to highway design. He further added to this challenge by mentioning the current economic climate. Meetings such as this can help to accomplish these goals.

GEOLOGY OF MONTANA

Richard B. Berg
Montana Bureau of Mines and Geology
Montana College of Mineral Science and Technology
Butte, Montana 59701

ABSTRACT

Igneous and sedimentary rocks metamorphosed 2,700 million years ago to gneisses, marbles and schists are now exposed in the mountain ranges of southwestern and central Montana. These metamorphic rocks are overlain by less intensely metamorphosed sedimentary rocks of the Belt Supergroup, also of Precambrian age. Sediments of the Belt Supergroup were originally deposited in a large, shallow sea that covered most of western and central Montana and northern Idaho. Some high-angle faults that were active at this time are thought to have been reactivated intermittently through most of geologic time, in some instances with movement continuing to the present. Most of the overlying Paleozoic and Mesozoic sedimentary rocks were deposited in marine environments. These rocks, widely exposed in central and western Montana, are important hydrocarbon reservoirs in the subsurface of the Montana plains. In the latter part of the Mesozoic Era, large slabs of rock in western Montana were thrust eastward for distances up to 100 miles (160 km). This activity was accompanied by folding of sedimentary rocks into anticlines and synclines. Cretaceous-age sedimentary rocks, consisting largely of shales deposited in extensive seas, are exposed in much of central and eastern Montana. While these seas covered what is now the Great Plains, granitic magma intruded the crustal rocks of western Montana to form igneous bodies, and surface eruptions formed a variety of volcanic rocks. One of the intrusive bodies, the Boulder batholith, is the host rock for the very large metal deposit at Butte. Later, igneous activity moved to the east, resulting in the emplacement of near-surface igneous rocks now exposed by erosion in the mountains of central Montana. The Fort Union Formation of Tertiary age, known for thick coal beds, overlies Cretaceous sedimentary rocks in much of eastern Montana. Sediment was also deposited during the Tertiary in intermontane basins of southwestern Montana. Igneous activity continued into the Quaternary, with igneous rocks only 115,000 years old exposed in Yellowstone National Park. The last advance of the continental ice sheet covered the northern quarter of the state, leaving a thin veneer of glacial deposits. Alpine glaciers sculpted the higher mountains of western Montana.

Many mineral commodities have been produced from deposits in Montana. Major metals that have been mined include copper, gold, silver, lead, zinc, manganese, antimony, and chromium, with the promise of platinum and palladium mining in the near future. Nonmetallic mineral commodities include vermiculite, barite, bentonite, gypsum, talc, and sapphires. Montana also produces substantial amounts of coal, oil and gas.

INTRODUCTION

Evidence of a long and diverse sequence of geologic events can be recognized in Montana. These events range from the metamorphism of igneous and sedimentary rocks 3,350 million years (m.y.) ago to recent faulting that caused the Hebgen earthquake and the resulting catastrophic landslide in 1959. The greatest diversity of geologic features can be seen in the mountainous southwestern part of the state (Figure 1). This variety of geologic features has led a number of universities to conduct their summer geological and geophysical field programs in this area. The divisions of geologic time referred to in the following sections are shown in Figure 2.

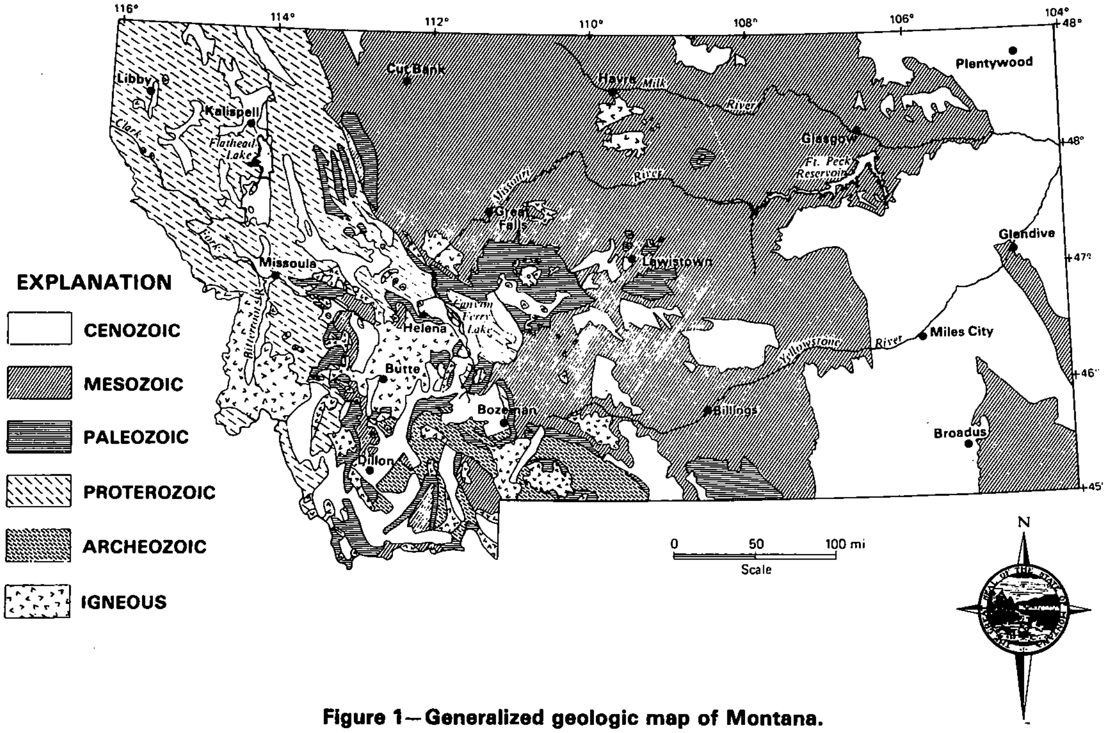
116°
114°
112°
110°
108°
106°
104°
48°
47°
46°
45°
Plentywood
Cut Bank
Havre
Milk
River
Libby
Kalispell
Flathead Lake
Glasgow
Ft. Peck Reservoir
Missouri
River
Great Falls
Glendive
Clark Fork
Missoula
Lewistown
Canyon Ferry Lake
Helena
Bitterroot
Butte
Yellowstone
River
Miles City
Bozeman
Billings
Broadus
Dillon
EXPLANATION
CENOZOIC
MESOZOIC
PALEOZOIC
PROTEROZOIC
ARCHEOZOIC
IGNEOUS
0
50
100 mi
Scale
N

Figure 1—Generalized geologic map of Montana.

ARCHEAN EON
(older than 2,500 m.y.)

Uplifted blocks of Archean metamorphic rocks form the cores of mountain ranges in southwestern Montana. Radiometric dates obtained from metamorphic rocks exposed in the Beartooth Mountains north of Yellowstone National Park indicate that some of these rocks were metamorphosed 3,350 m.y. ago (Mueller and others, 1985, p. 11). The precursor igneous and sedimentary rocks were obviously older, but how much older is not known. On the basis of the chemical compositions of these metamorphic rocks, Mueller and others (1985) inferred that the precursor igneous and sedimentary rocks were formed on an ancient

SUBDIVISIONS					Age estimates of boundaries in million years
PHANEROZOIC EON	CENOZOIC ERA	Quaternary Period		Holocene Epoch	0.010
				Pleistocene Epoch	2
		Tertiary Period	Neogene Subperiod	Pliocene Epoch	5
				Miocene Epoch	24
			Paleogene Subperiod	Oligocene Epoch	38
				Eocene Epoch	55
				Paleocene Epoch	63
	MESOZOIC ERA	Cretaceous Period		Late Cretaceous Epoch	96
				Early Cretaceous Epoch	138
		Jurassic Period			205
		Triassic Period			∿240
	PALEOZOIC ERA	Permian Period			290
		Carboniferous Periods	Pennsylvanian Period		∿330
			Mississippian Period		360
		Devonian Period			410
		Silurian Period			435
		Ordovician Period			500
		Cambrian Period			∿570
PROTEROZOIC EON	PROTEROZOIC Z				800
	PROTEROZOIC Y				1,600
	PROTEROZOIC X				2,500
ARCHEAN EON					

Figure 2—Subdivisions of geologic time with estimates of boundries (*from* Izett and others, 1986).

continent. Farther to the west in the Madison, Ruby and Gravelly Ranges and the Tobacco Root and Highland Mountains of southwestern Montana, igneous and sedimentary rocks were also metamorphosed to form rocks such as gneiss, amphibolite, marble, quartzite and schist. Although these rocks may have been metamorphosed 3,350 m.y. ago as were those in the Beartooth Mountains, a younger period of metamorphism 2,750 m.y. ago affected them (James and Hedge, 1980, p. 11). Metamorphism, caused by the confining pressure and high temperature of deep burial beneath overlying rocks since removed by erosion, was accompanied by stress within the crust of the earth which caused complex folding. About 2,700 m.y. ago magma intruded into metamorphic rocks in what is now the Beartooth Mountains and slowly cooled to form the Stillwater Complex (Lambert and others, 1985, p. 51). Tilting and subsequent erosion of this ultramafic complex situated along the northeast flank of the Beartooth Mountains has exposed layers of igneous rocks of differing composition. Layers of chromite-bearing rock near the base of this complex account for about 80 percent of the chromite reserves in the United States. During World War II and again during the Korean War chromite was mined from this deposit. More recently the copper and nickel resources of this complex have been investigated, and in 1973 a major platinum-palladium discovery was made. After extensive testing and development work, mining of part of this platinum-palladium deposit by the Stillwater Mining Company is planned for 1988.

Other important mineral deposits have been found in Archean metamorphic rocks. These include gold deposits in the Jardine district (north of Yellowstone National Park), Virginia City district south of Butte, Silver Star district also south of Butte and in the Tobacco Root Mountains southeast of Butte. Large bodies of unusually pure talc in marble layers are mined in the Ennis and Dillon areas. In addition, iron deposits occur in the Archean metamorphic rocks of southwestern Montana.

PROTEROZOIC EON
(2,500 m.y. to about 570 m.y. ago)

Archean metamorphic rocks were intruded by basic dikes between 1,455 m.y. and 1,120 m.y. ago (James and Hedge, 1980, p. 14). Concurrent with the intrusion of the earliest of these mafic dikes, a large northwest-trending basin developed in what is now northern Idaho, western Montana and southern Alberta. Sediment deposited in this basin, although subsequently metamorphosed to greenschist facies, retains features such as mud cracks, salt casts, ripple marks, and cut-and-fill structures indicative of shallow-water deposition. Principal lithologies of these metasediments of the Proterozoic Belt Supergroup are quartzite, siltite, argillite and lesser limestone and dolomite. The rocks of the Belt Supergroup form a very thick sequence of mostly shallow-water sediments at least 40,000 ft (12,200 m) thick near the center of the basin. Reconstruction of the stratigraphy and facies relationships of this sequence is difficult because most of the rocks of the Belt Supergroup now exposed in western Montana were thrust eastward, some for many tens of miles, near the end of the Mesozoic Era during the Laramide orogeny. Radiometric dates from the Belt Supergroup indicate that sediment was deposited from at least 1,500 m.y. ago to 900 m.y.

ago. During this interval of deposition, faulting in the basin probably contributed to variations in thickness and lithology. Gabbroic sills and basaltic flows within the Belt Supergroup are the result of two intervals of igneous activity at about 1,433 m.y. and 1,075-1,200 m.y. (Reynolds, 1984, p. 44-46) that are probably related to dikes intruded into Archean rocks at about the same times.

In the 1960s a large stratiform silver-copper deposit was discovered in metasedimentary rocks of the Belt Supergroup, in northwestern Montana. This deposit is now mined at Asarco's Troy mine. Since the development of this deposit another even larger silver-copper deposit, also in metasedimentary rocks of the Belt Supergroup was discovered in northwestern Montana and will be mined in the near future. Barite veins and a few gold deposits also occur in rocks of the Belt Supergroup.

PALEOZOIC ERA

(about 570 m.y. to 240 m.y. ago)

After uplift and accompanying erosion of Precambrian rocks, including both the Belt Supergroup and older Archean metamorphic rocks, Montana and surrounding areas were subjected to numerous invasions by marine waters. Because of gentle upwarping of land areas some seas were shallower than others, and fluctuating environments of deposition resulted in a variety of sediment types. The lowest formation of Paleozoic age is the Flathead Formation, a widespread sandstone or quartzite overlying Precambrian rocks and exposed in much of western and central Montana. Erosion of metamorphic rocks of the Canadian Shield to the northeast and rocks exposed on the Transcontinental arch to the east provided sand which was deposited on an extensive erosion surface that truncated both Archean metamorphic rocks and rocks of the Belt Supergroup (Peterson, 1981, p. 12). The Flathead Formation has been quarried for building stone at some localities where it has been metamorphosed to a quartzite. This distinctive Middle Cambrian formation is overlain by Cambrian shale, limestone and dolomite, which were deposited in a stable shelf environment with only minor fluctuations in sea level.

Ordovician sedimentary rocks in Montana are limited to one formation, the Bighorn Dolomite, exposed mainly in south-central Montana and encountered in oil wells in eastern Montana. Silurian sedimentary rocks have been encountered in drilling in eastern Montana, but are lacking in western Montana. Possibly they were never deposited in this area.

Most of Montana was covered by seas during the Devonian Period when conditions favored the deposition of fine-grained clastic sediments overlain by limestone and dolomite in turn overlain by shale. Some evaporite beds in this Devonian sequence contain halite ($NaCl$) and sylvite (KCl). In northeastern Montana these evaporite beds are found in drill holes at depths of more than 10,000 ft (3,000 m).

The Madison Group of Mississippian age is composed of limestone and dolomite and is one of the most widespread and easily recognizable stratigraphic units in Montana. Gray to buff cliffs of this limestone and dolomite are prominent on the flanks of most of the mountain ranges of southwestern and central Montana. Because carbonates of the Madison Group accumulated slowly in a sea far removed from land, these rocks are relatively free of land-derived detritus. Because of its cavernous nature and widespread distribution, the Madison Group is an important aquifer and, like some of the other Paleozoic formations, an important hydrocarbon reservoir. These beds are also a major source of limestone for the manufacture of portland cement and for other industrial uses.

Beds of upper Mississippian age overlying the Madison Group differ markedly from it because uplift and erosion of the Canadian Shield to the northeast and the Transcontinental arch to the east provided a supply of detritus. Although there are carbonate units in this younger sedimentary sequence, sandstone and finer-grained rocks predominate. In central Montana the Heath Formation (Big Snowy Group of Upper Mississippian age) contains black, organic-rich oil shale. The Kibbey Formation (the lowest formation of the Big Snowy Group) contains gypsum beds which are mined in central Montana.

Permian beds of phosphate, carbonate and chert were deposited in a sea that covered a large area of the northern Rockies, including southwestern Montana. The source area of clastic sediments deposited in this sea was to the north and east in Montana. The Permian Phosphoria Formation contains phosphorite beds mined for phosphate in Montana and Idaho.

MESOZOIC ERA
(about 240 m.y. to 63 m.y. ago)

During the Triassic Period sediment was deposited in a sea that covered much of the same area as that occupied by the Permian sea. Triassic beds in this area are composed of fine-grained clastic sediment. Jurassic marine rocks, also composed of fine-grained detrital sediments and carbonates, overlie the Triassic sedimentary rocks. A gypsum bed in the Jurassic Piper Formation is mined by U.S. Gypsum at their underground mine east of Lewistown. During the Jurassic period the sea withdrew leaving a broad coastal plain on which mud, silt and fine-grained sand were deposited. Abundant vegetation accumulated in poorly drained swampy areas to form the coal beds of the upper Morrison Formation which have been mined in parts of central Montana. The overlying Kootenai Formation of Cretaceous age was deposited in an extensive alluvial plain. Periodic uplift of the mountains to the west provided a source of much coarser sediments than in the underlying Morrison Formation. Both the Morrison and Kootenai formations contain ceramic-quality clay beds, some of which were mined in underground mines in central Montana.

Cretaceous rocks exposed over large areas in the plains of central and eastern Montana record shallow seas covering this area and receding to the north from the mountains. At least five cycles of the sea advancing to the south and then retreating to the north are recorded in Cretaceous sedimentary rocks. Cretaceous formations are characterized by a western nonmarine facies which is composed of detritus derived by erosion of the Rocky Mountains that were being uplifted at this time. Farther east, finer grained sediments were deposited in the sea to become the shale characteristic of many of the marine Cretaceous formations. Bentonite beds are prevalent in marine Cretaceous units and are an important source of this mineral commodity. Volcanic ash that fell into or was washed into the sea altered to the clay of these bentonite beds.

While Cretaceous seas covered eastern Montana, thrust faulting was occurring in western Montana. In southwestern and central Montana large slabs of rocks were thrust eastward as much as 100 miles (160 km) during the interval inferred to be between 100 and 75 m.y. ago (Ruppel, Wallace, Schmidt and Lopez, 1981, p. 149). Much of this thrust faulting involved rocks of the Belt Supergroup and most of the rocks of this supergroup now exposed in western Montana have been thrust to the east. At about this same time, magma cooled slowly to form the Idaho batholith, a large complex of granitoid plutons exposed in western Montana and extending into central Idaho. Emplacement of the Idaho batholith spanned a substantial time interval from about 110 to 55 m.y. ago (Armstrong, 1975, p. 4). Within the shorter time interval from 78 to 68 m.y ago igneous activity farther east in Montana produced the Boulder batholith (Robinson, Klepper and Obradovich, 1968, p. 566). This batholith, which extends from Butte on the south to Helena on the north, consists of at least 15 granitoid plutons, one of which is the host rock for the very large metal deposit at Butte. This deposit was mined extensively for copper, silver and many other metals for over 100 years until 1983 when mining was temporarily discontinued until 1986 when Montana Resources Inc. started mining. Volcanic activity related to the emplacement of the Boulder batholith may have produced volcanic ash that was deposited in a Cretaceous sea and subsequently altered to form bentonite beds in eastern Montana. In addition to the Boulder batholith, other granitoid plutons were emplaced in western Montana at about the same time.

CENOZOIC ERA
(63 m.y. ago to present)

The Cenozoic Era is divided into two periods, the Tertiary Period from 63 to 2 m.y. ago and the Quaternary Period from 2 m.y. ago to the present (Figure 2). During the Paleocene Epoch, the oldest epoch of the Tertiary Period, sediment of the Fort Union Formation was deposited in what was mainly a non-marine environment that covered much of eastern Montana and the western part of the Dakotas and northern Wyoming. Rocks of this group were deposited mainly in rivers, lakes and swamps. Accumulation of plant remains in these swamps resulted in the formation of thick beds of lignite and subbituminous coal now mined in the Powder River Basin of Wyoming and Montana.

Igneous activity that had begun in southwestern Montana during the Late Cretacous Period continued into the Eocene Epoch with the formation of both plutonic and volcanic rocks that range in composition from dacite to andesite. Igneous activity after the Eocene produced rhyolite and basalt and was accompanied by block faulting that formed the intermontane valleys of western Montana (Chadwick, 1981). From the late Eocene to the Pliocene these valleys were partially filled with detritus derived from the surrounding mountain ranges and with volcanic ash from more distant sources. During the interval from late Eocene to Pliocene the climate varied from wet to dry, with deposition of fanglomerates, debris flows and the development of braided streams during the drier times. During wetter times some of the sediment was removed from these basins by meandering streams. Fossil vertebrates are locally abundant in some of these beds and insect fossils are found at a number of localities. In central Montana numerous isolated mountain ranges such as the Sweetgrass Hills and the Highwood, Bearpaw, Little Rocky, Judith, Moccasin and Crazy Mountains were the sites of igneous activity, mainly between 65 and 48 m.y. ago (Marvin and others, 1980). In some of these mountains magma forced up the surrounding sedimentary rocks forming domes which were later eroded to sufficient depth to expose the igneous rocks; the Little Rocky Mountains are an example of such a structure. In other instances, intrusion of magma was accompanied by the emplacement of many dikes such as in the Crazy and Highwood Mountains. Because surrounding sedimentary rocks were more susceptible to erosion than the igneous rocks, they were eroded more rapidly, leaving the igneous rocks standing above the surrounding plains. Most of these igneous rocks are alkalic and, in the Judith, Little Rockies and Moccasin Mountains and in the Sweet Grass Hills, host gold deposits.

Igneous activity continued into the Quaternary in Yellowstone National Park and vicinity. Basalt flows exposed on the east side of the Yellowstone River north of Yellowstone National Park are 0.6 m.y. old (Chadwick, 1978, p. 26) and a rhyolite flow in the vicinity of West Yellowstone is only 114,500±7,300 years old (Pierce, Obradovich and Friedman, 1976).

Although there is evidence of continental glaciation of the plains of Montana before the Wisconsinian age of glaciation, most glacial features are attributed to Wisconsinian glaciation, the youngest of the Pleistocene stages. At that time the continental ice sheet covered the area roughly north of the present course of the Missouri River and extended west to the eastern front of the Rocky Mountains. Deposits of glacial till now cover the bedrock in most of this area. At the same time that this part of Montana was covered by the continental ice sheet, alpine glaciers occupied most of the mountain ranges of western Montana. Glaciers are now found only in a few localities in western Montana, with the greatest concentration in Glacier National Park.

Tectonic activity continues in western Montana. The most recent major earthquake in Montana was the 1959 Hebgen earthquake west of Yellowstone National Park. This earthquake of magnitude 7.5 caused a large landslide that dammed the Madison River to form a new lake appropriately named Earthquake Lake.

ACKNOWLEDGMENTS

Review of an earlier version of this paper by Susan M. Vuke-Foster and Robert N. Bergantino improved it substantially. Their comments and interest are sincerely appreciated. Editorial suggestions by Steve Blodgett were also very helpful.

REFERENCES CITED

Armstrong, R. L., 1975, The geochronometry of Idaho: Isochron/West, no. 14, p. 1-50.

Chadwick, R. A., 1978, Geochronology of post-Eocene rhyolitic and basaltic volcanism in southwestern Montana: Isochron/West, no. 22, p. 25-28.

________, 1981, Chronology and structural setting of volcanism in southwestern and central Montana, in Montana Geological Society Field Conference & Symposium Guidebook, T. E. Tucker (ed.): Montana Geological Society, Billings, p. 301-310.

Izett, G. A., Lanphere, M. A., MacLachlan, M. E., Naeser, C. W., Obradovich, J. D., Peterman, Z. E., Rubin, M., Stern, T. W., and Zartman, R. E., 1986, Major geochronologic and chronostratigraphic units: Isochron/West, no. 45, inside front cover.

James, H. L., and Hedge, C. E., 1980, Age of basement rocks of southwest Montana: Geological Society of America Bulletin, v. 91, p. 11-15.

Lambert, D. D., Unruh, D. M., and Simmons, E. C., 1985, Isotopic investigations of the Stillwater Complex: A review, in The Stillwater Complex, Montana: Geology and Guide, G. K. Czamanske and M. L. Zientek (eds.): Montana Bureau of Mines and Geology Special Publication 92, p. 46-54.

Marvin, R. F., Hearn, B. C., Jr., Mehnert, H. H., Naeser, C. W., Zartman, R. E., and Lindsey, D. A., 1980, Late Cretaceous-Paleocene-Eocene igneous activity in north-central Montana: Isochron/West, no. 29, p. 5-25.

Mueller, P. A., Wooden, J. L., Henry, D. J., and Bowes, D. R., 1985, Archean crustal evolution of the eastern Beartooth Mountains, Montana and Wyoming, in The Stillwater Complex, Montana: Geology and Guide, G. K. Czamanske and M. L. Zientek (eds.): Montana Bureau of Mines and Geology Special Publication 92, p. 9-20.

Peterson, J. A., 1981, General stratigraphy and regional paleostructure of the western Montana overthrust belt, in Montana Geological Society Field Conference & Symposium Guidebook to Southwest Montana, T. E. Tucker, (ed.): Montana Geological Society, Billings, p. 5-35.

Pierce, K. L., Obradovich, J. D., and Friedman, I., 1976, Obsidian hydration dating and correlation of Bull Lake and Pinedale glaciations near West Yellowstone, Montana: Geological Society of America Bulletin, v. 87, p. 703-710.

Reynolds, M. W., 1984, Tectonic setting and development of the Belt basin, northwestern United States, in The Belt, Abstracts and Summaries, Belt Symposium II, 1983, S. Warren Hobbs (ed.): Montana Bureau of Mines and Geology Special Publication 90, p. 44-46.

Robinson, G. D., Klepper, M. R., and Obradovich, J. D., 1968, Overlapping plutonism, volcanism, and tectonism in the Boulder batholith region, western Montana, in Studies in Volcanology, R. R. Coats and others (eds.): Geological Society of America, Memoir 116, p. 557-576.

Ruppel, E. T., Wallace, C. A., Schmidt, R. G., and Lopez, D. A., 1981, Preliminary interpretation of the thrust belt in southwest and west-central Montana and east central Idaho, in Montana Geological Society Field Conference & Symposium Guidebook to Southwest Montana, T. E. Tucker (ed.): Montana Geological Society, Billings, p. 139-159.

GEOTECHNICAL DESIGN CONSIDERATIONS FOR ROAD CONSTRUCTION ON AN ACTIVE TALUS SLOPE

by Walter V. Jones, P.E., and Alan Stilley, P.E.
Northern Engineering & Testing, Inc.

Abstract

Precious metal mining and timber harvesting in the early 1980s prompted construction of access roads into steep and mountainous terrain in the northern Rocky Mountains. South of Big Timber, Montana, one of the mining projects required a new road that would cross talus slopes with boulders to 30 feet in diameter and evidence of recent talus movement. Methods for design and construction of roads across active talus slopes are not well developed. The following article presents a case history for one such project.

Aerial photographs, helicopter reconnaissance and walking of the route were used to prepare geologic maps outlining dormant and active talus areas. Angles of talus slopes were measured at 25 to 38 degrees to the horizontal. Observations where stream erosion undercut talus slopes showed, if the talus is clean, cuts would stand at 36 to 38 degrees: where the talus contained significant fines, slopes at 45 degrees were stable. Descriptive terms were selected for talus size, activity of the talus slope, and steepness of terrain for communicating the information and as a support to design recommendations.

Although cuts in the talus slopes wide enough to create a benched road could be safely made and would be generally stable at one and one quarter horizontal to one vertical, rolling talus fed from above cliffs would endanger road users. Warning systems and protected vehicle turnouts would reduce the risk to road users, but the safest method of protection through the most active talus areas would be to place the road in a buried enclosure below ground surface. This would allow rolling talus to move over the road without affecting the roadway or causing danger to the road user.

INTRODUCTION

Precious metal prices in the early 1980s prompted the improvement or development of many mines in the Northern Rocky Mountains. One of these developments, about 35 miles south of Big Timber, Montana, in the Absorkee Mountain Range, required an access road to be constructed in steep mountainous terrain through active talus slopes. The original road would only be a 14-foot wide access road leading to a test adit, and after the determination of how profitable the mine would be, the road would possibly be enlarged to 24 feet wide. Both platinum and palladium were to be mined.

GENERAL GEOLOGIC CONDITIONS

The Absorkee range is part of the Northern Rocky Mountains and consists of high plateaus and peaks up to more than 12,000 feet in elevation. The proposed road would extend up a valley that is relatively U-shaped and broad in the lower reaches, becoming steeper and V-shaped in the upper reaches. A major geologic unit is the Stillwater Complex which is a unit of a large igneous intrusive formation uplifted to form the Absorkee Range. In the immediate project area, the exposed bedrock consists primarily of Pre-Cambrian granite rock or closely related types. Local mountain glaciation covered the Absorkee Range during the last ice age and extended down the valley. Considerable faulting of these units has occurred in the area. Of primary importance for the proposed roadway was the necessity to cross long talus slopes, some of which appeared to be active. The talus consisted of colluvial materials with boulders up to 30 feet in diameter which would topple from the steep cliffs at the head of the talus slopes. At some locations there were no remaining cliff faces while at other locations there were cliffs up to several hundred feet high feeding the top of the talus slopes. Large blocks appeared to break off as thick slabs from the cliff faces. Natural tension cracks, freeze-thaw, wet-dry, and temperature expansion and contraction contributed to the deterioration at the cliff face and the manufacture of broken rock for development of talus slopes below.

In the lower portion of the canyon, the creek meandered and ran rather gently at a slight gradient, but in the upper portions, the creek ran very rapidly, at steep gradients, and carried a considerable amount of bed load during the highest water periods. This caused downcutting and continual erosion away from the toe of some of the talus slopes and also triggered at least one major landslide which is not included in the discussion for this paper. At the undercut locations large steep slopes were exposed for observation. Where these contained considerable fines they ranged from approximately 45 degrees to near vertical.

METHODS OF INVESTIGATION AND FINDINGS

Because of the remoteness of the area, with no access other than foot travel, a helicopter was used in the early phases of the investigation, and was used for transportation from the end of an existing road to the project area during the later phases of the investigation. Aerial photographs similar to Photos 1, 2, and 3 had been taken and were used extensively, especially in evaluating where active talus slopes existed. After the surveyors had established a preliminary centerline alignment in the field, the entire alignment was walked and geologic conditions mapped. Existing slope angles were measured at many locations. Photographs were taken to illustrate important features.

TALUS SLOPES

Talus was generally present at intermediate elevations on most of the valley slopes. Several areas in the valley have active talus slopes: that is, rock is currently being deposited down the slopes. Aerial photographs were used to show the distribution of active talus slope areas.

PHOTO 1 - An overview of the steep valley where the upper road alignment was proposed. Note the variation in color of the talus slope.

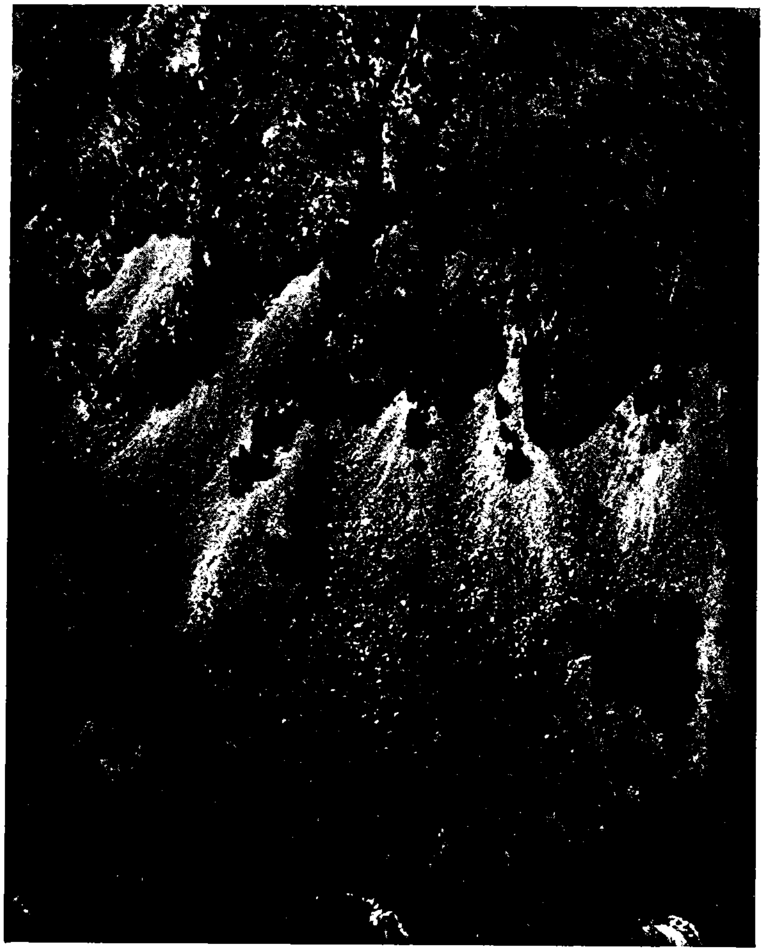

PHOTO 2 - The proposed road alignment crosses this steep talus slope. Light colored areas indicate active talus. Note distribution and distance individual rocks have rolled.

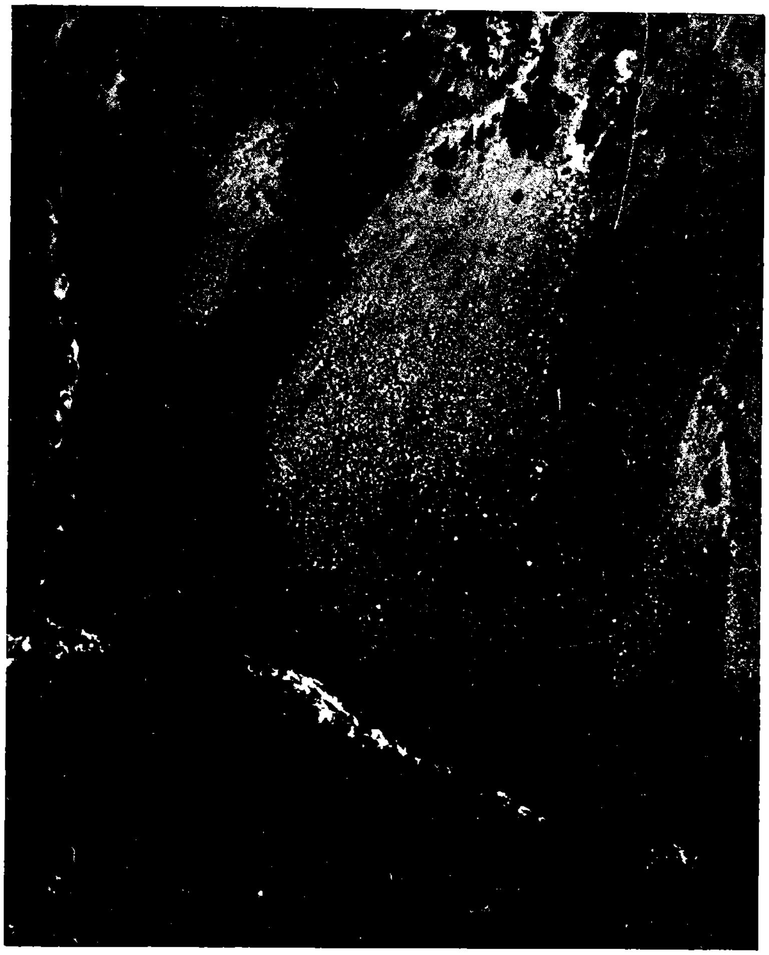

PHOTO 3 - This is one of the widest, most active talus areas the roadway would cross. Note that active movement of large blocks extends to the stream.

Generally the gravity deposition of the talus has resulted in the larger blocks of rock being deposited at lower elevations near the base of the slopes, while the finer material is deposited farther up the slopes (See Photo 4). Inactive areas of talus tend to have a brown color, characteristic of rock having been exposed to the elements for many years; while the active areas tend to have a light-gray color characteristic of freshly exposed rock. This is evident in several of the photos. The talus ranges from plate-like pieces to near cube shaped pieces. The flatter, platey pieces were generally distributed higher in the slope than the cube-like pieces which rolled farther down slope before stopping. A natural sorting of both sizes and shapes thus occurs.

Where movement by occasional toppling and mostly sliding has occurred, slope angles are steep. Where movement is by rolling and the slope is long enough for large momentum to develop, the blocks tend to roll to form flatter slopes as shown on Photo 6.

Measured slope angles ranged from about 25 to 38 degrees to the horizontal in the talus areas. An exception is near the toe of some talus slopes where massive blocks have "runout" and created very flat areas. Photo 7 taken along a talus slope shows the steepness, distribution of sizes, active and dormant areas, and the cliffs feeding the talus movement.

In many areas the "feed cliffs" provide enough new material to prevent vegetation establishment below them. Also fresh blocks of talus are scattered down the slope several hundreds of feet. An important factor in distribution of block size along the slope is the jointing and fracture patterns in the cliff rock. In several areas the patterns were closely spaced so all pieces were smaller than a few feet in diameter. At other locations widely spaced patterns produced rock sizes in excess of 30 feet in diameter. Photo 8 shows an area where joint and fracture patterns produced much smaller blocks than did the cliffs above Photo 6.

Another important item to the downhill movement and degree of activity of talus slopes shown in Photo 9 is the "slabbiness" of the rock in the "feed cliffs".

Most of the talus, where the proposed road crosses it, is relatively clean, i.e., free of fines in the upper several feet. Observation where stream erosion undercut the slopes indicates that where the talus is clean, slopes are relatively stable at about 36 to 38 degrees; where there is significant fine material in the talus, stable slopes were observed at angles of 45 degrees and steeper.

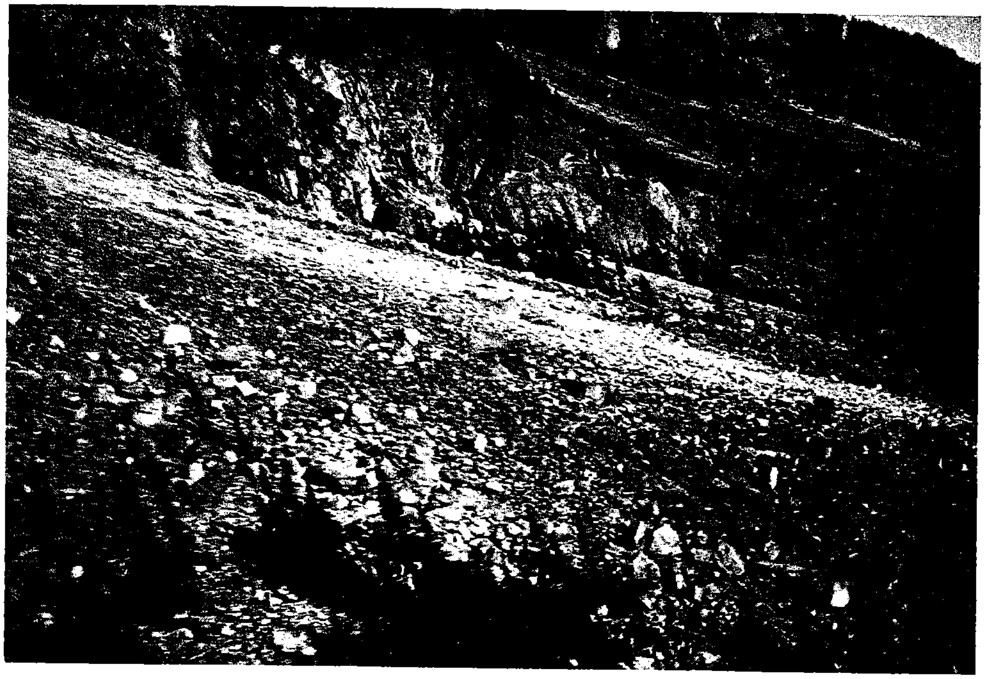

PHOTO 4 - Distribution of talus on near dormant to active slope. Finer material is deposited on upper slope while larger blocks roll to lower slope. Trees are partially buried and some active blocks are scattered amongst the trees. Lighter areas indicate recent rolling talus.

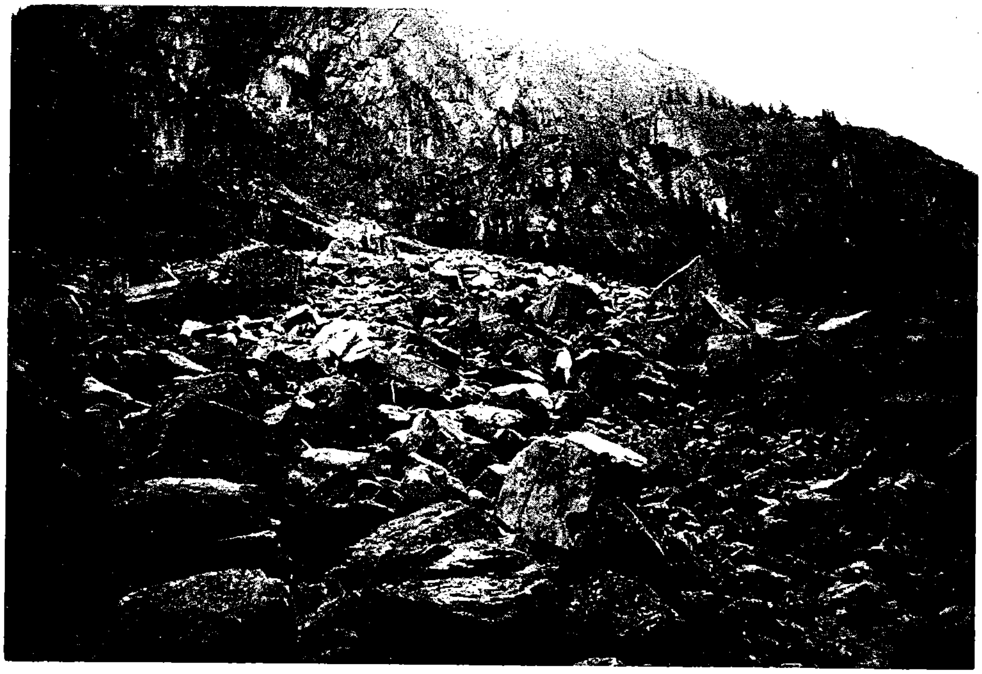

PHOTO 5 - A narrow active talus area. Note the block shape of most rocks in the near foreground. Very few fines have made it this far from the "feed" cliffs.

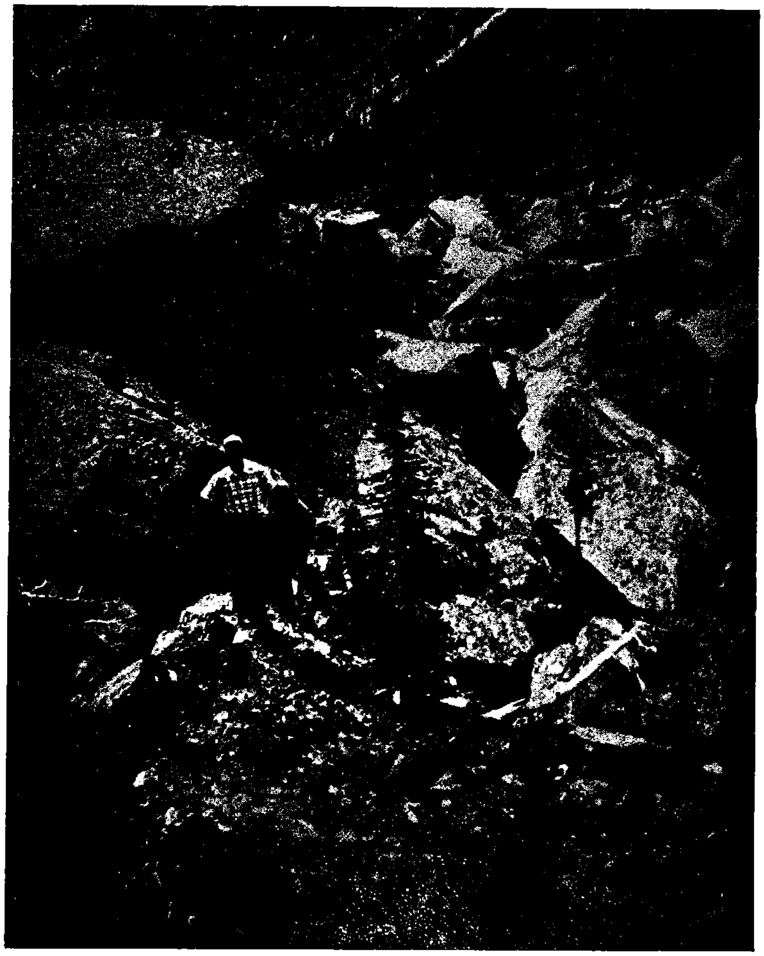

PHOTO 6 - Angle of talus slope is less than 20 degrees. Very large cube-like blocks had considerable momentum to "runout" at these flat slopes. Blocks to 30 feet in diameter were common in this area.

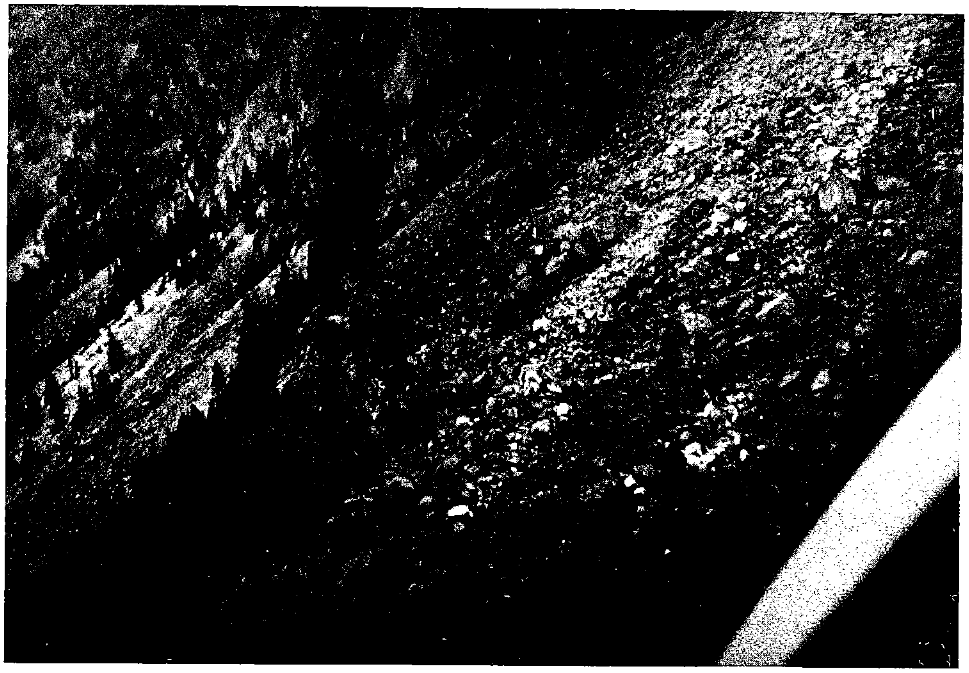

PHOTO 7 - Cliff areas interspersed in the talus slope. A very active area in upper right of photograph. Notice large pines growing in area protected from active talus by cliffs.

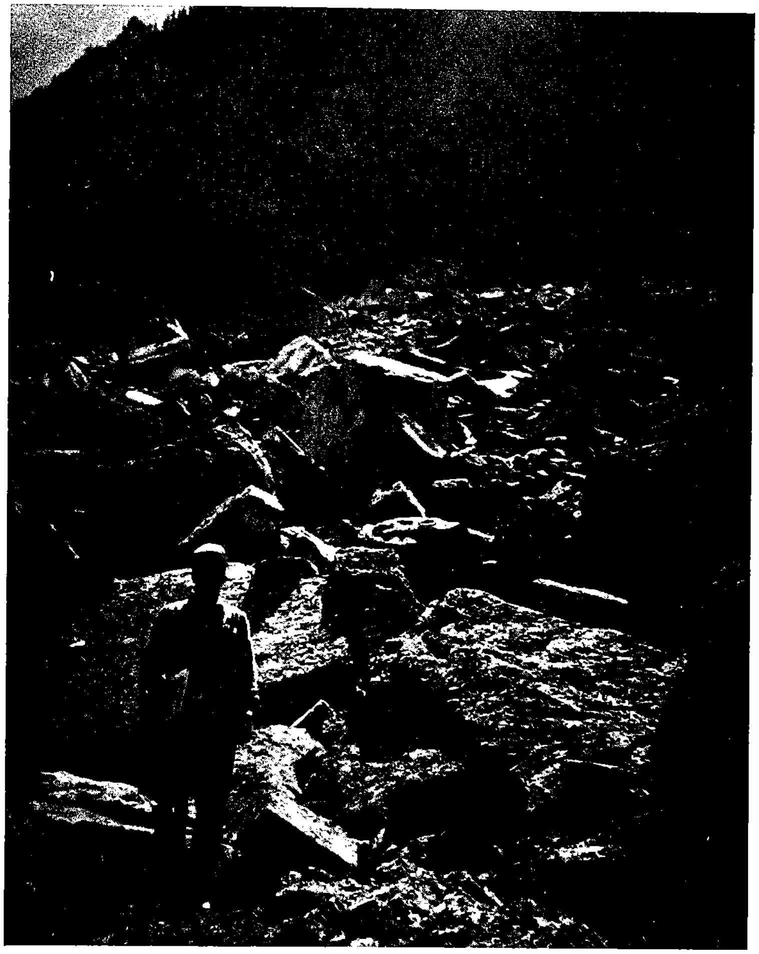

PHOTO 8 - Although not far from the feed cliffs this material is much smaller than that in Photo 6. This is a result of joint and fracture patterns in the cliff rock.

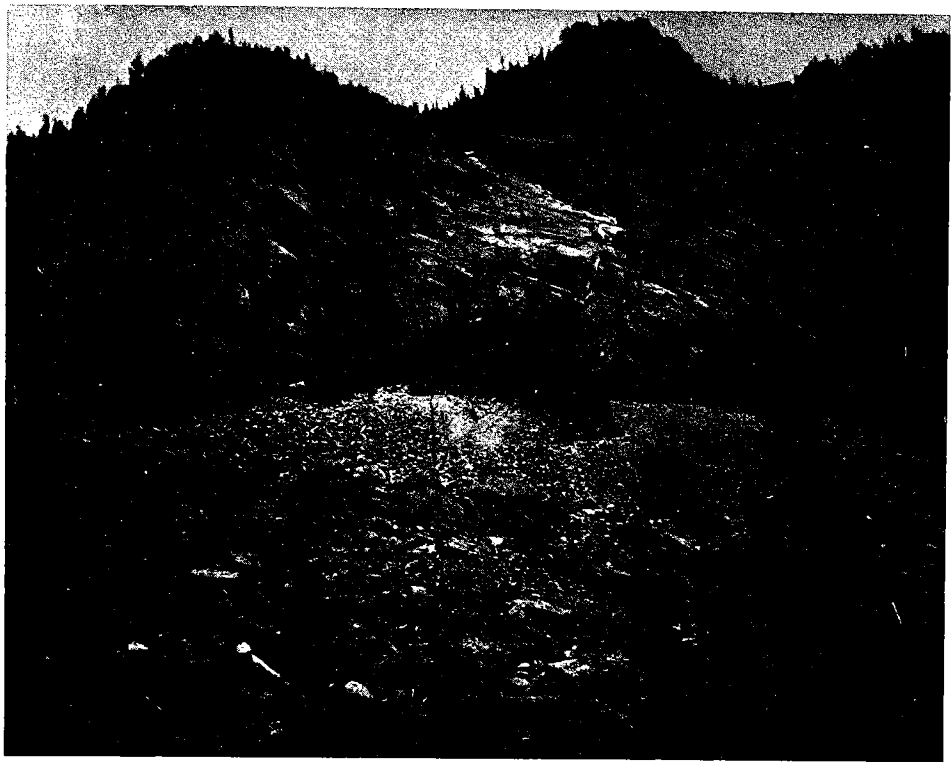

PHOTO 9 - Cliff rock at this location is "slabby" so active talus is confined close to the cliff face.

In order to communicate the actual conditions to engineers for design purposes, descriptive terms of the talus material were developed. The descriptive terms were with respect to size, activity, and steepness of the talus slope. These are listed as follows:

Talus Size

A. Small talus was described as that talus larger than one-half cubic yard in volume, and less than 10 feet in diameter. This material cannot be moved with scraper type equipment, but can generally be moved with bulldozers.

B. Medium talus is that material which can be moved with a bulldozer, but occasional ten foot diameter or larger material will need to be blasted.

C. Large talus is that material larger than ten feet in diameter which would normally require drilling and blasting to break it into smaller sizes prior to moving.

Activity of Talus Slopes

A. Dormant: No evidence of any recent talus movement. Characteristic color is dark. Possible areas of large old trees in talus. No special design needed.

B. Moderately Active: Some evidence of recent talus movement within the last few years. Possible areas of small young trees in talus. Will probably not require special design procedures.

C. Active: Evidence of recent talus movement, probably within the last year. Will require special design. Color is light, characteristic of freshly exposed rock. If trees were in talus, they showed signs of recent damage or of being partly to mostly covered.

Steepness of Terrain

A. Gentle: Majority of slopes less than 30 degrees to the horizontal.

B. Moderate: Ground slopes between 30 and 36 degrees to horizontal.

C. Steep: Most slopes are steeper than 36 degrees to horizontal.

These descriptive terms were used in a tabular form to list the conditions, station to station, in the talus portion of the roadway alignment.

An example of this listing is shown in Tables 1 and 2 below:

TABLE 1
NARRATIVE DESCRIPTION OF TALUS SLOPE CONDITION BY STATIONS

72+40 to 73+90 - This part of the route crosses an active talus slope composed of large sized talus blocks. There is evidence of recent movement of talus blocks up to five feet in diameter, over the proposed alignment. The exposed rock cliff east of the alignment is feeding the slope and appears to contain several areas of imminent rockfall. Special design procedures will be necessary to deal with the active talus hazard in this section. East of centerline the terrain is steep, while to the west it is moderate. Access will be difficult and large talus excavation methods will be required. Photograph 6 shows conditions east of centerline in this section.

73+90 to 84+50 - The line begins to traverse the toe of the large slide feature in this section. Medium sized talus, with considerable fines, apparently carried down by the slide, is present in this area. The road route also comes quite close to the river in this section with the alignment on steep slopes at the toe of the slide feature. There may also be some alluvial gravel deposits immediately adjacent to the river. In several areas, bin walls will probably be required to construct the road next to the river and on steep slopes. Tentatively, bin walls are planned between stations 75+50 and 77+90 and between 80+00 and 82+70. The talus material, or alluvium, should provide good support for bin wall structures. The deepest cut, approximately 30 feet, also occurs in this section at approximate station 79+00. It is difficult to judge, but surface observations of slopes eroded by the river in this area indicates this cut should be mostly in the talus material. Equipment access will be difficult and medium talus excavation methods are anticipated.

TABLE 2
AN EXAMPLE SUMMARY LISTING OF IMPORTANT FEATURES FOR TALUS SLOPE DESIGN

Station	Road Subgrade Material	Anticipated Excavation Conditions	Talus Activity	Remarks
63+50 to 65+50	Talus	Talus - Medium	Dormant to Moderately Active	1. Scattered trees. 2. Groundslope is moderate.
65+50 to 68+50	Talus	Talus - Large	Dormant to Moderately Active	1. Very difficult access and excavation due to large talus. 2. Terrain is moderate.
68+50 to 70+00	Talus	Talus - Medium	Dormant	1. Terrain is moderate.
70+00 to 72+40	Talus	Talus - Large	Dormant to Moderately Active	1. Rock cliff located immediately east of centerline. 2. Terrain is steep east of centerline and moderate to west. 3. Very difficult access and excavation conditions due to large talus.

TABLE 2 (CONT.)

Station	Road Subgrade Material	Anticipated Excavation Conditions	Talus Activity	Remarks
72+40 to 73+90	Talus	Talus - Large	Active	1. Evidence of recent talus movement. Blocks up to 5′. 2. Very difficult access and construction conditions. 3. Terrain is steep east of centerline and moderate west.
73+90 to 84+50	Talus	Talus - Medium	Dormant	1. Route traverses toe of slide feature. 2. Terrain is moderate to the east and steep immediately adjacent to river. 3. Possible bin walls at 75+50 to 77+90 and 80+00 to 82+70. 4. Route is heavily timbered.

DESIGN APPROACHES

Three main considerations were thought to be critical for the section of roadway through the talus slopes: 1) construction methods, 2) safety to roadway user, and 3) long term maintenance costs.

With respect to the construction considerations, the large talus not only would require special heavy equipment and blasting, but access would be difficult and some sort of a pad of finer material would need to be placed across it for getting equipment to the work area as well as providing a subgrade for the roadway system. During construction, workers would need to be careful and on the alert for natural or work related rolling talus rocks.

With respect to safety of the user the activity level of the talus was extremely important. Not only were shallow type creep movements to be considered, but of greater concern was the rolling large talus rocks that could strike vehicles traveling the roadway. Principally, there were two approaches to improving safety through the active talus slope areas. One was to devise a safety alarm network and safety turnout locations which would still have a considerable degree of risk associated for the road user. The other was to protect the roadway by burying it in an underground conduit through the active talus slope areas. In this way, as large talus rocks would topple down the slope, they would merely roll over the top of the roadway not threatening traffic or causing risk to anyone.

With respect to long-term maintenance costs, both the shallow creep and rolling talus movement were important. Roadway damage from either source would require expensive repairs to maintain a paved road on the steep hillside. Shallow creep type movements would crack and deform the pavement requiring crack maintenance and periodic overlays to smooth the road. Toppling boulders would puncture or crack the asphalt surface and damage guard rails or other restraining systems. Cut slope and fill slope slides would sever the roadway and render it unusable until repairs could be made. In general these slopes for the expected life of the roadway (less than 30 years) should be made as steeply as they will remain stable against slide type failures. This reduces the amount of new exposed surface to the elements. Recommended slope angles in the angular talus materials were:

Material Type	Slope Inclination Horizontal to Vertical
Cut Slopes	
Clean talus	1 1/4:1
Dirty talus (considerable fines)	1:1
Fill Slopes	
All talus	1 1/4:1

PHASED CONSTRUCTION

Construction of the roadway in two phases was appealing because this approach provided additional observation prior to making a decision to use expensive buried roadway sections. That is the original 12-foot wide road, which would carry little traffic during exploration of the adit, could be constructed in a conventional way through the active talus. This would allow evaluation of construction equipment, procedures, benching into the talus, activity of the talus (creep and rolling) and stability of cutslopes into the talus.

Then if the decision to develop the mine into a large scale operation was reached, better design and construction information would be available. A decision to use safety warning devices or a buried roadway would be more obvious and the locations where they would be most beneficial could be better pinpointed.

It is unfortunate that the project road was not constructed so that this case study could have included a complete evaluation of the methods of analysis, designing and constructing engineering projects across talus slopes.

CONCLUSIONS

Road design and construction across active talus slopes with boulders as large as 30 feet in diameter requires careful investigation, planning, and applied judgment. Methods of communicating field information to designers are extremely important. For this project several methods were used:

Geologic maps

Aerial photographs

On-the-ground photographs

Descriptive terms with respect to size, activity and steepness were tabulated for the entire alignment.

Written descriptions

A phased approach to the development of the final roadway section is preferable when possible. This allows a field testing of basic assumptions and judgments before applying them to the final design.

37th Annual Highway Geology Symposium, Helena, Montana, August 20-22, 1986

STATISTICAL ANALYSES OF FACTORS RELATED TO ROCK SLOPE STABILITY IN EASTERN TENNESSEE

Patrick T. Ryan and C. Allen Torbett
Department of Geological Sciences
The University of Tennessee in Knoxville

Eric C. Drumm and William F. Kane
Department of Civil Engineering
The University of Tennessee in Knoxville

Abstract

Rockslope failure in the Southern Appalachians of Eastern Tennessee/Western North Carolina has been a pervasive problem and increasing future development enhances the likelihood of greater damage. A systematic analysis was conducted of two stable and six unstable rock slopes occurring within the Blue Ridge Physiographic Province in folded and faulted metasediments of Cambrian and Precambrian Age. The slopes examined were comprised of slate, phyllite, quartzite and shale. The complex structural style of the region is the result of intense thrust faulting.

The field investigation employed standard geological techniques using a Brunton Pocket Transit. Geologic and geometric observations were taken on all major discontinuities including: faults, bedding, cleavage and joints. In addition, the slope height, slope orientation, and the presence and location of tension cracks and failure planes were recorded. Joint density and Schmidt hardness values along failure planes were obtained in an attempt to estimate the discontinuity shear strength.

A parametric study was conducted to determine the sensitivity of the calculated factor of safety with respect to the cohesion (Φ) and friction angle(Φ) of the failure surface. For the range of slope geometries encountered in this study, this parametric study indicated that FS and cohesion were sensitive to the tension crack location. FS was found not to be significantly affected by friction angle over the expected range of values (25°-40°). With the assumption that (Φ) has a minimal affect on the calculated FS, a representative value of Φ was chosen and the value of cohesion was back-calculated for each of the unstable slopes. Regression analyses was performed on the data set. Variables examined were joint cohesion, slope face angle, joint density, slope azimuth, slope height, tension crack size and position, Schmidt hammer values and safety factors as derived from limiting equilibrium analysis. Several strong correlations were suggested within the slope parameter data set and are summarized in the correlation coefficient matrix.

This study verifies the applicability of limiting equilibrium analyses in the Southern Appalachians. Simple field tests utilizing the Schmidt hammer are shown to be useful in estimating cohesion. In addition, the use of multivariant statistical techniques can be a valuable aid in determining causal components, as well as probabilistic aspects of rock slope stability.

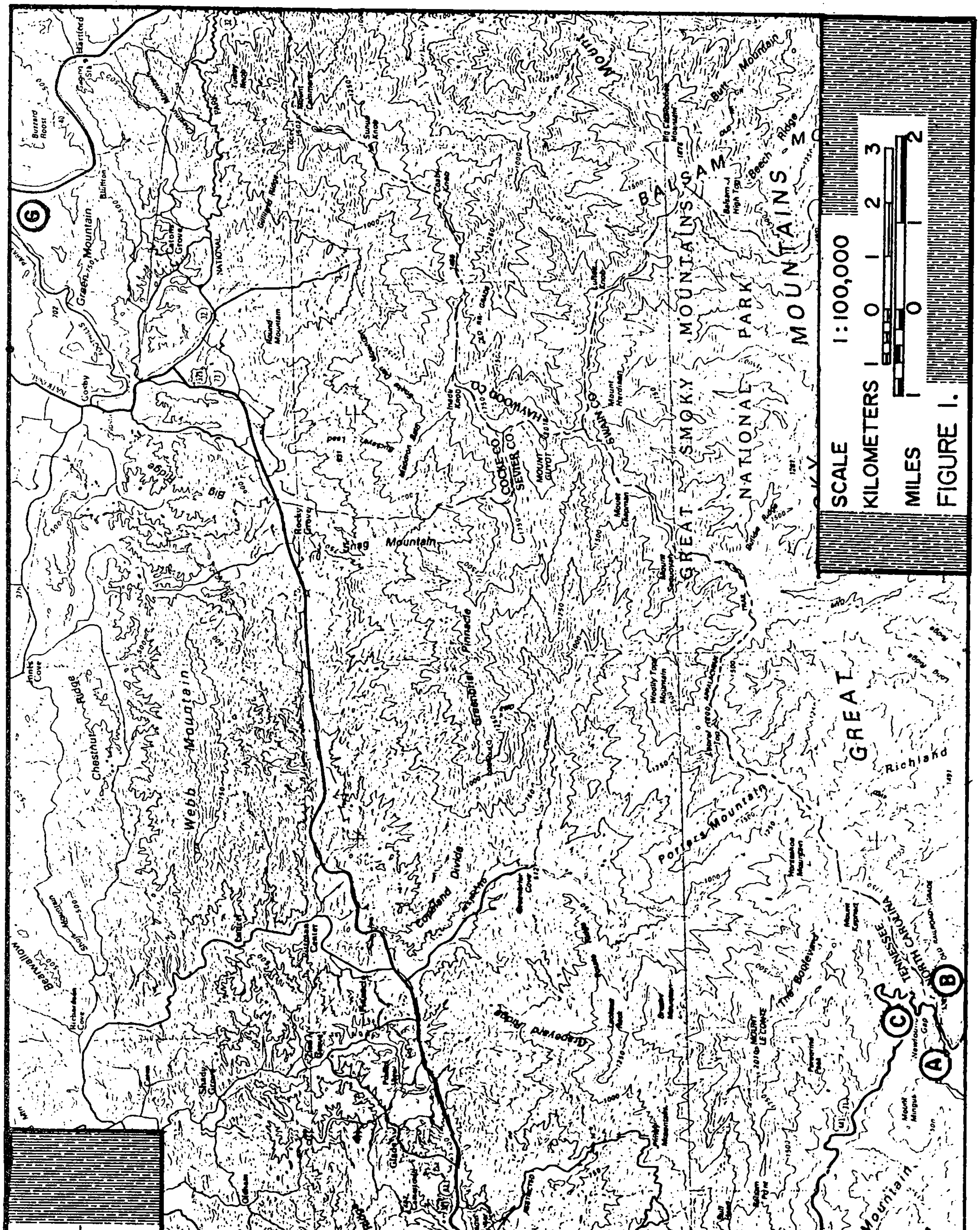
SCALE 1:100,000
KILOMETERS 1 0 1 2 3
MILES 1 0 1 2
N
GREAT SMOKY MOUNTAINS NATIONAL PARK
GREAT SMOKY MOUNTAINS
BALSAM MOUNTAIN
Sugarland Mountain
Webb Mountain
Chestnut Ridge
Big Ridge
Green Mountain
Snag Mountain
Copeland Divide
Porters Mountain
Greenbrier Pinnacle
The Boulevard
Richland
Butt Mountain
Beech Ridge
Mount Le Conte
Mount Guyot
Mount Cammerer
Newfound Gap
Gatlinburg
Rocky Grove
Cosby
Bluffton
COCKE CO.
SEVIER CO.
HAYWOOD CO.
SWAIN CO.
TENNESSEE
NORTH CAROLINA
A
B
C
D
E
F
G
M

FIGURE 1.

Introduction

Rockslope failure is a pervasive problem in mountainous regions and its likelihood of occurrence is often vastly increased due to human induced perturbations. Though not a new phenomenon in the Great Smoky Mountains, increased development in the area has renewed the interest and importance of understanding the mechanics of rockslope instability within the region. Several rock slides have occurred in the last few years, exemplifying danger to the public and to the transportation within the Great Smoky Mountains National park and along Interstate Route 40 between North Carolina and Tennessee.

Interstate Route 40 has experienced numerous slope stability problems along the Pigeon River Gorge since its opening in 1964, particularly along the west bound lane (Tice, 1981). The most recent failure occurred in February 1986 closing the I-40 westbound tunnel between North Carolina and Tennessee for several weeks. The rerouting of traffic along marginal routes ultimately led to several traffic fatalities. Though not leading to loss of life, failures along U.S. route 441 through the Great Smoky Mountains National Park have led to the formal assessment of slope stability (Federal Highway Administration, 1982). Since that time several slides have taken place that caused the highway to be closed for clean up and remedial correction.

A field study of slopes in eastern Tennessee and western North Carolina was conducted along selected segments of U.S. Highway 441 in the Great Smoky Mountains National Park and along Interstate 40 in the Pigeon River Gorge (Figure 1).

Geology

Geologically, the area lies within the Blue Ridge Physiographic Province and consists of a heterogeneous mass of intensely folded and faulted metasediments of Cambrian and Precambrian Age. The slopes examined were comprised of rocks from the Pigeon Siltstone and Rich Butt Sandstone of the Snowbird Group and the Thunderhead

FIGURE 2

STRATIGRAPHIC COLUMN OF THE CENTRAL GREAT SMOKY MOUNTAINS

SYSTEM	SERIES	GROUP	FORMATION	THICKNESS *
CAMBRIAN	LOWER CAMBRIAN	CHILHOWEE GROUP	HELENMODE FORMATION	200
			HESSE SANDSTONE	100-200
			MURRAY SHALE	500
			NEBO SANDSTONE	250
			NICHOLS SHALE	700
			COCHRAN FORMATION	1,000+
LATE PRECAMBRIAN	OCOEE SERIES	WALDEN CREEK GROUP	SANDSUCK FORMATION	2,000
			WILHITE FORMATION	3,500
			SHIELDS FORMATION	1,500
			LICKLOG FORMATION	1,500
		UNCLASSIFIED	RICH BUTT SANDSTONE	1,500
		GREAT SMOKY GROUP	UNNAMED SANDSTONE	4,500
			ANAKEESTA FORMATION	3,000-4,500
			THUNDERHEAD SANDSTONE	5,500-6,300
			ELKMONT SANDSTONE	1,000-8,000
		SNOWBIRD GROUP	PIGEON SILTSTONE	10,000
			ROARING FORK SANDSTONE	7,000
			METCALFE PHYLLITE	UNKNOWN

* APPROXIMATE THICKNESS IN FEET

ADAPTED FROM KING (1964)

Sandstone and Anakeesta Formation of the Great Smoky Supergroup (Figure 2). These groups comprise a major portion of the Ocoee Series of Upper Precambrian Age (King, et al., 1968). The Pigeon Siltstone is a uniform body of laminated siltstone containing coarse silt-sized grains of quartz and feldspar in a matrix altered to sericite and chlorite. The Thunderhead Sandstone is a heterogeneous body of orthoquartzite with numerous slate interbeds and is one of the principle ridge supporting units of the uplands in the area. The stratigraphically lower Anakeesta Formation is a dark, silty, pyritiferous argillite that has been largely metamorphosed to slate and phyllite. The Rich Butt Sandstone is an "unclassified" unit of questionable stratigraphic affinities occurring in association with the Snowbird Group. This unit is comprised of massively bedded, gray, fine-grained sandstone with several coarser grained interbeds. The investigated slope along the Pigeon River Gorge on I-40 occurs in the Lower Cambrian Hesse Sandstone of the Chilhowee Group (see Figure 2). The Hesse consists of massive bedded orthoquartzite with thin interbeds of a poorly indurated siltstone (King, et al., 1964) . Structural relationships in this portion of the Blue Ridge are rather complex and poorly exposed. The bedrock has been intensely folded and faulted resulting in a variable degree of metamorphism. Characteristic of this area is the extreme dissection of the bedrock strata by the three major northeast trending faults of the region: the Greenbrier, Great Smoky and the Gatlinburg thrust faults. These three thrust faults and their related splays have displaced strata by as much as 60 miles and have created the resulting complex imbricate relationship of the strata (King,et al., 1968).

Methods of Analysis

Eight rockslopes in roadcuts in eastern Tennessee and western North Carolina (Figure 1) were identified and mapped as summarized in Table 1. Six of the eight slopes have undergone varying degrees of planar failure while two are stable. Field investigation employed standard geological techniques using a Brunton Pocket Transit. Geologic and geometric observations and measurements were taken along all major

TABLE 1

COMPILED DATA SHEET

SLOPE		A	B	C	D	E	F	G	H	FOOT NOTES
LITHOLOGY		P	P	Q	MS	MS	MS	Q/SlSh	Sl/P	1
AZIMUTH		065°	065°	035°	074°	075°	060°	159°	138°	
PSI- P		54°	50°	N/A	N/A	35°	34°	36°	37°	2
PSI- F		85°*	85°*	75°	85°	80°	79°	70°*	76°	3
FAILURE		P	P	W	W/P	P	P	P	P	4
Z		10'	10'	N/A	N/A	25'*	28'*	15'	17'*	5
H		74'	74'	106'	40'	86'	86'	327'	50'	6
FS	(MIN)	.395	.430	N/A	1.37	.696	.719	.665	.741	7
	(MAX)	.441	.484	N/A	3.2	.789	.832	.702	.984	
C	(MIN)	11759	13176	N/A	102	5436	4400	11825	2090	8
	(MAX)	11936	13360	N/A	471	6000	5066	12058	2515	
JOINT DENSITY	⧫	.244	.244	.365	.335	.15	.183	.091	.445	9
	◆	.335	.335	.244	.503	.244	.427	.183	.762	
TENSION CRACK		SF	SF	N/A	N/A	SF	SF	SF	SF	10
SCHMIDT HAMMER		46.3	46.3	49.0	44.5	45.6	46.8	56.5	34.3	11

NOTES: SEE FOLLOWING PAGE

TABLE 1: NOTES

SLOPE #4- GEOMETRY OF SLOPE DOES NOT ALLOW FOR PLANAR NOR WEDGE GRAPHIC ANALYSIS:
AZIMUTH OF POSSIBLE FAILURE PLANES >20° FROM THE AZIMUTH OF SLOPE FACE: PSIP=90° & 50°
FOR PLANAR FAILURE; WEDGE ANALYSIS EXCLUDED BY THE UPPER SLOPE ANGLE (54°) > PSI5(25°)

1. LITHOLOGY: P-PHYLLITE, Q-QUARTZITE, MS-METASANDSTONE, Si-SILTSTONE, Sh-SHALE
2. PSI-P=ANGLE OF THE FAILURE PLANE
3. PSI-F= THE ANGLE OF THE SLOPE FACE
4. FAILURE (MODE): P-PLANAR, W-WEDGE
5. Z= DEPTH OF TENSION CRACK
6. H= HEIGHT OF THE SLOPE
7. FS (FACTOR OF SAFETY): COMPUTED OVER A RANGE OF C (COHESION) @ 1000,1500,& 2000 POUNDS/SQUARE FOOT; FS (MIN) @ ZW/Z=1 & C=1000, FS (MAX) @ ZW/Z=0 & C=2000;
SLOPE #5 - FS(MIN) IS FOR PLANAR FAILURE @ 1000 & ZW/Z=1 AND
FS(MAX) IS FOR WEDGE FAILURE @ 2000 PSF
8. C (COHESION): EXPRESSED IN POUNDS/SQUARE FOOT; COMPUTED @ FS=1 ; C(MIN) @ ZW/Z=0, C(MAX) @ ZW/Z=1 : SLOPE #5-(MIN) IS FOR PLANE "B" IN WEDGE ANALYSIS
AND (MAX) IS FOR PLANAR ANALYSIS @ ZW/Z=1
9. JOINT DENSITY: JOINTS/FOOT

DOWN SLOPE ⬍ CROSS SLOPE ⬌

10. TENSION CRACK :(LOCATION ON SLOPE): SF-SLOPE FACE, US-UPPER SLOPE, N/A-NO CRACK PRESENT
11. SCHMIDT HAMMER (HARDNESS): AVERAGE REBOUND NUMBER ON TYPE "N" HAMMER.
REBOUND NUMBERS AVERAGED ACCORDING TO ISRM SUGGESTIONS (BAMFORD AND OTHERS ,1981)

discontinuities including; faults, bedding, cleavage and joints. Additionally, the slope height, slope orientation, tension crack location, joint density and Schmidt hardness along the failure planes were noted. The above data was then used in graphic analysis using a Schmidt equal area stereonet with the original slope geometries estimated from adjacent slopes. The results of the graphic analysis were applied to a limiting equilibrium analysis as outlined by Hoek and Bray (1981).

The resulting data was then used to compute Factor of Safety (FS) values and back calculate cohesion (C) for FS=1. Correlation coefficients were computed and placed in a correlation matrix (see Table 2). It has been shown for the slopes investigated, varying Φ from 25°-40° exerts little influence on FS in limiting equilibrium analysis(Kane and Drumm,1986).

Results and Discussion

Analysis of the data set reveals two interesting relationships based on the tension crack location. This study found a 29.3% decrease in the calculated FS when the tension crack was located in the slope face as opposed to the upper surface. A four fold increase of C was required to maintain FS=1 when the tension crack was located in the slope face compared to tension crack in the upper surface. This implies that increased caution is warranted when tension cracks are located in the slope face as compared to the upper surface. Hoek and Bray (1981) state, ".....the presence of a tension crack in the slope face should be taken as an indication of potential instability...," (p.165). The authors of this paper would like to add an additional caveat: The location of a tension crack in the slope face is an important destabilizing parameter which requires serious concern regarding slope stability . Though not stated specifically, this is implied by Hoek and Bray (1981), figure 66, p.162.

The Beta correlation coefficient matrix (Table 2) reveals strong positive/negative relationships among several of the factors. These relationships can be

TABLE 2

BETA CORRELATION COEFFICIENT MATRIX

	AZ	PSIF	PSIP	Z	H	FS (MIN)	FS (MAX)	C (MIN)	C (MAX)	JT. DOWN	JT. CROSS	SCHDT HARD.
AZ	1											
PSIF	-.878	1										
PSIP	-.42	.74	1									
Z	-.152	-.271	-.821	1								
H	.659	-.752	-.293	.103	1							
FS (MIN)	.465	-.723	-.975	.784	.171	1						
FS (MAX)	.446	-.608	-.871	.691	.046	.956	1					
C (MIN)	-.098	.256	.691	-.737	.412	-.809	-.91	1				
C (MAX)	-.111	.258	.682	-.721	.415.	-.805	-.91	1	1			
JT. DOWN	.103	.2	.18	-.231	-.643	.031	.32	-.454	-.473	1		
JT. CROSS	.172	.009	.118	.058	-.566	.321	.576	-.674	-.689	.936	1	
SCHDT HARD	.086	-.281	-.01	-.071	.805	-.186	-.455	.665	.678	-.925	-.898	1

* SEE 'COMPILED DATA SHEET NOTES' FOR EXPLANATION OF ABBREVIATIONS USED ABOVE

categorized generally as those correlable to the factor safety (FS) and those to back calculated cohesion (C). Depth of the tension crack (Z) correlates positively to FS and negatively to the angle of the failure plane (PSIP): This is due to a simple geometric relationship; deeper tension cracks are associated with shallower angles of the failure plane angle (figure 3). The FS decreases as the slope face angle (PSIF) increases: Increasing the slope face angle allows the greater likelihood of a possible failure plane to daylight in the slope face, a necessary criterion for any slope failure (Hoek and Bray, 1981, p. 150). Back calculated cohesion (C) and FS exhibit a strong negative relationship which is not surprising, C is the value calculated to maintain FS=1. Thus, as C increases more force is required on a particular slope to maintain a stable geometry and the subsequent FS value decreases proportionally.

Five major factors were found to correlate significantly with cohesion: tension crack depth (Z), factor of safety (FS), joint density across the slope face (JT.CROSS), Schmidt hardness, and failure plane angle (PSIP), (see Table 2). Cohesion relates negatively to tension crack depth (Z), increasing Z decreases the angle of the failure plane. FS is negatively correlated to C: lower FS values for a given slope require larger back calculated C values to attain a FS>1. Cross slope joint density negatively correlates with back calculated cohesion (C); the greater the joint density the lower the cohesive force required along the failure plane to resist failure. This relationship plays an important role in the later discussion of the Schmidt hammer-cohesion model. As one would expect, a positive correlation exists between failure plane angle (PSIP) and cohesion (C); as PSIP increases, the gravimetric potential is increased and a greater amount of cohesive force is required to maintain slope integrity. Schmidt hammer hardness is positively correlated to C, as discussed later.

Linear regression analysis was used to develop a probabilistic model using Schmidt hammer rebound number (hardness) as a means of estimating C at FS=1. It was found that C and Schmidt hardness could be related to one another by a simple polynomial

FIGURES 3 A - B

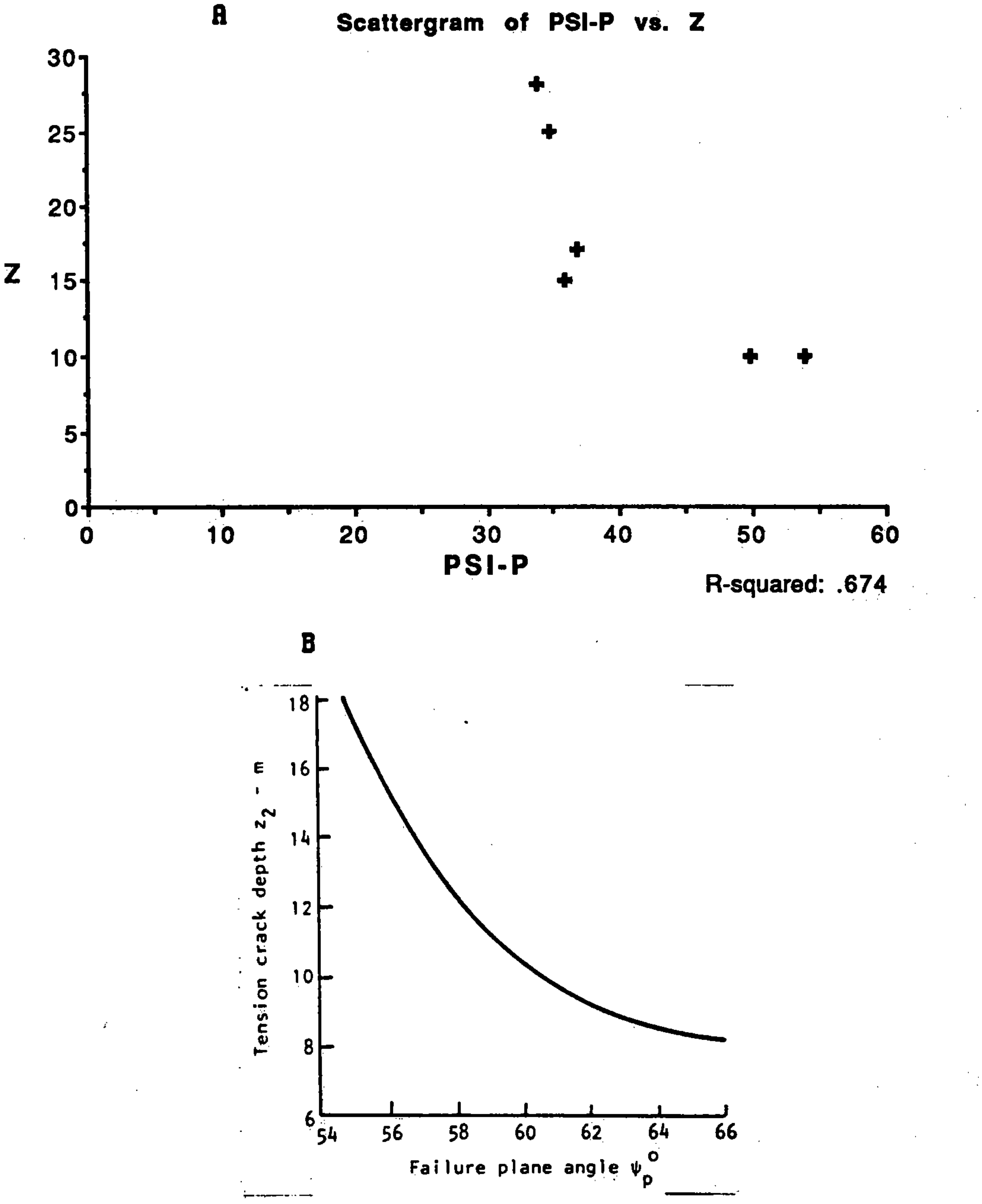

COMPARISON OF TENSION CRACK DEPTH TO FAILURE PLANE ANGLE: THIS DATA SET (A) AND FROM HOEK AND BRAY (1981), FIGURE 90, P.193 (B) expression for both the conservative estimate where the tension crack is in the slope face and full of water, C(max); and the less conservative estimate where the tension crack is in the upper slope and dry, C(min). The relationship between Schmidt hardness and cohesion can be expressed by:

$$C(max)=435.78X+(-11542.207) \qquad \text{(equation 1)}$$

and

$$C(min)=443.984X+(-12294.153) \qquad \text{(equation 2)}$$

where
X = Schmidt hammer rebound number
$C = \text{pounds/foot}^2$

(see figure 4)

These equations overestimate C by approximately 17% at FS=1. Due to the similarity of equations one and two, we propose a combined equation to be used in preliminary FS determination.

$$C = (A\ (X) + B)\ D \qquad \text{(equation 3)}$$

where
A = 440
B = -11918
$C = \text{Cohesion in pounds/foot}^2$
D = 0.83, correction for overestimation
X = Schmidt hammer rebound number

The support of this relationship is grounded in the fact that the Schmidt hammer measures the hardness of rock materials. The higher the Schmidt hardness the lower the joint density in the rock surface (Table 2). Jointing acts to increase surface roughness and to reduce the amount of C required to maintain slope stablity. A corollary to this is that higher joint densities may act to reduce the hydrostatic pore pressure beneath the rock slab by increasing drainage. These two relationships act in a complementary fashion influencing the value of C. Back calculated C, the value computed by equations 1, 2, 3 is the amount of cohesion (pounds/foot^2) required to maintain the slope at FS=1.

FIGURE 4

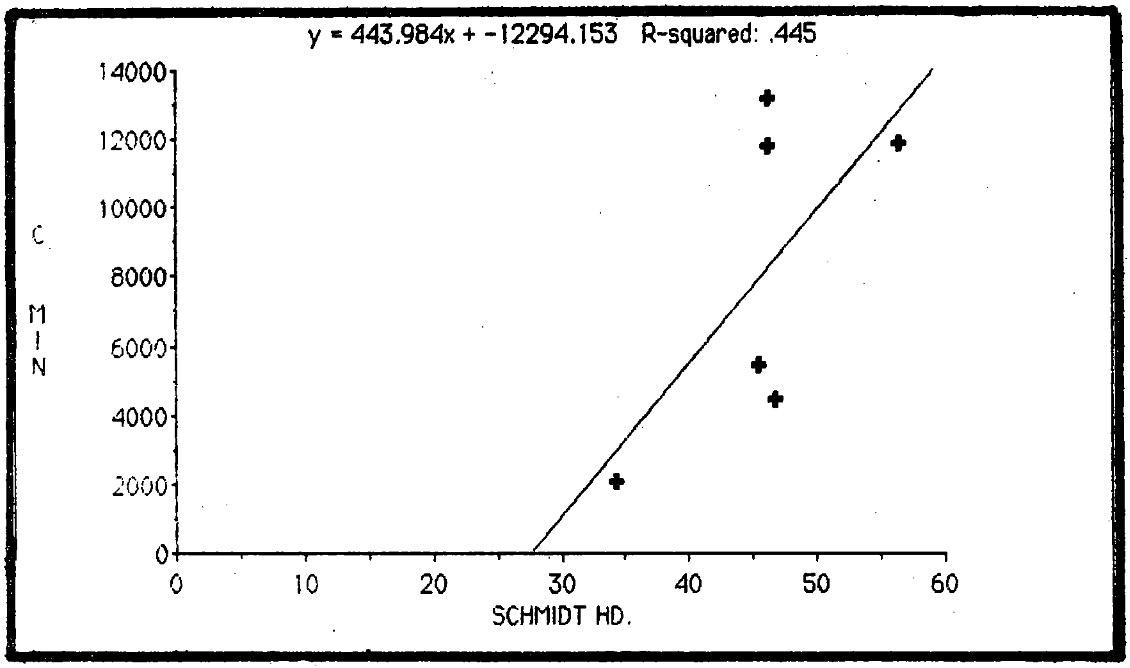

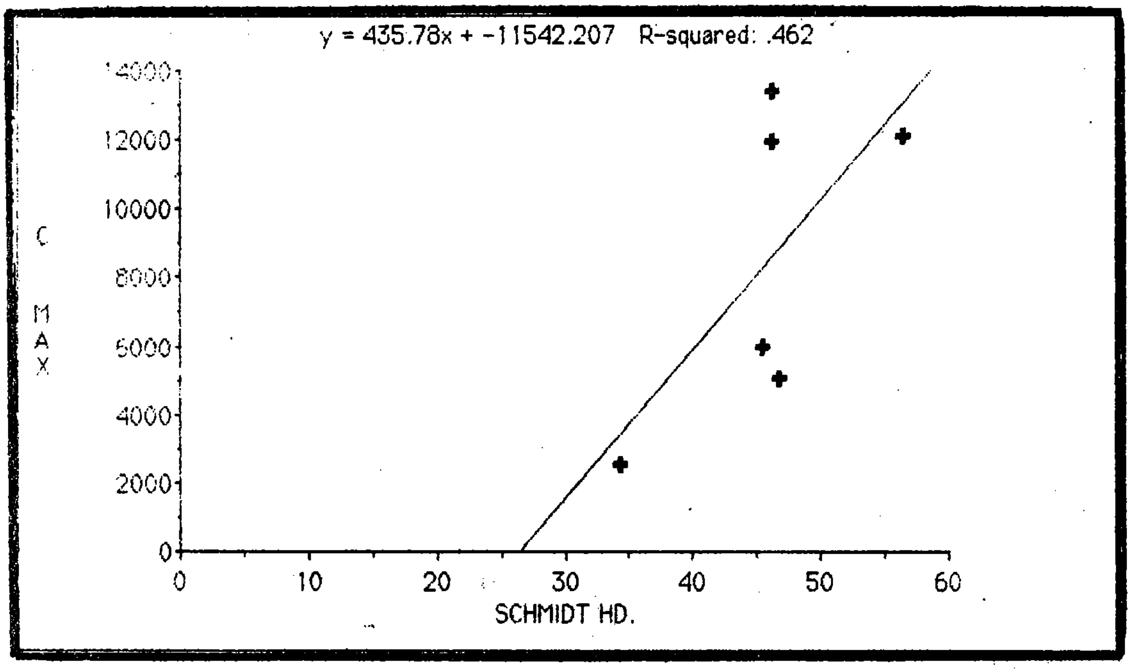

SCATTERGRAMS OF LINEAR REGRESSION RESULTS

Thus, this approach may prove a valid first approximation of relative slope stability in the field.

CONCLUSIONS AND FURTHER RESEARCH

Within this study it was verified that limiting equilibrium analysis is applicable to the Southern Appalachian region. Factor of Safety and Cohesion was found to be sensitive to tension crack location: A 29.3% decrease in FS is noted when the tension crack is located in the slope face as compared to upper slope position. A four fold increase of C was required to maintain a FS = 1 when the tension crack is located in the slope face as compared to upper slope location. Regression analyses on the data set revealed strong relationships among several of the factors. The strength of the relationship between C and Schmidt hardness enabled cohesion to be predicted; C was overestimated by 17.4%. This approach utilizes a simple field test device, the Schmidt hammer, to determine a difficult to measure parameter, cohesion.

The attempt of this study was to identify specific slope geometries and parameters that are problematic for rock slope engineering within the Southern Appalachian, Blue Ridge region. Continuance of this research aims toward developing first approximation of FS and C relationships in order to determine whether a slope in question warrants further, more rigorous consideration. Direct shear testing of representative rock types will lead to a better understanding of cohesion and the internal angle of friction. Ultimately, a probabilistic model could be developed for a region of similar structural style and stratigraphy. This model could be utilized to predict problematic slope orientations prior to construction, thus allowing the cost and/or efficacy of the site to be considered in overall planning. The development of stronger correlations and therefore a more reliable model is contingent on collecting a considerably larger data set and applying nonlinear regression to the data.

REFERENCES

Bamford, W.E. and others,1981 "Suggested Methods for Determining Hardness and Abrasiveness of Rocks,"Rock Characterization Testing and Monitoring , ed., E.T. Brown, Pergamon Press, New York, p. 101-103.

Federal Highway Administration, 1982, "Landslide Study, Great Smoky Mountains Park, Tennessee and North Carolina," Project Development Soils and Foundation, Report #11-82, 33 pp.

Hoek, E. and Bray, J., 1981, Rock Slope Engineering , 3rd Ed., Inst. of Mining and Metal., London, 402 pp.

Kane, William F. and Drumm, Eric C., 1986, "Geotechnical Factors Affecting Rock Slope Stability in Eastern Tennessee," Proceedings, 27th U.S. Symposium on Rock Mechanics,Tuscaloosa, Alabama, June 23-25, 1986, p. 107-111.

King, P.B., 1964, "Geology of the Central Great Smoky Mountains, Tennessee," U.S. Geological Survey Professional Paper #349-6, 148pp.

King, P.B., Neuman, R.B., and Hadley, J.B., 1968, "Geology of the Great Smoky Mountains National Park, Tennessee and North Carolina," U.S. Geological Survey Professional Paper #587, 23pp.

Tice, J.A., 1981, "The Hartford Slide-a case history,"Proceedings, 32nd Annual Highway Geology Symposium and Field Trip, Gatlinburg, Tennessee, p. 16-35.

STABILITY PROBLEMS OF ROCK CUTS
U.S. 23 IN EASTERN KENTUCKY

Earl M. Wright, Kentucky Department of Highways
Frankfort, Kentucky

Michal Bukovansky, Golder Associates
Denver, Colorado

INTRODUCTION

U.S. 23 in eastern Kentucky was constructed in approximately 1963 along the Big Sandy River. The river valley is steep-sided, with the sides formed by steeply inclined to vertical sandstone cliffs. A number of long and high rock cuts have been excavated along the highway; the cut heights vary between 70 and 130 feet. The highway section between Prestonsburg and Paintsville contains seven important and separate rock cuts with a combined length of approximately 3 miles.

All seven rock cuts are in Pennsylvanian sedimentary rocks. The formation is horizontally bedded and it contains a sequence of sandstones, shales, siltstones, and coal. In addition to horizontal bedding, vertical or subvertical jointing is pronounced in the sandstone units and to a lesser extent in other types of rock. In addition to vertical jointing, a system of stress relief joints can be documented in the area. Because this stress-relief system is of importance to cut stability, it will be discussed in detail later.

Ground water appears to occur in more permeable members of the formation. Wet spots can be documented at numerous cut faces. During very wet periods, ground-water inflows into the cuts increase.

Rock cuts along the highway were excavated mostly at vertical or subvertical slopes, most of them in uniform cut slopes over the entire cut height. Only a few cuts have been excavated in a benched configuration. Natural grades above cut faces are usually very steep; any flatter slopes or benched configurations increase the heights of the cuts significantly.

Numerous failures of cut faces have occurred during the lifetime of the highway. The yardages of some of these failures were significant. Widths of the catching berms at the toe of some cuts were frequently not sufficient to retain a failure, resulting in spillage onto the highway.

With regard to the importance of the highway and continuing hazard to traffic, the Kentucky Department of Highways (KDOH) decided to perform certain geotechnical studies and apply certain mitigating measures to reduce these hazards.

STABILITY PROBLEMS

Generally, little attention has been paid to stability problems in rock masses with horizontal bedding and vertical joints. If geologic formations of this type are homogeneous and of a sufficient strength, very high and steep cuts (frequently vertical) can be excavated without encountering any serious stability problems, with the possible exception of the rock fall (Bukovansky and Piercy, 1975).

Stability conditions may become very different when the rock mass is heterogeneous and/or anisotropic. Horizontally bedded rock masses where softer layers alternate with hard layers may feature important stability problems when steep or vertical cuts are designed in such conditions. Pennsylvanian formations in the U.S. and numerous other formations (such as the Cretaceous Mesaverde in Colorado, Utah, New Mexico, and Wyoming) are typical formations of this type. Extensive experience with rock masses of this type is available in Europe in the Alps and the vicinity. Such rocks are called a flysch there.

Alternating layers of soft and hard rocks in eastern Kentucky comprise precisely this rock type. In individual rock cuts, softer shales alternate with hard sandstones or siltstones. Coal also comprises a soft layer compared to sandstone. Softer shales tend to slake and slough from cut surfaces; more resistant sandstones above them are being progressively undercut and form overhangs, frequently of important dimensions. Large blocks of sandstone lose their support and, at a certain time, they topple. Slaking and sloughing of shale continue deeper into the slope and the failures continue. The rate of shale slaking and sloughing is frequently high so that failures may occur only a few years after the excavation of the cuts. A typical toppling-type failure is shown on Figure 1A.

Stability conditions of a rock cut with a vertical face become more critical with the presence of joints dipping steeply into the valley. Most slope stability problems along U.S. 23 have been caused by the presence of such steeply inclined joints.

Detailed geotechnical documentation of the cut faces confirmed the frequent presence of subvertical dividing planes. These subvertical dividing planes do not coincide with the vertical joints that are common in horizontally bedded rocks. Subvertical joints documented along U.S. 23 have been classified as stress relief joints. They are generally parallel with the surfaces of natural cliffs. They could be followed for large distances in cuts that have been excavated along the highway curves; the strike of these joints keeps changing as the direction of the valley changes. It is evident that these joints do not belong to any of the predominant joint sets. Slope stability problems caused by such joints may become serious, as shown on Figure 1B.

Development of stress relief joints is significantly different in formations that already contain systems of joints before stress relief. In such cases, stress relief resulted mostly in loosening and opening of the existing joints, as shown on Figure 2A. Cases of such relief are frequent in steep-sided canyons in the western United States. Pre-existing vertical joints have frequently been opened by stress relief so that opening reaches up to several feet (Bukovansky and Piercy, 1975).

Stress relief causes fracturing of the rock mass which contains either no or infrequent joints. Such may be the case in massive sandstones of the Pennsylvanian formation where vertical joints are either non-existent or extremely rare. It is probable that as a result of stress relief during erosion of the canyon, continuous stress relief joints were created (Figure 1B). The extent of these joints is very large; along U.S. 23, they can be followed for distances of 0.5 mile or more. The stress relief joints caused by tensile stresses are generally open and enable circulation of water along them. Almost without exception, all stress relief joints documented along U.S. 23 carried traces of water circulation.

The inclination of joints is on the order of 60 degrees. We suspect that this inclination (dip) coincides closely with the inclination of the original cliff surfaces prior to excavation.

The presence of these joints in cuts that were mostly excavated at vertical slopes is of an utmost importance for cut stability. Blocks or slabs separated from the rock mass by such joints will fail during the excavation or during the lifetime of the rock cut. The presence of a shale layer below a cut portion containing such stress relief joints will further contribute to local instability and failures.

It is very difficult to estimate spacing between individual stress relief joints that appear to be generally parallel each to the other. At several locations, spacing could be measured; it was on the order of 3 to 4 feet. At numerous locations, spacing of the stress relief joints dictated the thickness of the failed rock blocks.

It can be assumed that the spacing between successive stress relief joints increases with distance behind the slope face. It is evident that the frequency of the stress relief joints increases in the direction toward the previous cliff face. Stability conditions of individual cuts were always worse at locations where the thickness of the excavation (measured perpendicular to the cut slope) was small. In other words, thin, sliver-type excavations are more likely to cause stability problems in such geologic conditions than excavations that reach much farther behind the original cliff face.

Although the influence of ground water on the stability of individual cuts has not been studied in detail, we believe that it is important. In sedimentary rocks where sandstone layers alternate with shales and coal, fractured sandstone and coal usually comprise strata with higher permeabilities that may carry water. Ground water typically occurs in the lower part of sandstone strata, perched on underlying shale. If ground water occurs permanently, physical properties of the underlying shale may be modified and deteriorated. Such reductions in shale strength may unfavorably influence the stability of the cut.

The occurrence of ground water in horizontally bedded strata frequently depends on local dips of beds. If the strata dip into the valley even at very low angles of a few degrees, ground water may seep into the cut. If the strata dip into the slope, the probability is higher that no ground water would be seeping into the cut. In such conditions, the existence of a soft layer at the top of the shale is less likely, and the stability of the cut will probably be more favorable.

Accurate estimations of the orientation of the beds and local changes in dips and strikes are very difficult to obtain by direct measurement of the outcrops. Direct documentation of water seeps at individual locations probably comprises the most reliable method of evaluating groundwater occurrence.

ANALYTICAL METHODS AVAILABLE

Stability analyses of rock cuts excavated in horizontally bedded rock masses are infrequent, as stability problems in such conditions are rare. Finite element analyses have been used in the past to define zones of maximum shear and tensile stresses in such rock masses. It may be difficult to directly use results of such analyses for practical purposes.

In the presence of steeply inclined joints that are undercut by the cut face, a sliding block analysis can readily be performed. It is evident that the rock cuts along U.S. 23 are unstable wherever the cut face undercuts the stress relief joints that dip on the order of 60 degrees. The friction angle along these joints is lower than the dip of the joint, and any block limited by stress relief joints is unstable. A failure of such a block usually occurs in a very short period of time, even if no ground water is present.

Analyses of toppling-type failures caused by undercutting of hard sandstone ledges by slaking and sloughing shale are very difficult and, to our knowledge, have not been performed. Advanced analytical solutions using methods such as the finite difference method (Cundall et al, 1980) could probably be successfully applied, but data on time-dependent properties of the slaking shales would have to be empirically obtained.

Seegmiller (1984) provides a careful review of an identical stability problem as it may be encountered in open-pit mining. He emphasizes the importance of different Poisson's ratios of hard sandstone and soft shale. As a result of the difference, both rock types expand laterally quite differently; shale will expand much more than the hard sandstone. Underlying shale does not behave elastically because it is usually more densely broken than sandstone. Numerous fractures are evident in shale, and their extent increases considerably with time. The actual Poisson's ratio of such rock types is in fact considerably higher because of the presence of vertical fractures or joints. As a result, lateral deformations are much higher than those expected in an elastic medium. As a result, the shale disintegrates and slakes progressively. Air and water that can enter into the vertical fractures in the shale will further contribute to the loss of strength of the shale.

MITIGATING MEASURES AVAILABLE

For new rock cuts, the KDOH has been applying a concept of benched cuts (Wright, 1981, Figure 3). With this concept, the cut is divided into several benches, the elevation of which is determined by the rock mass lithology. Typical bench widths are 18 feet, but they will be modified according to weathering and other factors. Cut slopes are different in different rock types; the slopes range from 1:1

in soft and less resistant rock such as shale, to 1:20 (vertical) in hard and resistant rock such as sandstone, siltstone, or limestone. Benches are located so that the top of the bench is in the least resistant rock such as shale. With this arrangement, future slaking and weathering of shale will not cause undercutting of the harder layer overlying the shale. Sloughing and slaking will only cause loss of the crest of the bench. Other authors (Seegmiller, 1984) recommend locating the soft layer below a harder layer so that shale is protected by a hard cap. To prevent undercutting of the overlying sandstone, protecting the shale layer against slaking and sloughing is necessary in such a case.

This benching concept is entirely acceptable for the existing rock cuts along U.S. 23. Cut configurations can be designed according to the lithology of rocks exposed in cut faces. Benching of existing cuts would require, however, extensive excavations. Natural grades above the crests of existing cuts are very steep, and any additional excavation will significantly increase the height of the cut. For this reason, the KDOH has been investigating alternate methods of mitigating cut stability problems.

Artificial support, such as the use of bolting and anchoring, apparently comprises an alternative to large excavations. Although excavation is generally the prefered method of mitigating stability problems, bolting and anchoring can become attractive from a cost point of view. Artificial support can also be installed without significant traffic interruptions.

In geologic and geotechnical conditions such as those along U.S. 23, bolting and anchoring can effectively be applied to prevent toppling-type failures of sandstone ledges undercut partly by slaking and sloughing shale layers. Bolting and anchoring become expensive in cases where they are designed to support slabs resting on stress relief joints inclined on the order of 60 degrees into the valley. Bolting forces required to stabilize such blocks are very high as they approach the magnitude of the weight of the unstable blocks. Economically, excavating these blocks is nearly always less expensive than bolt or anchor support.

The most important problem in cut stabilization is the presence of slaking and sloughing shale. It is evident that to maintain long-term stability of the cuts, slaking and sloughing have to be prevented. Excavation of overhanging parts of sandstones would only temporarily eliminate the stability problem, frequently for a period of just several years.

Methods of protecting against slaking and sloughing are few and not well documented. It is evident that surface protection of vertical or subvertical cut surfaces excavated in shale would be required. Pneumatically-applied mortars or concrete (gunite or shotcrete) apparently comprise a logical choice for such protection (Figure 4). The Tennessee Department of Transportation (Trolinger, 1978) has successfully experimented with shotcrete reinforced by wire mesh and equipped with appropriate drainage systems consisting of drainage strips and drain holes in the shotcrete. Grouted dowels were used to install the wire mesh tightly against the cut face.

Similar systems have been used by the Alabama Department of Transportation. The same or modified methods of such protection have been used in coal mines in the western United States where coal seams outcrop in steep canyon walls or in mine benches. Coal seams are much softer than the overlying, hard sandstones; and by continuous slaking and sloughing, they undercut sandstone ledges. Wire mesh, anchored by means of non-tensioned dowels or by tensioned rock bolts, has usually been applied to prevent such sloughing. Shotcrete has been used less frequently.

Seegmiller (1984) proposes several systems for protection of such soft layers for open-pit mines. He proposes using various combinations of chain-link fabric, shorter bolts, and longer anchors combined with roof bolt mats. He also recommends horizontal drains in the overlying sandstone to decrease or eliminate flow of water along the shale surface.

It is apparent that not enough experience is available on the protection of the shale surface. It is also evident that protection of this rock is absolutely necessary if a shale layer is overlain by an important sandstone layer.

At the present time, the Kentucky Department of Transportation is considering various alternatives to mitigate the rock cuts at U.S. 23. With regard to considerable costs involved in mitigating stability problems, the KDOH is also considering the possibility of relocating the roadway away from rock cut toes so that an effective protective berm is created at the toe of the slopes. The final decision on an acceptable method will be made based mostly on the economic feasibility of each individual solution.

REFERENCES

Bukovansky, M. and N. H. Piercy, 1975. High Road Cuts in a Rock Mass with Horizontal Bedding. Proceedings, 16th Symposium on Rock Mechanics, Minneapolis, Minnesota.

Cundall, P.A., H. Hansteen, S. Lacasse, and P. B. Seines, 1980. Nessi-Soil Structure Interaction Program for Dynamic and Static Problems. Norwegian Geotechnical Institute, Report 51508-9.

Royster, D. L., 1979. Landslide Remedial Measures. Bulletin of Assoc. of Engineering Geology, Vol. XVI, No. 2.

Seegmiller, B.L., 1984. Rock Reinforcement Design for Surface Mine Bench Instabilities. Mining Engineering, November 1984.

Trolinger, W. D., 1978. Specialized Protection for Shale Cut Slopes. 37th Annual SASHTO Convention, Nashville, Tennessee.

Wright, E. M., 1981. Remedial Corrective Measures and State of the Art for Rock Cut Slopes in Eastern Kentucky. 32nd Annual Highway Geology Symposium, Gatlinburg, Tennessee.

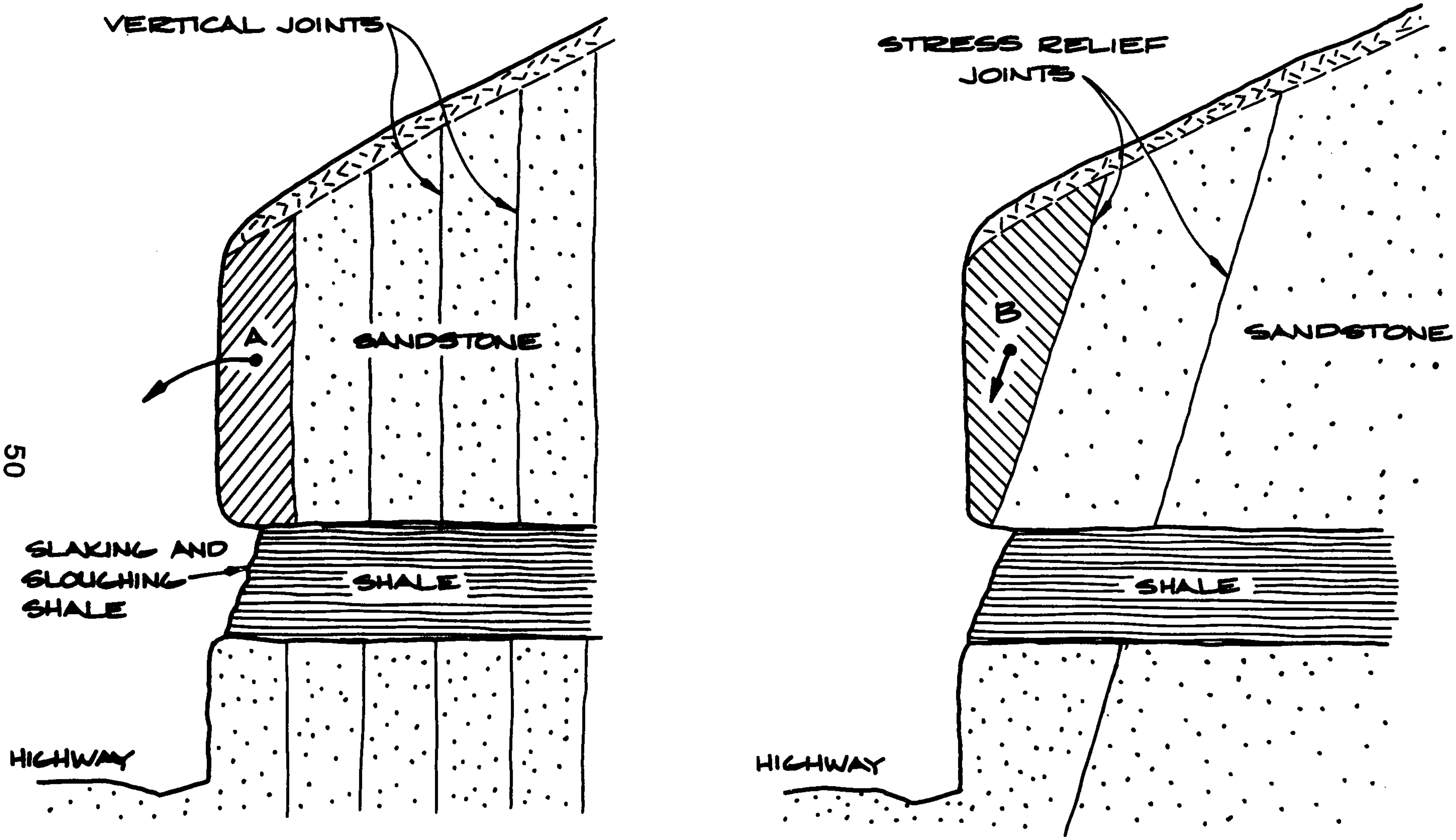
VERTICAL JOINTS
A
SANDSTONE
SLAKING AND SLOUGHING SHALE
SHALE
HIGHWAY
STRESS RELIEF JOINTS
B
SANDSTONE
SHALE
HIGHWAY

A. TOPPLING FAILURE
(BLOCK A)

B. SLIDING FAILURE
(BLOCK B)

FIGURE 1: INSTABILITY FEATURES

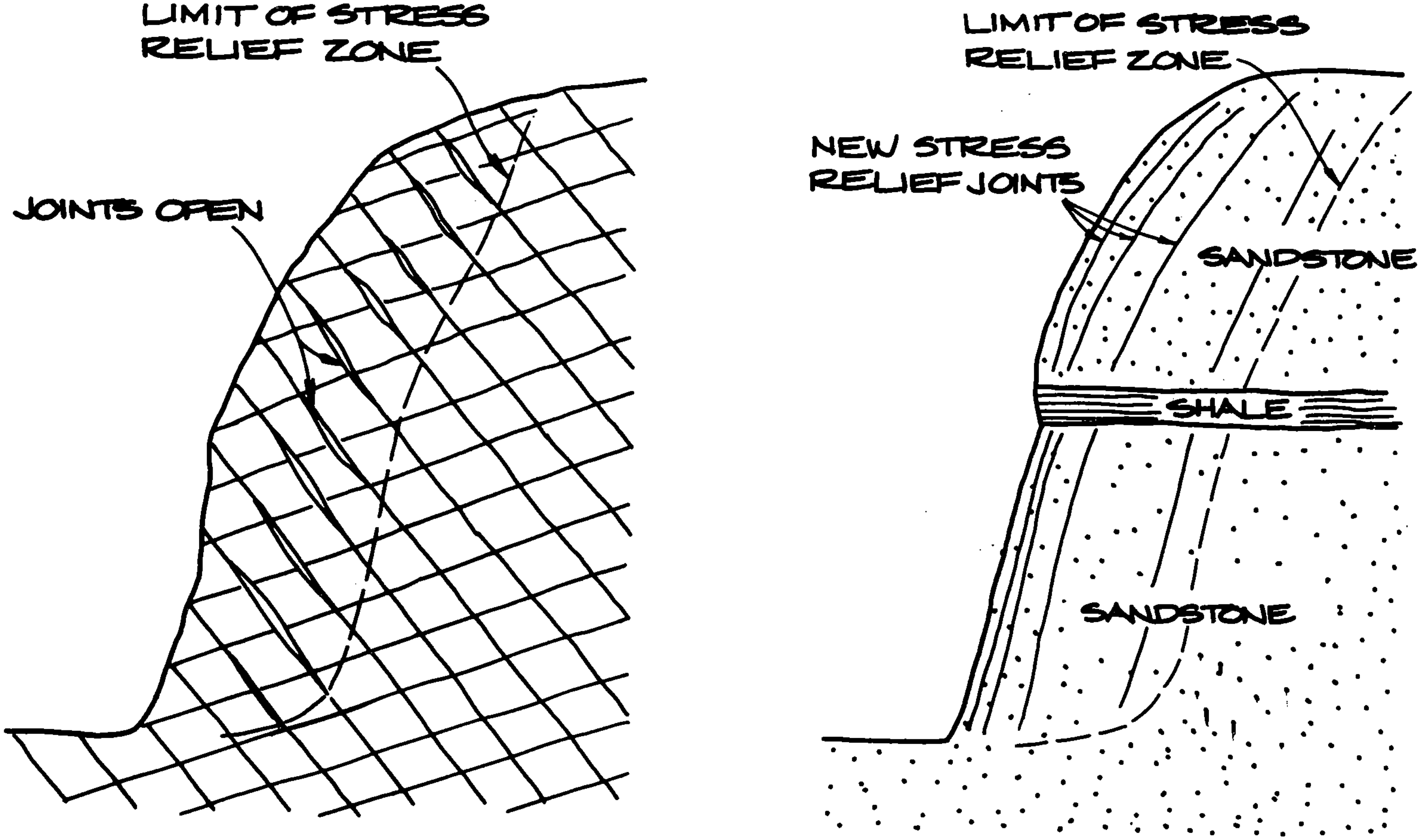
LIMIT OF STRESS RELIEF ZONE
JOINTS OPEN
LIMIT OF STRESS RELIEF ZONE
NEW STRESS RELIEF JOINTS
SANDSTONE
SHALE
SANDSTONE

A. IN A ROCK MASS ALREADY CONTAINING JOINTS, JOINTS WILL OPEN

B. IN A ROCK MASS WITH NO JOINTS, STRESS RELIEF JOINTS WILL BE CREATED

FIGURE 2: INFLUENCE OF STRESS RELIEF

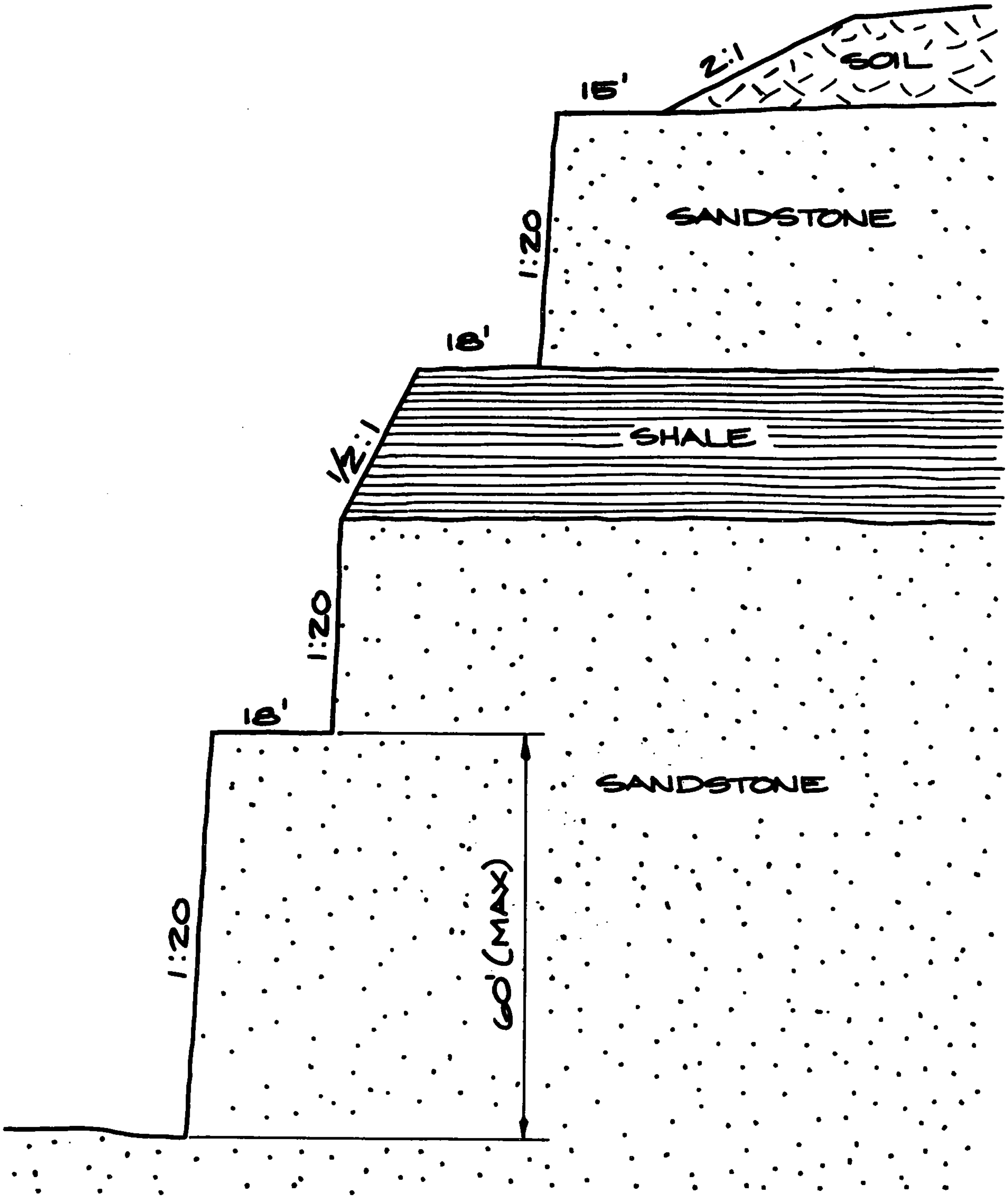
2:1
SOIL
15'
SANDSTONE
1:20
18'
SHALE
1/2:1
1:20
18'
SANDSTONE
1:20
60' (MAX)

FIGURE 3: BENCHING CONCEPT

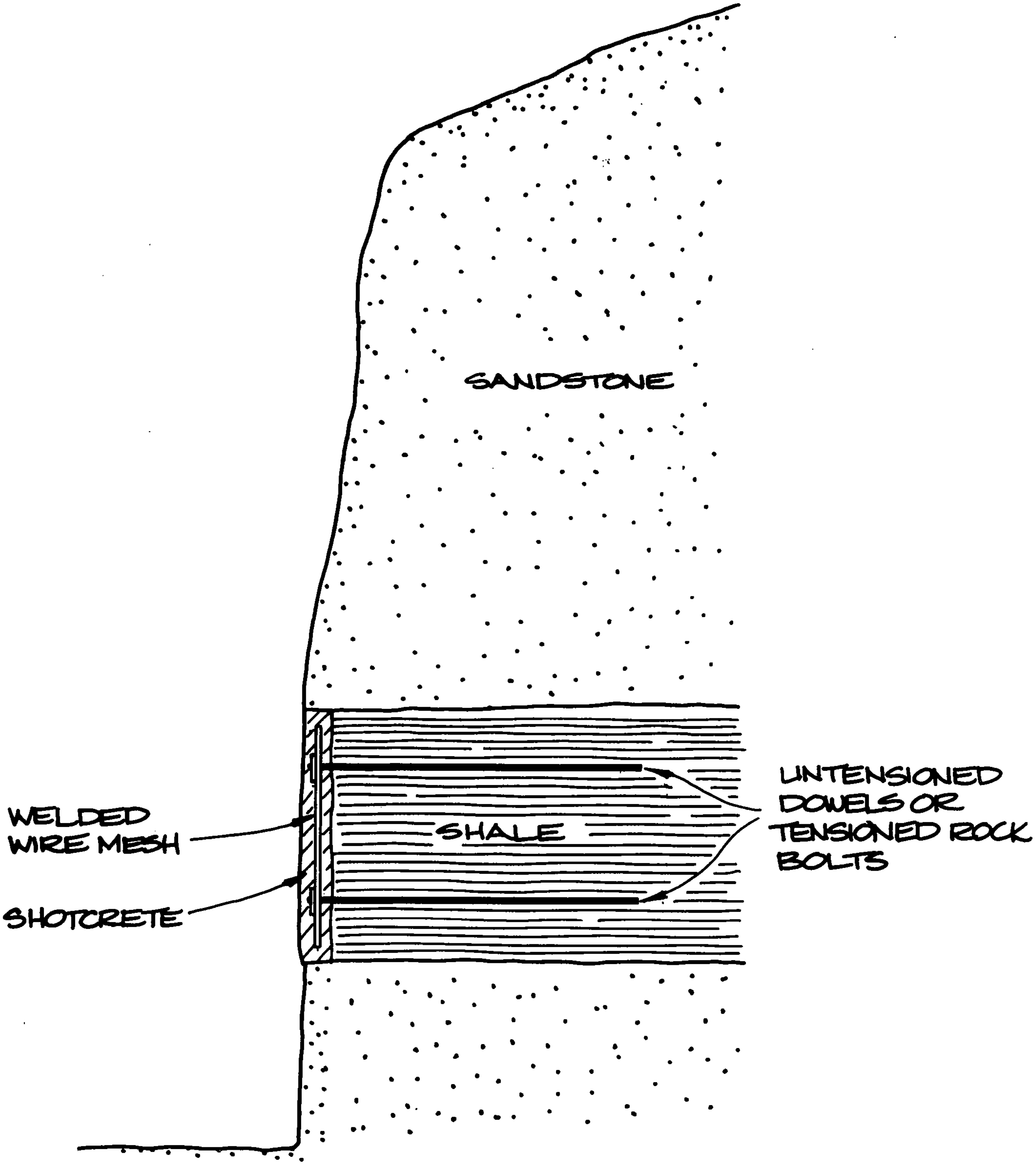
SANDSTONE
SHALE
UNTENSIONED DOWELS OR TENSIONED ROCK BOLTS
WELDED WIRE MESH
SHOTCRETE

FIGURE 4 : SHALE SURFACE PROTECTION

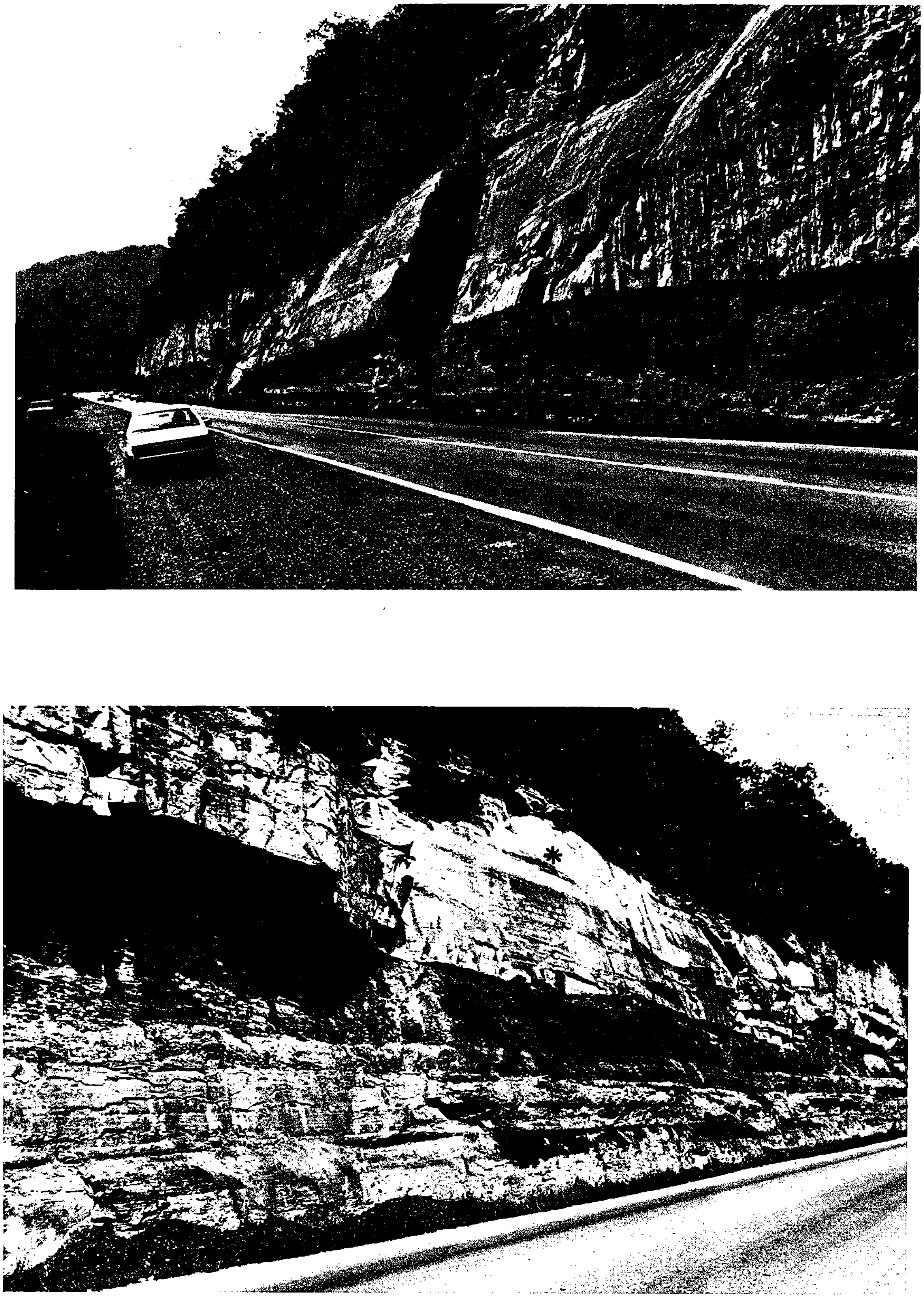

FIGURE 5: STRESS RELIEF JOINTS,* SLOUCHING SHALES AND CUT. FAILURES

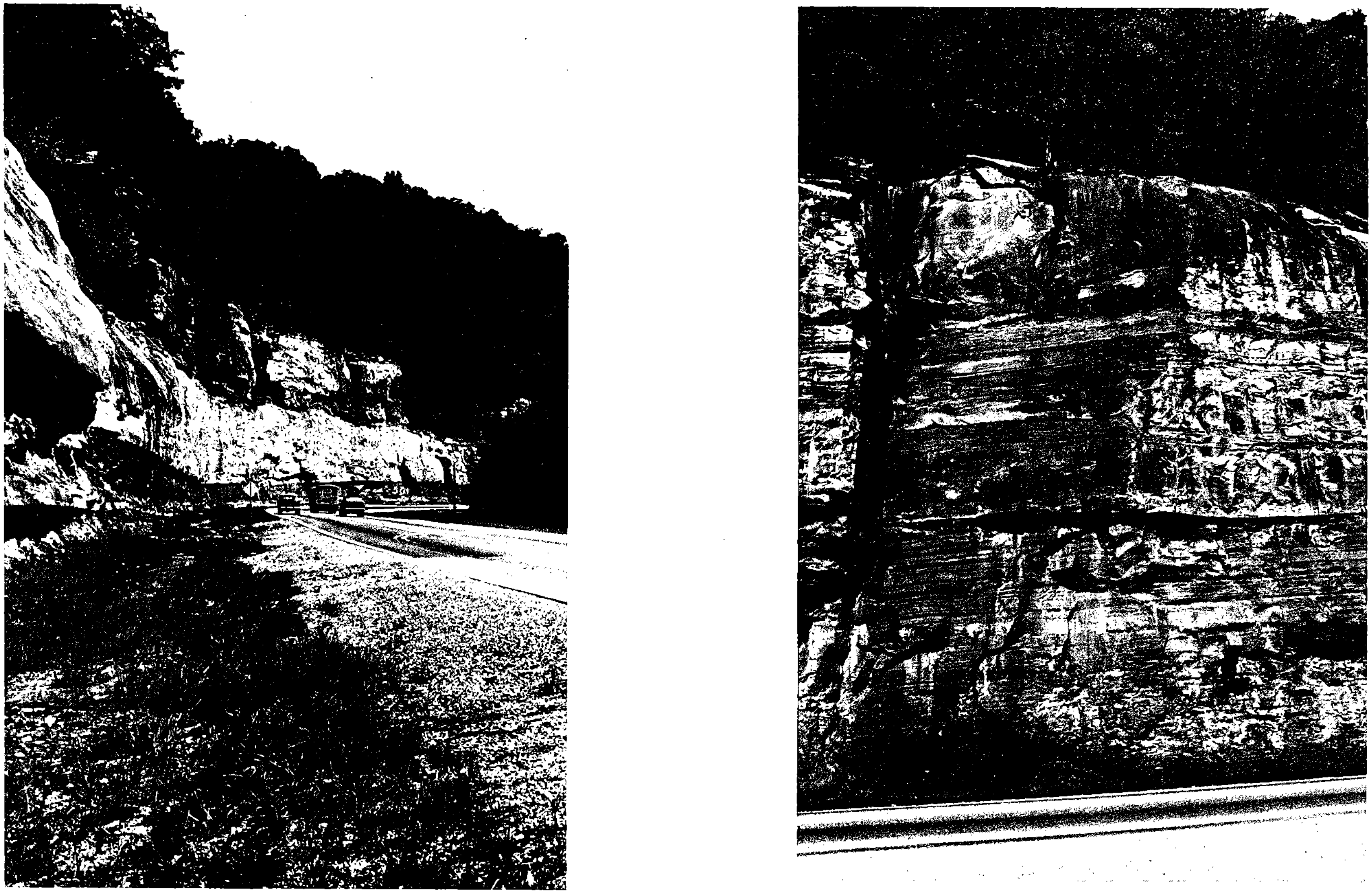

A. UNSTABLE CUT PORTIONS B. WEDGE-TYPE FAILURE

FIGURE 6. CUTS INSTABILITY

ANALYSIS AND REHABILITATION OF AGING ROCK SLOPES

by
Lee W. Abramson
and
William F. Daly

Parsons Brinckerhoff Quade & Douglas, Inc.
New York

ABSTRACT

Our great primary highway and interstate highway system was first conceived and constructed in the 1940's and 1950's, nearly a half century ago. Since then, rapidly increasing demands on the system have necessitated expansions and additions to the existing transportation network. These improvements during the 1960's and 1970's presented engineers with difficult challenges to add lanes where there was barely room on a hillside for the roadway in the first place. To accomplish this, fills were constructed using innovative solutions such as reinforced embankments or alternatively, larger cuts into the hillside were made. It is the performance of these original and expanded highway cuts in rock that is the subject of this paper.

Highway cuts are preferably made in hard, continuous, unweathered rock by blasting. However, alignment considerations often preclude construction within this ideal engineering material. In those cases a variety of design concepts are required to stabilize, reinforce or support the fractured and sometimes severely weathered rock adjacent to the roadway. The best of intentions during construction, unfortunately, have not always insured a permanently stable, inert rock slope after it is exposed to the forces of nature. Falling rock and occasionally catastrophic failures have occurred and seem to be occuring with increasing frequency as highway rock cuts grow older and older in age.

This paper provides an overview of the historical development and performance of highway rock cuts including recent examples of catastrophic slope failures, describes current slope condition survey techniques, methods of stabilization and improvement and long-term performance monitoring. Examples of recent rehabilitation programs incorporating these elements of analysis, design and construction are cited.

INTRODUCTION

To the maximum extent possible, initial development of the transportation network in the United States tended to follow natural drainage features to minimize the necessity for extensive cut-and-fill operations. When moving from one drainage basin to another, roads circumvented terrain obstacles rather than crossing them in deep cuts. When natural crossings of terrain obstacles, such as Cumberland Gap, were available, they were utilized even if their use required a significant detour. This transportation network was adequate for the nation's needs in the early 19th century when bulk goods moved primarily by water and the road net was used primarily for local transportation.

Development of railroads, starting in the 1830's, resulted in the first extensive use of rock excavations for transportation in the United States. Earlier rock excavations for canal construction in the first quarter of the century, had not required cuts of the same magnitude. Railroads crossing the Appalachians in the East and the Sierras and the Rockies in the West required extensive rock cuts. However, major rock excavation for roadway construction was minimal throughout the 19th century.

Development of the automobile and the truck in the early 20th century initiated the extensive highway construction which has continued to date, with the exception of the hiatus caused by the Depression and World War II. With the decline of the railroads, the nation relies on bulk transportation by truck for interurban movement of goods and services. The public has come to rely on the personal automobile as the principal means of travel, both for business and vacation. New construction and reconstruction of existing routes for vehicle traffic has resulted in extensive rock cuts of significant depth and length.

However, as the transportation network has aged, time and weather have adversely affected the stability of the deep rock cuts which are an integral and, in some cases, critical part of our national transportation network. For at least the next 25 years stabilization and rehabilitation of aging rock slopes in these cuts will be a major concern of Federal and state transportation agencies.

Some recent examples of rock slope failures affecting highway routes in North America are listed in Table 1. It can be seen that rock slope instability occurs across the continent and few states are immune from sudden catastrophic failures. Schuster and Fleming (1986) estimate that in the United States, the number of landslide related fatalities per year exceeds 25 and losses to public and private property exceed $1.5 billion per year.

Effective methods are currently available to evaluate the condition of rock slopes along transportation routes. Rock slope failure is often a progressive phenomenon. Timely implementation of control or mitigation procedures is essential to arrest this phenomenon. Slope condition assessment techniques, potential modes and causes of failure, slope rehabilitation, planning and monitoring methods are discussed below. A case history is also presented to demonstrate the usefulness of these concepts.

SLOPE CONDITION ASSESSMENT TECHNIQUES

The techniques used to investigate the condition of an existing natural or man-made slope are not unlike that for common geotechnical investigations. However, because an existing facility is involved there

Table 1
Some Recent Examples of Rock Slope Failures Affecting Highway Routes in North America (N.P. = Not Published)

Location	Original Slope Conditions			Type and Volume of Instability	Rehabilitation Methods	Cost $ (Date)	Remarks	Source
	Height (Feet)	Angle (Degrees)	Type of Rock					
Interstate 40, Haywood County, North Carolina	150	75	Quartzite interbedded with siltstone, slate and phyllite	Planar, 13,900 cy	Scaling, bolting, mesh, drainage and catchment	6.0 million (1985)	Destroyed adjacent tunnel portal	Abramson and Daly, 1986 (This paper)
State Route 31, Hawkins County, Tennessee	60	Vertical	Quartzose sandstone interbedded with shale and clay	Planar, 8,900 cy	Shot-in-place rock buttress	0.1 million (1985)	–	Moore, 1986
U.S. 460, Cedar Bluff, Virginia	100	Near-vertical	Limestone and dolomite	Wedge, estimated 1,000 cy	Removal	N.P. (1983)	Tension cracks observed at least 2 years prior to failure	Watts and West, 1985
Interstate 77, Canton, Ohio to Charleston, West Virginia	Varies	Vertical	Sandstone or limestone underlain by shale	Planar and wedge, volume N.P.	None to date	N.P. (1986)	Sections categorized stable, unstable, and potentially unstable	Shakoor and Weber, 1986
N.P., Spring Valley, Idaho	65	60	Granite	Planar, 500,000 cy	Relocation, drainage and buttress	0.5 million (1986)	–	Smith, 1986
Highway 60, Edmonton, Alberta	40	20	Mudstone, claystone and sandstone interbedded with coal and clay	Planar, estimated 10,000 cy	N.P.	N.P. (1965)	–	Eigenbrod and Morgenstern, 1972
U.S. 14 and 20, Cody, Wyoming	N.P.	Near-vertical	Schist, granodorite and granite pegmatite	Planar and wedge, 5,000 cy at portal	Scaling, protection	N.P. (1974)	Portals of three tunnels under construction	Sherman, 1974
Interstate 80, Nevada County, California	100	45	Granite	Rolling of weathered boulders of various sizes	Steepening slope to provide 20-foot-wide catchment	N.P. (1970)	Slope had benches that filled with debris but could not be accessed for clearing	Mearns, 1972
Highway 40A, Butte County, California	110	55	Phyllite	N.P.	Flatter slopes, drainage	0.5 million (1960's)	During construction when original design slopes were observed to be too steep	O'Neill, 1973
Interstate 93, Woodstock, New Hampshire	70	Near-vertical	Gneiss and schist with mylonite seams	Planar, 17,000 cy	Flatter slopes, catchment, bolts, tendons, drainage	N.P. (1972)	Slope redesigned during reconstruction after failure	Fowler, 1976
Interstate 40, Cooke County, Tennessee	Varies	Varies	Siltstone, slate and shale	Wedge, miscellaneous 1,000 to 10,000 cy	Drainage, removal, buttresses, bolts and catchment	N.P. (1985)	Rehabilitation program currently underway	Moore, 1985
Interstate 40, Station 0+00 to 211+00, North Carolina	Varies	Varies	Varies	Planar and wedge, varies up to 100,000 cy	Removal, catchment, relocation, bolts, mesh and drainage	4.0 million (1979)	Slope stability assessment report	NCDOT, 1979
River Bluff Road, Monroe County, Illinois	200	Near-vertical	Limestone	Planar, volume N.P.	Removal	N.P. (1972)	–	Killey et al, 1985
U.S. 23, Lawrence County, Kentucky	70-130	Near-vertical	Sandstone, siltstone, shale and coal	Planar, volume N.P.	Flatter slopes, bolts, shotcrete, mesh, drainage	N.P. (1985)	–	Wright, 1985
Interstate 15, Central Western Montana	Varies	Varies	Quartz monzonite	Miscellaneous	Barriers, mesh netting and drainage	N.P. (1986)	–	MTDOH, 1986

is usually more extensive background information available as well as unique project specific requirements governing modifications to the facility. The investigation should be divided into tasks as shown in Table 2 and as follows:

- Review of existing data
- Site reconnaissance
- Geologic exploration
- Analysis of potential failure modes
- Analysis of potential causes of failure
- Assessment of slope condition and rehabilitation planning

Review of Existing Data

Data review should include all accessible documents generated for the facility including: feasibility records; geologic explorations; design drawings, specifications and supporting calculations; construction records; maintenance records; and any relevant published literature. Among other things, feasibility records will show the envisioned purpose of the facility, reasons for site selection, traffic patterns, type of vehicle usage (e.g. campers versus semi-trailers), and economic considerations such as dependence of neighboring cities. Previous geologic explorations are often quite useful for assessing general geology, nature of overburden materials, rock type(s), rock quality and groundwater levels. Design documents will reflect how the original designer of the facility planned the geometrical lay-out, as well as excavations and slope support based on geological considerations. Construction records will show how easily these design concepts were implemented, how geologic conditions varied from the original assessments and any unusual occurrences during construction. Most highways have maintenance patrols, some which work around the clock. Maintenance records should be analyzed to determine geologic similarities between areas of frequent instability and the project site vicinity. Finally, relevant published literature should be researched including geologic papers, geotechnical papers, and local newspaper accounts of events pertinent to highway construction, maintenance or usage.

Site Reconnaissance

After or while background information is being collected and digested, members of the project team should go into the field to perform a detailed site reconnaissance. Spatial relationships of nearby cities and connecting highways should be determined. Current traffic patterns and highway usage should be observed. The accuracy of maps and as-built drawings should be verified. The topography, geology, climatology and general site conditions should be noted. If reliabile topographic maps do not exist, photogrammetric mapping may be required. Signs of imminent or previous rock slope instabilities should be investigated. Future geologic exploration methods and potential sites should be identified. Finally, preliminary rehabilitation concepts

TABLE 2

STEPS LEADING TO ASSESSMENT OF SLOPE CONDITION

DATA REVIEW

- Feasibility Studies
- Geologic Explorations
- Design Documents
- Construction Records
- Maintenance Records
- Published Literature

SITE RECONNAISSANCE

- Geography
- Patronage
- Topography
- Site Conditions
- Geology
- Climate
- Potential Exploration Sites

GEOLOGIC EXPLORATION

- Aerial Photograph Interpretation
- Borings
- Geologic Mapping
- Laboratory and Field Testing
- Geophysical Methods
- Data Interpretation

POTENTIAL FAILURE MODES

- Planar
- Wedge
- Toppling
- Circular
- Complex
- Calibration With Real Field Conditions

POTENTIAL CAUSES OF FAILURE

- Weathering
- Hydrostatic Pressure
- Freeze/Thaw
- Seismic
- Creep
- Progressive Failure

ASSESSMENT OF SLOPE CONDITION

- Classification of Problem Areas
- Prioritization of Rehabilitation Program
- Planning and Logistics

should be generated and checked to see whether site conditions are conducive to potential measures considered both from a constructibility standpoint as well as a user standpoint.

Geologic Exploration

After existing data have been reviewed, summarized, and then corroborated with field observations, the need to gather additional geologic information should be assessed. Usually, further exploration is required. The methods chosen will vary depending on the size of the site, accessibility, type of geologic formations, intended use of data, time constraints and economic considerations.

The most common method of exploration for slope stability is geologic mapping. Usually, it is not the intact rock itself that fails but the discontinuties in the rock mass. These discontinuities generally consist of partings along bedding or foliation, joints, shear zones and faults. The character of these features are mapped within each lithological zone requiring differentiation. Along with information regarding rock type, color, strength and hardness, the strike, dip, spacing, persistence, roughness, waviness, weathering, aperture, filling and staining of discontinuities is noted. The International Society for Rock Mechanics (1978) gives detailed descriptions of these parameters in "Suggested Methods for the Quantitative Description of Discontinuities in Rock Masses." An example of a form for this data acquisition is given in Figure 1. In addition to geologic mapping, aerial photography can be studied for past landslides, fault traces, drainage features and rock outcrops in the vicinity to be mapped.

Depending on accessibility, borings can be drilled to obtain: groundwater information; traditional RQD values; oriented core data; thickness and character of faults, shear zones, and joint fillings; samples of laboratory testing, and depth of weathering and blast disturbance. Laboratory testing can be conducted on samples to obtain values for unconfined compressive strength, tensile strength, elastic modulus, Poisson's ratio, strength along discontinuities, creep and swell potential, and strength of joint fillings. Large scale field tests are seldom conducted for slope stability problems but can include direct shear tests, water dye tests, overcoring, and rock fall simulations (Wu, 1985). Geophysical surveys are sometimes conducted to establish depth of overburden soils, seismic velocities of the rock, rippability, depth of disturbance due to previous blasting, depth of weathering and correlations with other strength parameters.

Interpretation of data should proceed during and after data acquisition and geologic exploration. Plans, profiles, block diagrams, and cross sections should be generated at this stage. Time and money can be saved by considering potential future use of these documents and formatting them appropriately. Will they become part of construction contract documents, will they be used in a geotechnical report, or both?

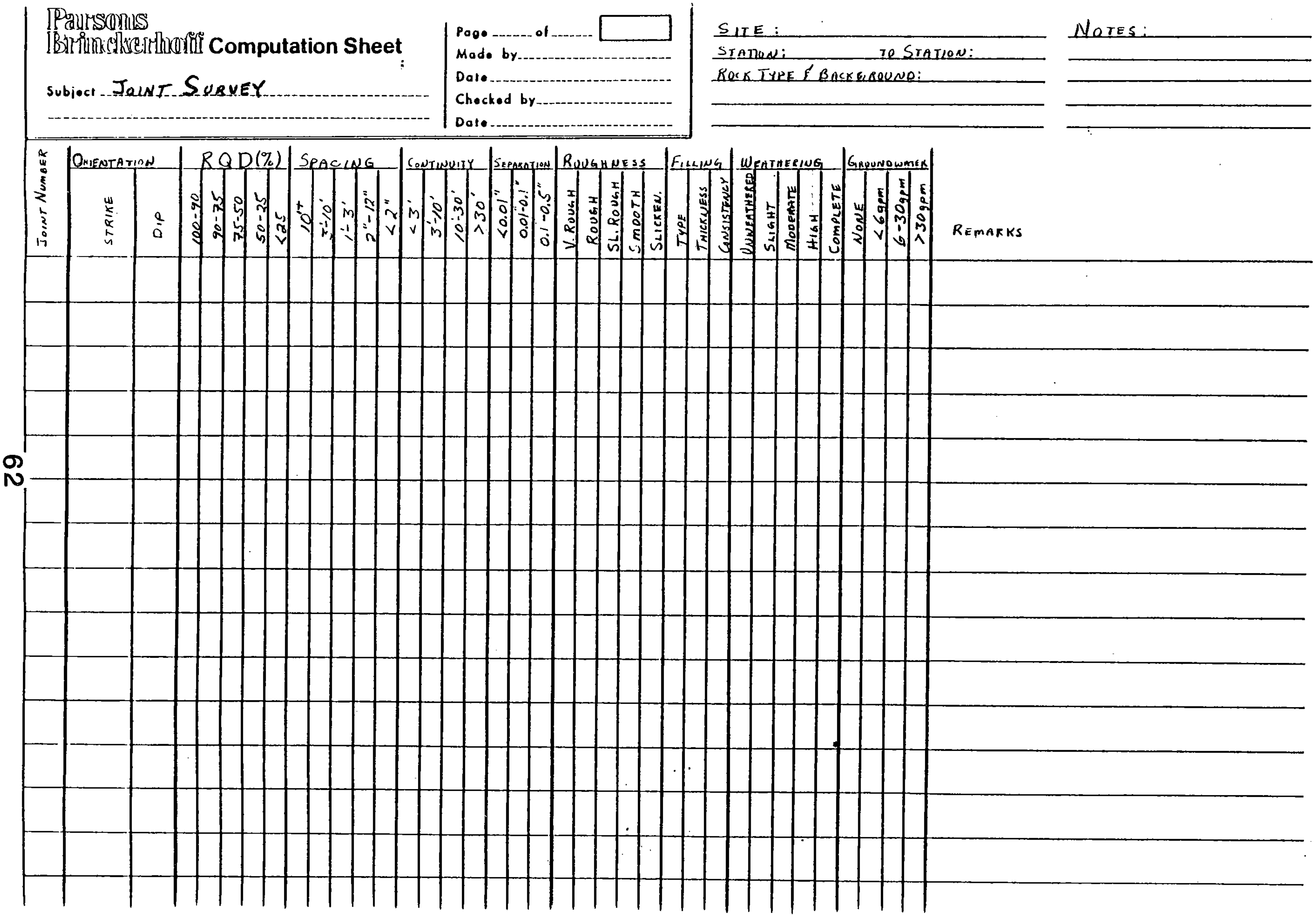

Parsons Brinckerhoff Computation Sheet

Subject JOINT SURVEY

Page ______ of ______

Made by ______

Date ______

Checked by ______

Date ______

SITE :

STATION: TO STATION:

ROCK TYPE & BACKGROUND:

NOTES:

JOINT NUMBER	ORIENTATION		RQD(%)					SPACING					CONTINUITY				SEPARATION			ROUGHNESS					FILLING			WEATHERING					GROUNDWATER				REMARKS
	STRIKE	DIP	100-90	90-75	75-50	50-25	<25	10'+	3'-10'	1'-3'	2"-12"	<2"	<3'	3'-10'	10'-30'	>30'	<0.01"	0.01"-0.1"	0.1-0.5"	V. ROUGH	ROUGH	SL. ROUGH	SMOOTH	SLICKEN.	TYPE	THICKNESS	CONSISTENCY	UNWEATHERED	SLIGHT	MODERATE	HIGH	COMPLETE	NONE	<6gpm	6-30gpm	>30gpm	

FIGURE 1. Joint Survey Data Form

Geologic mapping data should be summarized and plotted on a polar stereographic projection. This graphic technique is used to find trends in field mapping measurements. The basis of the technique is briefly discussed below. More detailed discussions on the methods and basis of stereographic projection are available in Methods of Geological Engineering by R.E. Goodman (1976) and Hoek and Bray's (1981) Rock Slope Engineering.

In adapting stereographic projection to structural geology, the traces of planes on the surface of a reference sphere are used to define the dips and dip directions of the planes. The great circle which is traced out by the intersection of the plane and reference sphere will define uniquely the inclination and orientation of the plane in space. Since the same information is given on both upper and lower parts of the sphere, only one of these need be used and, in engineering applications, the lower reference hemisphere is used for the presentation of data. In addition to the great circle, the inclination and orientation of the plane can also be defined by the pole of the plane. The pole is the point at which the surface of the sphere is pierced by the radial line which is normal to the plane. In order to communicate the information given by the great circle and the position of the pole on the surface of the lower reference hemisphere, a two dimensional representation is obtained by projecting this information onto the horizontal or equatorial reference plane.

An aid in the analysis of pole plots is the construction of contour pole plots. This can be done manually or by a computer. From the contoured plots, trends in the field data are depicted. The central value of highest concentration of poles can be taken as representing the mean orientation of the given set of discontinuities. Figure 2 illustrates the use of equatorial equal area nets for plotting both poles and great circles to represent typical rock mechanics problems, such as slope stability. Specific characteristics of each joint set can be used to further define the behavior of the rock mass using the Discontinuity Significance Index described by Watts and West (1986) or the like.

Potential Modes of Failure and Analysis

From the above data acquisition and interpretation, potential failure modes can be ascertained using the orientation, height and slope of an existing rock cut with the known geologic character of the rock mass. The predominant modes of failure along highway routes are planar and wedge although toppling, circular and complex failures occur frequently as well. Methods of analysis have been published by many authors including Hoek and Bray (1981), Goodman (1976 and 1980), and others. Now with the advent of personal computers, computation of apparent safety factors for a variety of assumed conditions and probabilities have never been easier (Abramson, 1985; Hendron et al, 1971; Kovari and Fritz, 1975; and Watts and West, 1985).

Unfortunately, our advancements made in computing factors of safety have not necessarily improved our ability to accurately model rock

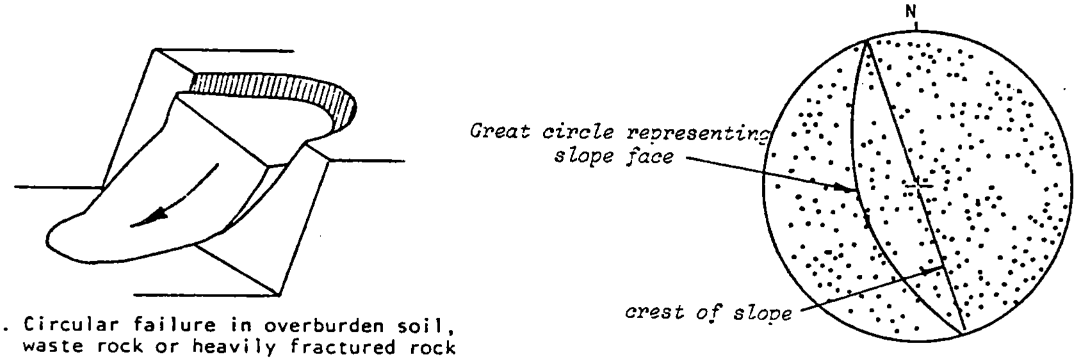
N
Great circle representing slope face
crest of slope

a. Circular failure in overburden soil, waste rock or heavily fractured rock with no identifiable structural pattern.

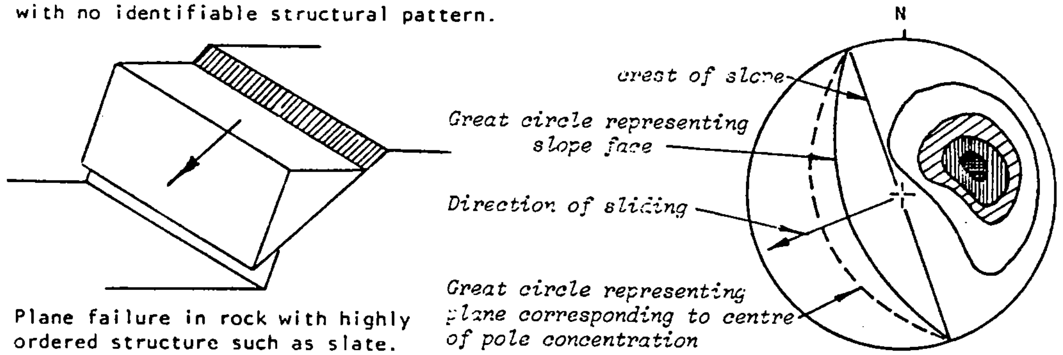
N
crest of slope
Great circle representing slope face
Direction of sliding
Great circle representing plane corresponding to centre of pole concentration

b. Plane failure in rock with highly ordered structure such as slate.

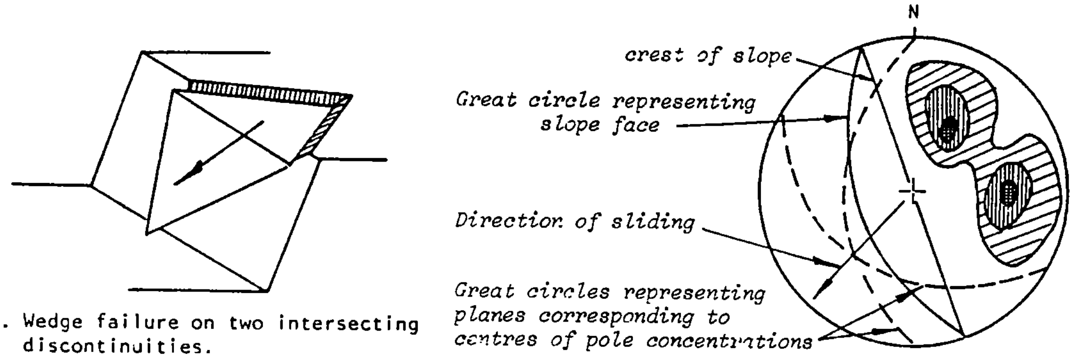
N
crest of slope
Great circle representing slope face
Direction of sliding
Great circles representing planes corresponding to centres of pole concentrations

c. Wedge failure on two intersecting discontinuities.

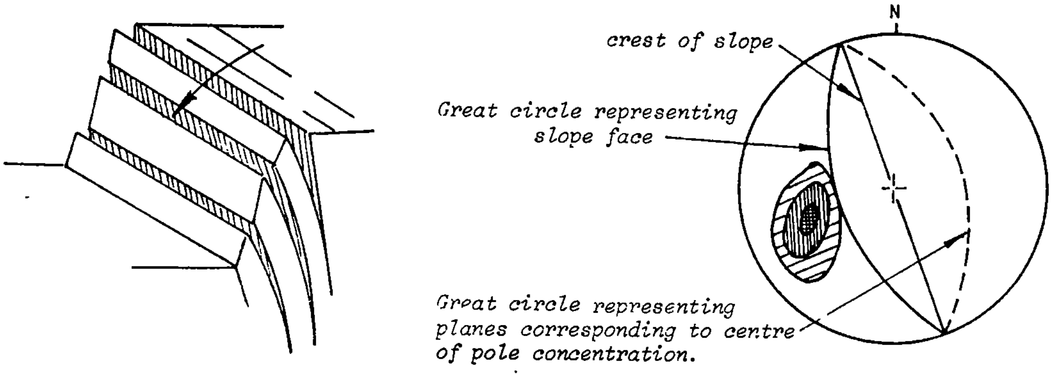
N
crest of slope
Great circle representing slope face
Great circle representing planes corresponding to centre of pole concentration.

d. Toppling failure in hard rock which can form columnar structure

FIGURE 2. Example Types of Slope Failure Shown by Stereoplots

(From Hoek and Bray, 1981)

masses which are heterogeneous, inelastic and discontinuous. The discontinuities in the rock mass are usually what control stability. The characteristics, strength, stress state, and stress history of discontinuities are still not clearly understood because of our inability to completely sample and test the rock mass. To further complicate the picture, the hydrologic characteristics of the rock mass, particularly the amount, pressure and seepage of groundwater between discontinuities, is seldom clearly known and is often responsible for the onset of failure.

Most states that have strong seasonal climate variations report a high incidence of failures during the spring months (Figure 3), when joint water that has become frozen and expanded over the winter begins to melt. The water tends to jack loosened rock blocks and wedges during the winter causing a transition from peak strength along discontinuities toward residual strength. During the spring, the ice melts subjecting the rock to hydrostatic loading and increased lubrication along joints. As the strength along discontinuities decreases, the stress increases. Sooner or later the stress will exceed the strength and failure occurs. While this concept is easy to verbalize, our ability to analyze real field conditions and to predict failures is quite handicapped by the lack of accurate engineering parameters.

Therefore, while typical modes of failure are well known and tools for analysis are plentiful, assumptions made and the accuracy of input data makes the results of analyses somewhat questionable and tenuous for use in determining engineering solutions to real stability problems. One way to enhance the results of our studies is to return to the field and confirm that what our computers are telling us truly is observable in the field. Isolated blocks are frequently observed in the field that would have calculated factors of safety less than 1.0 but are stable in reality due to factors such as joint irregularities or wedging effects. If failures are predicted by analysis, can any examples be found near the site? If so, are they large or small? For instance, if observed instabilities are large, reinforcement or removal is the only answer. However, if they are small, catchment may be a much more cost effective solution.

Potential Causes of Failure

Slopes do not fail because of the "modes of failure". Something causes this mode of failure to engage itself. Calculated factors of safety are essentially point measurements in time. Factors of safety change constantly during every season, every rainfall, every earthquake and over the years as the rock slope ages due to exposure to the elements. The rate of change from stability to instability can be instantaneous as in the case of an earthquake or can take tens of hundreds of years as in the case of slow degradation of a shale stratum underlying massive sandstone. In most cases, there are a variety of weakening forces acting on the slope with different rates of degradation and relative importance. Sometimes, these phenomena are products of

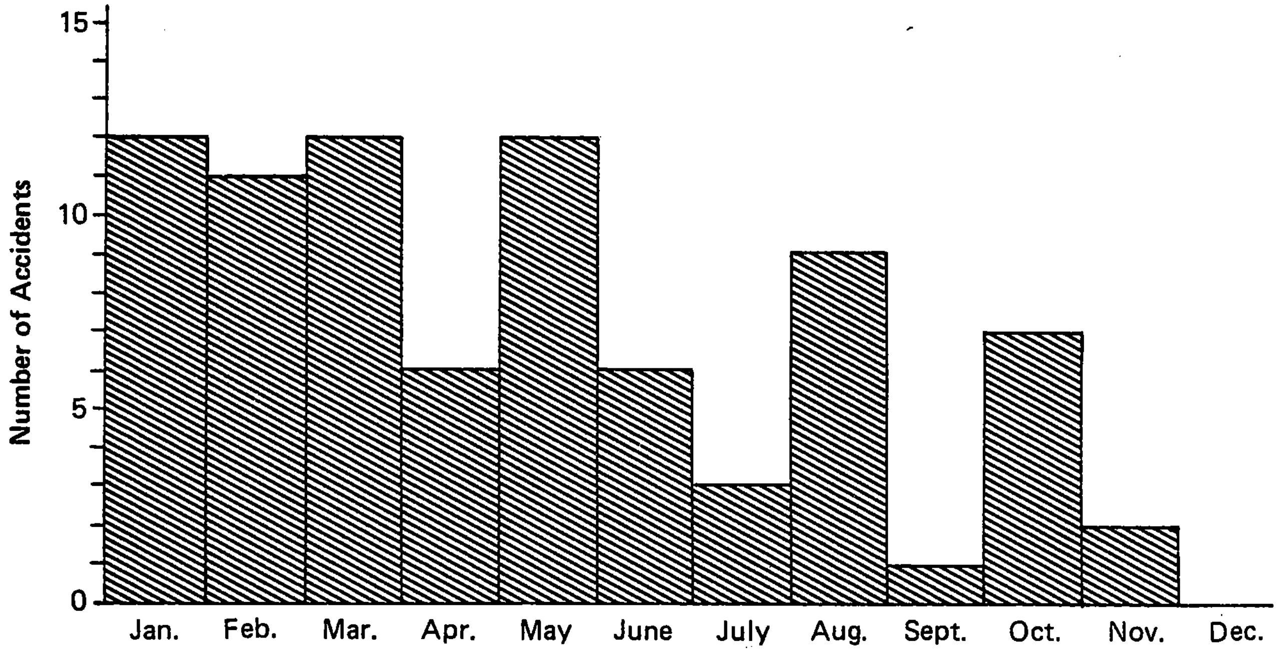

Figure 3. Frequency of Rockfall, Slides, and Related Accidents During Months of Year from the Year 1965 to September 1979 (Modified from NCDOT, 1979)

geologic transformation which have begun long before highways were invented. Stress relief jointing along river valleys is one common example.

Nevertheless, the principal causes of failure are often related to only a handful of natural processes: weathering; hydrostatic pressure; freeze/thaw cycles; seismic events; creep; and progressive failure which is a product of the other processes and their inter-relationships. Additionally, actions by man such as undercutting the toe of a slope, diverting surface run-off onto an unstable slope or increasing the driving force on a slope by surcharge loading can also contribute to a failure. However, the theme of this paper centers around aging slopes that are not being affected directly by man's activities.

Generally, the rock mass starts off with one or more sets of throughgoing discontinuities. Construction of a highway frequently causes these discontinuities to open due to stress relief and/or blasting gas pressure and vibration. These effects are most pronounced at the slope face and become less pronounced within the rock mass. A rule-of-thumb is that the depth of loosening is equal to the height of cut or valley. Typically instabilities occur within 50 feet of the slope face.

Weathering: Opening of joints allows water and air to get at the joint walls and fillings causing expansion and weakening of the materials.

Hydrostatic Pressures and Freeze/Thaw Cycles: The water within the rock mass, in addition to facilitating weathering processes, tends to freeze during the winter and melt during the spring. As described before, freezing of the groundwater tends to push loosened rock blocks out causing further loosening. Spring melt waters tend to impose hydrostatic forces on the bases and sides of discrete rock blocks, thereby increasing the magnitude of driving forces and decreasing the magnitude of resisting forces. This can occur within tension cracks and other open joints due to rainfall and snow melt whether a freeze cycle occurs or not.

Seismic Events: Seismic events tend to cause dynamic displacements of a loosened rock mass. The effects can be further loosening, displacement, rotation of discrete blocks or wedges, or complete failure.

Creep: When clay minerals are prevalent in the rock mass, either as a constituent of intact rock or along discontinuities, then creep (displacement at constant load) can occur along open joints particularly if the other processes described above are occurring also. We know from direct shear tests that re-adjustment of stress along joints occurs as irregularities are over-ridden, crushed, and/or sheared through. Therefore, it is easy to envision a block of rock creeping downslope, ever so slowly, redistributing its weight onto the most resistant surfaces until, finally, stress concentrations exceed the strength of potential support points and displacements accelerate until failure occurs.

Progressive Failure: The process by which most slope failures occur is called progressive failure. It essentially refers to the compounding of events which, over time, combine to cause ultimate instability of the slope. The processes described above can be divided into short-term and long-term events. Single rainfall or run-off induced hydrostatic pressures, freeze/thaw and earthquakes can be categorized as short-term events. Weathering, creep and cyclic hydrostatic pressures or freeze/thaw cycles can be categorized as long-term events. An aging rock slope is exposed to the long-term events usually as soon as the highway cut is made. A myriad of factors then will determine which processess are most deleterious to the slope and the time rate of degradation. This is as true for highway cuts as it is for ancient river valleys. The short-term events interplay with the long-term processes, usually resulting in local accelerations or changes in the nature of ongoing degradation. Tension cracks are often a common sign of large-scale progressive failure but as Hoek and Bray (1981) state:

> "It is impossible to quantify the seriousness of a tension crack since it is only the start of a very complex progressive failure process about which very little is known. It is quite probable that, in some cases, the improved drainage resulting from the opening up of the rock structure and the interlocking of individual blocks within the rock mass could give rise to an increase in stability. In other cases, the initiation of failure could be followed by a very rapid decrease in stability with a consequent failure of the slope."

Assessment of Slope Condition and Rehabilitation Planning

In summary, by processing site conditions and geologic data, potential slope failure modes can be analyzed. With this information, potential causes of failure can be investigated to see which are present and their relative importance. With this knowledge, a rehabilitation program can be planned. If merely one localized section of roadway is being studied, rehabilitation methods can be prescribed and implemented. If several locations or long stretches of roadway are being studied, the problem areas must be classified and prioritized. Limited funds are available for protection, rehabilitation or reconstruction of aging rock slopes. Effective utilization of these funds requires establishment of priorities for their expenditure.

The highest priorities should be given to choke points. Choke points are locations where rock slides could cause significant structural damage or economic dislocation due to long-term disruption of traffic. Examples would be:

- High rock slopes adjacent to tunnel portals or bridge approaches in which substantial masses of rock with high potential energy, sufficient to destroy or severely damage structures, could be included.

- Long, deep cuts where post-slide removal of large masses of rock and stabilization of remaining unstable masses could disrupt traffic and the economny for months.

Next highest priority should be given to roadway hazards. Many highways, including older portions of the interstate system, have near-vertical rock cuts immediately adjacent to the highway shoulder. As these cuts deteriorate, rock falls onto the roadway are increasingly common. Relatively minor rock falls on curved alignments can be deadly.

Third priority should be given to slopes where minimal potential for structural damage, economic disruption or personal injury exists. Within this category, slopes with significant annual maintenance costs should be considered for rehabilitation or reconstruction. Continued unrestrained deterioration may lead to major slides involving large rock masses, which could cause substantial economic disruption.

Once the problem areas are classified and prioritized, planning of design and construction are the next items of business. Like any infrastructure rehabilitation project, construction work usually must be done on or adjoining to an existing in-service facility. That presents many difficulties aside from the technical ones. Traffic flow patterns must be analyzed and maintained. Proper phasing of the work is necessary to re-route traffic at the appropriate times. During scaling operations and other types of debris removal, traffic may have to be stopped temporarily or intermittently. Weather may play a key role as in the I-40 Sterling Mountain slide rehabilitation described later in this paper. In that case, traffic had to be restored to the westbound lanes prior to mid-November when the roadway is prone to icing and hazardous driving conditions. Incidentally, repaving was being done east of the tunnel and slope rehabilitation in Tennessee was beginning west of the tunnel. Planning and logistics must consider work at the project site as well as work planned or ongoing on connecting roadways.

SLOPE REHABILITATION METHODS

The methods available for slope rehabilitation continue to be similar to those described by Piteau and Peckover (1978). There are typically six methods of rehabilitating a slope which can be used singly or in combination:

- Road relocation
- Warning/surveillance
- Removal of potentially unstable rock
- Reinforcement or supporting potential failures
- Relief of hydrostatic pressure by drainage
- Catchment of falling rock

These methods are listed in Table 3 and described in detail below.

A relative cost comparison is given in Table 4. Generally speaking, warning or surveillance methods are the cheapest rehabilitation measures which can be taken and removal of rock to

TABLE 3

REHABILITATION METHODS

WARNING/SURVEILLANCE

- Signs
- Patrols
- Electronic Devices

ROAD RELOCATION

REMOVAL OF MATERIAL

- Surface Scaling
- Flattening of Slope

REINFORCEMENT/SUPPORT

- Bolts/Dowels/Tendons
- Mesh
- Shotcrete
- Buttresses

DRAINAGE

- Surface
- Subsurface

CATCHMENT

- Shoulder
- Benches
- Fence
- Berm
- Barriers

TABLE 4

APPROXIMATE COST RANKING OF ROCK SLOPE REHABILITATION METHODS

(per 100 ft of roadway with 100 ft high vertical slope)

Description	Rehabilitation Type	Approximate Cost ($\$X10^3$)
Signs, Patrols or Warning Devices	Warning/Surveillance	less than 1
Earthen Berm	Catchment	2
Rock Fence	Catchment	3
Short Drain Holes	Drainage	10
Mesh	Reinforcement	10
Road Relocation (No cut or fill)	Relocation	30
Slope Surface Scaling	Removal	40
Shotcrete	Reinforcement	100
Long Drain Pipes	Drainage	120
Dowels, Bolts, Tendons	Reinforcement	150
Flatten Slope to 1H:4V	Removal	190
Flatten Slope to 1H:3V	Removal	250
Road Relocation*	Relocation	400
Widen Shoulder by 50 ft.	Catchment	740

* With reinforced embankment within new rock cut

relocate the road, flatten the slope or widen the shoulder are the most expensive. But rehabilitation method selection is usually not based solely on cost. Each site has different needs and constraints which must also be evaluated. Furthermore, rehabilitation methods are ranked by individual cost in the table without consideration of possible combinations which are commonly used. For example, road relocation normally requires cutting of the existing slope or construction of additional embankment. Considering combinations causes the cost to jump up by roughly an order of magnitude as shown in the table.

Warning/Surveillance

Many state transportation departments have found it necessary to patrol roads that have particularly frequent rock falls. While this method is fairly simple it does not mitigate the problem and can be very hazardous to the workers. Rock fall signs are intended to be temporary until hazardous conditions are eliminated. Yet if rehabilitation is a low priority, the signs sometimes remain in place indefinitely, serving no realistically practical purpose. Electronic devices are sometimes, but not commonly used as warning systems. These devices can include geotechnical instrumentation, electrical wire or fence, vibration monitors and television cameras. A symposium on landslide and slope stability monitoring was held at the 66th Annual Meeting of the Transportation Research Board where several current and new warning systems were introduced. The use of geotechnical instrumentation for rock slopes will be discussed in more detail later in this paper. It is important to note however, that eliminating potential rock fall hazards is preferable to monitoring and maintaining them for long periods of time.

Road Relocation

An alternative to patrolling the roadway is to relocate it away from the unstable area. Potential choices for re-alignment will depend on site conditions but may include moving the road away from the rock slope onto an embankment, tunneling through a mountain rather than going around it, or finding an alignment that misses the mountain altogether. In many cases it is most economically feasible to rehabilitate the existing slopes rather than move the road.

Removal of Potentially Unstable Rock

Removal of potentially unstable rock is typically necessary for slope rehabilitation whether it is to insure long-term performance or simply for worker safety. This may include removal of accumulated rock on benches, surface scaling by hand, explosive removal of overhangs, flattening of the slope and/or construction of additional benches. Breakage and removal of the rock is normally done using conventional rock excavation equipment. Access to the slope is sometimes limited and may require hand-carried equipment and rappeling expertise. Alternatively, scaling can be done using a crane with a specially designed "rake" or demolition ball.

Rock removal can be hazardous to the workers doing the work, as well as workers performing other tasks on-site. Additionally, vehicles passing nearby may be endangered. Therefore, traffic must be stopped or diverted and on-site personnel must be informed about the nature and timing of overhead activities. Protection of existing structures adjacent to the work may also be necessary.

Reinforcement or Support of Potential Failures

Unstable rock masses can either be reinforced to be self-supporting or can be supported externally. Common reinforcement methods include rock bolts, dowels or tendons, mesh and shotcrete.

Rock reinforcement dowels or bolts resist movement along joints and restrict block fallout and loosening. Tensioned reinforcement will change the stress state around the slope face by inducing compressive stresses, which provide confinement, thereby improving the strength of the rock mass. Steel fabric, straps or channels control rock falls between reinforcement elements.

Shotcrete is forced into open joints, fissures, seams, and irregularities in the rock surface and serves the same binding function as mortar in a stone wall. The adhesion of shotcrete to the rock surface, together with the shear strength of the shotcrete layer, provides resistance to the fallout of loose rock blocks as well as confinement of the rock mass. It will also seal rock which is prone to weathering due to exposure to the elements of nature.

Support of the rock can be accomplished with buttresses, bulkheads or retaining walls. These structures are typically constructed with cast-in-place, reinforced concrete, although stone or masonry can be used also. Recently, a new technique using the unstable rock as a "shot-in-place buttress" has been used successfully in Tennessee (Moore, 1986). Rock reinforcement is often used in combination with support methods.

Site specific conditions normally dictate whether to reinforce the rock or support it. Support methods are most commonly used to stabilize overhangs. Reinforcement is most commonly used to prevent ultimate sliding or rotational failure of potentially unstable rock massess along discontinuities. Also, surface protection using mesh and/or shotcrete can be used to prevent progressive ravelling and attack by sunlight, air and water.

Relief of Hydrostatic Pressure by Drainage

To limit the amount of water that accumulates along rock mass discontinuities, pressure relief drainage systems are used. This tends to prevent hydrostatic pressures from building up along discontinuities and also limits the volume of water that can freeze in the winter causing rock block displacement due to expansion. The two general forms of drainage are surface and subsurface. Surface drainage refers to diversion of surface run-off away from tension cracks or open rock mass discontinuities near the slope face. This can be accomplished with dikes, ditches or culverts. When discontinuity openings are particularly prone to water inflow the gaps may be sealed and filled with grout until no significant void space remains.

Shallow or deep subsurface drainage is usually accomplished with perforated PVC pipes which are grouted or dry-packed into place near the slope face. The holes are normally 2 to 3 inches in diameter and can be drilled to between 100 and 200 feet in length. Most times, every drain pipe will not intercept water bearing strata or discontinuities. A sufficient number must be installed to compensate for the "dry" ones. Also, they must be maintained in operating condition to be effective.

Catchment of Falling Rock

Regardless of which of the rehabilitation methods above are chosen, there is usually the need for catchment of falling rock. Most slopes contain small pieces of rock that could loosen in the future but do not require extensive removal or reinforcement. Furthermore, just as the original road design and construction does not eliminate future rock fall hazards, rehabilitation methods will not always be 100 percent effective due to the continual forces of nature. Catchment can consist of engineered benches, ditches, wide shoulders, berms, steel barriers, nets, fences, and/or concrete walls. Occasionaly, rock sheds or tunnels are used for protection from falling rock in extreme cases but are not common and will not be given further attention in this paper.

The type of catchment used depends largely on site conditions. Specifically, the height and angle of the slope and clearance between slope and roadway are important. This not only dictates how much space there is for catchment but it also relates to anticipated paths of falling rocks. Obviously the catchment area must be somewhere, along the path of the rocks, to be effective.

Generally, the flatter the slope is, the more likely falling rocks will bounce and/or roll. Simple rock falls (i.e. no bounce or roll) tend to occur on steep slopes and can be kept off of the roadway with benches, ditches, and shoulders of appropriate widths and locations. Bonazzi and Colombet (1984) aptly point out that design of such catchment areas "should also include provisions in the original design for permanent re-access, despite the cost involved, because ..... (if) there is a danger, it would be better to be able to do something about it before it can become critical". That is to say that sometimes the catchment areas become filled with talus forming a slope which can eventually direct subsequent rock falls onto the roadway. The catchment area then must be accessed periodically to remove such debris which potentially defeats the purpose of the catchment area.

For the flatter slopes where rock falls tend to bounce and/or roll, a barrier is needed to deflect rocks away from the roadway. Key considerations in the design of such barriers are height, location and strength. Berms, steel barriers, fences and/or concrete walls can be used for this purpose. These are normally used in conjunction with benches, ditches and shoulders.

If space does not permit the construction of adequate catchment areas and barriers near road level, potential rock debris must be held in place directly against the slope face. This can be accomplished using a net that is fastened to or over the slope. The netting commonly consists of chain link fence or gabion wire fabric held in place by rock bolts or cable tendons. These methods are currently being used on rehabilitation projects in Montana, Tennessee and North Carolina to name a few.

LONG-TERM PERFORMANCE MONITORING

Long-term monitoring of slope performance after rehabilitation can be accomplished using geotechnical instrumentation. In addition to performance monitoring, the instruments can be used to ensure safety, cost economy or design and construction method adequacy. The two main parameters measured are deformation and water levels. Deformation can be measured with optical survey points, inclinometers or extensometers. Water levels can be measured with observation wells or piezometers. These can be read manually or remotely.

The reliability of geotechnical instrumentation was the subject of a recent symposium of the Transportation Research Board. At the symposium, Dunnicliff (1985) listed the basic ingredients of a reliable instrumentation program: simplicity; self-verification; durability in the installed environment; thorough planning; installation care; regular maintenance and calibration; and care during data collection, processing and interpretation. Making these ingredients part of a slope monitoring program is essential for success.

Furthermore, a specific course of action in response to instrument readings is necessary. If the instruments are simply installed and read by field personnel without them understanding to whom results should be transmitted and how serious readings may be, then the instrumentation program is serving no purpose. The instruments must be read on a scheduled basis and data must be examined by a competent engineer or geologist in a timely manner. Limits for acton and type of action should be pre-determined and understood by all. For example, a schedule for action like the one below could be used:

Displacement	Code	Action
Greater than 2"	Red	Call chief geologist/engineer immediately
1 to 2"	Yellow	Read instruments weekly
Less than 1"	Green	Read instruments monthly

CASE HISTORY: I-40 STERLING MOUNTAIN PORTAL RECONSTRUCTION

Most of the concepts presented above were used for rehabilitation of a slope in North Carolina after one of the more dramatic failures of recent time. On March 5, 1985, a massive rock slide involving roughly 14,000 cubic yards of rock debris occurred at the eastern portal area of the twin tunnels which carry Interstate 40 through Sterling Mountain (Photograph 1). The 150-foot canopy or tunnel extension which had been built at the eastern end of the westbound tunnel to protect the interstate from falling rock was destroyed and the eastbound lane was also completely blocked (Photograph 2).

Good to excellent quality Longarm Quartzite can be seen above the tunnel under which is poor to fair quality Longarm Quartzite interbedded with siltstone, slate and phyllite. The Longarm Formation is one of four formations of the Snowbird Group which is one of three regional lithologic units of the Ocoee Series. The original Blue Ridge Mountains were eroded, producing large quantities of material which became the metasediments forming most of the Great Smoky Mountains. This mass of sediments is known as the Ocoee Series.

The knob of rock that failed was bounded by a fault trending nearly east-west, a major joint set trending northeast and bedding which strikes northwest. Because of the pre-existing discontinuities in the rock mass, the abundant water available to accelerate weathering along these discontinuities, and probably freeze-thaw pressures, the block of rock finally failed destroying the westbound portal section of the tunnel. A contractor on a nearby project was mobilized to clear the debris and to pave the construction road that passes around the outside of the mountain. Traffic was reinstated 18 days after the failure with westbound traffic going through the eastbound tunnel and eastbound traffic going along the construction road (Photograph 3).

After one month of geologic mapping, core drilling and frantic head scratching, a design concept was presented to North Carolina Department of Transportation and the Federal Highway Administration for reconstruction of the portal. The overall objectives were to reconstruct the westbound portal to the same general dimensions as it formerly had, repair any damage to the remaining structures, stabilize or remove any potential rock falls and re-open the highway to full use before winter. This involved demolition of badly damaged portions of the existing portal, construction of a new, cast-in-place concrete portal and retaining wall, the repair of damaged portions of the westbound tunnel, construction of a Reinforced Earth wall along the shoulder as a catchment area and stabilization of the adjacent rock slopes with a combination of scaling, reinforcement and drainage (Figure 4). Also advance procurement of the Reinforced Earth strips and panels was recommended since time was of the essence. These recommendations were promptly accepted. The design documents wee prepared and issued to five contractors within the next month. Three contractors bid the job within three working days at which time the lowest bidder, Oman Construction, was selected. The notice to proceed was issued the following day and construction began. The contract

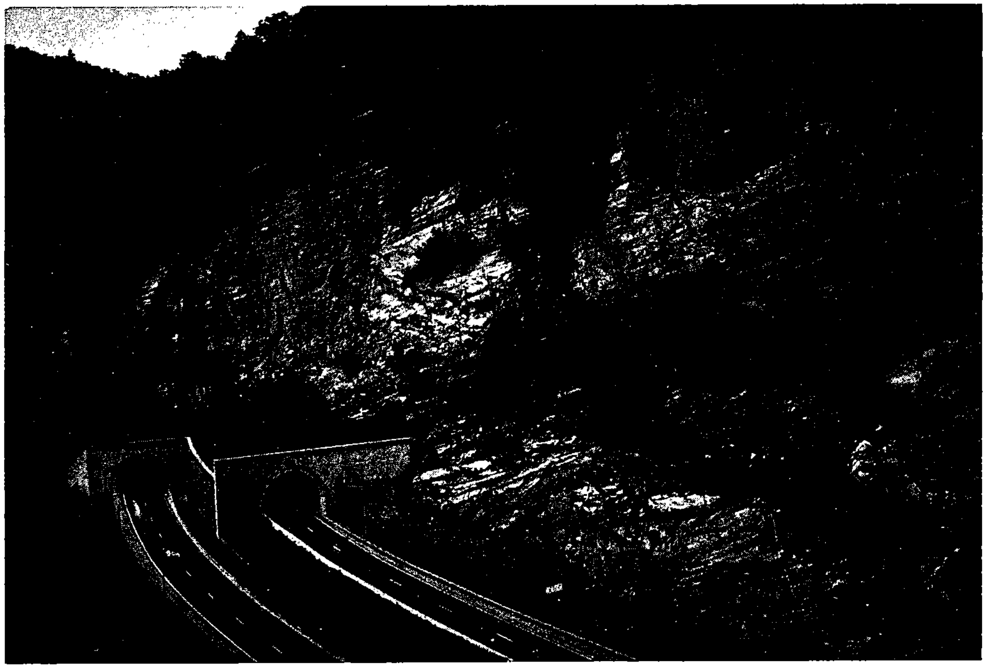

Photograph 1. Portal Prior to Slope Failure

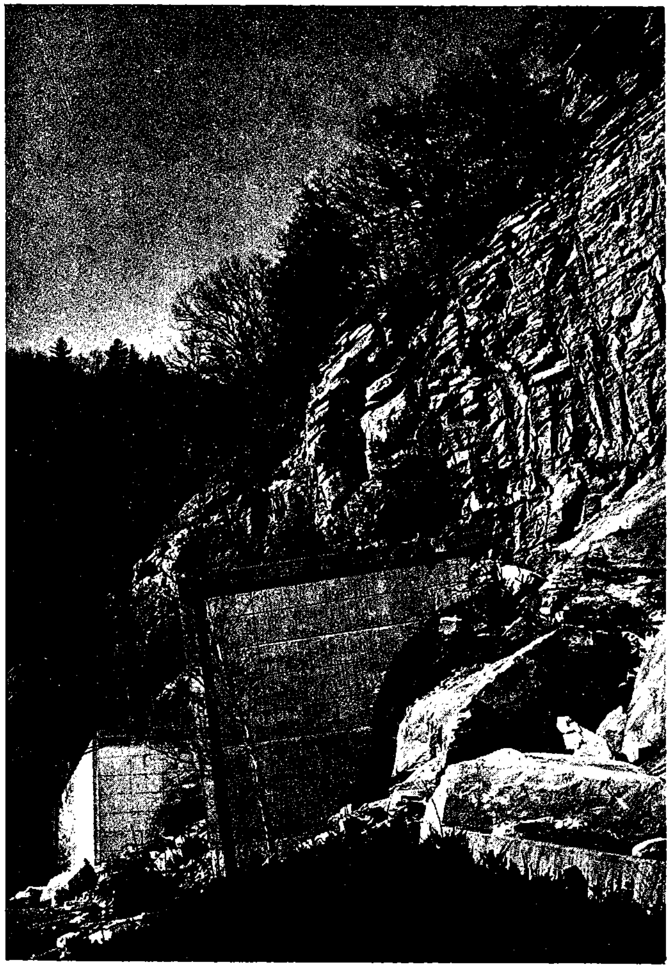

Photograph 2. Portal After Slope Failure

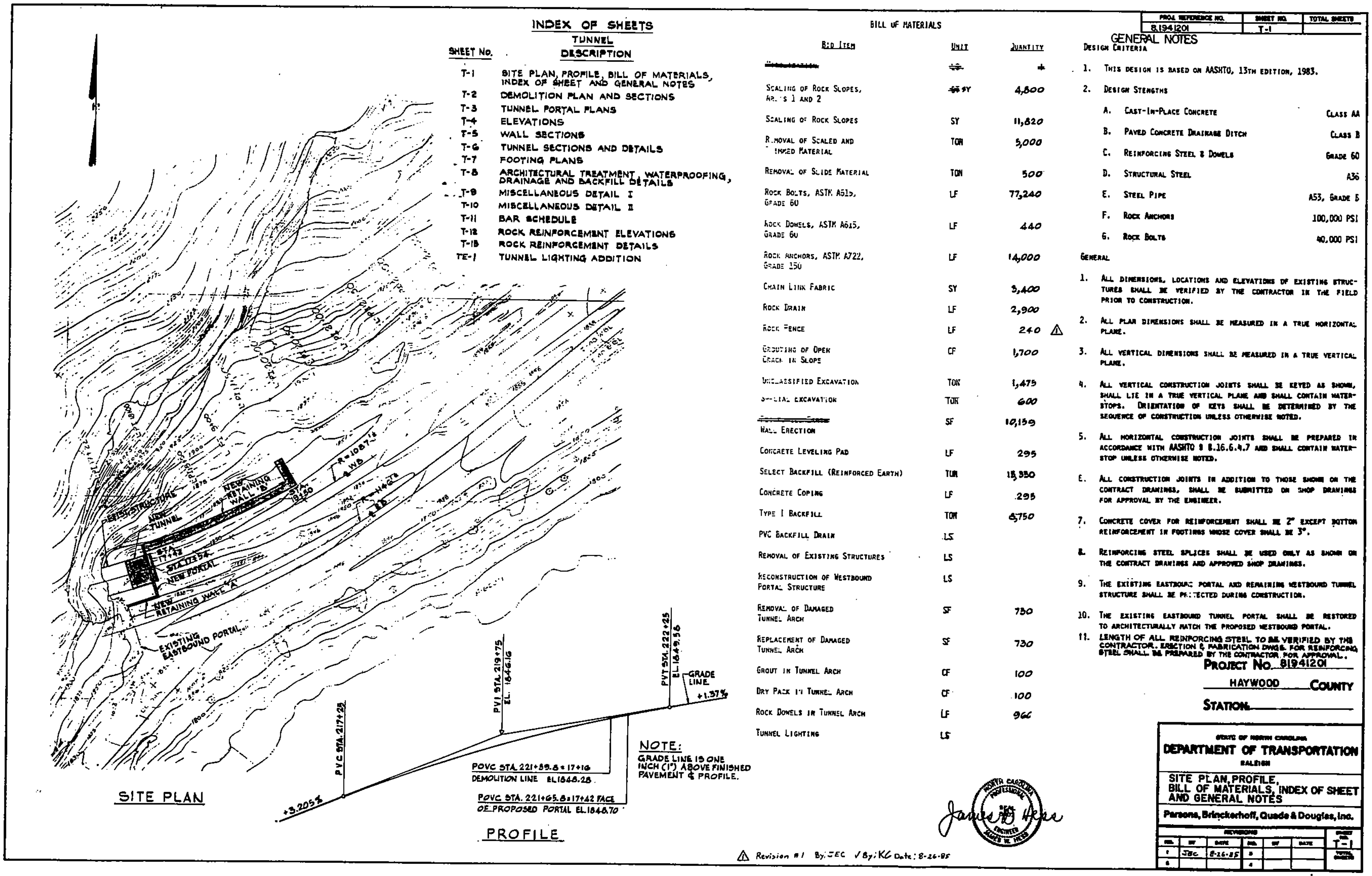
SITE PLAN
EXIST. STRUCTURE
NEW TUNNEL
NEW RETAINING WALL 'B'
STA. 19+50
STA. 17+42
STA. 17+54
NEW PORTAL
NEW RETAINING WALL 'A'
EXISTING EASTBOUND PORTAL
R=1087.1 WB
R=1146.0 EB
PROFILE
+3.205%
PVC STA. 217+25
PVI STA. 219+75 EL. 1846.16
PVT STA. 222+25 EL. 1849.56
GRADE LINE
+1.37%
POVC STA. 221+89.8 = 17+16 DEMOLITION LINE EL.1848.28
POVC STA. 221+65.8 = 17+42 FACE OF PROPOSED PORTAL EL.1848.70

NOTE:
GRADE LINE IS ONE INCH (1") ABOVE FINISHED PAVEMENT & PROFILE.

INDEX OF SHEETS

TUNNEL

SHEET No.	DESCRIPTION
T-1	SITE PLAN, PROFILE, BILL OF MATERIALS, INDEX OF SHEET AND GENERAL NOTES
T-2	DEMOLITION PLAN AND SECTIONS
T-3	TUNNEL PORTAL PLANS
T-4	ELEVATIONS
T-5	WALL SECTIONS
T-6	TUNNEL SECTIONS AND DETAILS
T-7	FOOTING PLANS
T-8	ARCHITECTURAL TREATMENT, WATERPROOFING, DRAINAGE AND BACKFILL DETAILS
T-9	MISCELLANEOUS DETAIL I
T-10	MISCELLANEOUS DETAIL II
T-11	BAR SCHEDULE
T-12	ROCK REINFORCEMENT ELEVATIONS
T-13	ROCK REINFORCEMENT DETAILS
TE-1	TUNNEL LIGHTING ADDITION

BILL OF MATERIALS

Bid Item	Unit	Quantity
~~[illegible]~~	~~LS~~	~~+~~
Scaling of Rock Slopes, Ar.'s 1 and 2	SY	4,800
Scaling of Rock Slopes	SY	11,820
Removal of Scaled and Trimmed Material	TON	5,000
Removal of Slide Material	TON	500
Rock Bolts, ASTM A615, Grade 60	LF	77,240
Rock Dowels, ASTM A615, Grade 60	LF	440
Rock Anchors, ASTM A722, Grade 150	LF	14,000
Chain Link Fabric	SY	3,400
Rock Drain	LF	2,900
Rock Fence	LF	240 ⚠
Grouting of Open Crack in Slope	CF	1,700
Unclassified Excavation	TON	1,475
Special Excavation	TON	600
~~[illegible]~~ Wall Erection	SF	10,159
Concrete Leveling Pad	LF	295
Select Backfill (Reinforced Earth)	TON	18,350
Concrete Coping	LF	295
Type I Backfill	TON	8,750
PVC Backfill Drain	LS	
Removal of Existing Structures	LS	
Reconstruction of Westbound Portal Structure	LS	
Removal of Damaged Tunnel Arch	SF	730
Replacement of Damaged Tunnel Arch	SF	730
Grout in Tunnel Arch	CF	100
Dry Pack in Tunnel Arch	CF	100
Rock Dowels in Tunnel Arch	LF	966
Tunnel Lighting	LS	

⚠ Revision #1 By: JEC ✓By: KC Date: 8-26-85

PROJ. REFERENCE NO.	SHEET NO.	TOTAL SHEETS
8.1941201	T-1	

GENERAL NOTES

Design Criteria

1. This design is based on AASHTO, 13th edition, 1983.
2. Design Stengths

A.	Cast-In-Place Concrete	Class AA
B.	Paved Concrete Drainage Ditch	Class B
C.	Reinforcing Steel & Dowels	Grade 60
D.	Structural Steel	A36
E.	Steel Pipe	A53, Grade B
F.	Rock Anchors	100,000 PSI
G.	Rock Bolts	40,000 PSI

General

1. All dimensions, locations and elevations of existing structures shall be verified by the contractor in the field prior to construction.
2. All plan dimensions shall be measured in a true horizontal plane.
3. All vertical dimensions shall be measured in a true vertical plane.
4. All vertical construction joints shall be keyed as shown, shall lie in a true vertical plane and shall contain waterstops. Orientation of keys shall be determined by the sequence of construction unless otherwise noted.
5. All horizontal construction joints shall be prepared in accordance with AASHTO § 8.16.6.4.7 and shall contain waterstop unless otherwise noted.
6. All construction joints in addition to those shown on the contract drawings, shall be submitted on shop drawings for approval by the engineer.
7. Concrete cover for reinforcement shall be 2" except bottom reinforcement in footings whose cover shall be 3".
8. Reinforcing steel splices shall be used only as shown on the contract drawings and approved shop drawings.
9. The existing eastbound portal and remaining westbound tunnel structure shall be protected during construction.
10. The existing eastbound tunnel portal shall be restored to architecturally match the proposed westbound portal.
11. Length of all reinforcing steel to be verified by the contractor. Erection & fabrication dwgs. for reinforcing steel shall be prepared by the contractor for approval.

PROJECT No. 8194120I
HAYWOOD COUNTY
STATION

STATE OF NORTH CAROLINA
DEPARTMENT OF TRANSPORTATION
RALEIGH

SITE PLAN, PROFILE, BILL OF MATERIALS, INDEX OF SHEET AND GENERAL NOTES

Parsons, Brinckerhoff, Quade & Douglas, Inc.

REVISIONS

NO.	BY	DATE	NO.	BY	DATE	SHEET NO.
1	JEC	8-26-85	3			T-1
2			4			TOTAL SHEETS

FIGURE 4. Rehabilitation Plan and Bid Quantities

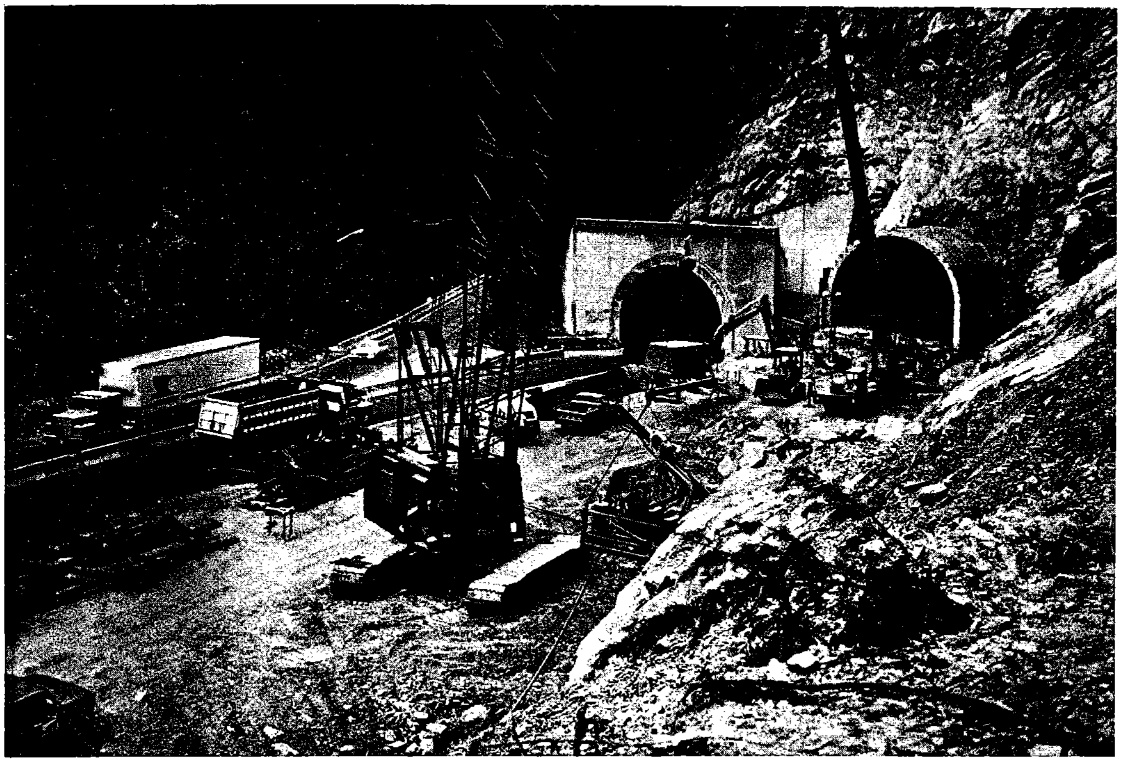

Photograph 3. Re-instatement of Traffic During Construction

Photograph 4. Rock Overhang Removal by Blasting

amount was for almost 6 million dollars, 5% within the engineer's estimate.

Scaling and removal of overhangs was the first order of business (Photograph 4). The contractor piled hay around the existing structure for protection. Explosives were used to remove the rock overhangs. The blaster pre-split a back line and then immediately fractured the freed blocks almost in mid-air. Scalers then rappelled down the side of the slope with pry bars, knocking loose any blocks or wedges that could conceivably be removed. Traffic was generally interrupted while scaling was being done.

After scaling was complete, demolition of damaged structures and construction of new ones proceeded. Repair of the concrete tunnel arch began (Photograph 5) and excavation for new structures was completed. Shoring of the remaining tunnel was also required. The contractor erected reinforcing steel and poured concrete for new footings, retaining walls and the portal structure while rock bolts were being installed concurrently (Photograph 6). The slope was divided into five reinforcement areas (Figure 5).

Areas 1, 3 and 5 required selective bolting using #9 bars of varying lengths on an as-needed basis. The location of these bolts was determined in the field by the designer and DOT's geotechnical and construction staff. Potential wedges in Area 2 were stabilized by pattern bolting and chain link fabric. Areas 4A and 4B were the most worrisome since large blocks remained which could fail in the same manner as the original failure. Here 40-foot long, high strength anchors were specified on a 10x15 foot pattern with 20-foot bolts to stabilize the surficial slabs in between. The resulting pattern was 5 foot x 5 foot. Rock bolting and mesh erection was generally done from cranes.

Additionally, a reinforced earth wall catchment area and rock fence were erected near the new portal to collect small-scale rock falls that may occur in the future (Photograph 7). Secondly, drain pipes were installed along the base of the slope to relieve future build-up of water along throughgoing rock mass discontinuities within the slope.

CONCLUSIONS

Several papers presented at this 37th Annual Highway Geology Symposium recognize the time-dependent nature of rock slope stability. Rock slope failure is often a progressive phenomenon. The accumulated result of small movements occurring over decades can severely reduce the shear strength of critical discontinuities.

This progressive failure is similar to the phenomena described by Skempton and Hutchinson (1969) and Bjerrum and Jorstad (1968) in their classic papers concerning the behavior of slopes in overconsolidated clays and clay shales. As in any progressive failure phenomenon, timely

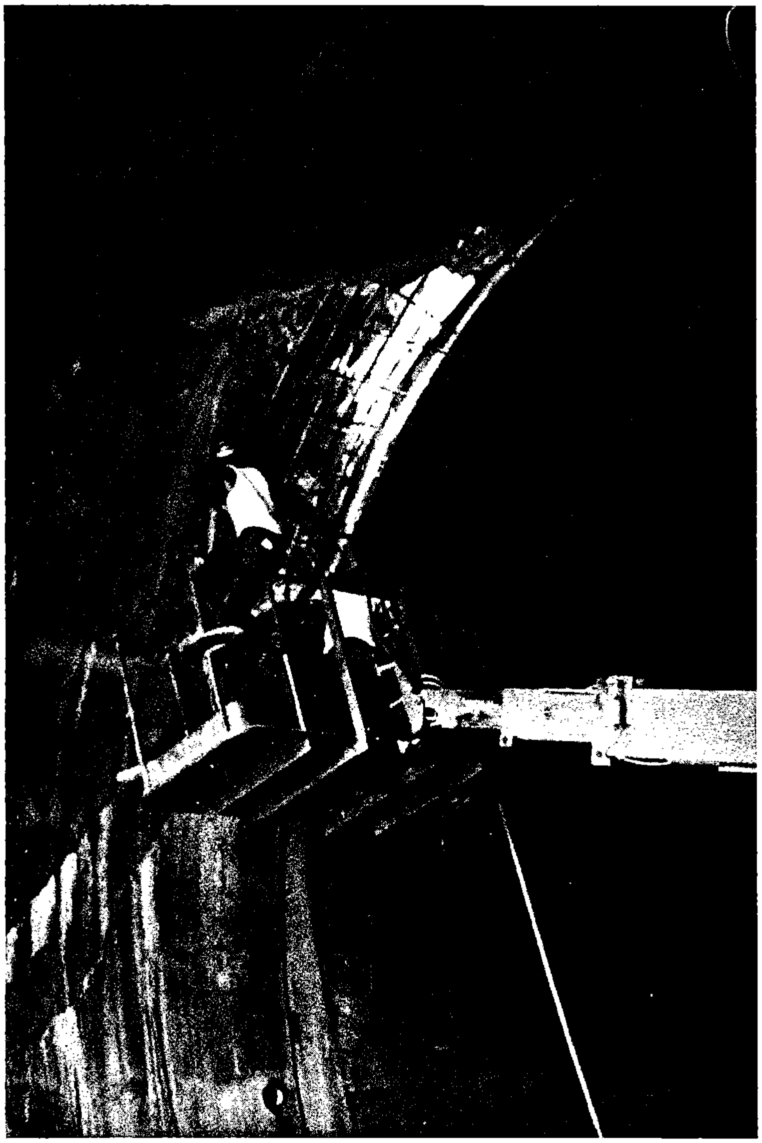

Photograph 5. Repair of Portal Structure

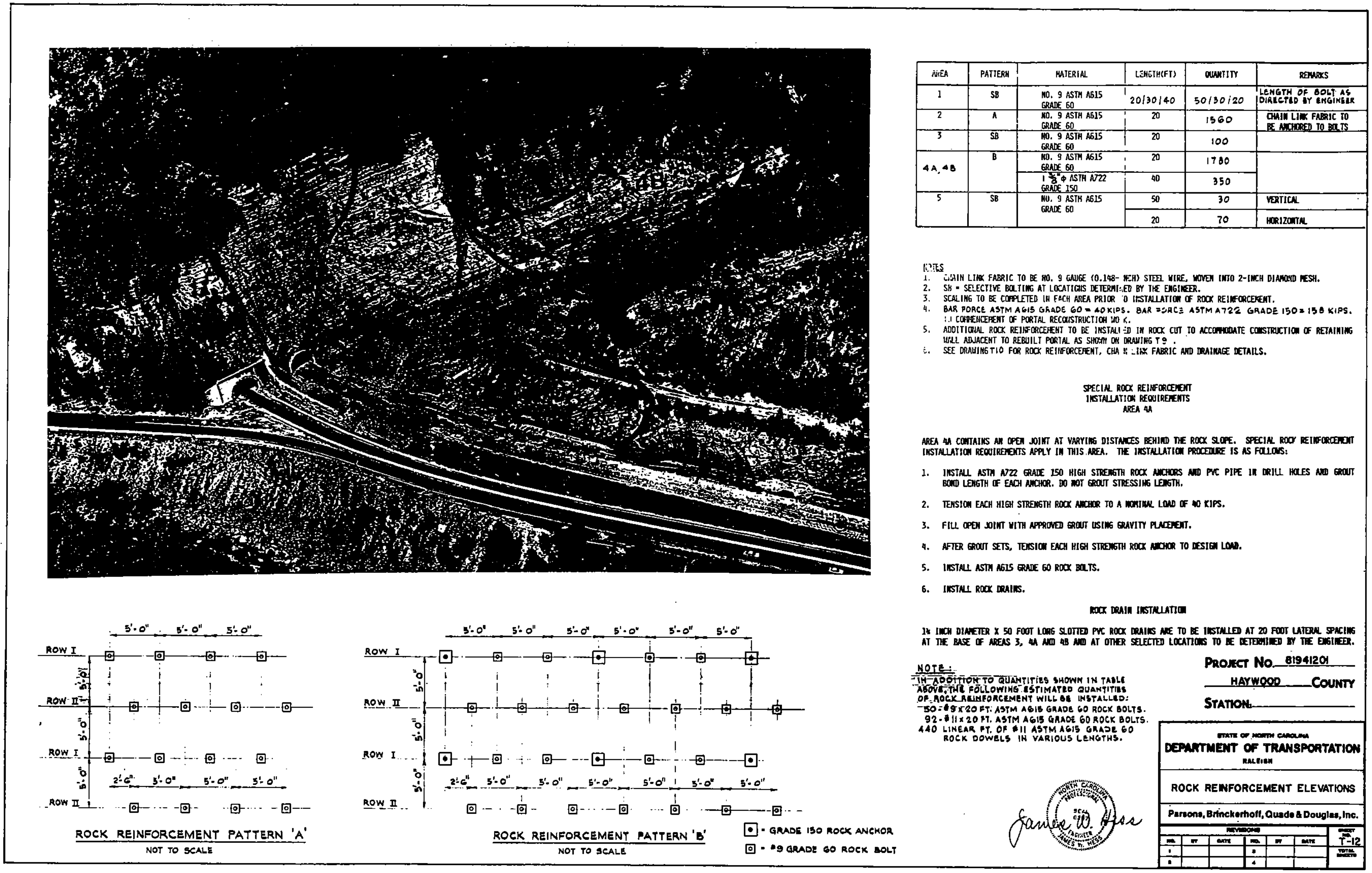
ROW I
ROW II
ROW I
ROW II
5'-0"
2'-6"
ROCK REINFORCEMENT PATTERN 'A'
NOT TO SCALE
ROW I
ROW II
ROW I
ROW II
5'-0"
2'-6"
ROCK REINFORCEMENT PATTERN 'B'
NOT TO SCALE
⊡ - GRADE 150 ROCK ANCHOR
⊡ - #9 GRADE 60 ROCK BOLT

AREA	PATTERN	MATERIAL	LENGTH(FT)	QUANTITY	REMARKS
1	SB	NO. 9 ASTM A615 GRADE 60	20/30/40	50/30/20	LENGTH OF BOLT AS DIRECTED BY ENGINEER
2	A	NO. 9 ASTM A615 GRADE 60	20	1560	CHAIN LINK FABRIC TO BE ANCHORED TO BOLTS
3	SB	NO. 9 ASTM A615 GRADE 60	20	100	
4A, 4B	B	NO. 9 ASTM A615 GRADE 60	20	1780	
		1 3/8"φ ASTM A722 GRADE 150	40	350	
5	SB	NO. 9 ASTM A615 GRADE 60	50	30	VERTICAL
			20	70	HORIZONTAL

NOTES

1. CHAIN LINK FABRIC TO BE NO. 9 GAUGE (0.148-INCH) STEEL WIRE, WOVEN INTO 2-INCH DIAMOND MESH.
2. SB = SELECTIVE BOLTING AT LOCATIONS DETERMINED BY THE ENGINEER.
3. SCALING TO BE COMPLETED IN EACH AREA PRIOR TO INSTALLATION OF ROCK REINFORCEMENT.
4. BAR FORCE ASTM A615 GRADE 60 = 40 KIPS. BAR FORCE ASTM A722 GRADE 150 = 158 KIPS. AT COMMENCEMENT OF PORTAL RECONSTRUCTION WORK.
5. ADDITIONAL ROCK REINFORCEMENT TO BE INSTALLED IN ROCK CUT TO ACCOMMODATE CONSTRUCTION OF RETAINING WALL ADJACENT TO REBUILT PORTAL AS SHOWN ON DRAWING T9 .
6. SEE DRAWING T10 FOR ROCK REINFORCEMENT, CHAIN LINK FABRIC AND DRAINAGE DETAILS.

SPECIAL ROCK REINFORCEMENT
INSTALLATION REQUIREMENTS
AREA 4A

AREA 4A CONTAINS AN OPEN JOINT AT VARYING DISTANCES BEHIND THE ROCK SLOPE. SPECIAL ROCK REINFORCEMENT INSTALLATION REQUIREMENTS APPLY IN THIS AREA. THE INSTALLATION PROCEDURE IS AS FOLLOWS:

1. INSTALL ASTM A722 GRADE 150 HIGH STRENGTH ROCK ANCHORS AND PVC PIPE IN DRILL HOLES AND GROUT BOND LENGTH OF EACH ANCHOR. DO NOT GROUT STRESSING LENGTH.
2. TENSION EACH HIGH STRENGTH ROCK ANCHOR TO A NOMINAL LOAD OF 40 KIPS.
3. FILL OPEN JOINT WITH APPROVED GROUT USING GRAVITY PLACEMENT.
4. AFTER GROUT SETS, TENSION EACH HIGH STRENGTH ROCK ANCHOR TO DESIGN LOAD.
5. INSTALL ASTM A615 GRADE 60 ROCK BOLTS.
6. INSTALL ROCK DRAINS.

ROCK DRAIN INSTALLATION

1½ INCH DIAMETER X 50 FOOT LONG SLOTTED PVC ROCK DRAINS ARE TO BE INSTALLED AT 20 FOOT LATERAL SPACING AT THE BASE OF AREAS 3, 4A AND 4B AND AT OTHER SELECTED LOCATIONS TO BE DETERMINED BY THE ENGINEER.

NOTE:
IN ADDITION TO QUANTITIES SHOWN IN TABLE ABOVE, THE FOLLOWING ESTIMATED QUANTITIES OF ROCK REINFORCEMENT WILL BE INSTALLED:
50 - #9 x 20 FT. ASTM A615 GRADE 60 ROCK BOLTS.
92 - #11 x 20 FT. ASTM A615 GRADE 60 ROCK BOLTS.
440 LINEAR FT. OF #11 ASTM A615 GRADE 60 ROCK DOWELS IN VARIOUS LENGTHS.

PROJECT No. 8194120I
HAYWOOD COUNTY
STATION

James W. Hess

JAMES W. HESS

STATE OF NORTH CAROLINA
DEPARTMENT OF TRANSPORTATION
RALEIGH

ROCK REINFORCEMENT ELEVATIONS

Parsons, Brinckerhoff, Quade & Douglas, Inc.

REVISIONS						SHEET NO.
NO.	BY	DATE	NO.	BY	DATE	T-12
1			3			TOTAL SHEETS
2			4			

FIGURE 5. Classification of Slope into Reinforcement Areas

Photograph 6. Rock Bolting Above Other Construction Activities

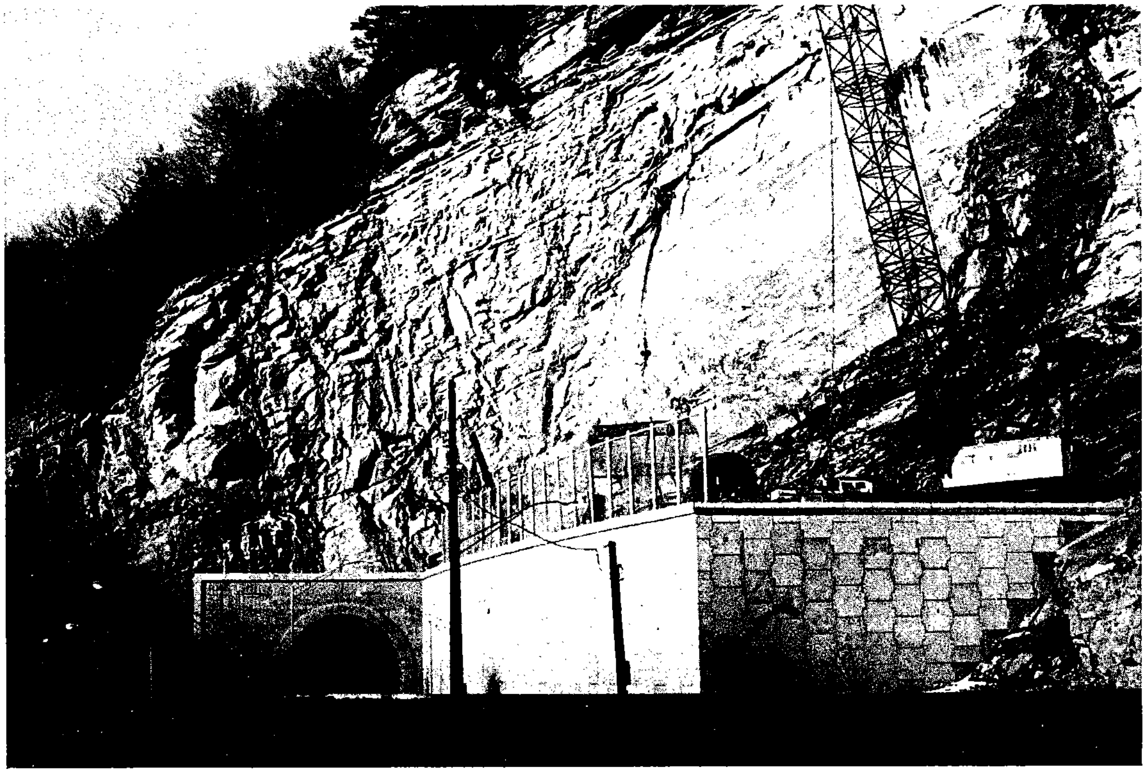

Photograph 7. Rehabilitated Structure

implementation of control or mitigation procedures is essential. Failure can be prevented or the severity of effects can be minimized if not prevented.

Effective methods are currently available to evaluate the present condition of rock slopes along transportation routes and potential for short-term or long-term failure. A wide range of proven techniques are available for preventing failure or minimizing its effects on the roadway and adjacent structures.

However, in many instances, these techniques are only used in post-failure movement rather than to prevent the onset of instability. It would be more cost-effective to utilize these techniques at a smaller scale and lower level of expenditure to prevent further deterioration of potentially critical slopes.

REFERENCES

1. Abramson, L.W. (1985), "Rock Wedge Stability Analysis on a Personal Computer," Proc., 26th U.S. Symposium on Rock Mechanics, Rapid City, South Dakota, Balkema, Rotterdam, pp. 675-682.

2. Bjerrum, L. and Jorstad, F.A. (1968), "Stability of Rock Slopes in Norway," Norwegian Geotechnical Institute, Oslo, Publication No. 79, 11 pp.

3. Bonazzi, D. and Colomet, G. (1984), "Restrengthening and Maintenance of Anchored Rock Slopes," Proc., International Conference on In Situ Soil and Rock Reinforcement, Paris, pp. 225-230.

4. Dunnicliff, J. (1985), "Closing Remarks on Reliability of Geotechnical Instrumentation," Transportation Research Record No. 1004, Transportation Research Board, National Research Council, Washington, D.C., pp. 46-49.

5. Eigenbrod, K.D. and Morgenstern, N.R. (1972), "A Slide in Cretaceous Bedrock, Devon, Alberta," Proc., 2nd International Conference on Stability in Open Pit Mining, Vancouver, AIME, pp. 223-237.

6. Fowler, B.K. (1976), "Construction Redesign - Woodstock Rockslide, N.H.," Proc., Specialty Conference on Rock Engineering for Foundations & Slopes, Volume 1, Boulder, Colorado, ASCE, pp. 386-403.

7. Goodman, R.E. (1976), Methods of Geologic Engineering in Discontinuous Rock, Chapter 3, West Publishing, St. Paul, Minnesota, pp. 58-90.

8. Goodman, R.E. (1980), Introduction to Rock Mechanics, Wiley, New York, pp. 34 and 42.

9. Hendron, A.J., Jr., Cording, E.J., and Aiyer, A.K. (1971), "Analytical and Graphical Methods for the Analysis of Slopes in Rock Masses," U.S. Army Engineer Explosive Excavation Research Office, Livermore, California, Technical Report No. 36, 148 p., NTIS No. AD-738-929.

10. Hoek, E. and Bray, J.W. (1981), Rock Slope Engineering, Revised Third Edition, Institution of Mining and Metallurgy, London, pp. 37-63 and 76.

11. International Society of Rock Mechanics (1978), "Suggested Methods for the Quantitative Description of Discontinuities in Rock Masses," International Journal on Rock Mechanics, Mining Science and Geomechanics Abstract, Volume 14, pp. 319-368.

12. Killey, M.M., Hines, J.K. and DuMontelle, P.B. (1985), "Landslide Inventory of Illinois," Illinois Department of Energy and Natural Resources, State Geology Survey Division, Circular No. 534, p. 4.

13. Kovari, K. and Fritz, P. (1975), "Stability Analysis of Rock Slopes for Plane and Wedge Failure with the Aid of a Programmable Pocket Calculator," Proc., 16th U.S. Symposium on Rock Mechanics, ASCE, New York, pp. 25-34.

14. Mearns, R. (1972), "Solving a Rockfall Problem in Nevada County, California," Highway Research News No. 49, Highway Research Board, National Research Council, Washington, D.C., pp. 14-17.

15. Montana Department of Highways (1986), 37th Annual Highway Geology Symposium Field Trip Guide, Helena, Montana.

16. Moore, H.L. (1985), "Wedge Failures Along Tennessee Highways in the Appalachian Region - Their Occurrence and Correction," Preprint, 28th Annual Meeting of the Association of Engineering Geologists, Winston-Salem, North Carolina, 47 pp.

17. Moore, H.L. (1986), "The Construction of a Shot-in-Place Rock Buttress for Landslide Stabilization," Proc., 37th Annual Highway Geology Symposium, Helena, Montana, 21 pp.

18. North Carolina Department of Transportation (1979), "I-40, Slope Stability Study, Final Report, Station 0+00 to 211+00," Volume 1.

19. O'Neill, A.L. (1973), "Slope Failures in Foliated Rocks, Butte County, California," Highway Research Record No. 135, Highway Research Board, National Research Council, Washington, D.C. pp. 40-42.

20. Piteau, D.R. and Peckover, F.L. (1978), "Engineering of Rock Slopes," Chapter 9 in Landslides - Analysis and Control, Transportation Research Board Special Report No. 176, National Academy of Sciences, Washington, D.C., pp. 192-228.

21. Schuster, R.L. and Fleming, R.W. (1986), "Economic Losses and Fatalities Due to Landslides," Bulletin of the Association of Engineering Geologists, Volume XXIII, No. 1, pp. 11-28.

22. Shakoor, A. and Weber, M.W. (1986), "Role of Shale Undercutting in Promoting Rock Falls and Wedge Failures Along Interstate 77," 29th Annual Meeting of the Association of Engineering Geologists, San Francisco.

23. Sherman, W.F. (1974), "Engineering Geology of Cody Highway Tunnels, Park County, Wyoming," Proc., 3rd International Congress on Rock Mechanics, Pennsylvania State University Experiment Station, University Park, Pennsylvania.

24. Skempton, A.W. and Hutchinson, J.N. (1969), "Stability of Natural Slopes and Embankment Foundations," Proc., 7th International Conference on Soil Mechanics and Foundation Engineering, Mexico, State-of-the-Art Volume, pp. 291-340.

25. Smith, R.M. (1986), "Spring Valley Slide," Executive Summary Report of the 12th Northwest Geotechnical Workshop, Helena, Montana, p. 1.

26. Watts, C.F. and West, T.R. (1985), "Electronic Notebook Analysis of Rock Slope Stability at Cedar Bluff, Virginia," Bulletin of the Association of Engineering Geologists, Volume XXII, No. 1, pp. 67-85.

27. Watts, C.F. and West, T.R. (1986), "Discontinuity Significance Index and Electronic Data Collection for Rock Slope Stability Studies," Bulletin of the Association of Engineering Geologists, Volume XXIII, No. 3, pp. 265-278.

28. Wright, E. (1985), "Rockfalls on Eastern Kentucky Highways," 28th Annual Meeting of the Association of Engineering Geologists, Winston-Salem, North Carolina.

29. Wu, S. (1985), "Rockfall Evaluation by Computer Simulation," Transportation Research Record No. 1301, Transportation Research Board, National Research Council, Washington, D.C., pp. 1-5.

A TIME-BASED MODEL TO HELP EVALUATE FUTURE STABILITY OF CUT SLOPES

Stanley M. Miller

Department of Geology and
Geological Engineering
University of Idaho
Moscow, Idaho 83843

ABSTRACT

Of the recognized time-related factors that influence stability of cut slopes within time periods shorter than 50 years or even 100 years, the most critical factor in many field situations is the character of precipitation activity. An extreme-value statistical model based on historical precipitation data can be linked with geotechnical slope stability models to provide a method for estimating the probability of slope failure within a given time period. Temporal slope stability predictions obtained from the analysis provide useful information for the design of cut slopes and for the development of slope maintenance programs. Two hypothetical examples are presented to illustrate the analytical techniques and to point out that additional research work is needed in the area of analysing groundwater response to precipitation activity.

INTRODUCTION

Time-related factors that influence the stability of cut slopes include conditions such as the degree of geologic weathering, the rate and amount of surface erosion, the creep-induced reduction in shear strength, and the character of precipitation activity. For the typical time span associated with the construction and maintenance of highway slope cuts (usually less than 50 years or perhaps even 100 years), the most critical of these factors is the precipitation activity. Highway maintenance crews are all too familiar with the cleanup and repair associated with slope failures initiated by heavy rainfall or rapid snowmelt events that cause a significant rise in the piezometric surface.

The common method for estimating the stability of a slope cut consists of applying proven two-dimensional, limiting equilibrium stability models to predicted failure geometries in the slope. Identification of these geometries, or failure modes, relies upon knowledge of the geologic materials present and the configurations of the natural ground surface and the proposed slope cut. Input data for the stability analysis include material properties (such as unit weight and shear strength) and site conditions (such as boundaries of geologic materials and height of piezometric surface). Although natural variabilities may be recognized in the input terms, mean values or conservative estimates are used in the stability analysis to calculate a mean or conservative factor of safety, which could better be termed a "stability ratio". This ratio often becomes the primary basis for slope design, even though it has not been evaluated by sensitivity studies and it does not incorporate measured variabilities in input properties or the influence of time. The assumption of "worst possible conditions" over the time period of interest leads to an overly conservative and overly expensive slope design.

Variabilities in input properties can be accounted for in a probabilistic slope stability analysis (Marek and Savely, 1978; Miller, 1984; Kirsten and Moss, 1985). The properties are random variables described by probability density functions (pdf) or by cumulative distribution functions (cdf). These functions are "input" to the limiting equilibrium equation to produce a pdf of the stability ratio (factor of safety). Several different analytical methods are available for this input operation, with the most simple being Monte Carlo simulation. Repeated calculation of stability ratios, each based on a unique set of input values (which are sampled, or drawn from their respective pdf's), produces a distribution of simulated stability ratios. The percentage of simulated stability ratios that are less than one is an estimate of the probability of failure. Although such procedures incorporate the variabilities and even perhaps the interdependencies in input properties, they cannot include directly the effects of varying piezometric levels over time.

EXTREME-VALUE STATISTICAL ANALYSIS

The statistical theory of extreme values (Gumbel, 1958) provides a convenient method for incorporating temporal piezometric conditions into the stability analysis. This technique uses historical records focused on the extreme (maximum) values taken on by the random variable of interest, X. The emphasis on extreme values is especially relevant to slope stability studies, because a slope design depends less on the accurate knowledge of random fluctuations in X (piezometric height) than on the largest value that X can assume within a given time period.

The time period spanned by the available historical record is divided into N equally spaced intervals. Only the extreme (maximum) value Y taken on by the random variable X within each interval is considered in the analysis. Most geographic regions have an annual wet season when abundant water infiltration causes a significant rise in the piezometric surface. In mountainous areas of the Western U.S. this wet season often occurs during the spring. Groundwater monitoring by U.S. Forest Service engineers has indicated that piezometric surfaces in typical mountainous areas tend to be quite stable except during the spring months, when significant increases are observed (Prellwitz and Babbitt, 1984). Consequently, a reasonable interval for this analysis is one year. The list of N maximum values is then used to obtain the mean and standard deviation of Y (denoted m_y and s_y respectively).

The maxima assume Gumbel's Type I distribution and can be used to predict the probability of exceeding a threshold value of X within a given number of intervals, or years:

$$P(X \geq x') = 1 - \exp[-T \cdot \exp(-B[x'-A])] \tag{1}$$

where: x' = threshold level of piezometric surface
T = time period in years
B = parameter of the extreme-value distribution
$= S_N/s_y$ (2)

A = parameter of the extreme-value distribution
$= m_y - (M_N/B)$. (3)

The terms M_N and S_N are the mean and standard deviation of Gumbel's "reduced" extremes. They depend on N and are tabulated accordingly by Gumbel (1958, p. 228).

Thus, the probability of exceeding a specified level of the piezometric surface within a given number of years can be estimated from historical information about the piezometric surface. However, this type of information hardly ever is directly available because long-term piezometric monitoring is rarely conducted. The information can be obtained indirectly from infiltration modeling based on historical precipitation records. Finite element computer models, such as UNSAT2 (Neuman and others, 1974), provide estimation tools for approximating the maximum rise in the piezometric surface due to precipitation and infiltration activity at a specific site. Minimal hydrogeologic information necessary to use such models consists of saturated hydraulic conductivity (obtained from laboratory tests or from auger-hole injection tests) and porosity (obtained from laboratory tests). Other required hydraulic inputs to the models then can be indirectly inferred from textbook generic data. If possible, results from the computer analyses should be verified by field data such as those presented by Prellwitz and Babbitt (1984). These procedures for estimating maximum annual levels in the piezometric surface obviously are unrefined and require further research and investigation.

TIME-BASED ANALYSIS OF SLOPE STABILITY

Monte Carlo simulation can be used in a time-based analysis of slope stability to estimate the probability of slope failure over a given time period. The temporal input to the analysis consists of cumulative distribution functions (cdf) of the level of the piezometric surface. This level is defined either as the height above a certain datum plane or as the depth below ground surface.

The cdf of piezometric level X for a given time period (in years) is derived from an extreme-value statistical analysis. A series of threshold values is defined for a given time period, and the exceedance probability P' for each of the thresholds is calculated according to equation (1). The probability that X takes on a value less than a given threshold x' is given by

$$P(X < x') = 1 - P(X \geq x') = 1 - P'. \tag{4}$$

The probability values given by equation (4) for the series of threshold values provide an estimated cdf of X. The entire computational process is repeated for each time period desired. Example cdf's of piezometric level X are presented in Figure 1.

During the Monte Carlo simulation that generates a distribution of stability ratios, a piezometric cdf is randomly sampled in a manner similar to that used in sampling from the other required input distributions (such as those for unit weight, shear strength, and other material properties). The probability of slope failure is thereby estimated for that particular piezometric cdf, which is representative of a given time period. The Monte Carlo simulation is then repeated for a different piezometric cdf, which is representative of another time period of interest. Intuitively, results from the simulations should show that the probability of failure increases as the time periods become longer.

EXAMPLES

Two hypothetical slope stability studies are presented to illustrate the computational procedures of the time-based analysis. The first study consists of a stability analysis based on the infinite slope stability model (after Ward and others, 1979), which considers a translational failure of soil material along a defined planar base. The second study relies on the step path model (after Jaeger, 1971) for analysing stability in a discontinuous rock mass.

Infinite Slope Model

A simplified version of the limiting equilibrium equation for the infinite slope stability model (Figure 2a.) is given by

$$S = \frac{s_r}{\sin(B)\cos(B)[D(H - H_w) + D_s H_w]} \tag{5}$$

where: S = stability ratio (safety factor)
B = slope angle = angle of sliding
D = unit weight of soil material
D_s = saturated unit weight of soil material
s_r^s = shear strength of soil material for a given effective normal stress
H = vertical height of soil element
H_w = vertical height of piezometric surface above datum plane.

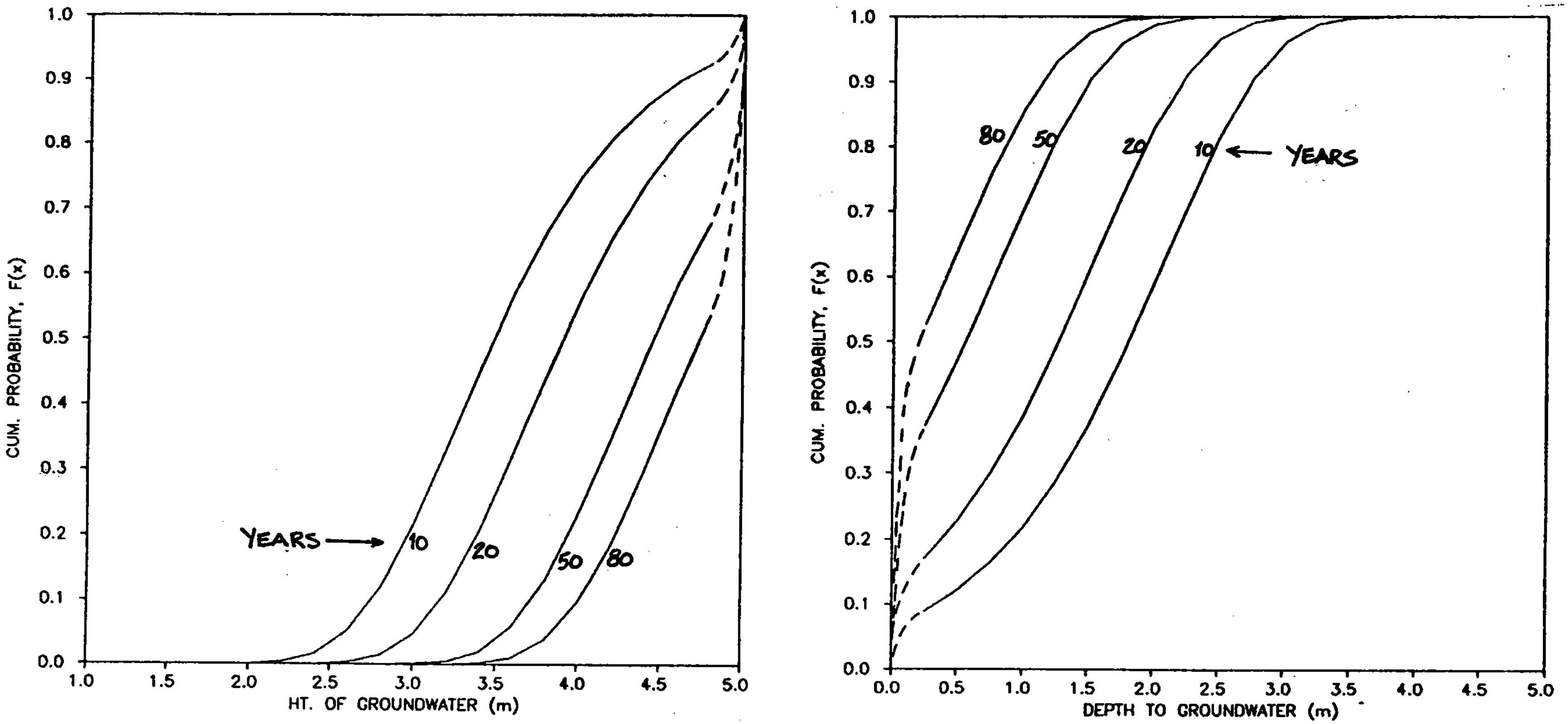

a. piezometric level defined as height above a datum plane H_w; N=50, m_y=2.2, s_y=0.7.

b. piezometric level defined as depth from ground surface D_w; N=50, m_y=3.45, s_y=0.9.

Figure 1. Time-related cumulative distribution functions for piezometric level estimated from an extreme-value statistical analysis.

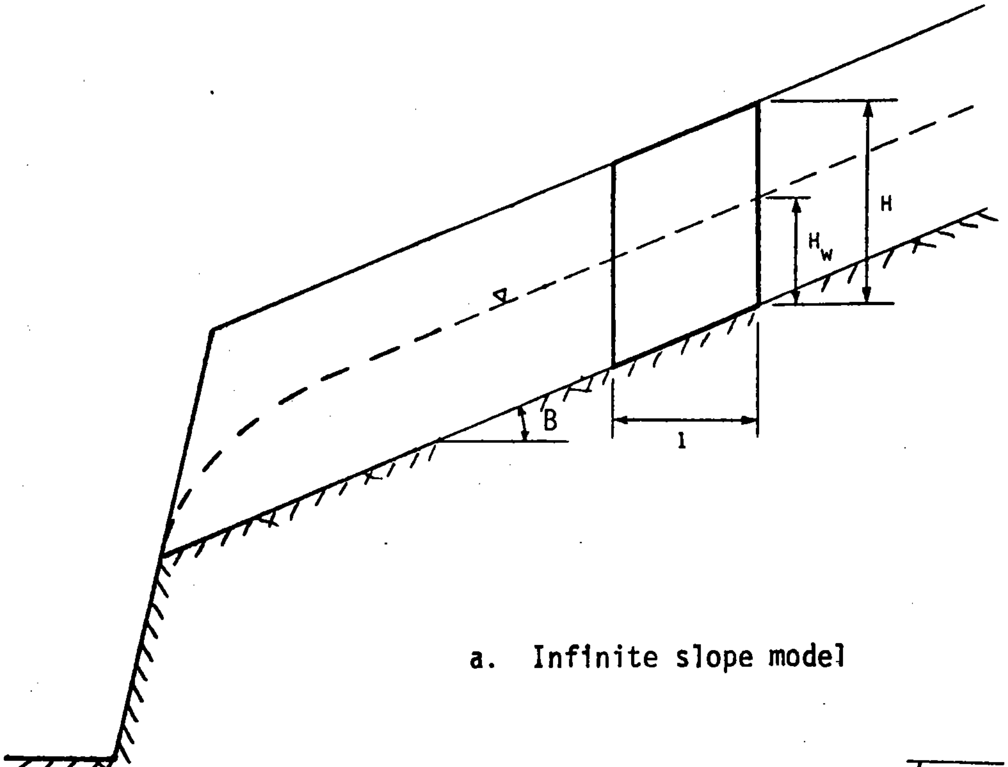

a. Infinite slope model

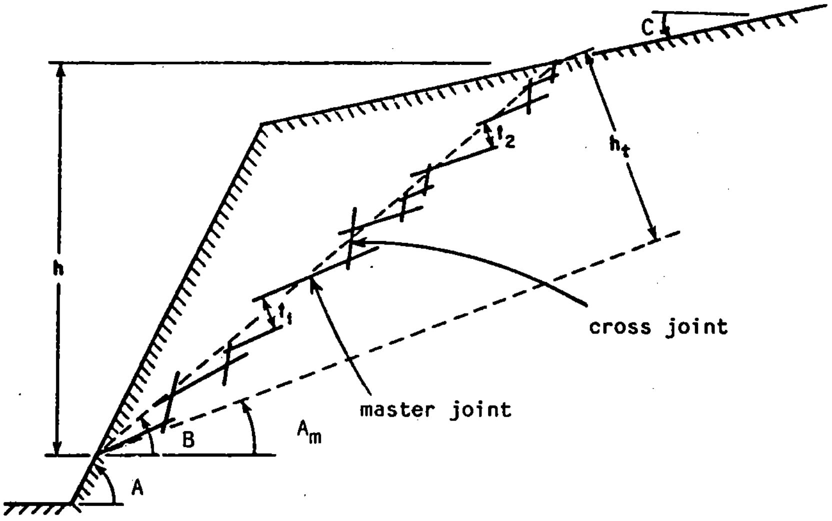
C
t_2
h_t
h
cross joint
t_1
master joint
B
A_m
A

A = angle of slope cut

B = step path angle

C = natural slope angle

t_1, t_2 = length of tensile rock bridges

Fraction of Tensile Intact Rock = $(t_1 + t_2)/h_t$

b. Step path model.

Figure 2. Slope stability models for the example problems.

For this example the slope angle B is set to 38 degrees and the vertical depth of soil H is set to 5 m. The unit weight, saturated unit weight, shear strength, and height of the piezometric surface are treated as random variables. The shear strength is considered a power function of effective normal stress, and the mean and standard deviation that define its normal distribution are estimated by laboratory direct shear tests and analytical procedures outlined by Miller and Borgman (1984). The shear strength curve used in this study is given in Figure 3. The cdf of the piezometric level, which is used in the calculation of effective normal stress, is defined in Figure 1a. The unit weight and saturated unit weight are assumed to be normally distributed with means and standard deviations as follows:

	Mean	S.D.
soil unit weight (tcm)	1.80	0.10
sat. unit weight (tcm)	1.86	0.12

During a given simulation "pass" the same random number is used to sample from the unit weight and the saturated unit weight distributions, thus ensuring that the two are directly correlated.

The simulations are conducted for time periods of 1, 10, 20, 50, and 80 years. An example distribution of simulated stability ratios indicates that the output values appear to be normally distributed (Figure 4a). The results given in Table 1 are from simulations consisting of 1,000 passes. The estimated probability of slope failure is observed to nearly double from a 10-year period to a 80-year period. It should be noted that results for time periods beyond 50 years have limited reliability because the time history used in this extreme-value analysis of piezometric level is limited to 50 years (N = 50).

Table 1. Results of time-based stability analyses for the infinite slope example.

Time Period (years)	Est. Probability of Slope Failure	Sim. Stability Ratio Mean	S.D.
1	0.13	1.51	0.52
10	0.26	1.26	0.43
20	0.34	1.17	0.40
50	0.43	1.09	0.40
80	0.49	1.05	0.39

Step Path Model

A version of the limiting equilibrium equation for the step path slope stability model (Figure 2b.) is given by

$$S = \frac{s_r L + W\cos(A_m)\tan(R) + T_s L}{W\sin(A_m) + V\cos(A_m)} \tag{6}$$

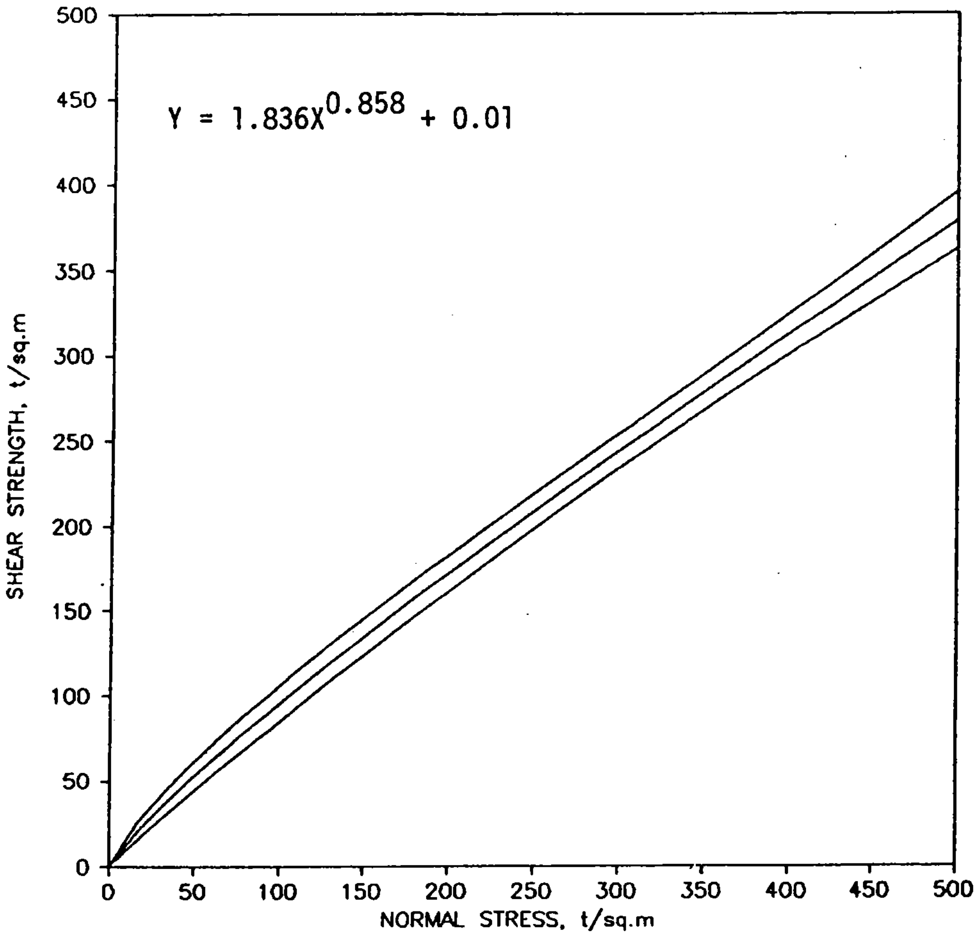

Figure 3. Shear strength as a power function of effective normal stress; the central curve represents the mean shear strength, while the two outer curves represent the mean plus or minus one standard deviation.

```
 NO. DATA =  250               MEAN =  .11156E+01
  MINIMUM =  .20498E+00        S.D. =  .39311E+00
  MAXIMUM =  .22593E+01        VAR. =  .15454E+00

     DATA CLASSES                  OBSERVED FREQUENCY

------------------------¦----+----¦----+----¦----+----¦----+----¦----+----¦
.10227E+00 - .24350E+00 ¦XXXX
.24350E+00 - .38473E+00 ¦XX
.38473E+00 - .52596E+00 ¦XXXXX
.52596E+00 - .66720E+00 ¦XXXXXXXXXXXXXXX
.66720E+00 - .80843E+00 ¦XXXXXXXXXXXXXXXXXXXXXXXXXXXXX
.80843E+00 - .94966E+00 ¦XXXXXXXXXXXXXXXXXXXXXXXXXXXXXXXX
.94966E+00 - .10909E+01 ¦XXXXXXXXXXXXXXXXXXXXXXXXXXXXXXXXXXXXXXXXXXX
.10909E+01 - .12321E+01 ¦XXXXXXXXXXXXXXXXXXXXXXXXXXXXXXX
.12321E+01 - .13734E+01 ¦XXXXXXXXXXXXXXXXXXXXXXXXXXXXXX
.13734E+01 - .15146E+01 ¦XXXXXXXXXXXXXXXXXXXXX
.15146E+01 - .16558E+01 ¦XXXXXXXXXXXXXX
.16558E+01 - .17970E+01 ¦XXXXXXXXXXXX
.17970E+01 - .19383E+01 ¦XXX
.19383E+01 - .20795E+01 ¦XXXXX
.20795E+01 - .22207E+01 ¦XXX
.22207E+01 - .23620E+01 ¦X
------------------------¦----+----¦----+----¦----+----¦----+----¦----+----¦
```

a. Infinite slope model; estimated probability of failure is 0.45.

```
 NO. DATA =  250               MEAN =  .11705E+01
  MINIMUM =  .23458E+00        S.D. =  .41469E+00
  MAXIMUM =  .25442E+01        VAR. =  .17197E+00

     DATA CLASSES                  OBSERVED FREQUENCY

------------------------¦----+----¦----+----¦----+----¦----+----¦----+----¦
.11910E+00 - .27789E+00 ¦X
.27789E+00 - .43667E+00 ¦XXXXXXX
.43667E+00 - .59546E+00 ¦XXXXXXXXXXXX
.59546E+00 - .75424E+00 ¦XXXXXXXXXXXXXXXX
.75424E+00 - .91303E+00 ¦XXXXXXXXXXXXXXXXXXXXXXXXXX
.91303E+00 - .10718E+01 ¦XXXXXXXXXXXXXXXXXXXXXXXXXXXXXXXXXXXXXXXXXXXXXX
.10718E+01 - .12306E+01 ¦XXXXXXXXXXXXXXXXXXXXXXXXXXXXXXXXXXXXXXXXXXXXXX
.12306E+01 - .13894E+01 ¦XXXXXXXXXXXXXXXXXXXXXXXXXXXXX
.13894E+01 - .15482E+01 ¦XXXXXXXXXXXXXXXXXXX
.15482E+01 - .17070E+01 ¦XXXXXXXXXXXXXXXXXXXXXX
.17070E+01 - .18657E+01 ¦XXXXXXXXXXXX
.18657E+01 - .20245E+01 ¦XXXXXXXX
.20245E+01 - .21833E+01 ¦XX
.21833E+01 - .23421E+01 ¦XX
.23421E+01 - .25009E+01 ¦X
.25009E+01 - .26597E+01 ¦X
------------------------¦----+----¦----+----¦----+----¦----+----¦----+----¦
```

b. Step path model; estimated probability of failure is 0.38.

Figure 4. Histograms of 250 simulated values of stability ratio for the example problems with time equal to 50 years.

where: L = effective sliding length
= $h \cdot \sin(A_c - B) / \sin(B)\sin(A_c - A_m)$

W = weight of potential failure mass
= (two-dimen. Area) x (unit weight)
s_r = shear strength along the master joints

R = waviness or roughness of master joints
T_s = tensile strength component of rock bridges
= (percent intact rock) x (rock tensile strength) x $[\sin(B - A_m)\sin(A_c - A_m) / \sin(A_c - B)]$

A_m = average dip of master joints
A_c = average dip of cross joints

B = overall dip of step path
h = vertical height of step path
V = horz. component of water forces acting in cross joints

The input properties that are treated as random variables are considered to be normally distributed with means and standard deviations as follows:

	Mean	S.D.
unit weight (tcm)	2.71	0.08
dip of step path (degrees)	52	2.8
percent intact rock (percent)	1.00	0.30
rock tensile strength (tsm)	450	40

The above estimates for step-path dip and for percent intact rock are obtained using step-path simulation procedures discussed by Call and Nicholas (1978). Unit weight and tensile strength are estimated by laboratory testing. Slope geometry and properties of the rock joints used in the example problem are defined as follows:

angle of slope cut, A	60 degrees
natural slope angle, C	38 degrees
height of slope cut	15 m
dip of master joints	46 degrees
dip of cross joints	85 degrees
waviness of master joints	1.5 degrees

The mean and standard deviation of shear strength are similar to those shown in Figure 3. The cdf of piezometric level, which is used in the calculation of effective normal stress, is defined in Figure 1b. For each simulation pass, a step path is assumed to initiate at a randomly assigned position on the lower half of the slope cut. This arbitrary assumption allows for only the "major" potential slope failures to be analysed (this condition can be modified to fit any particular needs of the project under study).

The step path stability simulations are conducted for time periods of 1, 10, 20, 50, and 80 years. An example distribution of simulated stability ratios indicates that the output values appear to be normally distributed (Figure 4b). The results given in Table 2 are from simulations consisting of 1,000 passes. The probability of failure significantly increases with longer time periods.

Table 2. Results of time-based stability analyses for the step path example.

Time Period (years)	Est. Probability of Slope Failure	Sim. Stability Ratio Mean	S.D.
1	0.07	1.91	0.63
10	0.20	1.45	0.58
20	0.26	1.34	0.53
50	0.35	1.20	0.46
80	0.43	1.14	0.42

CONCLUSIONS

A time-based model that incorporates historical precipitation records into probabilistic slope stability analyses can provide useful information for the design of cut slopes and for the development of slope maintenance programs. Model output includes a schedule of probabilities of slope failure referenced to time periods of various lengths. Graphs then can be constructed to provide a risk assessment for the slope under study (Figure 5).

For some slope failure mechanisms, such as that modeled by the infinite slope method, the time period for the risk assessment can not be referenced to any specific starting point, because the potential failure depends only on natural slope conditions and not on the man-made slope cut. For failure mechanisms that depend on the slope cut, such as a circular rotation through soil material or a fracture-controlled translation in a rock mass, the risk assessment period begins when the slope cut is made. Artificial stabilization efforts (rock bolts or tendons, horizontal drains, buttresses) can be analysed in the stability models to determine their influence on reducing the risk of slope failure in future years. Thus, a time-based stability model can assist in the evaluation of future stability of cut slopes.

Probabilistic output from the stability analysis provides richer information than that obtained by the deterministic calculation of a factor of safety. For example, let us assume that we analyse two slope cuts along a highway route. Geologic materials and failure mechanisms are different at the two sites, yet the calculated mean stability ratio (safety factor) is 1.2 for each slope. However, due to different variabilities in the two sets of input properties, the stability ratios for the two slopes have standard deviations of 0.2 and 0.5, respectively. Assuming the stability ratios are normally distributed, the probabilities of slope failure are estimated to be 0.16 and 0.34, respectively. In addition, probabilistic information associated with a risk analysis (such as shown in Figure 5) could be input into economic studies to help determine the most cost-effective alternatives for slope design, slope reinforcement, and slope maintenance in future years. Such an application would seem attractive in light of shrinking funds and tighter budgets for highway rehabilitation and maintenance.

The least reliable aspect of this type of time-based slope stability model is the estimation of groundwater response (piezometric surface) to precipitation and infiltration activity. As seen in the example problems, the calculated risk of future slope failures is directly related to the time history of annual maximum elevations of the peizometric surface. Thus, future research efforts in this geotechnical area should be directed toward cost-effective evaluation of near-surface hydrogeologic properties and toward numerical and empirical methods for modeling near-surface groundwater behavior.

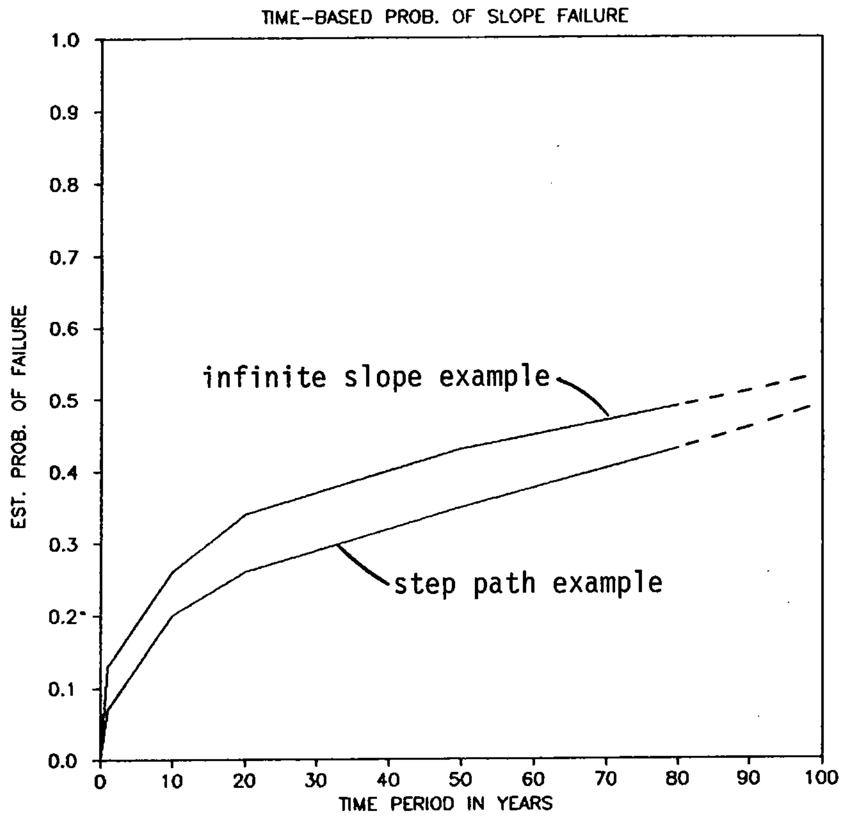

Figure 5. Probability of slope failure as a function of time for the two example problems.

REFERENCES

Call, R.D. and Nicholas, D.E., 1978, Prediction of step path failure geometry for slope stability analysis; paper presented at 19th U.S. Symp. on Rock Mechanics, Lake Tahoe, Nevada.

Gumbel, E.J., 1958, Statistics of Extremes; Columbia Univ. Press, New York, 375 p.

Jaeger, J.C., 1971, Friction of rocks and stability of rock slopes; Geotechnique, v. 21, no. 2, p. 97-134.

Kirsten, H.D. and Moss, A.S.E., 1985, Probability applied to slope design - case histories; in Rock Masses: Modeling of Underground Openings/ Probability of Slope Failure/ Fracture of Intact Rock, C.H. Dowding, ed., ASCE, New York, p. 106-121.

Marek, J.M. and Savely, J.P., 1978, Probabilistic analysis of the plane shear failure mode; in Proc. of 19th U.S. Symp. on Rock Mechanics, Lake Tahoe, Nevada, v. II, p. 40-44.

Miller, S.M., 1984, Probabilistic rock slope engineering; Misc. Paper GL-84-8, Geotechnical Lab, U.S.A.E. Waterways Exp. Station, Vicksburg, MS, 75 p.

Miller, S.M. and Borgman, L.E., 1984, Probabilistic Characterization of shear strength using results of direct shear tests; Geotechnique, v. 34, no. 2, p. 273-276.

Neuman, S.P., Feddes, R.A., and Bresler, E., 1974, Finite element simulation of flow in saturated-unsaturated soils considering water uptake by plants; Hydrodynamics and Hydraulic Engineering Laboratory, Israel Institute of Technology, Haifa, Israel.

Prellwitz, R.W. and Babbit, R.E., 1984, Long-term groundwater monitoring in mountainous terrain; paper presented at 63rd Annual Meeting of the Transp. Research Board, January.

Ward, T.J., Li, R.M., and Simons, D.B., 1979, Mathematical modeling approach for delineating landslide hazards in watersheds; in Proc. of 7th Annual Symp. on Engr. Geology and Soils Engr., Moscow, ID, p. 109-142.

WIRE NETTING FOR ROCKFALL PROTECTION

MASSIMO CIARLA*

ABSTRACT

ROCKFALL generates significant roadway safety and maintenance problems. It is caused by slopes cut too steep due to economic or other necessity. To alleviate the problems generated by rockfall road engineers have come up with alternate solutions consisting of methods of road protection, slope stabilization and/or simply warning and instrumentation methods.

The purpose of this paper is to illustrate the use of wire netting above the roadway as a method of protection against rockfall. Functional, practical and economical aspects of this method are discussed.

Projects carried out in the Western United States are presented to illustrate both existing applications of double twisted wire netting for rockfall protection and the effectiveness of such protective solution.

INTRODUCTION

As defined in reference[1], rockfall is "the relatively precipitous movement of a segment of rock of any size from a cliff or other slope that is so steep that the segment continues to move downslope." Road engineers from time inmemorial have had to contend with the problems of extremely high and steep slopes and the associated risks of rockfall. The engineers' task is to select among the possible horizontal and vertical route configurations the one that is most economical, in the initial outlay and subsequent periodical maintenance costs and, above all, assures the traveller safety in all circumstances against rockfall on the road bed.

---

*Assistant to the President, Terra Aqua Inc., Reno, Nevada

Among the principal causes for slope deterioration and the associated rockfall on the road bed the following are recalled: rainfall, freezing and thawing, wind, snow melt, springs and seepage.

The remedial measures for the rockfall in cut slopes can be grouped in three categories:

1. Slope stabilization
2. Protection methods
3. Warning methods.

The methods of cut stabilization aim to eliminate the movement of rock, that is, they aim to increase the forces resisting motion and to decrease the forces destabilizing the slope. Among these methods it is possible to single out: slope flattening, controlled blasting, cable lashing, anchored wire mesh, surface and subsurface drainage, scale or trim, rockbolts, shotcrete and gunite, concrete buttresses and retaining walls.

The protection methods aim to prevent the moving rocks from reaching the road bed. Among these methods the main ones can be summarized as follows: relocating the roadway, widening at grade, benches, draped mesh blankets, fences, catchment ditches, metal guard rail.

The warning methods are to be considered as emergency rather than long-term solutions. Among the various possibilities the following are noted: signs, monitoring, patrols, electric wire and fences.

The project engineer will select one or more of these solutions depending on the complex of characteristics proper to each situation.

In this paper the use of metallic mesh will be discussed both as a method of slope stabilization and as a protection of the road bed. The material, its functional characteristics and methods of installation will be discussed.

WIRE NETTING

This mesh can be utilized both as a simple protection device for the road bed, in this case it functions as draped mesh blanket, Fig. 1, as well as double acting device which protects the road bed and stabilizes the slope; in this case it functions as anchored wire mesh.

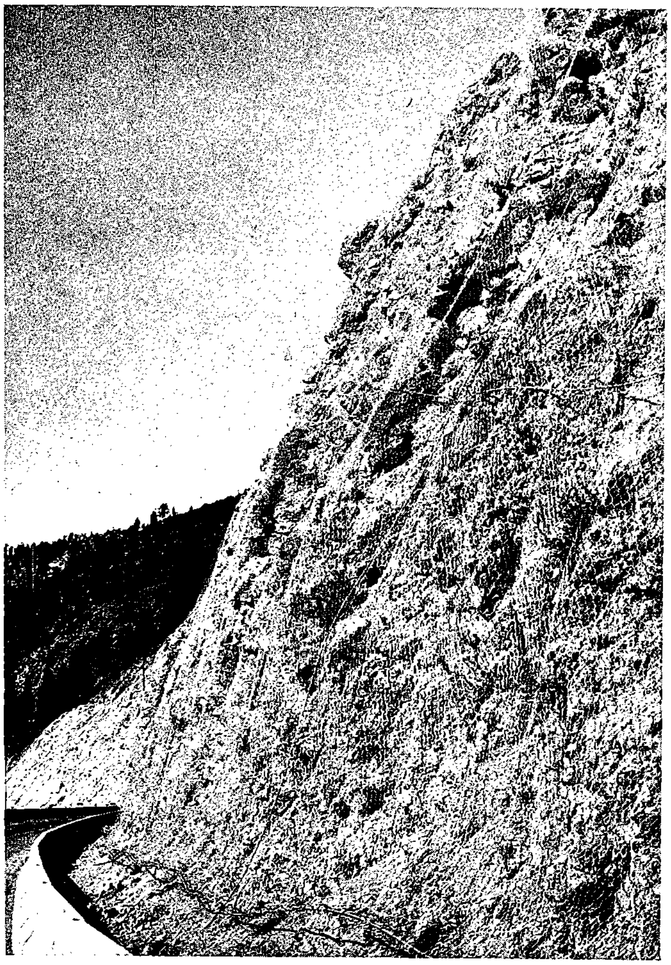

Figure 1. Draped wire mesh blanket completely covering a degraded slope along the Highway 80, west of Reno, in the State of Nevada

In both instances the mesh panels are tied continuously to each other, Fig. 2, and are anchored at the top of the cut slope by means of anchor bolts and wire ropes, Fig. 3. The wire ropes form a grid of 25' x 25' or 50' x 50' for the mesh to rest on and they cover the entire cut slope, Fig. 4. The mesh in turn is tied continuously to these wire ropes. In the case of the anchored wire mesh, the anchor bolts extend over the entire cut area, generally at 25' or 50' on center, and they keep the mesh pressing constantly on the slope. The larger rocks, therefore, tend to remain stable.

In the case of the draped mesh blanket method, the function of the mesh is to retain the falling stones behind the mesh while they fall to the toe of the cut, Fig. 5. The same effect of guiding the smaller stones to the toe of the cut is provided also by the anchored wire mesh method.

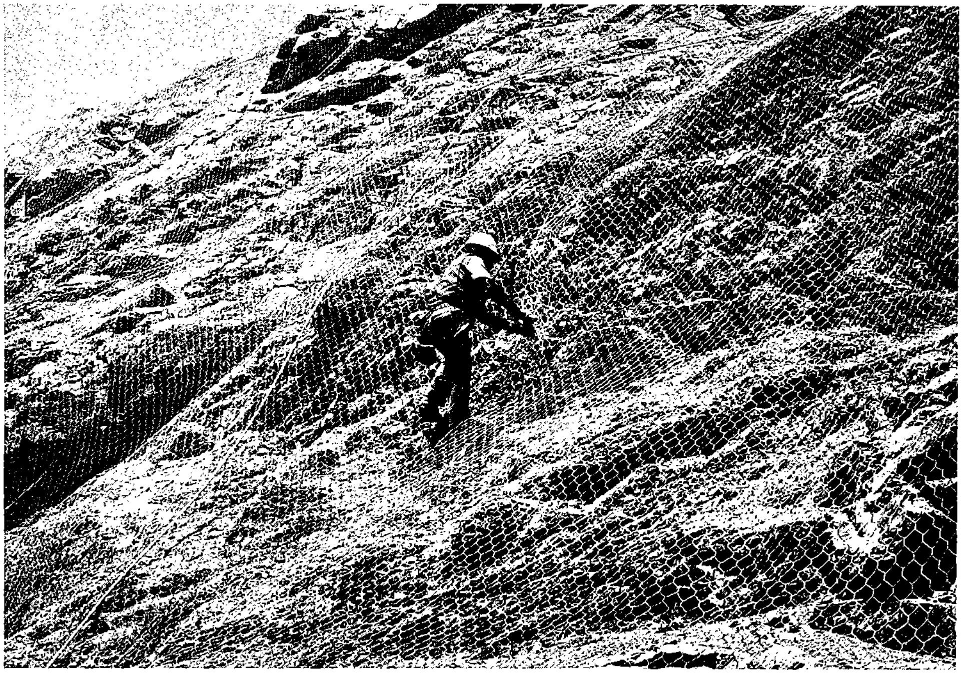

Figure 2. The wire panels are laced together to the grid of wire ropes to form a continuous shield for the falling rocks.

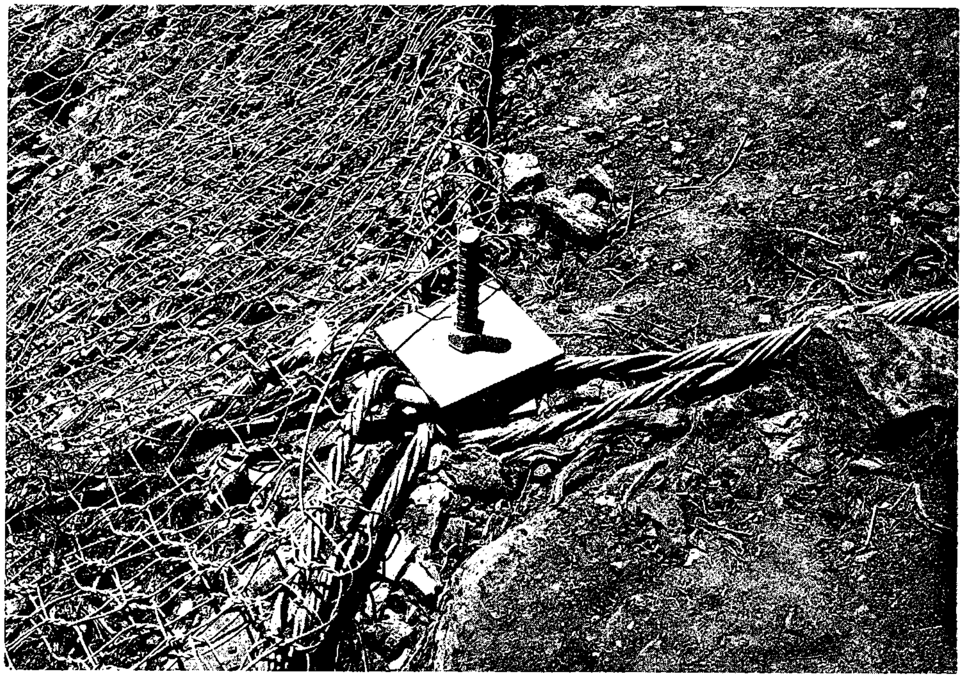

Figure 3. Detail of anchor bolt to which wire ropes are connected.

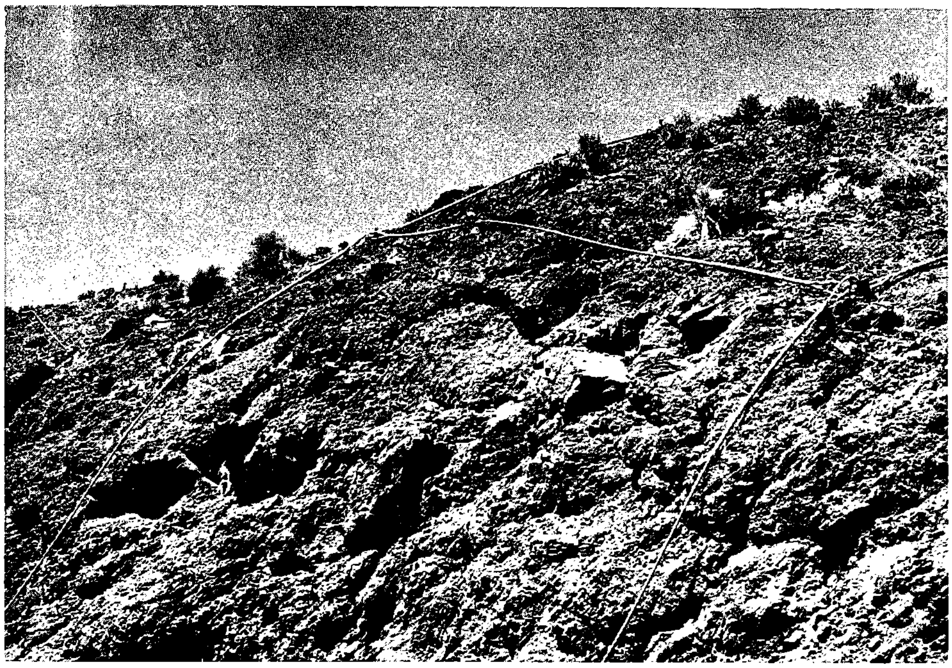

Figure 4. Detail of installed wire ropes forming a 50' x 50' grid. The wire mesh panels will be tied continuously to these cables.

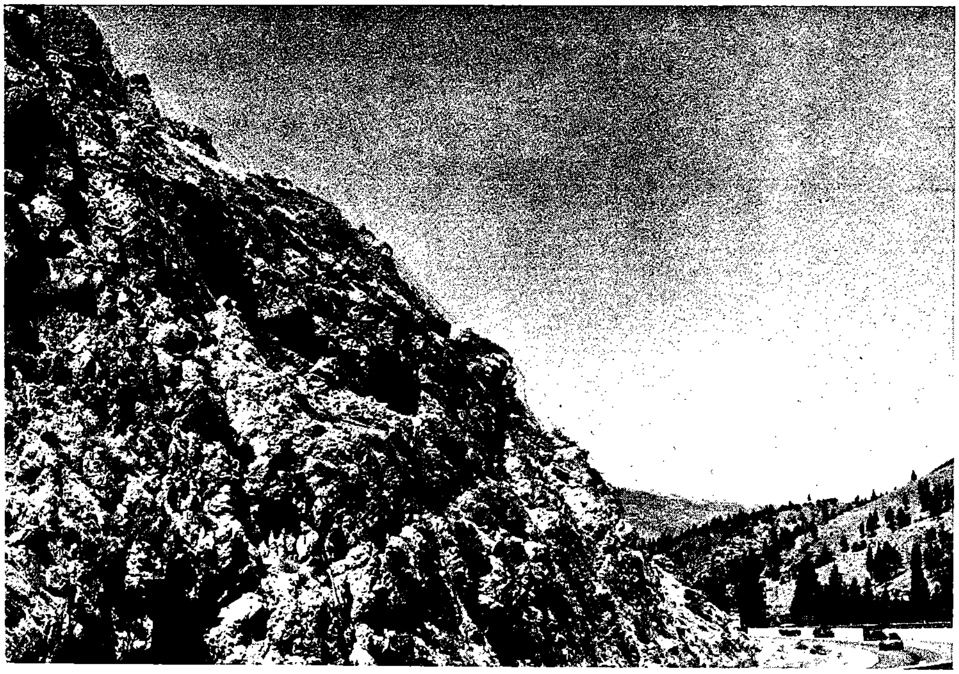

Figure 5. Highway 80 - Nevada. A draped wire mesh blanket retains this large rock which eventually will be guided to the toe of the cut and there removed.

MATERIALS

Originally public agencies used chain-link fence to contain falling rock. During recent decades the galvanized double twisted hexagonal gabion mesh has become the netting of choice, Fig. 6. This mesh has several advantages over the alternate. Among these as indicated in reference[2] the "gabion mesh has the advantage that it has double twist hexagonal weave which does not unravel, like chain-link mesh, when it is broken."

Also gabion mesh, because of its double twisted pattern, retains its general panel width while it is being spread or lifted on slopes, Fig. 7. This is a significant advantage over the condition with chain-link mesh which assumes its proper shape and width only when stretched.

In addition to the unravelling characteristic and installation advantages, the high flexibility in conforming to the large irregularity of the slope, the high mechanical strength and corrosion resistance and the ability of using galvanized mesh also coated with PVC in the worst corrosive environments, are significant functional characteristics.[5]

INSTALLATION PHASES

The mesh installation process, while affected by the special conditions of each site, can be summarized into four main phases:

1. Preparation of the slope to be protected (scaling and clearing).
2. Installation of anchor bolts and wire rope grid.
3. Spreading the mesh on the slope.
4. Alignment and lacing of the mesh panels to each other and to the wire rope grid.

Concerning the third phase, two main methods of spreading the rolls of mesh over the slope are considered.

The first method consists of carrying the entire rolls to the top of the cut and then, once they are anchored in their proper place, they are unrolled down the slope. This method is normally used when:

- the top of the slope is accessible to vehicles.

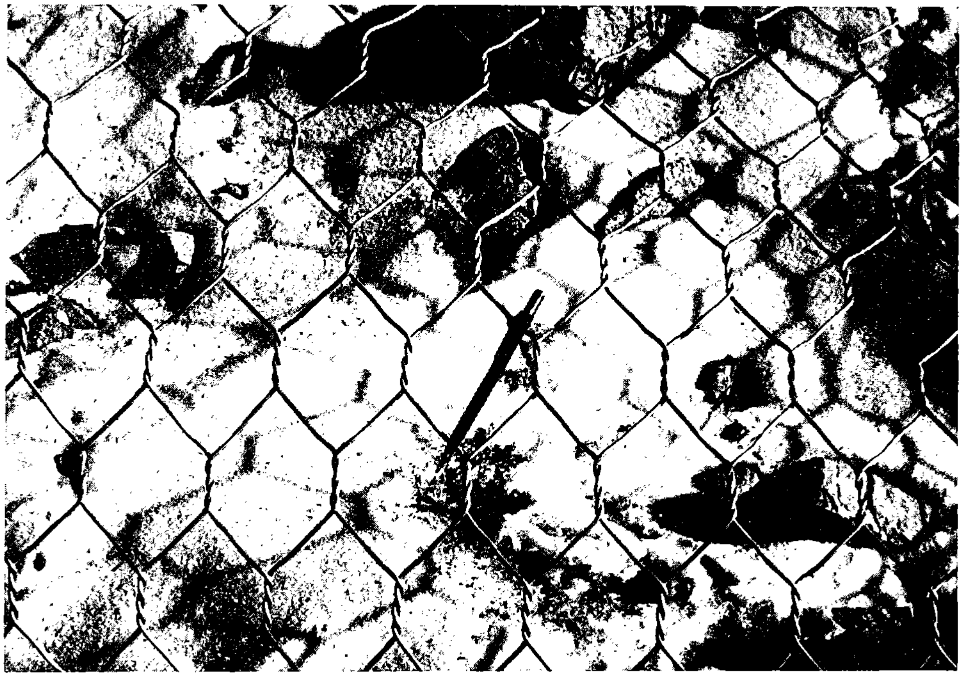

Figure 6. Detail of the heavily galvanized double twisted hexagonal mesh.

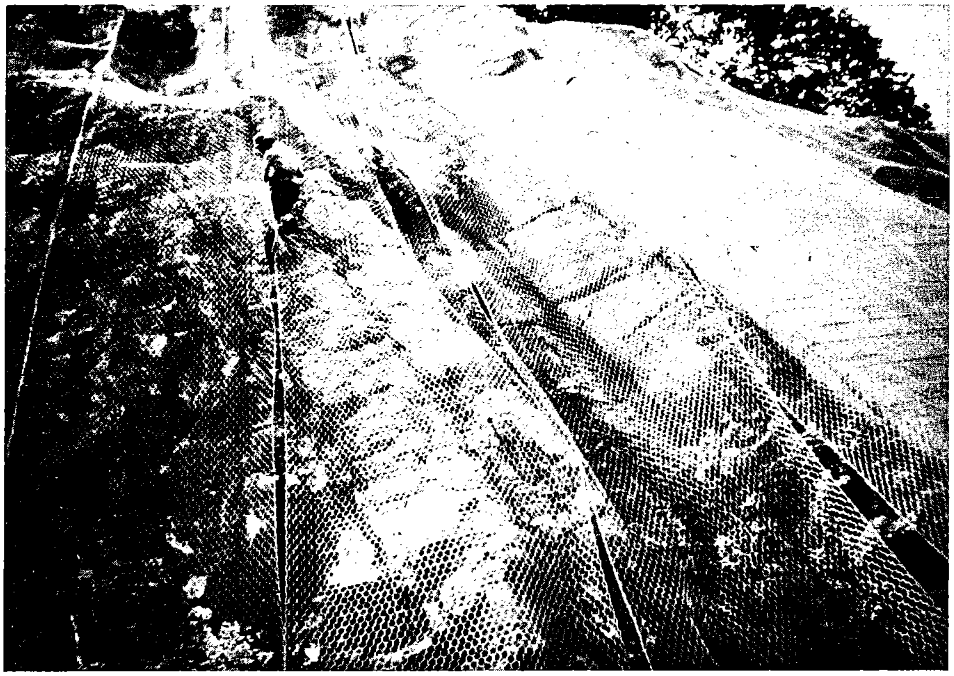

Figure 7. Lacing operation of the mesh panels spread on slope. The constant panel width retained in this operation results in significant saving in time and effort for the mesh installation.

- impediments such as telephone or electric cables or a railroad line exist at the top of the slope.

The means of transportation for the mesh can be a tractor, a crane, a winch, or a helicopter. This last is used almost exclusively on slopes exceeding 150 to 200 feet.

The second method consists in starting with the entire roll at the toe of the slope, hooking one end of it and unwinding the roll up to the top of the slope, where it is anchored. For the lifting it is possible to use a helicopter, a winch, a crane or any equipment such as a jeep, a truck, a tractor, which, remaining at the toe of the slope, can pull a cable through a pulley mounted at the top of the slope. The helicopter is more and more frequently used: Fig. 8. Its higher hourly cost is compensated for by a decidedly greater production. Nonetheless, in order for this procedure to be truly efficient it requires following some important precautions: radio contact between all the members of the crew and in particular between the pilot and the people on the ground; maximum accord among the men and a careful preparation for promptly securing the mesh at the top of the slope to avoid useless waste of time.

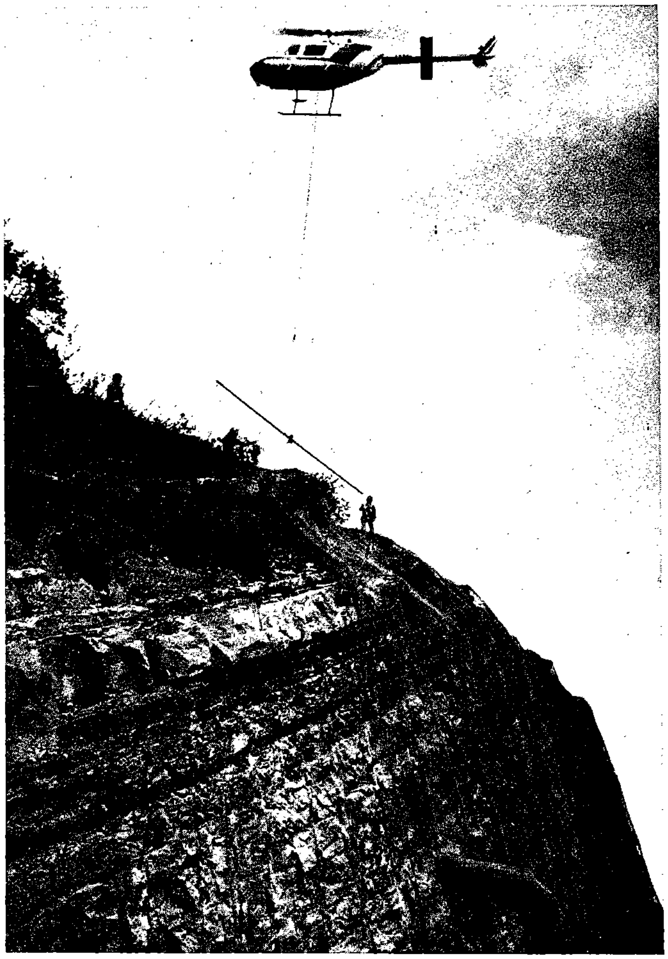

Figure 8. The helicopter is used here for the lifting of unrolled panels to the top of the slope.

SIGNIFICANT PROJECTS

In the following pages, the use of double twisted hexagonal heavily galvanized mesh in projects completed in Montana and Nevada, will be presented to illustrate the validity of these protective solutions and of the materials.

HIGHWAY 15 - MONTANA

During recent years the Montana Department of Transportation has undertaken to enlarge from two lanes to four lanes it major highway network. Highway 15, connecting Helena to Butte, is part of this highway improvement program. In the stretch between Bernice and Basin, at approximately mile post 155, in order to avoid traffic interruption during the construction phase, a detour road to serve later as a frontage road for local traffic became necessary.

To provide this detour road and to satisfy the geometrical requirements of the new Highway 15, a 200 foot high slope was cut in fractured rock formation. At that point the project designers had to provide rockfall protection for both roadways and stabilization of the slope. The option to flatten the slope was unworkable and similarly were also the other options of local stabilization, namely the use of rockbolts, cable lashing, etc., which could not be used due to the length of the slope and the highly fractured condition of the rock.

The possibility of using metallic mesh anchored to the slope with rock bolts and cables was studied, its economic consequences checked and, finally, in 1984, it was approved by the Department of Transportation. The job started in mid-December, 1984, and by mid-February, 1985, the Contractor had finished installing approximately 10,000 square yards of metallic mesh. To lift the mesh panels a 270 foot boom crane was used, Fig. 9. The 13 foot wide, 300 foot long mesh rolls were positioned at the toe of the slope and hooked on one edge to the crane which lifted it up to the summit. At the top the mesh was secured to a #6 rebar which in turn was tied to a 1 inch diameter rebar dowel anchor by means of a 3/4 inch diameter wire rope. Once all the mesh rolls were unrolled over the slope, they were tied to each other and to the cable grid which in turn was anchored to the slope with rebar anchors. The anchors were set 25 feet on center on the upper portion of the slope and at 50 feet on center on the lower portion. All the lacing operations were performed by workmen from a work cage supported from the boom crane, Fig. 10.

The adaptability and flexibility of this type of hexagonal double twisted mesh turned out to be fundamental requirements in providing an easy installation without gaps and excessive overlaps, Fig. 11. The total cost of the installation was $177,000 unquestionably an economic solution in comparison with the other alternatives considered. After two winter seasons and spring break-up, this metallic mesh protection shows no noticeable deterioration and a significant amount of small debris has been collected at the toe of the slope.

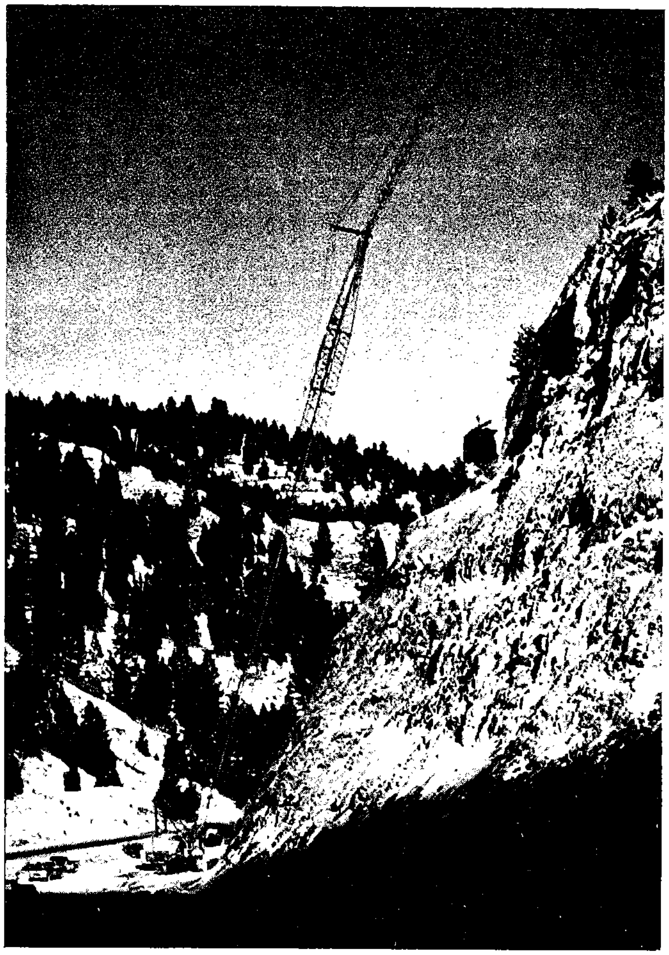

Figure 9. Highway 15-Montana. The rolls of mesh positioned at the toe of the slope were hooked on one end and lifted up to the top of the cut using this 270' boom crane.

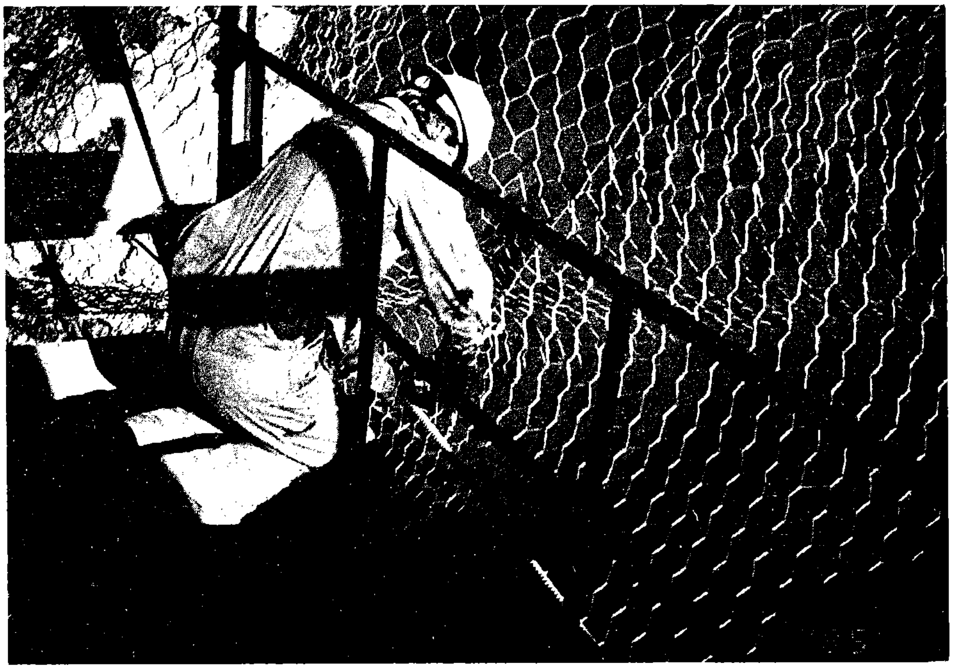

Figure 10. The mesh blanket is laced to the cable grid; the workman works from a work cage supported from the crane.

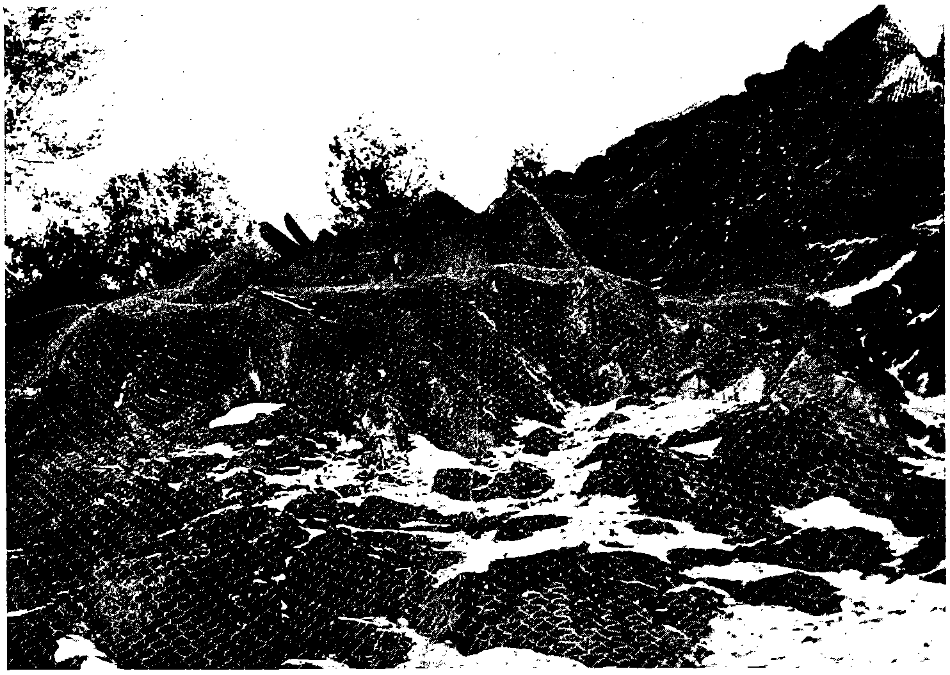

Figure 11. The installation of the double twisted mesh panel protection is completed.

STATE ROUTE 207 - KINGSBURY GRADE - NEVADA

In recent years the area of Gardnerville and Minden in Nevada has witnessed a very substantial population growth. This population's daily commute to the tourist and commercial areas of Lake Tahoe, uses State Route 207, the Kingsbury Grade. This road, built originally in the 30s using standards appropriate for the traffic of that period, soon became inadequate to carry this heavy commute. Thus, through various phases starting in 1966 through 1985, Route 207 was completely upgraded. The designers' objective being primarily to lower the grades, realign the route, and widen the pavement section. These improvements have involved sizable cuts, as high as 125 feet, in decomposed granite and construction of large fill embankments and their subsequent protection from erosion, due primarily to the freezing and thawing, the snow melt and the meteoritic rain which is abundant in this region.

As a solution to this problem, the Department of Transportation of the State of Nevada studied a scheme of double twisted hexagonal metallic mesh draped over the cut slopes and on the fill embankments of the road, a scheme which turned out to be very efficient.

To protect the road bed the mesh panels joined to each other were anchored with double anchors at the top of the cut, Fig. 12. Along the slope they were tied to a 50' x 50' cable grid. The rocks, instead of falling onto the road bed, rolled or slid behind the metallic mesh and were subsequently removed from the toe of the slope, Fig. 13.

For the stabilization of the fill embankments, the mesh panels tied to each other were simply kept adherent to the slope by means of light anchors made of two feet long steel staples of 3/8 inch diameter and spaced 25 feet on center, Figs. 14 and 15. The snow collecting on the fill embankments and that blown by the snow removal equipment did not cause significant erosive problems on these protected slopes. Overall, 20,000 square yards of rockfall protection were installed on the cut slopes at a total cost of $156,000. An equal amount of 20,000 square yards of metallic mesh were spread over the fill embankments of the road at a total cost of $101,000.

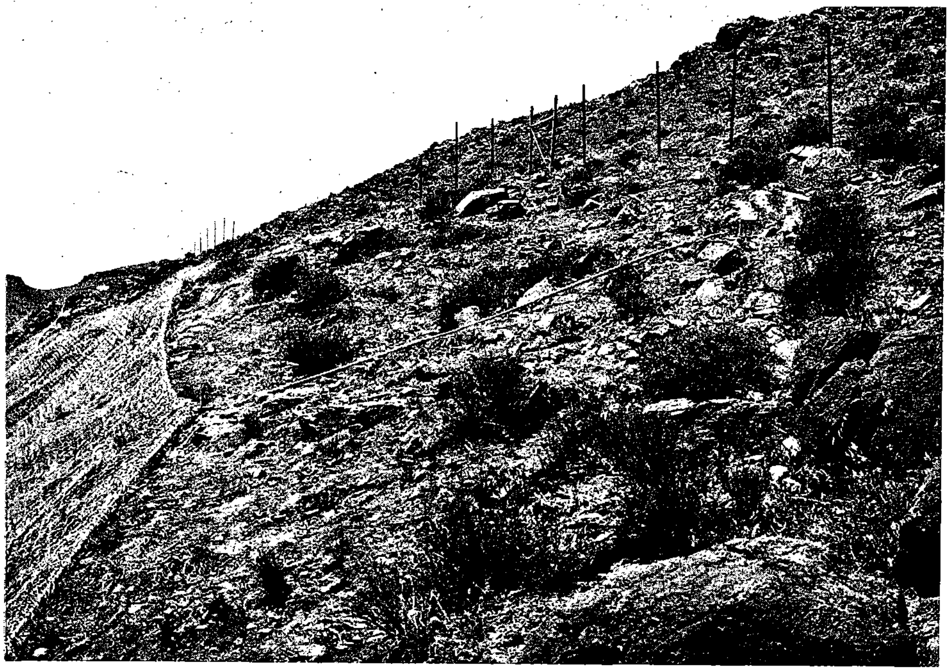

Figure 12. Detail of the anchor bolts, spaced 15', and connected by a wire rope.

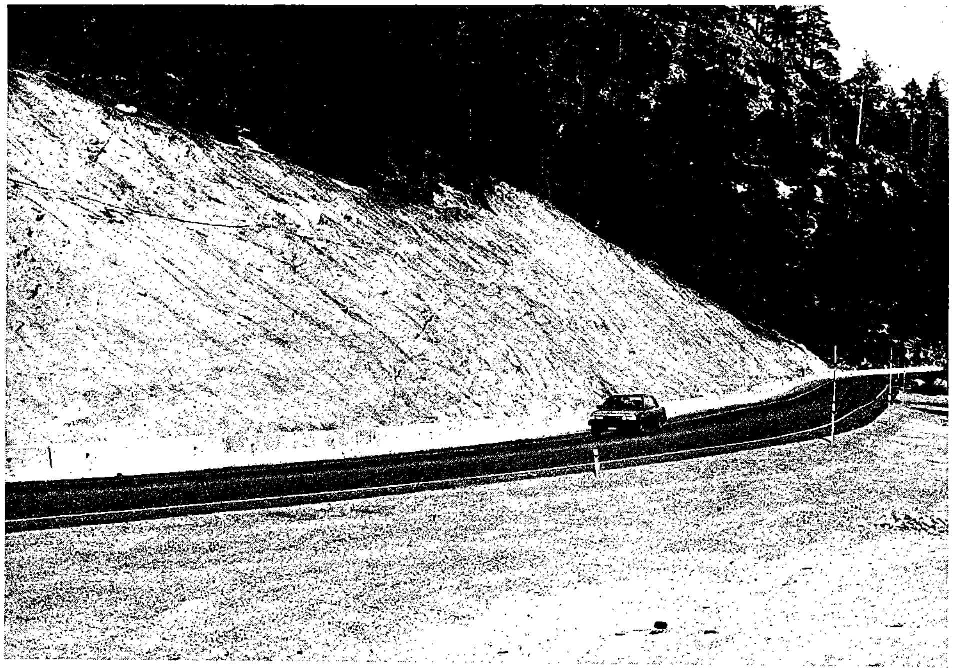

Figure 13. Wire mesh blanket laid on the decomposed granite slope, protects the State Route 207 from rockfall.

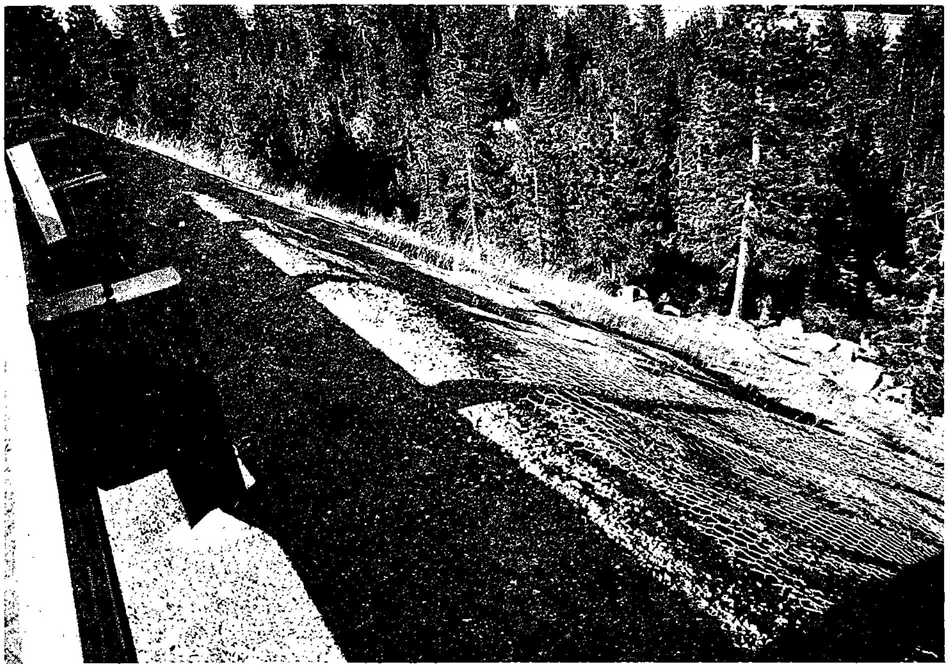

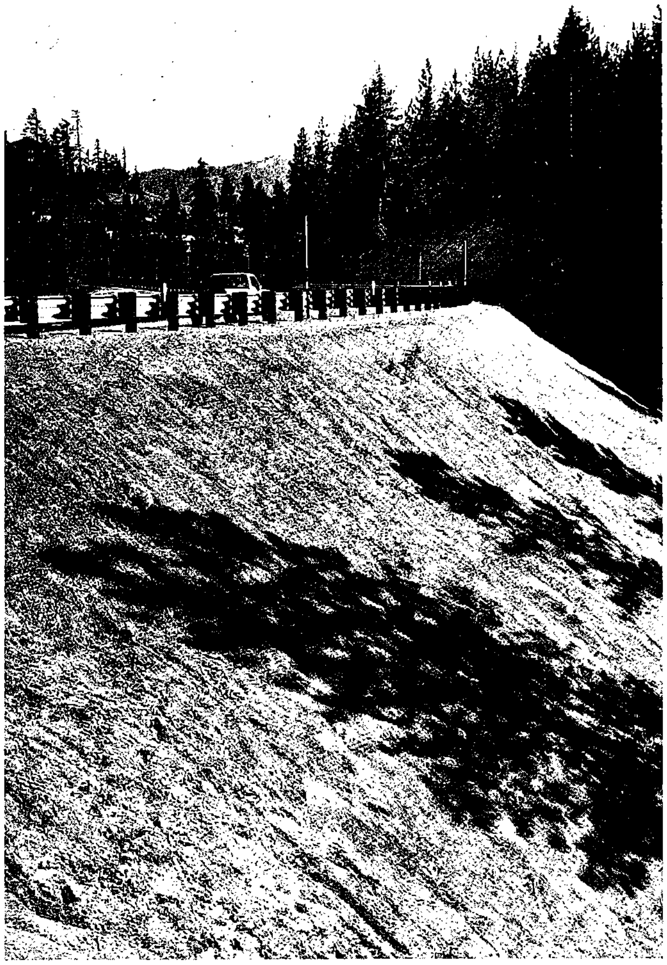

Figures 14-15. Metallic mesh panels laced together have stabilized the slopes of fill embankments of the State Route 207.

HIGHWAY 80 - EAST OF SPARKS, NEVADA

The degradation of the cut slopes along the major Highway 80 have always been sources of problems for the safety of vehicular traffic and always involved major upkeep and maintenance expenditures for the Highway Department, Fig. 16. To resolve these problems the Transportation Department of the State of Nevada, starting in 1980, has made recourse with ever greater frequency to the rockfall retaining metallic mesh which safely directs the rocks to the toe of the slopes, thus preventing their falling over the road bed. The Figures 17 and 18 show views of a project carried out in 1980, in which 37,000 square yards of mesh were installed at a cost of $175,000. The Figures 19 and 20 show instead a very recent project along the Truckee Canyon in which 79,000 square yards of rockfall safety mesh have been installed at a cost of $458,000.

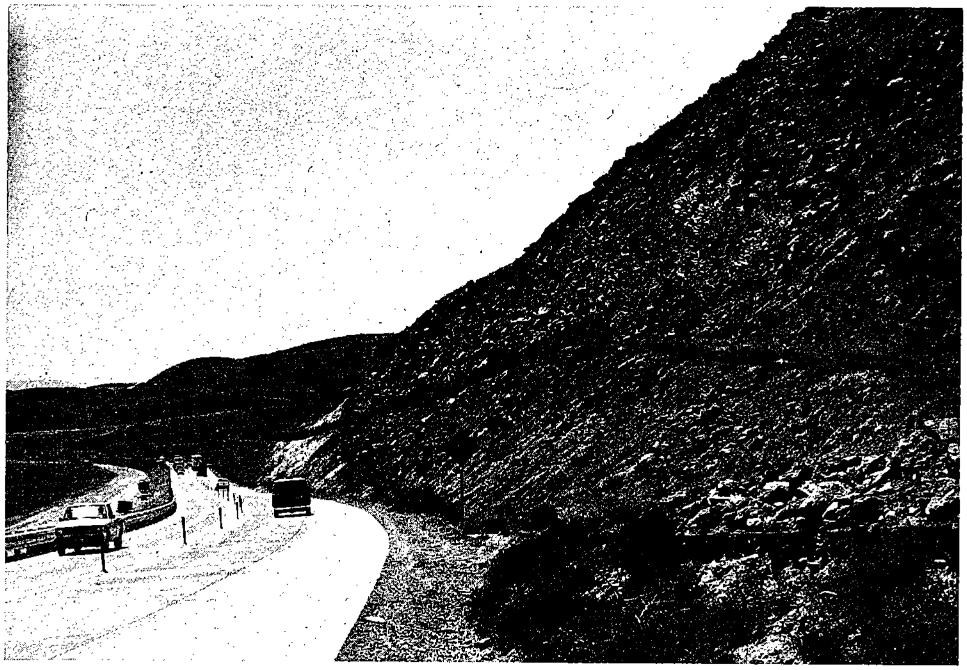

Figure 16. Highway 80 east of Sparks - Mid-slope bench and wire mesh fence are used in this stretch of the Highway 80 as rockfall mitigation measure.

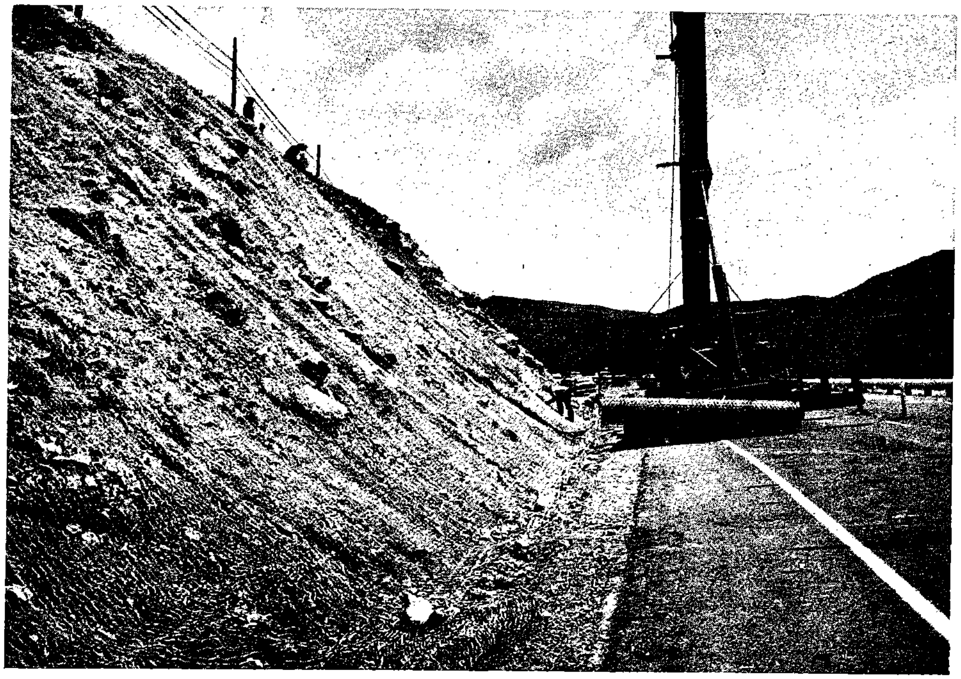

Figure 17. Highway 80 - Nevada, 1980. The rolls of wire mesh were lifted to the top of the slope, anchored in their proper place and unrolled downward.

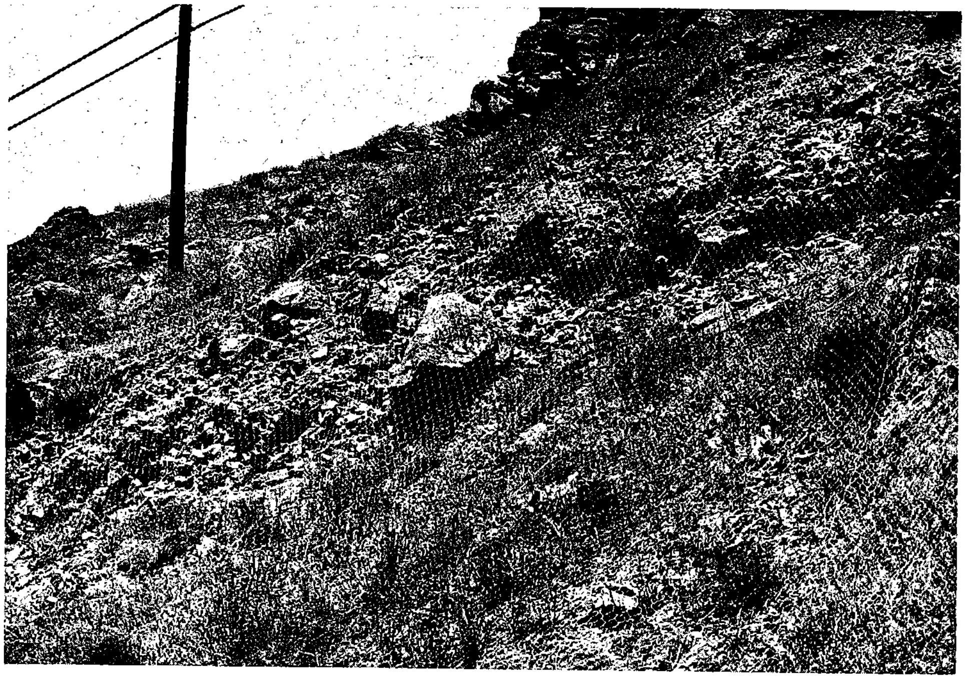

Figure 18. The same wire mesh protection showed in Figure 17 after six years of service. A significant amount of debris are collected at the toe of the slope.

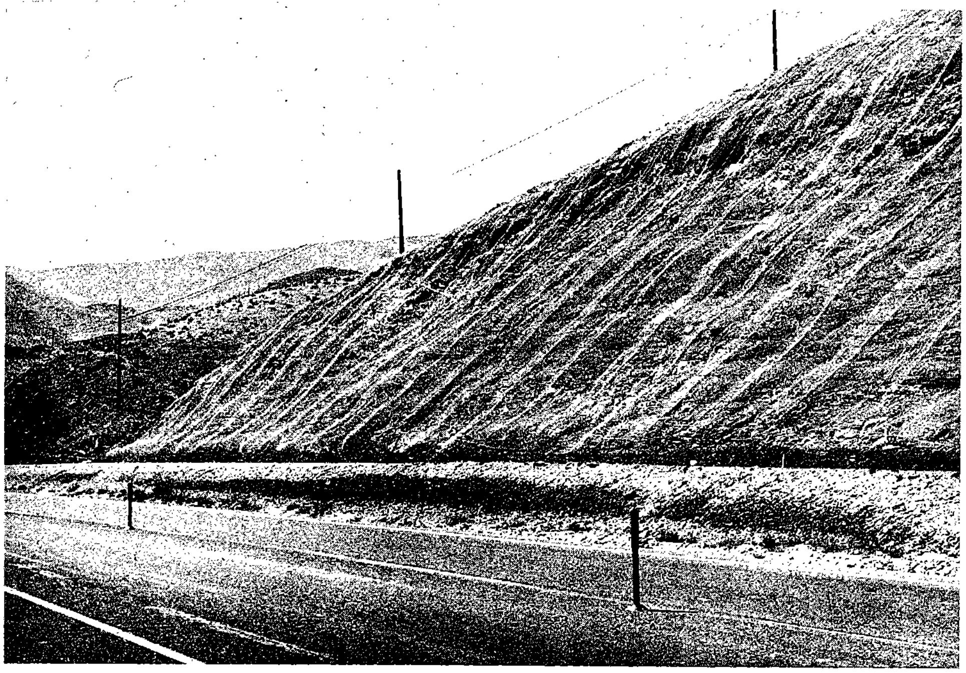

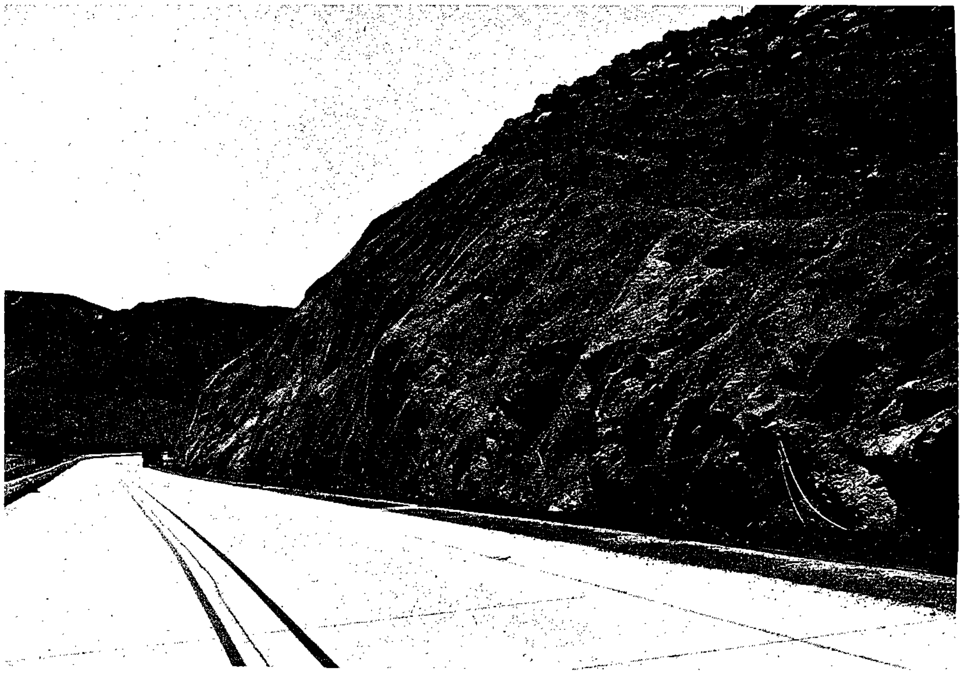

Figures 19-20. Highway 80 east of Sparks in the Truckee Canyon. Draped wire mesh blankets protect the road bed of the Highway 80 from rockfall.

CONCLUSIONS

The use of heavily galvanized double twisted hexagonal mesh stretched and anchored on slopes is widely recognized as an effective and economical solution to the problem of slope stabilization and as a road bed protection against rockfall.

The environmental impact constitutes an important decisional factor. The use of this mesh on the slopes assuredly supports vegetation growth which in time contributes to the slope stabilization.

The use of PVC coated mesh in areas of high corrosive potential is an important factor for the overall efficiency of the protective blanket.

Projects completed in the States of Montana and Nevada in recent years provide corroborating evidence for the functional validity of this rockfall restraining mesh.

ACKNOWLEDGEMENTS

The author gratefully thanks the individuals who have provided assistance in collecting the information about the projects discussed, in particular he thanks Mr. Dennis Keaster of the Department of Transportation of the State of Montana and Mr. Jack Lane of the Department of Transportation of the State of Nevada, who by their kindly collaboration have greatly facilitated this data gathering.

REFERENCES

1. State of California, Department of Transportation. Rockfall mitigation. 1986.

2. Federal Highway Administration. Rock Slopes. Design, excavation, stabilization. November 1981.

3. Piteau & Associates. Workshop on rock slope engineering. Planning, design, construction and maintenance of rock slopes for Highways and Railways. Vancouver B.C..

4. E. R. Magni. Rock cut stability along Ontario Highways. Paper presented at the 4th International Symposium on Landslides, Toronto, Canada. September 1984.

5. Officine Maccaferri. Rockfall protection netting. Off. Maccaferri S.P.A. Bologna 1985.

The Author: Massimo Ciarla is a graduate of the Hydraulic Engineering School of the University of Rome, Italy (1975). He has been a member of the Association of Professional Engineers of Rome, Italy, since 1978.

ROCK FALL MITIGATION AS A FUNCTION OF COST BENEFIT AND PROBABILITY ASSESSMENT

BY

ROBERT J. WATTERS[1] AND LYN KARWAKI[2]

1. Geological Engineering Division, Mackay School of Mines, University of Nevada-Reno, Reno, Nevada 89557

2. Civil Engineering Department, University of California, Berkeley, California 94720.

ABSTRACT

Techniques are presently available to provide effective mitigations for rockfall. The mitigations can produce safe highways if the problem is realized and an effort is made to solve the problem. A cost benefit analysis combined with probabilistic approaches to establish an effective mitigation which the practicing designer or maintenance personnel can use is presented.

The selection of the best mitigation for a site specific locality is not as simple as it at first appears. Factors such as geometries of the slope(s) and highway involved, availability of maintenance equipment and personnel, traffic flow, history or frequency and consequence of rock fall and available funds, together with geotechnical conditions, are all points which must be considered to obtain the optimum solution. Due to the number of factors which should be considered, the ideal solution may not be easy to discern.

A sample analysis is presented of mitigations applied to rock slopes in the Tahoe - Reno area with emphasis on Interstate I-80 along the California - Nevada border.

INTRODUCTION

In the last 25 years, due to more stringent construction and highway safety requirements, more thought and design has been given to the problem of rock fall. The effects of rock fall are greatest on highways due to vehicular traffic often moving at high speeds, colliding with fallen rock. Hence, rock fall mitigation has been researched mainly from the standpoint of highway design (Ritchie, 1963). The seriousness of the problem as it impacts highways can be gauged by study of California Highway Patrol records for a five year period ending December 1975, indicating that over 500 accidents were due to rock on the highway.

Direct costs incurred by rock falls include the maintenance required for work such as scaling and clearing ditches, cost of patrols in bad weather at particularly dangerous locations, delays and rerouting of traffic, and damage claims due to accidents. In 1980 California used $1,725,000 just for rock and sand patrols.

Indirect costs incurred by rock fall involve the loss of life, losses due to injuries, and property damage resulting from rock fall induced accidents. California Highway Patrol records indicate that for a five year period ending in December of 1975, 876 accidents on California State Highways resulted from natural material on the roadway. A sample of these accidents indicates that rock was involved in approximately 515 instances. For the period between March 1, 1974 and November 30, 1976, Board of Control records indicate that 34 claims arising from 32 accidents caused by rock on roadways were filed against the State of California. One death and 21 injuries were involved in these claims. Claims filed against the State of California as a result of rockfall caused accidents averaging over one million dollars per year. Statistics from other state highway departments show similar problems due to rock fall.

At engineering construction sites where excavations are required for building, etc., rock fall manifests itself either during the excavation phase and subsequent construction of the facilities, or during the operation and maintenance phase (Fookes and Sweeney, 1976; Watters and Kinney, 1979). Techniques in controlling rock fall are similar whether used at construction sites or for highways.

NATURE OF ROCK FALL

Rock fall(s) occur when a rock or group of rocks dislodge from a face or slope. Unstable rock masses are usually fractured, and failures involve individual rocks or relatively small rock masses. This instability can be external or internally caused. Some typical external influences would be chemical weathering, temperature variations, frost wedging, water running on the surface or stream erosion at the toe of the slope, and prying by the roots of vegetation. Internal factors include residual stresses from geological influences such as orientation and spacing of rock defects, water pressure vibrations.

Two particularly important factors are pressure from groundwater in joints and fissures, and frost wedging. The importance of these factors have been shown by Peckover and Kerr (1977) in studies relating total rock fall per month and direct correlation between rock fall and climatic conditions.

It is important to emphasize the difference between rock fall and slope failure. In slope failure a major part of the slope undergoes significant movement which markedly changes the slope and excavation geometries, the failure involves large volumes of material. Rock fall does not significantly change geometries, and generally only involves a maximum of one or two cubic yards of material. The type of project and size of the excavation are key components as to what constitutes rock fall. In open pit mining excavations, with overall slopes in excess of 1000 feet in vertical depth, a volume of rock of say 100 cubic yards can be generally regarded as minor, whereas on a highway slope 50 feet high, it would probably be regarded as a major rock slide. In a highway situation, a rock nine inches in diameter from a rock fall can seriously impact a car and cause fatalities. A similar sized rock at a construction site may just be one of many and go unnoticed.

COLLECTION OF ROCK FALL MITIGATION INFORMATION

Sixteen state highway departments were contacted and information requested on their rock fall mitigation techniques. It rapidly became apparent that states handle the administrative problem differently. Some states, like California and Idaho, are broken into districts; each district handles their own day to day rock fall problems, unless major designs are required. Arizona Department of Transportation, for example, established a Geotechnical unit within its materials section to handle rock stability problems. The majority of states contacted have a centralized administrative approach.

Once all the data was collected and synthesized, the techniques used could be divided into two main types -- stabilization or protection methods. These two methods could then be further subdivided. The actual costs of the different mitigation techniques were obtained where these were itemized, but where they were incorporated into say general highway maintenance, they were difficult to break out with any degree of accuracy. Tables 1 and 2 detail the main rock fall techniques utilized by individual states. Further information on each state's techniques are given in a recent paper by Nichol and Watters (1983).

ROCK FALL AND STABILIZATION COSTS

The cost of stabilization and protection against rock fall is highly dependent of the site specific details, e.g., site access or if the "fix" is applied during or after slope excavation, Table 3 lists the costs associated with different measures. Some techniques like slope modification or bench construction are site specific, but measures consisting of shotcrete application can be approximately costed.

The decision to utilize a particular rock fall mitigation is based not only on cost but on the effectiveness and the probability of the rock fall occurring.

DECISION THEORY FUNDAMENTALS

Applying decision analysis to rock fall yields the expected costs on which to base an informed decision. The technique requires the identification of all the consequences that can arise from the situation. To each consequence, a probability and cost must be assigned. In the area of slope stabilization, one set of consequences is whether or not the rock falls, and if the rock falls, the various consequences which result. Decision-making is essentially a process of making the most prudent choice among several alternative activities in a world of unknowns.

MITIGATION

STATE	FENCE	DITCH	BOLTING AND DOWLING	WIRE MESH BLANKETS	SHOT-CRETE	SCALING	BENCHES
ALASKA		X	X	X		X	
ARIZONA	X	X				X	
CALIFORNIA	X	X	X	X	X	X	
COLORADO		X	X	X	X	X	X
HAWAII	X			X			
IDAHO	X	X		X			
MONTANA	X	X		X	X	X	X
NEVADA	X	X		X		X	X
NEW HAMPSHIRE	X	X	X	X		X	
NEW MEXICO	X	X	X	X	X		
OREGON	X	X	X	X	X		
UTAH	X	X		X		X	
VERMONT			X				
WASHINGTON	X	X		X			
WYOMING	X	X	X	X	X		
BRITISH COLUMBIA	X	X	X	X	X	X	

TABLE 1.
MAIN ROCK FALL MITIGATION TECHNIQUES BY STATES

	MITIGATION				
STATE	GABION WALLS	SKEWED MULTIPLE ANGLE SLOPES	PRE-SPLITTING	DRAINAGE	SLOPE FLATTENING OF EXISTING SLOPES
ALASKA	X		X	X	
ARIZONA			X		
CALIFORNIA			X		
COLORADO	X				
HAWAII			X		
IDAHO	X		X		
MONTANA	X		X		
NEVADA	X				X
NEW HAMPSHIRE					X
NEW MEXICO	X	X		X	X
OREGON					
UTAH					
VERMONT			X		X
WASHINGTON	X				
WYOMING			X		
BRITISH COLUMBIA			X	X	

TABLE 2.
MAIN ROCK FALL MITIGATION TECHNIQUES BY STATES

Table 3
Stabilization Methods and Related Costs

Control Method	Cost	Year
Stabilization methods:		
Scaling	Site Specific	
Trimming	Up to $150/cy	1976
Slope Modification	Site Specific	
Drainage	$8-15/lf	1976
Shotcrete	$280-$500/cy	1976
Weep Holes	$30-$50 each	1976
Support & Restraint		
Buttresses	Site Specific	
Retaining Walls	Site Specific	
Rock Bolts	$240/bolt & assembly	1983
Rock Dowel	$18-$38/lf	1976
Protection Methods		
Benches	Site Specific	
Bench Fence	$20/lf	1982
Anchored Wire Mesh	$5-$30/sy	1982
Shaped Ditches	Site Specific	
Wire Mesh Catch Nets & Fences	$15-$30/lf	1982
Hanging Rock Fence	$38/lf^2	1982
Gabions	$30/cy	1968
Rock Sheds & Tunnels	$400-$1,500/lf	1976

The next step is to establish probabilities for the different events. The assignment of probabilities can be either subjective or objective. A subjective probability is basically the probability an engineer assigns on the basis of experience. First, the assessment depends on the engineer's outlook, optimism, pessimism, even the mood at the time. Second, is that experimental evidence has proven that people tend to overestimate the probability of a rate event. Due to these difficulties, it is wiser to use objective probabilities if they are available. An objective probability is based on actual or historical data.

Assigning costs to each consequence is almost as difficult as assigning probabilities. For example, if two accidents occur as a result of the same cause, there are still a myriad of other events which affect the outcome, such as if the accident occurred on dry or wet pavement, different costs will result. If there is enough historical or sample data to work with, a weighted average would best represent the cost.

Once these items have been established, or the best estimate determined, the decision analysis begins. The most common techniques used are the payoff matrix or the decision tree. A decision tree facilitates decision making when uncertainty prevails, especially when the problem involves a sequence of events. In a sequential decision problem in which the consequences of one stage depends on consequences which occurred earlier, the evaluation of alternatives can become very complicated. The decision - tree technique facilitates the stabilization evaluationequential decision problem in which the consequences of one stage depends on consequences which occurred earlier, the evaluation of alternatives can become very complicated. The decision - tree technique facilitates the stabilization evaluations by enabling the engineer geologist to write down all the future possible events, as well as their monetary outcomes in a systematic manner.

Having derived the decision tree, the expected cost for each branch is calculated. Then the stabilization technique with the least expected cost is chosen. This optimal decision is reached by a process known as "averaging out" or "folding back" the tree. The process begins with the events that comprise the tips of the branches. The expected values are calculated back to the decision point.

In summary, the decision tree technique permits us to transport ourselves in conceptual time to the extremities of the tree, where expectations are calculated in terms of the alternative outcomes and their probabilities of occurrence. We then work our way back by folding back, so to speak, the branches of the tree, choosing only those paths that yield the minimum expected cost at each decision junction.

TYPES OF DATA

There are three general types of information required in order to perform a decision analysis on the situation of rockfall from slopes adjacent to highways.

The first type of information needed is a record of rockfalls. This record should include the location, the frequency, and the consequences of rockfall. Most state departments of transportation rely on accident reports filed with the highway patrol to provide their information. An accident report lists the milepost location, the date and a code describing the cause of the accident. This establishes the location and the frequency, but not the consequences. The codes do not adequately describe rock-related accidents. The specific code used most often is "Object in Roadway". The safety engineer must then review each such report to determiine if the object is a rock. In the six-year period beginning in 1977 and continuing through 1982, there were only two types of accidents reported in Nevada:

A. Object in roadway/rock in roadway
B. Out of control vehicle/rock in roadway

The ambiguity of these descriptions makes it difficult to determine the actual events - did the rock impact the car, cause a delay, etc.?

Even though these ambiguities cause problems for the analysis, it is highly unlikely that the highway patrol will change their accident report forms, though a follow-up call by the engineering staff could be made to gather the additional information if it is not on the report.

The third type of information is the physical and geological characteristics of the slopes. This information is used to find the likely cause of failure and to judge if further falls are likely. If further falls are judged likely, then stabilization techniques should be considered. The possible failure types and surfaces will determine which stabilization techniques will be included in the tree diagram.

SAMPLE APPLICATION

In 1982, the Nevada Department of Transportation installed wire mesh on the rock slopes on the western side of I-80 between mile posts 0.00 and 1.00 as measured from the California-Nevada border. Similar mesh had been installed further east on I-80. The stretches of highway which were originally blasted through the hills have always been a problem area due to rock slides and rock falls. The Nevada Department of Transportation had been forced to run a plow truck through the area seven days a week to clear fallen rock from the road surface. In spite of these efforts, the sections of I-80 had a very high level of accidents caused by drivers being struck or swerving to avoid fallen rocks. The possible solutions to this problem were to acquire additional right-of-way which would be excavated in order to flatten the slope, grout the slopes, or use gabion wire mesh. The first two alternatives were considered much too costly, so the third was attempted. Thus far the wire mesh has proven to be successful.

Utilizing the information from mile posts 0.00 to 1.00, there were 13 rock-related accidents from 1977 to 1982 when the wire mesh was installed. Twelve of the accidents were rock in roadway and only one

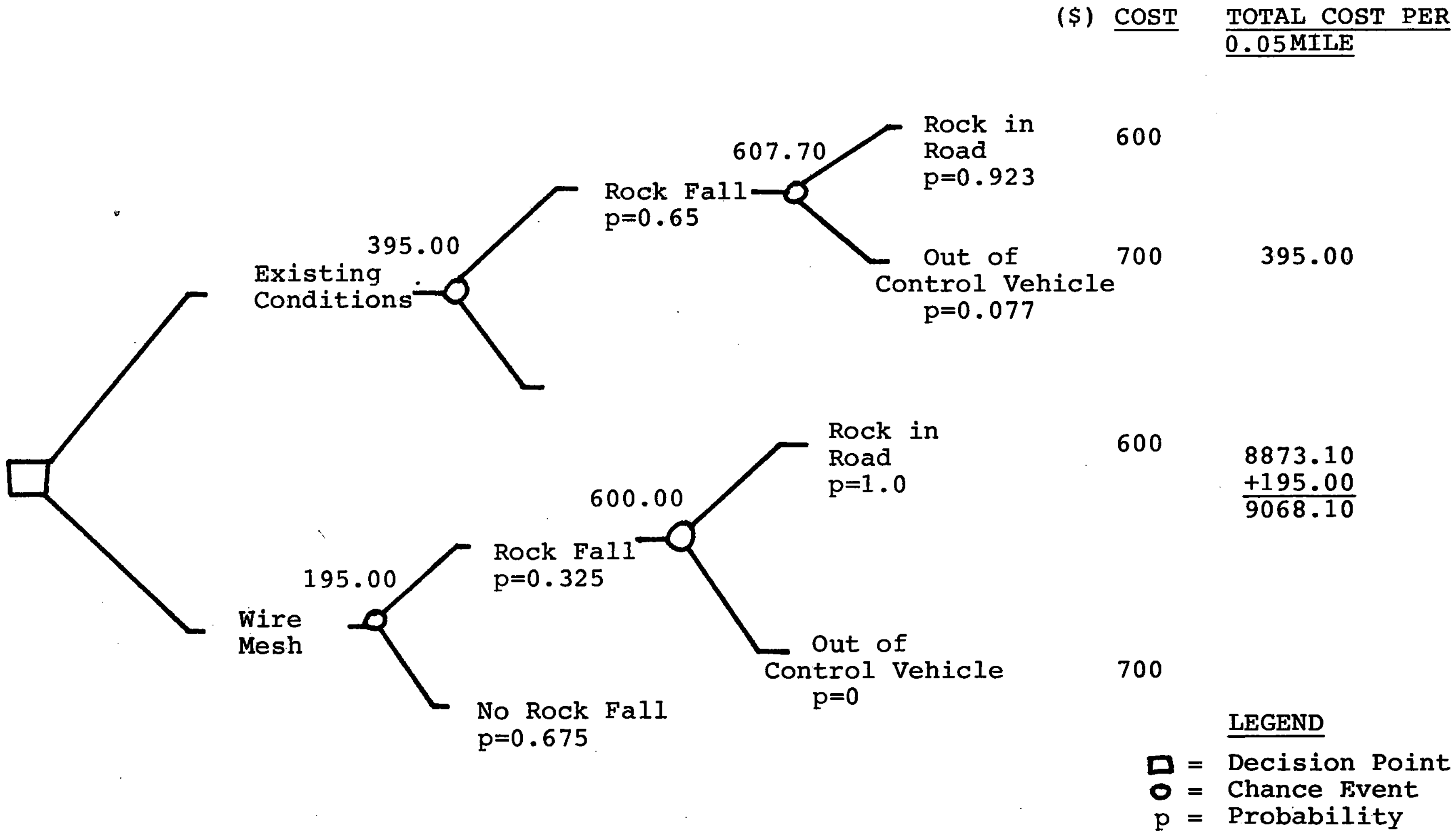
($) COST
TOTAL COST PER 0.05MILE
Existing Conditions
395.00
Rock Fall
p=0.65
607.70
Rock in Road
p=0.923
600
Out of Control Vehicle
p=0.077
700
395.00
Wire Mesh
195.00
Rock Fall
p=0.325
600.00
Rock in Road
p=1.0
600
8873.10
+195.00
9068.10
Out of Control Vehicle
p=0
700
No Rock Fall
p=0.675
LEGEND
□ = Decision Point
○ = Chance Event
p = Probability

Figure. 1 - Decision - probabilities and costs per 0.05 mile segment.

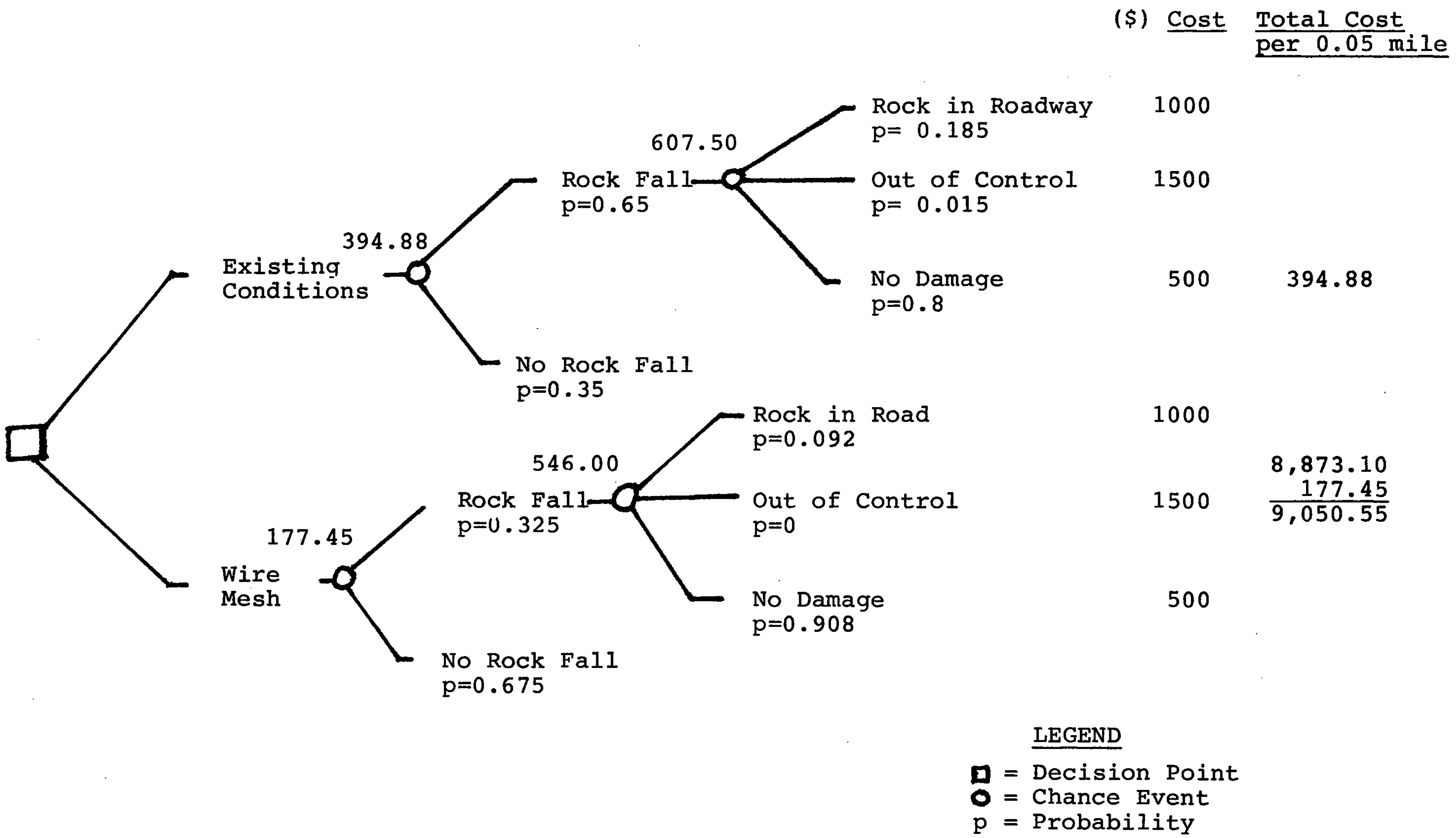
($) Cost
Total Cost per 0.05 mile
Existing Conditions
394.88
Rock Fall p=0.65
607.50
Rock in Roadway p= 0.185
1000
Out of Control p= 0.015
1500
No Damage p=0.8
500
394.88
No Rock Fall p=0.35
Wire Mesh
177.45
Rock Fall p=0.325
546.00
Rock in Road p=0.092
1000
Out of Control p=0
1500
No Damage p=0.908
500
8,873.10
177.45
9,050.55
No Rock Fall p=0.675
LEGEND
□ = Decision Point
○ = Chance Event
p = Probability

Figure. 2 - Decision - Probabilities(1 : 5) and costs per 0.05 mile segment.

was vehicle out of control. The one mile section was divided into 20 0.05 mile segments. The probabilities derived are as follows:

P(Rockfall in .05 mi segment) = 13/20 = 0.65
P(Rock in road) = 12/13 = 0.923
P(Out of control vehicle) = 1/13 = 0.077

The actual cost of vehicular damage is unknown and therefore we have made the arbitrary assumption that only minor damage occurred. Assigned costs of $100 for rock in roadway accidents and $200 for out of control vehicles plus the $500 for maintenance was used.

In 1983 there were two rock-in-roadway accidents. This represents a 50% reduction in the number of accidents from 1982. The probabilities are shown in Figure 1.

The expected cost of no stabilization is $395 per 0.05 mile. The expected cost per .05 mile for the wire mesh is $195. At face value, it appears that the wire mesh is the least cost choice. However, the cost of the wire mesh installation was $177,462 or $8,873.10 per 0.05 mile. The comparison is between $395 with no stabilization versus $9,068.10 with wire mesh (per .05 mi.). If these assumptions were anywhere close to approximating the actual costs, then no stabilization would be the appropriate choice.

These monetory figures do not consider legal costs to the State of defending a claim, even if defended successfully. If, however, the decision had been made already to stabilize, then the analysis would be applied to the various mitigation techniques.

It must be noted that the conditional probability used to revise the probability of rockfall is subjective. The only other possibility of deriving this conditional probability would be to examine the data from similar types of slopes in other locations that used that stabilization technique.

Now, assuming that only one accident in every five is reported, the analysis can be applied again. This has been done, and the results are presented in Figure 2. This is a much more realistic assessment than the above example. The addition of a category representing no damage allowed me to properly treat the branch tips and to revise the probabilities accordingly. Assume that the unreported accidents were all no damage. The decision remains the same; $394.88 versus $9,050.55, but the analysis is more indicative of the real world and of the proper application of the analysis.

CONCLUSIONS AND RECOMMENDATIONS:

Currently, most departments of transportation decide if a slope may require stabilization by the number of accident reports in Nevada. If there are 3 accidents per year for 3 years in succession in rural areas and 10 accidents per year for 3 years in urban areas, the slope is designated as a potential risk and stabilization is considered. If a significantly higher number of accidents occur, the slope is considered a high risk and it is stabilized. Other slopes are labeled as potential problems. Potential problems cause difficulties in deciding if preventative stabilization be undertaken.

Once the slope is considered for stabilization, cost-benefit analyses can be run to determine cost effectiveness. The same criteria of accidents/year could be used to identify problem slopes. However, a decision program is much simpler, direct and easier to run than a cost-benefit analysis. Several bonuses are that the probability of rockfall is now included in the analysis, the need to determine an appropriate discount rate is bypassed and the information is more readily determined than future benefits, expecially for potential problem slopes.

The problems involved in applying decision analysis to slope problems is that unless there is a relatively high probability of expensive accidents, the no-stabilization program will be generally the choice with the lowest expected cost.

Further research using actual costs due to a rock fall incident should include legal costs for both plaintiff and defense and award, if any, forestalled costs due to the successful application of the mitigation. For a mitigation to be deemed successful, an adequate data base on rock fall, both before and after installation of the mitigation, is required.

ACKNOWLEDGMENTS

Information supplied by Mr. Frank Page, Nevada Department of Transportation, on costs and rock fall on I-80 is gratefully acknowledged.

REFERENCES

Fookes, P.G. and M. Sweeney, 1976, Stabilization and Control of Local Rock Falls; Quarterley Journal of Engineering Geology, Volume 9, pp. 37-55.

Nichol, M.R., and R. J. Watters, 1983, Comparison and Effectiveness of Rock Fall Mitigation Techniques in the U.S.A. and Canada, Proceedings of the 20th Annual Engineering Geology and Soils Engineering Symposium, Boise, Idaho, pp. 123-142.

Peckover, F.L. and J.W.G. Kerr, 1977, Treatment and Maintenance of Rock Slopes on Transportation Routes. Canadian Geotechnical Journal, Volume 14, pp. 487-507.

Piteau, R., and F.L. Peckover, 1978, Engineering of Rock Slopes, Chapter 9. In Landslide Analysis and Control, Transportation Research Board, National Academy of Sciences, Washington, D.C., pp. 192-228.

Ritchie, A.M., 1963, The Evaluation of Rock Fall and Its Control, Highway Research Record, Volume 17, pp. 13-28.

Watters, R.J., and R.P. Kinney, 1979, Design Safeguards for Potential Slope Instability and Rockfall Affecting the Integrity of the Trans Alaska Oil Pipeline, 20th U.S. Rock Mechanics Symposium, University of Texas at Austin, pp. 357-362.

STATE-WIDE INVENTORY AND HAZARD ASSESSMENT OF DEEP-SEATED LANDSLIDES IN MONTANA

Edith M. Wilde and Mervin J. Bartholomew
Montana Bureau of Mines and Geology
Montana Tech, Butte, MT 59701

ABSTRACT

The Montana Bureau of Mines and Geology, in conjunction with the U.S. Geological Survey are compiling a deep-seated landslide inventory at a scale of 1:500,000; and are generating an accompanying computerized data base. Landslides are characterized by the following parameters: types of landslide features; age or date of initiation of sliding; location and size; and source rock or material.

The study involves the assessment of the deep-seated landslide hazard in Montana relative to: identified landslide-prone lithologies; Quaternary faults and historic seismicity; costs of remedial actions; and hydrology-related factors. Although not a specific part of this study, regions are also identified that are likely to have a high incidence of shallow-landsliding under acute meteorological and/or hydrological conditions.

INTRODUCTION

The National Research Council's Task Group on Landslides and other Ground Failures highlighted, in their 1981 report, ground failures as the nation's most economically significant class of natural hazards. Much of the Rocky Mountain region is characterized by unstable slopes. Population growth, increasing development of energy and mineral resources, and increasing use of large areas for recreation in the Rocky Mountain states indicate an increase of landslide-related losses during the next few decades.

DISCUSSION

Landslide identification and delineation are fundamental to any hazard reduction or mitigation program. Staff of the Montana Bureau of Mines and Geology in Butte and the U.S. Geological Survey in Denver and Menlo Park are currently compiling an inventory of Landslide locations in Montana. The personnel involved in this project are Mervin J. Bartholomew, Edith M. Wilde, Michael C. Stickney, Faith E. Daniel and Hugh W. Dresser from Montana Tech and Roger B. Colton and Earl E. Brabb from the U.S. Geological Survey.

Landslide locations are being compiled at scales of 1:100,000 and 1:250,000 for a final map at the 1:500,000 scale. The greatest part of the state is being covered by use of aerial photographs. Where possible, landslides identified by air-photo interpretation are being verified by field checking. Areas lacking air-photo coverage or geologic maps are being covered by either aircraft or ground reconnaissance. In addition, an accompanying computerized database is being prepared containing references for specific landslide locations;

currently this bibliography has about 300 references to site-specific landslides in Montana.

This study is involved with the assessment of the deep-seated (usually involving more than a few meters depth of material) landslide hazard in Montana. From this study the Bureau expects to target areas in the state for more detailed investigation of landslide hazards. Although shallow landsliding, generally associated with acute meterological or runoff conditions, should be considered as an equally serious hazard, the identification of all these features is beyond the capabilities of this project. This project will show the distribution of known landslides relative to: (1) selected lithologies (such as Cretaceous and Tertiary shales and Pleistocene lake deposits) which are landslide-prone, (2) faults known to have experienced surface rupture during the later Quaternary, and (3) historic seismicity. Historically active landslides will be indicated where known as well as those potentially or actually related to manmade features such as highways, dams, mines, canals, and buildings.

"Landsliding" is a general term for the more rapid and often catastrophic form of the geologic process of mass wasting. In the United States, most classification systems for types of mass wasting (landslides) are based on 3 factors: 1) the type of material which is set in motion, 2) the rate of movement, and 3) the type of movement involved. Landslide movements are of 3 primary types (which can also be subdivided): 1) SLIDE (or slip), 2) FLOW, and 3) FALL. Gravity, of course, is the ultimate driving force for all types of landslide movements, but a number of other factors determine whether or not movement will occur; and, as it does, the rate of movement. Conditions favoring landsliding may exist for a long time without any movement actually occurring; but once started, an individual landslide may be intermittantly active over a considerable span of geologic time. Thus older slides, of say Pleistocene or earlier Holocene age may experience reactivation under the right conditions. From a practical standpoint, no large landslide of Quaternary age should be considered "dead".

Both meteorological conditions and seismicity may serve as triggering mechanisms for both individual and groups of landslides. Among the many other factors which initiate landsliding are: 1) the degree of the slope; 2) the nature of the material on the slope; 3) the amount of water present in slope materials, 4) the kind and amount of vegetation cover, and 5) the attitude or dip of bedrock. However, even if the slopes are relatively stable, landsliding may be triggered by heavy or frequent vibration (such as an earthquake or mine blasts), by loading the head or slope, by removal of toe material, by changing the physical characteristics of the slope material, or by removal of interlocking root systems due to timbering or fires.

Landsliding may be either rapid or slow depending on the nature of the factors listed above which are involved. Slow movement includes a range of geologic processes from creep, solufluction and gelufluction to earth-, debris-, and mudflows. These geologic processes are often shallow-seated features involving only the top few meters of vegetation, soil, and saprolite. Although it is not a specific part of this study, some areas, particularily in the mountainous northwestern portion of the state, have been identified that are likely to have a high incidence of shallow-landsliding and snow avalanching under acute meteorological and/or hydrologic conditions. Of these types of relatively shallow, slow landsliding, we have specifically tried to identify mainly the larger flow-type features. These flow-type features are often responsible for extensive property damage and loss of life.

Rock or debris falls are the free-fall, bounce or roll of broken pieces of bedrock debris down a steep slope or vertical cliff. Locally, human habitation may necessitate a closer look at rock falls. For example, near the airport in Billings a housing development is located below an active rockfall. Large boulders broken away from the cliff face above the housing development may be expected to accumulate at its base. High potential for property damage exists locally in this and other areas, particularily if severe seismic shaking should occur. The accumulated debris (broken rock fragments) from this form of mass wasting and from snow avalanches forms the talus slopes nearly always present at the base of cliffs and steep hills, particularly in western Montana. Along the highway between Butte and Great Falls are many areas of active talus which contain active slides, as well.

Of course, human habitation and large landslides, such as near Virginia City, are equally likely to lead to serious environmental problems if such major slides are reactivated. On a smaller scale, as urban areas such as Great Falls expand, investigation of the relationships among landslide-prone lithologies, natural or induced hydrologic conditions, and slope stability will be needed to avoid man-induced landsliding.

Rapid landsliding includes the geologic processes implicit in the terms debris-, earth-, or rock avalanche, slump, or slide. Because of their potential for destruction and the often awesome power associated with their emplacement, these rapid forms of mass wasting are more familiar to most of us. Such rapid movement types of landsliding are most prevalent in mountainous regions.

The type of landsliding which involves movement by slide or slip has numerous examples in Montana. Movement can either be along a slide plane more or less parallel to the slope, or along a rotational plane. The former movement is simply known as a slide, while the latter is called a slump. Many of these small slumps and slides are located along the course of rivers, lakes, highways and railroads in Montana where Tertiary and Pleistocene sediments, such as along Lake Koocanusa, seem preferentially susceptible to numerous, small failures. In many cases, however, it is often difficult from air-photo interpretation to determine whether a larger landslide is a slide or a slump. Many landslides which begin as slump features also contain flow features; thus landslides, particularly in Cretaceous and Tertiary shales of eastern Montana are really composite landslide features. Good examples are found along the margin of the the Fort Peck Reservoir where many slump features were initiated by wave undercutting. In addition, many large-scale composite features are present along the Yellowstone River.

Southwest of Helena is the seismically active portion of Montana in which 22 faults have been identified as having had surface rupture during the late Quaternary. Lateral spreads and landslides are found at the ends and along segments of some of these faults such as the Centennial, Madison, Red Rock and Lima Reservoir faults; however, many other large landslides in this region are undoubtedly earthquake induced. The well known and catastrophic Hebgen landslide was a rock slide which blocked the path of the Madison River. It was initiated by earthquake activity, but the slope had been unstable for some time. A similar large rockslide may have occurred near the Canyon Ferry Dam.

South and east of Dillon is a large portion of the state underlain by Quaternary tuffaceous material and Cretaceous shale which are highly prone to landsliding on a very large scale. Southeast of Virginia City is one of the largest landslides in the state; this feature covers many square miles. Another typical landslide in this region is the well known slide adjacent to the Interstate 15 route south of Dillon. A few miles south, the new highway appears to cross the toe of yet another of these large landslides; several other large slides are also found in this vicinity. Some classic examples of debris flows, such as on the northeastern flank of Dixon Mountain, also are found in this seismically active area.

Landsliding occurs in every state in the nation and is an economically significant natural hazard in more than half. According to the 1985 report of the National Resource Council in the U.S., losses from landsliding and other ground failures exceeds losses from all other natural hazards combined (National Resource Council, 1985). Landsliding causes at least $1 to $2 billion in economic losses, and 20 to 50 deaths each year. Despite a growing geologic understanding of landsliding processes and a rapidly developing engineering capability for landslide control, losses from landsliding are continuing to increase. This is partially a consequence of residential and commercial development expanding onto steeply sloping terrain that is prone to landsliding.

Appropriate land use management, effective building and grading codes, the use of well designed engineering techniques for landslide control and stabilization, the timely issuance of emergency condition warnings, and the availability of landslide insurance could significantly reduce the catastrophic effects of landsliding. However, one of the most obvious ways to avoid problems with landsliding is to avoid building on slopes that are likely to experience landsliding. Any of these preventive approaches require, as a starting point, the identification of areas where landslides are likely and the representation of these hazardous locations on maps.

The purpose of this study is to provide a map which locates landslides, identifies landslide prone lithologies and areas as subject to seismically induced landsliding. We expect this map to be available (at least informally) for use by private or government agencies along with an accompanying report by early in 1987. As a sort of generalization Montana can be characterized as having three regions of slightly different landslide hazards. The eastern two thirds of the state contains vast areas of landslide-prone lithologies which need only the addition of precipitation or runoff to induce failure. In the mountainous northwestern Montana Cenozoic sediments fill the valleys and are prone to smaller slides but the steep, rugged terrain coupled with high precipitation, snow melt, and runoff create a high potential for shallow landslide hazard, as well as snow avalanches. Landslide hazard is perhaps highest in the seismically active southwestern part of Montana where extensive landslide-prone lithologies underlie topographically rugged regions which also have high runoff during a portion of the year.

REFERENCES

Bloom, Arthur L., 1978, Subaerial destructional (erosional) processes and erosional landforms: Chapter 8: Mass-wasting and hillslope evolution, in Geomorphology: A systematic analysis of late Cenozoic landforms, Prentice Hall, p. 163-196.

Bradshaw, Michael J., A. J. Abbott and A. P. Gelsthorpe, 1978, Mass movement and slope development, in The earth's changing surface: John Wiley & Sons, p. 98-114.

Leet, Don L., Sheldon Judson, Marvin E. Kauffman, 1978, Mass movement of slope material in Physical Geology: Prentice-Hall, p. 240-254.

Levin, Harold L., Mass movement of earth materials, 1981, in Contemporary Physical Geology: CBS College Publishers, p. 399-414.

National Research Council, Committee on Ground Failure Hazards, and Commission on Engineering and Technical Systems, 1985, Reducing losses from landsliding in the United States: National Academy Press.

National Research Council, 1981, Report to the Commission on sociotechnical systems, National Research Council, by the Task Group on Landslides and Other Ground Failures (unpublished).

National Research Council, 1982, Selecting a Methodology for Delineating Mudslide Hazard Areas for the National Flood Insurance Program, Committee on Methodologies for Predicting Mudflow Areas: National Academy Press, Washington, D.C.

Plummer, Charles C. and David McGeary, 1985: Mass Wasting in Physical Geology: Wm. C. Brown Co. Publishers, p. 165-182.

Ritter, Dale E., 1978, Physical weathering, mass movement, and slopes, in Process Geomorphology: Wm. C. Brown Co. Publishers, p. 127-168.

Strahler, Arthur N., 1977, Weathering, soils, and mass wasting: Principles of Physical Geology, Harper and Row, Pub. Inc., p. 239-256.

Strahler, Arthur N. and Alan H. Strahler, Modern Physical Geography: John Wiley & Sons, p. 256-269.

The Construction of a Shot-in-Place
Rock Buttress for
Landslide Stabilization

BLOCK GLIDE LANDSLIDE

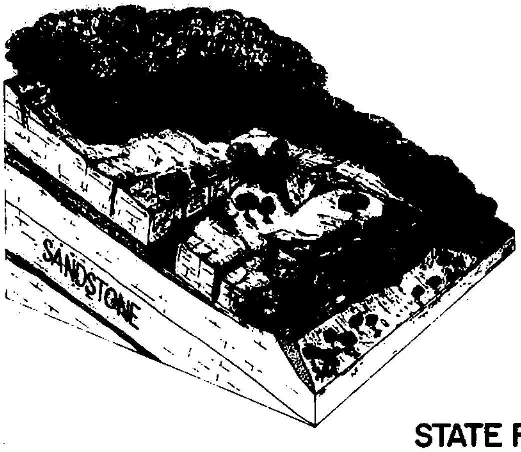

STATE ROUTE 31
HAWKINS COUNTY

By Harry Moore
Geotechnical Operations
Tennessee Department of Transportation

Prepared for presentation at the 37th Annual Highway Geology Symposium, August 20-22, 1986, Helena, Montana.

"THE CONSTRUCTION OF A SHOT-IN-PLACE ROCK BUTTRESS FOR LANDSLIDE STABILIZATION"

Introduction

During the past decade the Tennessee Department of Transportation has experienced landslide conditions requiring special treatment. Block glide type landslides where dipping strata are undercut by roadway cutslopes present unique situations for remedial work. New construction in regions where block glide conditions exist has resulted in an increase in their occurrence.

The block glide landslides occurring on mountain sides or large ridges usually involve beds of dipping strata which may extend upslope in excess of 500-700 feet. Providing restraint for this type of unstable material requires both a fast approach and a method of preventing continued up-slope migration of the landslide during repair.

The utilization of the shot-in-place rock buttress concept along Tennessee Highways has provided 'tested' results for continued implementation of this treatment. This narrative discusses the design and implementation of the shot-in-place rock buttress concept for landslide stabilization as experienced by the Geotechnical Section of the Tennessee Department of Transportation.

The first documented use of the shot-in-place rock buttress in Tennessee was on Interstate 40 at the Waterville Exit (near the North Carolina State Line) in Cocke County (Trolinger, personal communication, 1985). During the late 1960's a rock fill slope was constructed on a steep rock surface at the Waterville Interchange. This fill slope later resulted in a fill slide. A series of 'shot holes' were drilled through the failed fill material into the underlying bedrock. The resulting blast broke the bedrock and fill material destroying any continuous failure plane. The embankment stabilized and is functional today . . . the first documented use of the shot-in-place buttress concept.

New road construction across Clinch Mountain in Grainger County in the mid to late 1970's resulted in numerous block glide landslides requiring the use of shot-in-place rock buttresses. This marked the second and most widespread use of this concept. The engineering geology of this Clinch Mountain project has been accurately described by Jim Aycock (1981). The use of the shot-in-place buttress concept on the Clinch Mountain project was described by David L. Royster (1979).

Royster (1979) states that "The idea was to 'relax the slope' by breaking up the bedding planes along which sliding was taking place and use the shot rock to act as a buttress against further upslope movement." This 'idea' was employed on the Clinch Mountain project and as a result six 100' high and two 30' high shot-in-place rock buttresses were constructed between 1976 and 1980. These shot-in-place buttresses were designed to provide a factor of safety against upslope movement of approximately 1.3

At present the eight shot-in-place gravity structures have functioned as designed with no buttress failures as of this writing.

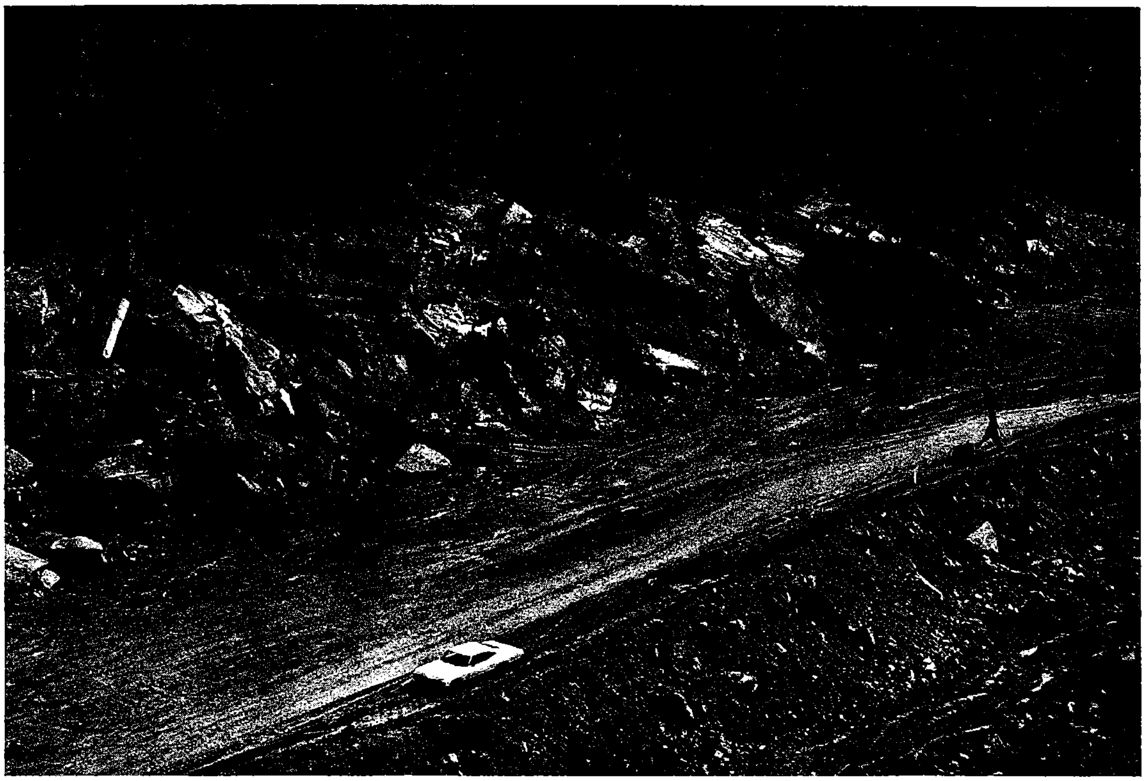

This block glide landslide occurred during the construction of a new 4-lane highway (U. S. 25-E) over Clinch Mountain in Grainger County, TN (1976).

Block glide landslides which occurred on U. S. 25-E in Grainger County were stabilized by the construction of shot-in-place rock buttresses such as the one pictured above. Note that it has vegetated and appears as a normal cut slope.

The shot-in-place rock buttress concept has been successfully employed along Tennessee Highways to provide restraint for block glide landslides. The project described in this text is the most recent implementation of this concept in Tennessee. Detailed in this narrative are conceptual design parameters, actual construction techniques and procedures, and a discussion of problems/concerns/ benefits surrounding the shot-in-place rock buttress concept.

CONCEPTUAL DESIGN

The use of the shot-in-place rock buttress concept requires the normal stability analysis computations for an 'ordinary' buttress type gravity structure. Again, the main purpose of the shot-in-place buttress is to 'relax the slope' by breaking up the planes of bedding along which movement is taking place.

The geologic data required for the remedial design includes the dip and strike of the bedrock, angle along which sliding is taking place, groundwater conditions, and lithology type and thickness.

Other criteria required for the buttress design includes knowing the blasting plan and resulting Ø of the shot material, unit weight and cohesion of the shot material, and the required safety factor.

By obtaining this information and incorporating it into the required computations, a satisfactory design can be effected.

Briefly, the shot-in-place rock buttress conceptual procedure is as follows:

*Investigating and analyzing the block glide landslide.
*Designing the required buttress and blasting plan.
*Stripping the vegetation off the failed material.
*Laying out, drilling and blasting the shot holes.
*Dressing up the buttress face and removing any 'swell material.
*Seed and provide drainage ditches, etc.

The concept is very straight foreward and does not require any unusual or 'out of the ordinary' construction procedures. In addition, standard computer programs set up for the design of gravity type buttresses can be used.

S. R. 31 PROJECT ON CLINCH MOUNTAIN

The subject project is a block glide landslide which occurred along the southeastern slope of Clinch Mountain on Tennessee State Route 31 six miles north of Mooresburg in Hawkins County (East Tennessee). The cut slide initially occurred in the early spring of 1984. Additional movement within the slide area enlarged the slide mass, damaging the roadway shoulder, deforming the roadway pavement and necessitated remedial measures.

The slide area is underlain by the Silurian Age Clinch Formation. The rock strata consist of medium to thick beds of well indurated quartzose sandstone with very thin (½" to 2" thick) interbeds of shale and clay. The strike of the rock strata is approximately N 20° E with a dip of 23° to the southeast.

The construction of the two-lane S. R. 31 highway over Clinch Mountain (some 40 years ago) required making cut slopes into the

LOCATION OF REPORT AREA HAWKINS CO. TENNESSEE

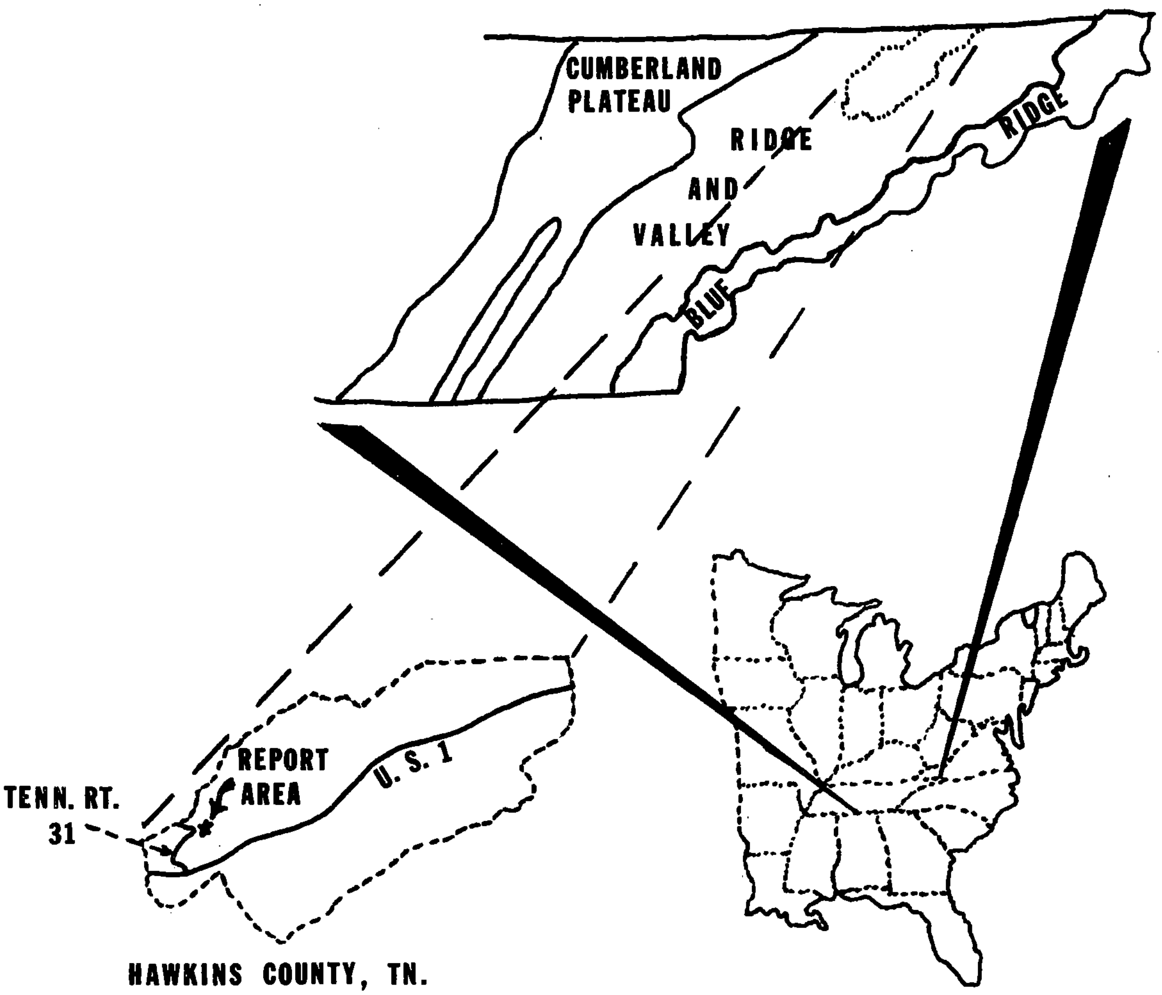
CUMBERLAND PLATEAU
RIDGE
AND
VALLEY
BLUE
RIDGE
TENN. RT. 31
REPORT AREA
U. S. 1
HAWKINS COUNTY, TN.

The location of the project area is on the south slope of Clinch Mountain in Hawkins County; the slope of the mountain corresponds to the direction of dip of the sandstone beds (arrow indicates project site).

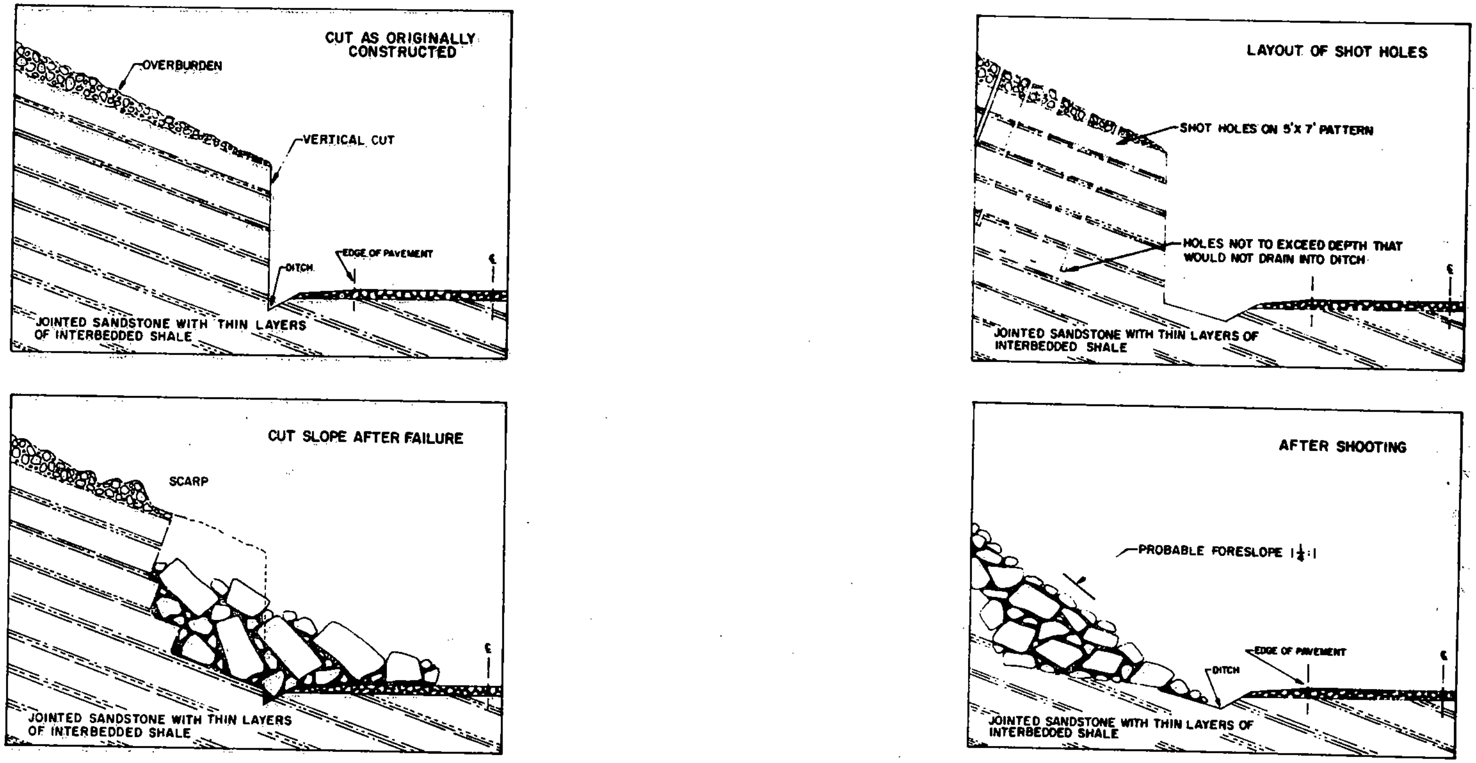
CUT AS ORIGINALLY CONSTRUCTED
OVERBURDEN
VERTICAL CUT
DITCH
EDGE OF PAVEMENT
℄
JOINTED SANDSTONE WITH THIN LAYERS OF INTERBEDDED SHALE
CUT SLOPE AFTER FAILURE
SCARP
℄
JOINTED SANDSTONE WITH THIN LAYERS OF INTERBEDDED SHALE
LAYOUT OF SHOT HOLES
SHOT HOLES ON 5'X 7' PATTERN
HOLES NOT TO EXCEED DEPTH THAT WOULD NOT DRAIN INTO DITCH
℄
JOINTED SANDSTONE WITH THIN LAYERS OF INTERBEDDED SHALE
AFTER SHOOTING
PROBABLE FORESLOPE 1¼:1
EDGE OF PAVEMENT
DITCH
℄
JOINTED SANDSTONE WITH THIN LAYERS OF INTERBEDDED SHALE

The two drawings on the left illustrate a typical cut section and failure experienced along S. R. 31 on Clinch Mountain. At right the two schematic drawings diagram the shot holes for a shot-in-place buttress and the finished shot-in-place rock buttress.

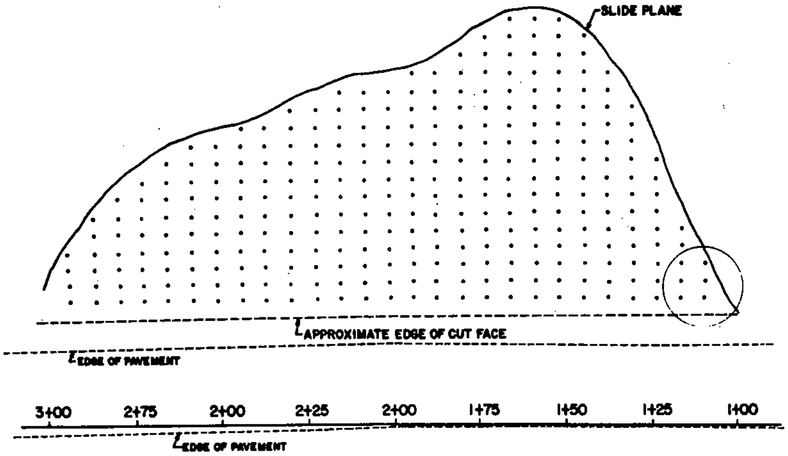
PLAN VIEW OF CUT SLOPE
AND
PROPOSED DRILL HOLE SHOT PATTERN
FOR "SHOT IN-PLACE" BUTTRESS
STATE ROUTE 31, HAWKINS COUNTY

SLIDE PLANE
APPROXIMATE EDGE OF CUT FACE
EDGE OF PAVEMENT
3+00
2+75
2+00
2+25
2+00
1+75
1+50
1+25
1+00
EDGE OF PAVEMENT

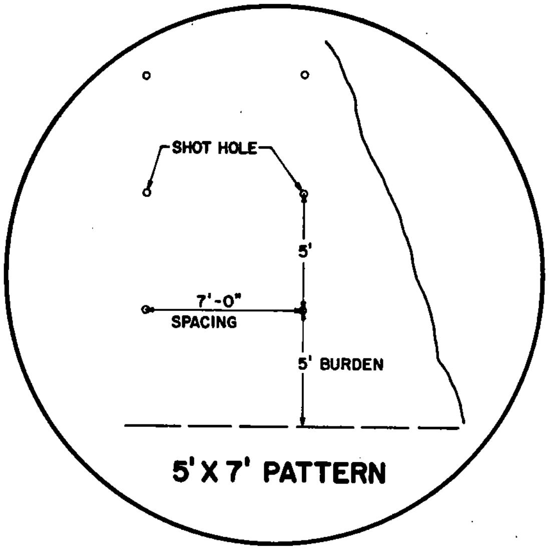
SHOT HOLE
5'
7'-0"
SPACING
5' BURDEN
5' X 7' PATTERN

These two drawings illustrate the proposed blasting pattern for the shot-in-place rock buttress on S. R. 31, Hawkins County, TN.

SHOT IN-PLACE BUTTRESS
(TYPICAL SECTION)

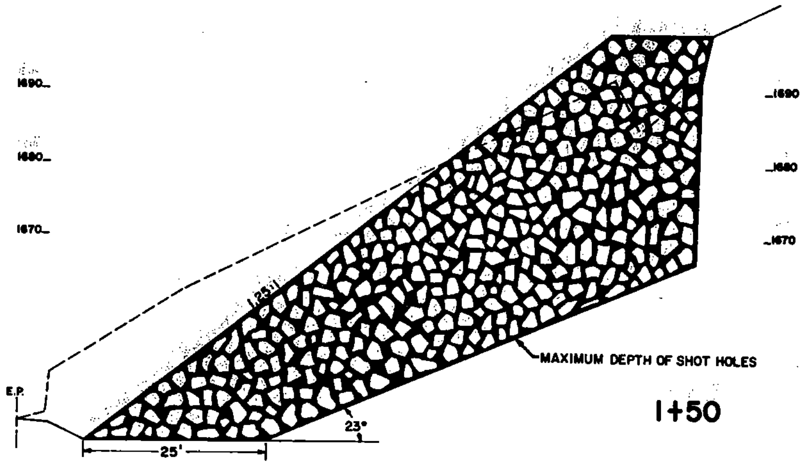
1690
1680
1670
1690
1680
1670
1.25:1
MAXIMUM DEPTH OF SHOT HOLES
1+50
E.P.
25'
23°

The above drawing illustrates the typical section of the proposed shot-in-place rock buttress. The front slope is on a 1.25:1 slope with the bottom of the buttress to approximate a 23° angle.

dipping sandstone strata. In numerous instances the cut slope undercut the dipping beds of rock and exposed the bedding planes of the strata (resulting in the rock strata dipping into the highway).

As weathering continued to enlarge joints in the bedrock, groundwater percolating along the joints and thin clay/shale interbeds has enabled a build-up of hydrostatic pressures downslope (relative to the top of the mountain) in the rock units.

With the "greasing" action that the saturated clay interbeds provided, the exposed and unrestrained bedding planes were free to slide downslope into the roadway. This resulted in a block of rock roughly 100 feet long, 200 feet wide and 12 feet thick to slide producing a classical "block glide" type landslide consisting of approximately 5200 cu. yds. These same type landslides were experienced during the recent construction of U. S. 25-E over Clinch Mountain in Grainger County in the 1970's (See Aycock, 1981).

If this particular landslide was left unrestrained, then the slide area would have enlarged headward by continuous blocks of bedrock sliding downslope into the original failed area. Eventually, this would have undercut the roadway upslope as the highway switches back above the slide area in order to cross the mountain.

Due to the field conditions and landslide type it was recommended that a "shot-in-place" rock buttress be utilized to correct and restrain the subject slide.

During the investigation it was determined that the ϕ of the "shot" material would be approximately 38^{o} with a unit weight of 2243 kg/cu meter (140 pcf). The cohesion of the shot rock was considered to be 0. In addition, the buttress was designed to provide a safety factor of 1.30 against future upslope movements.

The base of the buttress was designed to be 25 feet in width at an elevation equal to the roadway ditch elevation. The back limits of the buttress coincided with the slide scarp. From the back edge of the 25' wide buttress base the shot rock material was to slope up to the base of the scarp at a 23^{o} angle. A minimum 14' wide berm was left at the top of the buttress.

A blasting plan was also devised during the remedial design to insure proper breakage of the bedrock. The blasting design utilized a 5 foot burden and 7 foot spacing (5 x 7) with a drill hole diameter of 2.5 inches. The explosive used was Anfo at 1.92 lbs. per linear foot. Hole depths were approximately 20 feet. The stemming required was 3.8 feet and subdrilling calculated to 1.6 feet.

The contract was let to bid in August of 1985, for approximately $108,000.00. A total of 50 working days were set up for the contract.

Actual construction was initiated in early October. The rock buttress was completed by November 8, 1985, with only seeding and re-paving of the road remaining.

Construction began by clearing the slide area of vegetation. After the clearing and grubbing was completed, then the layout of the drill holes was required.

It was the contractor's choice to either drill and shoot the slide with one shot or to drill and shoot in several separate sections. The contractor elected to drill and shoot the slide mass in six separate sections.

PRE-SLIDE CONDITIONS
STATE ROUTE 31
HAWKINS COUNTY

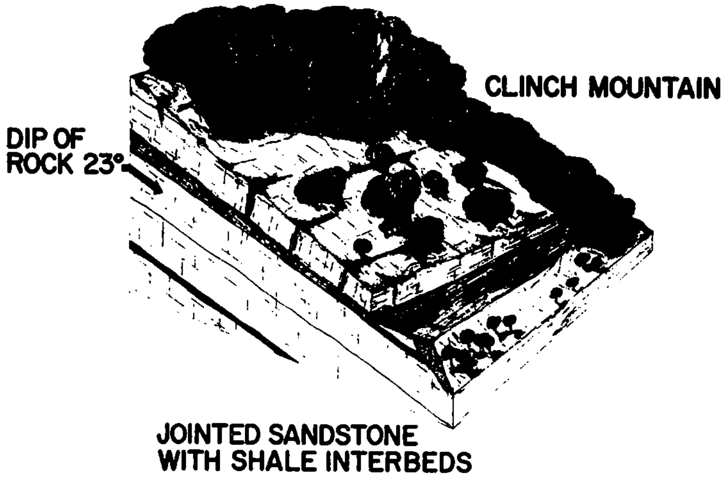
CLINCH MOUNTAIN
DIP OF ROCK 23°
JOINTED SANDSTONE WITH SHALE INTERBEDS

BLOCK GLIDE LANDSLIDE

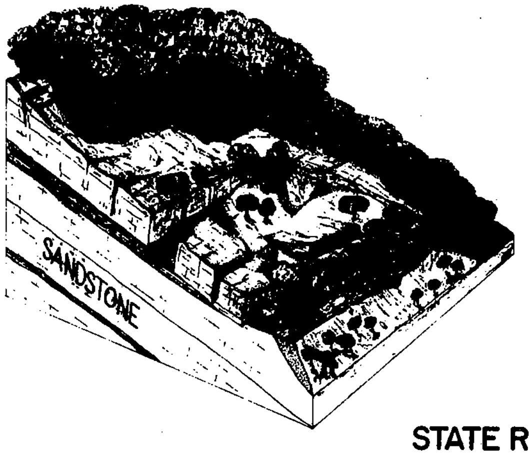

STATE ROUTE 31
HAWKINS COUNTY

These schematic block diagrams show the geologic conditions previous to and after the block glide failure along S. R. 31 on Clinch Mountain, Hawkins County, Tennessee.

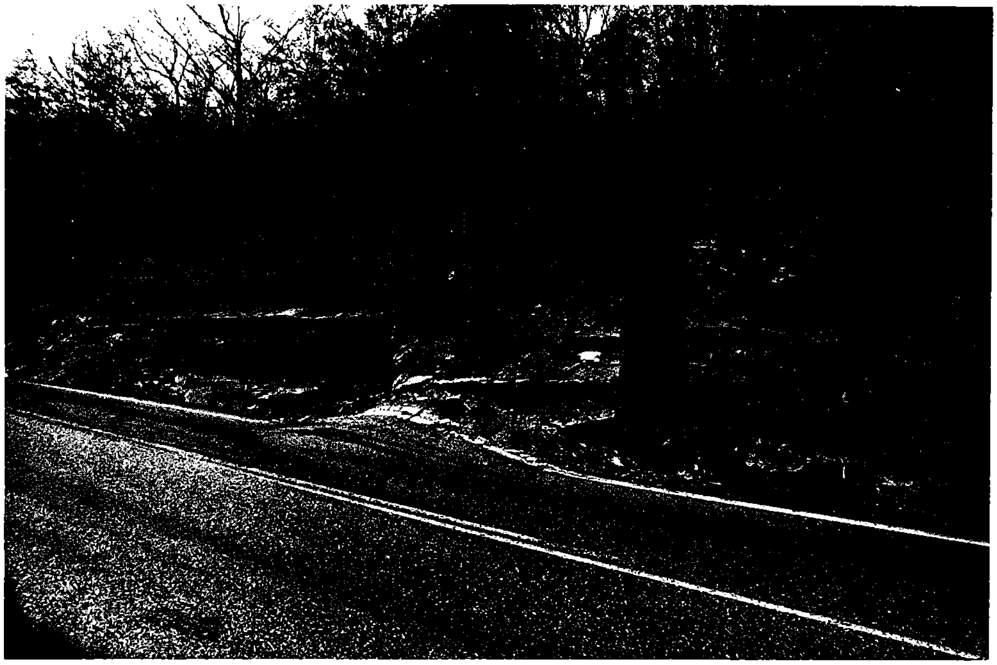

The block glide landslide at the project site resulted from movement along an interbed of clay within the bedrock mass. A joint has opened approximately 3.5 feet marking the slide boundary; note how the roadway shoulder has been 'plowed' by the moving bedrock.

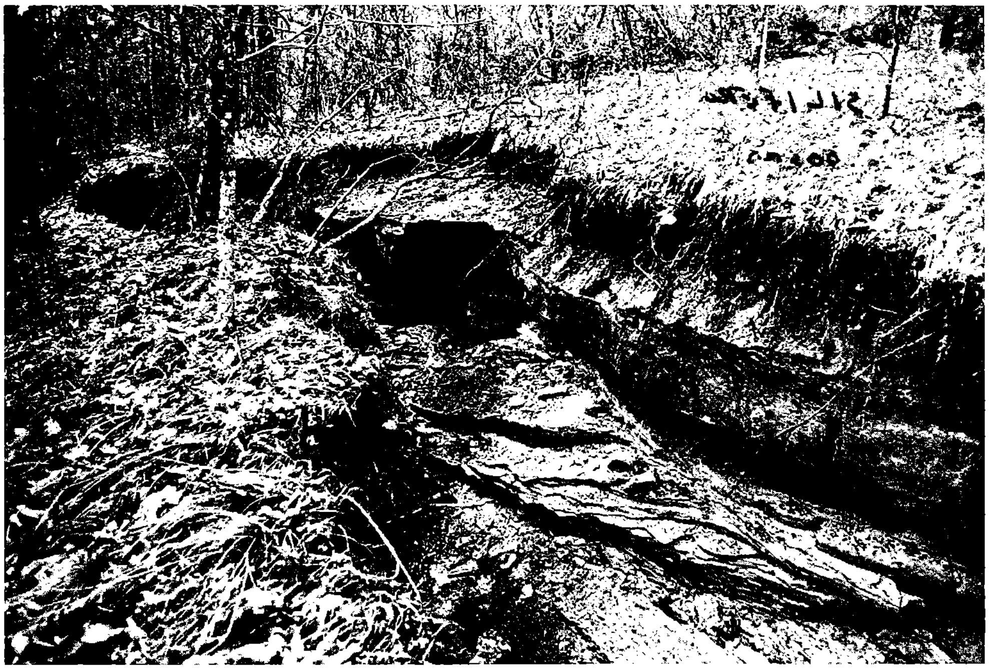

The up slope limit of the subject slide was marked by an eight foot wide scarp, varying up to 15 feet deep.

DRILLING PATTERN FOR SHOT-IN-PLACE BUTTRESS

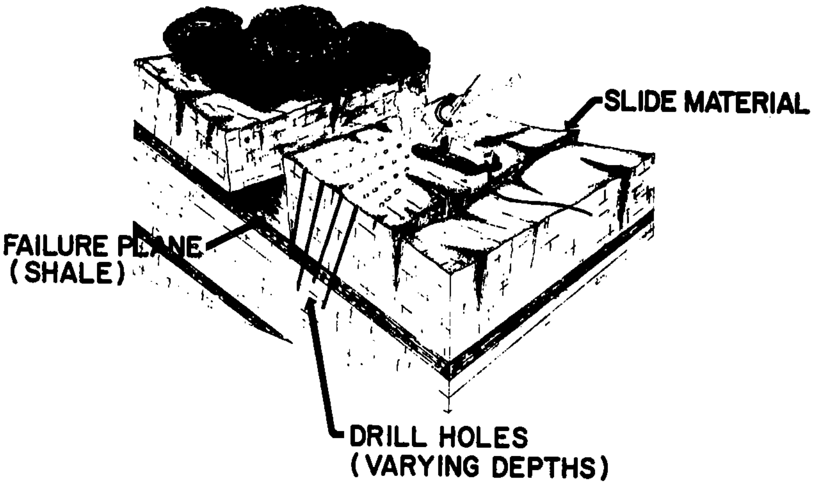
SLIDE MATERIAL
FAILURE PLANE
(SHALE)
DRILL HOLES
(VARYING DEPTHS)

BLASTING SLIDE MATERIAL FOR SHOT-IN-PLACE BUTTRESS

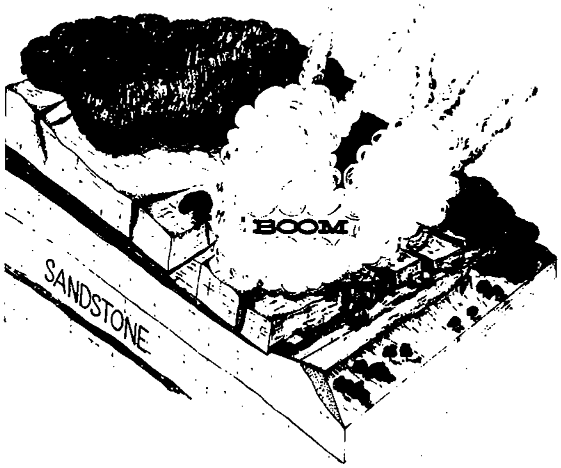
BOOM
SANDSTONE

Illustrated above are schematic drawings of drilling blast holes and eventually blasting the rock for a shot-in-place rock buttress.

Upon letting the slide repair to contract the contractor quickly began clearing operations; note large opened joint.

Drilling shot holes for the shot-in-place buttress was accomplished with standard track drill equipment.

After blasting the rock the slide became a jumble of large rock fragments; note the different orientation of the rock boulders which resulted from the blasting process.

This is a view from the top of the shot-in-place rock buttress on Clinch Mountain, Hawkins County, TN.

After blasting the rock the contractor used a bulldozer and a highlift to reshape and grade down the 'swell' of the shot rock.

This is a view of the completed shot-in-place rock buttress which now appears as an irregular soil and rock cut slope.

The adjacent highway remained open to traffic with flagmen control through-out the construction period. After each shot the road was cleared and reopened to traffic.

Due to the swell of the bedrock after blasting, there were approximately 2500 cu. yds. of excess material on the project. This rock and sand material was wasted nearby requiring a short haul.

Dressing up of the buttress face and top proceeded along with the completion of each blasting section. The final dressed face was on a 1.25:1 ratio.

A passer-by would only notice what would appear as a somewhat irregular cut slope. With an adequate seeding mixture the apparent cut slope became a grassy slope covering a rock buttress with no signs of once being a landslide.

PROBLEMS/CONCERNS/BENEFITS

With the utilization of new techniques comes the required evaluation process. Reflecting on the subject project brings to discussion certain problems, concerns, and benefits pertaining to the new concept.

The main problem experienced on this project was control of the blasting design. Since few Transportation Departments have personnel experienced in blasting design it has been historically left up to the contractor to provide the required blasting design (without any checks and balances). It is traditionally the aim of the contractor to 'shoot' rock in order to facilitate hauling (i. e. the smaller the rock the easier it is to load and haul). This situation requires considerable diligence on the part of the Project Engineer or Geotechnical Representative along with adequate backup within the 'chain of command'.

Another problem that must be considered is traffic control. In most instances it is desirable to maintain traffic throughout the construction project. The use of flagmen (sometimes on a 24 hour basis) and proper clean-up after blasting will facilitate the situation.

The greatest concern from the view point of the Geotechnical Personnel is what actually is happening to the bedrock after it is blasted. The situation within the buttress mass itself is unknown and presumed to be as designed. However, questions regarding rock break-up, amount of fines, drainage, and the interlocking character of the shot rock still remain.

Probably the greatest benefits to the shot-in-place buttress concept is that it is relatively inexpensive to construct and can be completed within a short amount of time. In addition the concept has some flexibility in it's use (i. e. possible use with some fill slide situations and other cut slope stability problems).

CONCLUSIONS

The design and construction of a shot-in-place rock buttress project for the stabilization of block glide type landslides can be effectively achieved. A geotechnical investigation, standard stability analysis and a blasting design are required prior to

SHOT-IN-PLACE BUTTRESS

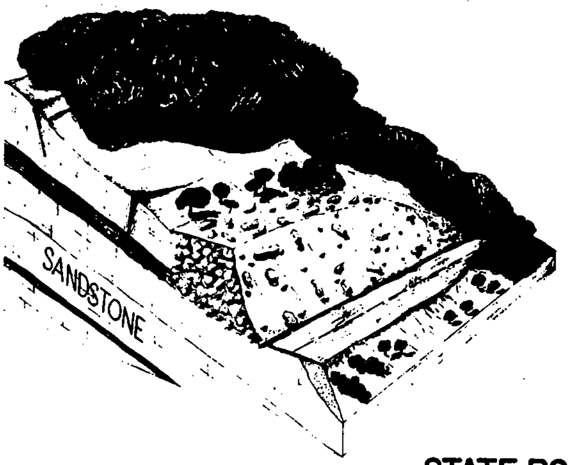

STATE ROUTE 31
HAWKINS COUNTY

This schematic block diagram shows a typical shot-in-place rock buttress as was constructed on S. R. 31 in Hawkins County.

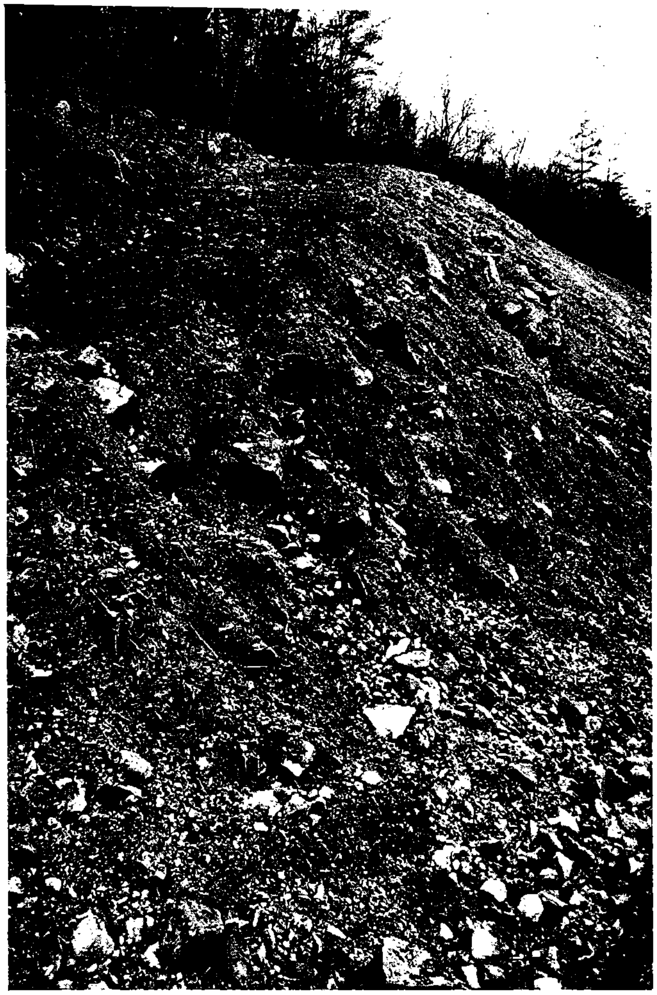

This view shows the top and fron slope - geometry of the shot-in-place rock buttress upon completion.

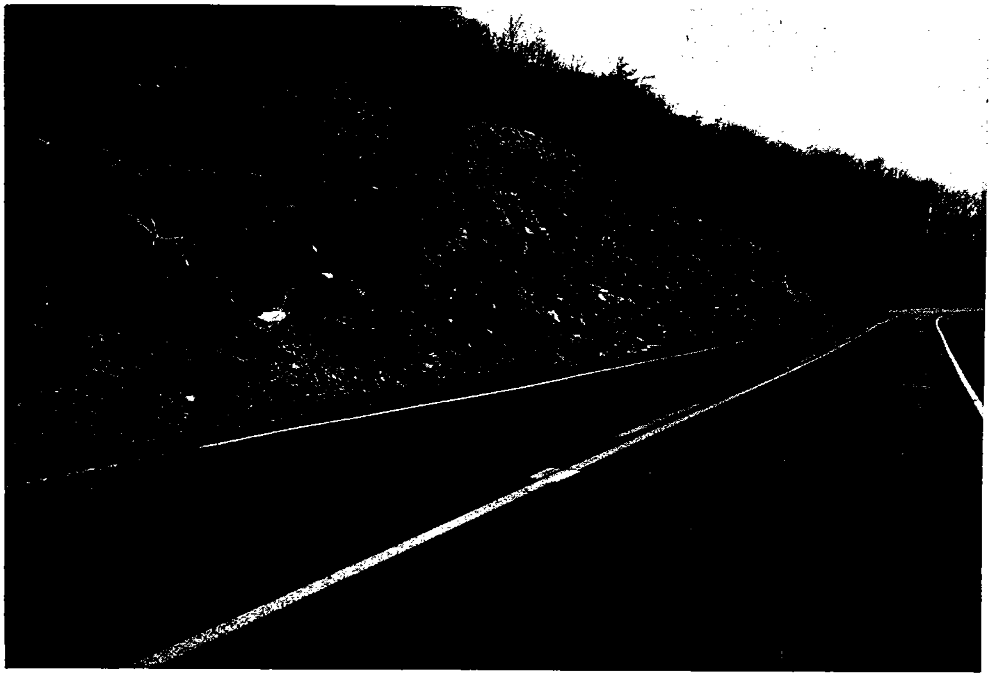

Shot-in-place rock buttress as constructed on Clinch Mountain along State Highway 31 in Hawkins County, Tennessee.

construction. Proper control of the blasting procedure, drill hole layout, traffic, and inspection are mandatory. A shot-in-place rock buttress can be constructed relative inexpensively and fast depending on the site conditions and weather.

At present the subject landslide is stabilized and the highway is functional. The shot-in-place rock buttress concept has proven to be a most expedicious method for stabilizing block glide landslides along highways in East Tennessee.

REFERENCES CITED

Aycock, James H., 1981, "Construction Problems Involving Shale in a Geologically Complex Environment, S. R. 32 - Appalachian Corridor "S", Grainger County, Tennessee"; proceedings of the 32nd Annual Highway Geology Symposium, Gatlinburg, Tennessee, May.

Royster, David L., 1979, Landslide Remedial Measures; Bull. Association of Engineering Geologists, Vol. XVI, No. 2.

Trolinger, William, 1985, Personal Communication, Manager, Geotechnical Operations Section, Tennessee Department of Transportation, 2200 Charlotte Ave., Nashville, TN 37219.

APPLICATION OF PERSONAL COMPUTER MODELS FOR THE STABILITY ANALYSIS OF THREE LANDSLIDES NEAR VAIL, COLORADO

A. Keith Turner
Professor of Geological Engineering
Colorado School of Mines
Golden, Colorado, 80401

ABSTRACT

Three landslides located near Vail Colorado were monitored for the Colorado Division of Highways during the spring and summer of 1985. Field investigations involved traditional methods for monitoring ground water conditions and movements of the slide masses.

These field data identified the probable failure mechanisms, but could not supply precise values for the mechanical properties of the slide materials. Preliminary stability analyses were performed on IBM-PC's, using the best estimates of landslide geometries and a range of assumed values for the mechanical properties. The materials values which best satisfied the factor of safety criteria and observed failure patterns were selected from these analyses.

Groundwater conditions were critical in all three slides. The efficiency and effectiveness of alternative drainage schemes were studied by seepage simulation programs. Some remedial actions were shown to be effective for all reasonable permeability values. Others increased the chances of failure under some permeabilty conditions. Since true field permeability data are hard to obtain, such remedial actions were identified as undesirable.

By combining the capabilities of these programs in a series of iterations, the anticipated benefits of alternative remedial measures were assessed in a cost-effective manner. The availability of powerful analytical programs on personal computers makes such assessments much more convenient and economical.

INTRODUCTION

Landslide reactivation has become an important consideration to highway authorities in Colorado, as well as other Western States, in recent years. Precipitation patterns which were particularly favorable to the initiation or reactivation of landslides occurred during the winters of 1982-83 and 1983-84. As a consequence many older and some new failures occurred which threatened to severely disrupt transportation facilities.

During the winter of 1984-85 the Colorado Division of Highways (CDH) began field investigation programs at three landslides near Vail, Colorado (see Figure 1). Drilling at these sites to install piezometers and inclinemeters continued during the winter months. However, it became obvious that sufficient manpower was not available within the CDH to take frequent observations of these installations, and to conduct other needed field observations, during the spring and early summer of 1985. Accordingly, the CDH contracted with the Colorado School of Mines (CSM) to conduct the necessary field observations and subsequent data reduction and analyses.

The three landslides were all fairly large masses, in excess of one million cubic yards each, and all were apparently due to reactivation of older prehistoric slides due to a combination of highway construction activities and the prevailing climate conditions. However, the slides did differ considerable in their geometries and dominant modes of failure.

The three landslides are referred to as follows:

1) Battle Mountain slide located on US 24 about 2 miles south of Minturn and about 7 miles south of Vail.
2) Wolcott slide located on Interstate-70 about 15 miles west of Vail; and
3) Vail slide located in the town of Vail on Interstate-70 one mile east of the Vail interchange.

All three slides are located on figure 1. The bulk of the field observations were conducted in a six week period in May and June of 1985, when all three slides were moving most rapidly. Sporadic observations continued at all three sites during the remainder of 1985.

The analyses of the field data extended through the winter of 1985-86 and were not completed until the summer of 1986. During this period the analysis techniques evolved. Evaluation of the Battle Mountain slide was completed first (Shine, 1985). It was followed by the Wolcott slide (Nasser, 1986), and then by the Vail slide (Fernandez, 1986).

The analyses involved traditional data reduction and correlation processes. These were assisted by the use of an Autotrol CAD graphics display system in the case of the Battle Mountain and Vail slides. However, stability analysis is central to all landslide studies. These were conducted with heavy reliance on modern computer programs for both stability analysis and assessment of drainage modification methods. Much of the computer computations were performed on IBM PC computers.

Because these landslides represent a range in types, and yet were analyzed using the same computer programs and similar approaches, the results reported here concerning the utility of modern PC-based computer programs should be of benefit to highway engineers.

DESCRIPTION OF THE LANDSLIDES

In order to fully evaluate the utility of the computer-based analysis methods, some knowledge of the basic characteristics of each slide is required. Accordingly, the following brief descriptions of each landslide are included in this paper. The interested reader is referred to the full reports on each landslide for further details concerning both field observations and analysis techniques (Shine, 1985; Nasser, 1986; Fernandez, 1986).

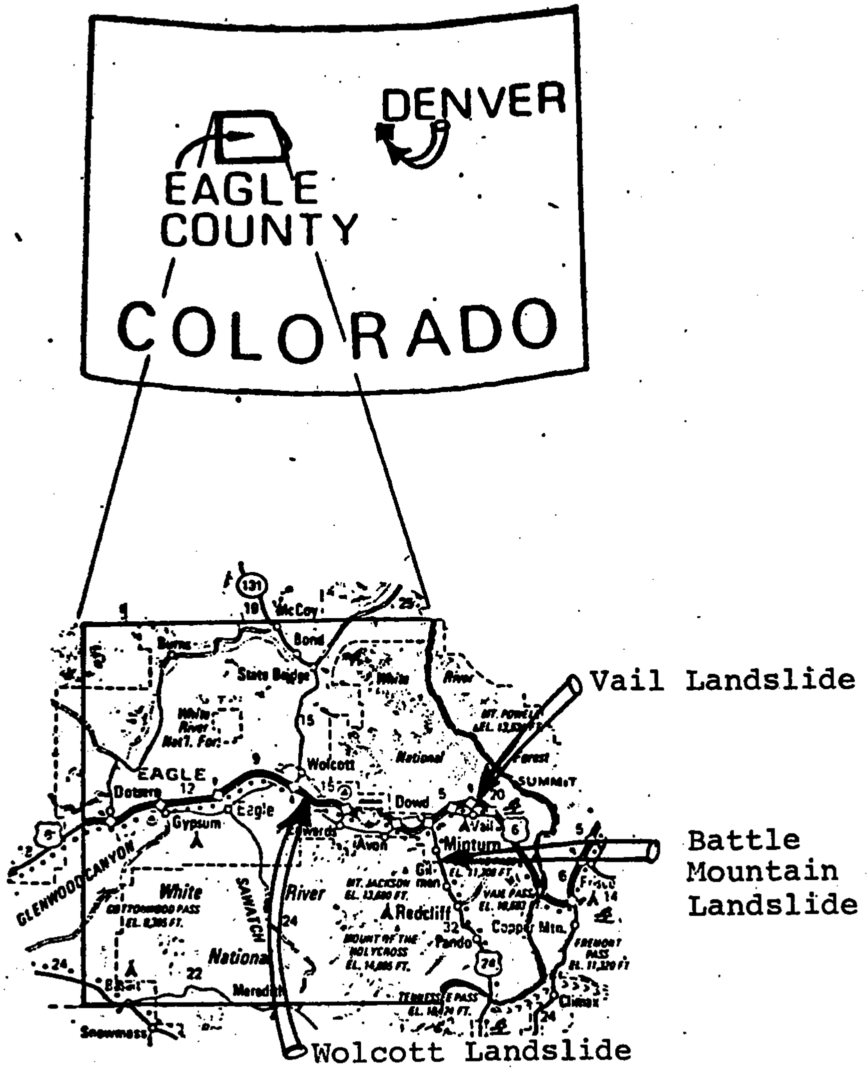
DENVER
EAGLE COUNTY
COLORADO
Vail Landslide
Battle Mountain Landslide
Wolcott Landslide
McCoy
Bond
State Bridge
White River Nat'l. For.
EAGLE
Dotsero
Gypsum
Eagle
Wolcott
Dowd
Edwards
Avon
Vail
Minturn
Gilman
Redcliff
Pando
Copper Mtn.
Climax
SUMMIT
GLENWOOD CANYON
White River National
SAWATCH
Meredith
Snowmass

FIGURE 1. Location Map of the Three Landslides.

Battle Mountain Landslide

Geologic Setting

The slide is located on the site of a larger prehistoric landslide below the cliffs opposite Cross Creek south of Minturn. During the Pinedale glaciation a glacier deposited morainal materials on the west side of the Eagle Valley. The Eagle River was diverted eastward and undercut the cliffs composed of Belden and Minturn formations which subsequently failed. It is unknown if this slide was ever completely stable, but movements became of concern once U.S. 24 was routed across the slide, and these movements seem to be slowly accelerating over the past few years.

The bedrock is sedimentary rocks of Pennsylvanian age. The lower Belden Formation consists mostly of marine shales and some limestones. The overlying Minturn Formation is composed of siltstones, sandstones, shales and some carbonate units. Accordingly, the lower Belden rocks are believed to be less permeable than the overlying Minturn units. The rocks are gently deformed in the immediate area, and the contact between the Belden and Minturn dips below the road and into the slide along its southern flank.

Critical Field Observations

Saturation of the slide mass is the basic cause of movement. Water table elevations rose by up to 12 feet during the spring snowmelt period; and during this time movements of up to 14 inches were observed along the road. Intense summer rainfalls do not seem to cause any appreciable change to the ground water levels, and thus do not seem to be a significant cause for failures.

The 16 observation wells and one inclinometer installed on the slide allowed the construction of the major failure surface for the slide. All available data were combined to create digital maps of the topography, water table, and failure surfaces of the slide using an Autotrol CAD system which allowed for the computation of slide volumes. The slide involves about one million cubic yards.

Groundwater seepage from the toe of the slide was collected along the old road grade. A maximum flow of over 14 gallons/minute was measured in early May, but this dropped rapidly to around 2 gallons/minute in early June and around 0.5 gallons/minute in early July.

Mechanisms of Movement

Analysis of movement data, combined with observations of surficial features, suggest that the slide consists of at least four zones (labelled A-D on figure 2). Observed rates of movement indicate that the slide mostly fails first in its lower portions, and then the movement retrogresses to its head. The cracks and distortions on the outer shoulder along U.S. 24 in the southern part of the slide (zone A) appeared to be more severe during the spring of 1985 than in previous years. The slide toe seems to be located at the old abandoned road.

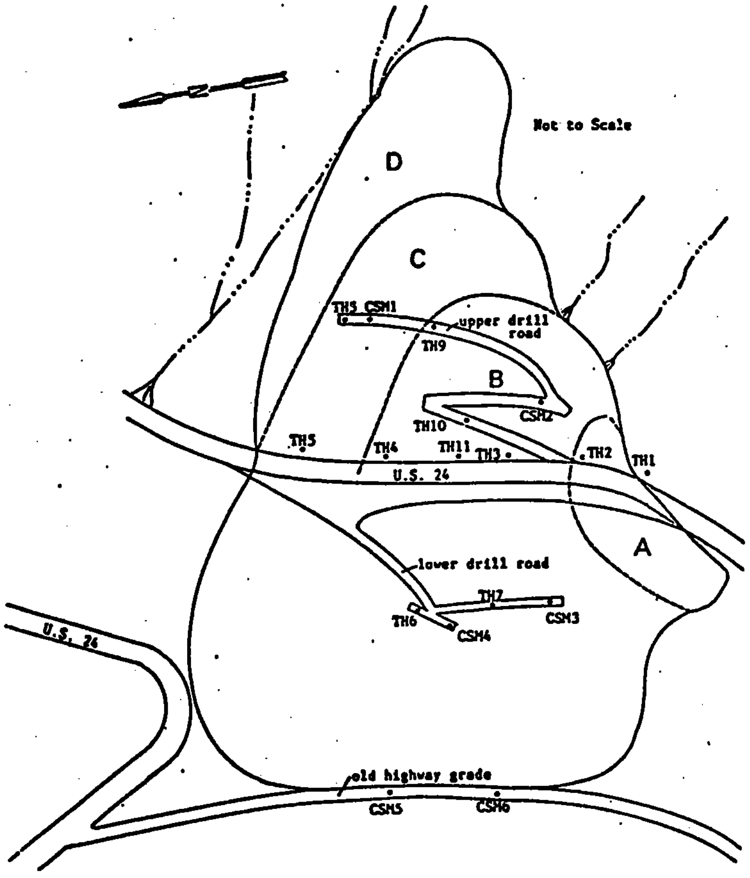
N
Not to Scale
D
C
B
A
TH8
CSM1
upper drill road
TH9
CSM2
TH10
TH5
TH4
TH11
TH3
TH2
TH1
U.S. 24
lower drill road
TH7
TH6
CSM4
CSM3
U.S. 24
old highway grade
CSM5
CSM6

FIGURE 2. Sketch map of the Battle Mountain Landslide showing locations of exploratory holes and major movement zones.

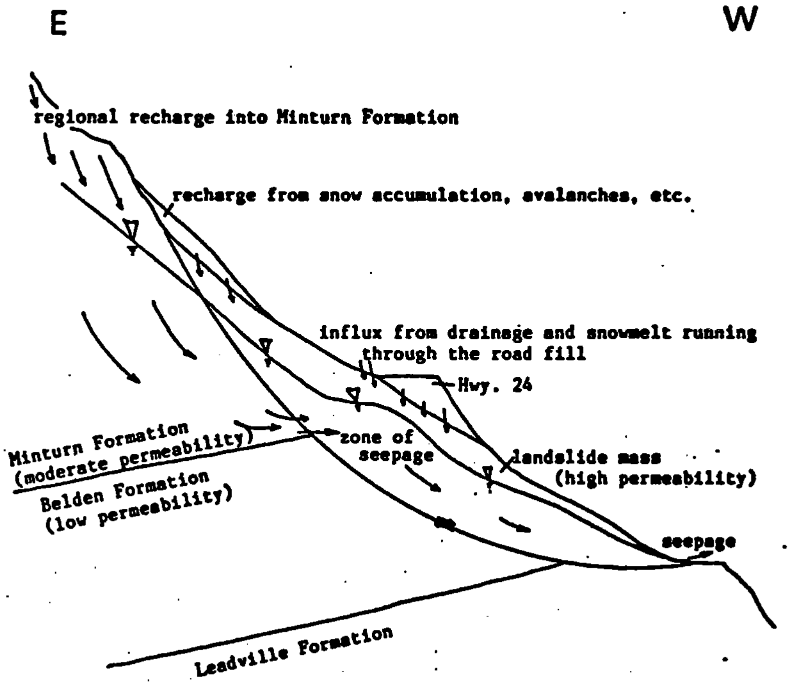
E
W
regional recharge into Minturn Formation
recharge from snow accumulation, avalanches, etc.
influx from drainage and snowmelt running through the road fill
Hwy. 24
Minturn Formation (moderate permeability)
Belden Formation (low permeability)
zone of seepage
landslide mass (high permeability)
seepage
Leadville Formation

FIGURE 3. Cross-section through the Battle Mountain Slide, looking south and showing suspected hydrology.

The water table data show a distinct flattening of this surface in the lower central portions of the slide (see figure 3). Such a pattern can be best explained by an inflow of water from the bedrock along the Minturn-Belden contact into the slide mass. Other important sources of water include direct recharge from the surface of the slide and through the road fill material.

All available movement data suggest the slide is relatively deep seated, with a primary failure zone passing roughly 100 feet below the highway (see figure 4).

The Wolcott Landslide

Geologic Setting

The slide is located near the axis of the Wolcott Syncline, in the siltstones and shales of the Benton Formation. The regional structure tends to direct groundwater toward the slide, and artesian or near-artesian conditions may exist in the Dakota sandstone units immediately below the slide.

The slide is shallow, with failure surfaces at about 12 and 19 feet below the surface. Sliding occurs within layers that contain bentonite. The rock units underlying Bellyache Ridge, on which the slide is located, dip toward the Eagle River. A meander of the river is undercutting the toe of the slide. The entire surface of Bellyache Ridge is composed of highly fractured siltstone,sandstone and shale, and is much disturbed, so that recharge from snowmelt each spring is very easy.

Critical Field Observations

Saturation of the slide causes the movement. Recharge through the surface of the slide, and throughout the slope above it, is quite easy due to the broken nature of the materials. The water table within the slide rises to within 8 feet of the surface in several areas. An extensive seepage zone near the eastern edge of the slide, above I-70, was measured, and produced 18 gallons/minute. Other smaller seepages occur, and surface ponding and saturated conditions occur at several locations in the I-70 and U.S. 6 rights-of-way during the snowmelt (see figure 6).

Existing culverts under U.S. 6 remain dry, and appear to predate the I-70 construction which obviously disturbed local drainage patterns. An existing French Drain along the south shoulder of I-70 does not appear to be working properly.

Movements have now begun to affect the grade of an irrigation ditch below U.S. 6, so that it overflowed in late May and introduced a new source of saturation to the lowest portion of the slide (see figure 6). This triggered a second wave of failures, after the main slide mass had stopped moving.

The Eagle River meander is undercutting the toe of the slide. The

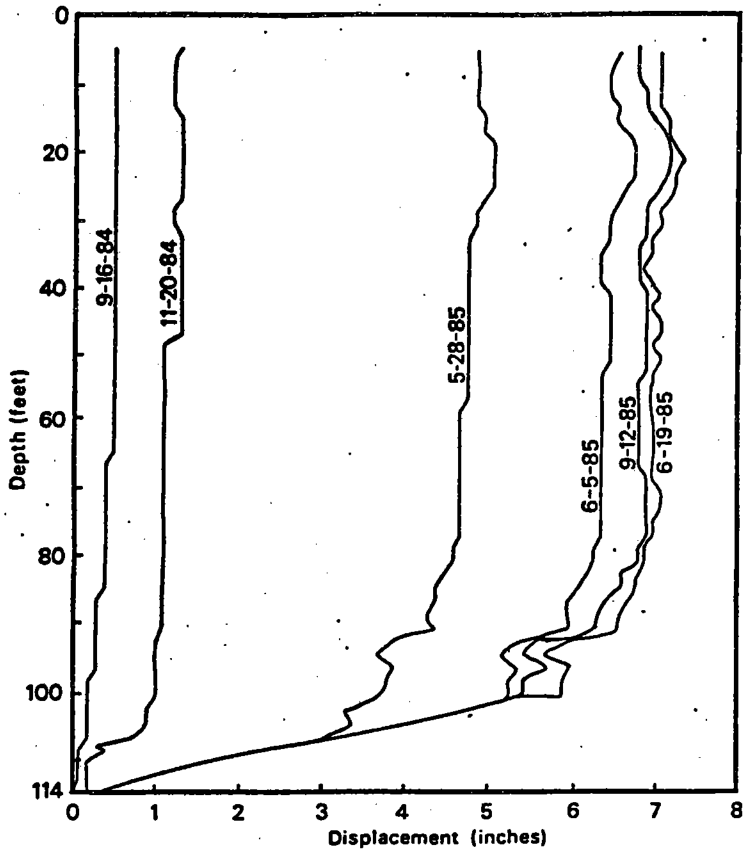

FIGURE 4. Inclinometer data from the Battle Mountain slide.

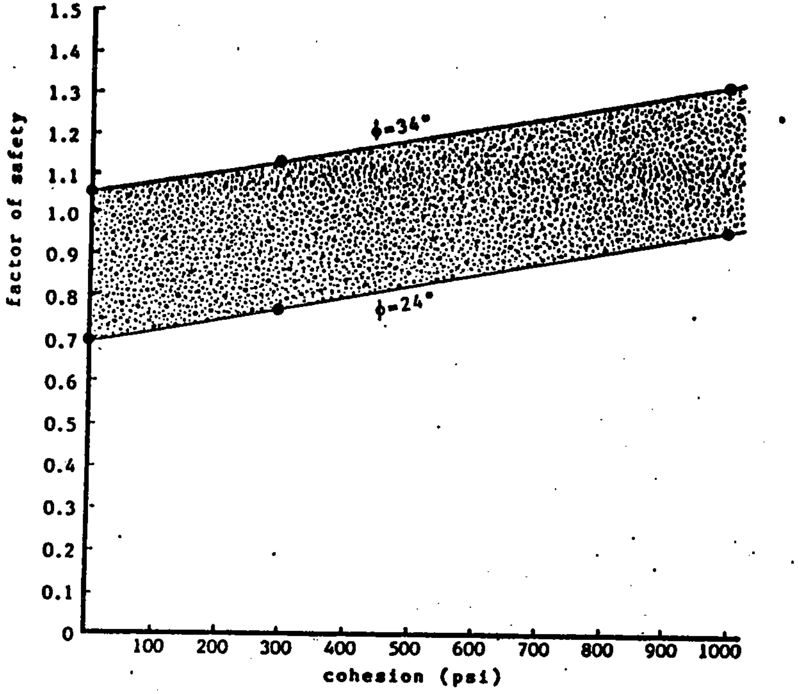

FIGURE 5. Results of sensitivity analysis of soil strength parameters and FOS for most critical surface for the Battle Mountain slide.

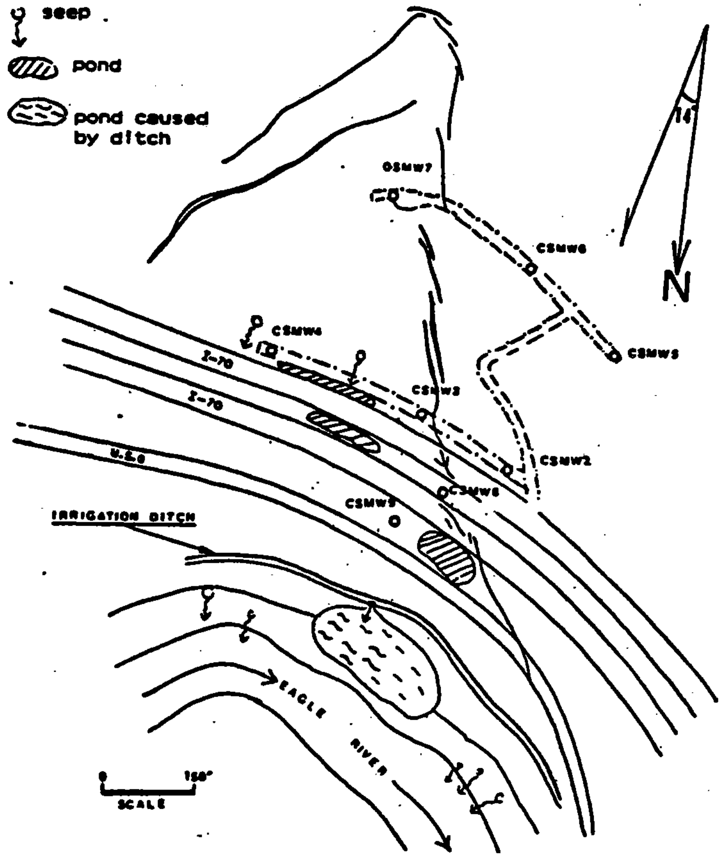
seep
pond
pond caused by ditch
N
14°
CSMW7
CSMW6
CSMW5
CSMW4
CSMW3
CSMW2
CSMW8
CSMW9
I-70
I-70
U.S.6
IRRIGATION DITCH
EAGLE RIVER
0
150'
SCALE

FIGURE 6. Sketch map of the Walcott slide showing locations of ponding and seepage areas.

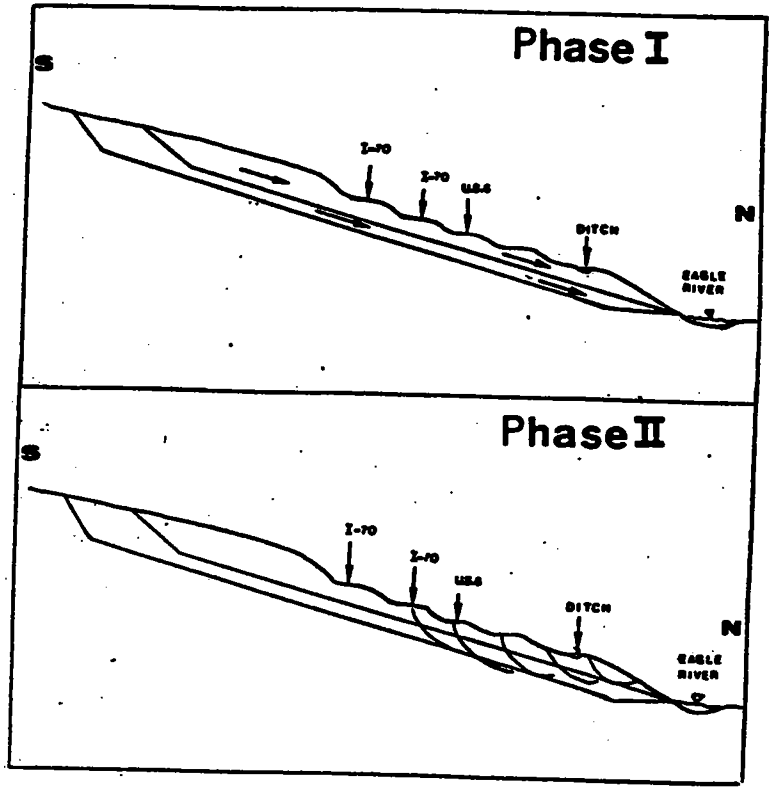
Phase I
S
I-70
I-70
US6
DITCH
N
EAGLE RIVER
Phase II
S
I-70
I-70
US6
DITCH
N
EAGLE RIVER

FIGURE 7. Conceptual cross-section of the Wolcott slide showing the suspected modes of movement for each phase.

exposed cliff of slide materials exhibits several seepage zones. Extensive instability in this toe area results from this undercutting and a "disturbed zone" of slump blocks and scarps is found above the meander and below the irrigation ditch.

Mechanisms of Movement

Subsurface investigations suggest that the movements are relatively shallow dip-slip failures. Two major slide planes at about 12 and 19 feet below the surface have been identified. These seem to form two slide masses, with the shallower mass contained within the larger deeper one.

During the spring of 1985, movement occurred, as shown in figure 7, in two phases:

1) During and subsequent to the snowmelt, saturation occurred at several locations above and under the highways. Part of this was due to inoperative surface drainage components. Movements initiated when the groundwater levels rose to within 12 feet of the surface over most of the slide area but the movement continued for some time after the levels receded.
2) Leakage from the irrigation ditch in late May caused local saturation in the toe area below the highways. Retrogressive failure began in this area and spread up the slope across U.S. 6 and into the westbound lanes of I-70.

The Vail Landslide

Geologic Setting

The Vail landslide is located on the north side of the Gore Valley, opposite the Vail golf course and 1 mile east of the main Vail interchange. Recent movements have affected the westbound lanes of I-70 to a greater extent than the eastbound lanes, and represent a reactivation of an older, prehistoric, post-glacial landslide. This older landslide appears to have resulted from the over steepening of the Minturn Formation valley walls by glacial erosion and their subsequent failure where the rock was weakened by the Spraddle Creek Fault Zone.

The slide materials are thus derived from the various units of the Minturn Formation forming the cliffs behind and above the slide. Drilling has determined that the lower reaches of this slide, at least, have over-ridden gravels which are believed to be outwash from the Pinedale glaciation. In this respect the slide is similar to the Whiskey Creek Slide located a few miles to the west. It is suspected that the slide receives water from the bedrock behind the slide, possibly through fractures associated with the Spraddle Creek Fault, and drains into this gravel layer.

Critical Field Observations

The existing monitoring efforts have been restricted to the lower portions of the slide within 600 feet of I-70 by economic considerations. The current slide movements appear to be mostly restricted to this lower zone, and appear to be a response to the undercutting of the toe of the older large landslide by the construction of Interstate-70. It is unclear at this time whether the upper portions of this old landslide are moving or not. No evidence for such movement was found; however the area is large, steep, and difficult of access, so features suggesting such movement are extremely difficult to find.

Drilling found that the old slide mass appears to have over-ridden a gravel layer which is believed to be glacial outwash associated with the younger Pinedale glaciation (see figure 8). Because the piezometer holes penetrated this gravel layer, and were fully perforated, they appear to have acted as local drains, and for most of the observation period have monitored the water levels in this gravel. The gravel appears to have a water level which is similar to the Gore Creek level; it is significantly below the slide failure plane.

Other observations suggest that the slide probably contains perched water tables and locally saturated zones at much higher elevations than shown by these piezometer holes. Observed seepage from the exposed face on the eastern portions of the slide, poor drainage and ponding along the north shoulder and median of Interstate-70, and infiltration of surface water into the slide all point to the conclusion that locally saturated conditions exist within the lower portions of the slide.

Movements were measured by use of six EDM reflector stations which were observed from a single instrument station. These stations became operative after the bulk of the 1985 movements had occurred. Relative movements were obtained by surveying along 4 stake lines on the lower portions of the slide, and by measuring offsets along the inside edge of pavement of the westbound lanes of the Interstate. These measurements indicate that the lower portions of the slide are moving as two different zones.

The movements of the slide in recent years have destroyed or distrupted the original drainage facilities along the Interstate. Ponding of surface water, and saturation of the pavement subgrade results. This saturation locally aggravates the pavement distress.

Mechanisms of Movement

The currently available data serve to characterize the basic movement phenomena for the Vail slide, but are inadequate to fully define such movements or to fully evaluate the effectiveness of remedial measures. Further monitoring seems warranted.

As was noted above, the lower portions of the slide appear to be moving as two different zones. The eastern zone appears to be failing as a series of relatively shallow slumps, probably due to the removal of the toe material by the Interstate construction. The western zone appears to be a more deep seated rotational failure. The movement of this western portion is causing the distortion of the Interstate-70 pavement

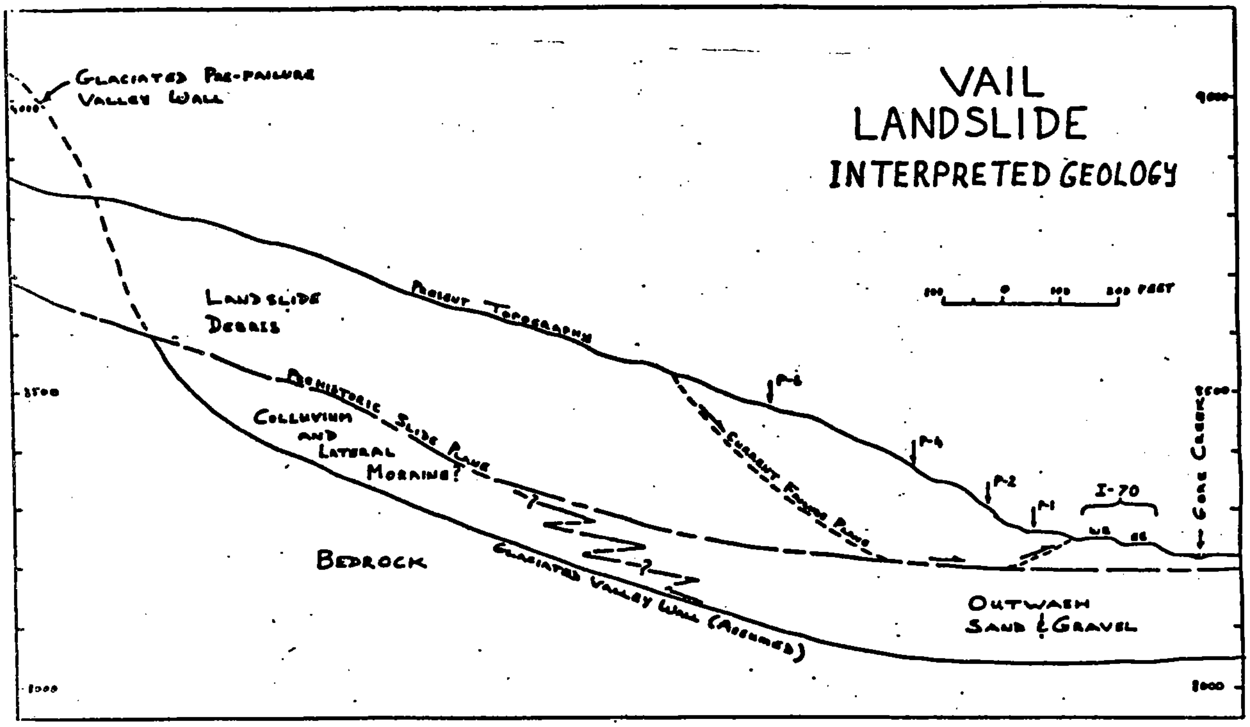
VAIL
LANDSLIDE
INTERPRETED GEOLOGY
Glaciated Pre-failure Valley Wall
Landslide Debris
Present Topography
Prehistoric Slide Plane
Current Failure Plane
Colluvium and Lateral Moraine?
Bedrock
Glaciated Valley Wall (Assumed)
Outwash Sand & Gravel
P-6
P-4
P-2
P-1
I-70
WB
EB
Gore Creek
100 0 100 200 FEET
9000
8500
8000

FIGURE 8. Cross-section of the Vail Landslide.

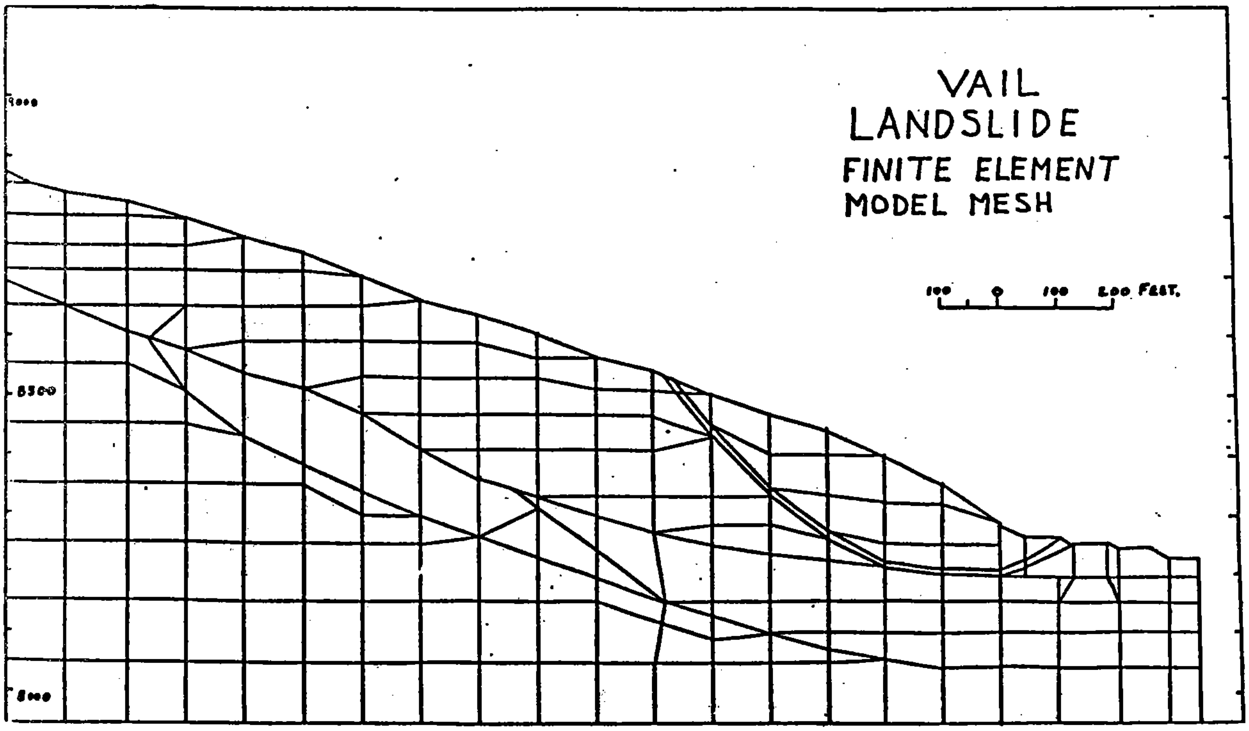
VAIL
LANDSLIDE
FINITE ELEMENT
MODEL MESH
100 0 100 200 FEET.
9000
8500
8000

FIGURE 9. Finite element model mesh for the Vail Landslide.

structures. The two zones appear to be diverging slightly, with the western zone having a westward component of movement, and the eastern zone having an eastward component of movement. Such a pattern of movements suggests, but does not prove, that upper portions of the slide may also be moving and are supplying a driving force to the lower sections.

SELECTED COMPUTER PROGRAMS

STABL Program for Slope Stability Analysis

This project used a computer code STABL developed at Purdue University in 1975 (Seigel, 1975a; 1975b) and since reported in the open literature (Boutrop and Lovell, 1980; Siegel and others, 1981) and adapted by several agencies. The program has evolved through several generations in the intervening years; the version used in these studies is referenced as STABL3. In 1985 an enhanced version, called STABL4 was announced (Lovell and others, 1985), along with an IBM-PC version called PCSTABL4 (Carpenter, 1985). However, these newer versions were not available at the time these anlayses began and their enhancements were not critical to this study.

STABL performs slope stability analysis by a 2-D limiting equilibrium method. It uses the method of slices to analyze the slope and calculates the factor of safety (FOS) according to the simplified Janbu or Bishop methods for non-circular and circular surfaces, respectively. STABL is the only known program to contain searching routines for shapes other than circles. This was important in analyzing the Wolcott slide which had markedly non-circular failures.

The STABL3 coding was initially operated on the CSM VAX-8600 computer. It was subsequently modified to run on an IBM-PC, following the recommendations given in Lovell and others (1985). The versions used here did not have operational plotting facilities. This was due largely to hardware and software support restrictions, caused by a facilities upgrading that was currently underway at the CSM computing center. The lack of such plotting facilities was an inconvenience.

Accuracy of Stability Analysis Calculations

The authors of STABL have addressed the concerns about the inherent accuracy of the answers derived by STABL. For some situations, it is possible to run comparisons with other available programs. This was performed for some analyses at the Vail slide and very close agreement was obtained between the values provided by STABL and those by another PC-computer based Bishop circle program.

A series of standard problem examples, with solutions are available in the STABL documentation, and these were used to check results.

As a result of these considerations, the current analyses support the contention of the Purdue researchers that STABL supplies generally conservative FOS values.

Seepage Assessment Program

In order to assess the effect of an interceptor drain on the stability of the landslide, a reasonable estimate of the upgradient and downgradient influence of the drain is required. A PC-based computer program to solve for Glover's solution for the groundwater flow into a trench was used (McWhorter and Sunada, 1974; Nasser, 1986). This method assumes non-steady flow in a homogeneous, isotropic aquifer of infinite extent, relatively small drawdowns compared to the saturated thickness, and other assumptions which are likely to be only approximately true in a landslide mass. However, the approach seemed a reasonable approximation for the Wolcott and Vail landslides.

Required data includes values for permeability and porosity. When these are not accurately known, a range of values may be selected and drawdown values for each produced. Data for the Wolcott landslide are given in Table 1 to illustrate this process.

STABILITY ANALYSIS PROCEDURE

The procedures used to perform the stability analysis and then to evaluate the effectiveness of remedial measures were similar for all three landslides. They involved six steps:

1) Identify the appropriate geometries for the STABL3 computer model;
2) Perform a sensitivity analysis to determine the effects of changing the strength parameters for cohesion (C) and angle of internal friction (phi) on the FOS calculations;
3) Selection of the characteristic values of cohesion and angle of internal friction which appear to best explain the field behavior of the landslides;
4) Perform stability analysis computations to define the failure mechanism(s) using the values determined in the previous steps;
5) Analyze the effects of drainage on the water table geometries by appropriate methods; and
6) Apply the results of such drainage estimates to modify the field conditions being modelled, and reanalyze the stability using STABL3.

Importance of Sensitivity Analysis Process

The stability of the landslide will obviously change when the material properties change. Unfortunately, laboratory determinations of soil parameters such as cohesion and angle of internal friction (phi) often are not fully representative of these values for the landslide mass. This may be due to inherent inhomogeneity within the sliding material, or "scaling-up" problems between the small laboratory samples and the much larger landslide mass. Such changes in the FOS are not readily predictable for all combinations of c and phi. Accordingly the procedure followed in all these studies, and recommended for any future studies, was to run a series of analyses with varying values of c and phi and prepare a diagram such as shown in figure 5 which relates the most critical FOS to such changes.

Using this diagram, it was then possible to choose a few (perhaps two or three) combinations of c and phi which would give a most critical FOS of around 0.97 to 0.98. Such a FOS was chosen because all these landslides were known to be failing.

A sequence of further STABL3 analyses were run using the selected combinations of c and phi to determine if any, or even all, of them produced failure surface geometries that satisfied the field observations. The combination of such values which most closely replicated failure geometries observed in the field was then used in further analyses.

These analyses showed that phi generally was more critical than c in affecting the stability and geometries of failure in these landslides. Some additional analyses of this type were repeated on the Vail landslide with different assumed density values for the sliding materials. In this case, it was found that as the density of the sliding material was reduced, the other factors kept constant, the FOS of the slide was reduced. This result could not have been predicted without such sensitivity analyses.

Evaluation of Drainage Measures

In all these landslides, drainage was the most logical stabilization method. The size, topography, and geohydrological conditions at each site dictated such a solution. The methods for evaluating the effects of drainage on the landslides varied from site to site.

At Battle Mountain, the steep terrain and geometry of the failure surface suggested the use of horizontal drains to produce the necessary drainage. No simple method of assessing the hydrological effects of such drains appeared appropriate, so the existing water table was simply lowered five and ten feet below its present position, and new FOS values were computed. These showed marked improvements and accordingly a horizontal drain installation has been proposed.

At Wolcott, the shallow planar failure and generally even shallower depths to water, suggested the installation of a French Drain to capture and drain the subsurface water (see figure 10). The effect of such a drain was modelled on the IBM-PC using a program which implemented Glover's solution for seepage into a trench (McWhorter and Sunada, 1974; Nasser, 1986). A series of analyses were performed with different values of permeability and drainable porosity to assess the probable effectiveness of such an installation (see Table 1).

Such values were then used to revise the ground water table elevations and new FOS values were computed using STABL3. Results obtained for Wolcott are shown in Table 2. Figure 11 shows the resulting relationships between the hydraulic conductivity and the factor of safety for the Wolcott landslide. The FOS for both failure surfaces increased with increasing hydraulic conductivity. Higher hydraulic conductivity increases the radius of influence of the drain, thus increasing its

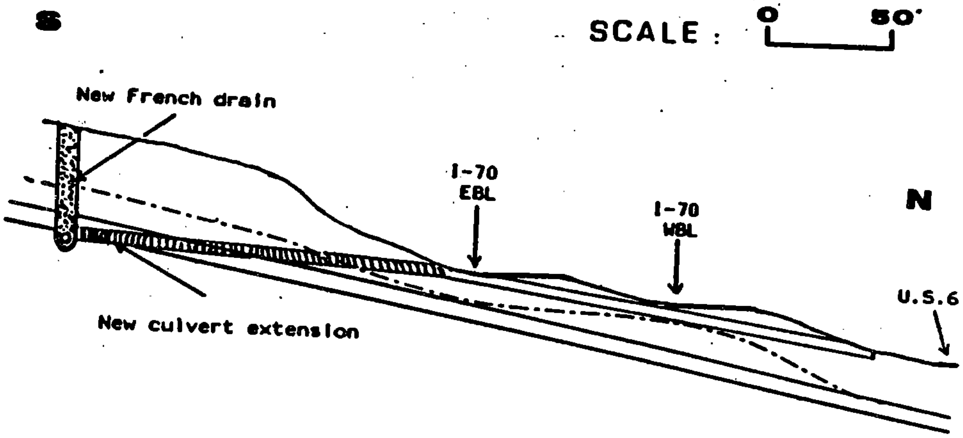
S
SCALE : 0 50'
New French drain
I-70
EBL
I-70
WBL
N
U.S.6
New culvert extension

FIGURE 10. Proposed new drainage system for the Wolcott landslide.

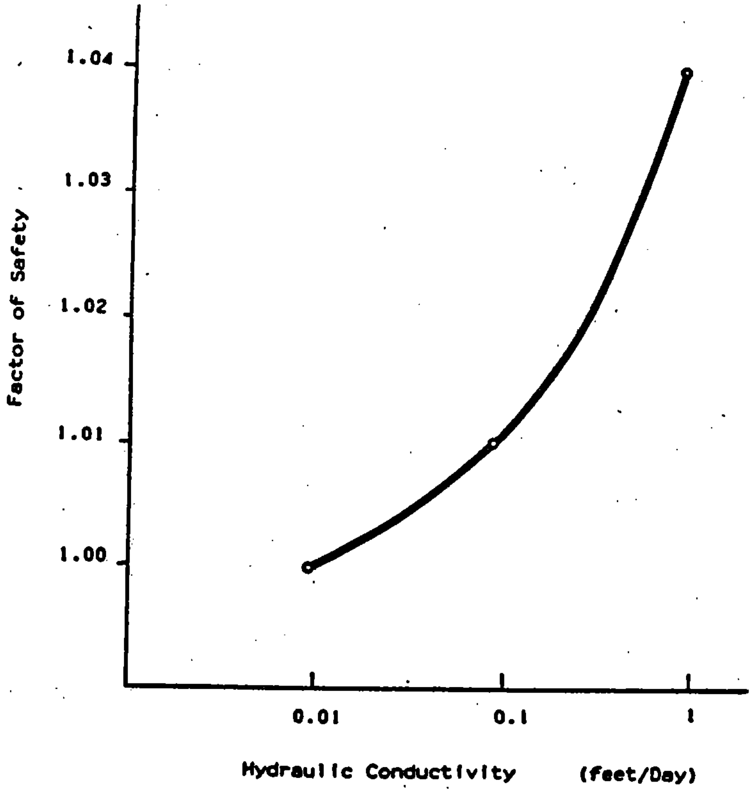

FIGURE 11. Relationship between factor of safety and hydraulic conductivity for drained conditions at the Wolcott landslide.

TABLE 1

DRAWDOWN DATA FOR THE WOLCOTT SLIDE USING GLOVER'S EQUATION

Distance,(ft)	Drawdown,(ft)					
	K=0.01 ft/day		K=0.1 ft/day		K=1 ft/day	
	t=1 year	t=2 years	t=1 year	t=2 years	t=1 year	t=2 years
50	1.9576	4.8367	12.013	14.225	17.370	18.136
100	0.0186	0.3848	5.903	9.183	14.812	16.298
200	0.0000	0.0000	0.725	2.774	10.158	12.793
300	0	0	0.037	0.527	6.413	9.650
400	0	0	0.000	0.061	3.708	6.982
500	0	0	0.000	0.004	1.957	4.836
600	0	0	0	0.000	0.940	3.203
700	0	0	0	0.000	0.409	2.026
800	0	0	0	0	1.617	1.222
900	0	0	0	0	0.058	0.703

Average saturated thickness: 25 feet
Drainable formation porosity: 0.02
Drawdown at interface: 20 feet

TABLE 2

STABILITY ANALYSIS OF THE WOLCOTT SLIDE

Failure Surface	Factor of Safety	Factor of Safety		
	At Maximum Observed water table	Drained After 1 Year		
		K=0.01	K=0.1	K=1 (ft/Day)
Deeper	0.949	1.003	1.015	1.045
Shallower	0.994	1.034	1.042	1.063

efficiency in dewatering the landslide, and this in turn causes an increase in the FOS. Even with a very low value for hydraulic conductivity, the factor of safety of both failure surfaces increased above 1.0. Because the results seemed favorable throughout the anticipated range of values for these parameters, a French Drain installation is among the stabilization measures recommended at Wolcott.

At Vail, the solution to the drainage problem is more complex. Horizontal drains cannot be located to reach adequately into the slide. Similarly, the slide is too deep for a traditional French Drain. However, the apparent draining effect from the slide into the underlying gravels, caused by the piezometer installations, suggested that a line of large diameter wells might be effective drains. Much further testing remains to prove this concept workable, however, some initial computations were undertaken.

The Glover seepage model was again used to assess the drawdown effects of a line of wells at three different locations, with different effective drainage rates and different permeability and porosity values. There are many approximations and assumptions made with this approach and the results are very approximate. They do show, however, that if such drainage can be achieved, the landslide FOS will be increased by 3 to 12 percent and stability is likely to be achieved. They also showed that, under some rather extreme conditions, drainage in the immediate toe area, caused by a lined of drains on the north shoulder of I-70, might temporarily reduce the FOS. Accordingly such a remedial measure was not recommended.

FURTHER WORK

The analysis of the proposed drainage measures at the Vail Slide uncovered the limitations of using Glover's solution to evaluate drainage systems. Methods are needed which would allow modelling of the hydrodynamics of the suspected subsurface flow systems within the sliding mass. This can be accomplished with finite element flow modelling techniques.

At the present time a finite element ground water model is being modified to operate on the IBM-PC. A finite element mesh has been designed for the Vail slides to allow such experimentation (see figure 9). Further analyses of the Vail slide using these tools are planned.

The Vail Slide reactivated after a wet period in July 1986. New damage to the I-70 pavement occurred which required some regrading and repaving. Concerns about a truly catastrophic failure have once again been raised. It is hoped that the use of a combination of these analytical tools will help evaluate the Vail Slide and demonstrate the value of these methods.

CONCLUSIONS

The use of modern computer programs on personal computers to perform slope stability analysis is becoming commonplace in many engineering offices. A variety of these programs are offered by several vendors with a wide range of prices. No attempt has been made to evaluate these competing programs.

The family of STABL computer programs developed over the past decade at Purdue University with FHWA financial support do represent a powerful and convenient-to-use system. Our experience indicates that the system developers have provided easy to manage data entry requirements and data checking with understandable error messages. This is important to many engineers who may use the programs on an irregular basis.

The FOS values by computed by STABL appear to be conservative, and for those situations which can be checked by other procedures, the values are in close agreement. We have not had the opportunity to try the latest versions, STABL4 and PC-STABL4, but would recommend that these packages be considered when slope stability programs are begin acquired.

The use of PC-computers offers considerable economic advantages. However, adequate capacity on the PC is absolutely essential, as is the mathematical co-processor (the 8087 chip). We operated on a PC-computer having 640K memory and dual floppy drives. A hard disk would be helpful.

We did not have access to plotting facilities during these analyses, for reasons which were beyond our control. The lack of such plotting capabilities was inconvenient, but they are not mandatory. Nevertheless, efficiency of the analysis would be markedly improved with plotting capability.

Computations are slower on the PC than on the mainframe. On the other hand, the computer usually can still produce more calculations in a given time than the engineer can properly evaluate. Costs of a PC machine are relatively modest and are basically a fixed, one-time, capital cost. The cost of computing several alternatives is thus negligible, in contrast to the time and resource charges encountered on time-sharing mainframes.

When these considerations are combined with the ability to perform a variety of hydraulic simulations on the PC, and thus iteratively evaluate alternative remedial measures to stabilize a slope, the advantages of working with PC-based programs become very large.

REFERENCES CITED

Boutrup, E. and Lovell, C.W., 1980, "Searching Techniques in Slope Stability Analysis", Engineering Geology, Vol. 16, No. 1/2, July. Special Issue on Mechanics of Landslide and Slope Stability, pp. 51-61.

Carpenter, J.R., 1985, "PCSTABL4 User Manual", Purdue University, School of Civil Engineering, West Lafayette, Indiana, 87 pp.

Fernandez, Javier, 1986, "Analysis of a Landslide along Interstate-70 at Vail, Colorado," Master of Engineering Report, Colorado School of Mines, Golden, Colorado (in press).

Lovell, C.W., Sharma, S., and Carpenter, James R., 1985, "Introduction to Slope Stability Analysis with STABL4", Purdue University, School of Civil Engineering, West Lafayette, Indiana, 124 pp.

McWhorter, D.B., Sunada, D.K., 1974, "Groundwater Hydrology and Hydraulics," Water Resources Publications, Fort Collins, Colorado, 345 pp.

Nasser, Khalil, 1986, "Slope Stability Analysis of the Wolcott Landslide, Eagle County, Colorado", Master of Engineering Report, ER-3110, Colorado School of Mines, Golden, Colorado 111 pp.

Shine, Brendan, 1985, "Engineering Geology of the Battle Mountain Landslide, South of Minturn Colorado," Master of Engineering Report ER-3139, Colorado School of Mines, Golden, Colorado 125 pp.

Siegel, R.A., 1975a, "Computer Analysis of General Slope Stability Problems," Joint Highway Research Project No. 75-8, School of Civil Engineering, Purdue Univeristy, West Lafayette, Indiana, May, 210 pp.

Siegel, R.A., 1975b, "STABL User Manual," Joint Highway Research Project No. 75-9, School of Civil Engineering, Purdue University, West Lafayette, Indiana May, 104 pp. (Revised by E. Boutrup, June, 1978).

Siegel, R.A., Kovacs, W.D., and Lovell, C.W., 1981, "Random Surface Generation in STability Analysis", Journal, Geotechnical Engineering Division, ASCE, GT7, July, pp. 996-1002.

GENERAL METHOD FOR THREE DIMENSIONAL SLOPE STABILITY FEATURING RANDOM GENERATION OF THREE DIMENSIONAL SURFACES

by
Jose Eduardo Thomaz[1]
Charles William Lovell[2]

SYNOPSIS

The popularity of the computer program STABL (Siegel, 1975), and the promising results found in former studies at Purdue University, using three dimensional surfaces, encouraged the authors to expand the concepts of random generation of surfaces to three dimensions. The method of analysis proposed by Chen (1981) was expanded to accept more complex soil profiles. These methods and the results of a few parametric studies are presented in this paper.

INTRODUCTION

In the last two decades, the area of slope stability analysis has received a lot of research attention. Most of these approaches have been developed in the search of a better, more realistic, representation of the physical phenomena involved in a landslide. These approaches include limit equilibrium analysis, finite element analysis and, more recently, variational calculus techniques. Nevertheless, most of the work currently available in the literature approaches the problem two dimensionally.

Since all slides are three dimensional and there are many practical situations where two dimensional analysis can be non-representative, the authors developed a program with features to let the three dimensional analysis of slopes be performed with relative simplicity. For this purpose, a routine for the generation of three dimensional surfaces was developed. This routine will let the program perform an automatic search for the critical 3D-surface, inside a specific region of the slope. A general method for the analysis of the equilibrium equations was also incorporated, and both forces and moment equilibrium are satisfied. The resulting program, called 3D-PCSTABL (Thomaz, 1986), runs on IBM-PC microcomputers or compatibles, with 256 Kb of memory and two disk drives.

RANDOM GENERATION OF THREE DIMENSIONAL SURFACES

The first problem to be addressed was to find a way to define the geometry in such a way that different soil and water conditions could be represented. It should also contribute to efficiency in the process of searching for the critical surface.

---

1. Research Assistant, and 2. Professor of Civil Engineering, Purdue University, West Lafayette, Indiana.

The system for representing the geometry of the problem consists of a three dimensional cartesian system. The engineer will define three orthogonal axes, ""X", "Y" and "Z". The horizontal plane will be defined by axes"X" and "Y". The axis "Z" will represent the elevations of the layers and ground profiles (Figure 1). The next step consists of defining the points (coordinates) that will represent the geometry. The way these coordinates are to be defined can be seen in Figure 2. The user defines a grid, consisting of cross sections parallel to the "X" and to the "Y" axis. The spaces between these cross sections do not need to be the same. Nevertheless, it is highly recommended that they do not present large variations. The intersection of these cross sections are the points that will define the geometry of the problem. They can be perceived as boreholes, where the elevations of the ground, different soils, and ground water are to be defined. The coordinates should be defined so that the slide occurs in the "Y" direction.

DEFINITION OF SEARCHING BOUNDARIES

In order to optimize the surface searching process, appropriate boundaries must be defined. The choice of appropriate boundaries is important to reduce the amount of time involved in the search, by avoiding the generation of "useless" surfaces. "Useless" surfaces are those with little or no probability of being critical (as surfaces passing through sound rock, for instance). Some engineering judgment is thus required, when defining the region to be searched. It should be noted that even if the boundaries are very wide, the resulting critical region will still be the same. Nevertheless, the amount of time necessary to arrive at this final region will be much larger, since a higher percentage of the surfaces generated will probably lie outside of the critical region of the slope.

The user has to define a main axis of sliding, which will govern all the surface generation process. The process will take place on the left and right sides of the axis, independently. This axis would be the axis of symmetry if symmetric surfaces were to be generated.

Boundary restriction must be defined in both "X" and "Y" directions. These boundaries will be used to generate the intersection between the ground surface and the sliding three dimensional surface. Boundary restrictions in the "Z" direction also must be defined, and will be used to form the "body" of the sliding surface. Figures 3a and 3b show the way these boundary limits are established.

The points that will form the three dimensional surfaces are then generated randomly inside the pre-defined boundaries. In order to keep the surfaces with acceptable shapes, there are random angular restrictions, which vary according to the position of the points being generated. Figure 4 shows how the generation of

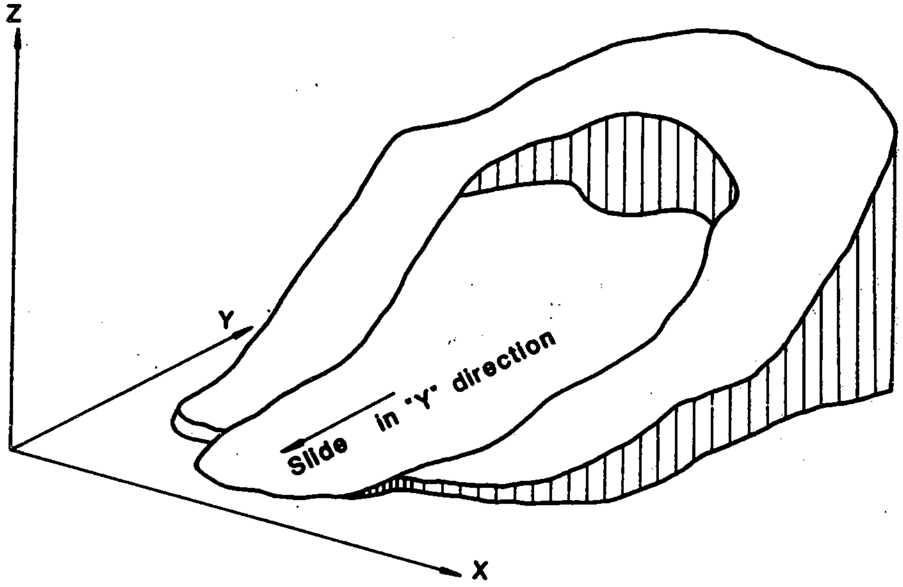
Z
Y
X
Slide in "Y" direction

Figure 1 - System of Coordinates

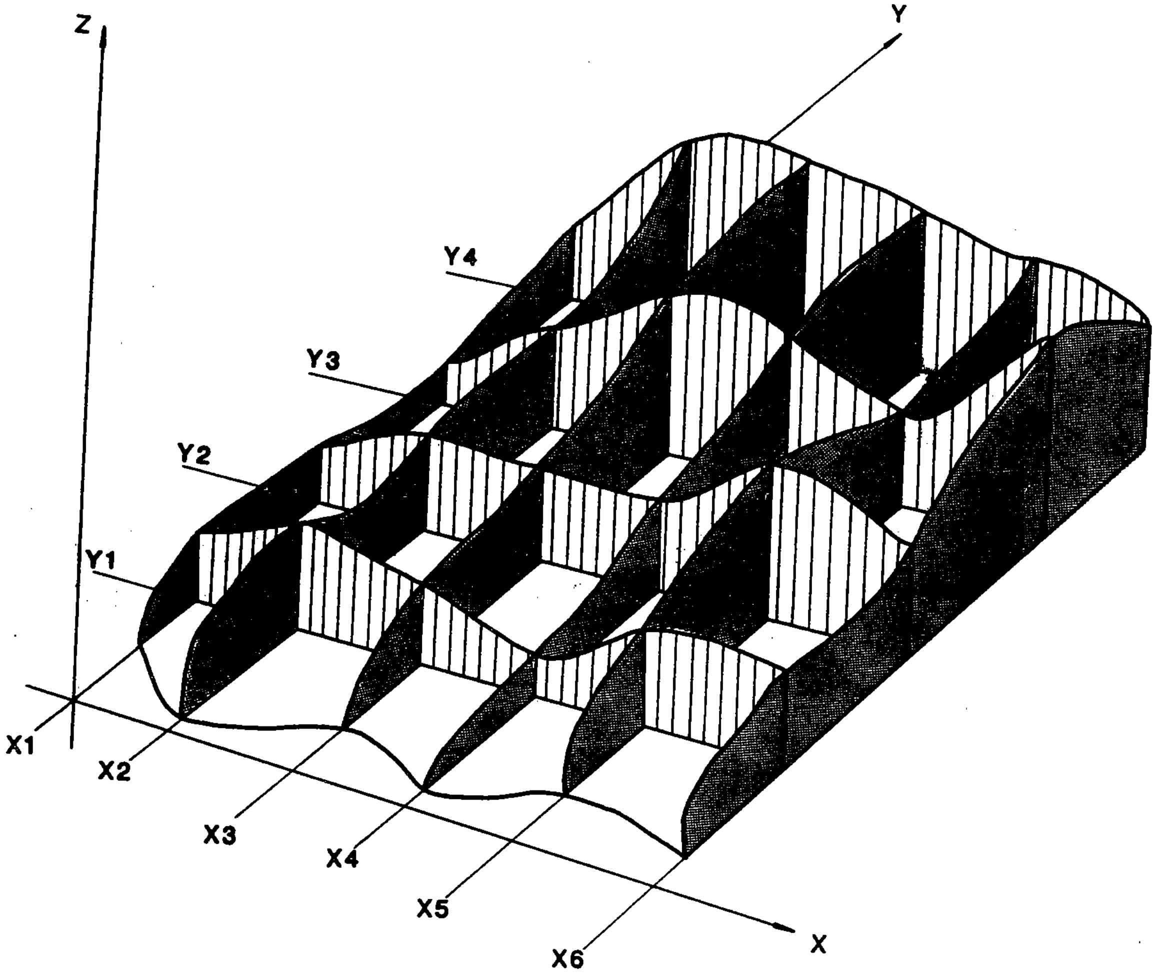
Z
Y
Y4
Y3
Y2
Y1
X1
X2
X3
X4
X5
X6
X

Figure 2 - Grid of Cross Sections

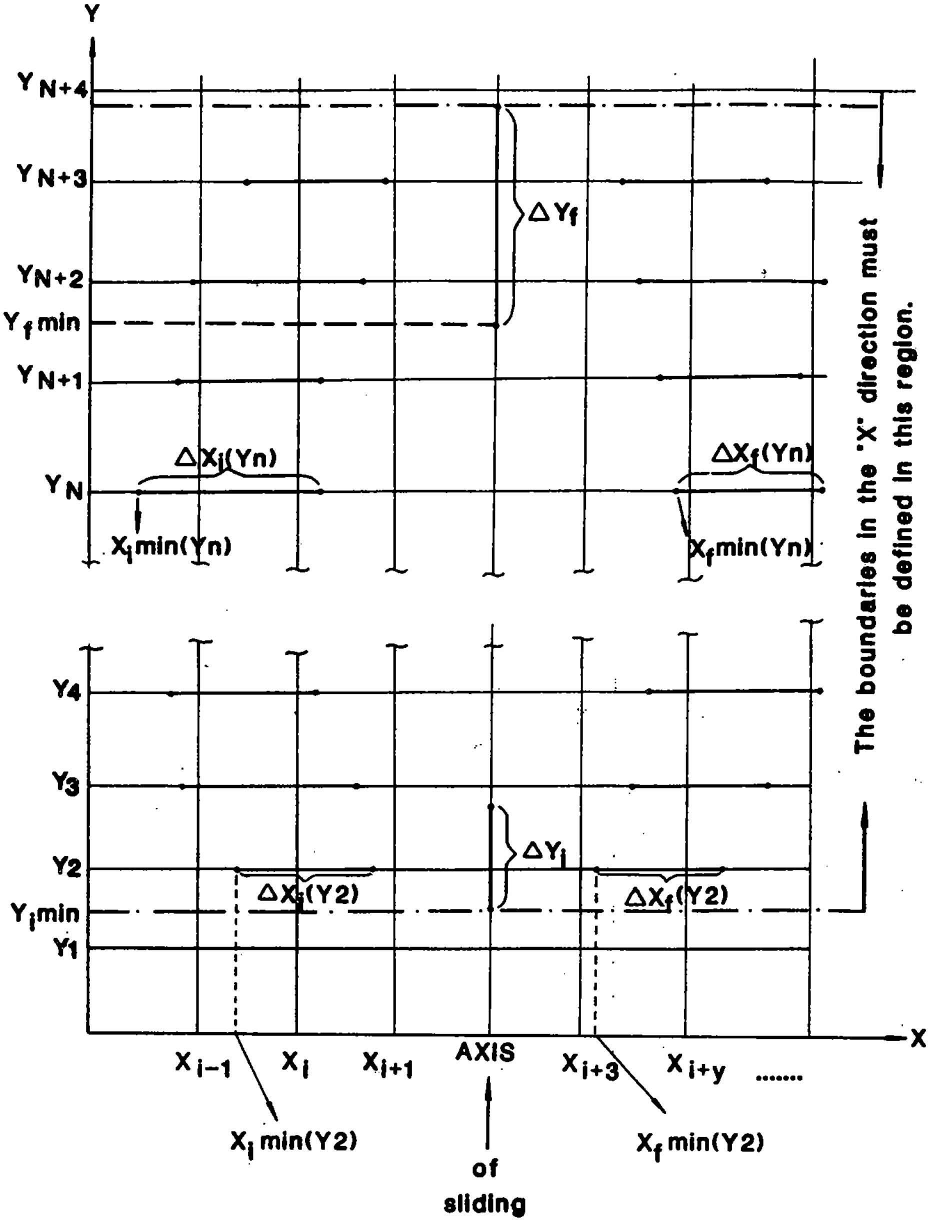
Y
Y_{N+4}
Y_{N+3}
ΔY_f
Y_{N+2}
Y_f min
Y_{N+1}
$\Delta X_i(Y_n)$
$\Delta X_f(Y_n)$
Y_N
X_i min(Yn)
X_f min(Yn)
The boundaries in the 'X' direction must be defined in this region.
Y_4
Y_3
ΔY_i
Y_2
$\Delta X_i(Y2)$
$\Delta X_f(Y2)$
Y_i min
Y_1
X
X_{i-1}
X_i
X_{i+1}
AXIS
X_{i+3}
X_{i+y} ....
X_i min(Y2)
of sliding
X_f min(Y2)

Figure 3a - Searching Boundaries in the "X" Direction

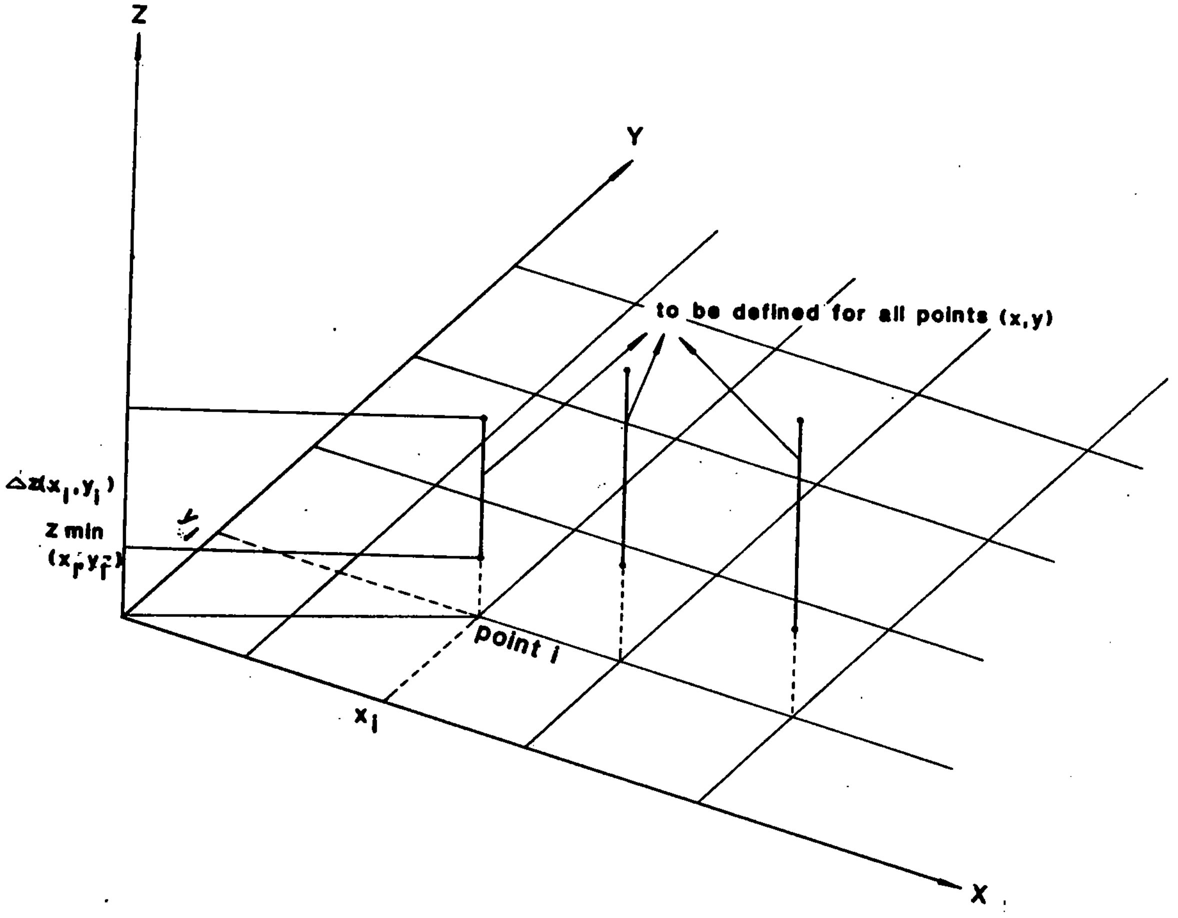

Z
Y
to be defined for all points (x,y)
Δz(x_i,y_i)
z min
(x_i,y_i)
y_i
point i
x_i
X

Figure 3b - Searching Boundaries in the "Z" Direction

TOP VIEW OF PART OF A SURFACE

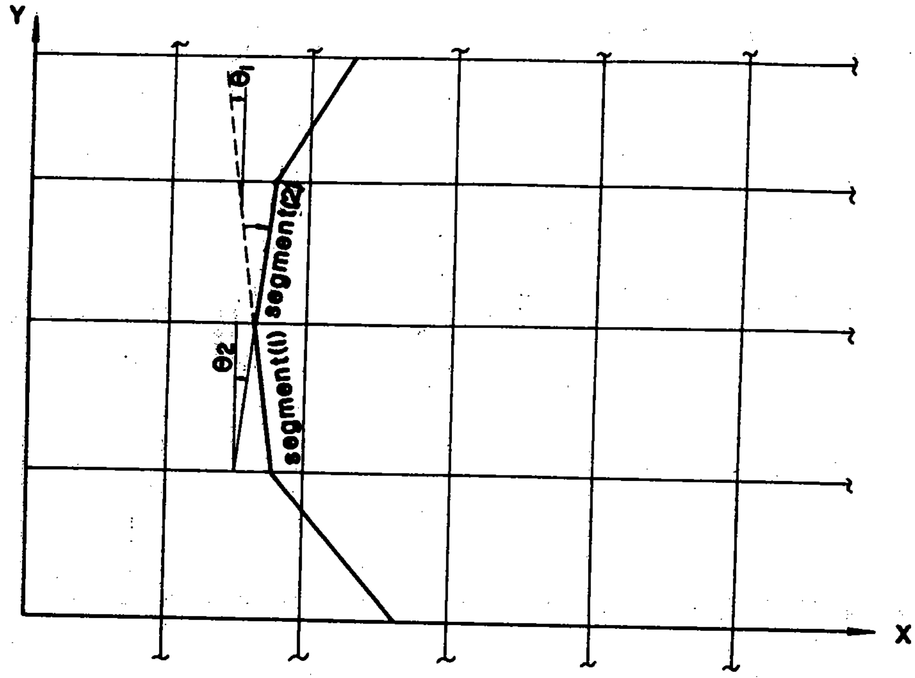
Y
X
θ1
θ2
segment(1)
segment(2)

$$\Delta\theta = \theta_1 - \theta_2 = -45° R_1^2 + (45° R_1^2 + 45°) R_2^{R2}$$

Figure 4 - Angular Restriction Criteria for Surface Generation

the surface's is controlled by the angular restrictions, and Figure 5 displays a general view of how the surfaces are formed.

METHOD OF ANALYSIS

The previous item presented the methodology for the generation of three dimensional surfaces. It became evident that the failure surfaces generated have a very general nature and can cover a large variety of shapes. The surfaces will represent slides that can have either a translational or a rotational nature, and in order to calculate the factor of safety of both types, a general method of analysis had to be developed.

Similarly to the usual method of slices, the approach used was to divide the soil mass in columns. As it was shown by Chen (1981), the number of parameters included in a three dimensional analysis is much larger than in a two dimensional analysis. Figure 6 shows the forces acting on a column. In order to decrease the level of indetermination of the problem, assumptions were made to eliminate or fix the value of some unknowns. The assumptions made in this work follow the ones proposed by Chen (1981), and are listed as follows:

- The failure mass is symmetrical about the main axis of sliding.

- Direction of movements along the "Y" direction only, and consequently the shear stresses along the "X" direction are zero.

- The forces on the sides of the columns will be assumed as acting along the central vertical line of each side.

- The intercolumn shear forces are assumed to be parallel to the bottom of the side of the column. The cohesive part of the shear force will act at a half height from the bottom and the frictional part of the shear force will act at the centroid of the normal stress distribution along the sides, which is considered linear between layers. The inter-column shear forces at the two ends of each column are assumed to be a function of their positions, taking the largest values a the outmost points and decreasing to zero at the central section because of no relative movement in the middle section of the surface.

- The interslice forces on the sides of the column are assumed to have the same inclination (Theta) throughout the whole failure mass.

After using the above assumptions to reduce the number of unknowns of the problem, and bringing the system to equilibrium of forces and moments, we arrive at a system of two non-linear equations and two unknowns: (1) The interslice force inclination and (2) the factor of safety of the failure surface. The system of equations can be solved by successive iterations, using a

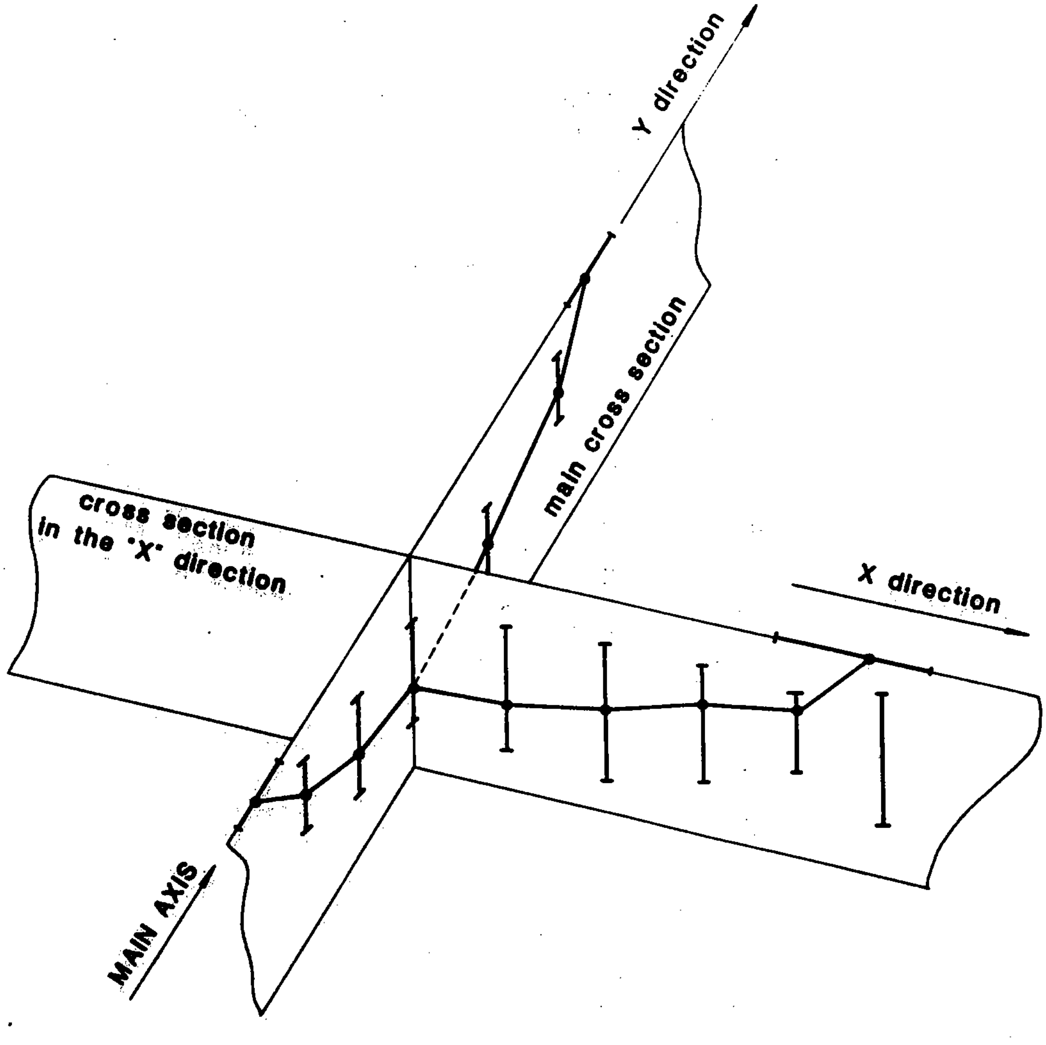
Y direction
main cross section
cross section
in the 'X' direction
X direction
MAIN AXIS

Figure 5 - Process of Generation of 3D Surfaces

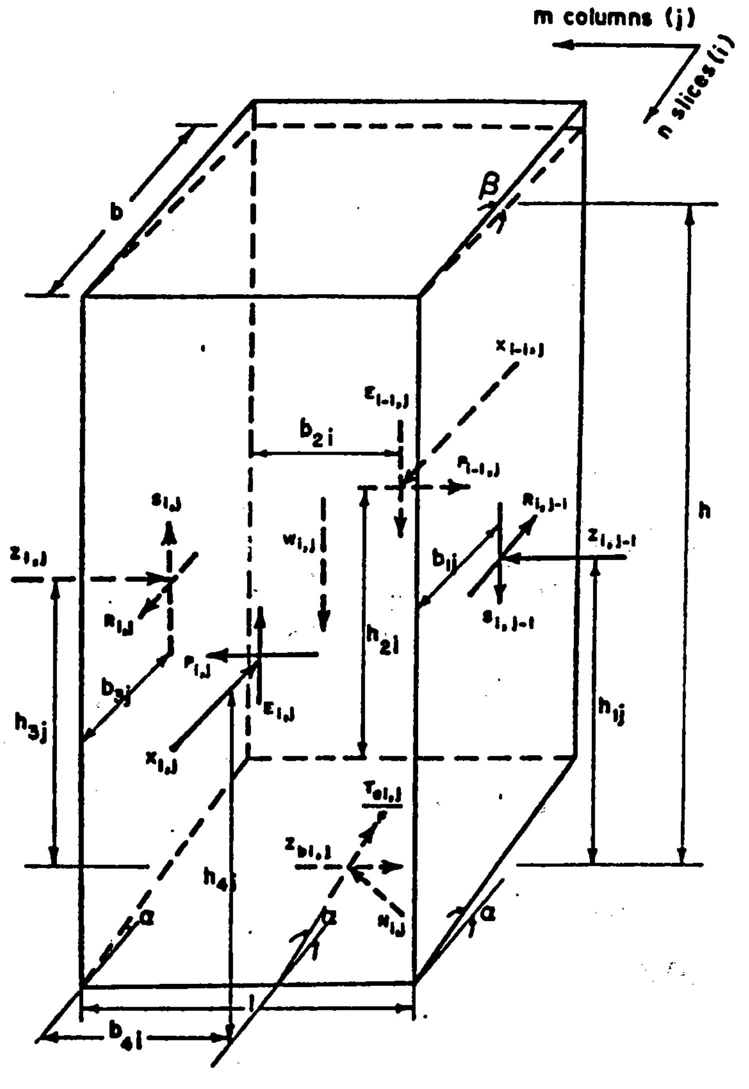
m columns (j)
n slices (i)
b
β
h
x i-1,j
E i-1,j
b2i
P i-1,j
S i,j
W i,j
R i,j-1
Z i,j-1
Z i,j
b1j
R i,j
P i,j
h2i
S i,j-1
b3j
E i,j
h1j
h3j
X i,j
T αi,j
Z bi,j
h4i
α
N i,j
l
b4i

Figure 6 - Free Body Diagram of a Column
(from Chen, 1981)

modified Newton's method.

RESULTS AND COMPARISONS

After the methods were implemented in a computer program called 3D-PCSTABL, a series of studies were performed comparing its results with the ones obtained by the program PCSTABL5 (Carpenter, 1985), which incorporates conventional methods of slices, as Simplified Bishop, Simplified Janbu and Spencer, as well as routines for random search of two dimensional surfaces.

These analyses addressed four major independent variables:

1. Influence of the strength parameters and slope inclination on the ratio between three and two dimensional factors of safety.
2. Influence of the strength parameters and slope inclination on the agreement between the position of the three dimensional and the two dimensional most critical surfaces (checked on the main axis cross section).
3. Influence of the strength parameters and the slope inclination on the shape of the most critical surfaces.
4. Influence of pore water pressure.

In all the cases, the soil is assumed to be homogeneous, and the searching boundaries were initially very general, being progressively refined until the critical surface was established. Different combinations of cohesion intercept and friction angle were tried, and the trends in the shapes of the most critical surfaces, and the position agreement between the 3D and the 2D critical surfaces, and the ratio between the 3D and the 2D factors of safety were observed. The slope characteristics remained the same. The height of the slope was 6.1 m (20 ft), and the slope was variable, assuming inclinations of 1.5:1, 2.5:1 and 3.5:1. The density (unit weight) of the soil was considered to be 1930 kg/m3 (120 pcf). Cases were studied for two different water conditions: slope without water (ru = 0) and slope with ru = 0.5. The most interesting results are summarized in the following paragraphs.

The values of the critical factors of safety found by the two programs, for all cases analyzed, are presented in Table 1, and the curves for the values of the ratios between the 3D and the 2D factors of safety are plotted in Figure 7 (for ru = 0.0). It is noted that:

Table 1 - 3D and 2D Factory of Safety

Slope Angle	Case	ru = 0.0 Factors of Safety 2D	ru = 0.0 Factors of Safety 3D	ru = 0.5 Factors of Safety 2D	ru = 0.5 Factors of Safety 3D
1.5:1	1	1.608	1.875	0.770	0.897
	2	2.019	2.080	1.556	1.596
	3	2.439	2.456	2.165	2.188
2.5:1	1	2.538	2.560	1.206	1.129
	2	2.717	2.789	1.932	2.060
	3	3.245	3.339	2.587	2.965
3.5:1	1	2.540	2.530	1.440	1.525
	2	3.313	3.605	1.006	1.206
	3	3.157	4.181	2.691	3.639

1 - $c' = 0.0$ kPa $\phi' = 40^{o}$

2 - $c' = 14.4$ kPa $\phi' = 25^{o}$

3 - $c' = 28.7$ kPa $\phi' = 15^{o}$

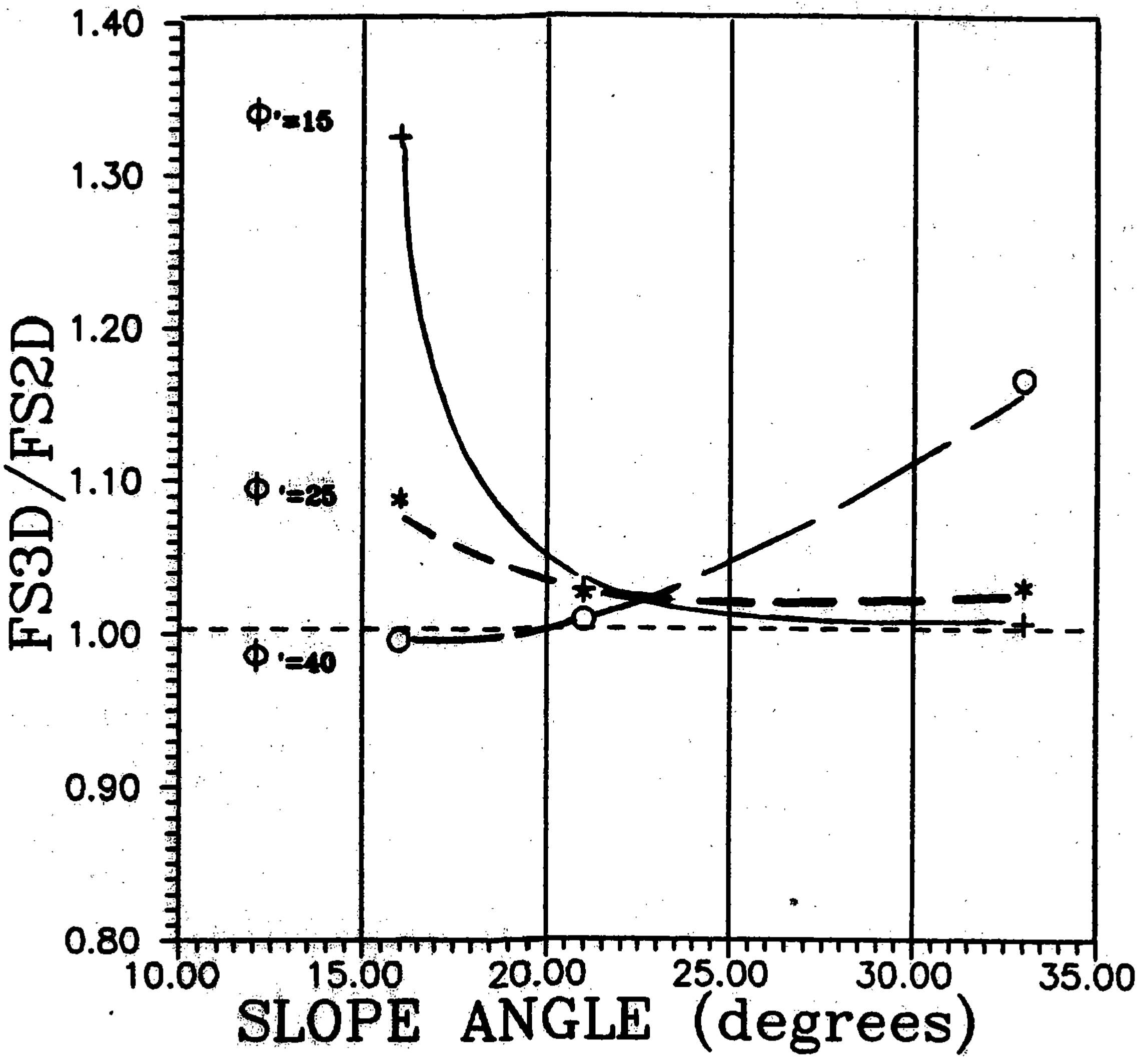

Figure 7 - Ratios Between 3D and 2D Factors of Safety (ru = 0.0)

For cohesive soils:

- The ratio between FS3D and FS2D is always greater than one. This ratio can be as large as 1.3 for gentle slopes, decreasing to almost 1.0 as the slope gets steeper. This is apparently related to the three dimensional shape of the most critical surfaces, which become wider at the foot of the slope and narrower at the top, as the slope flattens.

For cohesionless soils:

- The ratio between FS3D and FS2D can be less than one for gentle slopes, increasing as the slope inclination increases. The maximum ratio was of the order of 1.15, for a slope of 1.5:1.

In order to show the agreement between the position of the two and the three dimensional most critical surfaces, the range of the average depth of typical three dimensional critical surfaces was plotted in Figures 8 and 9 for cohesive and cohesionless soils, respectively, as well as the corresponding two dimensional critical surfaces. From the different cases studied, it became clear that:

For cohesive soils:

- There is good agreement between the cross sections displaying the average depth of the most critical three dimensional surfaces and the two dimensional most critical surfaces. Apparently the agreement gets better as the cohesive intercept of the soil increases, and as the slope becomes flatter. For steep slopes, there was a tendency for the three dimensional critical surfaces to start beyond the toe of the slope.

For cohesionless soils:

- The cross sections displaying the average depth of the most critical three dimensional surfaces are always deeper than the two dimensional most critical surfaces. For steep slopes, just as for cohesive soils, there was a tendency for the three dimensional critical surfaces to start beyond the toe of the slope.

Another aspect investigated was the three dimensional shapes of the slides. Figures 10 and 11 are representative of the results obtained for cohesive and cohesionless soils, respectively. The conclusions can be summarized as follows:

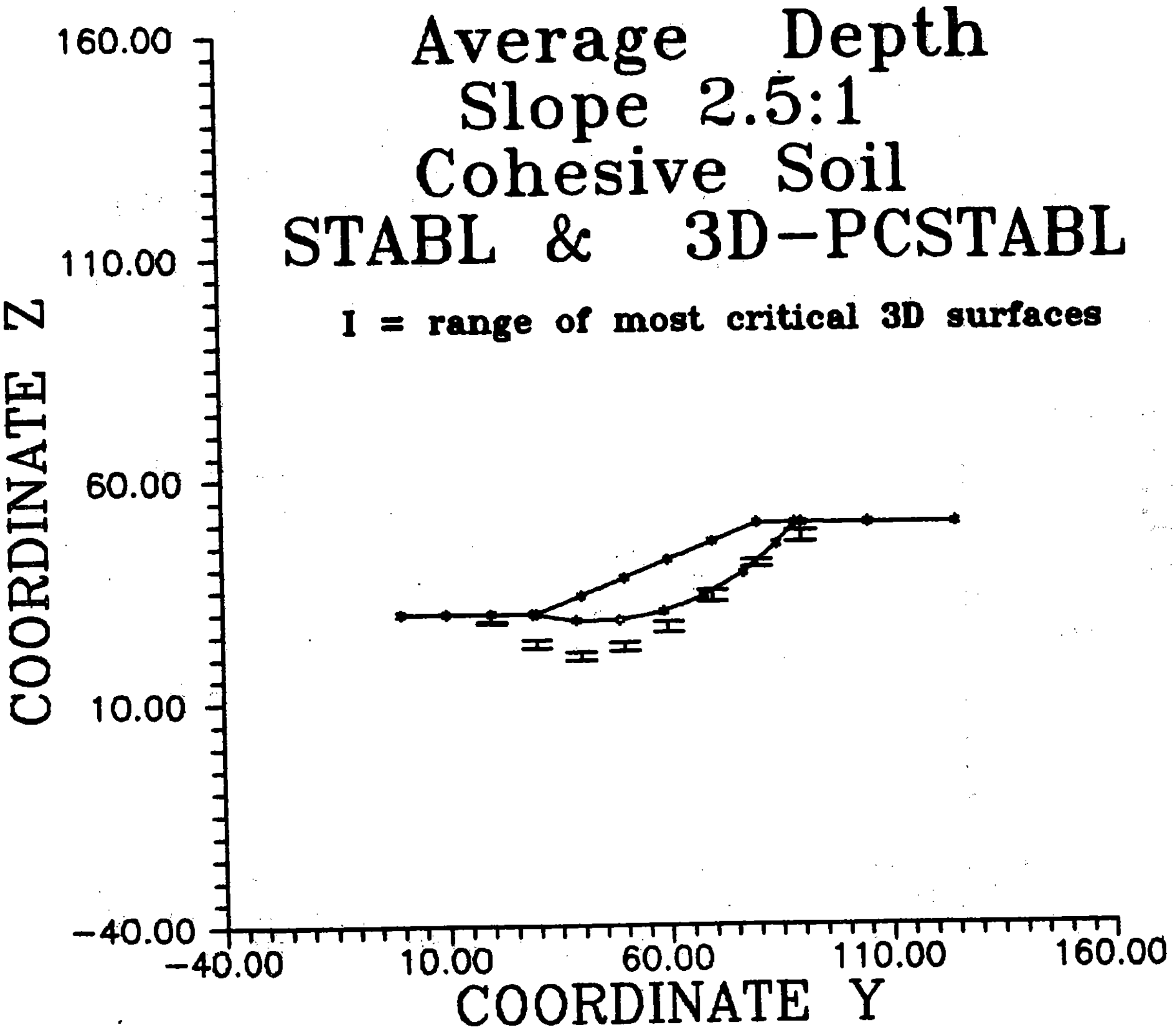

Figure 8 - Typical Average Depth of 3D and 2D Surfaces for Cohesive Soils

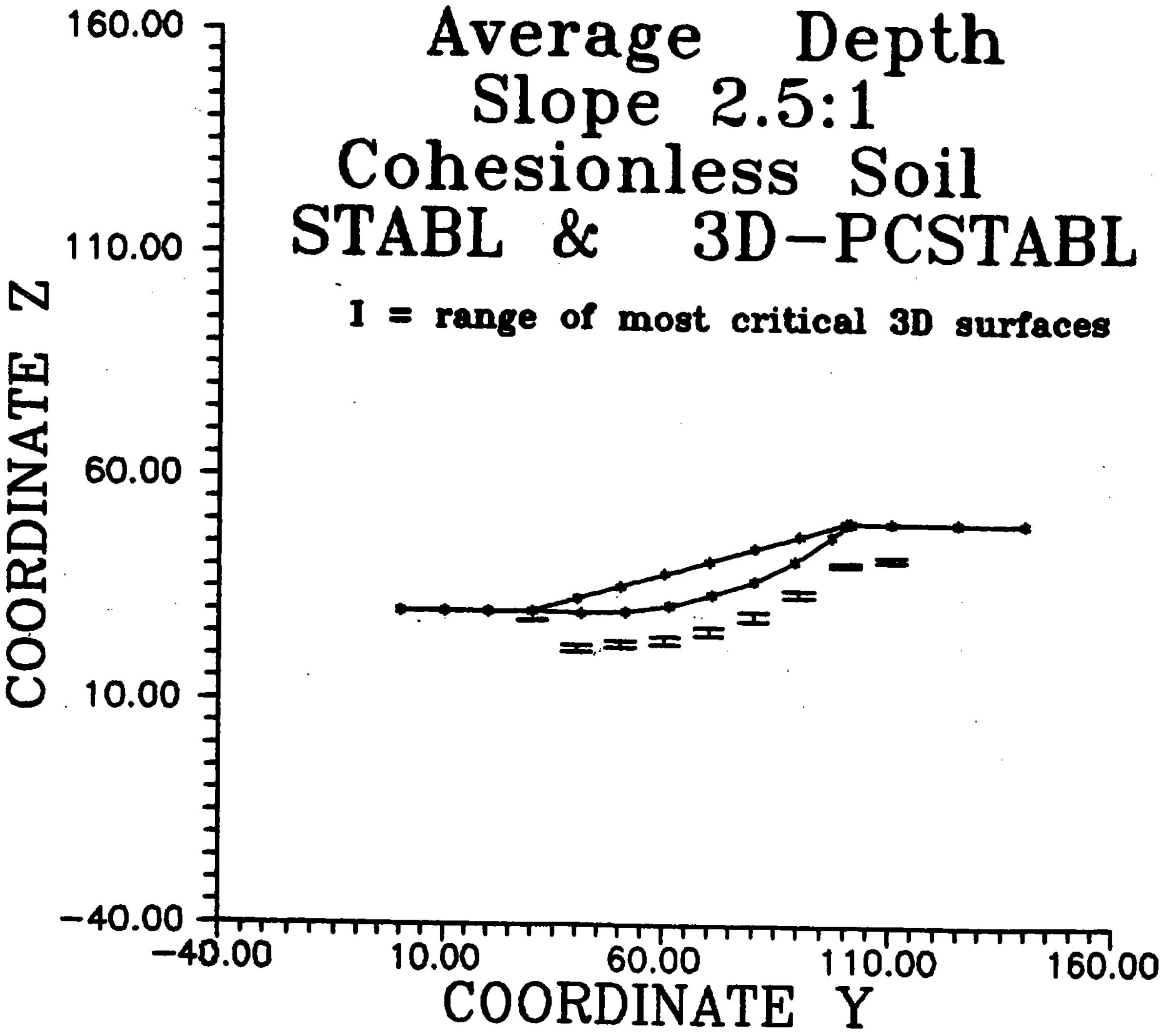

Figure 9 - Typical Average Depth of 3D and 2D Surfaces for Cohesionless Soils

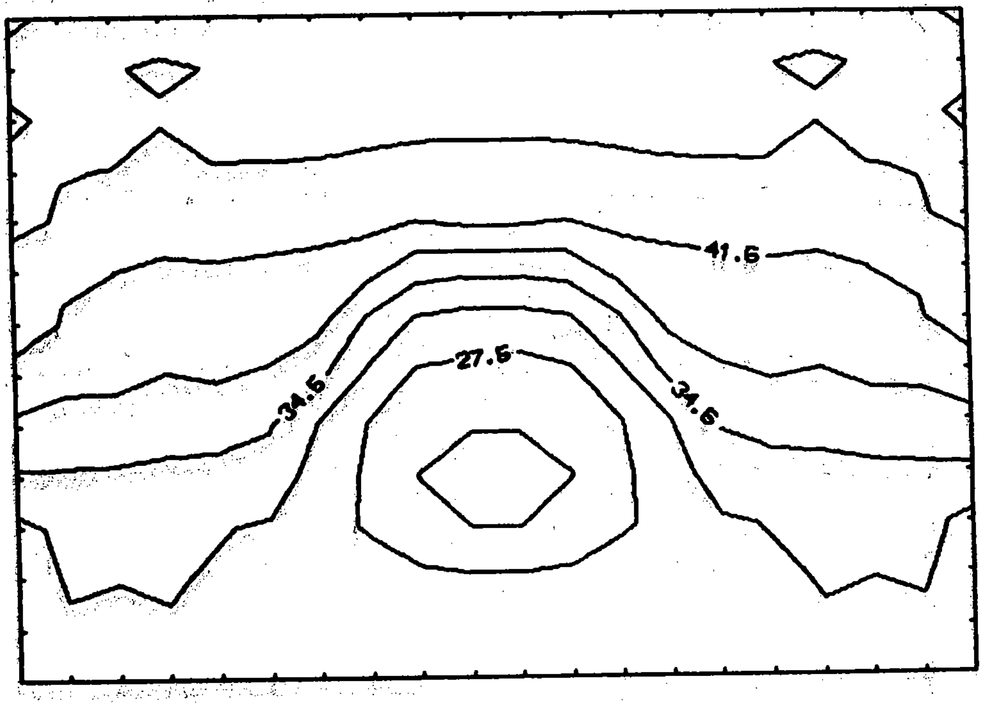

Figure 10 - Contour Plot of 3D Surfaces in Cohesive Soils (Contours Indicate Points of Equal "Z" Value) (Numbers Indicate Value of the "Z" Coordinates)

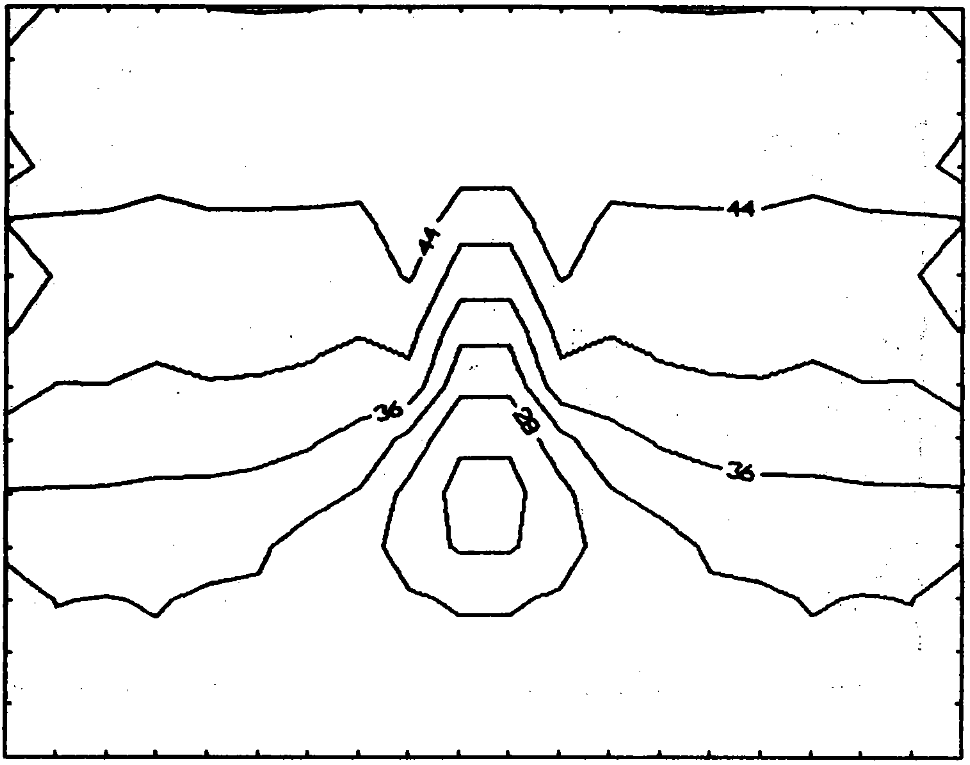

Figure 11 - Contour Plot of 3D Surfaces in Cohesionless Soils (Contours Indicate Points of Equal "Z" Value) (Numbers Indicate Value of the "Z" Coordinates)

For cohesive soils:

- The three dimensional surfaces tended to have elliptical and spherical shapes. As the slope flattens, it becomes more difficult to establish the exact shape of the surface, since the surfaces become wider, and many surfaces lead to essentially the same factor of safety.

For cohesionless soils:

- The three dimensional surfaces tended to be approximately block shaped. There seems to be no definite relation between the shape of the surfaces and the inclination of the slope.

From the parametric studies performed, the overall conclusion is that the three dimensional behavior of a landslide is related to the amount of shear strength and cohesion of the soils involved. As landslides in cohesive and cohesionless soils have different, and sometimes opposite characteristics, it can be very difficult to estimate how conservative or unconservative a two dimensional analysis is, if the soil profile to be analyzed is formed by soils with substantial shear strengths and cohesive intercepts. In addition, as Figure 12 shows, if water pressure exists, the three dimensional effect on the factor of safety can be even greater.

SUMMARY

This work presented a methodology to generate random three dimensional sliding surfaces and evaluate their factors of safety. The method employs random numbers to create a surface within boundaries defined by the user. Angular restrictions are imposed in order to keep the surface kinematically compatible. The soil is divided in columns, and the forces on the sides are calculated. The equilibrium of forces and moments is satisfied. The methodology was implemented in a program that runs on IBM microcomputers. The program code is called 3D-PCSTABL and can be obtained from Purdue University. Some cases were run comparing the effects of the inclination of the slope and of the strengt parameters on the shape of the critical surfaces and on the ratio between the 3D factor of safety and the traditional 2D factor of safety.

It has been found that the steeper the slope, the lower the ratio between 3D and 2D factors of safety for medium and highly cohesive soils. For cohesionless soils the behavior is the opposite, with the ratio increasing for steeper slopes. In cohesionless soils, the critical three dimensional surfaces were found to be deeper than the most critical two dimensional surfaces, for all slopes. The higher the cohesion of the soil, and the flatter

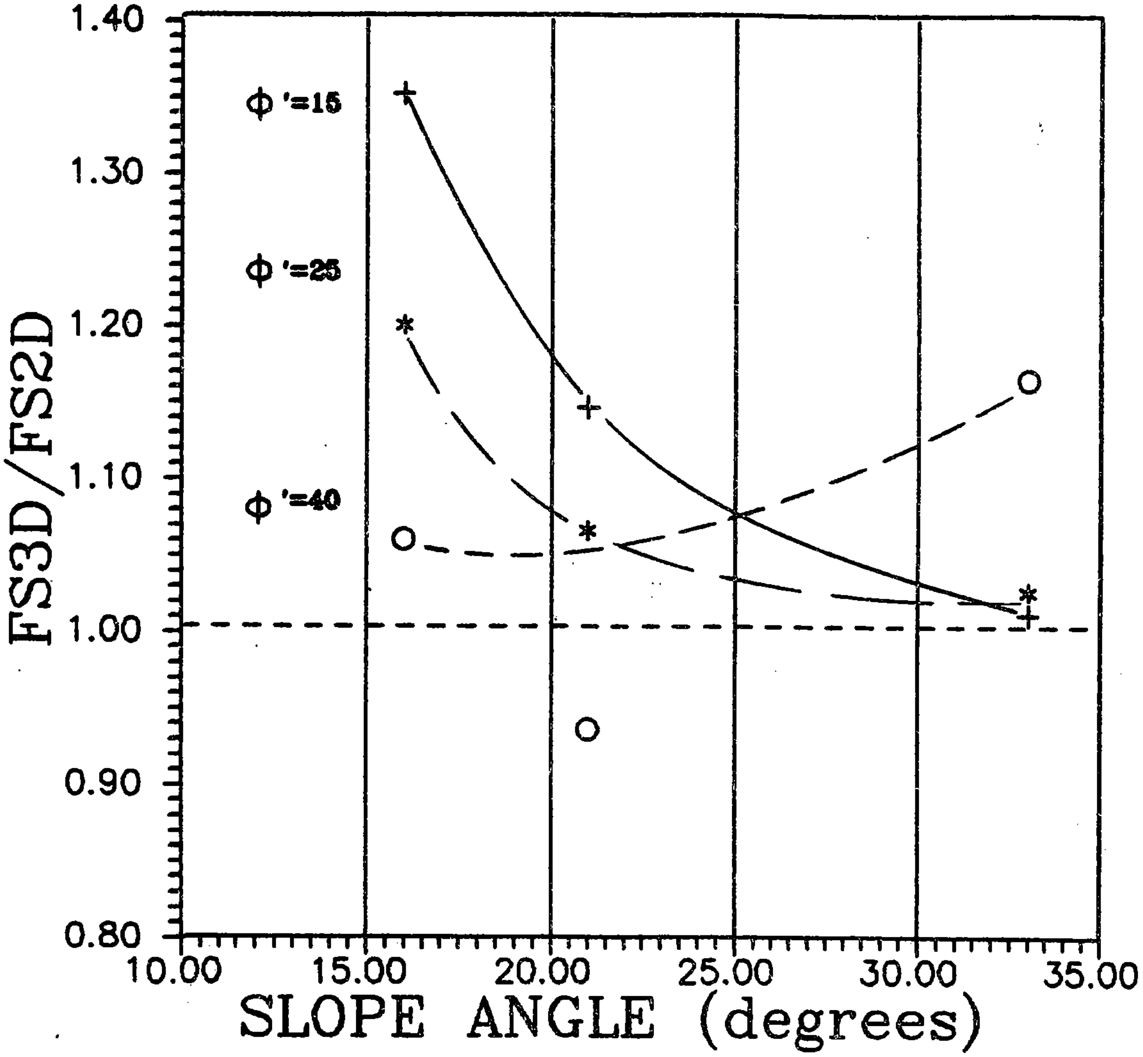

Figure 12 - Ratios Between 3D and 2D Factors of Safety (ru = 0.5)

the slope, the better the agreement between the depths of the two and three dimensional most critical surfaces. The three dimensional shapes of the surfaces were found also to be related to both the strength parameters and the inclination of the slope. Cohesionless soils in general showed narrower, block-like surfaces, with a tendency to widen as the slope flattens. Cohesive soils on the contrary showed a tendency to have wider, ellipsoidal or spherical surfaces.

REFERENCES

Carpenter, J. R. (1985), "STABL5...The Spencer Method of Slices: Final Report", Report JHRP-85-17, Purdue University, West Lafayette, Indiana.

Chen, R. H. (1981), "Three Dimensional Slope Stability Analysis", Report JHRP-81-17, Purdue University, West Lafayette, Indiana.

Siegel, R. A. (1975), "Computer Analysis of General Slope Stability Problems", MSCE Thesis, Purdue University, West Lafayette, Indiana, (also report JHRP-75-8).

Thomaz, J. E. (1986), "A General Method for Three Dimensional Slope Stability Analysis", MSCE Thesis, Purdue University, West Lafayette, Indiana.

POLYMER GEOGRID REINFORCED SOIL SLOPES REPLACE RETAINING WALLS

by

Michael J. Cowell, Ron Anderson and Robert Anderson

INTRODUCTION

The application of soil reinforcement techniques over the past few decades have concentrated on solving the problems of building vertical walls. Systems involving metal strips, metal grids, polymer grids and geotextiles have all been used to economize retaining wall construction. While the competition between these different systems has reduced the cost of retaining walls, a new technique has emerged which dramatically drives down the construction costs. It is reinforced steepened slopes.

The use of retaining walls for a highway or site development are typically the result of insufficient right-of-way to allow a conventional soil embankment to be constructed. For example, if the shear strength of the local soil only allows embankments to be constructed safely at a 3 horizontal to 1 vertical slope angle , and the right-of-way constraints will only allow a 1.5H to 1V slope to be built, then a retaining wall must be constructed. While soil reinforcement techniques can be used to construct this retaining wall more economically than a conventional wall, these same techniques can also be used to reinforce the 1.5H to 1V slope at a greater savings.

The purposes of this paper are to describe how the economics of constructing reinforced steepened slopes provide significant savings, present a simplified method for designing steepened slopes, and describe a recent project where a reinforced slope has been used successfully to replace a retaining structure.

ECONOMICS

The savings that can be realized by steepening slopes using soil reinforcement techniques is illustrated in Figure 1 and Table 1. The comparisons made are between a 20-foot-high reinforced 1.5H to 1V slope, a 10-foot-high retaining wall with a 3H to 1V surcharge slope,and a 20-foot-high reinforced soil wall. The relative economics show the reinforced soil slope as approximately 40% less than the wall and slope option and 65% less than a full-height reinforced soil retaining wall. This comparison is conservative in that it has assumed all backfill soils are the same quality. This is an accurate assumption for metal reinforcement, however, if polymer geogrids are used, common borrow can be used for backfill which would increase the economic advantages of the reinforced steepened soil slope.

Table 1 - Cost Comparison Between Reinforced Soil Embankments and Conventional Retaining Walls for Options Shown on Figure 1

	Construction Costs $/Lineal foot	Subtractions or Additions $/Lineal foot	Total Cost $/Lineal foot
1. 20' high TENSAR Geogrid steepened reinforced soil slope	$200	0	$200
2. 10' high retaining wall	$300	+$25 more earthwork	$325
3. 20' high retaining wall	$600	-$42 less earthwork required	$558

Note: All costs are in lineal feet of running slope or wall length.

To date this concept of strengthening common borrow with polymer reinforcement to construct reinforced steepened soil slopes has been used by a number of highway departments (2, 6), federal agencies, and developers over the past four years. While most of these projects involved replacement of retaining structures, several were a substitute for conventional flat embankments. The design of these structures have been performed both in-house by government agencies, and by consultants using rigorous hand methods or detailed computer program(s). Recently a simplified method (4) has been developed to advance the use of reinforced soil slopes. Details for this simplified design method follow.

Simplified Design Methods

The design of a reinforced soil slope can be visualized as the addition of tensile strength to soil. Placement of the high-tensile-strength geogrids in a soil slope is a function of the over-all stability of that slope. A sufficient number of geogrid layers must be placed so that failures do not occur between geogrid layers; and the embedment length of these layers must be long enough to provide sufficient anchorage behind all potential failure surfaces.

For reinforced soil slopes constructed over stable foundation soils, the amount of reinforcement required is a function of the shear strength and density of the embankment fill, the geometry of the slope (height and slope angle), and any surcharge acting on top of the slope. For these conditions, a series of charts have been developed (Figures 2, 3 and 4) based on conventional limit equilibrium analyses (1, 3, 4, 5). These charts provide a means for calculating the total tensile force required for equilibrium and determining the embedment length required for anchorage behind potential failure planes. The charts for embedment length take into account the length required to resist sliding and pullout using polymer geogrids manufactured by The Tensar Corporation. The assumptions associated with these charts and an example of how they are used follows.

The stability analyses from which the charts were developed assume the following conditions:

- Fill material is characterized by a friction angle only, $(c' = 0)$.
- Porewater pressures are zero $(u = o)$.
- Slopes are supported by competent, level foundations.
- The slope face is planar and inclined in the range of 30° to 80°; the crest is horizontal.
- The fill material is uniform throughout.
- Surcharge loads, if any, are uniformly applied along the slope crest, and are small in comparison to the slope height.
- Layers of reinforcement are horizontal and continuous; discrete reinforcements are not considered.
- Seismic forces are negligible.

To determine the number of geogrid layers, and the distribution of these layers in the slope, the following steps are performed:

1. Determine the minimum number of geogrids required.

$$N = \frac{T}{T_a}$$

where: N = minimum number of geogrid reinforcement layers

T = required gross tensile reinforcement force per unit length of embankment

T_a = long-term allowable tensile force per unit width provided by the reinforcement

To calculate T the following steps are performed.

From Figure 2 the horizontal earth pressure coefficient. K, is obtained to calculate T.

$$T = 1/2\ K\ \gamma\ (H')^2$$

where: T = required gross tensile reinforcement force per unit width of slope
K = horizontal earth pressure coefficient
γ = unit weight of soil
H' = effective height of the slope

H' is termed the "effective" height of the reinforced soil slope in order to incorporate surcharge loads into the simplified design method. The use of H' is valid when H' is less than 1.2 x H. The surcharge load can be expressed as an equivalent thickness of soil, and added to the slope height as below:

$$H' = H + \frac{q}{\gamma}$$

where: H' = effective slope height
H = actual slope height
q = uniformly distributed surcharge load on the crest
γ = unit weight of soil

Use of Figure 2 requires knowledge of the slope angle, B and the factored soil angle of internal friction, ϕ'_f. The design factor of safety (F.S.) against slope failure is applied to the friction angle of the soil as follows:

$$\tan \phi'_f = \frac{\tan \phi'}{F.S.}$$

where: ϕ'_f = factored angle of internal friction

ϕ' = angle of internal friction

F.S.= gross factor of safety

$$\text{thus, } \phi'_f = \tan^{-1}\left(\frac{\tan\phi'}{F.S.}\right)$$

2. Determine the distribution of the reinforcement within the slope.

   The N layers of reinforcement calculated in the first step must be distributed in a way that ensures internal stability of the reinforced slope at all elevations. The amount of reinforcement required at each elevation varies linearly with the depth, z below the crest of the slope.

   The type and vertical spacing of geogrids can be optimized using the following equation:

$$s_v = \frac{T_A}{K\gamma z}$$

   where: s_v = maximum spacing between geogrid reinforcement layers for depth z
   z = depth below crest of slope

   Using this equation,the optimum geogrid type and spacing can be calculated as illustrated in Figure 5.

3. Determine the minimum embedment length requirements.

   From Figures 3 or 4 the minimum embedment length at the top and bottom of the slope can be determined as a function of the effective slope height, H'. The minimum length of each layer can then be calculated or determined graphically. Actual design lengths should be kept as uniform as possible to balance the number of different lengths versus waste.

4. Design Layout.

Figure 6 shows the layout for a 38-foot-high 1H:1V slope with a 2-foot surcharge based on the strength properties and spacing results shown on Figure 5. The final layout shows the primary reinforcement needed for internal and external stability, as well as the intermediate reinforcement required for constructability and stability of the slope face. The layout also shows how the lengths of grids were adjusted to provide both stability and uniformity of grid lengths. This final layout is then checked against N to assure enough reinforcement has been used to provide an internally stable structure.

The simplified design method is a quick method to design steepened soil slopes using TENSAR Geogrids for projects with stable foundations. The following section discusses a project where a polymer geogrid reinforced slope replaced a retaining wall.

CASE HISTORY

There has been a number of projects documented in North America (2,6,7) where slopes reinforced with polymer geogrids have been used. A recent project which provides an example of how a reinforced soil slope replaced a standard retaining wall is the MARTA (Metropolitan Atlanta Rapid Transity Authority) steepened embankment project in Atlanta, Georgia. This project involved construction of a steepened reinforced embankment for the new MARTA rail spur which connects downtown with the airport. On much of the rail line reinforced soil walls using metal strips and granular backfill were used to meet the grade and right-of-way constraints of the project.

For the airport yard spur, a combination of walls and conventional flat slopes were proposed. As the design progressed, problems arose in areas originally designed for conventional slopes because more right-of-way was needed for future expansion of the adjacent interstate highway, I-85.

The alternatives proposed were a 20-foot-high TENSAR Geogrid reinforced steepened slope and a 10-foot-high wall with a 2H:1V surcharge slope. A preliminary design and cost estimate was performed for each design. The steepened slope alternative saved over $100 per lineal foot of slope. The project went to bid with both alternatives and the steepened slope design was selected by the contractor. In addition to the savings inherent to the steep slope design, additional savings were realized through the use of the local borrow soils. The local regional silty clay soils which had a low friction angle (28°) and are corrosive to metal were used with polymer goegrids.

Figure 7 shows the final design for the MARTA project. The design incorporated high strength SR-2 (T_A = 2000 lbs/ft). At the base of the slope where the stresses would be higher, and lower strength SS-2 (T_A = 500 lbs/ft) at the top. In this way, the most economic geogrid ($/lb) was used. The primary reinforcements for internal and external stability of the structure were the 32-foot-long layers of SR-2 and SS-2. Shorter layers of SS-2 were also used near the slope face. The purposes of these layers were to provide internal stability near the slope face under the construction loads and to obtain better compaction and greater erosion resistance at the face of the slope. For final slope face protection, polymer reinforced straw mats were used to prevent erosion and promote vegetation.

SUMMARY

The use of polymer geogrids for the reinforcement of soil slopes is the latest refinement of soil reinforcement technology. The use of polymer geogrids to construct a steepened slope provides a more economical structure than conventional reinforced soil retaining walls. Savings are realized in the amount of soil reinforcing materials, facing treatments, and often earthwork costs when local borrow is used.

A simplified design method has been presented to demonstrate the mechanics of designing a reinforced soil slope. The method is based on conventional limit equlibrium techniques.

Finally, a case study illustrating the use of reinforced soil slopes as a cost saving alternative to conventional retaining walls has been presented.

REFERENCES

1. Bonaparte, R., Holtz, R.D., and Giroud, J.P., 1985. Soil Reinforcement Design Using Geotextiles and Geogrids. Geotextile Testing and the Design Engineer, A Symposium Sponsored by ASTM Committee D-35 (in draft).

2. Devata, M.S., 1985. Geogrid Reinforced Earth Embankments with Steep Side Slopes. Polymer Grid Reinforcement: Proceedings of a Conference Sponsored by the Science and Engineering Research Council and Netlon, Ltd., Thomas Telford, Ltd.: 82-87.

3. Jewell, R.A., Pain, N., and Woods, R.I., 1985. Design Methods for Steep Reinforced Embankments. Polymer Grid Reinforcement: Proceedings of a Conference Sponsored by the Science and Engineering Research Council and Netlon, Ltd., Thomas Telford, Ltd.: 11-17.

4. The Tensar Corporation, 1986. Slope Reinforcement with TENSAR Geogrids Design and Construction Guideline, Tensar Technical Note TTN:SR1.

5. The Tensar Corporation, 1986. "NEWSLOPE" User's Manual, an in-house computer program (unpublished).

6. Forsyth, R.A. and Bieber, 1985. LaHonda Slope Repair with Geogrid Reinforcement. Polymer Grid Reinforcement: Proceedings of a Conference Sponsored by the Science and Engineering Research Council and Netlon, Ltd., Thomas Telford, Ltd.: 54-57.

7. Busbridge, J.R., 1985. Stabilization of Canadian Pacific Railway Slip at Waterdown, Ontario. Polymer Grid Reinforcement: Proceedings of a Conference Sponsored by the Science and Engineering Research Council and Netlon, Ltd., Thomas Telford, Ltd.: 58-63.

DESIGN OPTIONS:

1. STEEPENED TENSAR GEOGRID REINFORCED SLOPE
2. CONVENTIONAL 10' HIGH RETAINING WALL
   WITH 3 : 1 SURCHARGE
3. CONVENTIONAL 20' HIGH RETAINING WALL

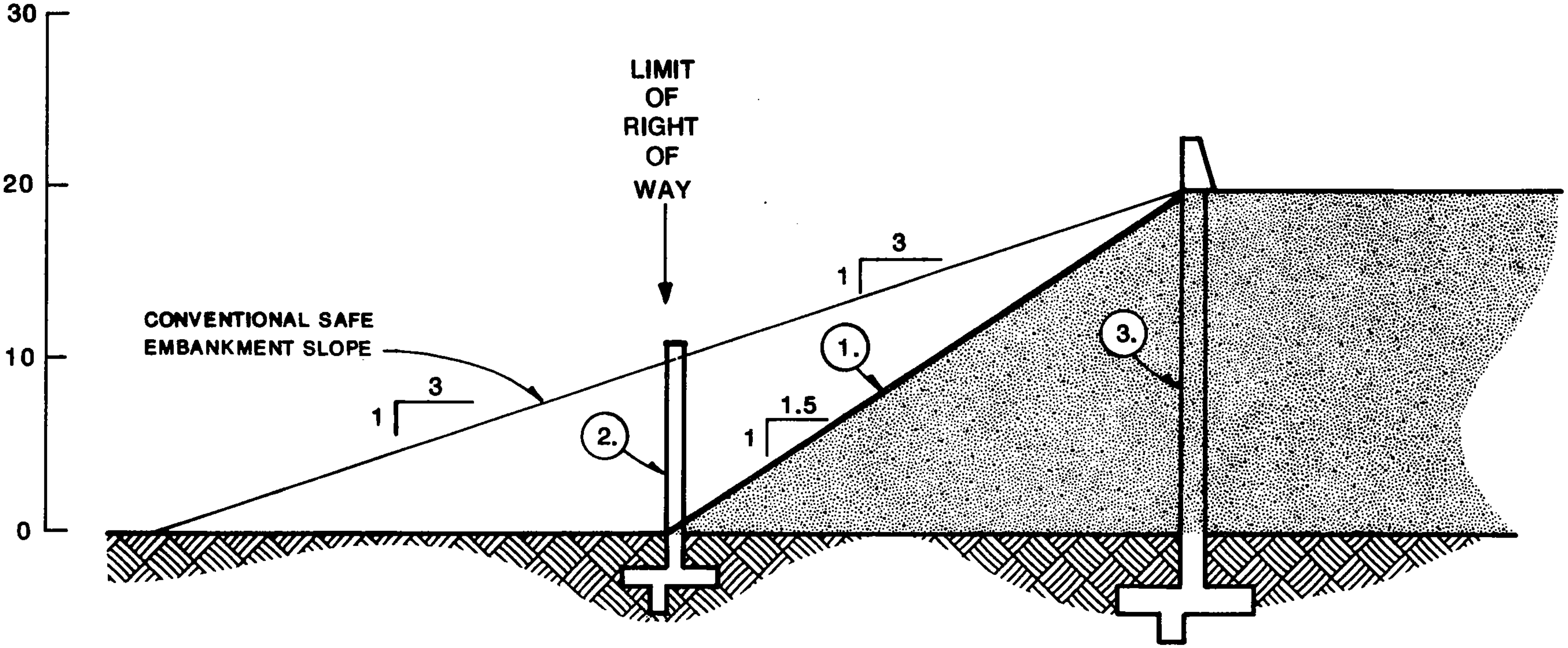
30
20
10
0
LIMIT OF RIGHT OF WAY
CONVENTIONAL SAFE EMBANKMENT SLOPE
3
1
3
1
1.5
1
1.
2.
3.

Fig. 1 EXAMPLE OF DESIGN OPTIONS TO MEET R.O.W. RESTRICTIONS

© THE TENSAR CORPORATION,1986

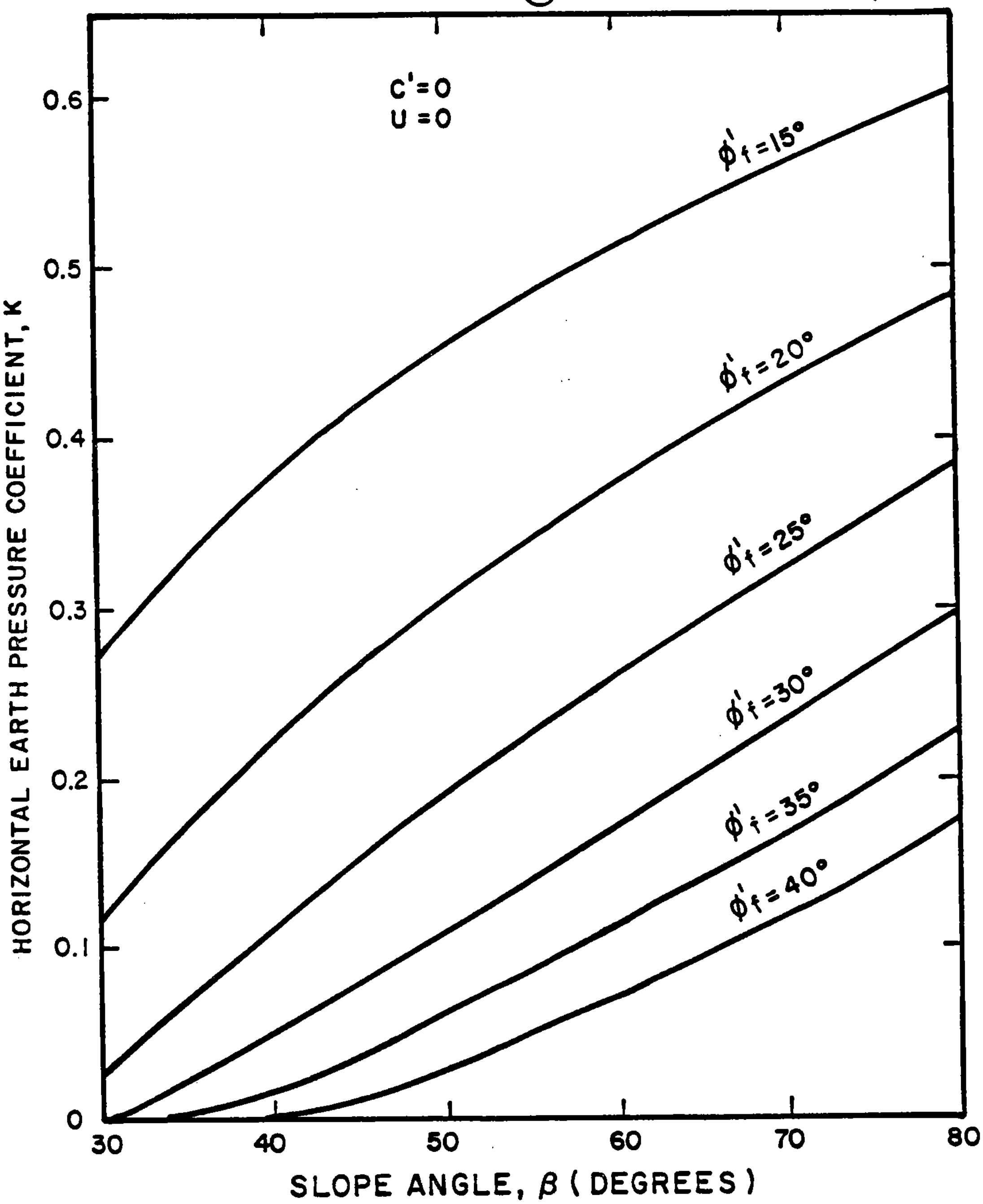

Fig. 2 HORIZONTAL EARTH PRESSURE COEFFICIENTS IN UNREINFORCED SOIL SLOPES.

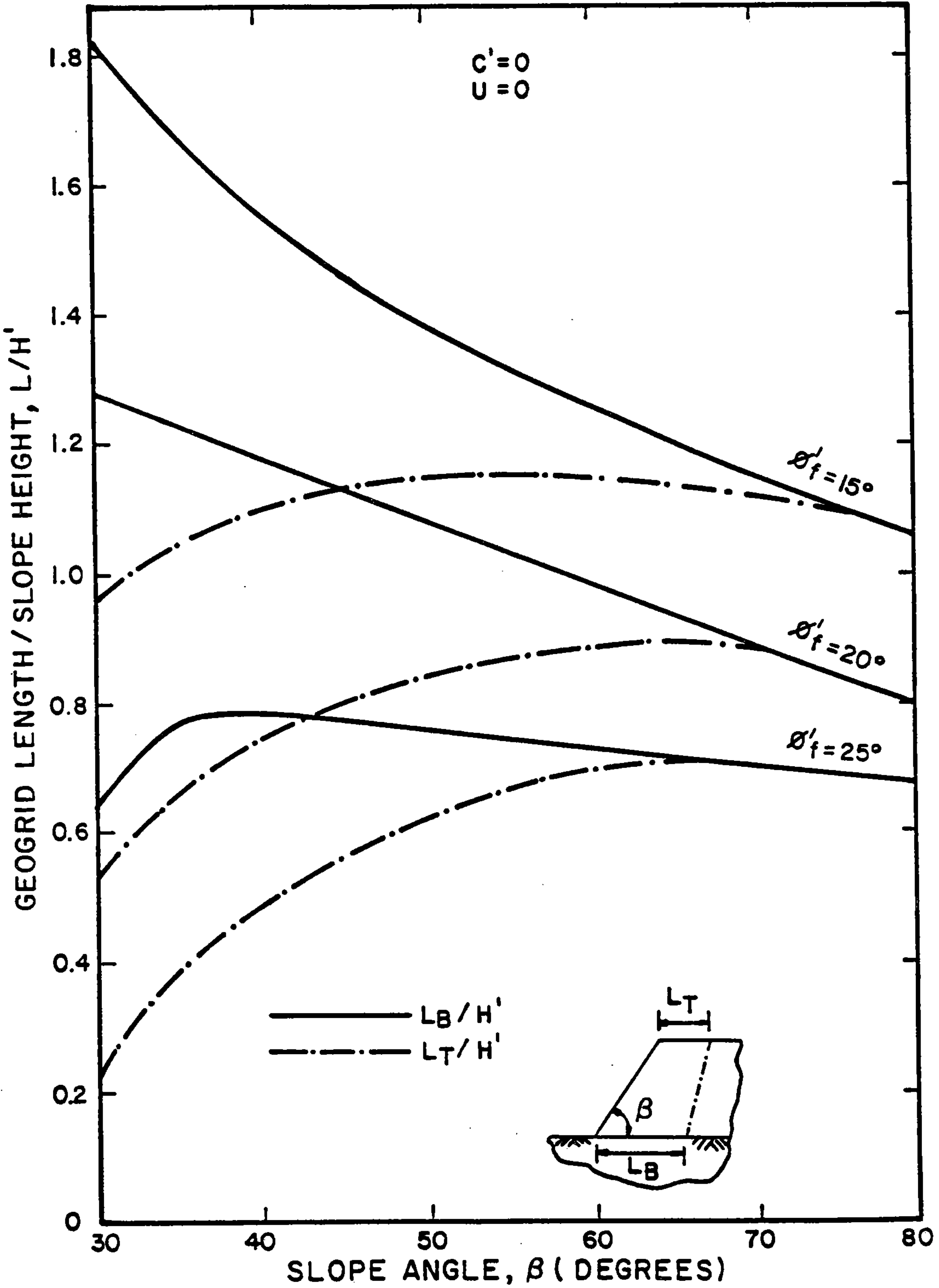
© THE TENSAR CORPORATION, 1986

Fig. 3 GEOGRID EMBEDMENT LENGTHS FOR ϕ'_f =15° TO ϕ'_f = 25°

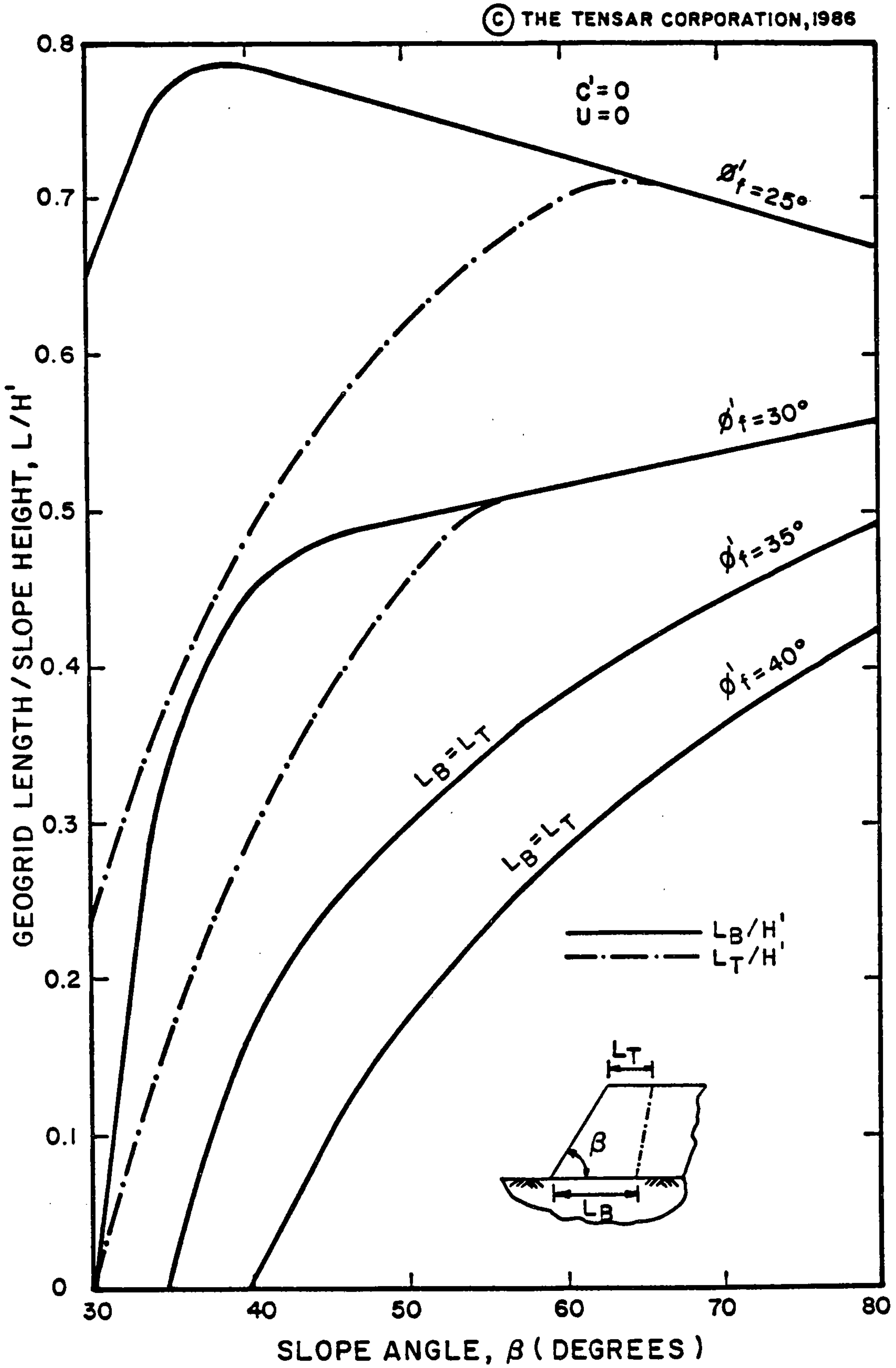

Fig. 4 GEOGRID EMBEDMENT LENGTHS FOR $\phi'_f = 25°$ TO $\phi'_f = 40°$

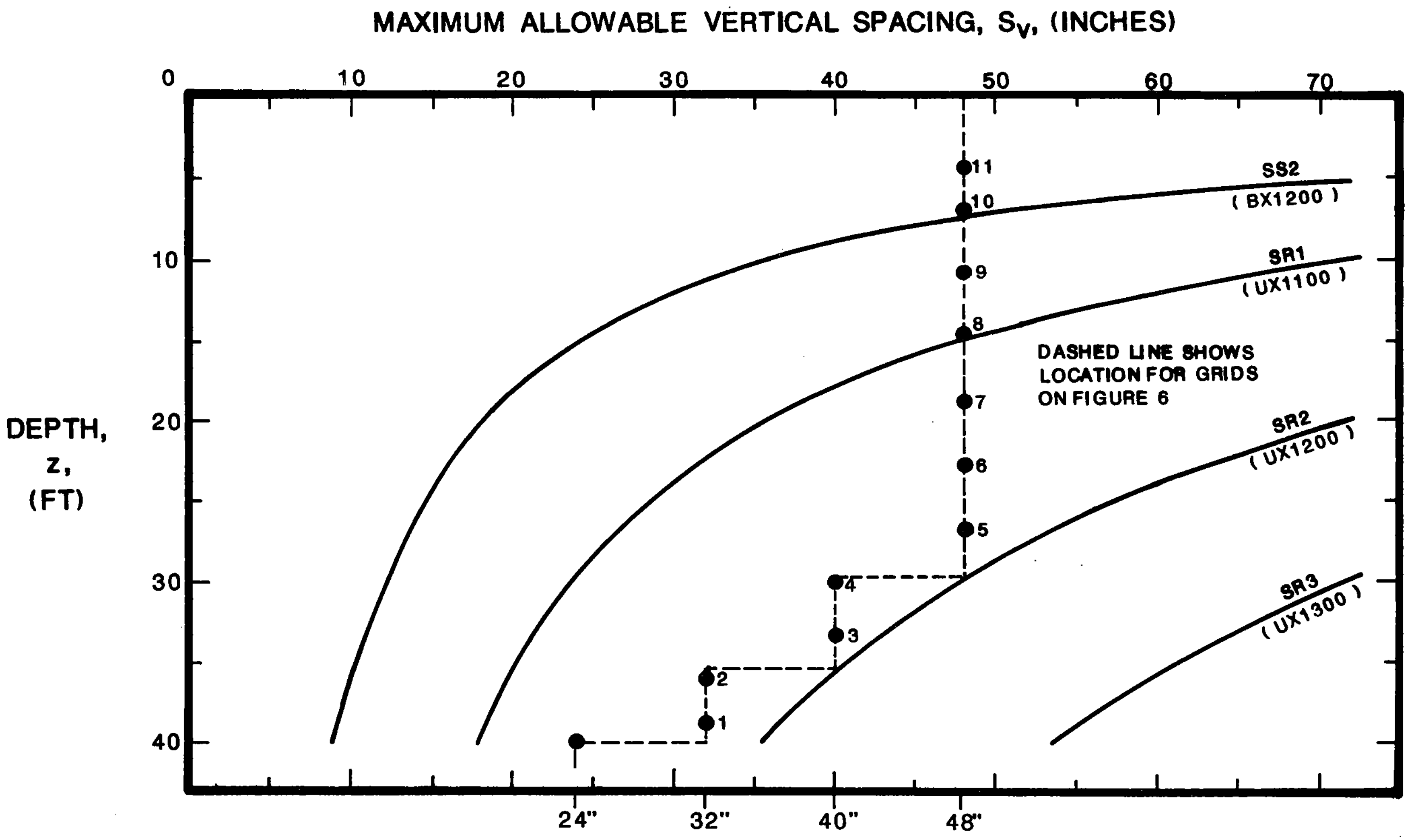

Fig. 5 MAXIMUM ALLOWABLE VERTICAL SPACING, S_v, VERSUS DEPTH, z, FOR $H = 40'$, $\phi' = 32^\circ$, $K = 0.14$, $\gamma_m = 120$ pcf, $\beta = 1:1$

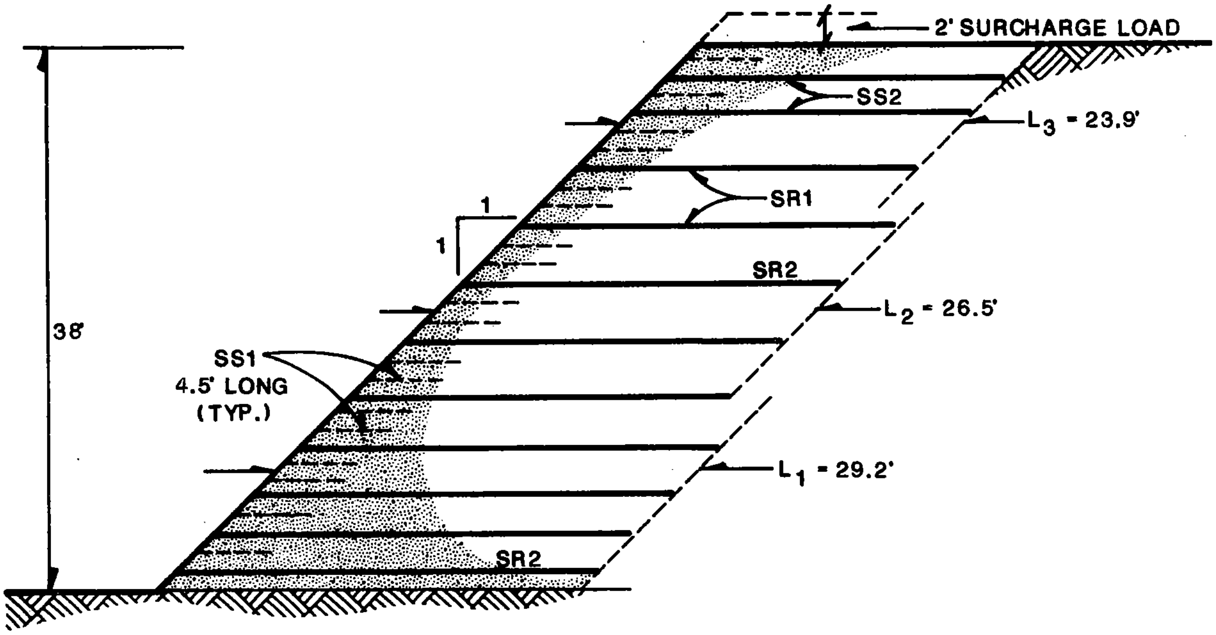
2' SURCHARGE LOAD
SS2
L3 = 23.9'
SR1
1
1
SR2
L2 = 26.5'
38'
SS1
4.5' LONG
(TYP.)
L1 = 29.2'
SR2

Fig. 6 GEOGRID LAYOUT FOR DESIGN EXAMPLE

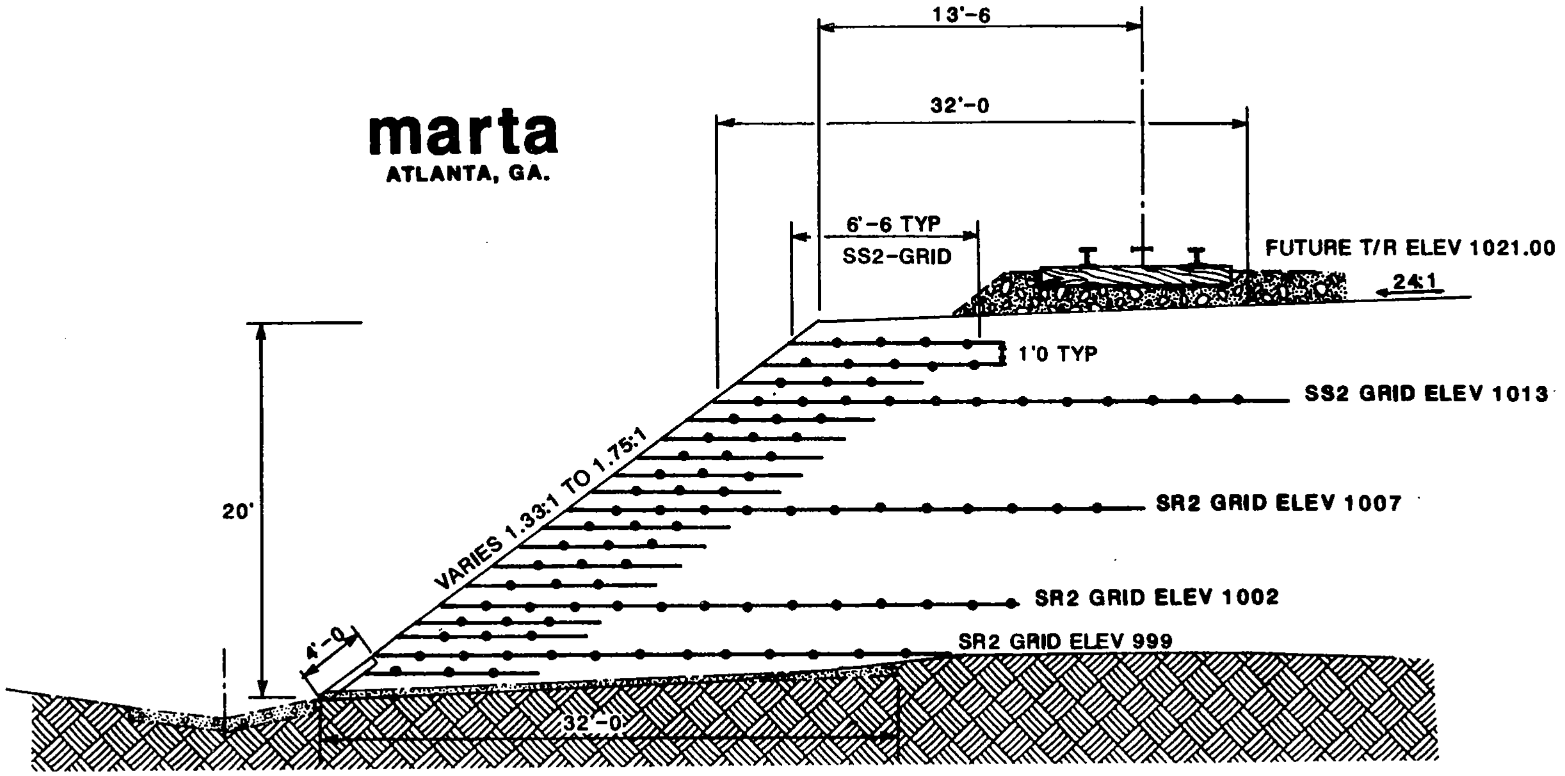
marta
ATLANTA, GA.
13'-6
32'-0
6'-6 TYP
SS2-GRID
FUTURE T/R ELEV 1021.00
24:1
1'0 TYP
SS2 GRID ELEV 1013
SR2 GRID ELEV 1007
SR2 GRID ELEV 1002
SR2 GRID ELEV 999
VARIES 1.33:1 TO 1.75:1
20'
4'-0
32'-0

Fig. 7 TYPICAL CROSS SECTION OF TENSAR REINFORCED SOIL SLOPE FOR MARTA

DESIGN AND SPECIFICATION OF TIED BACK RETAINING WALLS

by Ronald B. Reeves

Lang Tendons, Inc.
Newark Road
Toughkenamon, PA 19374
Telephone (215) 268-2221

presented August 20, 1986
at the 37th Annual
HIGHWAY GEOLOGY SYMPOSIUM
Helena, Montana

CONTENTS

SUMMARY 1

SECTION 1. DESIGN LOAD FOR TIED BACK WALLS SUPPORTING EARTH CUTS.......2

Restraint Force
Stability
Design Details

SECTION 2. CORROSION PROTECTION OF PERMANENT TIEBACKS.................5

2.1 THE CORROSION PROCESS IN TIEBACKS.........................5
Galvanic Corrosion
Stray Current Corrosion
Hydrogen Embrittlement

2.2 CORROSION PREVENTION IN PERMANENT TIEBACKS................8
Passivators
Organic Inhibitors
Coatings and Encapsulation
Ground Conditions

2.3 CORROSION PROTECTION DETAILS FOR 7-WIRE STRAND TIEBACKS..11
Bond Length
Unbonded Length
Anchorage

SECTION 3. PERFORMANCE SPECIFICATION OF TIED BACK WALLS...............18

Wall Description
Material Quality Level
Contractor Requirements

SECTION 4. FIELD LOAD TESTING OF TIEBACKS.............................21

4.1 BACKGROUND FOR LOAD TESTS.................................21
Load Test Parameters for Acceptance of Tiebacks

4.2 DESCRIPTION OF FIELD LOAD TESTS...........................22
Performance Test
Proof Test
Creep Test
Lift-Off Test

4.3 QUALITY CONTROL FOR TIEBACK LOAD TESTS...................27

APPENDIX A. GUIDE SPECIFICATION FOR PERMANENT STRAND GROUND ANCHORS...A1

INDEX TO FIGURES

1. ESTIMATING EARTH PRESSURE DISTRIBUTIONS FOR ANCHORED WALLS.....2
2. TYPICAL GALVANIC CORROSION CELL.................................5
3. LONG LINE CORROSION CELL..6
4. CORROSION BY STRAY ELECTRIC CURRENTS............................7
5. CORROSION PROTECTED EXTRUSION COATED 7-WIRE STRAND..............9
6. SIMPLE CORROSION PROTECTED PERMANENT TIEBACK...................12
7. GROUT COVER DEFICIENCIES IN SIMPLE CORROSION PROTECTED TIEBACKS..13
8. ENCAPSULATED CORROSION PROTECTED PERMANENT TIEBACK.............14
9. AVENUES FOR CORROSION ATTACK ON ANCHORAGES....................16
10. CORROSION PROTECTION FOR ANCHORAGES...........................17
11. PERFORMANCE TEST RESULTS......................................24
12. PROOF TEST RESULTS..25
13. CREEP TEST RESULTS..26

SUMMARY

Tied back retaining walls provide an efficient and economical method for supporting earth and rock cuts. Current design and construction practice has evolved from over 25 years of world wide experience with safe and economical tied back walls.

To realize the benefits of tied back retaining walls, the engineer must understand and apply current design and specification practice. Safe, efficient, and economical tied back walls result from 1) specifying reasonable and safe design loads, 2) understanding corrosion in tieback tendons and how it can be efficiently prevented, 3) using performance specifications that include materials specified by quality level, and 4) specifying prescriptive field load tests.

Design loads for tied back walls should be determined using methods developed for designing support for braced cuts. These methods will produce design loads that allow an efficient and safe structure.

Corrosion of tieback tendons is caused by formation of galvanic cells. Passivators, organic inhibitors and coatings will prevent galvanic corrosion of tieback tendons. Corrosion protection details depend on the function of the part of the tendon and on ground conditions. In non-aggressive conditions, grout cover provides corrosion protection to the bond length and an extruded sheath over the strand that is completely filled with corrosion inhibitor grease provides corrosion protection to the unbonded length. In aggressive conditions, a corrugated sheath protects the grout cover in the bond length and the same extrusion coated strand used in non-aggressive conditions provides corrosion protection to the unbonded length. The anchorage, which is the tendon part most susceptible to corrosion, requires special attention to corrosion protection details. These include anchorhead protection/cover, trumpet design and electrical isolation of the tendon from the structure.

Performance specifications, rather than prescriptive, will assure that the wall meets the owner's needs for a safe and economical structure that will perform satisfactorily over its design life.

Finally, each tieback should be load tested because the interaction between the tieback tendon and the ground cannot be predicted, and the quality of grouting work cannot be precisely verified visually. Prescriptive test procedures verified by quality control procedures will assure uniform data and will give confidence that the test parameters measure tieback behavior and are free from the effects of variations in the test procedures.

SECTION 1. DESIGN LOADS FOR TIED BACK WALLS SUPPORTING EARTH CUTS

Tied back walls and braced sheeting support earth cuts in the same way. As with the braced cut, each tier of a tied back wall supports the cut as the excavation proceeds from the surface to final grade. After the cut reaches the necessary depth, the first tier of tiebacks is installed and post-tensioned. The tiebacks limit strain in the soil behind the wall until the lateral earth force against the soldier beam is greater than the force exerted by the tieback. The restraint force for tied back walls should be calculated from the earth pressure envelopes given in Soil Mechanics in Engineering Practice (Terzaghi & Peck, 2nd ed.) for braced cuts. Like braced cuts, tied back walls designed using these earth pressure envelopes have given satisfactory performance. This method, using the shear strength parameters for the soil at the site, will give factors of safety of 1.3 to 1.4 when the cut is analyzed for stability using limit equilibrium methods.

Restraint Force

The restraint force is the horizontal component of the tieback lock-off load and is distributed to the soil as a line load by the soldier beam. The restraint force, calculated using the earth pressure envelopes shown by Figure 1 gives the upper limit for the lateral earth pressure along the soldier beam. The actual pressure distribution depends on the magnitude of the restraint force and on the stiffness of soil which supports the soldier beam.

SOIL TYPE: SAND — SOFT TO MEDIUM CLAY (q_u = 0.25-1.0 TSF) — STIFF TO HARD CLAY (q_u > 1.0 TSF)

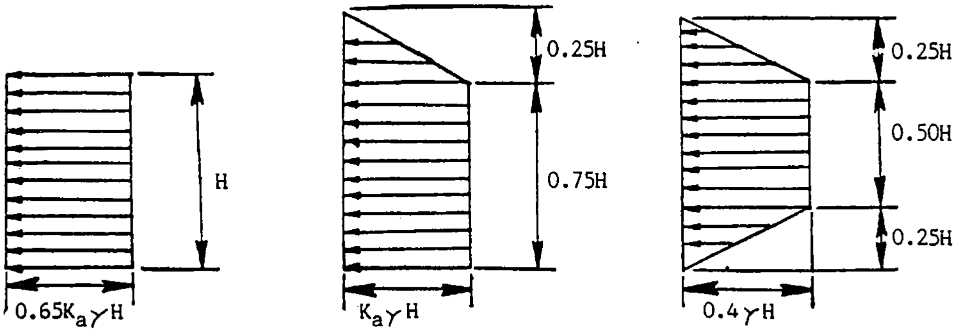

$K_a = \tan^2 45-\phi/2$

$K_a = 1 - m\,(2q_u/\gamma H)$

m = 1 for overconsolidated clays

m < 1 for normally consolidated clays

Value of 0.4 should be used for permanent walls; Values between 0.4 and 0.2 may be used for temporary walls

NOTATION:

H - Final wall height

γ - Soil unit weight

ϕ - Angle of internal friction

K_a - Active earth pressure coefficient

m - Reduction factor

q_u - Unconfined compressive strength, TSF

FIGURE 1. ESTIMATING EARTH PRESSURE DISTRIBUTIONS FOR ANCHORED WALLS

Actual pressure distribution can be estimated by analyzing the soldier beam as a beam on an elastic foundation. The restraint force causes the soldier beam to exert pressure on the face of the cut. As long as this pressure exceeds the lateral earth pressure, the strain in the soil at the bottom of the cut is less than that required to satisfy conditions for plastic equilibrium. As a result, there is little or no restraint force from the interaction between the soil and the soldier beam at the bottom of the cut.

Since the soldier beam distributes the restraint force to the soil or rock as if it were a beam on an elastic foundation, none of the restraint force is directly transmitted to the wall surface. The wall surface receives no direct load until the lateral earth force exceeds the restraint force or until the inward movement of the soldier beam pushes the wall surface against the soil or rock. Field observations have shown that the usual case is for the wall surface to be loaded only by inward movement of the soldier beams. Lock-off loads are usually set at 80 percent of the design load in order to limit inward movement of the soldier beams and to set the restraint force at the level of the lateral earth force.

Stability

If the tieback is anchored in the soil or rock beyond any possible failure surface, the restraint force gives stability to the wall and to the supported soil or rock mass. This condition is met when the unbonded length of the tieback extends beyond the failure surface. This surface can be located by plastic equilibrium methods or by limit equilibrium methods. The failure surface is commonly determined by using the active Rankine (plastic equilibrium) state.

Design Details

Since the design model for tied back walls is empirical, it is valid as long as specific conditions are satisfied. These conditions are as follows:

1. The clear space between soldier beams should not exceed 8 feet. This assures that the lagging or the surface between the soldier beams carries no force except that caused by inward movement of the soldier beams.

2. To eliminate the need for toe restraint, the height of walls using one tier of tiebacks should not exceed 25 feet. Field observation of temporary cuts supported by braces or tiebacks support this conclusion.

3. The soil behind the wall must be drained so the pheratic surface does not intersect the wall.

4. The coefficient of active earth pressure should be determined as shown by Figure 1.

5. Lateral force due to surcharge, to point loads, and to line loads must be included by superimposition on the envelopes shown in Figure 1.

SECTION 2. CORROSION PROTECTION OF PERMANENT TIEBACKS

2.1 THE CORROSION PROCESS IN TIEBACKS

Tieback tendons are susceptible to galvanic corrosion, stray current corrosion, and hydrogen embrittlement. Galvanic corrosion of steel occurs in the presence of water and oxygen. The oxygen creates the galvanic cell and the water becomes the electrolyte. Galvanic corrosion reduces the cross section by pitting and creates conditions favorable for hydrogen embrittlement and stress-corrosion cracking. Hydrogen embrittlement and stress-corrosion cracking cause corrosion which penetrates the cross section and causes brittle failure of the steel.

Galvanic Corrosion

Galvanic corrosion occurs in the presence of water and oxygen. Concentration of the oxygen on the surface of the steel makes one area electrically positive with respect to another area. This creates an internal system for flow of electrons in the metal from the anode to the cathode. Internal flow of electrons reduces potential differences and produces excess electrons at the cathode and free iron ions at the anode. Water in contact with the surface ionizes into hydroxyll ions (OH^-) and hydrogen ions (H^+) and creates a weak electrolyte. As shown in Figure 2, hydroxyll ions migrate to the anode and chemically combine with iron ions (Fe^{++}) to form corrosion products and create a pit in the surface of the steel. In a similar manner, hydrogen ions migrate to the cathode, capture an excess electron and become molecular hydrogen or water.

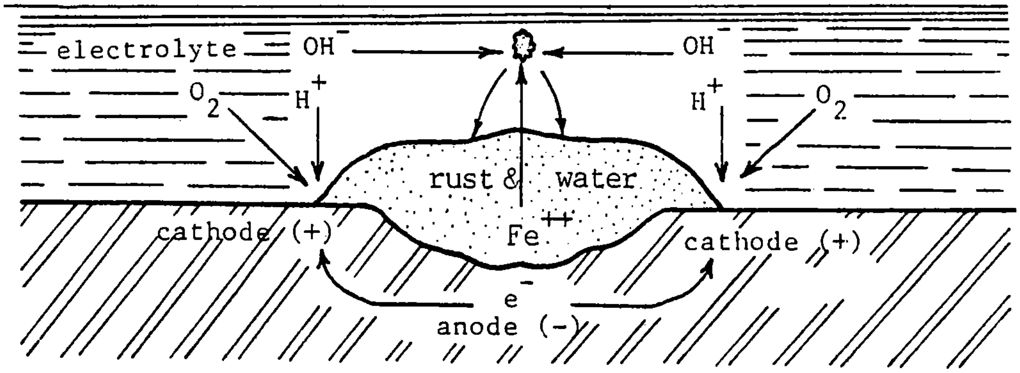

FIGURE 2. TYPICAL GALVANIC CORROSION CELL

There are two types of galvanic cells: local and long line. **Local galvanic cells** (Figure 2) occur when cathodes and anodes are adjacent. Local cells are created when bare steel is exposed to the atmosphere. The corrosion spreads by repetitive formation of adjacent cathodes and anodes. Local cells do not occur if oxygen or water is absent. For tiebacks, local cells will occur in regions of saturation and aeration. The bond length and unbonded length occur in regions deficient in oxygen; thus, formation of local corrosion cells on the bond or unbonded lengths of tiebacks is unlikely. However, formation of local corrosion cells is very probable at the anchorage.

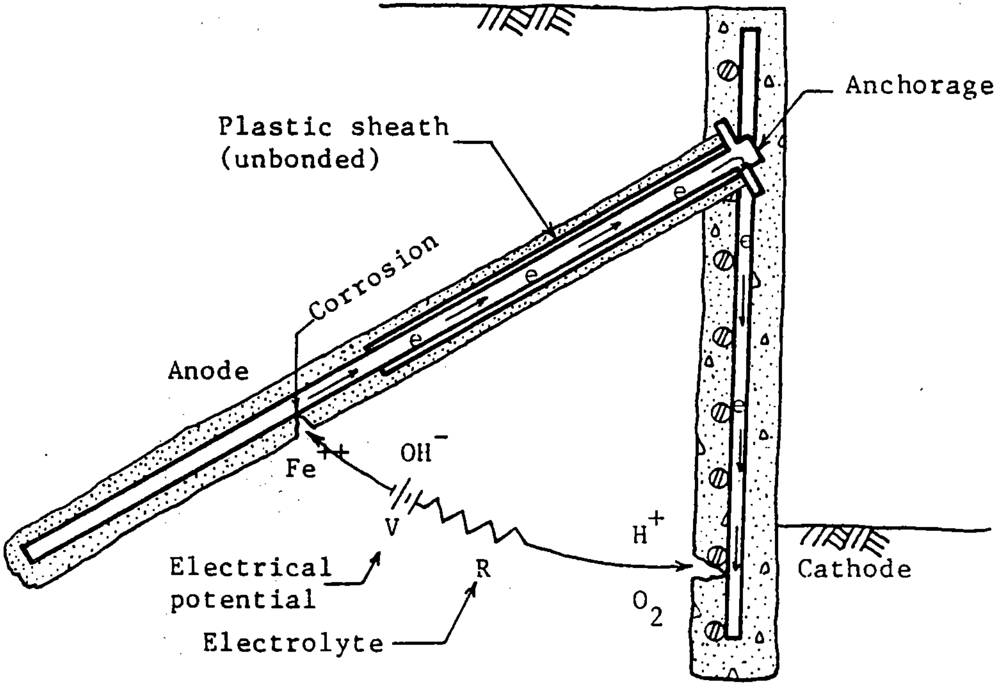

FIGURE 3. LONG LINE GALVANIC CORROSION CELL

Long line galvanic cells (Figure 3) may form when the steel internally connects a region deficient in oxygen with a region abundant in oxygen, and the two regions are externally connected by an electrolyte formed from ground water. In the absence of protective systems, long line galvanic cells are the most probable cause of corrosion to the bond lengths of tiebacks with simple corrosion protection. Even if the soil electrolyte is very weak (soil resistivity greater than 2,000 ohm-cm), this cell operating over several decades may cause pitting of the steel in the bond length of the tieback.

However, galvanic corrosion can be prevented by one or a combination of several methods. Coating systems keep water and oxygen from the surface of the steel, passivation of the steel prevents the formation of differential cells in the presence of oxygen, and organic inhibitors form ion diffusion barriers that prevent the chemical reactions at the anode and cathode.

Stray Current Corrosion

Stray currents may damage the tieback tendon by pitting the area where the the current leaves the tendon. This system, illustrated by Figure 4, requires stray currents in the ground and conditions necessary for the tieback to become a part of the circuit. The current, I, enters at a location, point A or B, and returns to the ground at point C. At C electrons are removed from the iron and the iron ions chemically combine with ions from the electrolyte, ground water, to form corrosion products and pits in the surface of the steel. Electrical insulation of the tendon from the ground by encapsulation prevents stray current corrosion.

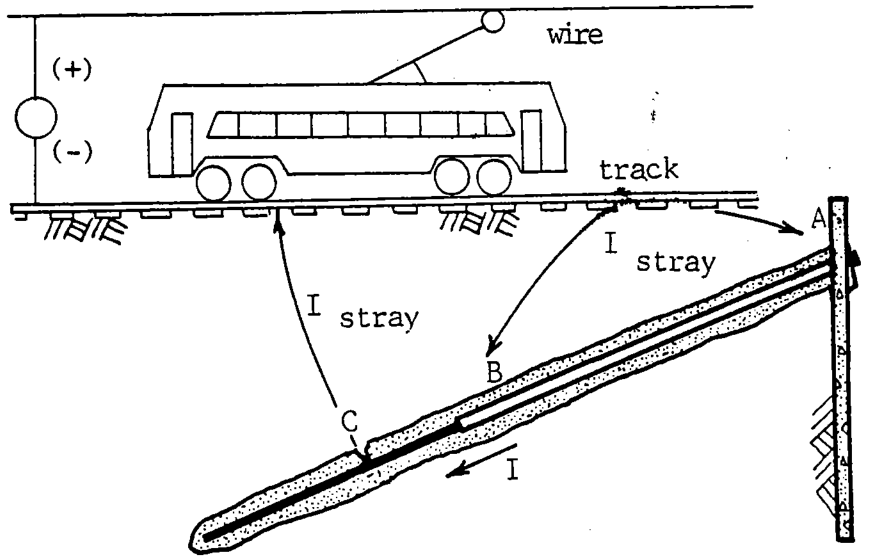

FIGURE 4. CORROSION BY STRAY ELECTRIC CURRENTS

Hydrogen Embrittlement & Stress-Corrosion Cracking

Hydrogen embrittlement and stress-corrosion cracking have caused brittle failures of high strength steels at tensile stresses less than the yield stress. These failures occur because ions enter the lattice of the steel, become molecules and, in concert with the tensile force, crack the section normal to the direction of the tensile force. The corrosion processes are not well understood, but the effects have been observed and documented. However, steels meeting the requirements of ASTM-A416 and ASTM-A722 have not been found subject to brittle corrosion failures, provided the steel has been protected from galvanic corrosion.

2.2 CORROSION PREVENTION IN PERMANENT TIEBACKS

Three material groups -- passivators, organic inhibitors, and coatings -- prevent corrosion of the steel strand in tieback tendons. Passivators create a surface condition on the steel that prevents formation of differential aeration cells. Organic inhibitors form a thin film on the surface of the steel that acts as a diffusion barrier and prevents passage of ions between the surface of the steel and the electrolyte. Coatings cover the surface of the steel and exclude water and oxygen from the surface of the steel. Encapsulation is a polymer coating which protects the passivator or inhibitor from hostile environments.

Passivators

Passivity is a property acquired by a metal that prevents oxygen from forming differential aeration cells on the surface. Passivators are usually inorganic substances that form adsorbed films over the metal surface and shift the corrosion potential several tenths of a volt in the positive direction, which in turn reduces the corrosion rate to very low values.

Portland cement grout in contact with bare steel passivates the steel. The grout produces a pH of 12.5. In this alkaline condition, the initial corrosion product is a thin film of hydrous ferrous oxide which passivates the steel and prevents further corrosion. This film is maintained as follows:

- In non-aggressive conditions, cover the bare steel with a minimum thickness of 0.5 in. (13 mm) of portland cement grout.

- In aggressive conditions, cover the bare steel with a minimum thickness of 0.2 in. (5 mm) of portland cement grout and encapsulate the grout with a smooth or corrugated high density polyethylene, polyvinyl-chloride or polypropylene sheath. The 0.2 in. (5 mm) grout cover provides sufficient cement paste to maintain alkaline conditions, and the encapsulating sheath protects this grout cover from damage by the surrounding aggressive ground conditions.

Organic Inhibitors

Organic inhibitors form a thin film on the surface of the steel that acts as a diffusion barrier and prevents passage of ions between the surface of the steel and the electrolyte. This barrier prevents the chemical reactions that cause pitting and formation of corrosion products.

Corrosion inhibitor grease is an organic inhibitor. It adsorbs to the steel surface by its bipolar structure and forms a diffusion barrier. It also serves as a lubricant to reduce friction between the steel and the smooth plastic sheath that surrounds the corrosion inhibitor. Corrosion is prevented so long as the adsorbed film of inhibitor grease covers all the steel surface as shown in Figure 5.

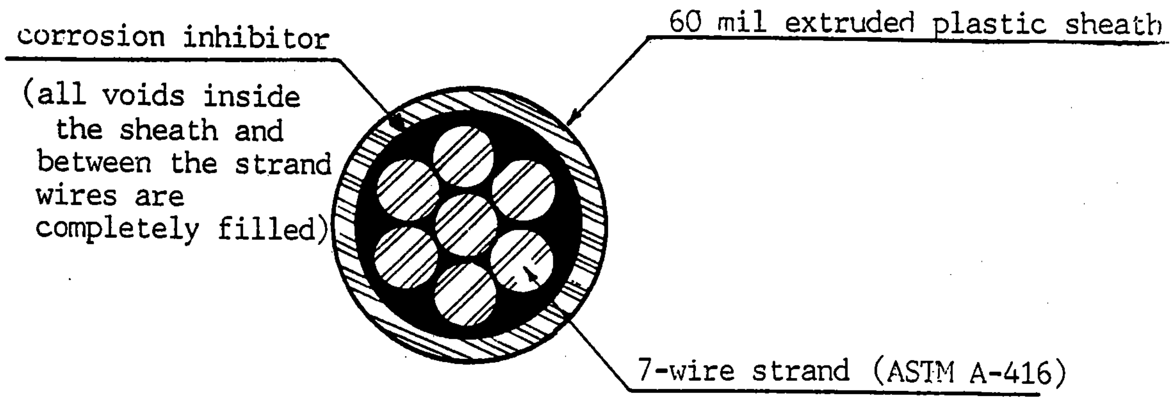
corrosion inhibitor
(all voids inside the sheath and between the strand wires are completely filled)
60 mil extruded plastic sheath
7-wire strand (ASTM A-416)

FIGURE 5. CORROSION PROTECTED EXTRUSION COATED 7-WIRE STRAND

Because the corrosion inhibitor grease dissolves when exposed to fresh portland cement paste and slowly degrades when exposed to moving water, it must always be protected by a smooth plastic sheath. In addition, all voids inside this smooth plastic sheath must be filled by corrosion inhibitor. The best way to satisfy both these requirements is to extrusion coat the strand as follows:

- Coat the exterior, exposed surface of the steel with corrosion inhibitor so the minimum film thickness after application of the encapsulating plastic sheath is 0.005 inch (0.13 mm).
- Hot melt extrude a seamless plastic sheath having a minimum wall thickness of 0.060 inch around the strand and corrosion inhibitor insuring that all voids inside the plastic sheath, including the volume between the wires of 7-wire strand (ASTM A-416), are completely filled with corrosion inhibitor (Figure 5). Post-tensioned, unbonded strand tendons (ASTM A-416) have failed by corrosion when coated by corrosion inhibitor that did not completely fill the plastic sheath. No failures of completely filled sheaths (extrusion coated strand) have been reported. Therefore, an extrusion coated unbonded length will require no additional encapsulation in either aggressive or non-aggressive conditions.

Coatings and Encapsulation

Coatings cover the surface of the steel and exclude water and oxygen from contact with the surface of the steel. Coatings differ from passivators and inhibitors in that they do not alter the basic tendency of the metal to corrode.

Encapsulation with a polymer coating protects a passivator or inhibitor from the effects of water and oxygen and also acts as an electrical insulator against stray electrical currents.

Encapsulation of the bond length with corrugated plastic sheathing, necessary only when ground conditions are aggressive, protects the passivation provided by portland cement grout on the bare steel. However, encapsulation of the unbonded length with a smooth plastic sheath over the corrosion inhibitor is always necessary to protect the corrosion inhibitor grease which in turn prevents corrosion.

Ground Conditions

Ground conditions defined by the parameters pH, resistivity, presence of sulfides, corrosion history of buried steel structures and stray electrical currents indicate the level of protection necessary to prevent corrosion of the tieback tendon. Ground conditions have been described as aggressive or non-aggressive depending on their expected effect on the passivator, organic inhibitor or coating. Ground conditions have been classified as follows:

Non-aggressive	Condition	Aggressive
4.5	**Ground < pH <**	4.5
2,000 ohm-cm	**< resistivity ≤**	2,000 ohm-cm
not present	**chlorides or sulfides**	present
no record	**damage to buried steel**	record
not present	**stray current**	present

Ground water with a pH less than 4.5 will depassivate steel by preventing the formation of the passivating film on the surface of the steel or by dissolving it. Then if oxygen is present, corrosion will occur. Soils with **resistivities** less than 2,000 ohm-cm indicate the presence of electrolytes that will cause corrosion of depassivated steel in the presence of oxygen. **Sulfides** act as a catalytic poison which prevent formation of hydrogen gas at the cathode; hence atomic hydrogen can invade the steel lattice and cause hydrogen embrittlement. **Chlorides** depassivate the steel. A history of corrosion **damage to buried steel** in the area indicates aggressive conditions. Tiebacks attract **stray currents** because concentration of oxygen at the anchorage makes the anchorage positive with respect to the bond length and the steel tendon is an excellent conductor.

2.3 CORROSION PROTECTION DETAILS FOR 7-WIRE STRAND TIEBACKS

Details for corrosion protection are dependent on the function served by the particular part of the tendon. The parts of a tendon divided by function are bond length, unbonded length and anchorage. Corrosion protection materials and their configuration are designed to prevent formation of galvanic cells and when necessary further protect the corrosion protection system from deterioration.

Bond Length

The bond length anchors the tendon to the soil or rock with portland cement grout. Grouts used will produce a pH = 12.5 at the surface of the steel, which passivates the steel. As long as the passivation exists, the steel will not corrode in the presence of water and oxygen. Tiebacks are usually anchored in undisturbed soil or in rock where oxygen is not present. This condition, combined with experience that steel failures in tiebacks have not occurred in the bond lengths, strongly supports using portland cement grout to protect the steel from corrosion when subsurface conditions are non-aggressive.

Simple corrosion protection is the system used to protect the bond lengths of tiebacks in non-aggressive soils and rocks. Details for this system are shown by Figure 6. All strands of the tendon in the bond length must be surrounded with portland cement grout which has a cement factor equal to or greater than 9 bags of cement per cubic yard of grout. In addition, the grout cover over the strand must be at least 0.5 inch.

This 0.5 inch cover has been prescribed from practice and there is no evidence that greater cover gives better corrosion protection. Unless ground pH in the bond length is less than 4.5, which is nearly always associated with soil resistivities less than 2,000 ohm-cm and/or the presence of sulfides, simple corrosion protection is satisfactory and represents good engineering practice.

The FIP Working Group on Ground Anchorages reported on 34 tieback failures of which 2 were in the bond length. One partially grouted tendon exposed to ground water containing chlorides and sulfides failed by severe galvanic corrosion after 5 years of service. The other had only 0 in. to 0.25 in. of grout cover. Both failures involved tendons with problems shown by Figure. 7.

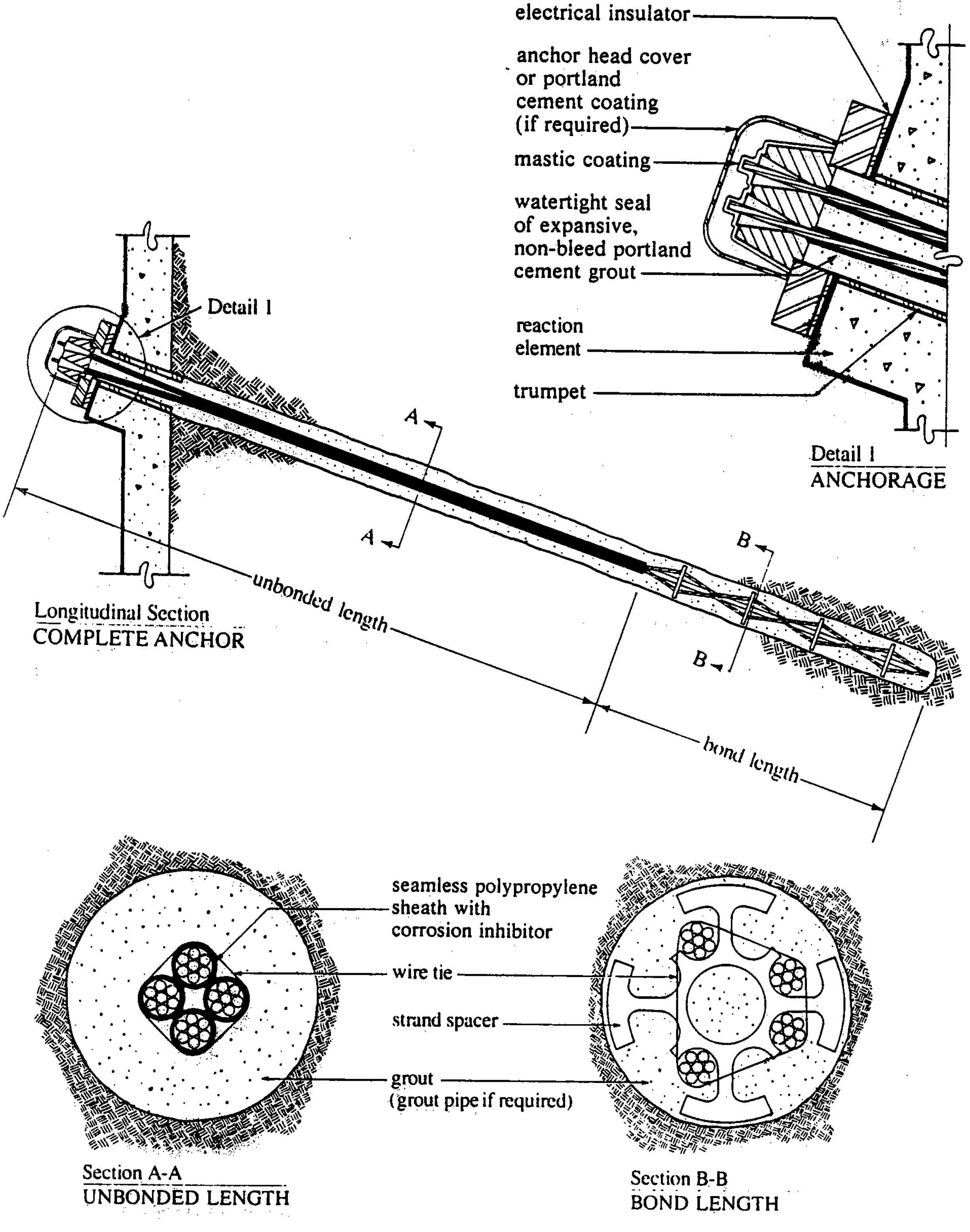
electrical insulator
anchor head cover or portland cement coating (if required)
mastic coating
watertight seal of expansive, non-bleed portland cement grout
reaction element
trumpet
Detail 1
ANCHORAGE
Detail 1
A
A
B
B
Longitudinal Section
COMPLETE ANCHOR
unbonded length
bond length
seamless polypropylene sheath with corrosion inhibitor
wire tie
strand spacer
grout
(grout pipe if required)
Section A-A
UNBONDED LENGTH
Section B-B
BOND LENGTH

FIGURE 6. SIMPLE CORROSION PROTECTED PERMANENT TIEBACK

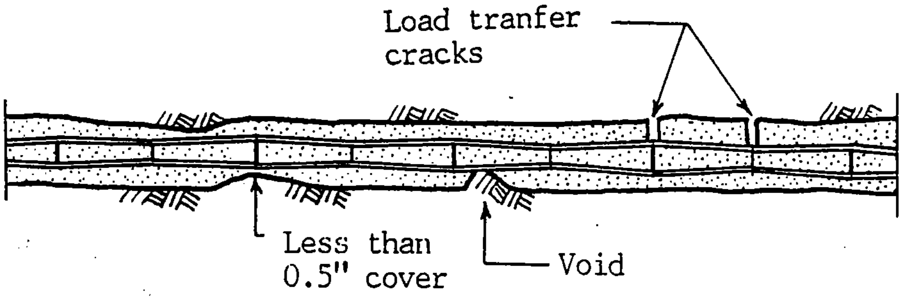

FIGURE 7. GROUT COVER DEFICIENCIES IN SIMPLE CORROSION PROTECTED TIEBACKS

Bond length encapsulation is a coating of corrugated plastic sheath which covers the portland cement grout. Details for this system are shown by Figure 8. This cover prevents water with pH less than 4.5 from coming into contact with the surface of the steel. A pH less than 4.5 will cause the steel to depassivate or will prevent passivation. Since the oxygen necessary to form local galvanic cells is not generally present in the bond length, encapsulation serves only to prevent formation of long line galvanic cells and prevent sulfides and chlorides from coming in contact with the tendons. Encapsulation works in conjunction with passivation and is not corrosion protection in itself except that it acts as an electrical insulator that protects the tieback from stray electrical currents or that prevents formation of long line galvanic cells.

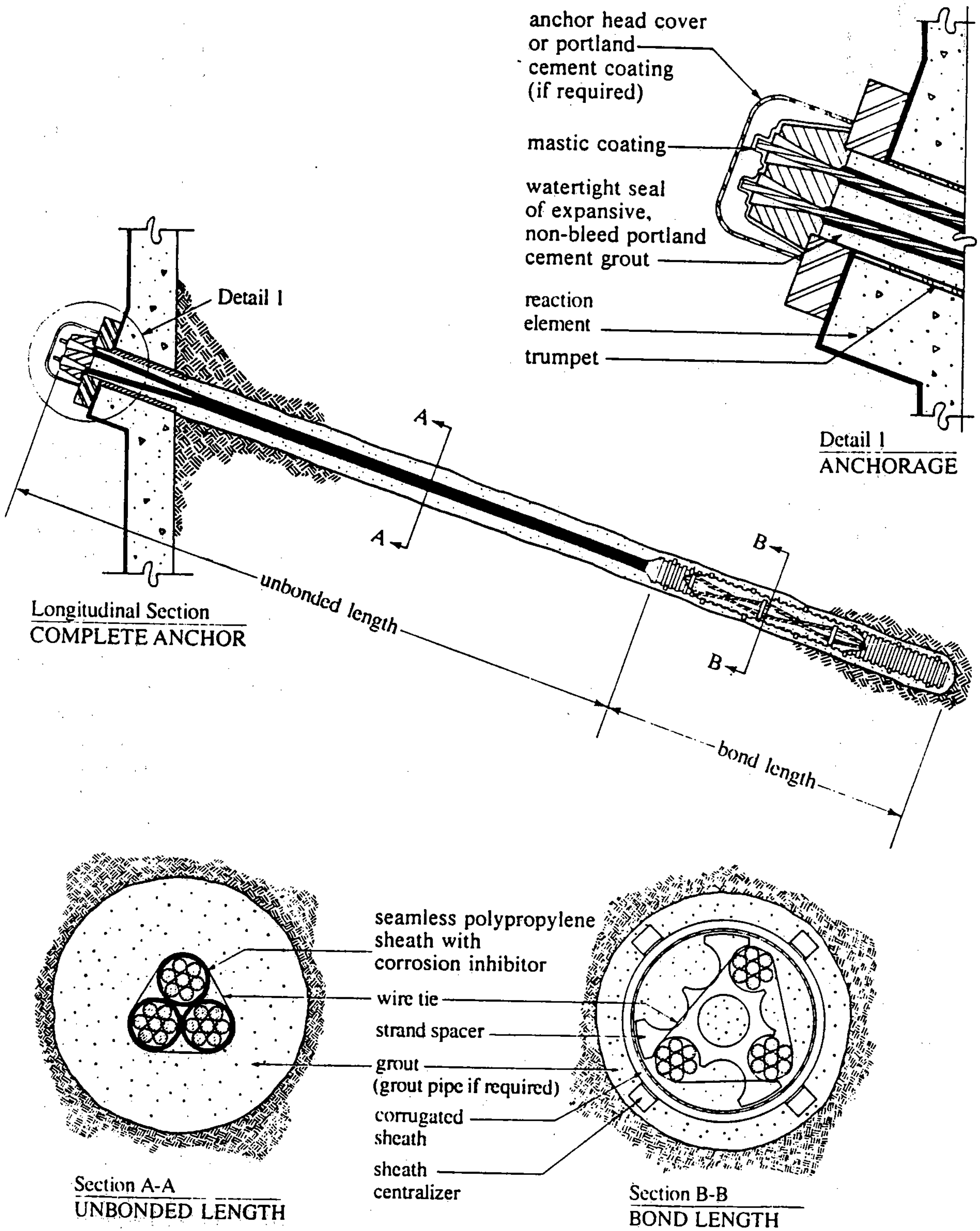
anchor head cover
or portland
cement coating
(if required)
mastic coating
watertight seal
of expansive,
non-bleed portland
cement grout
reaction
element
trumpet
Detail 1
ANCHORAGE
Detail 1
A
A
B
B
unbonded length
bond length
Longitudinal Section
COMPLETE ANCHOR
seamless polypropylene
sheath with
corrosion inhibitor
wire tie
strand spacer
grout
(grout pipe if required)
corrugated
sheath
sheath
centralizer
Section A-A
UNBONDED LENGTH
Section B-B
BOND LENGTH

FIGURE 8. ENCAPSULATED CORROSION PROTECTED PERMANENT TIEBACK

Unbonded Length

The unbonded length transfers the post-tension force from the anchorage to the anchor length of the tieback tendon. Most tiebacks are grouted in a single stage; hence, the unbonded length is designed to transfer this force undiminished and simultaneously give corrosion protection to the tendon. These objectives are accomplished by coating the strand with corrosion inhibitor grease and subsequently encapsulating the grease coated strand in a manner to fill all the spaces between the wires of the strand and the space between the strand and the inner wall of the sheath (Figure 5).

The detail shown by Figure 5 permanently protects the steel in the unbonded length from galvanic corrosion in both aggressive and non-aggressive ground conditions. **Additional encapsulation of the unbonded length is unnecessary unless there is doubt whether or not all space inside of the single strand encapsulation is completely filled with corrosion inhibitor.** When doubt of complete filling of individual strand encapsulation exists, the detail shown in Permanent Ground Anchors, FHWA-DP-68-1, for "Encapsulated Double Corrosion Protected Tendons," should be followed. This figure was detailed to compensate for incomplete filling of the sheath around the individual strands; hence, rigid application of these details eliminate price savings to the project provided by current technology (extrusion coated strand).

Extrusion coated strand is the only system which insures complete filling of all the space inside the plastic sheath with corrosion inhibitor. The extrusion process forces corrosion inhibitor between the 7 wires of the strand and limits sheath shrinkage to a surface that resists further shrinkage. A smooth exterior surface indicates that shrinkage was limited by the corrosion inhibitor film covering the exterior of the steel strand; thus, the sheath is completely filled.

Anchorage

The anchorage allows the lock-off of the tieback post-tension force and permits necessary relative movement between the tieback tendon and the wall. It is highly vulnerable to corrosion because oxygen and water are always present. Figure 9 shows the avenues by which galvanic corrosion attacks the anchorage. The 34 case histories of tieback failures collected by the FIP Working Group on Ground Anchorages showed nineteen failures occurred at or within 3.5 ft. of the anchorage; 20 failures, some included in the 19, occurred in the unbonded length, and 2 failures occurred in the bond length. This data and the exposure of the anchorage to water and oxygen direct special attention to corrosion protection details for the anchorage. These details include anchorhead protection/cover, trumpet design and electrical isolation of the tendon from the structure.

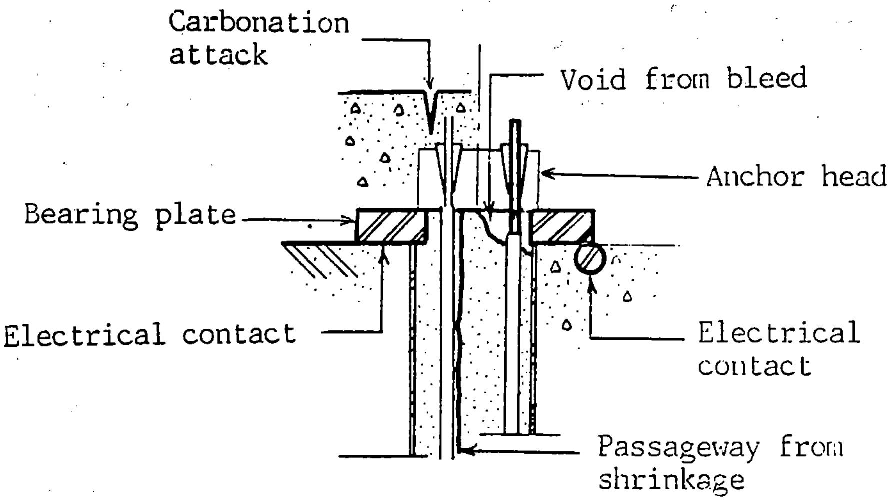

FIGURE 9. AVENUES FOR CORROSION ATTACK ON ANCHORAGES

Anchorheads are field coated with a mastic manufactured to provide corrosion protection to steel and are then covered by steel or plastic caps or by portland cement concrete as shown in Figure 10. The mastic protects the anchorhead from corrosion by calcium carbonate formed by reaction between absorbed carbon dioxide and hydrated cement paste.

Trumpets make a structural void which permits relative movement between the tieback tendon and the wall when the tieback is post-tensioned. They also permit spreading of the strands from the outside diameter of the tendon strand bundle to the strand pattern of the anchorhead. The trumpet can be plastic or steel pipe or tubing or it can be a hole cored through a portland cement concrete structure. The details should be suitable for the application. As shown in Figure 10, the trumpet is filled with expansive, non-shrink portland cement grout after lock-off of the post-tension force. This grout forms a water- and air-tight seal at the underside of the anchor head. This prevents corrosion of the tendon and the underside of the anchor head.

Electrical Isolation prevents corrosion in the bond length by interrupting the internal path for electron flow between the bond length and the steel in the wall exposed to oxygen, thus preventing formation of the long line corrosion cell, shown by Figure 3. Bond length encapsulation also accomplishes this objective by preventing the ground water (electrolyte) from coming into contact with bare steel in the bond length. As shown in Figure 10, electrical isolation adds a mastic coating over the exposed surface of the bearing plate and a sheet of 0.0625 inch thick ultra high molecular weight polyethylene between the anchorhead bearing plate and the structure. Electrical isolation should be used for **ALL** simple corrosion protected permanent tiebacks.

Electrical isolation eliminates the need for encapuslation of the bond length except where sulfides, chlorides, oxygen and/or stray currents are present in the bond length of the tieback. Using electrical isolation instead of bond length encapsulation will substantially reduce the price of the installed tieback without changing the quality.

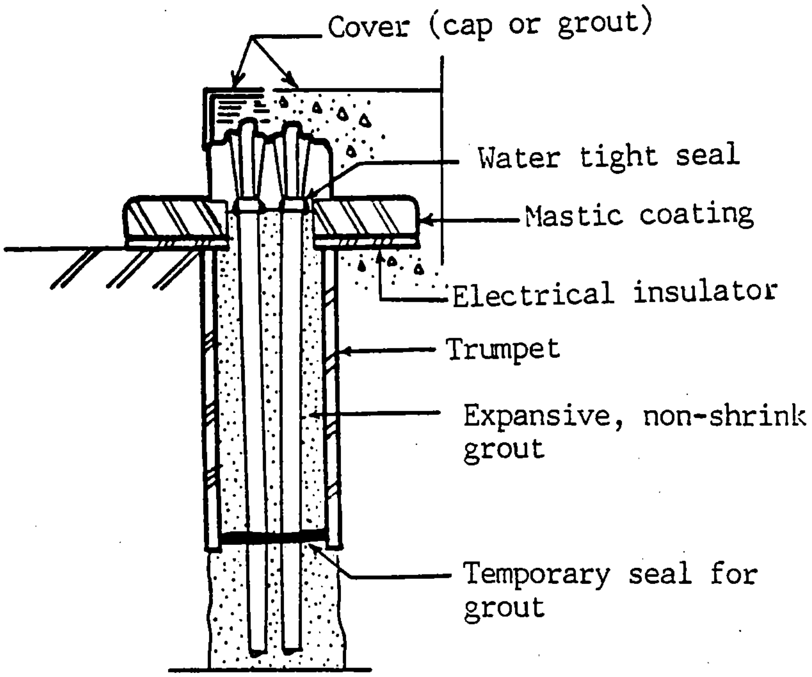
Cover (cap or grout)
Water tight seal
Mastic coating
Electrical insulator
Trumpet
Expansive, non-shrink grout
Temporary seal for grout

FIGURE 10. CORROSION PROTECTION FOR ANCHORAGES

SECTION 3. PERFORMANCE SPECIFICATION OF TIED BACK WALLS

Tied back walls are specified two ways: prescriptive specifications and performance specifications. Prescriptive specifications enlist only the construction expertise of the contractor. Performance specifications enlist both the engineering and the construction expertise of the contractor. Owners can increase the value of their construction by maximum use of performance specifications. This serves to join the owner, the engineer and the contractor in a professional partnership which achieves both quality and value in the completed project.

Performance specifications should include detailed wall descriptions and design parameters, material quality levels based on recognized industry standards, contractor qualification and submittal requirements and prescriptive field load test requirements.

Wall Description

The drawings and specifications should give a geotechnical description of the region that will be occupied by the wall and the tiebacks. The design loads should be given in terms of lateral earth pressure envelopes together with surcharge loads. The final wall dimensions and surface specifications should take into consideration aesthetic and service requirements.

Geotechnical investigations should cover the region occupied by the wall and the tiebacks. These investigations should provide information necessary for design and construction. Since the results of these investigations will be the basis of the design, disclaimers of responsibility should not be used. As a minimum, the following information should be provided:

Shear strength parameters, mechanical analysis, Atterburg limits, water content and standard penetration values for the region between the wall and the estimated shear failure surface.

Rock Quality Index (RQD) for rock in the bond length.

Mechanical analysis, Atterburg limits, standard penetration test values and water content for soil in the bond length.

Resistivity, pH and presence of sulfides and of chlorides in bond length.

Measurement for stray electric currents, if necessary.

Design parameters should include lateral earth pressure envelopes, specify the minimum unbonded length, specify the maximum tendon length if limited by easement, and specify the level of corrosion protection. The earth pressure envelopes should include the factor of safety for the wall along with factored surcharge loads. The minimum unbonded length is specified to satisfy the design requirement that the anchor zone be formed beyond the estimated shear failure surface. Bond length details, except as limited by easements, should be determined by the contractor.

Test load requirements should follow the recommendations of the Post-Tensioning Institute. The overload factor should be specified.

Description of the finished wall should show the overall dimensions of the finished wall in plan and profile. The description specifies the kind of wall surface with respect to acceptable materials and aesthetic quality. Interface requirements of the wall with other parts of the product are defined.

Material Quality Level

Quality is a specific condition which makes material or workmanship good enough to satisfy the service needs of the tied back wall. Permanent strand tiebacks should be specified by quality level based on industry standards. Tieback tendon suppliers have unique designs which satisfy the basic requirements for corrosion protection. However, an element by element comparison of one tendon with another does not establish equivalency. One tieback tendon is equivalent to another tendon if both satisfy the design requirements. Recommended guide specifications for permanent strand tiebacks appear in Appendix A.

Material quality levels should cite recognized industry specifications which are applicable to the materials to be incorporated in the tied back wall. ASTM, AASHTO, PTI, ACI, AISC, and federal and state agencies have published quality level specifications which define the quality level parameters for tied back walls. Quality level specifications should be cited for the following materials:

High strength prestressing steel
Structural steel
Ductile iron
Corrosion inhibitor grease
Plastics used for encapsulation
Portland cement
Admixtures for grout

Material quality levels should be verified by submittals which should include the following:

> Prestressing steel: mill certification reports for each heat used in fabrication of the tieback tendons; one 10 ft sample from each pack of post-tensioning steel used in fabrication of the tieback tendons.
>
> Ductile iron products: foundry heat test reports.
>
> Shop drawings for the tieback tendons and for the tieback anchorage.
>
> Manufacturer's literature for plastics, for corrosion inhibitor and for portland cement admixtures.
>
> Certificates of compliance for all materials.

Contractor Requirements

Contractor prequalification requirements and design documents required for submittal should be included in the specifications. These requirements should be structured to assure that the owner has the opportunity to be satisfied with the design concept before the opening of bids and that the owner can assure that the successful contractor is competent to build the wall.

Contractor prequalification should include the owner's usual requirements for competency and require submission of the design required for preliminary review. The contractors qualified by experience and by an approved design should be exclusively listed in the bid documents as the only contractors qualified to bid the tied back wall specified by the performance specifications. This will ensure a competent wall design by an experienced contractor. The general contractor should specify in its bid the tied back wall offered on by naming a contractor from the approved list. Specifying the tied back wall contractor should be a condition of the offer tendered by the bid.

Submittals required should be specified by scope and schedule. Required design calculations, including software documentation, should be specified. A review schedule should recognize the contractor's need for timely approvals and be closely followed by the engineer/owner to prevent delays in mobilization and materials acquisition.

SECTION 4. FIELD LOAD TESTING OF TIEBACKS

4.1 BACKGROUND FOR LOAD TESTS

Each tieback should be field tested to determine its acceptability. Prescriptive test procedures have been developed for tiebacks to establish uniform practice for acceptance and to allow comparison of test results. Four tests are prescribed to determine acceptability of tiebacks: performance, proof, creep and lift-off. Since this practice has been developed through the world wide experience of engineers, prescribed procedures should be altered only when there is a body of new or local experience that supports the change.

The Post-Tensioning Institute (PTI) has published the current testing practice in its "Recommendations for Prestressed Rock and Soil Anchors," a part of the Post-Tensioning Manual, 4th Ed (1985). The PTI testing recommendations are prescriptive and should be carefully followed in the field. This will assure uniform data with respect to procedures and give confidence that the parameters measure tieback behavior.

Load Test Parameters for Acceptance of Tiebacks

Acceptable tiebacks satisfy prescribed creep and elongation parameters at the specified test loads. These parameters are index properties developed from load tests of tiebacks which have satisfied actual service conditions.

Test Load is the design load times a factor that assures that all probable values for the creep rate at the design load will be less than the creep rate measured at the test load. The PTI recommends that the design load include the factor of safety for the design and that the ratio between the test load and the design load be 1.33. Tiebacks tested with this overload factor have proved safe and economical, without excessive steel or unnecessarily large drill holes.

The test load factor is not a part of the factor of safety against failure. The test load measures a creep rate which is the upper limit for all creep rates probable for the tieback at the design load. For example, if the test load factor is 1.5, if the design load does **not** include a factor of safety, and if the measured creep rate at the test load is 0.08 inch per decade, the design load factor of safety would be 1.5/1.33 or 1.13, not 1.5.

Total Elastic Elongation is a parameter that shows that the post-tensioned force has been transferred to the desired place in the soil or rock. The PTI acceptance criteria recommends a lower and an upper limit for total elastic elongation of tiebacks anchored in rock and **only** a lower limit for tiebacks anchored in soil.

Because a tieback anchored in rock behaves like a straight shaft in a uniform material, the upper limit (theoretical elastic elongation of the stressing length plus 50% of the bond length) is valid. This criteria is not valid for soil anchors because they do not behave as straight shafts in a uniform material. The upper limit approximates how much of the bond length has been mobilized in transfer of the post-tension force to the rock. The upper limit alone should not be used to disapprove a production tieback. Creep behavior should also be considered, and a decision based on both parameters.

The lower limit (80% of the theoretical elastic elongation) should always be satisfied in both rock and soil. This indicates that the post-tension force has been transferred to the soil or rock beyond the failure surface. Tiebacks which have less than 80 percent of the theoretical elastic elongation of the stressing length may permit unacceptable post-construction movements of the wall which will result in settlement behind the wall. The 80 percent factor comes from practice and arbitrary increase is not recommended.

Creep is change in strain at a constant load. In tieback load tests this movement occurs at the grout-soil/rock interface under repeated loading. Creep measurements made by load tests indicate a creep range because a specific value for the actual creep cannot be predicted. In general, the relationship between creep displacement and time is an exponential function: a straight line when plotted to a semi-log scale. The slope of this line is the creep rate.

The creep rate recommended by the PTI is a parameter which has been developed from field experience. Load tested tiebacks with creep rates equal to or less than the recommended value have not failed. The creep rate shows that the tieback will be safe; however, the creep rate will not accurately predict magnitude of creep which may be expected over the life of the structure. For this reason, the creep rate is determined at a test load greater than the design load to assure that it represents an envelope which will contain all probable creep values for that design load.

4.2 DESCRIPTION OF FIELD LOAD TESTS

Field load tests of tiebacks verify the design load for each production tieback by measurement of elastic elongation and creep parameters. This verification is necessary because of variations in ground conditions and lack of visual verification of installation work. Further, testing of each production tieback eliminates the need to compound the factor of safety to include variations in workmanship.

Four types of field load tests are used to confirm tieback acceptability: performance, proof, creep, and lift off tests. Performance, proof and creep test verify the capacity of each tieback. Lift-off tests verify that the restraint force in the tieback equals the specified lock-off load. Performance, proof and lift-off test should always be specified. Creep tests are specified only for anchors in cohesive soils (soils with a plasticity index greater than 20) or creep sensitive sedimentary rock.

Performance Test

The performance test measures the apparent elastic elongation of the tieback and the creep rate at the test load. Performance tests should always be carried out on the first three anchors and a percentage of the remaining anchors. In the performance test the anchor is incrementally loaded and then unloaded back to the initial alignment load according to a schedule of successively higher loads up to the test load. The test load is then held constant for 10 minutes to measure the creep rate.

The time for the creep measurement at the test load starts when the load application from the next lower increment begins, and the first reading occurs at 60 seconds. Once the test load is applied, it must be maintained as constant. This may require some repumping of the hydraulic jack to compensate for small movements or minor hydraulic oil seepage, but care should be taken not to exceed the value of the test load.

If recorded movement for the load hold period exceeds the acceptance criteria, the load is held for an additional period. A sample performance test pattern is shown in Figure 11.

The difference between the total elongation at a load increment and elongation at the subsequent alignment load is the apparent elastic elongation of the tieback. The apparent elastic elongation parameter indicates that the post-tension force has been transferred to the soil or rock along the bond length and not along the unbonded length.

The creep rate is the elongation per decade measured for constant test load. The creep rate is an indicator of whether or not the tieback will maintain the lock-off load during the design life of the structure. It is affected by the rate of incremental loading and by whether the test load was maintained at a constant value during the load hold period. These effects are normalized if the time interval between successively higher load increments is less than 60 seconds and each load increment, except the test load, are held only long enough to read and record the elongation of the tendon.

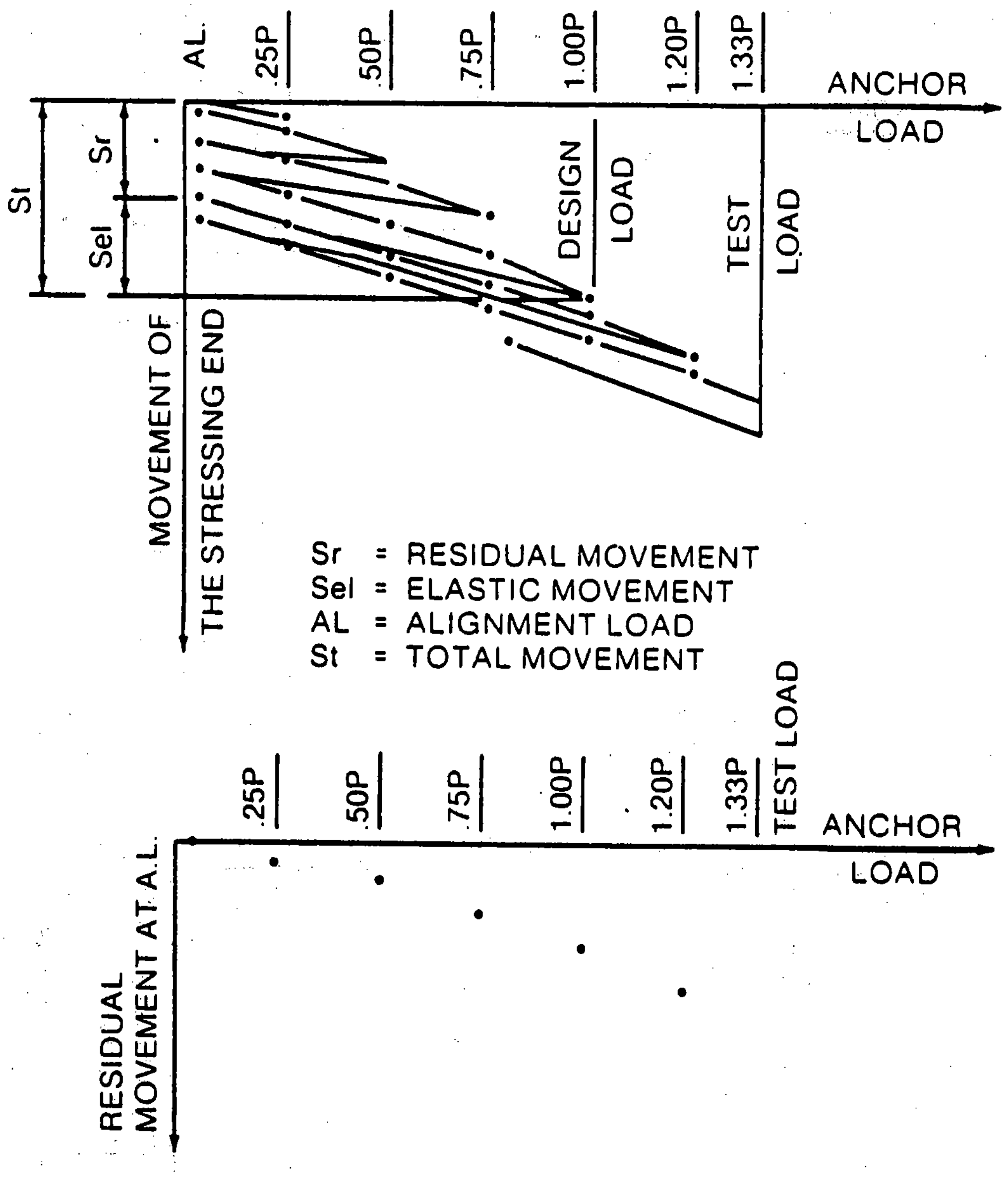

FIGURE 11. PERFORMANCE TEST RESULTS
(Figure reprinted from "Prestressed Rock and Soil Anchors," published by the Post-Tensioning Institute, Phoenix, AZ. Used by permission.)

Proof Test

The proof test measures the total elongation of the tieback and the creep rate at the test load. All anchors which are not performance tested are proof tested. The proof test also incrementally loads an anchor in accordance to a schedule, but differs in that the loads are only indexed upward to the test load. The test load is held constant for a load hold period similar to the performance test, and then, if the recorded movement is acceptable, the tieback is adjusted to the lock-off load. A sample proof test pattern is shown in Figure 12.

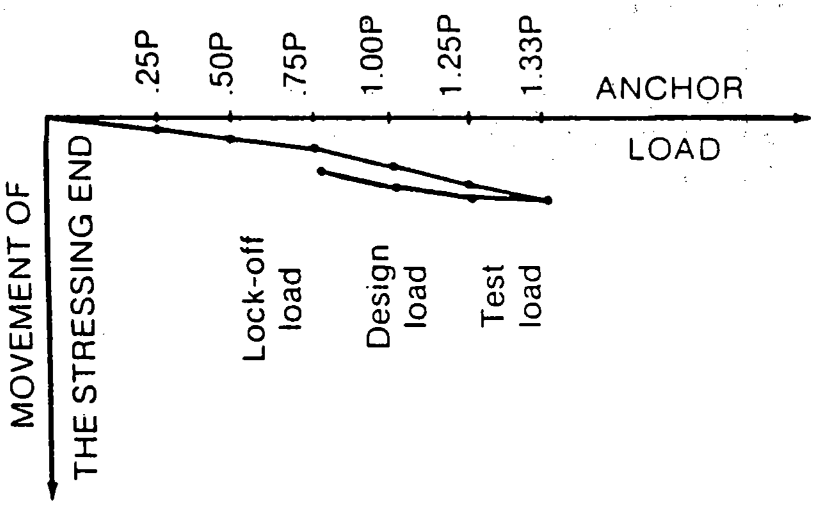

FIGURE 12. PROOF TEST RESULTS
(Figure reprinted from "Prestressed Rock and Soil Anchors," published by the Post-Tensioning Institute, Phoenix, AZ. Used by permission.)

The total elongation and creep rate should be comparable to neighboring performance tested tiebacks. The magnitude of the test load, and time for the load hold period, should be the same for proof and performance tests; otherwise, there is no basis for comparison of results between the two tests. Total elongation at the test load in the proof test may be less than for the comparable performance test because the duration of the loading is less in the proof test. Creep rates for load hold periods up to 60 minutes may be greater in the proof test than those for comparable performance tests.

As described for the performance test, the creep rate during the prescribed test period depends upon the rate of incremental loading and upon whether the test load was maintained at a constant value. The time intervals for applying and holding the test loads and the need for maintaining constant test load also applies to proof tests.

Creep Test

Creep tests measure the apparent elastic elongation of the tieback, the creep rate at all load increments up to and including the test load, and the failure load of the tieback. The creep test determines the suitability of tiebacks anchored in cohesive soil and the ultimate capacity of the tieback. While both performance and proof tests also measure the creep rate, the creep test measures creep rate over a longer time period to evaluate creep sensitivity. In the creep test, each load increment is held for a prescribed length of time. Temporary anchors are typically held at the test load for 100 minutes and permanent anchors for 300 minutes. Movement recorded at each load hold is plotted on a log scale to describe the creep rate, which is evaluated to predict future movement or creep failure. Typical creep test results are illustrated in Figure 13.

Total elongations at the test load will be greater for the creep test than those recorded for corresponding performance tests. Creep rates for time less than 60 minutes will be less for the creep test than creep rates recorded for corresponding performance tests.

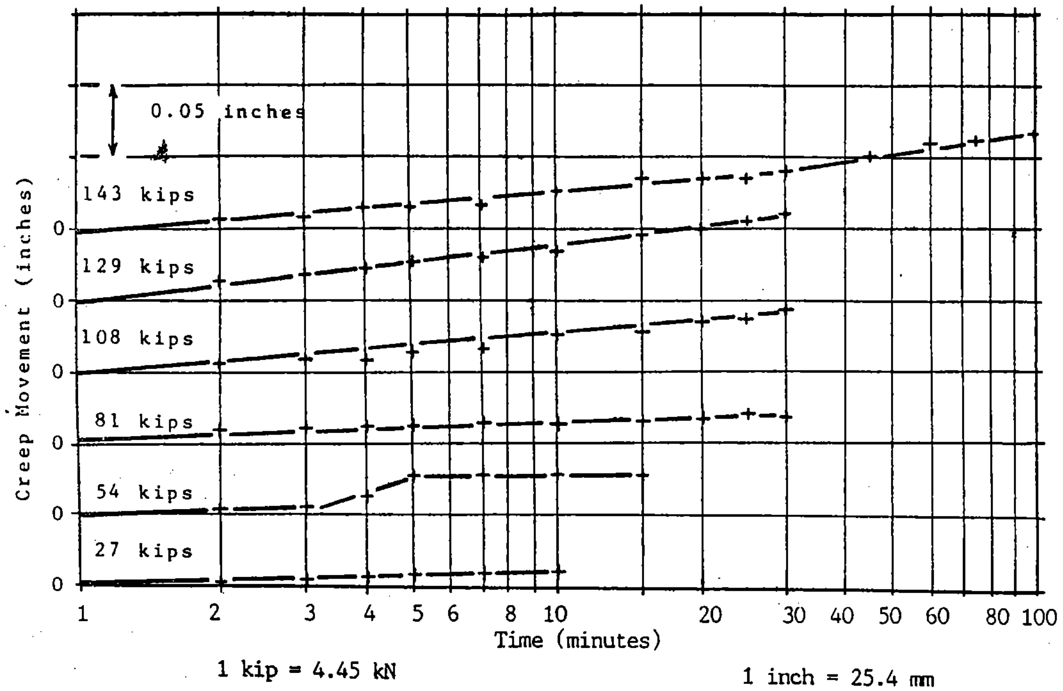

FIGURE 13. CREEP TEST RESULTS

The plot of the creep rate at a particular load increment vs. the load increment should be a straight line and be less than 0.08 in. per decade of time. Creep failure is indicated as this plot becomes an arc. Such a plot, examined by the method of double tangents, indicates the failure load, which is greater than the load for which the creep rate is less than or equal to 0.08 inch per decade.

As described for performance and proof tests, the creep rate at a given load depends upon the rate of incremental loading and upon whether the test load was maintained at a constant value. The time for increasing the load to the next higher increment must be less than 60 seconds, and the load at each increment must be maintained at a constant value. The time for holding constant load at each increment must start when load application from the next lower increment begins. Following of the prescribed procedures assures that the measured creep rate will show whether or not the soil is suitable for permanent tiebacks.

Lift-Off Test

Lift-off tests measure the post-tension force in the tendon after transfer of the post-tensioning force to the anchorage. The test involves jacking to determine the load at which the stressing anchorage lifts off the bearing plate or the wedges move off the anchor head to verify that the actual restraint force in the anchor is the specified lock-off load, less time dependent losses. The PTI divides this test into 2 parts: initial lift-off readings and lift-off test. Initial lift-off readings should be made for each production tieback. This assures that the lock-off procedures produce reliable and accurate lock-off loads.

Lift-off tests, typically done on randomly chosen anchors, may be done 24 hours to 7 days after lock-off. If tiebacks are properly load tested and lock-off loads are within specification limits, any recorded loss of post-tensioning load is probably due to inward movement of the wall. The significance of this movement depends on the particular job.

4.3 QUALITY CONTROL FOR TIEBACK LOAD TESTS

Quality control for load tests assures that the test parameters were accurately measured using established procedures. The results can then be compared with the results of other tests for the job and for other related work. Effective quality control requires understanding the basis for the prescriptive requirements of the load test specifications and insisting that the procedures are followed. In addition, certain precautions must be observed to prevent damage to the tendon and assure proper lock-off of the tieback.

Procedures

A copy of "Recommendations for Prestressed Rock and Soil Anchors" (available from the PTI) should be kept by the inspector on the job and used to supplement and support project specifications. These recommendations have commentary which provides background for the test procedures. Tiebacks load tested using these procedures and satisfying the specified acceptance criteria have given satisfactory performance.

Acceptance criteria are based on creep rate at the test load. The magnitude of the creep displacement during a time interval depends on the strain history prior to the time interval. Holding the load longer than necessary to stabilize the load at that increment while recording the elongation is unnecessary and undesirable when performing performance and proof tests.

Equipment

Test equipment includes a hydraulic ram, an electric hydraulic pump, pressure gages accurate to 100 psi, a 4 inch dial gage extensometer, and, if creep tests are required, a load cell. All equipment must be in good working order.

Hydraulic rams should be free of leaks and calibrated; the calibration chart shall be at the site. Rams shall not leak hydraulic fluid and pistons shall be clean and free running in the ram cylinder. Load readings less than 10 percent of the capacity of the ram are often nonlinear; therefore, the capacity of the ram should be no greater than twice the test load. Rams used with multistrand tendons shall be capable of simultaneous stressing of all strands in the tendon.

Two **certified pressure gages** should be provided, one gage used for testing and one gage used to recertify the production gage at the beginning of each shift. If the ram was calibrated with a certified gage, any certified gage can be used for the load test. Certified gages used with calibrated rams in good working order will measure tieback test loads to a tolerance of ± 5 percent.

Extensometer dial gages have become the standard device to measure tieback elongation under test loads. The plunger should be free moving and clean. A gage with a four inch travel is recommended so resetting the gage during a load test will not be necessary. While resetting is permissible, it introduces the possibility of errors in data reduction.

Load cells are recommended only for use during creep tests. Load cells allow maintenance of a more constant load than is possible with a pressure gage alone, and give a sharp benchmark against which very fine load adjustments can be made during the extended load hold periods of the creep test. For performance and proof tests however, anchorage tolerances and site conditions do not permit load cell installation that will give accurate and repeatable measurements. For these tests, certified pressure gages used with calibrated jacks give sufficiently accurate and repeatable measurements.

Inspectors' Check List

Accurate test results will be obtained if pre-test, in-test and post-test inspections are made. Tieback failures other than failure between the anchor grout and the soil or rock are usually due to improper procedures which can be prevented by inspection.

Pre-test inspections establish that conditions necessary for a successful test are satisfied. The recommended check list for strand anchors follows.

Ensure that:

1. Hydraulic ram has been calibrated and calibration chart is available.

2. Two certified gages are available and the production gage has been job certified against the job reference gage.

3. Hydraulic ram does not have hydraulic leaks, and the piston travels freely in its cylinder.

4. Load increments can be applied in less than 60 seconds.

5. The tendon alignment is verified as follows:

   The tendon passes through the trumpet and bearing plate such that it will not bind over sharp edges when stressed.

   The hand fit of the anchorhead in the bearing plate is such that the angle between the top of the bearing plate and the bottom of the anchorhead is less than or equal to 3 degrees.

6. The hydraulic ram and other parts of the stressing system are centered on the axis of the stressed tendon within an off-center tolerance of ± 1/16 inch.

7. The dial gage is mounted on a frame of reference independent of the movement of the anchorage or the wall.

In-test inspections assure that the test parameters will be properly measured and recorded. The recommended check list for strand tiebacks follows.

Ensure that:

1. All reusable strand wedges in the stressing head stop moving at the same time during the application of the alignment load.

2. The time interval between application of successive load increments is less than 60 seconds. Load increments less than the test load are held no longer than necessary to stabilize the load and measure the elongation.

3. The time for the load hold period starts when the load is applied from the next lower increment.

4. The test load is maintained, so far as practical, at a constant value and elongation measurements are made at the specified times.

5. Results of the load test are recorded on the specified form as the test proceeds.

Post-test inspections assure that the post-tension force is within the limits specified for the lock-off load. The recommended check list for strand tiebacks follows.

Ensure that:

1. Initial lift off tests made on each production tieback are within prescribed limits.

2. Wedges are evenly seated — the difference between the tops of the wedge halves should be less than 1/8 inch. Transverse cracks in the tops of these wedges occur but do not reduce the load holding capacity of the wedges.

3. Results of all load tests are recorded, plotted and submitted to the engineer for approval.

APPENDIX A. GUIDE SPECIFICATION FOR PERMANENT STRAND GROUND ANCHORS

1.0 Scope

This specification establishes the quality level for corrosion protection of 7-wire, grade 270 K, prestressing steel used for permanent ground anchors.

2.0 Reference

Except as modified by this specification the corrosion protection shall comply with the following:

2.1 "Recommendations for Prestressed Rock & Soil Anchors", Post-Tensioning Manual, 4th Edition (1985), Post-Tensioning Institute, Phoenix, AZ.

2.2 Tiebacks, FHWA/RD-82/047, Federal Highway Administration, Washington, DC., July, 1982.

3.0 Material

The material shall be as follows:

3.1 Prestressing steel shall be 7-wire strand, grade 270K, stress relieved or low relaxation steel, ASTM A-416.

3.2 Corrosion Inhibitor shall be as follows:

3.2.1 Drop Point - 300° F min. - by ASTM D-566 or ASTM D-2265,
3.2.2 Flash Point - 300° F min. - by ASTM D-92,
3.2.3 Water Content - 0.1% max. - by ASTM D-95,
3.2.4 Oil Separation - 0.5% by weight max. @ 160° F - by FTMS 791B, Method 321.2,
3.2.5 Corrosion Test - 5% salt fog @ 100° F, 5 mils (Q panel type S) - normal conditions: rust grade 7 or better after 720 hrs., aggressive conditions: rust grade 7 or better after 1,000 hrs.- by ASTM B-117 and ASTM D-610,
3.2.6 Soak Test - 5% salt fog @ 100° F, 5 mils (Q panel type S), immerse panels in 50% salt solution and expose to 5% salt fog - no emulsification after 720 hrs. - by ASTM B-117 modified,
3.2.7 Water Soluble Ions:
Chlorides - 10 ppm max. - by ASTM D-512
Nitrates - 10 ppm max. - by ASTM D-992
Sulfides - 10 ppm max. - by APHA 427D (15th Ed),
3.2.8 Sheathing Hardness and Volume Change - 10% max. for volume, 15% max. for hardness after 40 days @ 150° F - by ASTM D-4289,
3.2.9 Sheathing Tensile Strength Change - 30% max. after 40 days @ 150° F - by ASTM D-638.

Corrosion inhibitor shall be Viscosity Oil Co. VISCONRUST 4600 or an approved equal.

3.3 Polymer sheathing shall be as follows:

3.3.1 Polypropylene: Designation type II 26500D - by ASTM D-2146.

Polypropylene shall be Ashland Chemical Co. PROFAX 6823 and 7823 or an approved equal.

3.3.2 Polyethylene: High density polyethylene cell classification 334413 -by ASTM D-3350.

3.4 Cement grout shall be as follows:

3.4.1 Cement: Type I, II, or III - by ASTM C-150.

3.4.2 Admixtures which develop higher early strength or which prevent bleed and shrinkage shall be approved for grout used to fill bond length encapsulating sheaths and to fill the trumpets provided these admixtures do not cause corrosion of the steel.

Nonbleed expansive admixture shall be Celtite, Inc. CONBEX-209X or an approved equal.

Accelerator admixture shall be Fox Industries, Inc. FX-32 or an approved equal.

3.5 Metals shall be as follows:

3.5.1 Steel: bearing plates and anchorheads -by ASTM A-36.

3.5.2 Cast ductile iron: anchorhead -by ASTM A-536 grade 80-55-06.

4.0 Submittals

The contractor shall submit the following for approval:

4.1 Mill certifications for steel.

4.2 Foundry test reports for all cast items.

4.3 Proof test certifications for anchorheads.

4.4 Certifications of compliance for all materials.

4.5 Material samples shall include as a minimum a five foot sample of strand from each pack used for the production tiebacks.

4.6 Shop drawings showing tendon and anchorage details.

4.7 Description of equipment and procedures proposed for field load testing of the tiebacks.

4.8 Design mix for grout.

5.0 Corrosion Protection

5.1 Corrosion protection requirements shall be determined by ground conditions:

Non-aggressive ground conditions exist when:
1) pH greater than 5.0,
2) Soil resistivity less than 2,000 ohm-cm,
3) Sulfides not present,
4) No recorded deterioration of buried portland cement concrete structures.

Aggressive ground conditions exist when:
1) pH less than 5.0,
2) Soil resistivity greater than 2,000 ohm-cm,
3) Sulfides present,
4) Recorded deterioration of buried portland cement concrete structures.

5.2 Corrosion protection for non-aggressive conditions shall be "simple corrosion protection" as follows:

5.2.1 Bond length shall be clean, bare prestressing steel and shall have a cover of at least 0.5 inch of Portland cement grout.

5.2.2 Unbonded length shall be fully coated by corrosion inhibitor and then encapsulated by a seamless polypropylene sheath.

5.2.2.1 The corrosion inhibitor shall fill all space between the strand wires and between the strand and the extruded sheath. The diameter of the corrosion inhibitor film covering the strand shall be 0.005 to 0.010 inches greater than the diameter of the bare strand.

5.2.2.2 The encapsulation sheath shall have a wall thickness of 0.06 inch. This sheath shall be hot-melt extruded over the corrosion inhibitor encased strand.

5.2.3 The anchorage shall insulate the tendon from electrical grounding using a method approved by the Engineer.

5.2.4 The extruded polypropylene sheath shall have a watertight seal with the base of the anchor head, using a method approved by the Engineer.

5.3 Corrosion protection for aggressive conditions shall be "encapsulated corrosion protection" as follows:

5.3.1 Bond length shall be clean, bare prestressing steel that is centralized and encapsulated with portland cement grout inside of a corrugated polypropylene or polyethylene sheath.

Corrugated sheath shall cover the bonded length plus 2 feet of the unbonded length and shall be covered by at least 0.5 inch of Portland cement grout.

5.3.2 Unbonded length shall be fully coated by corrosion inhibitor and then encapsulated by a seamless polypropylene sheath.

5.3.2.1 The corrosion inhibitor shall fill all space between the strand wires and between the strand and the extruded sheath. The diameter of the corrosion inhibitor film covering the strand shall be 0.005 to 0.010 inches greater than the diameter of the bare strand.

5.3.2.2 The extruded sheath shall have a wall thickness of 0.06 inch. This sheath shall be hot-melt extruded over the strand that is coated by corrosion inhibitor.

5.3.3 The extruded polypropylene sheath shall have a watertight seal with the base of the anchor head, using a method approved by the Engineer.

5.4. Grout shall be made from neat portland cement paste or from portland cement and sand. The grout strength shall be 3,000 psi when the tieback is tested as determined by ASTM C-109-80.

5.5. After lock-off of the post-tension force, the trumpet shall be filled with non-bleed, expansive grout. The exposed surface of the anchorage shall be coated with mastic and covered by a plastic or metal cap or covered by portland cement concrete.

6.0 Load Tests

Load tests shall be as set forth by "Recommendations for Prestressed Rock and Soil Anchors," Post-Tensioning Institute, 1985.

7.0. Quality Control

7.1 Manufacturer of the permanent ground anchors shall certify that the requirements of this specification have been satisfied.

7.2 Field inspection of the unbonded length shall verify the following:

7.2.1 Full coating with corrosion inhibitor. Determine by visual inspection smoothness of extruded polypropylene sheath. Reject if the helical lay of the strand wire is seen as relief on the exterior of the polypropylene sheath.

7.2.2 Minimum wall thickness of polypropylene sheath. Reject if outside diameter of extruded sheath is less than diameter of bare prestressing strand plus 2 times the specified wall thickness.

7.2.3 Integrity of the polypropylene sheath. Inspect for presence of corrosion inhibitor. Remove corrosion inhibitor and examine for sheath damage. Repair polypropylene sheath in accordance with the recommendation of the manufacturer.

PERFORMANCE OF INTERNALLY REINFORCED SOIL RETAINING WALLS

by
A. Kulathu Aiyer **

INTRODUCTION:

Several internally reinforced soil systems are now being used by highway engineers for retaining walls, bridge abutments, stabilization of slopes and embankments and for a variety of other uses. These systems are generally cost effective, resulting in savings of about 10% to 50% over traditional systems. They are also simple to construct and can accomodate greater differential movements than conventional systems. They have, in general, good performance record but occasional failures are not uncommon. This paper discusses some of the factors which influence the performance of reinforced soil retaining wall systems.

THE BASIC SYSTEM:

A typical section of a reinforced soil retaining wall is shown in Fig.1 . The wall has basically two main components: a system of reinforcements and a compacted select backfill in which the reinforcements are embedded. The reinforcements may be of metal or polymer and may have different configurations like strips, bars, wires, wiremeshes, sheets or grids. The reinforcements interact with the backfill to form a coherent mass of reinforced soil. Cohesionless free-draining soils have some desirable characteristics and are generally preferred for backfills; however, select cohesive soils have also been used. In some systems, the reinforcements are tied to wall facing panels which merely help to hold the soil in place near the wall face and give the wall a pleasing appearance.

DESIGN CONSIDERATIONS:

An internally reinforced soil retaining system has to satisfy both external and internal stability criteria.

External stability computations are made by assuming the reinforced soil mass to be a rigid body . This rigid body is subject to overturning forces generated by the random backfill and externally applied loads (Fig.2). External stability is accomplished by ensuring adequate factors of safety

---

** Associate Professor of Civil Engineering, New Mexico State University, Las Cruces, NM 88003.

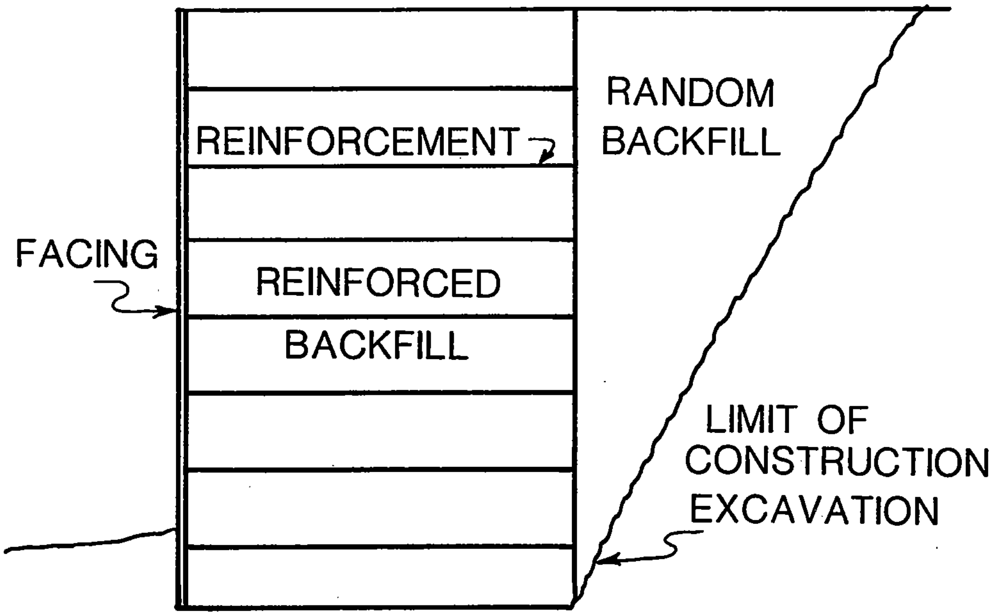
RANDOM
BACKFILL
REINFORCEMENT
FACING
REINFORCED
BACKFILL
LIMIT OF
CONSTRUCTION
EXCAVATION

Fig 1.

TYPICAL SECTION OF A REINFORCED SOIL RETAINING WALL

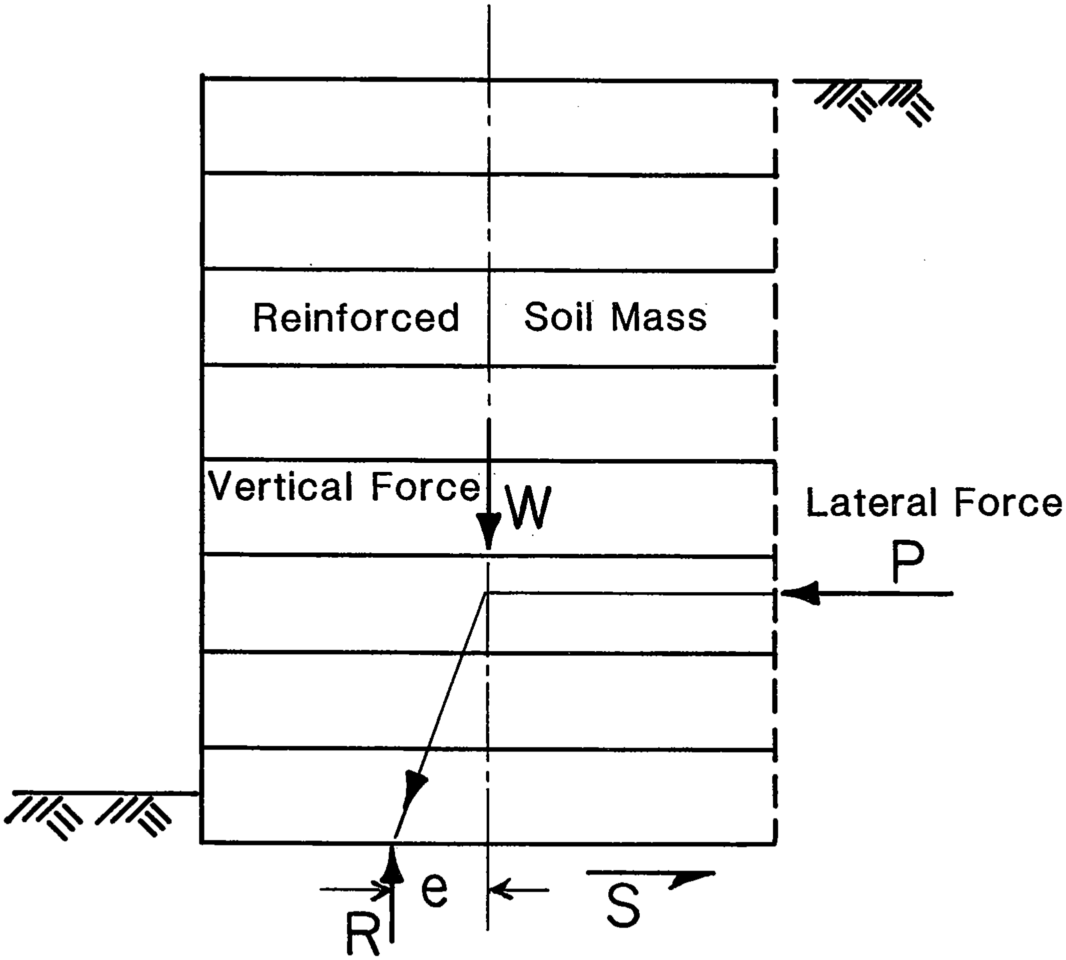
Reinforced
Soil Mass
Vertical Force
W
Lateral Force
P
R
e
S

Fig 2. EXTERNAL STABILITY

against failure by the following modes:

overturning of the wall about the toe,
sliding of the wall along the base,
bearing capacity of the foundation soil,
and overall rotation/translation of the wall.

Internal failure of the wall system can result either from a breakage of the reinforcements when their tensile resistance is not large enough to resist the maximum tensile forces mobilized in the reinforcements or from a slippage of the reinforcements when the soil-reinforcement interactions are not sufficient to resist the mobilized pullout forces (Fig.3). Internal stability can therefore be accomplished by satisfying the following two failure criteria:

(i) Maximum mobilized tensile force in the reinforcement shall be less than the permissible tensile strength
(ii) Maximum mobilized tensile force in the reinforcement shall be less than the permissible pullout resistance

The maximum mobilized tensile force in the reinforcement is estimated as the product of the internal horizontal stress within the compacted backfill at the level of the reinforcement and the vertical contributory area of the reinforcement.

The permissible tensile strength of the reinforcement is calculated from the cross-sectional and material properties of the reinforcement.

The permissible pullout resistance of the reinforcement is usually estimated on the basis of data obtained from laboratory or field pullout tests. The pullout resistance is based on the capacity achieved either at a specified maximum deformation (say, 0.75 in) or at a specified factor of safety with respect to the peak pullout capacity, whichever is less. Design for internal stability should ensure that both the tension and pullout criteria are satisfied during the entire design life of the retaining structure.

PERFORMANCE:

The field performance of an internally reinforced soil retaining system depends on three major groups of factors:

1. Quality of input data or parameters used for design
2. Adequacy of design methods and validity of assumptions
3. Quality of field construction and control

The factors in each of these groups are discussed further in the following paragraphs.

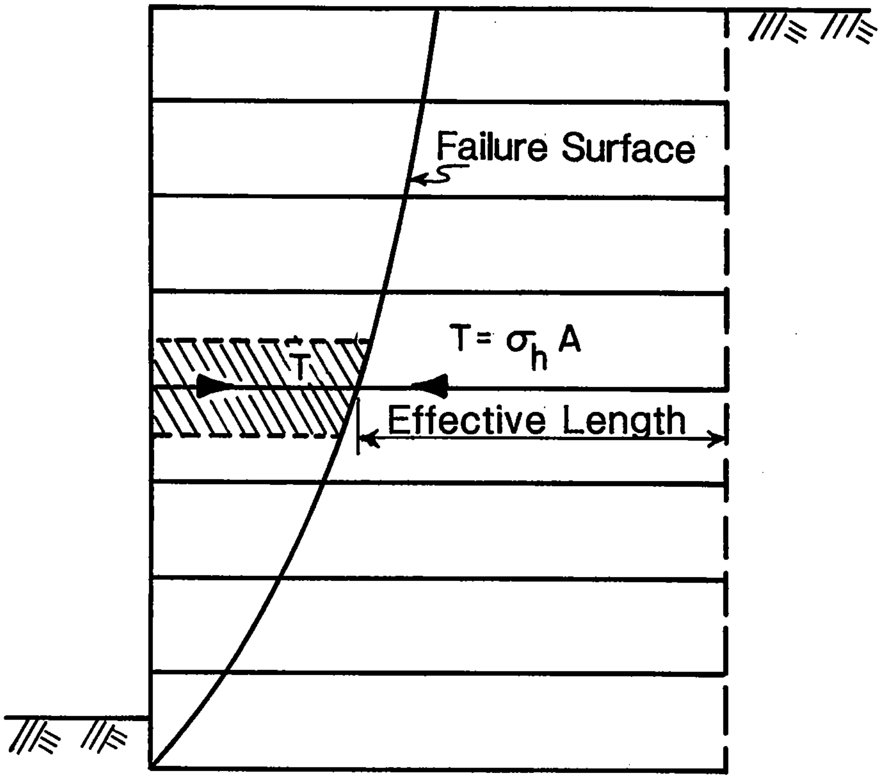
Failure Surface
T = σ_h A
T
Effective Length

Fig 3. INTERNAL STABILITY

QUALITY OF INPUT DATA OR PARAMETERS:

Design input parameters include the geometry of the wall, the loading conditions, the arrangement of the reinforcements and the properties of the backfill and reinforcement materials. The material properties used in the design must be so chosen as to be consistent with the stress, deformation, temperature and other environmental factors likely to exist under the field conditions. Of these parameters, the soil properties are perhaps more difficult to be determined correctly.

The significant soil properties are the unit weight and the shear strength parameters. These properties must be reliably known for the random and compacted backfills and for the foundation soil. The random backfill properties determine the lateral pressure acting on the reinforced soil mass and the compacted backfill properties govern primarily the internal stability conditions of the wall. If the backfill materials have been identified and are available for testing, then their properties must be determined under conditions duplicating as closely as possible the expected field conditions. But often, the true nature of the fill material and the physical conditions within the reinforced soil structure can be determined only during or after construction and therefore, not available to the designer. An engineering solution that is usually adopted in such a case, is to use typical or reasonable soil properties for design and then to have rigid specifications and construction codes to ensure the achievement of these properties during construction. The success of this approach depends primarily on the quality of field construction and control.

An internally reinforced soil retaining wall, even though based on an innovative technique, has to satisfy the same foundation conditions as for a traditional retaining wall. In other words, the foundation must be strong enough to support the reinforced soil mass without the possibility of a shear failure or excessive settlement of the foundation. So the correct determination of the strength and compressibility characteristics of the foundation soils is very important to ensure a satisfactory performance of the wall and this points to the necessity of having an adequate and well planned soil investigation prior to the design of the wall. As the soil borings are generally made only at specific intervals, the possibility of distinct changes in soil profile and properties between borehole locations has always to be kept in mind during design and construction stages. If foundation conditions that are different from those revealed by borings, are encountered during construction, then the effect of these changed foundation conditions must be very carefully evaluated and if necessary, changes must be made in the design and construction of the wall.

ADEQUACY OF DESIGN METHODS AND VALIDITY OF ASSUMPTIONS:

External Stability:

The lateral earth pressure on the reinforced soil mass is usually determined by using Rankine's active earth pressure theory. Even though field measurements of reinforced soil wall sytems have indicated variations from Rankine distribution, experience has shown that this approach is sufficiently accurate for most design purposes. Federal Highway Administration (FHWA) recommends the use of a maximum friction angle of 30 degrees for the random backfill unless specific project data indicates that a higher value is warranted. This limitation is also recommended when determining the coefficient of sliding friction at the wall base.

Water pressures are not normally included in the design calculations for retaining wall systems and therefore adequate provisions must be made for both surface and subsurface drainage of the backfill. If the drainage provisions are inadequate or become ineffective, excessive pore pressures may develop in the backfill resulting in excessive deformations or a failure of the wall.

Calculations for overturning of the wall are usually made about the toe and a minimum factor of safety of 2 is normally used. However, if the foundation conditions are not uniform and there is a weak layer under the toe, a tilting of the wall about an interior point along the base of wall may result with a consequent decrease in the factor of safety against overturning. This type of situation can occur when soil investigations are limited to locations along the centerline of a retaining wall alignment over dipping layers of soil. The possibility of lateral variations in soil characteristics must always be recognized and provided for.

Non-uniform foundation conditions may also cause load transfers by arching from weaker to stiffer zones in the foundation soil and this can result in a redistribution of the pressure at the base of the wall. If the toe soils are weaker and more compressible that those at the heel, the base pressure redistribution moves the base reaction toward the heel thereby increasing the overturning moment and decreasing the stability of the wall.

The estimation of the allowable base pressure of the foundation soil shall be made on the basis of both bearing capacity and settlement considerations taking into account the inclination and eccentricity of loading at the wall base.

The overall slope stability condition, which the retaining wall may only be a part of, should always be checked in accordance with standard procedures to ensure a satisfactory performance of the wall.

Internal Stability:

Shape and location of the failure surface: The failure surface behind a retaining wall divides the backfill into two distinct zones - the active zone, representing the sliding soil mass and the resistant zone, representing the remainder of the backfill. The location and shape of this failure surface is important in the analysis of internal stability because the pullout resistance of the reinforcement is dependent on the effective length or the length of embedment in the resistant zone. There is no uniformity among the various systems regarding the assumed location of the failure surface. Some wall systems use the planar Rankine failure surface rising at 45 + O/2 with the horizontal. It is well known that the shape and location of the failure surface are largely dependent on the actual deformation and boundary conditions associated with the wall and therefore, can differ from the planar Rankine surface. Field observations have indicated that the failure surfaces in some wall systems are indeed curved and therefore, these systems have recommended the use of bilinear approximations to the curved failure surface. However the use of the planar surface is simpler and is on the conservative side.

Internal vertical stresses: The vertical effective stress distribution within the reinforced soil mass must be known for establishing the minimum reinforcement length required to resist the mobilized tensile forces. These stresses at any reinforcement level depend on the magnitude and distribution of the vertical and lateral forces acting on the reinforced soil mass above that elevation and are influenced by the stress-deformation and interaction characteristics of the soil-reinforcement system. The actual vertical stress distribution is generally indeterminate; however, to keep the analysis simple, the internal vertical stresses are estimated by proportioning the vertical base pressure as calculated for external analysis linearly from the base to the depth of interest.

Internal horizontal stresses: The horizontal stress at each reinforcement level is computed by multiplying the internal vertical stress by a coefficient of earth pressure. Different soil retaining systems use slightly different methods of estimating this earth pressure coefficient. This is justifiable because of the differences in the deformation conditions inherent in each system. Some systems assume that the coefficient varies linearly from an at-rest value at the ground surface to the active value at a depth of 20 feet below ground surface. Below a 20 feet depth, the active coefficient of earth pressure is used. A number of systems are designed using a constant value, say the active coefficient of earth pressure or some other empirical value, for the earth pressure coefficient throughout the entire wall height. These assumptions are usually based on the results of field evaluations and are acceptable from a design point of view.

Pullout resistance: Some reinforced soil wall systems have accumulated extensive pullout data and have developed empirical analytical relationships to evaluate the pullout resistance as a function of ths soil and reinforcement type. But for systems where such data are nonexistent or insufficient, actual laboratory pullout tests should be conducted under simulated project conditions to clearly define the behavior of the system. The permissible pullout resistance of a reinforcement should be based on an adequate factor of safety with respect to the peak pullout capacity or on the capacity achieved at a given maximum deformation, whichever is less. A preliminary study of the available pullout test data seems to indicate that the former criterion generally governs when the backfill is cohesionless and the latter criterion governs when the backfill is cohesive.

Laboratory pullout tests should be conducted prior to construction, preferably before or during design stage. In situations where pullout capacities assumed in design differ unconservatively from actual values, appropriate changes in backfill and/or reinforcement lengths will have to be made. At present no standard pullout test procedure exists and several possible test methods are available.

Several systems boast of very high pullout capacities, thereby suggesting reduced design lengths for reinforcements. In practice, however, external stability and internal deformation requirements invariably govern the minimum reinforcement length. FHWA recommends a minimum reinforcement length of 70% of wall height but not less than 8.5 feet. In addition it is recommended that the reinforcement lengths be uniform throughout the entire height of the wall.

Other considerations: Allowances for corrosion of metal reinforcements are usually made by having protective coatings (of epoxy, zinc etc.,) for the reinforcements and/or by providing sacrificial material based on the rate of corrosion and the design life of the structure.

Creep characteristics of reinforcements have also to be properly evaluated and provided for in design. Geotextiles are subject to deterioration by exposure to solar ultraviolet light and so, when these materials are used for the wall systems,sufficient protection must be provided for their exposed surfaces by spraying with gunite or shotcrete.

QUALITY OF FIELD CONSTRUCTION AND CONTROL:

The performance and cost of a soil retaining system are primarily dependent on the characteristics of the backfill material. Proper care and control must be exercised in the selection of the backfill material and in its placement. The desirable characteristics of a select backfill are: high strength, good compactability, durability, free-draining, non-swelling, non-frost susceptible, non-creeping, and non-corrosive. Non-plastic, granular backfills with good drainage characteristics generally prove better than cohesive soils. In recent years, the high cost of procuring a granular select backfill has, in some cases, forced engineers to consider the possibility of using locally available, perhaps "not so good", cohesive or semicohesive soils as backfill. One of the problems of such soils as backfill is the lag in the shear strength increase with vertical loading. Adequate shear strength between the soil and the reinforcement may not develop sufficiently quickly to resist the additional vertical stresses as the height of the fill is increased. This fact is very significant and has to be properly taken into account in design and construction.

The characteristics of a backfill are controlled to a large extent by specifying its gradation, plasticity, corrosion and soundness characteristics. Specifications commonly used are:

Gradation:	Sieve size	% passing
	6"	100
	3"	75 - 100
	#200	0 - 15

Plasticity: Plasticity Index - not more than 6

Corrosion:
Resistivity > 3000 ohm-cm
pH = 5 to 9
Chlorides < 200 ppm
Sulphates < 1000 ppm
Sulphides < 300 ppm

Soundness: Magnesium sulphate soundness loss (AASHTO T-104) after 4 cycles not more than 30%

The compaction and placement of the select backfill is also very important to make sure that it is adequate, uniform and is as per specifications. Backfill compaction shall be accomplished without disturbance of distortion of the reinforcements. Compaction near the face of the wall shall be achieved by using light compacting equipment so as not to distort the wall excessively by high construction stresses in the backfill.

Adequate provisions should be made for the drainage of the backfill and for keeping the drainage effective during the entire life of the retaining structure.

It is also important to check for uniformity and adequacy of the foundation medium below the base of the wall. If less desirable soils are encountered within the zone of stress increase, they may either be replaced with select material for adequate depth or be properly taken into account in design.

Other stability problems that may arise are the local and general failure of the facing panels and the panel-reinforcement connections. These are usually due to excessive stress concentrations at junctions between facing panels and in the connections between the panels and the reinforcements. Stress concentrations are also conducive to accelerated corrosion and must always be minimized. This can be achieved by proper design and placement of the facing panels and by using well designed connections between the facing panels and the reinforcements.

CONCLUSION:

The general principles of design of internally reinforced soil retaining wall systems are reasonaly well understood by engineers. However, the field performance of these systems is dictated more often by the quality of soil investigations and the details of field construction than by the adequacy of the design methods. Adequate soil investigation prior to construction and good field inspection and quality control during construction are equally, if not more, important as the design procedures. A satisfactory performance can result only if all the parameters assumed in the design are effectively achieved under field operating conditions.

REFERENCES:

1. Guidelines for the Analysis of Internally Reinforced Retaining Systems, Memorandum, Federal Highway Administration U.S. Department of Transportation, August 1983.

2. Proceedings of the ASCE Symposium on Earth Reinforcement, Pittsburg, 1978.

ROADWAY STABILIZATION

USING A

TIEDBACK WALL

by

John A. Franceski

Branch Manager

SCHNABEL FOUNDATION COMPANY

8000 E. Girard Avenue, Suite 317

Denver, Colorado 80231

Prepared for Presentation
at the
37th Annual Highway Geology Symposium
August 20-22, 1986
Helena, Montana

ROADWAY STABILIZATION USING A TIEDBACK WALL

ABSTRACT

In the Spring of 1985, a series of small slope failures threatened to close the entrance road to the Mesa Verde National Park, the only public access. As the Spring run-off continued, the clayey talus material, on which the road was founded, began to move. Small scarps which developed in the shoulder of the downhill side of the road had progressed into the paved area.

The Federal Highway Administration Central Direct Federal Division immediately began a geotechnical investigation and analysis in order to identify the geometry and forces associated with the failure. Once these parameters were established, a tiedback wall was selected as the best method to stabilize the roadway because of time and access constraints. Design and installation of the soldier piles for the tiedback wall were done with the consideration that a second tier of tiebacks could be added at some future time should the need arise.

This paper presents the sequence of events from initial identification of the failure parameters through completion of the wall construction. The design criteria used to establish the size and strength of the wall components, details of the construction, and performance of the tiedback wall will be presented.

INTRODUCTION

Grouted rock and soil anchors, called tiebacks, were originally developed as an alternate to bracing or massive cantilever sheeting for temporary excavation support. Their history of excellent performance and easy verification of capacity has led to their use as a permanent means of supporting retaining walls. These walls are typically called tiedback walls or permanently anchored walls, and have gained wide acceptance on public and private projects.

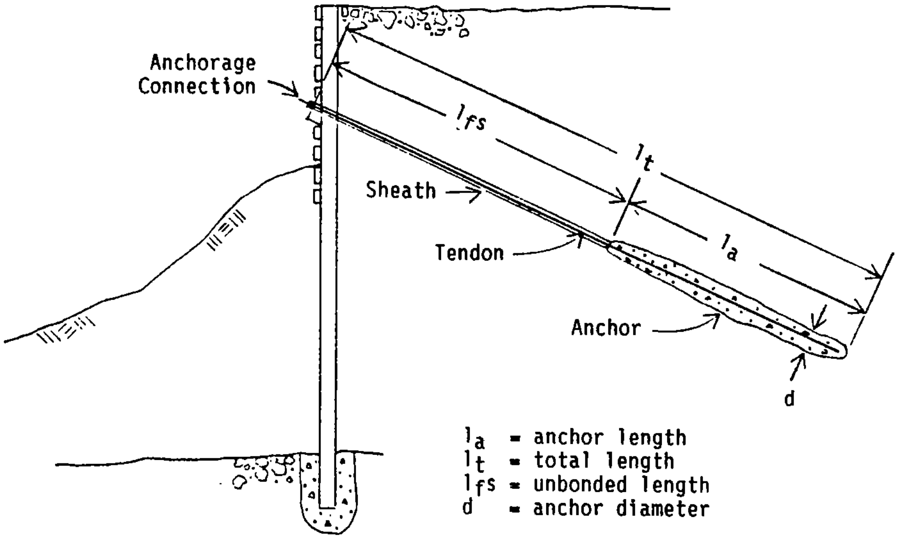

FIGURE 1. COMPONENTS OF A TIEBACK

Tiedback walls have several structural members (see Figure 1). First, the tieback itself is a grouted anchor which transmits force to the wall through a post-tensioned tendon. This force is resisted by adhesion of the anchor to the soil or rock in a zone called the anchor length. The portion of the tendon that is between the anchor length and the wall is called the unbonded length and it elongates elastically when post-tensioned. Tiedback walls may have horizontal support members called elements (see Figure 2) or vertical support members called soldier beams. The space between support members may be covered to further reduce soil movement or erosion. This cover is called the facing and it is usually cast-in-place or pre-cast concrete, shotcrete or treated timber.

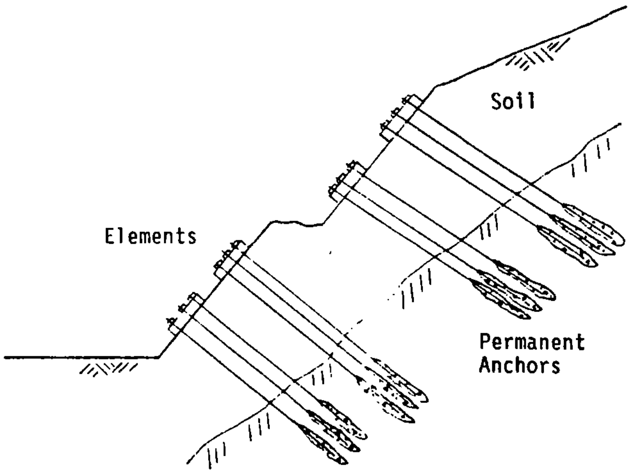

FIGURE 2. TIEDBACK ELEMENT WALLS

EXISTING CONDITIONS

The entrance road to Mesa Verde National Park winds steeply from the valley below transversing the canyon walls to the mesa above where historic ruins are located. The paved two-lane road serves as the only access into and out of the park. The grades along sections of the road exceed six percent and the natural hillside slope is at least 45 percent. The combination of these features have been the cause of continued maintenance problems. A variety of methods have been used to stabilize portions of the road in previous years.

The section of road which was failing in the Spring of 1985 had not been repaired for several years, however, the increase in Spring run-off, and subsequent saturation of the clayey talus material on which the road was founded, caused the downhill shoulder of the road to begin to move.

SUBSURFACE INVESTIGATION

The Federal Highway Administration Central Direct Federal Division recognized that an immediate repair would be required in order to keep the road in service during the busy summer season. A thorough geotechnical investigation was authorized for the purposes of identifying the geometry and loads associated with the failure. Initially, it was not known whether the slope failures were a localized wedge type failure or if the problem was a landslide with the overburden slipping on the soil rock interface.

Borings were taken along the section which was to be repaired. The profile at the roadway showed a sandy, clayey talus type material extending from the surface to an approximate depth of 20 feet. Interspersed throughout the overburden were sandstone cobbles and boulders. The material was similar to that which could be seen in the excavated slope on the uphill side of the roadway.

From approximately 20 to 25 feet, a brown weathered shale was encountered. The depth of this layer varied somewhat before running into a blue-gray shale formation which extended on to the terminations of the borings. The blue-gray shale was classified as hard. Core samples of blue-gray shale were taken for laboratory testing. Slope indicators were installed in selected holes which would be monitored to identify the location of a deep-slip surface, if any existed.

Groundwater was found in several borings at the overburden shale interface while groundwater was not indicated in other borings. This was later confirmed during the drilling of tieback anchor holes when ground water was encountered in a hole which was only six feet from a dry hole.

Additionally, samples of the overburden soil and groundwater were tested for pH, resistivity and the presence of sulfides. The results of this testing would be used to decide on the level or corrosion protection needed for the tieback anchors.

DESIGN

The monitoring of the inclinometers during the month following installation showed no detectable movement within the overburden beneath the roadway, but it was visually apparent that the slope on the downhill side of the road was continuing to move. Unconfined compressive strength tests confirmed the blue-gray shale competent for tieback anchors. Testing of the overburden soil provided the designers the information required to develop a loading diagram and subsequently tieback loads. A decision had to made at this point as to what kind of slope failure was to be corrected. As mentioned earlier, the inclinometer data indicated no deep seated movement characteristic of of a landslide. It was observed that the embankment downhill of the road, for approximately eight to ten feet, was sliding away and that these movements were damaging the road.

The decision was made to design the wall for a rectangular-shaped failure diagram with a height of 30 feet. This would take into account all overburden pressures to rock. Although the wall would be constructed to a height of only 15 feet during this phase of construction, the soldier beams and tiebacks were sized for a wall 30 feet high (see Figure 3). The soldier piles were designed to be placed in 30-inch-diameter holes drilled though the overburden and into the blue-gray shale for a minimum toe penetration of seven-and-one-half feet. Structural concrete was poured for the toe embedment in shale and the remainder of the hole filled with a lean concrete mix. The wall was designed for a single tier of the tiebacks at an elevation six to eight feet below the top of the wall.

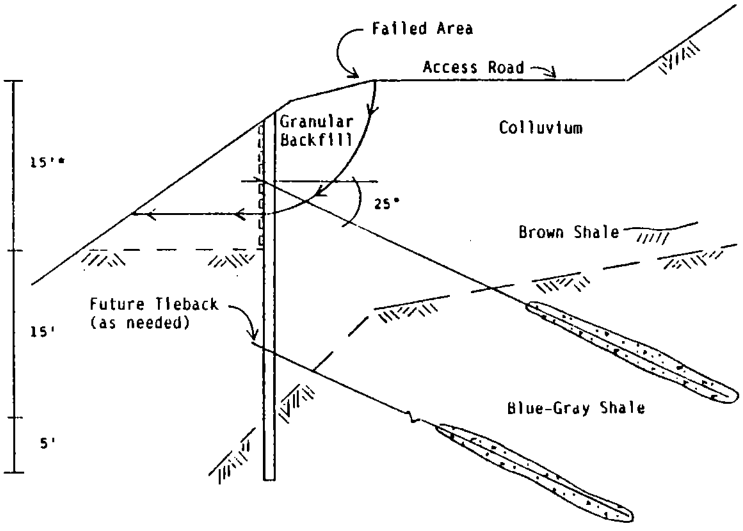

*Can be extended at some future time by adding lagging

FIGURE 3. A TYPICAL DESIGN SECTION FOR A TIEDBACK WALL

The structure was designed to allow for the addition of lateral support should the need arise. The following situations could be dealt with if they occurred: 1) overburden downhill from the wall could begin to move in the future thereby relieving the passive pressure in front of the wall and increasing the active pressure behind the wall and 2) the development of a landslide along the soil rock interface. Both situations could be dealt with efficiently by the addition of tiebacks at some future time.

The history of erratic soil movement along the access road dictated a design that not only would provide an efficient solution to the existing problems, but would provide for the economical correction of anticipated problems in the future.

CONSTRUCTION AND PERFORMANCE

A set of plans and specifications were prepared which detailed soldier beam size, minimum penetration into shale, waler size, connection detail, lagging thickness, tieback type and tieback details. Double corrosion tendons were specified with a minimum unbonded length of 30 feet. The type of tendon, bonded length and installation technique were left for the contractor to determine. A design load of 100 kips for each anchor and a maximum test overload of 150 percent were specified and established the criteria for the selection of tendon size.

Soldier beams were placed in drilled shafts and concreted in accordance with the plans. The next procedure was to excavate material behind the wall which had been disturbed when the slope failed. Select borrow material was compacted behind the wall as lagging and walers were connected to the soldier beams. Once the walers were in place, tieback drilling commenced. It was decided by the contractor to install anchors with 45 feet of unbonded length and 25 feet of bonded length. This decision was based on the estimated point where the tieback would intercept the blue-gray shale, because the shale had adequate capacity for the anchorage. All tendons were shop fabricated based on this estimate.

In the field, the blue-gray shale was encountered between depths of 30 and 40 feet. All drilling was done with air, which enabled the contractor to determine which holes were dry and which produced groundwater. After tendons were inserted into the drilled holes, grout was pumped through a grout pipe from the bottom of the hole to the surface (see Photo 1). The grout was allowed to cure for five days prior to testing of the anchors. Testing included performance tests on a select number of anchors, proof tests on each anchor and a creep test on one anchor. Five of the 28 anchors had lift-off tests performed eight months after the initial testing. All lift-off tests verified that the anchors maintained a capacity within five percent of the lock-off load.

Four of the tendons failed to meet the movement criteria established for a test load of 150 percent of the actual design load. However, all four tiebacks were capable of holding 140 percent of the design load without exceeding the test criteria. It was only the application of the final ten percent of overload that resulted in excessive movement. No conclusion could be drawn as to why these four anchors, all in a row, did not meet the test criteria. However, it was noted groundwater was encountered at the soil-rock interface in the area of these tiebacks. Replacement anchors identical to the original anchors were installed and successfully tested.

The entire project was completed (see Photo 2) in approximately 30 working days allowing the road to be opened for the busy summer tourist season, and if the potential problems do occur in the future, they can be corrected economically without interruption of traffic.

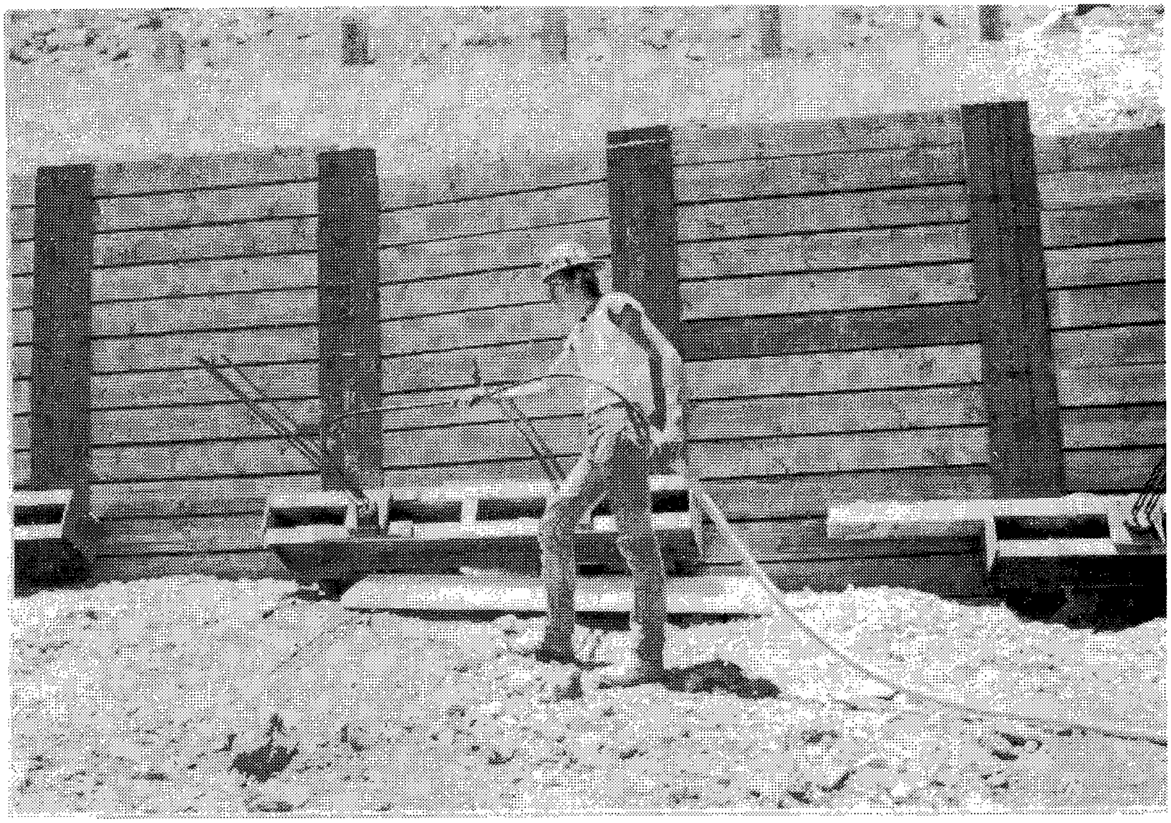

PHOTO 1. GROUTING TIEDBACK TENDONS

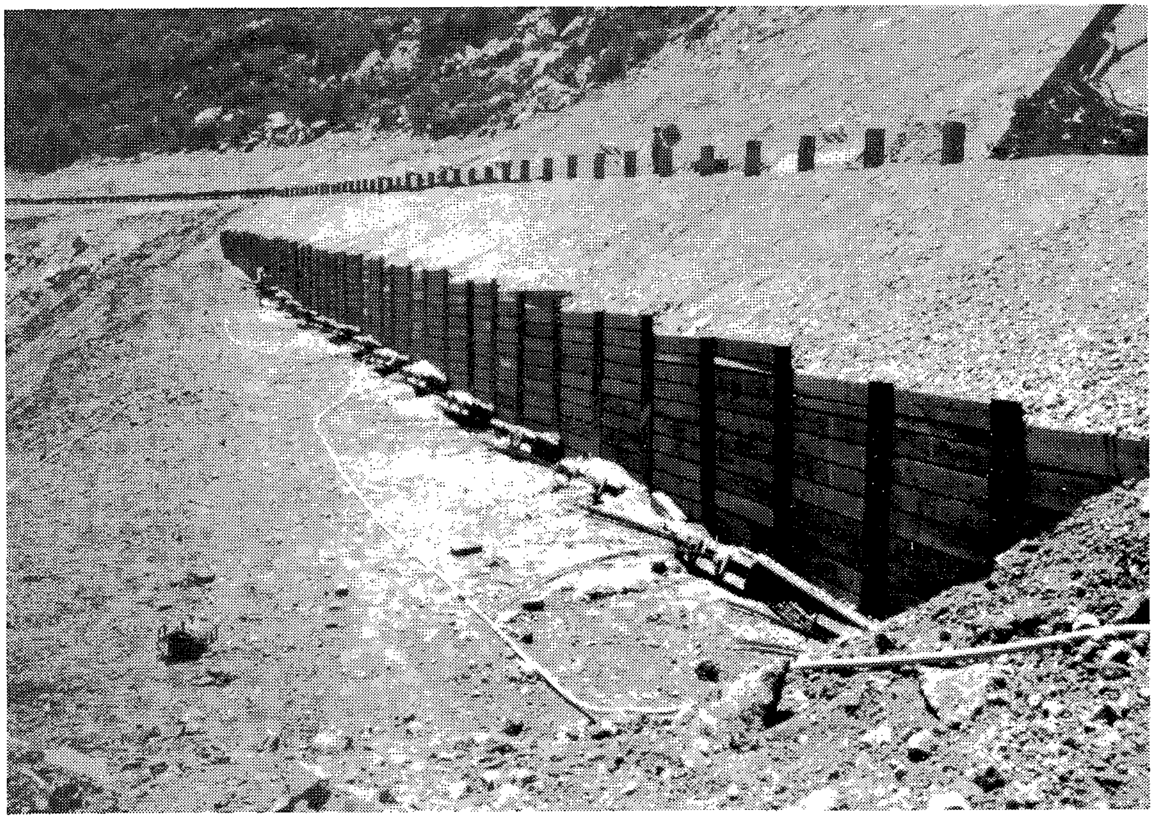

PHOTO 2. COMPLETED TIEDBACK WALL

RESILIENT MODULUS - WHAT IS IT?

BY

Sam I. Thornton and Robert P. Elliott
University of Arkansas
Fayetteville, AR 72701

ABSTRACT

The Resilient modulus test is a repeated load triaxial test. Loads and confining pressures are low in order to simulate highway traffic.

Loading conditions are different for fine grained soils and coarse grained soils. Fine grained soils are loaded from 1 psi to 10 psi with chamber pressures from 0 psi to 6 psi. Coarse grained soils are subjected to loads of 1 psi to 20 psi at confining pressures from 1 psi to 20 psi.

The resilient modulus, M_R, is the stress divided by recoverable strain. Because the modulus varies with the load and chamber pressure, M_R is reported as a plot of the variations of M_R with the deviator stress and the confining pressure. For granular soils, a log-log plot of M_R versus the sum of the principal stresses (θ) is used. The granular soil results are also reported as an equation taking the form: $M_R = k\ \theta^n$ Coarse grained results are reported in this form because data usually plot near a straight line. The parameters k and n determine the intercept and slope of the line. Larger values of k and n mean the soils should provide better roadway support.

For cohesive soils, M_R is reported using arithmetic plots of M_R versus deviator stress for each confining pressure.

The effect of several factors which affect resilient modulus are discussed. These factors include stress duration, load frequency, soil grain size, density ratio, degree of saturation, confining pressure and stress level.

INTRODUCTION

The resilient modulus is a fundamental material property that is similar in concept to the modulus of elasticity. That is, resilient modulus is a stress-strain relationship. The resilient modulus is determined from a repeated load triaxial compression test. In this test the resilient modulus is calculated using the recoverable or resilient deformation.

$$M_R = \frac{\text{Stress Amplitude}}{\text{Strain Amplitude}}$$

where

stress amplitude = load/area of the specimen
strain amplitude = recoverable deformation/original height

An example of typical behavior is demonstrated in Figure 1. As the load is applied, the stress increases as does the strain. When the stress is reduced, the strain also reduces but all of the strain is not recovered. The total strain, therefore, is composed of both plastic (permanent) and resilient (elastic) strain. Only the resilient strain is used in calculating the resilient modulus.

Resilient modulus is of current interest because the new AASHTO Guide for the Design of Pavement Structures (1985) requires its use in order to design a flexible pavement.

RESILIENT MODULUS TEST

The resilient modulus test is designed to simulate the behavior of soils and granular materials within a pavement system subjected to traffic loading. Consequently, the sample preparation, conditioning, and testing are conducted so as to simulate field conditions. The following describes the standard AASHTO test method (T274).

Under AASHTO, cohesive soils may be compacted by either gyratory, static, or kneading methods. The method to be used depends upon the expected moisture conditions during compaction and later when the pavement is in service. If the degree of saturation immediately following compaction is less than 80% and not expected to increase, any method may be used. If, however, the in-service water content is expected to increase, static compaction (Figures 2 and 3) is recommended (although kneading compaction followed by back pressure saturation can be used). Kneading compaction (Figure 4) is required if the compacted water contents exceed 80% saturation.

Granular soils are compacted using a split mold and vibrator. Samples are compacted in layers, normally 1 to 1.5 inches thick, with a vibrator such as a small, hand operated air hammer. Before removing the mold, a vacuum is applied to prevent sample collapse before the test is begun.

During testing, confining pressures are kept low in the resilient modulus test to simulate stresses caused by highway traffic. In the standard AASHTO test (T 274), the confining pressure for cohesive soils varies from zero (0) to six (6) pounds per square inch. In coarse grained soils, the confining pressures are varied from one (1) to twenty (20) pounds per square inch. Loads are varied as well as confining pressures and 200 repetitions of load are

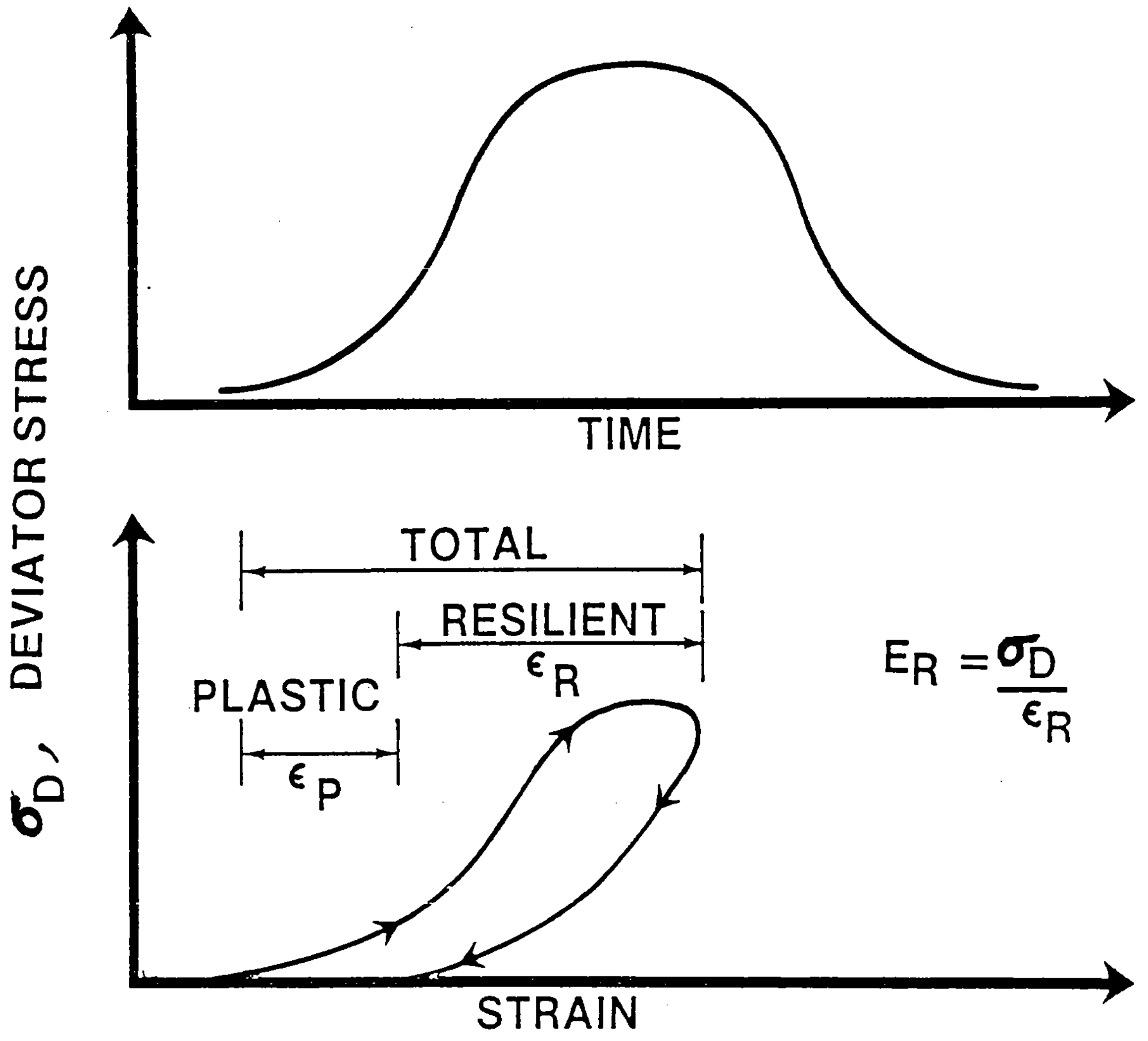
DEVIATOR STRESS
TIME
σ_D, DEVIATOR STRESS
TOTAL
RESILIENT
ϵ_R
PLASTIC
ϵ_P
$E_R = \frac{\sigma_D}{\epsilon_R}$
STRAIN

Figure 1 Typical Repeated Load Response (from National Highway Institute)

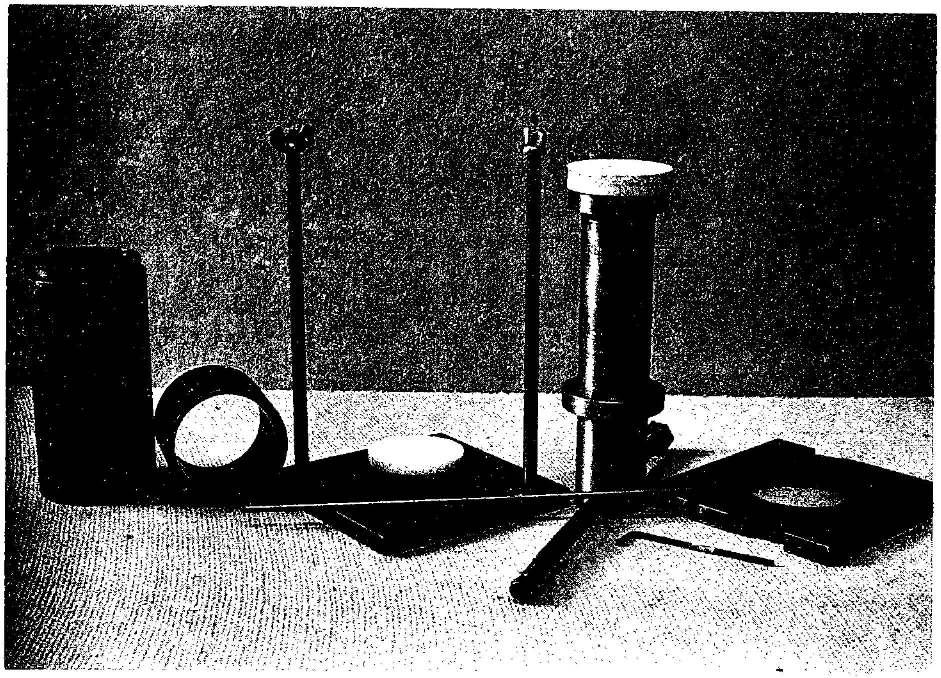

Figure 2   Mold and piston used for static compaction of Resilient Modulus samples

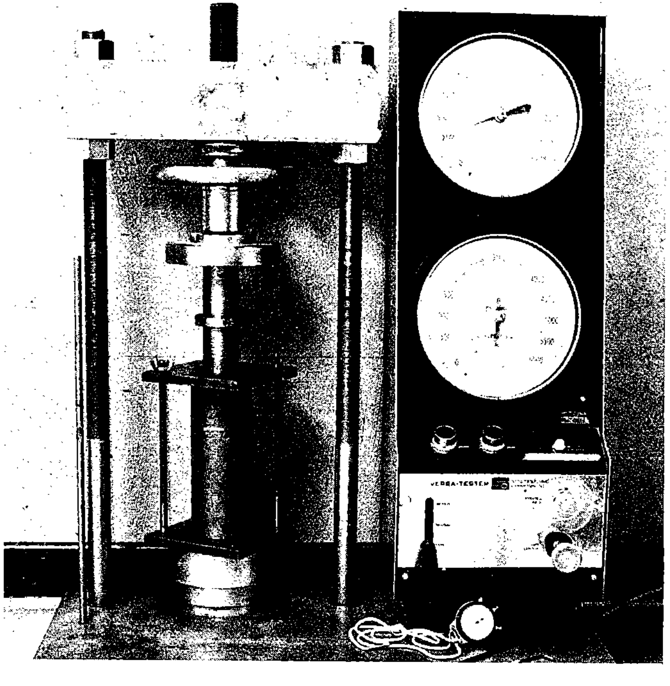

Figure 3   Static compaction of Resilient Modulus samples

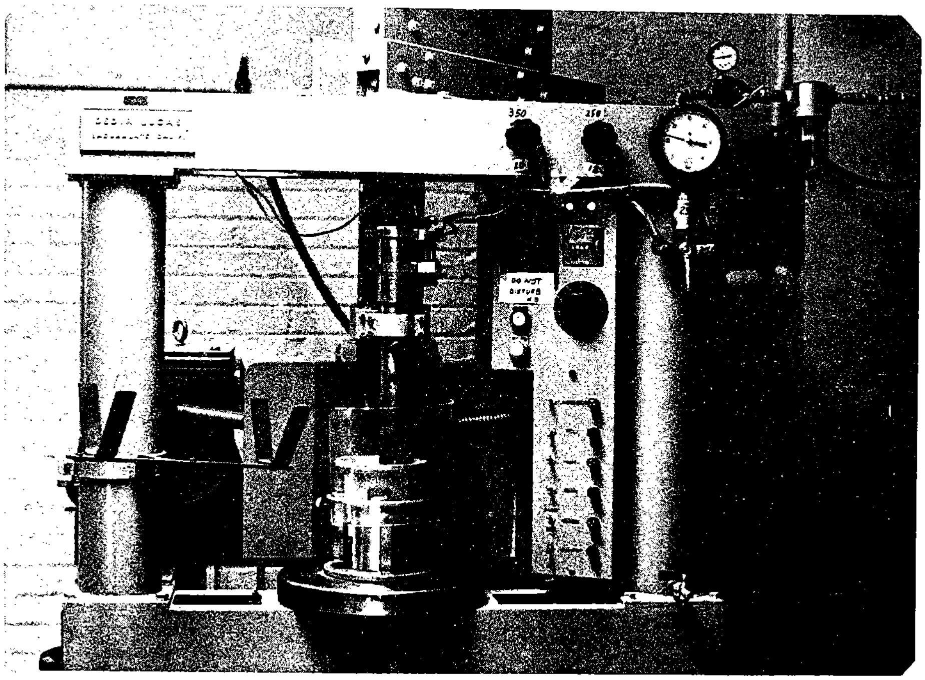

Figure 4   LUCAS Kneading Compactor

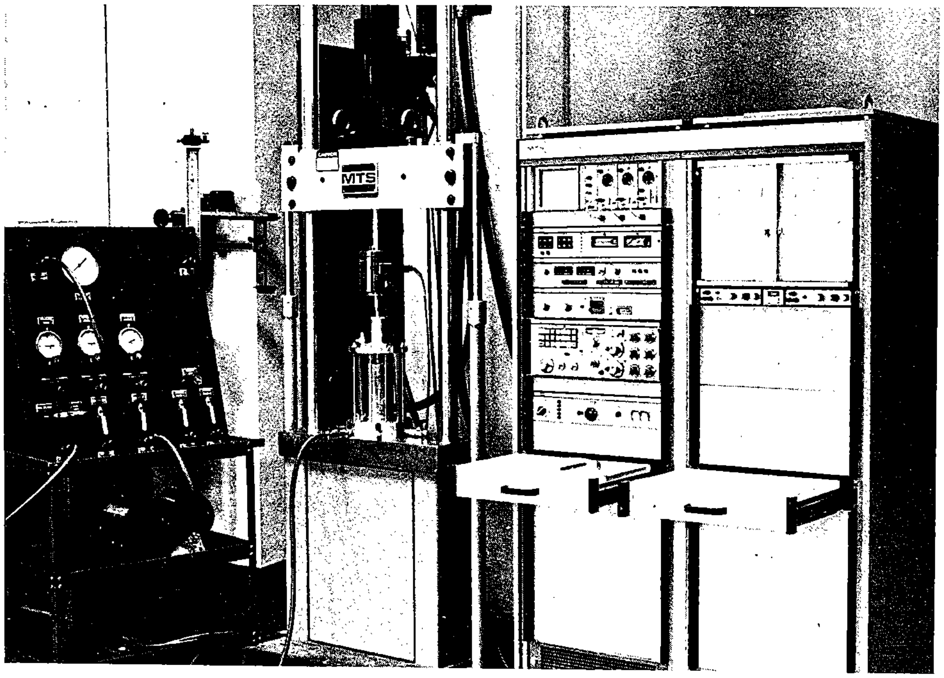

Figure 5   Resilient Modulus Test in progress

applied at each combination of confining pressure and load. This causes the number of load applications to be large.

For cohesive soils, the AASHTO test requires that the sample be tested first at 1 psi with a confining pressure of 6 psi, then 3 psi and 0 psi for a total of 600 applications of the 1 psi load. This sequence is repeated for loads of 2 psi, 4 psi, 8 psi, and 10 psi. The total number of load applications for testing a cohesive soil is 3000. Sample conditioning before testing adds another 1000 applications for a total of 4000 load repetitions.

In granular soils, the confining pressure is first set at 20 psi and 200 load applications of 1 psi followed by 2, 5, 10, 15, and 20 psi are made for 1200 load applications. The sequence is repeated for confining pressures of 15, 10, 5 and 1 psi. Total load applications for testing a granular soil are 6000 not including the 1200 repetitions required for conditioning.

Each load is applied for 0.1 seconds and cycle duration is usually 2 seconds (cycle duration must be from 1 to 3 seconds). For the number of repetitions required by the AASHTO test, the testing and conditioning time is 2 hours 20 minutes for a single cohesive soil specimen and 4 hours 12 minutes for a granular soil specimen. This includes no time for sample preparation, placing the sample in the machine, or making machine adjustments.

Sophisticated equipment is required to conduct the resilient modulus test. A photograph of the equipment used at the University of Arkansas is shown in Figure 5.

DISPLAYING RESULTS

Most of the early resilient modulus studies were concerned with the behavior of granular base materials. These found that a plot of the log of the resilient modulus versus the log of the sum of the three principal stresses (θ) resulted in a straight line plot. This straight line can be expressed as an equation:

$$M_R = k\,\theta^n$$

where

k & n = regression coefficients the straight line

By the AASHTO test procedure, the results of testing granular soils are reported as a log-log plot and a straight line regression equation (Figure 6).

For cohesive soils, the effect of confining pressures is not as great. As a result, the resilient modulus of a cohesive soil is more a function of the deviator stress. By AASHTO, cohesive soil test results are reported as an arithmetic plot of resilient modulus versus deviator stress for each confining pressure (Figure 7).

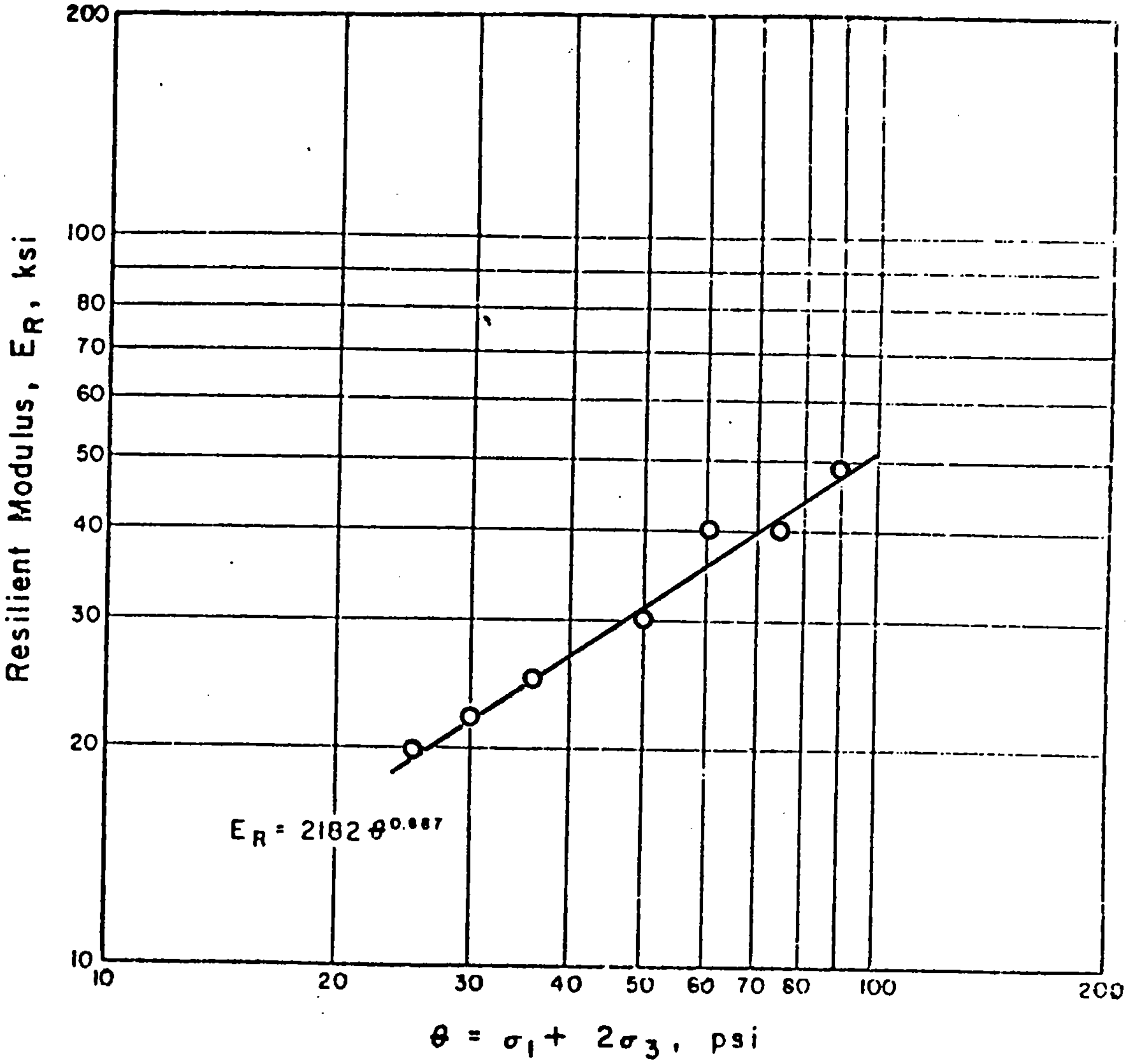

Figure 6 Resilient Modulus-Stress Relationship for Non-Cohesive Soil (from National Highway Institute)

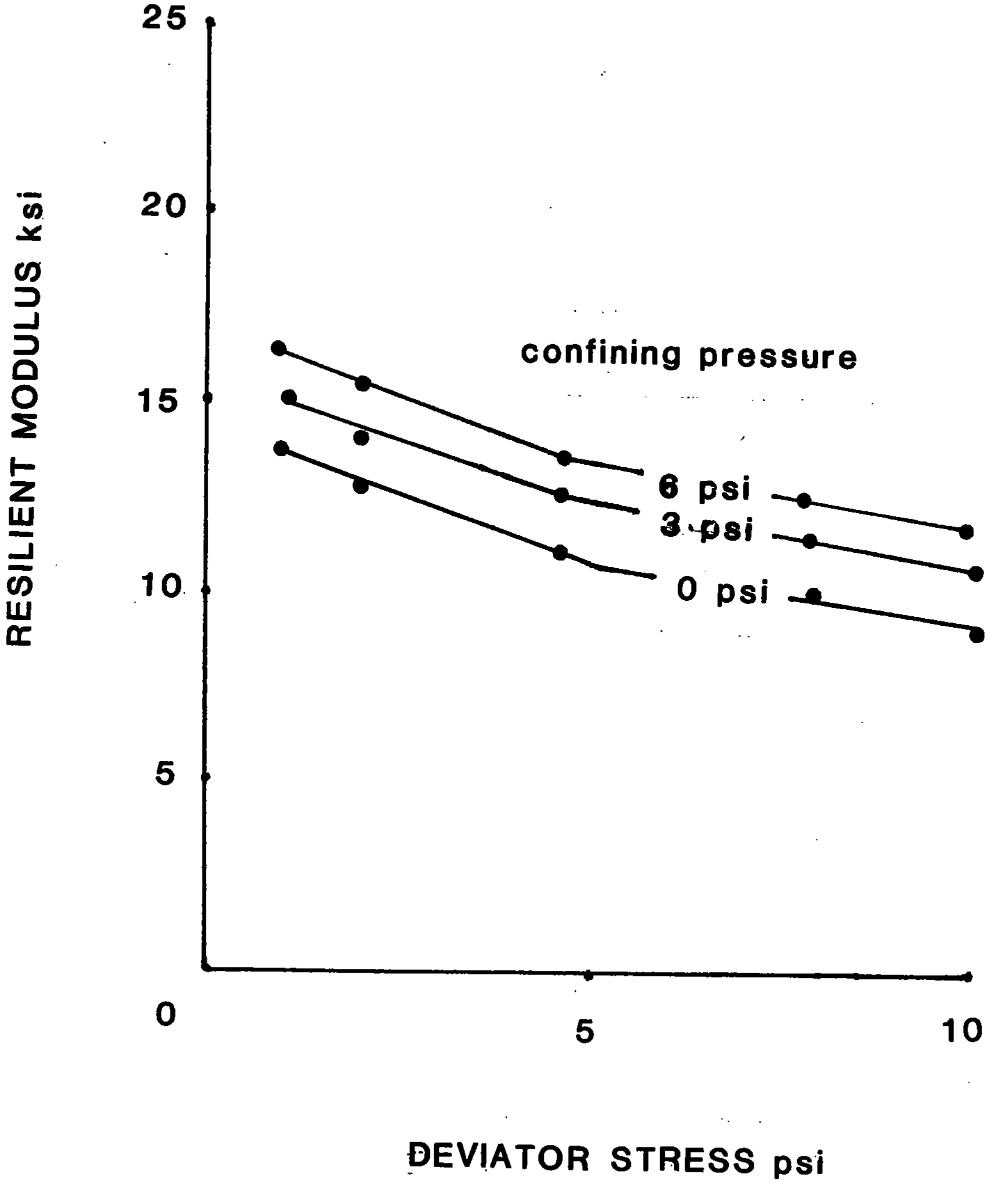

Figure 7 Resilient Modulus Results for Cohesive Soil

FACTORS AFFECTING RESILIENT MODULUS

A number of factors effect the resilient modulus of a given soil. Among these are load or stress duration, load frequency, confining pressure, stress level, grain size and distribution, void ratio or density, and degree of saturation. With regard to the first four of these, Seed et al (1967, p 24) stated:

"The rate of load application, although having an influence, is not of major importance - a reasonable loading rate consistent with moving traffic can be utilized. Frequency, on the other hand, may influence results significantly, and some indication of the frequency of load applications should be considered. A representative number of repetitions consistent with the field conditions should also be used. The major difficulty is to define the stress conditions under which the resilient behavior of the material should be measured".

A summary of the effects of the various factors as reported by several investigators (Seed, et al, 1967, p 24; Majidzadeh, 1978, p 134; Lottman, 1976, p 55) is presented in Table 1.

TABLE 1

Factors Affecting the Resilient Modulus

Stress Duration	M_R increases slightly when time of load application is reduced
Frequency	M_R increases with increased frequency of load application
Grain Size	M_R - moisture and density relation is dependent on soil types
Saturation	M_R decreases as a result of saturation
Confining Pressure	Increases in confining pressure result in large increases in M_R
Deviator Stress	In granular soils, deviator stress level has little effect on M_R so long as the sample has little plastic deformation

Of the factors listed in Table 1, all except saturation are controlled either by the AASHTO test requirements or by the sample itself. However, the density and degree of saturation (or moisture content) are selected by the one person responsible for testing and using the test results. An understanding of the significance of these factors can be useful.

The influence of moisture content is illustrated by Figure 8. For example the resilient modulus of the Wisconsinan Loam Till drops from 11 ksi at optimum water content to 4 ksi at about 2% above optimum. Therefore, the selection of an appropriate, representative water content can be crucial.

Selection of an appropriate test density is not as critical. Figure 9 has the results for two different soils tested at 95% and 100% of Standard Proctor. Although the higher density results in a higher resilient modulus, the difference is small.

Perhaps the method of compaction is more significant. Figure 10 compares two soils compacted by static and kneading methods. For both soils, the static compaction has a higher resilient modulus. Note that AASHTO T-274 specifies the method of compaction and would require the kneading compaction for these samples.

In addition to the factors listed in Table 1, the resilient modulus of a subgrade is affected by climatic factors, the most significant of which is freezing and thawing. Robnett and Thompson (1976) investigated the effect of freeze-thaw cycles on the resilient modulus of fine grained soils (Figure 11). One freeze-thaw cycle caused a dramatic reduction in the resilient modulus. Subsequent cycles caused additional, but minor, reductions.

ESTIMATING A RESILIENT MODULUS

The AASHTO Guide recognizes the difficulties of resilient modulus testing, particularly for those highway agencies that do not have the sophisticated test equipment needed. To accommodate these agencies, relationships between CBR and R-value are reported that may be used to estimate resilient modulus. The relationships are poor.

For example, in studying 15 Arkansas soils, Thornton (1983) found no significant correlation of resilient modulus with either CBR or R-value. Similarly, Robnett and Thompson (1973) tested eight Illinois soils. Figure 12 is a plot of CBR versus resilient modulus for these soils. The data scatter demonstrates the weakness of any correlation between CBR and resilient modulus.

There is hope that good estimators will be developed. For example, Thompson and Robnett (1976) developed reasonable equations for Illinois soils that involved factors such as clay content, silt content, organic carbon content, plasticity index, liquid limit, and group index. Although these are not ready for universal use, reasonable estimmators are possible.

USE

This paper has 1) defined resilient modulus, 2) described the test method and equipment, 3) listed several factors which affect the resilient modulus, and 4) explained how results from the test are displayed.

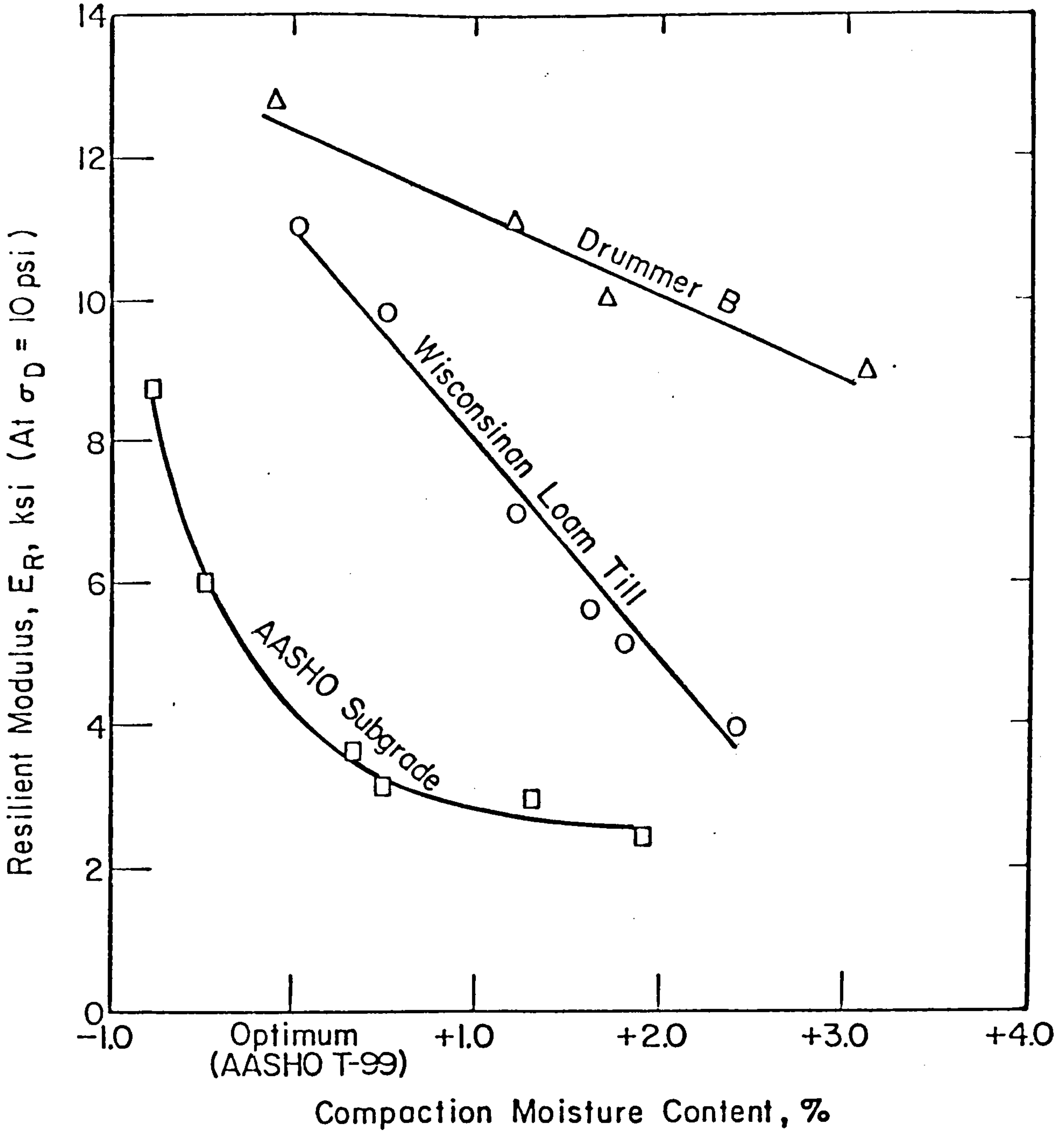

Figure 8 Effect of Compaction Moisture on Resilient Modulus (from Robnett and Thompson, 1976)

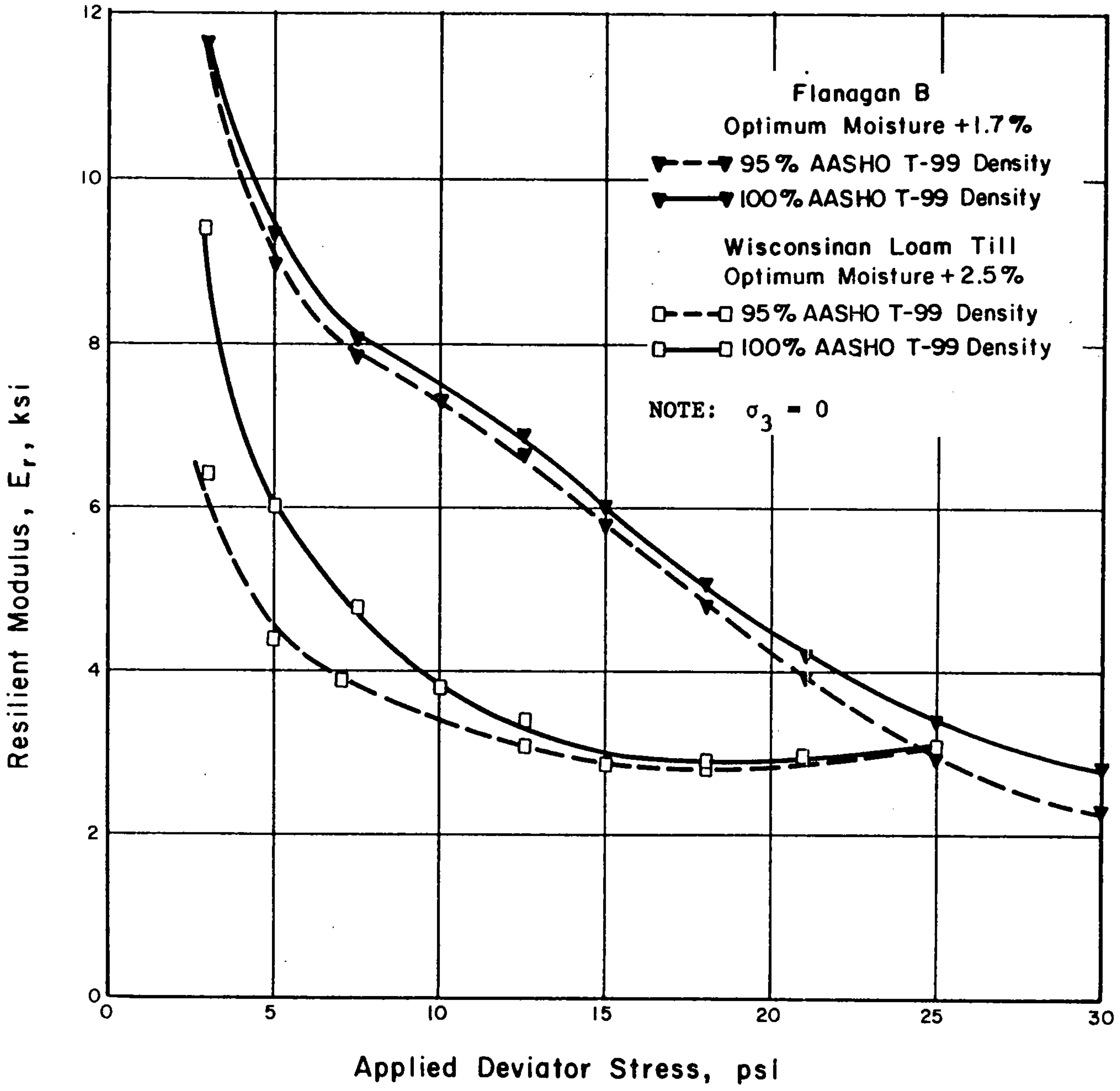

Figure 9 Effect of Density on Resilience of Specimens Compacted with Kneading Compactor (from Robnett and Thompson, 1973)

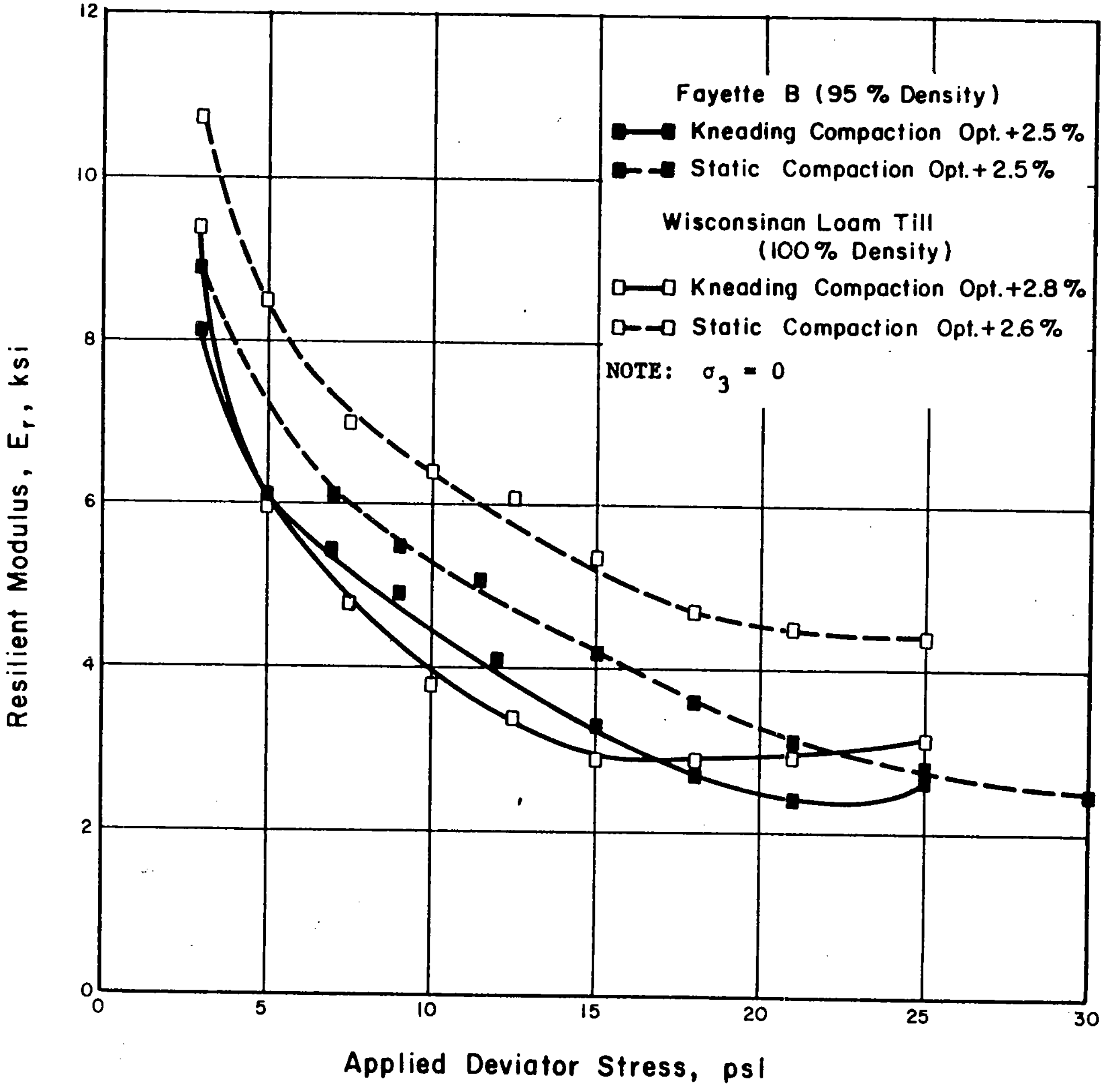

Figure 10 Influence of Compaction Method on Resilience (from Robnett and Thompson, 1973)

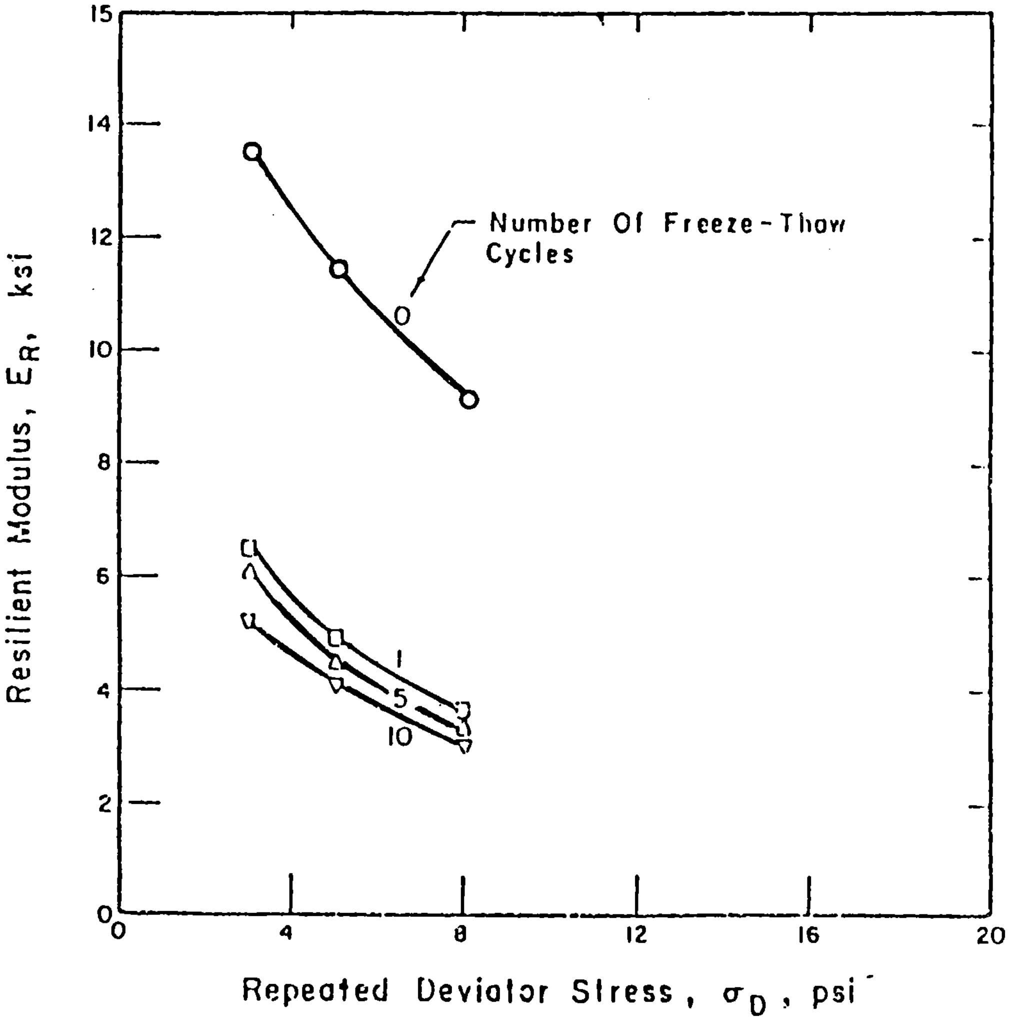

Figure 11 Effects of Freeze-Thaw on Resilient Modulus (from Robnett and Thompson, 1976)

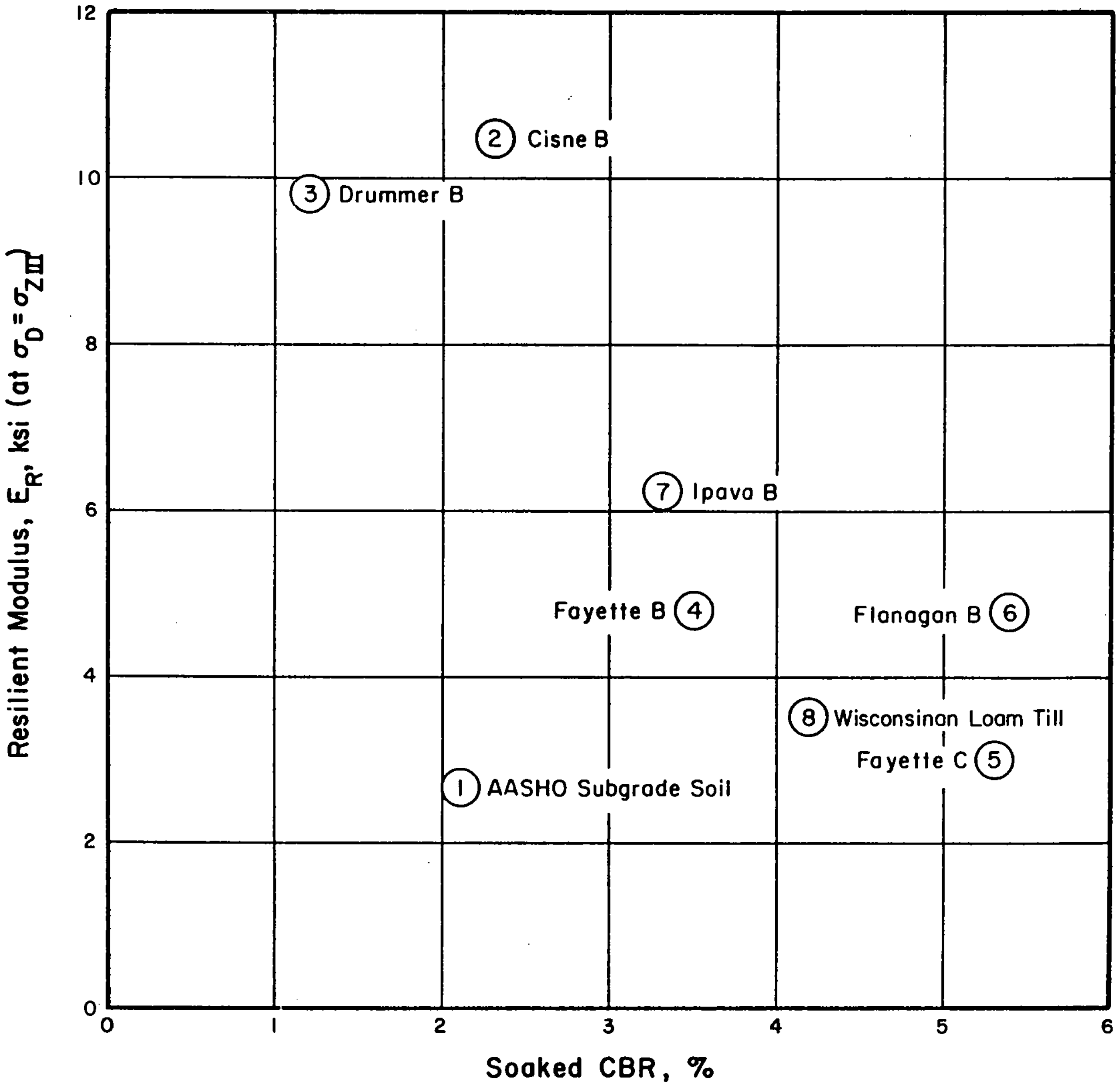

Figure 12 Plot of Soaked CBR and Resilient Modulus for Subgrade Soils Compacted to 95% AASHO T-99 Density.

A designer must still select the water content, in order to prepare the sample, and choose a value of M_R to be used in the AASHTO procedure. How this is done is explained in the companion paper, "Resilient Modulus - What Does it Mean?", which is included in this conference.

REFERENCES

AASHTO, 1985, "Proposed AASHTO Guide for Design of Pavement Structures", NCHRP Proj. 20-7/24.

AASHTO, 1982, "Resilient Modulus of Subgrade Soils", Standard Method of Test, American Association of State Highway and Transportation Officials, Designation AASHTO: T 274-82.

Hsu, Shih-Ying, and Vinson, Ted S., 1981, "Determination of Resilient Properties of Unbound Materials with Repeated Load Triaxial and Diametral Test Systems," Oregon Department of Transportation, Salem; Oregon State University, Corvallis, Oregon.

Lottman, Robert P., 1976, "Practical Laboratory Measurement and Application of Stiffness or Resilient Properties of Soils and Granular Base Materials for Idaho Flexible Pavement Design Procedures," Idaho Transportation Department, Boise, Idaho, 83707.

Majidzadeh, K., Khedr, S., and Bayomy, F., 1978, "A Statewide Study of Subgrade Soil Support Conditions," Ohio State University, Department of Civil Engineering, Columbus, Ohio, 43216.

Medina, Jacques de, and Preussler, Ernesto S., 1981, "Resilient Characteristics of Brazilian Soils," Journal, Geotechnical Engineering Division, ASCE 108, No. GT5, May, pp. 697-712.

National Highway Institute, 1984, "Techniques for Pavement Rehabilitation," Federal Highway Administration.

Robnett, Q.C. and Thompson, M. R., 1976, "Effects of Lime Treatment on the Resilient Behavior of Fine-Grained Soils," Transportation Research Record 560, Transportation Research Board.

Robnett, Q.C. and Thompson, M. R., 1973, "Interim Report, Resilient Properties of Subgrade Soils, Phase I - Development of Testing Procedure", Transportation Engineering Series No. 5, University of Illinois, Urbana.

Seed, H.B., 1967, "Factors Influencing the Resilient Deformations of Untreated Aggregate Base in Two-Layer Pavements Subject to Repeated Loading," Highway Research Record No. 190, pp. 19-57.

Thornton, Sam I., 1983, "Correlation of Subgrade Reaction", Final Report of HRC 67, Arkansas Highway and Transportation Department, PO Box 2261, Little Rock, AR 72203.

RESILIENT MODULUS
WHAT DOES IT MEAN?

Robert P. Elliott and Sam I. Thornton
Associate Professors, Department of Civil Engineering
University of Arkansas, Fayetteville, Arkansas

ABSTRACT

The new AASHTO Guide for the Design of Pavement Structures incorporates the resilient modulus test as the method for evaluating flexible pavement soil support. For those not familiar with the development and purpose of the test, there are many questions regarding its significance and why it was adopted. This paper discusses how the test relates to the structural capacity and performance of flexible pavements and how a resilient modulus value can be selected for design.

A strong relationship between the amount that a pavement deflects under load and the length of satisfactory service life has been demonstrated. Pavements that deflect more develop distress more quickly. Since most of the deflection (60 to 80%) develops within the subgrade, a measure of the soil's deflection behavior is a fundamental property that needs to be considered in rational pavement design. The resilient modulus is a measure of this behavior.

There is no single value for the the resilient modulus of a soil. Resilient modulus is affected by many factors that vary and change throughout the life of a pavement. The impact of these factors on design are examined. The paper concludes with an example of how the resilient modulus is included, selected and used in the new AASHTO guide.

INTRODUCTION

The new AASHTO Guide for the Design of Pavement Structures (1) requires the use of the subgrade resilient modulus to design a flexible pavement. The design nomograph for the new Guide is shown in Figure 1. The scale in the middle of the nomograph is for the Effective Roadbed Soil Resilient Modulus. Resilient modulus is also included as a test that can be used to establish the structural layer coefficient for base and subbase materials.

How does the resilient modulus relate to the "real world" structural capacity and performance of flexible pavements? How is a resilient modulus value selected for design? How is resilient modulus used in design? These questions are particularly bothersome because the standard test (AASHTO T-274) is quite time consuming.

Before trying to understand the resilient modulus, the need to replace the soil support scale that was used in the previous Guide for Design of Pavement Structures (2) should be recognized. The fundamental basis for both guides is the AASHO Road Test that was conducted in 1958-1960. Although the Road Test is the most comprehensive pavement research project ever undertaken, it did not (and could not) include all variables that can affect the performance of a pavement. One major factor not examined was subgrade soil strength. Only one type of soil was used in the Road Test.

Following the Road Test, pavement design procedures were developed from the research findings. The design procedures required some method for considering different subgrade soil types. For rigid pavements, a rational method for including subgrade soil was available that involved incorporating Westergaard's modulus of subgrade reaction (k value) and Spangler's theoretical formula for corner stresses (3). However, no similar approach was available for the flexible pavements.

For flexible pavements, a "soil support" scale was established using engineering judgement supplemented with limited data from Road Test sections having the greatest thickness of crushed stone base. This scale was not based on any particular method of test. Each highway agency was left to adopt a test method and establish or select a relationship between the test selected and the soil support scale. Without an analytical basis and a unified method of test, there is little possibility of improving the soil support scale.

BASIS FOR RESILIENT MODULUS TESTING

The AASHO Road Test demonstrated that pavement surface deflection under load is a strong indicator of how well a pavement will perform (4).

> "The performance of the flexible pavements was predicted with essentially the same precision from load-deflection data as from load-design information."

Other studies (5,6,7,8,9) found similar relationships between pavement deflection and performance (Figure 2).

Surface deflection results from the accumulation of load induced strain within the pavement and subgrade with the subgrade being a major contributor. At the AASHO Road Test (4), 60 to 80 percent of the deflection measured at the surface was found to develop within the subgrade. Consequently, the stress-strain relationship for the subgrade (resilient modulus) is a major factor contributing to surface deflection. It follows that subgrade resilient modulus is also a major factor in flexible pavement performance.

SIGNIFICANCE OF RESILIENT MODULUS

Surface deflection is not itself detrimental to the pavement. However, deflection is an indicator of the factors that are detrimental.

NOMOGRAPH SOLVES:

$$\log_{10}W_{18} = Z_R{*}S_o + 9.36{*}\log_{10}(SN+1) - 0.20 + \frac{\log_{10}\left[\frac{\Delta PSI}{4.2 - 1.5}\right]}{0.40 + \frac{1094}{(SN+1)^{5.19}}} + 2.32{*}\log_{10}M_R - 8.07$$

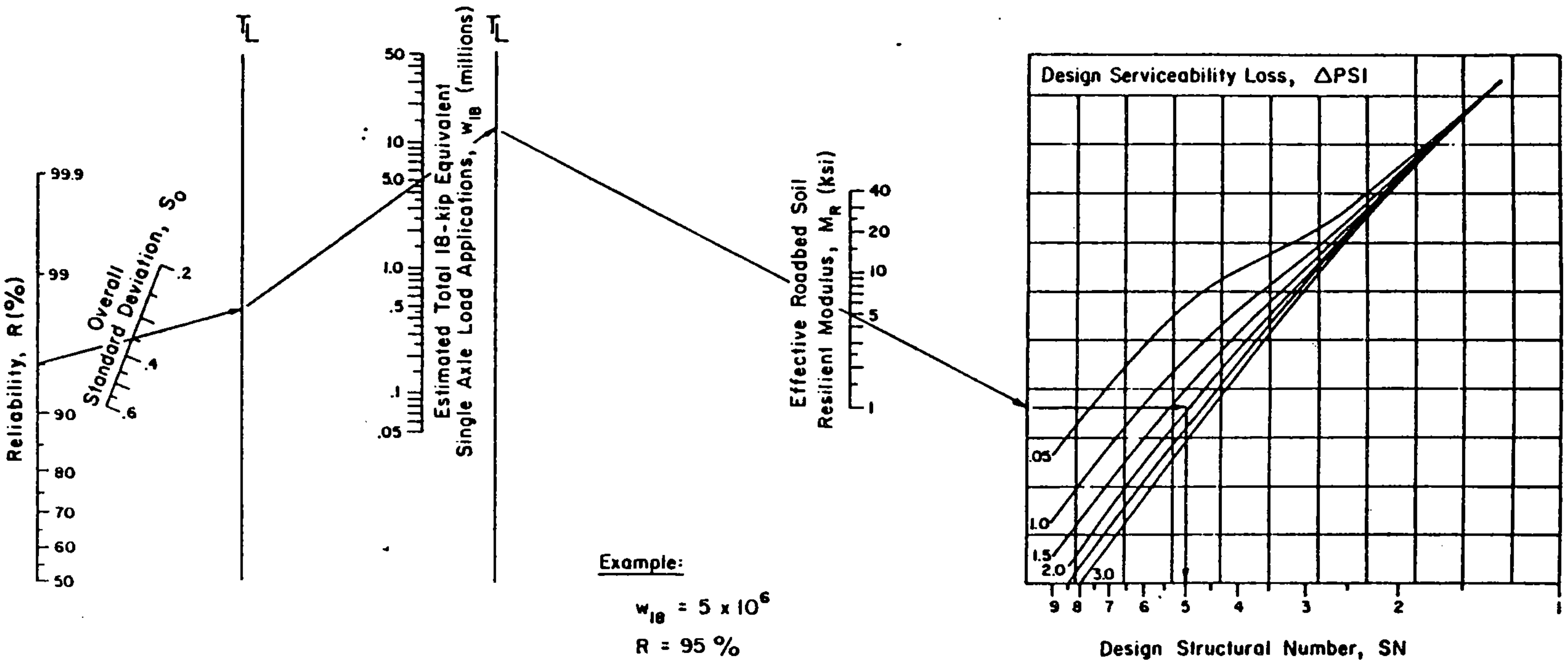

Example:

$w_{18} = 5 \times 10^6$

R = 95 %

$S_o = 0.35$

$M_R = 5000$ psi

ΔPSI = 1.9

Solution: SN = 5.0

Figure 1. AASHTO Nomograph for Flexible Pavement Design.

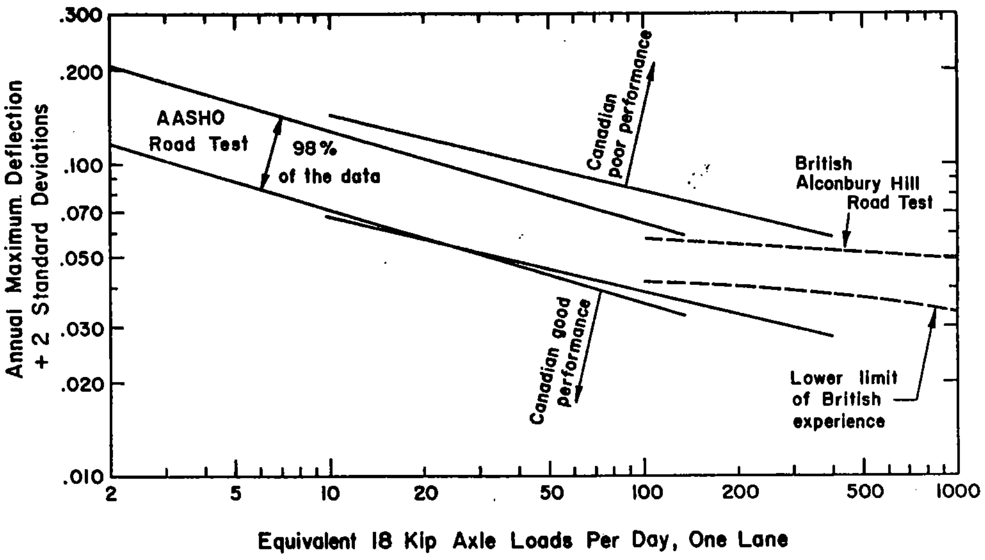

Figure 2. Reported Deflection-Life Relationships (Ref. 10)

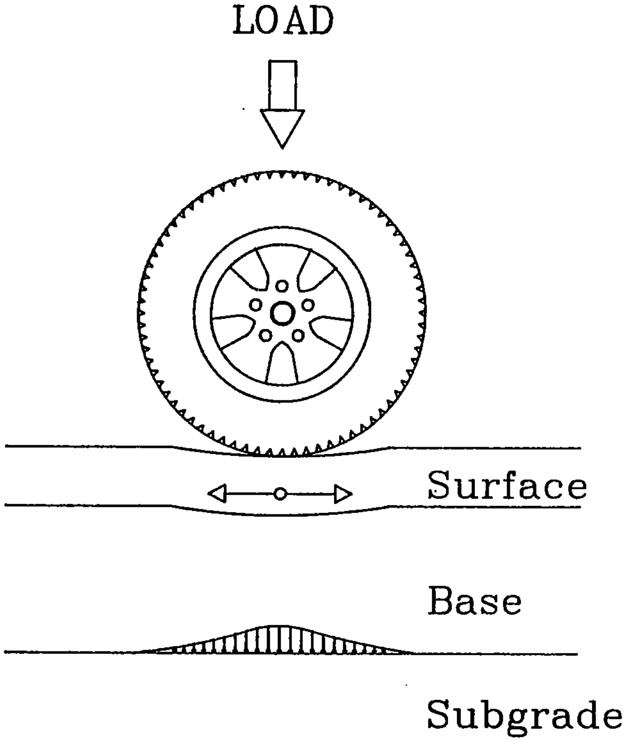

LOAD
Surface
Base
Subgrade

Figure 3. Illustration of the Primary Structural Responses that Control Pavement Performance.

There are two major types of load induced flexible pavement failure - fatigue cracking and rutting. Figure 3 illustrates the two prime structural parameters contributing to failure: the tensile strain that develops in the bottom of the asphalt (AC) layer and the stress or strain applied to the top of the subgrade.

Figures 4 and 5 illustrate the effect of subgrade resilient modulus on the AC tensile strain and the subgrade stress. These plots were developed using the ILLI-PAVE design algorithms developed by Thompson and Elliott (11). They represent the structural response of a conventional flexible pavement having a 3" AC surface and a 12" aggregate base when subjected to a 9000 pound wheel load.

In Figure 4, the AC strain decreases as the resilient modulus of the subgrade increases. A strain decrease increases the fatigue life (load applications before cracking) for the AC surfacing.

Figure 5 shows the change in subgrade stress ratio with resilient modulus. The stress ratio is the load induced vertical stress on the subgrade divided by the unconfined compressive strength of the soil. In analyzing the performance of the AASHO Road Test pavements, Elliott and Thompson (12) found a strong relationship between subgrade stress and load applications prior to cracking. As a result, the stress ratio was selected as the design parameter to guard against overstressing the subgrade. In Figure 5, the stress ratio decreases as the resilient modulus increases indicating an increasing pavement life.

EFFECT ON DESIGN BY THE AASHTO GUIDE

Figures 6, 7, and 8 illustrate the effect of subgrade resilient modulus based on the new AASHTO Guide.

Figure 6 is the relationship between resilient modulus and design traffic life. Relative traffic life is expressed as the total 18-kip equivalent single axle loads for any given resilient modulus divided by a base value. For this figure, the base value is the total 18-kip equivalent single axle loads for a resilient modulus of 5 ksi. For example, a pavement constructed on a subgrade having a resilient modulus of 10 ksi will carry approximately 10 times the traffic that the same pavement could carry if the resilient modulus were 5 ksi. Similarly, the 5 ksi soil would permit the pavement to carry nearly 10 times as much traffic as it could if built on a soil having a resilient modulus of 2 ksi.

Figure 7 is the relationship between resilient modulus and the design structural number. For Figure 7, a structural number of 5.0 was used with a resilient modulus of 5 as the base. For the same traffic conditions, a structural number of 6.6 would be needed on a subgrade having a resilient modulus of 2 ksi. If the resilient modulus were 10 ksi, the required structural number would be 4.0.

Figure 8 was prepared to show the effects of resilient modulus on pavement thickness. The structural numbers from Figure 7 are converted to equivalent Full Depth asphalt thicknesses. The conversion

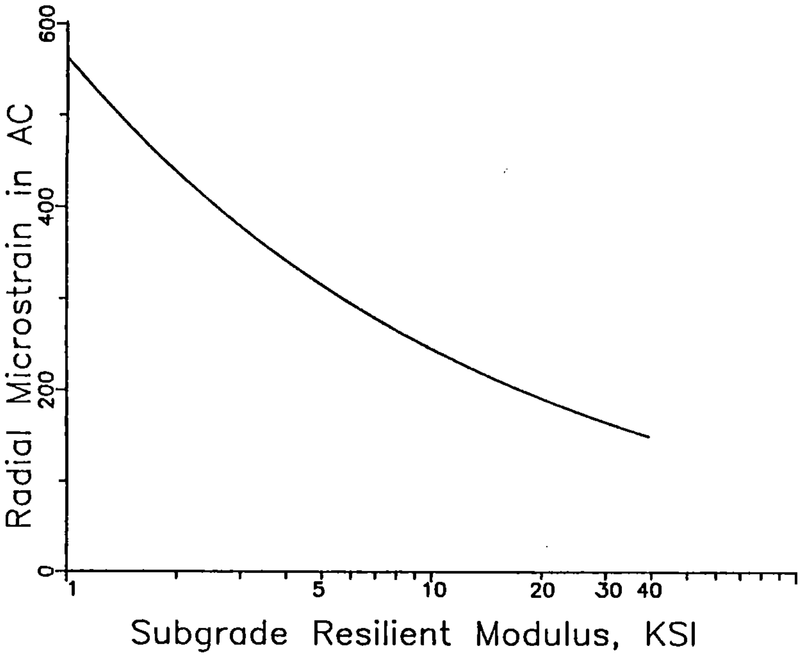

Figure 4. Effect of Subgrade Resilient Modulus on AC Radial Strain.

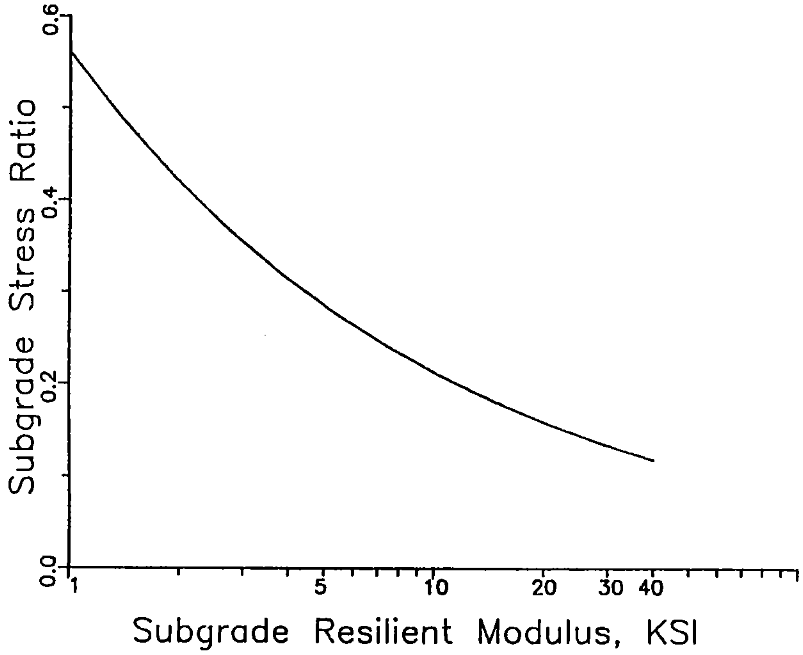

Figure 5. Effect of Subgrade Resilient Modulus on Subgrade Stress Ratio.

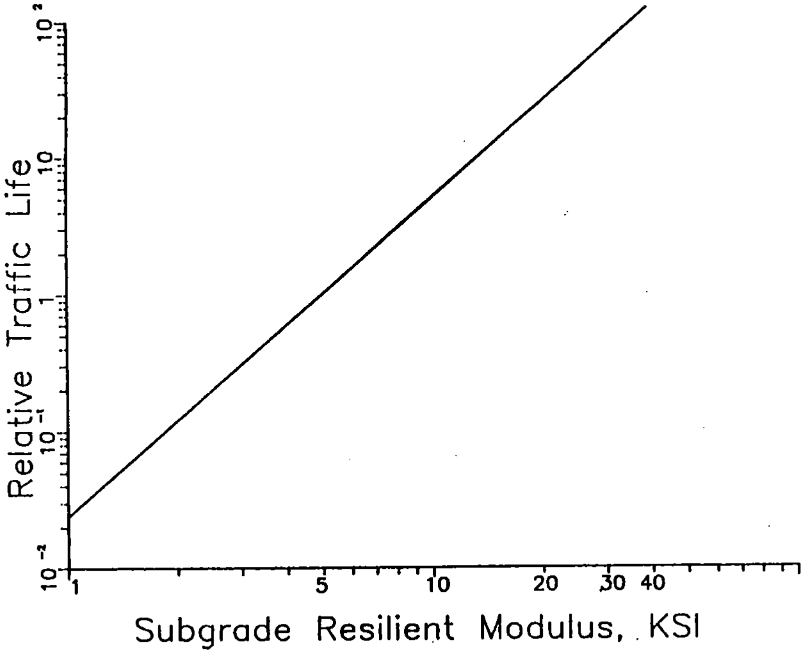

Figure 6. Effect of Subgrade Resilient Modulus on Relative Traffic Life.

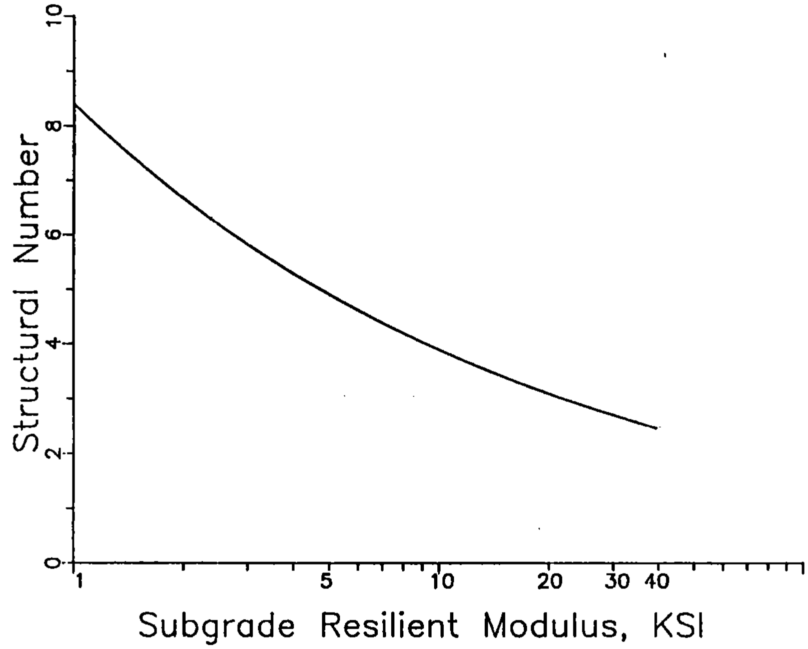

Figure 7. Effect of Subgrade Resilient Modulus on the Design Structural Number.

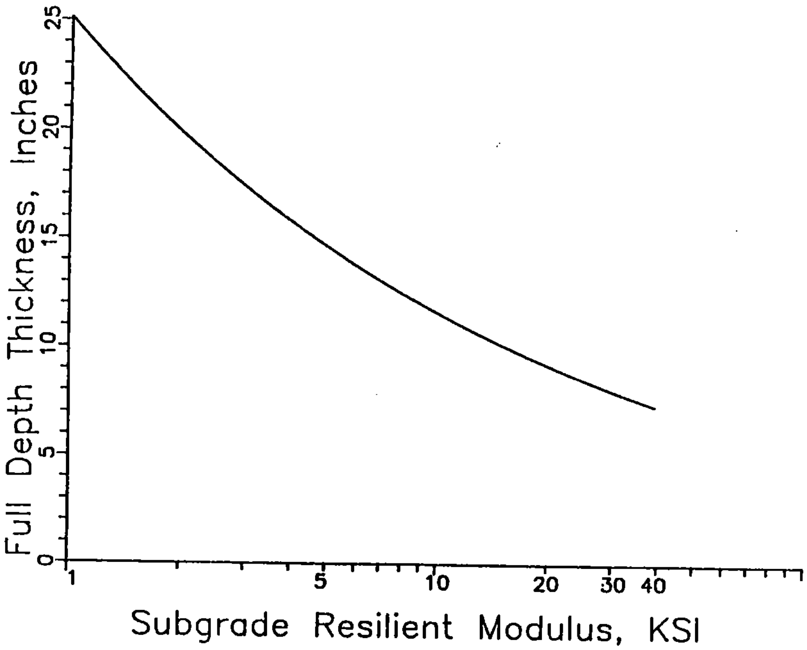

Figure 8. Effect of Subgrade Resilient Modulus on Pavement Thickness.

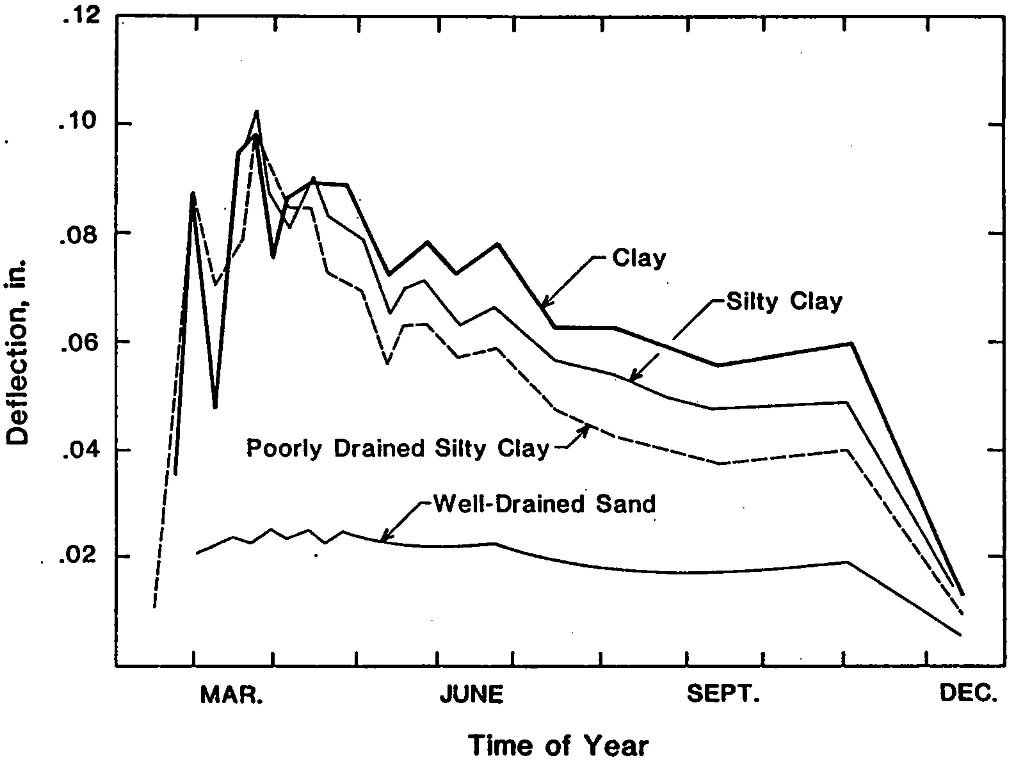

Figure 9. Seasonal Pavement Deflections for Various Soils Types.

was made using structural layer coefficients of 0.44 and 0.30 for the AC surface and bituminous base, respectively; and assuming that the base thickness would be 3 times the surfacing thickness. For this example, the Full Depth thickness would range from 19.8" to 14.9" to 11.8" for resilient moduli of 2, 5, and 10 ksi respectively.

In practical terms, Figures 7 and 8 indicate that a 30% error in the resilient modulus will result in an error of 1 to 1.5 inches in selecting the appropriate total asphalt thickness.

SEASONAL VARIATIONS

Unfortunately, there is no simple test that will give "The" resilient modulus of a soil. In fact, the subgrade resilient modulus is not a single, fixed value. Rather, the resilient modulus changes due to a number of factors throughout the pavement's life.

Several factors that affect the resilient modulus of a soil were discussed in the companion paper presented at this symposium, "Resilient Modulus - What is it?" (13). Of concern in this paper is how these factors can influence the seasonal variation of the subgrade. A seasonal variation is to be expected because, in most areas of the country, roadbeds are softer in the spring than they are at other times of the year. This is demonstrated by the seasonal variation in pavement surface deflections. However, the seasonal variation is more pronounced for some soils than it is for others (Figure 9).

Much of the variation in resilient modulus can be attributed to seasonal moisture changes. Figure 10 illustrates the effect of moisture content found by Thompson and Robnett (14) when testing the AASHO Road Test subgrade. However, the springtime peak deflection commonly noted in northern states is also indicative of the effect of freeze-thaw. Robnett and Thompson (15) also investigated the freeze-thaw effect finding that one freeze-thaw cycle caused a dramatic reduction in the resilient modulus with subsequent cycles causing additional, but minor, reductions (Figure 11).

SELECTION OF A DESIGN VALUE

The selection of a single resilient modulus value to be used in design can be quite complex. The object, of course, is to select a single value that is representative of the entire year.

Elliott and Thompson (12) conducted an analysis to find the appropriate "time of year" condition that would be representative of the entire year for the AASHO Road Test pavements. The study included 1) an investigation of the seasonal variation of resilient modulus at the AASHO Road Test and 2) a determination of the seasonal load damage effects for pavements with various thicknesses of asphalt. Their study was based on asphalt fatigue damage effects and included consideration of seasonal variation in the AC stiffness modulus as well as the subgrade resilient modulus.

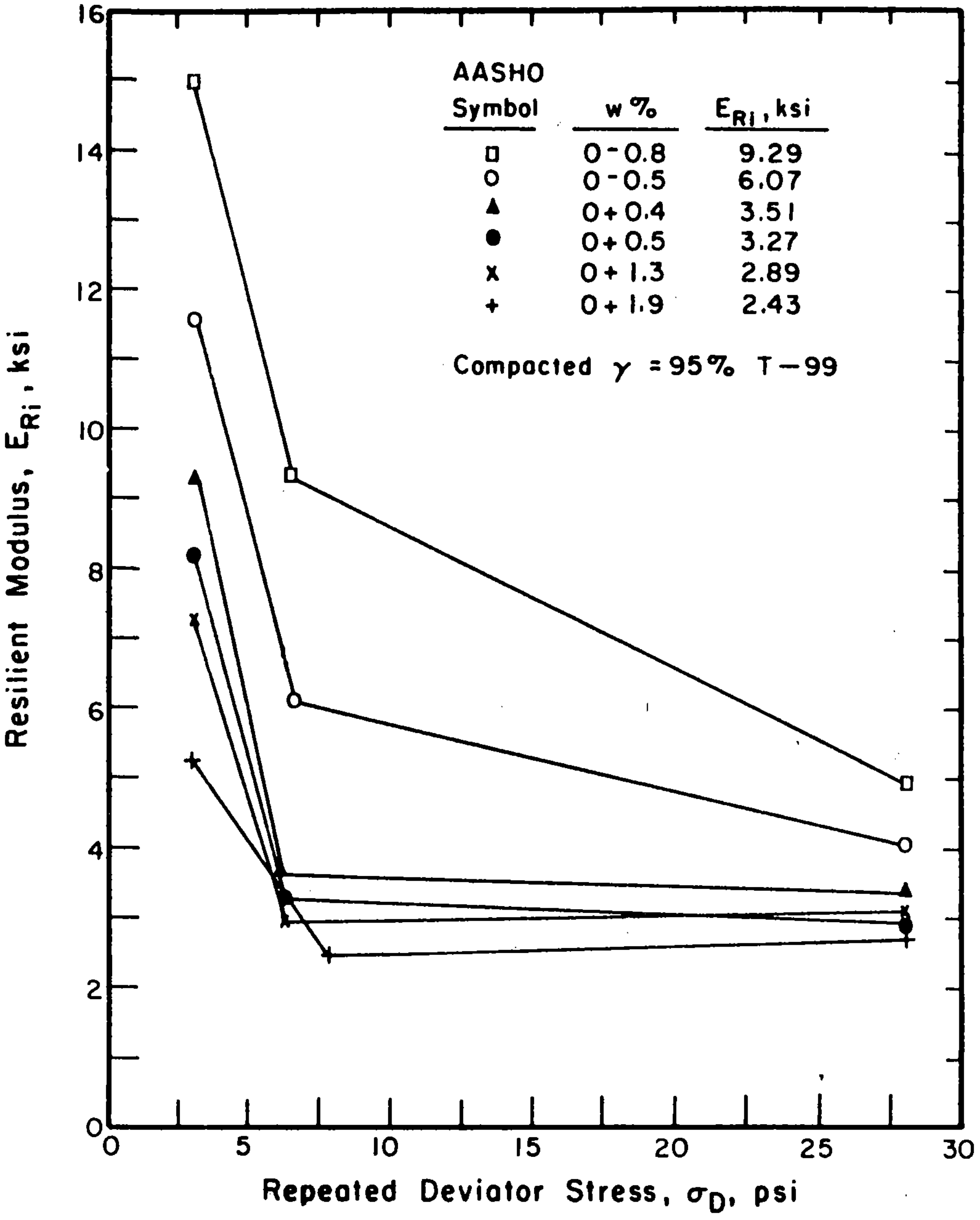

Figure 10. Effect of Moisture Content on the Resilient Modulus of the AASHO Road Test Subgrade (Ref. 14).

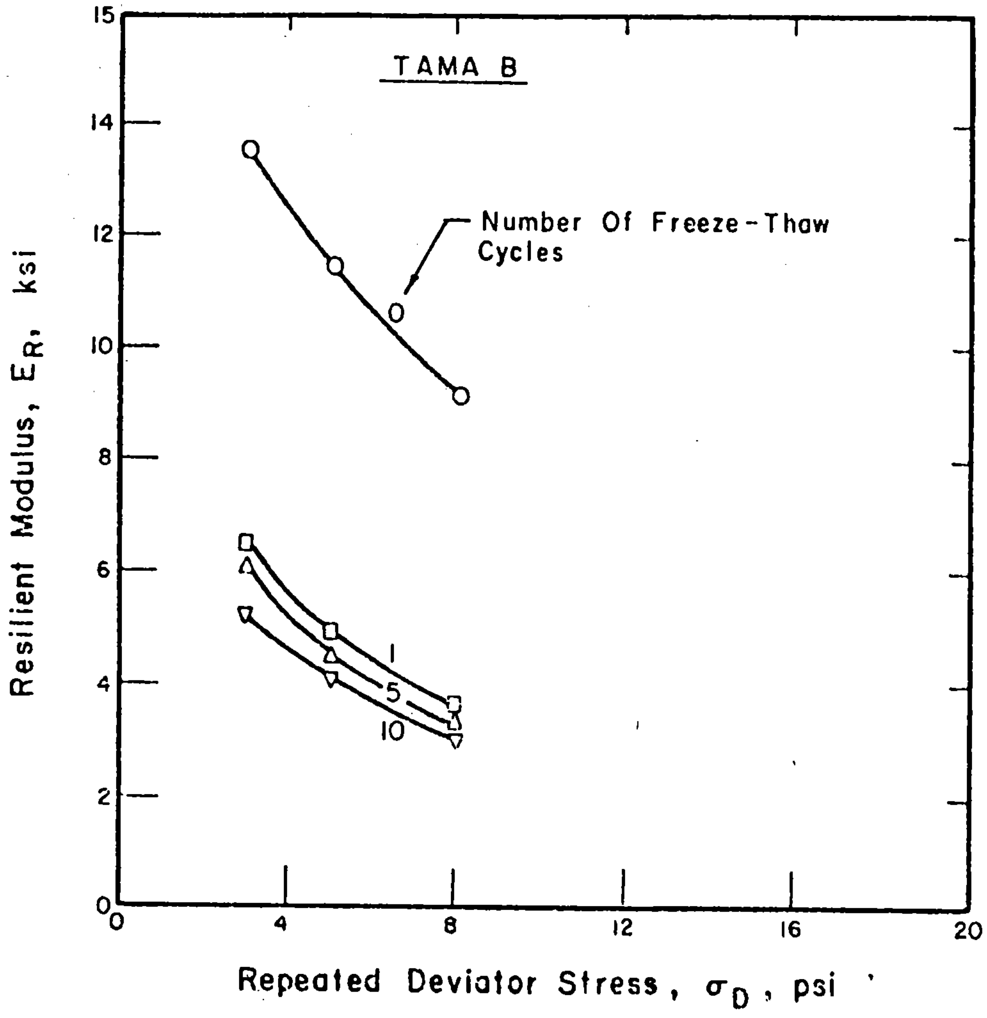

Figure 11. Effect of Freeze-Thaw on Resilient Modulus (Ref. 15).

The seasonal subgrade resilient modulus variation (based on analysis of deflection measurements taken during the AASHO Road Test) is shown on Figure 12. Figure 13 is the seasonal load damage effects expressed as a Weighting Factor.

Elliott and Thompson concluded that no single resilient modulus could truly represent all pavement thicknesses. However, since all curves intersected in a fairly tight pattern in late April and mid-October, they stated that conditions during either of those periods should be acceptable for design purposes.

EXAMPLE SUBGRADE RESILIENT MODULUS SELECTION

The new Guide contains a specific recommended method for selecting the subgrade resilient modulus. It consists of estimating seasonal variations in resilient modulus and assigning relative damage factors on a monthly or bi-monthly basis. The damage factors are summed and the average determined. The resilient modulus corresponding to the average damage factor is then used for design. The following steps are involved in selecting the subgrade resilient modulus.

Step 1. Develop a relationship between resilient modulus and subgrade moisture content.

This involves conducting resilient modulus tests on the subgrade soil at various moisture contents representing the range of moisture variation expected. For example, using the AASHO Road Test soil data (Figure 10), a relationship between resilient modulus and moisture content is developed (Figure 14).

Step 2. Estimate the seasonal variation in moisture content.

For this example it is assumed that moisture contents were determined four times during the year on a similar subgrade soil from a nearby pavement. From these a seasonal variation has been estimated as shown in Figure 15.

Step 3. Determine the monthly (or bimonthly) resilient modulus.

Figures 14 and 15 are used to estimate the resilient modulus for each month of the year. The monthly values are entered on the AASHTO form (Figure 16). For example, the moisture content in March is about 16.8%, which is 1.8% above optimum. The resilient modulus for 16.8% moisture content is 2,200 psi. Except for January and February, the resilient modulus for other months are found in a similar fashion. For January, it is assumed that the subgrade will be frozen resulting in a very high resilient modulus. February is assumed to be a period of thawing. To account for the freeze-thaw effect discussed earlier (Figure 11), the resilient modulus is determined in the normal fashion and reduced by 50%.

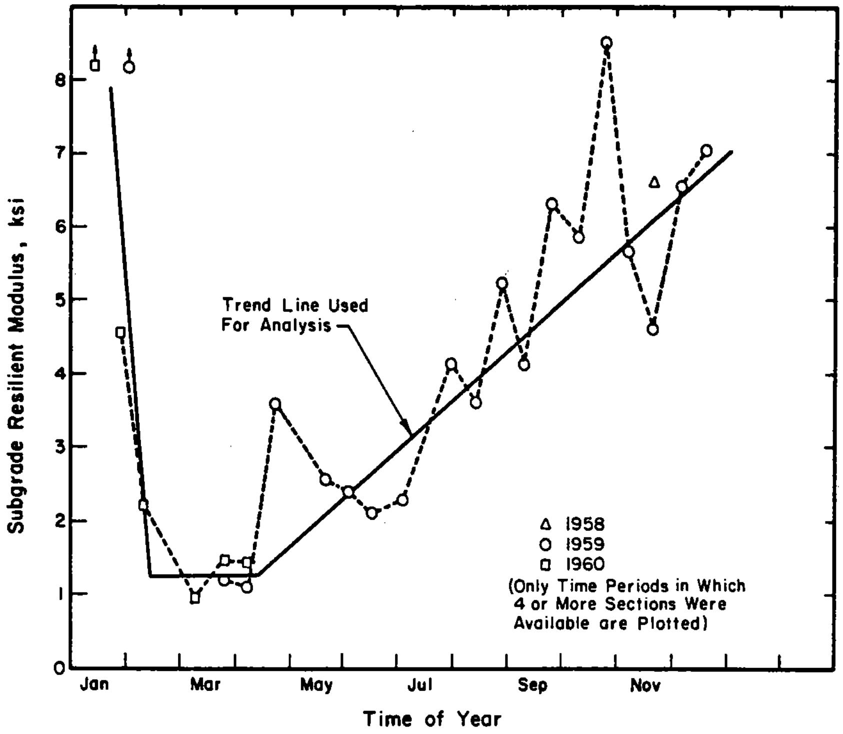

Figure 12. Variation in Subgrade Resilient Modulus at the AASHO Road Test (Ref. 12).

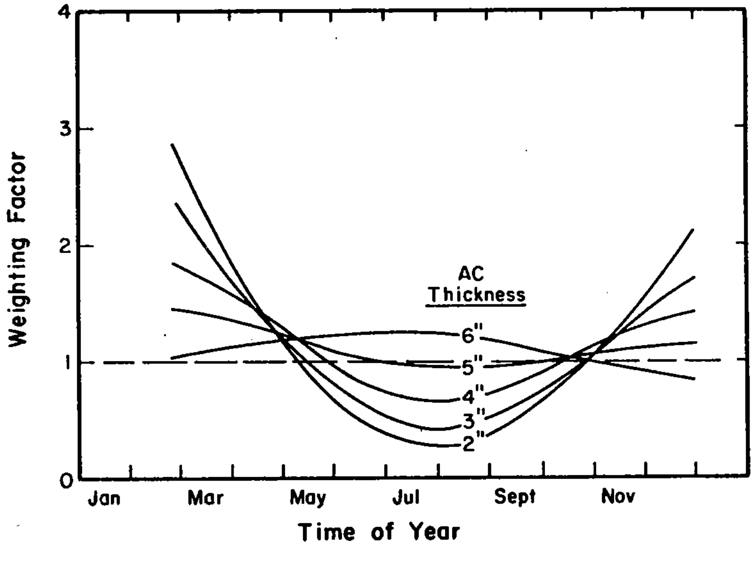

Figure 13. Seasonal Weighting Factors for Various Thicknesses of AC Surfacing (Ref. 12).

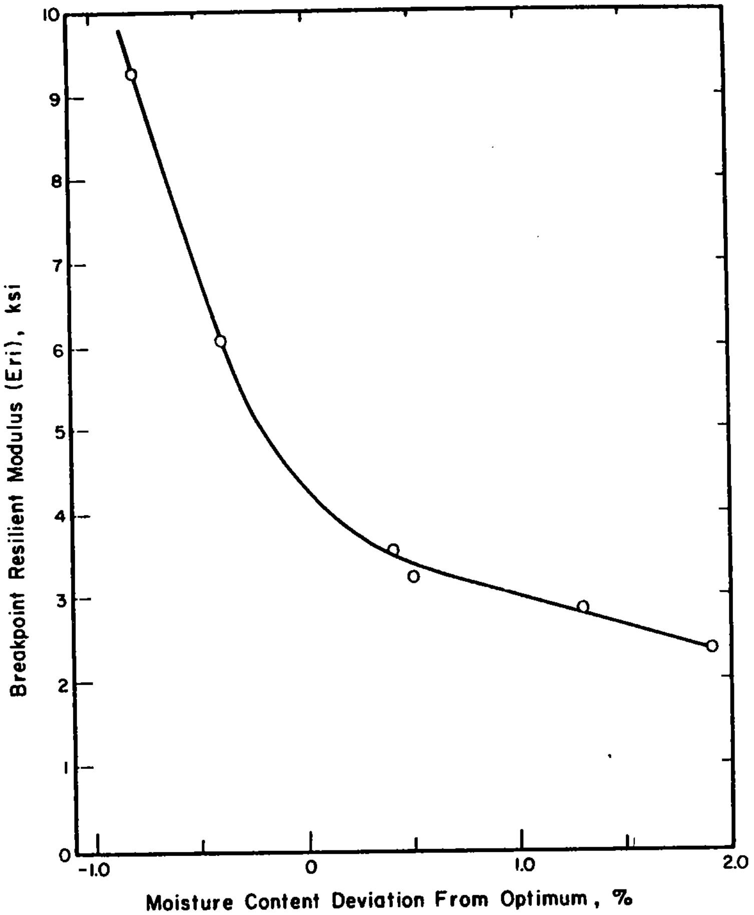

Figure 14. Moisture Content-Resilient Modulus Relationship for the AASHO Road Test Subgrade.

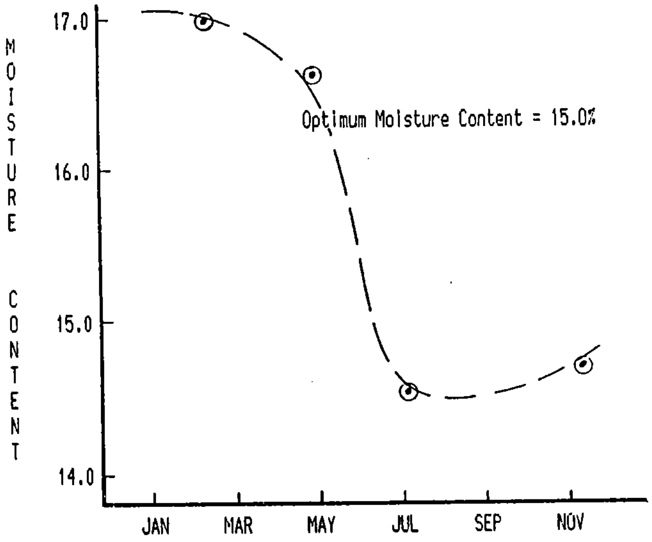

Figure 15. Seasonal Moisture Content Varialtion Used in Example.

Month	Roadbed Soil Modulus, M_R (psi)	Relative Damage, u_f
Jan.	Frozen	0
Feb.	1,100*	10.4
Mar.	2,200	2.1
Apr.	2,200	2.1
May	2,700	1.3
June	3,900	0.6
July	6,000	0.2
Aug.	6,800	0.2
Sept.	6,800	0.2
Oct.	6,000	0.2
Nov.	5,400	0.3
Dec.	4,500	0.4
	Summation: Σu_f =	18.0

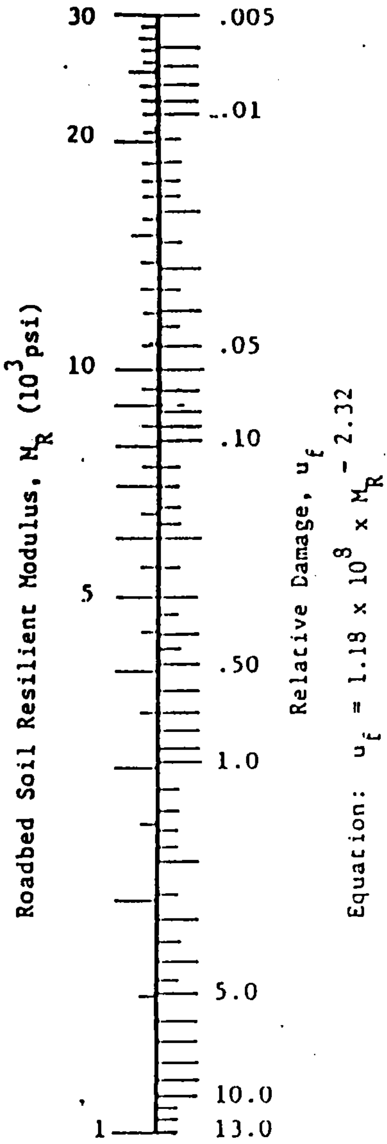

Average: $\bar{u}_f = \frac{\Sigma u_f}{n} =$ 1.5

Effective Roadbed Soil Resilient Modulus, M_R (psi) = 2500 (corresponds to $\bar{u}_f$)

*Reduced 50% to account for Freeze-Thaw.

Figure 16. Example Determination of Resilient Modulus for Use in Design.

Step 4. Select a relative damage factor for each resilient modulus.

Relative damage factors corresponding to the monthly resilient modulus values are selected using the scale on the right side of Figure 16. For the frozen subgrade (January), the resilient modulus would be high resulting in a low relative damage factor. For practical purposes a damage value of 0.0 is assigned.

Step 5. Use the average monthly relative damage factor to select the Effective Roadbed Soil Resilient Modulus.

The average damage value (1.5) is used with the scale on the right side of Figure 16 to select an effective roadbed soil resilient modulus (2,500 psi) to be used with the design nomograph (Figure 1).

RESILIENT MODULUS IN PERSPECTIVE

Resilient modulus is a significant and rational material property that needs to be included in the pavement design process. However, the resilient modulus does not represent all properties of a subgrade or granular layer that can affect the performance of a pavement.

The most direct evidence that other properties are also significant this comes from the AASHO Road Test (4). Two granular materials were used - a crushed stone and a gravel. Of these, the gravel base sections deflected less. Inch for inch, the gravel was more effective in reducing the deflections. This suggests that the gravel possessed the higher resilient modulus. Nevertheless, the crushed stone sections had the superior performance. As stated in the Road Test report:

> "Perhaps the gravel possessed less internal stability than the stone; yet it may have been somewhat less resilient." (i.e. higher resilient modulus)

Similarly, Figure 17 indicates that density has only a limited effect on resilient modulus. This could lead one to conclude that density is not significant. However, Figure 18 shows that density is significant relative to permanent deformation (strain).

Resilient modulus reflects only the rebound or resilient deformation behavior of the material. In so far as this relates to the load induced stresses, strains, and deflections, resilient modulus is important and significant. However, the resilient modulus tells absolutely nothing about the permanent deformation behavior of the material. For many materials, the permanent deformation behavior may well be the factor controlling pavement life. Therefore, resilient modulus must not be the only property considered in designing and selecting materials for a flexible pavement.

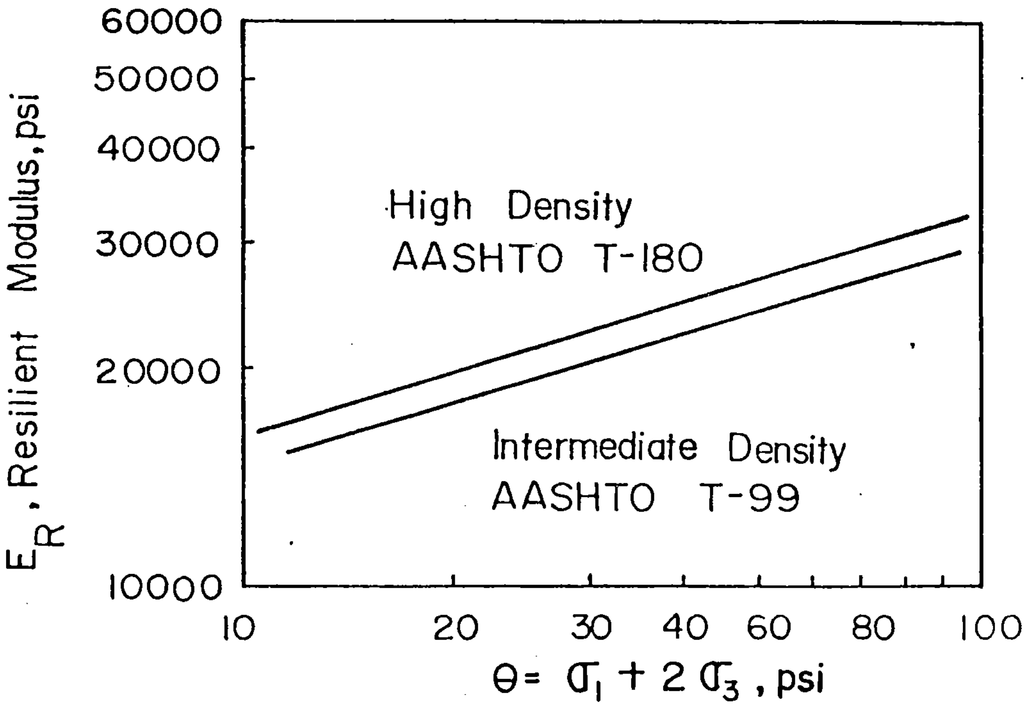

Figure 17. Effects of Density on Resilient Modulus (Ref. 16).

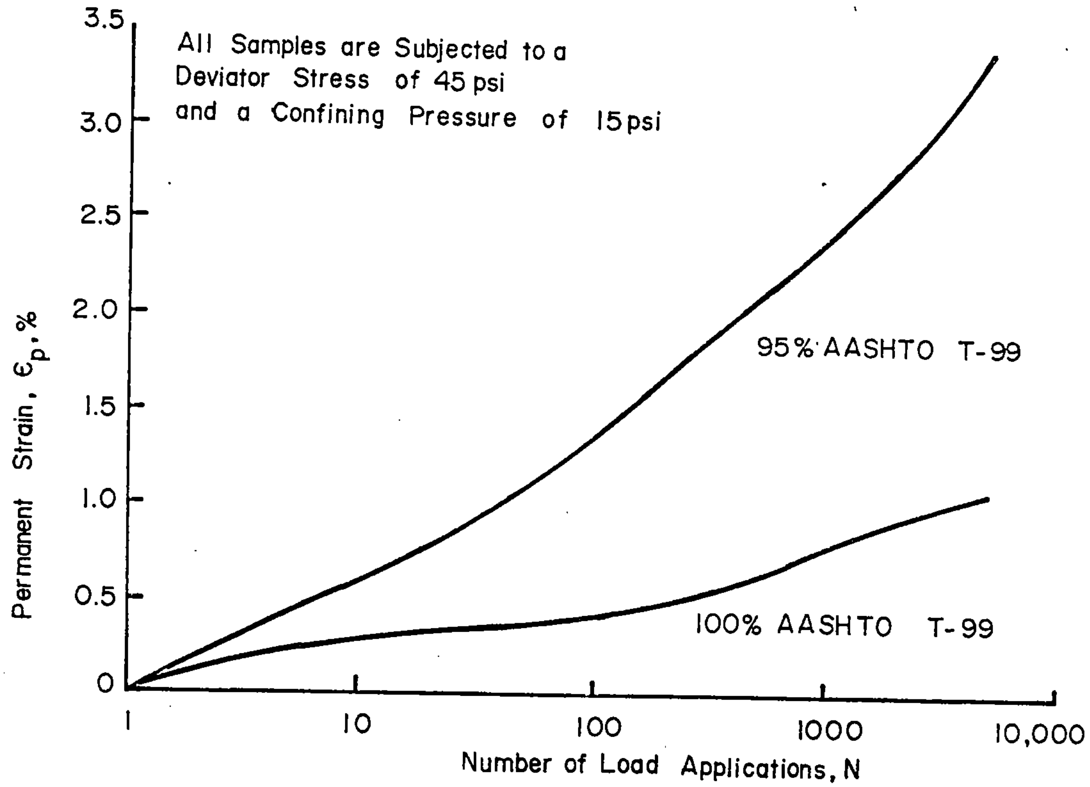

Figure 18. Effects of Density on Permanent Deformation (Ref. 16).

CONCLUSION

Resilient modulus is a fundamental material property. It relates to pavement design and performance for the same reason that surface deflection relates. It provides a measure of the load induced stress-strain behavior of the soil which in turn governs the load response of the pavement system.

Many factors affect the resilient modulus causing it to vary seasonally throughout the life of the pavement. Consequently, the selection of a single value for use in design can be complicated. While on paper the Guide procedure presented above appears to be straight forward, the estimation of seasonal moisture variation can be quite nebulous. Also the test procedure as presently set forth by AASHTO is very time consuming.

Because of this complexity, it is likely that highway agencies will develop methods of estimating subgrade resilient modulus based on other, easier to determine parameters. While to some, this may appear to be but little changed from the old soil support approach, it will have the decided advantage that it is based on an analytical approach with a rational test and can therefore be improved as the state of knowledge improves.

ACKNOWLEDGEMENTS/DISCLAIMER

This paper is in part based on Project TRC-94, "Resilient Properties of Arkansas Soils", which is being conducted by the Arkansas Highway and Transportation Research Center.

TRC-94 is sponsored by the Arkansas State Highway and Transportation Department and the U.S. Department of Transportation (Federal Highway Administration).

The contents of this paper reflect the views of the authors who are responsible for the facts and accuracy of the data presented herein. The contents do not necessarily reflect the official views or policies of the Arkansas State Highway and Transportation Department or the Federal Highway Administration. This paper does not constitute a standard, specification, or regulation.

REFERENCES

1. ______, "Proposed AASHTO Guide for Design of Pavement Structures," NCHRP Project 20-7/24, National Cooperative Highway Research Program, July 15, 1985.

2. ______, "AASHO Interim Guide for Design of Pavement Structures," American Association of State Highway Officials, 1972.

3. Langsner, G., Huff, T.S., and Liddle, W.J., "Use of Road Test Findings by AASHO Design Committee," Special Report 73, Highway Research Board, 1962.

4. ______, "The AASHO Road Test, Report 5, Pavement Research," Special Report 61E, Highway Research Board, 1962.

5. ______, "The WASHO Road Test, Part 2, Test Data, Analysis, Findings," Special Report 22, Highway Research Board, 1955.

6. Hveem, F.N., "Pavement Deflections and Fatigue Failures," Bulletin 114, Highway Research Board, 1955.

7. Nichols, F.P., "Deflections as an Indicator of Flexible Pavement Performance," Highway Research Record 13, Highway Research Board, 1963.

8. Canadian Good Roads Association, "Field Performance Studies of Flexible Pavements in Canada," Proceedings of the Second International Conference on the Structural Design of Asphalt Pavements, Ann Arbor, Michigan, 1967.

9. Burt, M.E., "Progress in Pavement Design," TRRL Report LR 508, Transport and Road Research Laboratory, Department of the Environment, England, 1972.

10. Kingham, R.I., "Development of the Asphalt Institute's Deflection Method for Designing Asphalt Concrete Overlays for Asphalt Pavements," Research Report 69-3, The Asphalt Institute, 1969.

11. Thompson, M.R. and Elliott, R.P., "ILLI-PAVE-Based Response Algorithms for Design of Conventional Flexible Pavements," Transportation Research Record 1043, Transportation Research Board, 1985.

12. Elliott, R.P. and Thompson, M.R., "ILLI-PAVE Mechanistic Analysis of AASHO Road Test Flexible Pavements," Transportation Research Record 1043, Transportation Research Board, 1985.

13. Thornton, S.I. and Elliott, R.P., "Resilient Modulus - What is it?," Paper presented at the Highway Geology Symposium, Helena, Montana, 1986.

14. Thompson, M.R. and Robnett, Q.C., "Final Report, Resilient Properties of Subgrade Soils," Transportation Engineering Series No. 14, University of Illinois, Urbana, 1976.

15. Robnett, Q.C. and Thompson, M.R., "Effects of Lime Treatment on the Resilient Behavior of Fine-Grained Soils," Transportation Research Record 560, Transportation Research Board, 1976.

16. ______, "Techniques for Pavement Rehabilitation," National Highway Institute, Federal Highway Administration, 1984.

DYNAMIC PILE MONITORING AND PILE LOAD TESTS IN UNCONSOLIDATED SANDS AND GRAVELS, WYOMING

Michael P. Schulte
Engineering Geologist
Wyoming Highway Department

INTRODUCTION

The Wyoming Highway Department made a formal request to the Federal Highway Administration in September, 1984, for the Demonstration Project No. 66 "Design and Construction of Driven Pile Foundations." The Project consists of conducting static load tests on driven piling. Selected piling is monitored with Dynamic Pile Monitoring Equipment (Pile Analyzer) which determines the ultimate static resistance, maximum measured force, maximum allowable compressive stress, maximum transfer energy and the transfer efficiency (actual hammer energy). The purpose of requesting this test program was to provide an opportunity to compare the W.H.D. static analysis (The Nordlund Method) for the type of foundation materials present at the two proposed bridge sites with newer and more accurate methods of analysis. Wyoming has a relatively small percentage of bridges founded in unconsolidated granular material with pile type design foundation and our static design parameters may be conservative for this type of foundation.

Location and Structure Foundation Information

Two separate bridges over the North Platte River were to be replaced. The foundation materials present at both sites are alluvial flood plain deposits consisting of layered to heterogeneous mixtures of silty sands and gravels ranging in depth from 77'+ to 110'+. Bedrock consists of claystones and siltstones of the Tertiary Brule Formation.

Design Requirements

The proposed bridge foundation designs called for HP 12 x 53 steel "H" pile at all abutment locations and HP 14 x 73 "H" pile at all pier locations. All piles were to be fitted with pile tip protection. The design load requirements for the bridge No. 1 consisted of 69 tons/pile at the abutments and an average of 87 tons/pile at the piers. Design load requirements for Bridge No. 2 consisted of 52 tons/pile at the abutments and an average of 89 tons/pile at the piers.

Hammer Data

The following hammer system was selected by the contractor:

Mitsubishi MH-15 single acting diesel hammer
Rated energy at maximum 8.5' stroke = 28,100 ft. lbs.
Ram weight = 3,310 lbs.
Hammer cushion - Alternate layers of micarta and aluminuim
totaling 3 inches in thickness.

Load Test and Dynamic Monitoring Procedure

Two load tests were chosen for this project; one at each bridge location. Bridge site No. 1 was set up to test the HP 12 x 53 pile and Bridge site No. 2 was set up to test the HP 14 x 73 pile. The static load tests consisted of driving four reaction piles in a 7.5' x 24' rectangular pattern with one centered compression pile. Piling was driven in 40' sections. The compression and two of the reaction piles were monitored at each site and driving was to be stopped when twice the pile design bearing was reached as measured by the Pile Analyzer. The compression piles were monitored and retapped with the hammer after 24 hours to ensure the soil resistance had been maintained and to determine the amount of additonal resistance gained due to soil setup. The load frame was then setup over the compression pile and anchored to the reaction piles. The ASTM D 1143-81 quick load test procedure was utilized at both sites. The applied load was measured by electronic load cells placed between the hydraulic jacks within the load frame and the 5" steel bearing plate placed on the compression pile and also by a pressure gauge. The pile top deflection was measured by two vertical dial gauges placed 180° apart. After a plunging failure had been reached, the load was reduced to obtain the pile rebound and residual pile settlement.

Test Site No. 1, HP 12 x 53 piling:

The monitored 12" compression pile was driven to 70' with an ultimate resistance af 150 tons. Retapping to 72' after 24 hours indicated an additional 8 tons soil setup resistance had been gained. The last 5' of driving averaged 38 blows per foot with a 6.12' average stroke. Due to the relatively low blow counts being obtained, it was decided to monitor one of the reaction piles without pile protection. Figure 1 is the summary of Dynamic Monitoring for this test site.

From the static testing with the load frame, a plunging failure occurred between 170 and 175 tons. Plotting the load settlement curve, Figure 2, as per the "Davisson Criteria", provided for a failure load at 140 tons. The rebound curve shows a residual pile settlement of 0.4 inches after load removal.

After testing, the contractor extracted all piling with an ICE vibrator driver/extractor. No damage was noted on either the tip protected piles or the unprotected piles.

With the conditions present at the time of testing, the initial static analysis indicated a soil resistance of 172 tons per pile at a depth of 72'. In discussing the analysis with FHWA Geothechnical Personnel, it appeared that while some of the input parameters were conservative, other parameters were liberal for this type of material. The parameters apparently compensated for one another in the analysis and it was in part a coincidence that the results obtained compare so close to the static load test plunging failure. Other methods of analysis included the Wave Equation Analysis for Pile Driving (WEAP) program and the Modified Engineering News formula. After refinement of the static analysis and it's input into the WEAP program. an ultimate resistance between 130-135 tons was obtained based on the blow counts. The Modified Engineering News formula indicated 57.5 tons resistance for the blow count obtained. Table 1 is a comparison summary of the results obtained.

TABLE 1

Method used for determining ultimate pile resistance	Ultimate resistance
W.H.D. Static Analysis	172 tons
Dynamic Monitoring Prediction	158 tons
Static Load Test	170-175 tons
"Davisson Criteria" for failure	140 tons
Wave Equation Analysis for Pile Driving	130-135 tons
Modified Engineering News	57.5 tons

Site No. 2, HP 14 x 73 piling:

The monitored compression pile was initially driven to a depth of 85' with an ultimate resistance of 165 tons. Retapping to 86' after 24 hours gave a resistance of 180 tons indicating a 15 ton gain due to soil setup. Only one reaction pile, No. 4, was fitted with tip protection. Figure 3 is the summary of Dynamic Monitoring for this site. The contractor was given permission to drive and have monitored a 16 3/4" O.D., 3/8" wall closed end pipe pile at this site (this was not covered under the contract). This pipe pile, placed outside the load test area, was driven to 65' with a resistance of 193 tons.

The plunging failure for the compression pile occurred at approximately 240 tons. Utilizing the Davission Criteria, Figure 4, failure occurred between 210-220 tons resistance. The additional 35 tons ±

between that predicted by the Pile Analyzer and the static load test was attributed to soil setup. Approximately 4 days elapsed between pile driving and actual load testing of this site while only 24 hours elapsed between driving and testing at site No. 1. The rebound curve shows a residual settlement of .55 inches after load removal.

The static analysis indicated an ultimate resistance of 238 tons at 86' but again the same conservative/liberal parameters were used and the close comparison between the static load test is only coincidental. With refinement of the input parameters the WEAP program indicated an ultimate resistance between 140-145 tons. The Modified Engineering News formula indicated 56.7 tons for the actual blow count recorded. Table 2 is a comparison summary of the results obtained.

TABLE 2

Method used for determining ultimate pile resistance	Ultimate resistance
W.H.D. Static Analysis	238 tons
Dynamic Monitoring Prediction	180 tons
Static Load Test	240 tons
"Davisson Criteria" for failure	210-220 tons
Wave Equation Analysis for Pile Driving	140-145 tons
Modified Engineering News	56.7 tons

SUMMARY AND CONCLUSIONS

The Pile Analyzer's predicted ultimate load capacities compare well with the results from the static load tests. The additional 35 tons of resistance encountered at test site 2 is attributed to soil setup.

The initial static analysis results, although close to the static load test, did not compare well with the Pile Analyzer at various embedment depths. With the information obtained from the dynamic monitoring and the static load tests, static design back analyses were performed with more realistic input parameters as suggested by FHWA personnel for this type of material, such as the actual (net) pile tip areas for determining end bearing, the projected pile perimeters (i.e. 4 x 12" and 4 x 14") for determining skin friction along with higher phi angles. Pile lengths and capacities were then determined for various sizes of "H" and pipe piles and the results were transmitted to the W.H.D. Bridge Section for cost comparisons and final selection.

The WEAP program was rerun using the adjusted static analysis. The results for 12" piling were very close to the actual conditions, however, the 14" results were still slightly conservative at 140 tons resistance for the blow count obtained.

The Modified Engineering News formula as used in the W.H.D. Specifications gave the most conservative results based on the actual blow count obtained and its use for this type of foundation material may be suspect.

In future situations where this type of granular foundation material is encountered, several considerations should be made:

1) The net end area of the pile should be used in end bearing computations unless the pile tip is founded in predominantly cobble to boulder size material.

2) When utilizing the WEAP program, the correct skin and toe dampening factors are critical. Material gradations must be determined to obtain the proper dampening values.

3) The Modified Engineering News formula is very conserative for this type of situation and other methods such as the WEAP program for determining ultimate bearing values should be used in its place whenever possible.

4) The use of displacement-type piles such as a closed end pipe pile should be considered with this type of situation. At these particular sites, an average 18% pile length reduction could have been realized and similar savings could be anticipated at other sites.

5) Pile tip protection (points) may not always be necessary unless large diameter material, cemented zones or other difficult driving conditions are anticipated.

Also mentioned as a point of interest is the ease and simplicity of pile extraction in this type of material when using a vibrator driver/extractor. The ICE extractor used on this project was considered more than adequate and could extract a 40' section of pile in less than three minutes.

SUMMARY OF DYNAMIC MONITORING RESULTS

TEST SITE NO. 1 (12x53 H-PILES)

PILE TIP DEPTH BELOW GROUND	ULTIMATE PILE LOAD CAPACITY IN TONS		
	TEST PILE (COMPRESSION) (WITH PILE TIP)	REACTION PILE NO. 1 (WITH PILE TIP)	REACTION PILE NO. 4 (WITHOUT PILE TIP)
5'	15	11	
15'	16	27	7
20'	19	34	31
25'	30		44
30'	38	40	52
35'	53	49	58
40'	70	58	76
45'	83	74	90
50'	106	90	101
55'	120	108	122
60'	123	117	120
65'	129	129	140
66'	127	128	147
67'	137	131	149
68'	143	132	149
70'	150	139	157
71'	158 — Retap	143	END OF DRIVING
72'	153 — After 24 Hours	139	NO RETAPPING
73'	END OF DRIVING	144	
74'		145	
75'		145	
		END OF DRIVING	
		NO RETAPPING	

FIGURE 1

TEST SITE #1 HP 12x53

DEFLECTION OF PILE = $\frac{PL}{AE}$

P=Load
L=Pile Length - 70'
A=Cross Section Area - 15.5sq.in.
E=Mod of Elastisty - 29×10^{6} psi

"DAVISSON CRITERIA" $.15+\frac{D}{120}=.25"$

40 TONS $\frac{(80,000)^{\#}(840)\text{in.}}{(15.5\text{sq.in.})\ (29,000,000)\ \#/\text{in.sq.}} = .15\text{in.}$

60 TONS $\frac{(120,000)\ (840)}{(15.5)\ (29,000,000)} = .22\text{in.}$

80 TONS $\frac{(160,000)\ (840)}{(15.5)\ (29,000,000)} = .30\text{in.}$

100 TONS $\frac{(200,000)\ (840)}{(15.5)\ (29,000,000)} = .37\text{in.}$

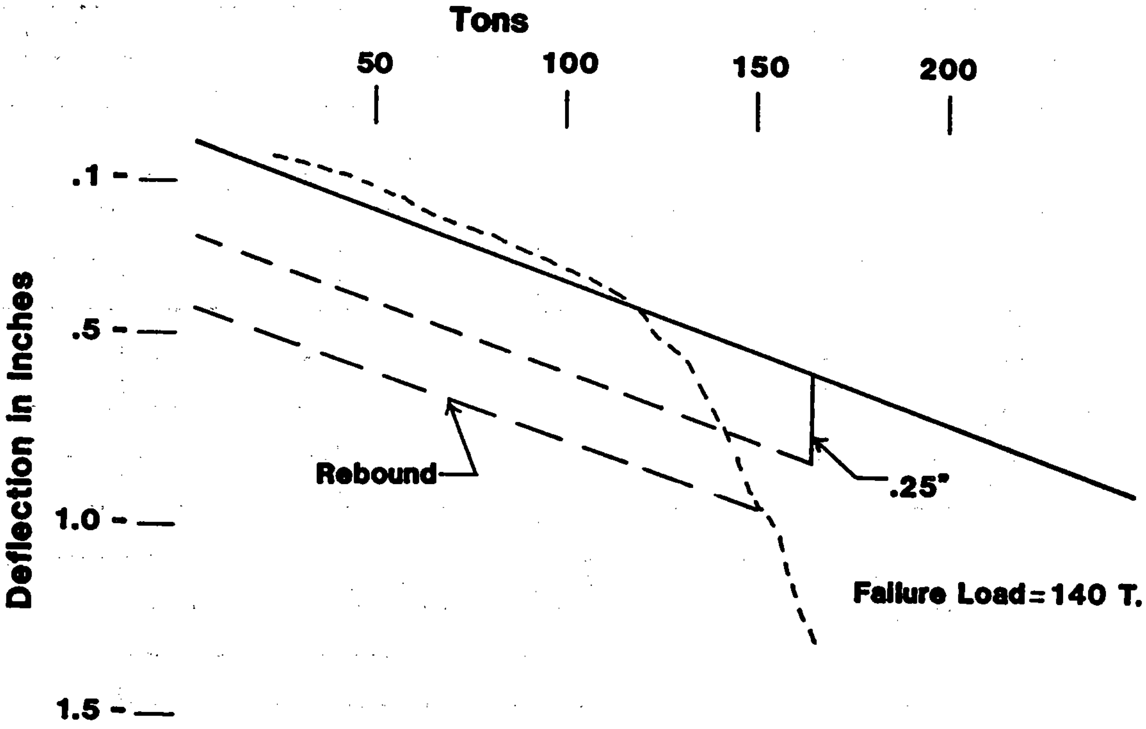

DATA FOR PILE LOAD TEST

FIGURE 2

SUMMARY OF DYNAMIC MONITORING RESULTS

TEST SITE NO. 2 HP 14x73 & 16" O.D. 3/8" WALL PIPE PILE

PILE TIP BELOW GROUND	ULTIMATE PILE LOAD CAPACITY IN TONS				REMARKS
	COMPRESSION PILE	REACTION PILE. NO. 2	REACTION PILE NO. 4	PIPE PILE 16" O.D. 3/8" WALL	
5	0	0	6	60	Pipe Pile
10	0	0	15	96	Driven At The
15	5	7	21	127	Request of
20	15	15	26	104	Contractor. Pipe
25	30	27	37	109	Pile Cost
30	39	41	47	112	Assumed By
35	45	60	54	123	Contractor.
40	71	67	66	123	
45	85	93	86	143	
50	101	121	95	153	
55	116	116	109	167	Pipe Pile
60	122	140	115	180	At Depth of
65	139	149	124	193	63' - 187 Tons
70	155	157	135		64' - 187 Tons
75	159	170	150	CLOSED END	
80	157	174	148		
85	165	176	160		
RETAP	180 FIRST 6 BLOWS	NO RETAP	NO RETAP		
86	165	179	167		
87		175	181		
88		175			
	NO TIP	NO TIP	TIP ATTACHED		

FIGURE 3

TEST SITE #2 HP 14x73

DEFLECTION OF PILE = $\frac{PL}{AE}$

P=Load
L=Pile Length -86'
A=Cross Section Area -21.5sq.in.
E=Mod of Elastisty - 29×10^{6} psi

"DAVISSON CRITERIA" $.15+\frac{D}{120}=0.27"$

40 Tons $\frac{(80{,}000)\#\ \ (1{,}032)\text{in.}}{(21.5)\text{sq.in.}\ \ (29{,}000{,}000)\#/\text{sq.in.}} = 0.1324\text{in.}$

80 Tons $\frac{(160{,}000)\ (1{,}032)}{(21.5)\ (29{,}000{,}000)} = 0.2648\text{in.}$

120 Tons $\frac{(240{,}000)\ (1{,}032)}{(21.5)\ (29{,}000{,}000)} = 0.3972\text{in.}$

160 Tons $\frac{(320{,}000)\ (1{,}032)}{(21.5)\ (29{,}000{,}000)} = 0.5297\text{in.}$

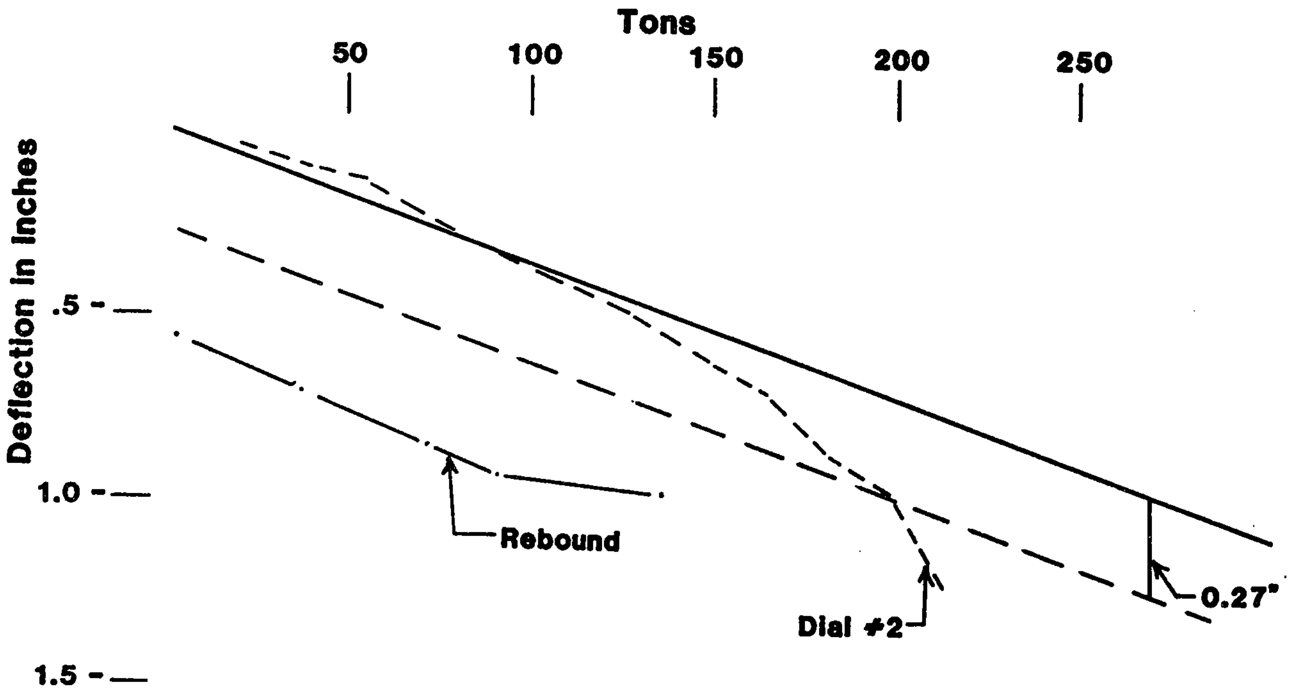

DATA FOR PILE LOAD TEST

FIGURE 4

SURVEY OF NONDESTRUCTIVE WAVE PROPAGATION TESTING METHODS FOR THE CONSTRUCTION INDUSTRY

Larry D. Olson, P.E. and Edward O. Church, P.E.*

ABSTRACT: Advances in research and technology have resulted in the availability of many new nondestructive testing (NDT) and evaluation (NDE) methods for applications to the construction industry. The NDT and NDE methods presented in this paper are based on elastic wave propagation theory, and the principles of geophysics and mechanical vibration engineering. Discussions are presented of various nondestructive methods and their applications to test raw sites, embankment and concrete dams, drilled shafts, driven piles, pavements, and structures. Case histories from engineering investigations and applied research studies by the authors are presented to illustrate applications of the NDT and NDE methods. The case histories and research demonstrate that NDT and NDE investigations can provide large amounts of reliable data economically for design, forensic and quality control engineering purposes for the construction industry.

INTRODUCTION

Rapid advances in electronics, computers and research have resulted in the current availability of new nondestructive testing (NDT) and evaluation (NDE) methods for applications to the construction industry. This paper focuses on NDT and NDE methods based on the propagation of elastic waves, and principles developed for geophysics and mechanical vibration engineering purposes. Applications of the NDT and NDE methods discussed in this paper to construction projects include:

1. in situ measurement of dynamic soil and rock properties;
2. integrity and length of drilled shafts and driven piles;
3. void detection, and moduli and thicknesses of layers for pavements;
4. integrity of structural concrete, masonry, wood and steel;
5. integrity evaluations of earth and concrete dams; and
6. monitoring, analysis and control of vibrations.

The NDT and NDE wave propagation methods have broad applications for dynamic design, quality control and forensic engineering investigations for the construction industry today. Until recently, many of the methods would have been impractical because they would have required a roomful of expensive equipment. The test equipment is now durable and portable enough to be airfreighted or put in a van and driven to the construction site. This has made the NDT and NDE methods much more economical and practical for field tests.

*Olson-Church, Inc., 925 East 17th Avenue, Denver, Colorado 80218

The advantages of nondestructive and destructive testing are presented below followed by descriptions of the NDT and NDE methods. Applications of the methods to subsurface conditions, drilled shafts, rigid pavements, and concrete structures are illustrated by case histories and the results of applied research studies by the authors.

ADVANTAGES OF NONDESTRUCTIVE AND DESTRUCTIVE METHODS

The nondestructive methods have several distinct advantages in comparison to destructive methods. Some of these advantages are:

1. Rapid testing and analysis so that construction can proceed,
2. Data on intact structures in the field rather than laboratory testing of specimens obtained destructively,
3. Much more economical test coverage of large areas,
4. Define the limits and nature of a defect without causing damage due to the testing,
5. Portable equipment and the ability to test in confined areas, and
6. Detailed evaluation of specific conditions that cannot be adequately defined with destructive tests.

The principal advantages of destructive testing are:

1. Direct measurement of material properties like strength and density,
2. Accepted standard for quality control of construction,
3. Tests are familiar to engineers, architects and contractors, and
4. Testing standards are set by ASTM, ACI, and Building Codes.

Both nondestructive and destructive methods have their place in the construction industry. In fact, many times nondestructive test results are correlated with destructive test results to best meet engineering investigation goals.

NDT AND NDE METHODS

Fundamental to all of the NDT and NDE methods is the measurement of wave propagation velocity through the test medium. Compression waves have the highest velocity, while surface waves have the lowest velocity. Surface wave velocity is about 0.9 times the shear wave velocity in a material. Compression wave velocity ranges from 1.4 to 2.4 times shear wave velocity for Poisson's ratios of 0 to 0.4, respectively.

The methods use compression, shear and surface (Rayleigh) waves from which the maximum small strain moduli or "stiffnesses" are calculated based on elastic theory. The measurement of stiffness at small strains is directly related to the stress-strain behavior of soils, deep foundations, pavements, and structures. For example, in soil dynamics models have been developed to predict the dynamic moduli for soils at larger strains based on the small strain moduli. Additional information is provided by more sophisticated analyses which compare amplitude and frequency responses between an impulse and a receiver or between receivers.

The wave propagation methods presented below are discussed in the order of subsurface investigations, deep foundations, pavements, structures, and construction vibrations. Many of the methods were initially developed for testing in just one of the above areas, but since have been successfully applied to other areas. The extension of wave propagation methods into areas other than which they were originally developed for has been the norm rather than the exception.

Downhole and Crosshole Seismic Tests. Compression and shear wave velocities in soils and rock are most commonly measured in situ with the downhole and crosshole seismic tests. Technically, these tests are destructive since borings are required. However, in comparison to dynamic laboratory tests on "disturbed" soil samples, the in situ measurement of dynamic soil properties with these seismic tests is "nondestructive" with respect to disturbance.

Both tests involve mechanically generating compression and shear wave energy and then measuring the times for the waves to travel known distances to velocity transducers or "geophones." The downhole test is less expensive to perform than the crosshole test since the wave energy source is on the surface and velocities of wave travel are determined to various depths of a geophone in a single boring (Fig. 1). However, the downhole test is not as accurate as the crosshole test, particularly at layered sites. The crosshole test involves drilling three borings and then generating the wave energy with a source in one of the end borings and recording the wave energy arrival times to receivers in the other borings as indicated on Fig. 2 (Stokoe and Hoar, 1978).

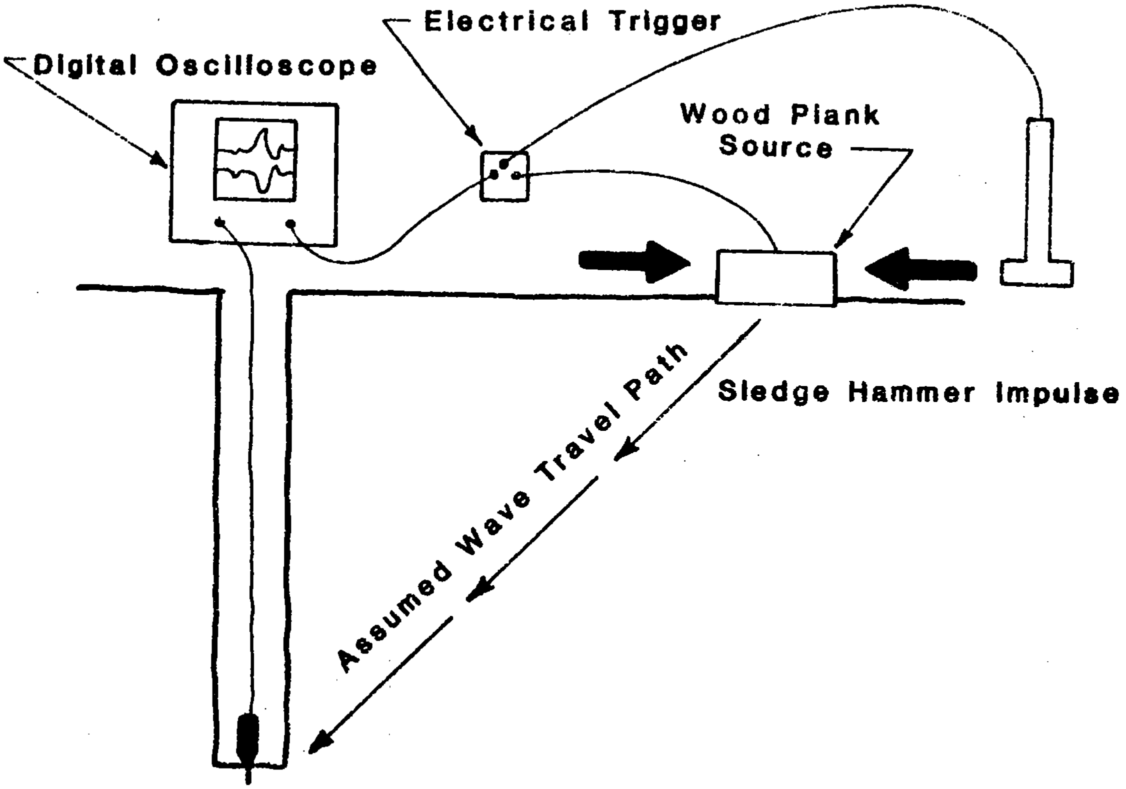

Fig. 1 - Downhole Seismic Test

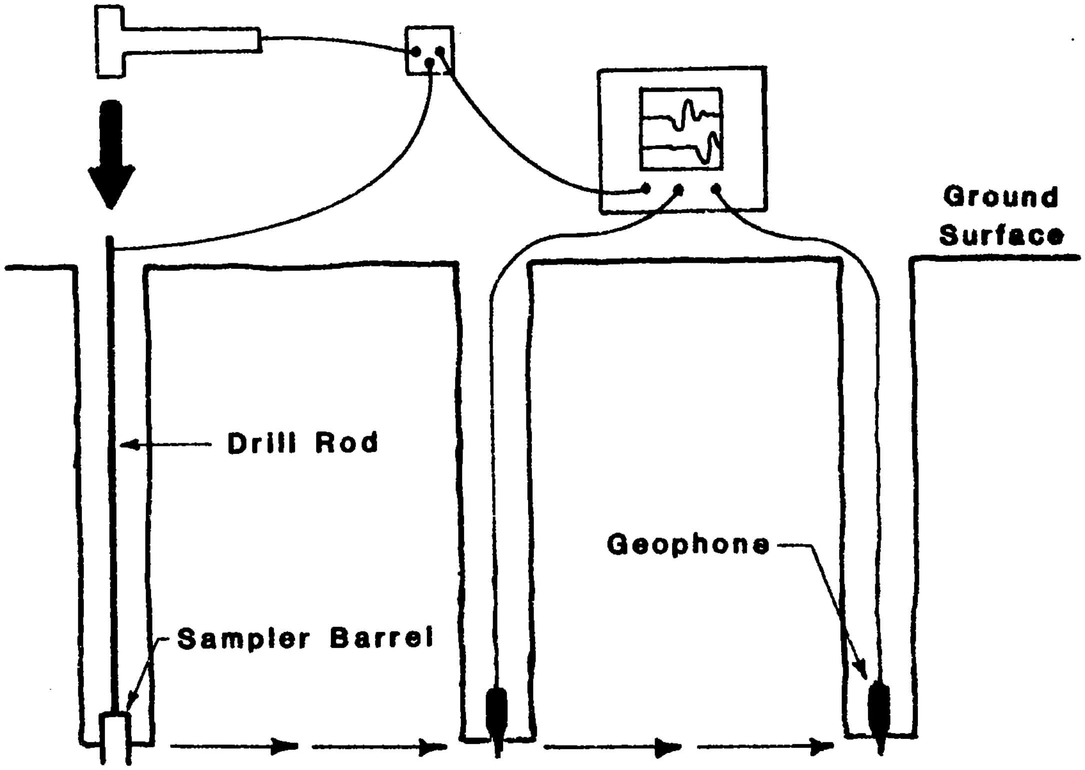

Fig. 2 - Crosshole Seismic Test

Woods and Stokoe (1985) have presented a comprehensive review of shallow seismic methods in soil dynamics. Robertson and Campanella et al (1986) have developed a cone penetrometer tool which contains geophones so that the downhole seismic measurements can be made in conjunction with obtaining cone penetration data.

Spectral Analysis of Surface Waves (SASW). The SASW method is a new geophysical method that was originally developed for rigid and flexible pavements to predict moduli and thickness of pavement layers (Stokoe and Nazarian, 1985). The SASW method has proven to be quite versatile already and has been applied to soil sites for liquefaction studies, earth dams, concrete dams, and compacted fills.

The method is based upon the measurement of surface waves propagating between two receivers as indicated on Fig. 3. The pair of geophones are expanded about a centerline in the "common receiver midpoint geometry" to test to greater depths (Fig. 3b). The method is used to determine the surface wave velocity and layer thickness profile at sites to depths of 50 to 100 feet. Moduli profiles determined with the SASW method have been found to closely agree with crosshole test results by Stokoe and Nazarian (1984). One of the most exciting capabilities of the method is its capability to detect a lower velocity layer underlying a higher velocity layer (overcoming a significant limitation of the seismic refraction method).

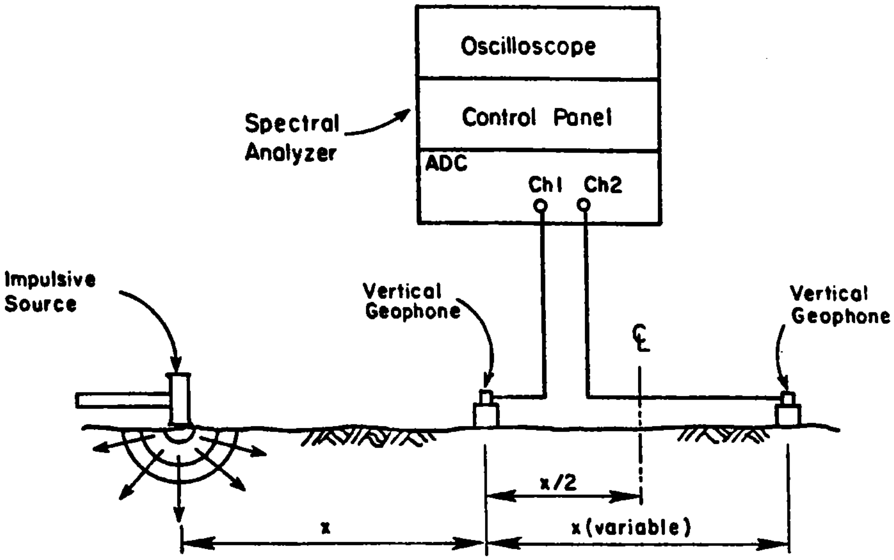
Oscilloscope
Control Panel
Spectral Analyzer
ADC
Ch1
Ch2
Impulsive Source
Vertical Geophone
Vertical Geophone
℄
x/2
x
x (variable)

(a) General Configuration of SASW Tests

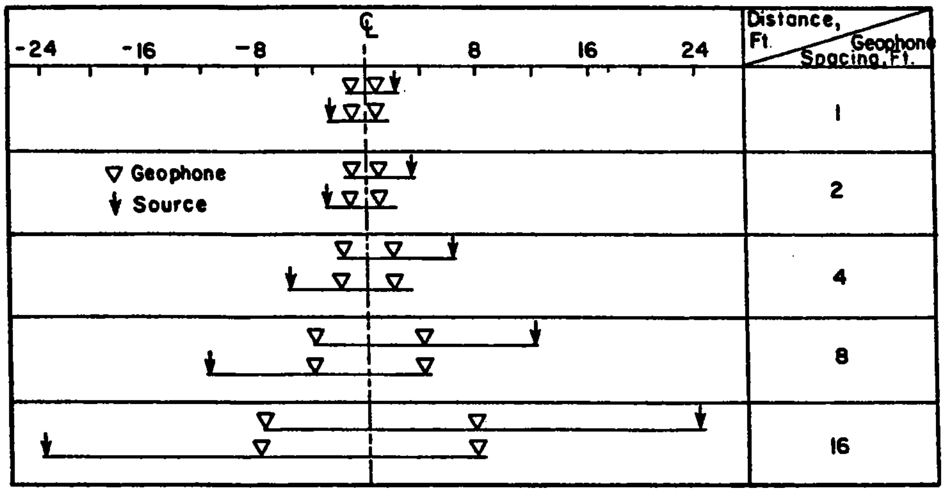
℄
-24
-16
-8
8
16
24
Distance, Ft.
Geophone Spacing, Ft.
1
2
4
8
16
▽ Geophone
Source

(b) Common Receivers Midpoint Geometry

Fig. 3 - Spectral Analysis of Surface Waves (SASW) Method (after Stokoe and Nazarian, 1985)

Stress Wave Reflection Methods. Geophysical principles of the seismic reflection survey using compression or "stress" waves have been adapted for a wide range of engineering purposes. Stress waves are used to test drilled shafts and driven piles (Stress Wave or "Seismic Echo" method), thicknesses of metals and other homogeneous materials (Ultrasonic Pulse Echo techniques discussed in a later section), for the detection of voids in concrete slabs and walls (Impact or Pulse Echo Method), and recently for NDE strength prediction for wood. All of these methods involve striking the test object to generate stress wave energy and then monitoring the arrival times of reflected stress wave energy. If the velocity of the stress wave is known, then the depth of the reflector can be calculated by multiplying the stress wave velocity by the reflection arrival time and dividing this quantity by two.

The stress wave method for testing deep foundations is illustrated on Fig. 4. The method can be applied with only surface receivers or with embedded geophones as well. The embedded geophones permit direct measurement of stress wave velocity and tracking of wave travel and attenuation down and back up a shaft. Capabilities and limitations of the stress wave method for drilled shafts are discussed in more detail by Hearne, Reese and Stokoe (1981), and Olson and Thompson (1985). The method has been widely used in Europe to test precast piling and drilled shafts with length to diameter ratios of less than 20:1. As shafts and piles become increasingly slender, stress wave attenuation may be so great that stress wave reflections cannot be identified. Embedment of geophone receivers at appropriate depths in shafts will mitigate the attenuation problem.

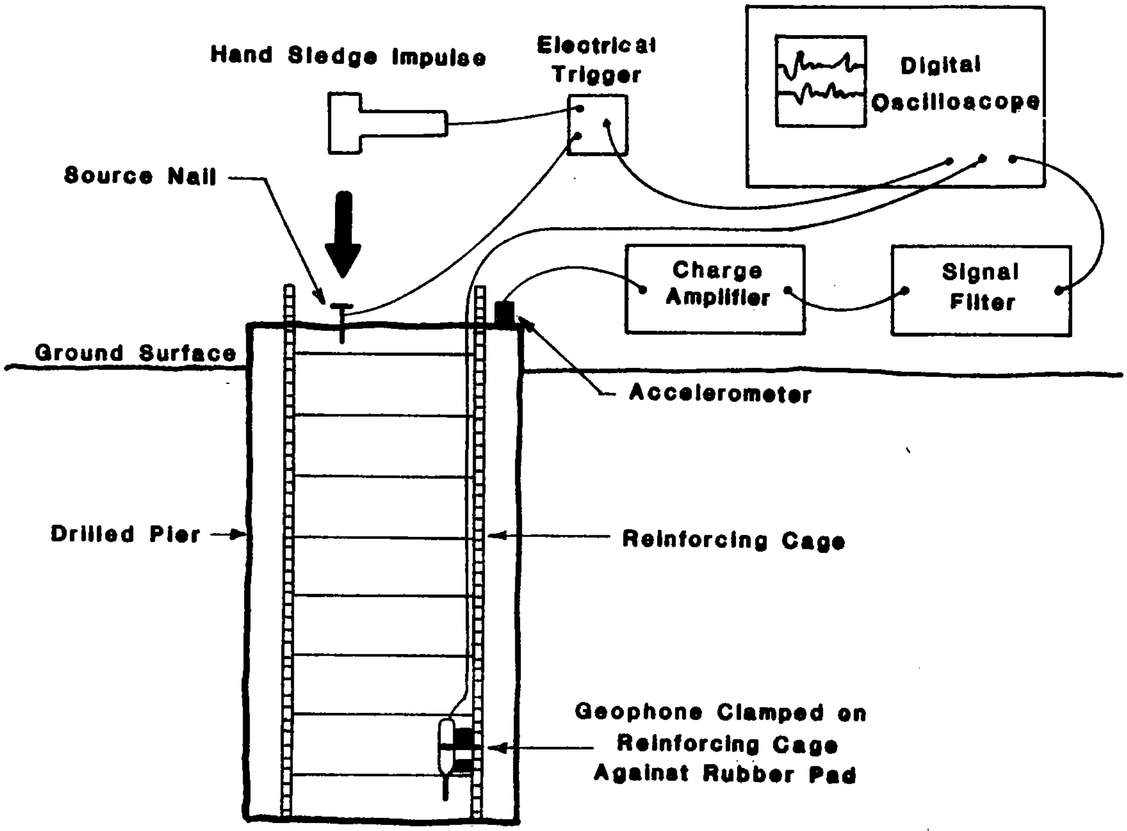
Hand Sledge Impulse
Electrical Trigger
Digital Oscilloscope
Source Nail
Charge Amplifier
Signal Filter
Ground Surface
Accelerometer
Drilled Pier
Reinforcing Cage
Geophone Clamped on Reinforcing Cage Against Rubber Pad

Fig. 4 - Stress Wave Method for Deep Foundations

Another solution to the attenuation problem for long, critical shafts involves embedding steel or PVC tubing in shafts to permit "Sonic Logging." A sonic log involves lowering a stress wave energy source into one of the water-filled tubes and a receiver tool into another tube. The test consists of simultaneously withdrawing both tools from the bottom of a drilled shaft and recording the time for the stress wave energy to travel from the source to the receiver. Shaft defects are indicated by increases in the wave travel time and loss of signal between the tubes. Sonic logging is also suitable for investigation of the integrity of concrete slurry walls and concrete cutoff trenches.

Research is currently being conducted on the Impact Echo technique for detection of flaws in concrete by the Structures Division of the National Bureau of Standards. Carino, Sansalone and Hsu (1986) have reported significant developments regarding equipment and analysis procedures for locating flaws at shallow depths in concrete slabs from surface tests. The method is based on identifying reflections of stress wave energy to predict the thickness of a sound concrete member or the depth of a defect. Research is continuing on the method to better define its sensitivity and develop automated testing procedures.

Current research and development efforts have resulted in a new NDE approach to predict the strength of wood members. Stewart, Brunette, and Goodman (1986) report that sonic NDE methods have been developed which predict the strength of wood with good accuracy. The method is based on initial correlation of NDE measurements and companion destructive strength tests using multiple regression analysis methods. Results of subsequent NDE tests are analyzed with the developed correlation to predict the strengths of utility poles and other wood structural members. The information is typically used to identify which wood members need replacing.

Ultrasonic Pulse Velocity (UPV) Methods. High frequency or "Ultrasonic" methods have been used to test concrete, masonry and wood structures since the 1940's. Even higher frequency methods are commonly used to measure thicknesses and locate flaws in metals, ceramics and other homogeneous materials with echo methods.

The UPV method of testing concrete involves measuring the time for an ultrasonic pulse to travel from a source to a receiver. Equipment consists of an electronic timer, a pulse wave source and a receiver. Measurements can be made directly through a wall with the receiver opposite the source (direct test), through the corner of a column with the source and receiver on adjacent column faces (semi-direct), and with both the source and receiver on the same surface (indirect). For direct and semi-direct tests, pulse velocities are calculated by dividing the distance between the source and receiver by the pulse travel time. For the indirect test, the pulse travel time is plotted as a function of receiver-to-source-spacing for several spacings. The inverse of a best-fit straight line through the data points is the pulse velocity.

The UPV method is very rapid and can identify such concrete conditions as void, cracking, frost damage, fire damage and crack depths by slower velocities in comparison to "good concrete." Good correlations between pulse velocity and concrete compressive strength have also been achieved during the first three days of concrete curing.

Consequently, the UPV method has been used to predict in-place concrete strength to determine when sufficient strength had been achieved to permit raising of slip-forms to the next level. Many different papers regarding the UPV method are presented in the American Concrete Institute SP-82 Publication, In-Situ Nondestructive Testing of Concrete, edited by V. M. Malhotra, 1984.

Impulse-Response Method. This method is a development of forced response vibration testing to characterize the dynamic response of machines to vibration for mechanical engineering design. A building institute in France, CEBTP, adapted the forced response technique to test the integrity of drilled shafts and driven piles in the late 1960's. Initial testing was accomplished by recording the vibration response of a geophone to the excitation force of a vibrator over a frequency range of at least 20 to 1000 Hz as discussed by Stain (1984). The equipment needed to perform the test today is portable and consists of a spectral analyzer, impulse hammer (special hammer with a force transducer to measure the impact force), and a geophone (Fig. 5).

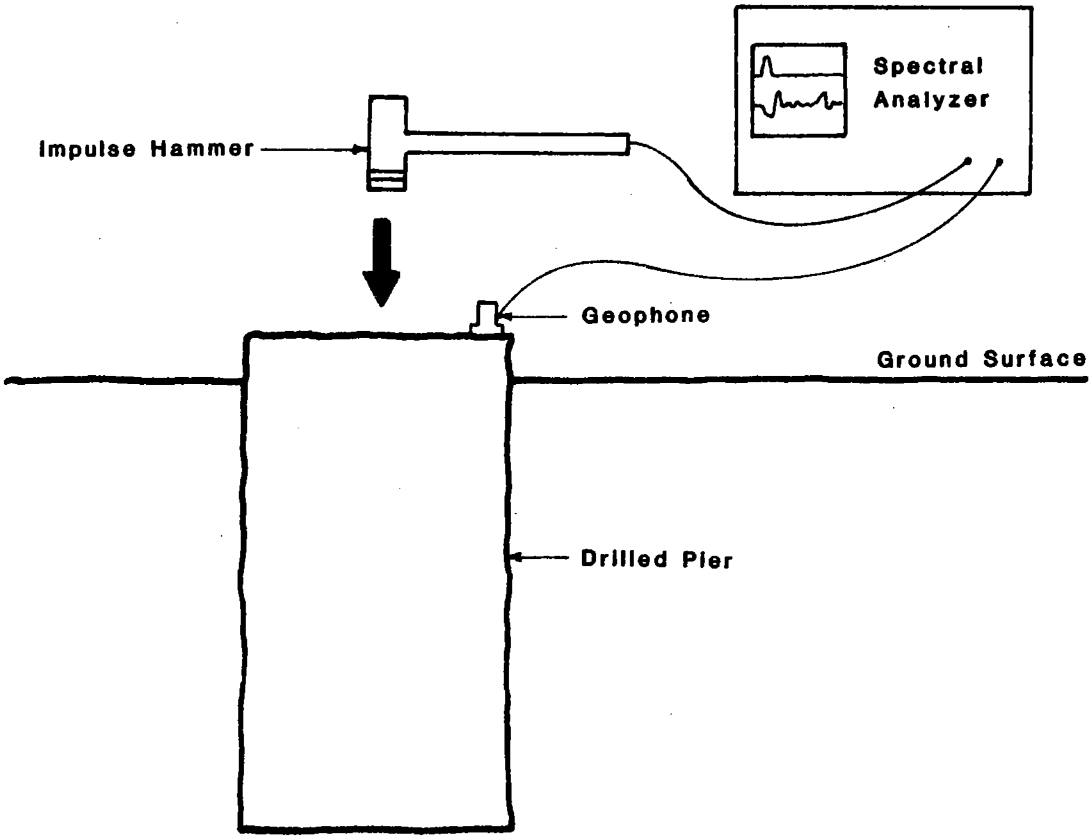

Fig. 5 - Impulse-Response Method for Deep Foundations

An impulse-response test measures the dynamic stiffness at the head of a drilled shaft or driven pile. Dynamic stiffness may be thought of in static terms as a spring constant with units of pounds force per inch displacement. Foundations bottomed in soft soils have lower dynamic stiffnesses than for the same foundations bottomed in bedrock. Foundations with defects such as necking and soil inclusions have lower dynamic stiffnesses in comparison to sound foundations. Enlargements and bulbs in shafts will produce larger dynamic stiffnesses. In addition, the presence of stress wave reflections from the bottom of a shaft, and reflections from bulbs and necks are indicated by resonant peaks in the impulse-response test records.

Soil-structure interaction effects and the nature of defects are characterized by dynamic stiffness. Typically, measured dynamic stiffnesses are evaluated comparatively for a number of foundations at a site and based on experience with similar shafts in similar soil conditions. Ideally, dynamic stiffness measurements are correlated with the static stiffness measured at low strains in axial load tests. Site-specific correlation permits predictions of working settlements to be made for shafts tested with the impulse-response method alone, based on the dynamic stiffness to static stiffness correlation. Normally, dynamic stiffness is 1 to 2 times the static stiffness measured from load tests.

Recently, the impulse-response method has been adapted to test rigid pavements to locate voids, delaminations and identify areas of poor versus good subgrade support. An applied research study was recently conducted using the impulse-response method to test a nine inch unreinforced concrete pavement (Pederson and Senkowski, 1985). The results of this study indicate very good agreement between the subgrade support conditions predicted using the impulse-response method and the results of cores and lifting of slabs. The impulse-response method is capable of detecting voids as thin as 1/16 inch or less. In comparison, ground penetrating radar at present cannot resolve voids much thinner than 1/2 inch. Pavement slabs are typically tested on a grid basis.

The impulse-response method can also be used to examine the dynamic responses of structures. This type of study is generally done to characterize the response of a structure to wind, wave, impact and earthquake loading. Test results can be compared to the results of structural dynamics analyses to model system responses.

Monitoring, Analysis and Control of Construction Vibrations. The availability of portable spectral analyzers provides a greatly increased capability for measurement and analysis of construction vibrations (Hall, 1985). In the past, vibrations have largely been measured in the time domain to record peak amplitudes generated by blasting, construction traffic, etc. The use of a spectral analyzer provides information on the variation of amplitude with vibration frequency. Such data can be of critical importance in evaluating vibration effects on existing structures, since resonance effects can greatly magnify vibration amplitudes. A prime example of the effects of resonance on buildings is the 1985 Mexico earthquake where buildings with resonances similar to soil resonances were severely damaged. Examples of this type of testing include evaluation of the effects of wind, earthquakes, impact loading, and vibrating machinery on foundations and structures.

APPLICATIONS OF NDT AND NDE WAVE PROPAGATION METHODS

The applications of NDT and NDE methods discussed below are from the authors consulting and applied research experience. Applications are discussed for crosshole seismic measurement of dynamic soil and rock properties, integrity of drilled shafts, detection of void below rigid pavements, and detection of honeycomb void in concrete structures.

Crosshole Seismic Investigation. This investigation was performed to provide accurate data on dynamic moduli of fill, sand and sedimentary sandstone bedrock for design of large natural gas compressor foundations. Knowledge of the shear wave modulus profile with depth is critical for machine foundation design. Crosshole seismic tests were made by drilling three borings along straight lines at compressor locations. Previous boring data indicated sedimentary sandstone bedrock at shallow depths of 15 feet or less. Consequently, it was possible to advance the three borings simultaneously to each desired crosshole test depth. Where deeper measurements are required, verticality of the holes becomes a problem. Deep borings must be cased with grouted PVC tubes and the holes logged with an inclinometer to accurately determine wave travel path distances between the cased holes.

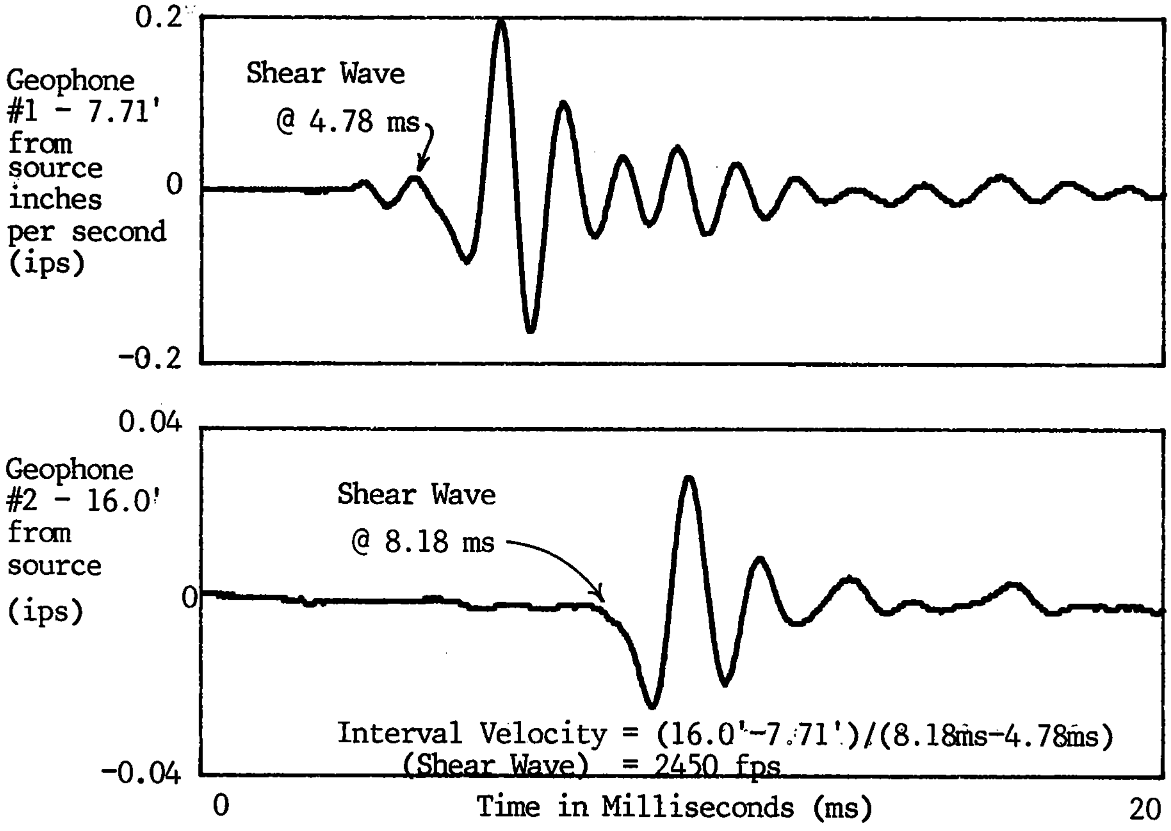

Fig. 6 - Crosshole Seismic Test Record in Sandstone Bedrock

A standard penetration sampler was used as the compression and shear wave energy source. Geophone receivers were planted in the bottoms of each of the receiver holes at distances of approximately 8 and 16 feet from the source hole. Tests were made every 3 to 5 feet depending on the soil profile. A crosshole test record is presented on Fig. 6 for sandstone bedrock at a depth of 14 feet. The arrival of the high amplitude shear wave energy is readily apparent in each of the vertical geophone responses. A shear wave velocity of 2,450 feet per second (fps) was calculated for the sandstone bedrock between the two geophones. Shear modulus is equal to the mass density of the sandstone multiplied by the square of the shear wave velocity. Based on a unit weight of 135 pounds per cubic foot for the very hard sandstone, a shear modulus of 175,000 psi was calculated. In comparison, the upper fill and sands had shear moduli between 12,000 and 56,000 psi.

Integrity of Drilled Shafts. One of the key questions regarding the suitability of an NDE method to evaluate the integrity of a drilled shafts concerns what size of defect can be detected for a given depth. The answer to this question depends on a complex interaction of factors such as shaft diameter, soil types and stiffnesses, and the nature of the defect.

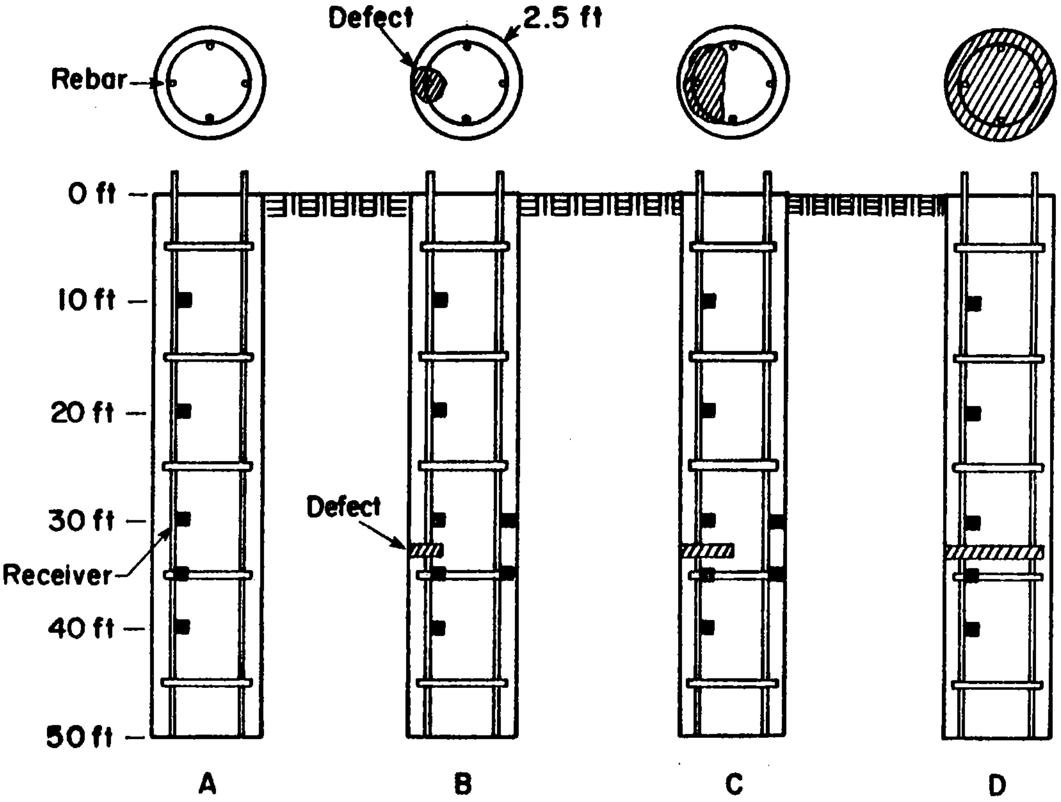

Fig. 7 - Drilled Shaft Research Site in Houston, Texas
(after Harrel and Stokoe, 1984)

Harrel and Stokoe (1984) evaluated the sensitivity of the stress wave propagation method by drilling three shafts with known defects and one sound shaft as a control in Houston, Texas in 1981. The shafts were 2.5 feet in diameter, 50 feet in length and instrumented with numerous embedded geophone receivers as indicated on Fig. 7. The defects consisted of clay soil cuttings from the holes wrapped in burlap bags that covered 1/4, 1/2 and the full cross-sectional shaft areas at depths of 32 feet in Shafts B, C and D, respectively (Fig. 7). Their research study demonstrated substantial benefits of using embedded geophones, particularly for direct measurement of stress wave velocity, studies of stress wave attenuation with depth and tracking of stress wave energy propagation through drilled shafts. However, stress wave reflections were not apparent in time domain records for the 1/4 area defect at the 32 feet depth.

The authors had the opportunity to conduct additional research on the sensitivity of the stress wave method at the site last fall with improved equipment. In addition, the four shafts were also tested with the impulse-response method. A stress wave record for Shaft A (sound shaft) is presented on Fig. 8. The upper half of the figure is the response of the surface accelerometer receiver on top of the shaft. The lower response is for an embedded geophone at a depth of 20 feet. The travel of the stress wave energy down the shaft and then back up the shaft is indicated on Fig. 8. A stress wave velocity of 13,600 fps was calculated for this shaft.

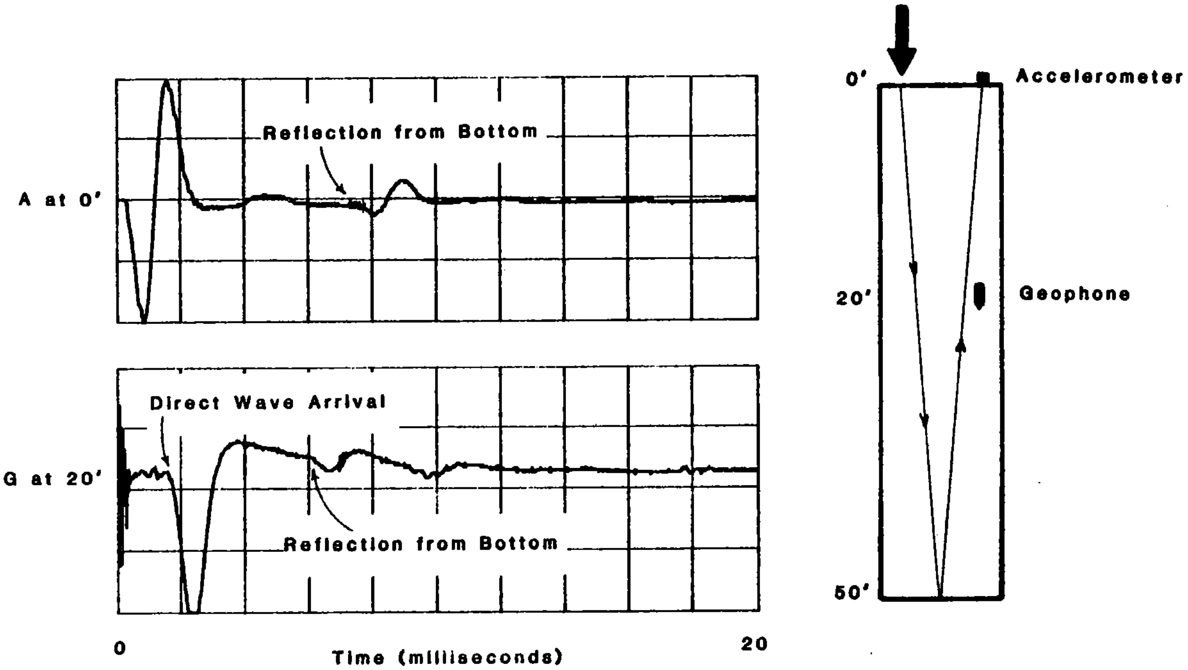

Fig. 8 - Stress Wave Test Record For Drilled Shaft A (Sound)

A stress wave record for an accelerometer on the surface of Shaft B (1/4 area defect) is presented on Fig. 9. A small reflection event and a second larger amplitude reflection event are indicated on Fig. 9. The small reflection corresponds to stress wave energy reflected from the defect while the larger reflection is from the bottom of Shaft B as indicated on Fig. 9. A stress wave velocity of 14,700 fps was calculated for this shaft. The identification of a stress wave reflection from the 1/4 area defect in time domain records is believed to be due to equipment improvements and the first author's experience in using the stress wave method since the earlier study by Harrel et al.

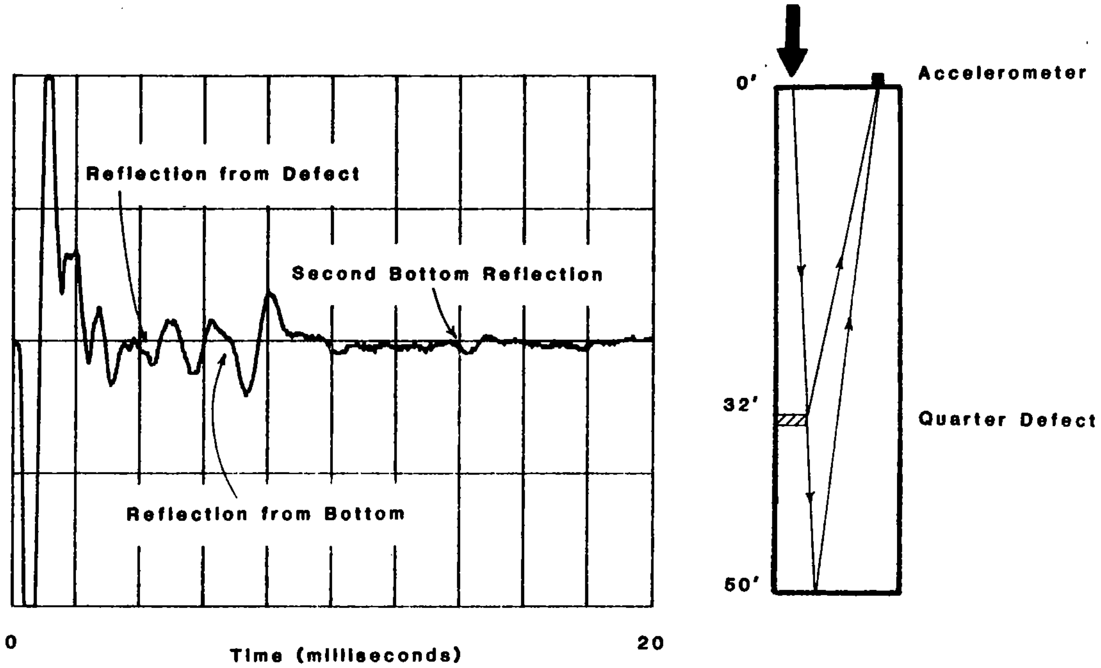

Fig. 9 - Stress Wave Test Record for Drilled Shaft B (1/4 area defect)

Impulse response test results are presented for Shaft A (sound) and Shaft D (full area defect) on Figs. 10 and 11, respectively. The vertical axis of the plot is the geophone vibration velocity (V) divided by the impulse hammer force (F). The horizontal axis is vibration frequency. The plot of V/F or "mobility" versus frequency is a known as a mobility plot. Dynamic stiffness can be calculated from the initial straight line portion of the plot at low frequencies or directly by integration using the spectral analyzer. At low frequencies the soil and shaft move together which permits the measurement of dynamic stiffness due to the soil-structure interaction effect. Examination of the plot indicates that mobility is higher for Shaft D than Shaft A at low frequencies of less than 50 Hz which indicates Shaft D is less stiff than Shaft A. Measured dynamic stiffnesses were 12,300 and 9,800 kips per inch for Shafts A and D, respectively. The full defect resulted in Shaft D being 20 percent less stiff than Shaft A.

Resonant peaks for each shaft are also apparent in the mobility plots for Shafts A and D (Figs. 10 and 11). Average changes in frequency between the peaks were calculated as 138 and 193 Hz for Shafts

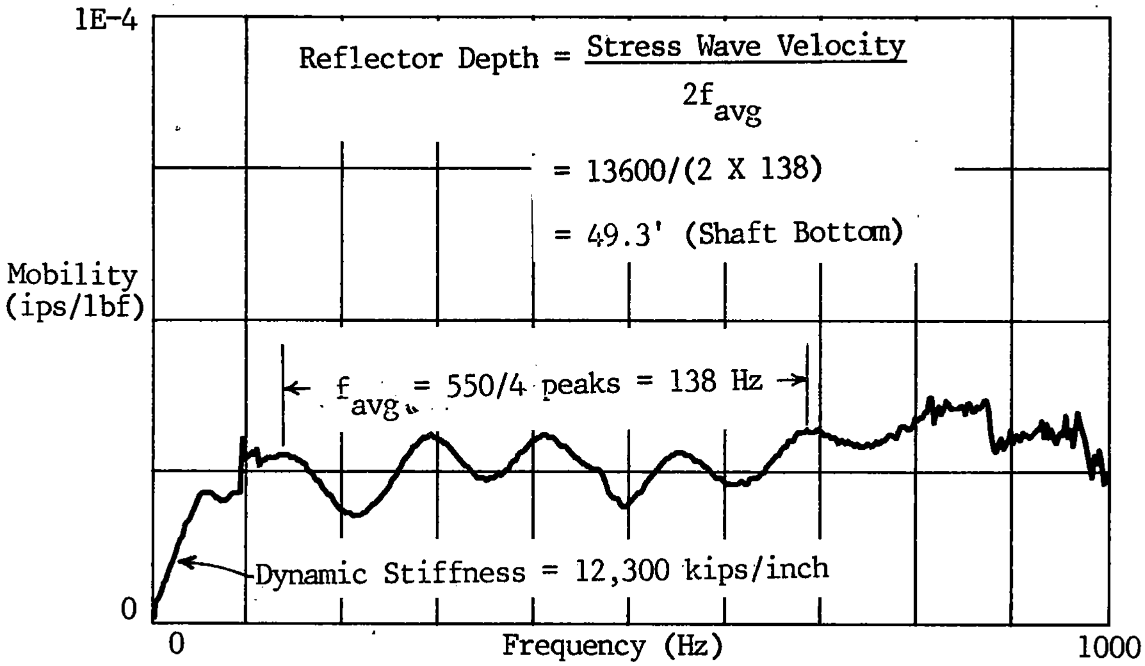

Fig. 10 - Mobility Plot for Shaft A (sound)

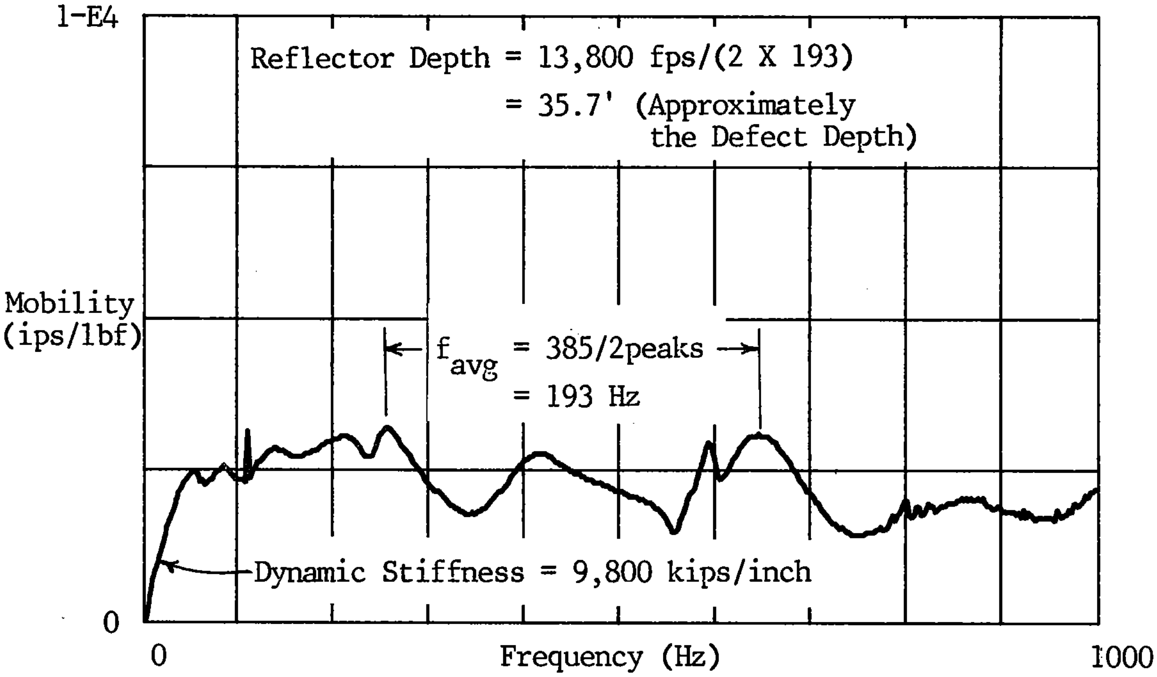

Fig. 11 - Mobility Plot for Shaft D (full area defect)

A and D, respectively. The resonances for sound Shaft A are more regular than those for Shaft D with the full defect. The depth of a reflector can be calculated by dividing the stress wave velocity by twice the change in frequency between resonances. Reflector depths of 49.3 and 35.7 feet were calculated for Shafts A and D (Figs. 10 and 11). These depths correspond correspond reasonably well to the bottom of Shaft A and the full defect at a depth of 32 feet in Shaft D.

Void Detection Below Rigid Pavement. For years, heavy chains and wrecking bars have been used to "sound" concrete pavements and slabs to hear "hollow" void areas. The first author took this approach a step further beginning a few years ago by dropping a rod and then recording the slab vibration response with an accelerometer receiver. A high degree of correlation was found at 5 sites between slab support conditions and the duration time of vibrations from the impact. Slabs underlain by void vibrated for significantly longer times than slabs with good subgrade support. This procedure required that a calibration be developed at each site for conditions of known void and good subgrade support.

The recent application of the impulse-response method to rigid pavements provides a much more powerful NDE method to evaluate slab subgrade support conditions. The authors recently performed a research demonstration of the ability of the impulse-response method to detect known void below a rigid pavement. The research demonstration was performed in association with Dr. Kenneth H. Stokoe, II of the Civil Engineering Department of the University of Texas at Austin. Impulse-response test records for mobility plots from void and good subgrade support areas are presented on Fig. 12. Major differences in the mobility plots are apparent between the void and good subgrade support conditions. The mobility is much higher and more irregular for the void versus the good subgrade support condition.

Integration of the mobility plots produced a plot of displacement (D) per impulse force (F) as presented on Fig. 13. The plot of D/F or "flexibility" is the inverse of dynamic stiffness (F/D). Examination of Fig. 13 indicates the concrete pavement test point with good subgrade support has one-half the flexibility or twice the dynamic stiffness of the pavement test point underlain by the void.

Different responses indicative of poor subgrade support and delamination (loss of bonding) can also be identified from mobility plots. As discussed earlier, the impulse-response method is capable of detecting voids as thin as 1/16 inch and thinner. The impulse-response method will define the area, but not the thickness of void. Practically, this limitation is not too important for most investigations, since once a void is located grouting is performed to fill the void and volumes of grout can be recorded to indicate void size. The method can be applied to test rigid pavements to define areas in need of grouting repairs and then used to re-test pavements to evaluate the effectiveness of the grouting program.

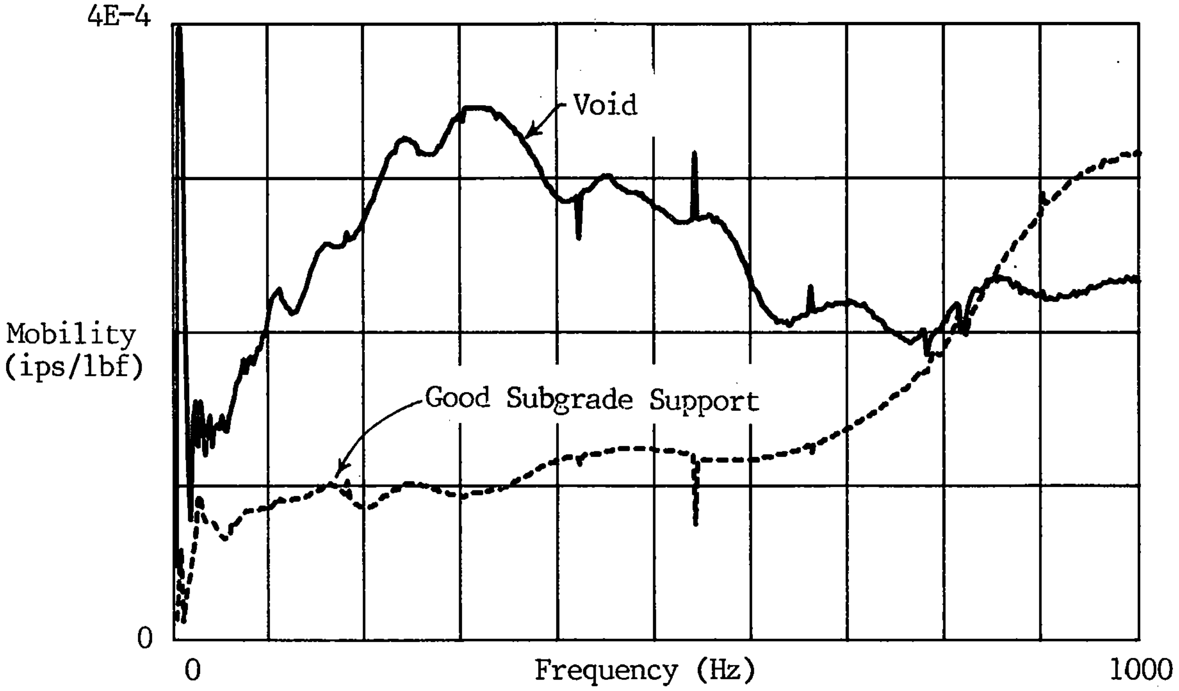

Fig. 12 - Mobility Plots for Concrete Pavement for Void and Good Subgrade Support Conditions

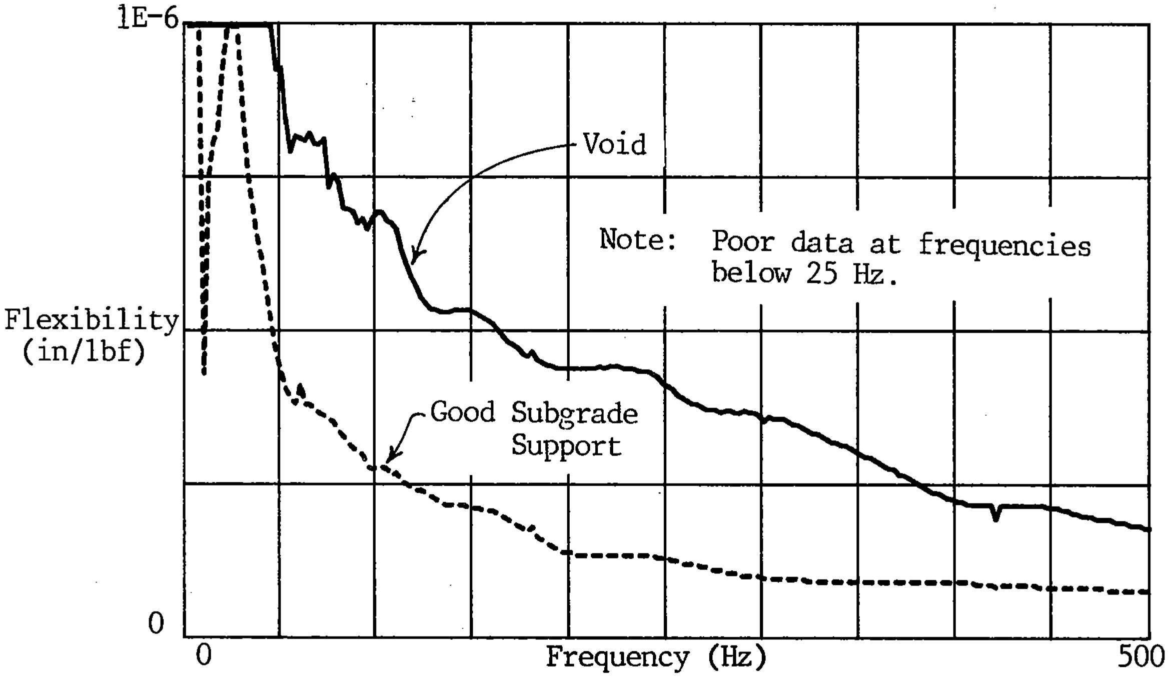

Fig. 13 - Flexibility Plots for Concrete Pavement for Void and Good Subgrade Support Conditions

Detection of Honeycomb Void in Concrete Structures. An ultrasonic pulse velocity investigation was performed to investigate concrete integrity for two water tanks. The water tanks were designed as post-tensioned tanks with anchorages in four pilasters around the tank. Concrete spalling and bending of a thick steel anchor plate occurred during stressing operations for post-tensioning cables at one of the pilaster anchorages. Examination of the spalled area indicated the presence of fine honeycomb voids in the critical zone immediately behind the anchor plate. Because of concern over the possibility of additional failures as unstressed anchorages were tensioned, it was decided to test the remaining anchorages with the pulse velocity method to evaluate concrete integrity.

Ultrasonic measurements were made directly through the 26 inch thick pilaster section on a 3 inch vertical by 4 inch horizontal grid as indicated on Fig. 14. Semi-direct measurements were made by placing the source on the outside edge of the pilaster behind the anchor plate and measuring travel times to receivers on the pilaster face. Pulse travel times were measured for 25 anchorages of the water tanks for a total of over 700 measurements.

The pulse travel time data was entered into a spreadsheet computer program for calculation of pulse velocities and statistical analyses. Review of the data and statistics indicated pulse velocities less than 11,500 fps and standard deviations greater than 500 fps were good predictors of questionable concrete areas. This value of pulse velocity is comparable to the suggested pulse velocity rating for questionable concrete presented in Table I below.

TABLE I

QUALITATIVE CONCRETE RATING BASED ON
ULTRASONIC PULSE VELOCITY MEASUREMENTS
(FROM MALHOTRA, 1976)

Ultrasonic Pulse Velocity (fps)	General Concrete Condition
Above 15,000	Excellent
12,000 to 15,000	Good
10,000 to 12,000	Questionable
7,000 to 10,000	Poor
Below 7,000	Very Poor

Note: The above values for pulse velocity should be reduced by 10 percent for evaluation of drilled shaft concrete quality based on stress wave velocity according to Harrel and Stokoe, 1984.

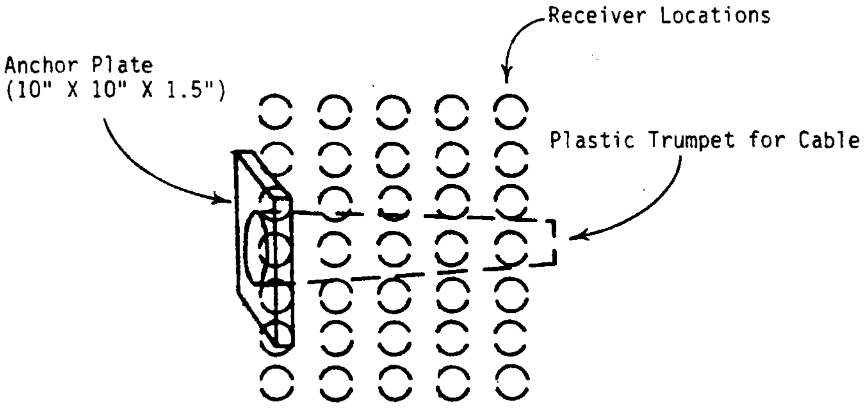
Receiver Locations
Anchor Plate
(10" X 10" X 1.5")
Plastic Trumpet for Cable

A. Projection of Direct Measurement Receiver Locations on the Pilaster Face

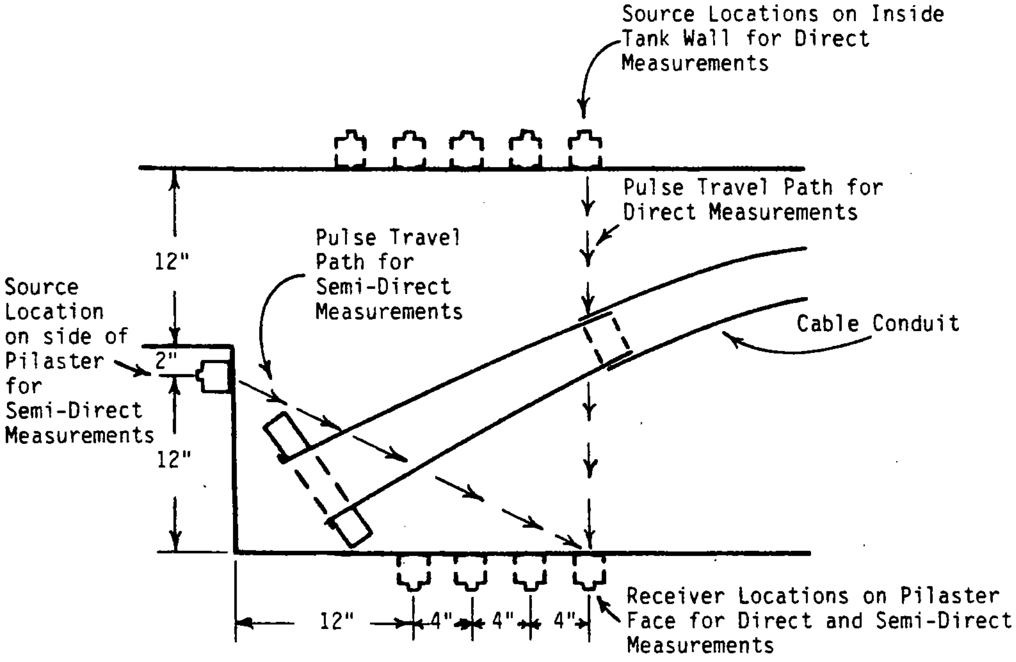
Source Locations on Inside
Tank Wall for Direct
Measurements
Pulse Travel Path for
Direct Measurements
12"
Pulse Travel
Path for
Semi-Direct
Measurements
Source
Location
on side of
Pilaster
for
Semi-Direct
Measurements
2"
12"
Cable Conduit
12"
4"
4"
4"
Receiver Locations on Pilaster
Face for Direct and Semi-Direct
Measurements

B. Pilaster Cross-Section at Anchorage Level

Fig. 14 - Ultrasonic Pulse Velocity Test Pattern for the Anchorages

Three areas of questionable or damaged concrete were identified by the ultrasonic pulse velocity tests. Because much of the water tank had already been tensioned, epoxy injection repair methods were used to fill voids and repair the damaged areas. The specialty contractor reported that vacuum drilling for injection tubes and grout takes confirmed the existence of voids and questionable quality concrete exactly as mapped by the pulse velocity tests.

The water tanks were subsequently tensioned without additional concrete failures. The tanks are full of water and in service today.

The ultrasonic pulse velocity testing program saved considerable expense by eliminating the drilling of unnecessary holes by the epoxy injection contractor. This shortened the time needed for repairs substantially, and allowed construction to resume sooner than would have ordinarily been possible.

SUMMARY

Nondestructive wave propagation methods are now available that can provide a large amount of data regarding subsurface conditions, and the integrity of deep foundations, rigid pavements and structures. The wave propagation methods are particularly valuable because they measure small strain moduli and stiffnesses which can be directly related to stress-strain behavior. The rapid testing associated with NDT and NDE investigations allows a great deal of information to be gathered more economically than ever before for small structures, such as a single drilled shaft, to large structures, such as dams and highways. Key factors in successful application of NDT and NDE methods to construction projects are: 1. investigations should be conducted by experienced engineers who have a thorough understanding of the capabilities and limitations of various nondestructive methods, and 2. the engineers must have a good understanding of construction practices and problems.

REFERENCES

Carino, N.J., Sansalone, M., and Hsu, N.N., "A Point Source-Point Receiver, Pulse-Echo Technique for Flaw Detection in Concrete," Journal of the American Concrete Institute, Proceedings V. 83 No. 2, 1986.

Hall, J.R., Jr., "Limits on Dynamic Measurements and Instrumentation," Richart Commemorative Lectures, ed. by Richard D. Woods, ASCE Fall Convention, Detroit, Michigan, October, 1985.

Harrell, S.A., and Stokoe, K.H., "Integrity Evaluation of Drilled Piers by Stress Waves," Research Report 257-1F, Center for Transportation Research, University of Texas at Austin, January, 1984.

Hearne, T.M., Stokoe, K.H., and Reese, L.C., "Drilled-Shaft Integrity by Wave Propagation Method," ASCE Geotechnical Engineering Journal, Vol. 107, No. 10, October, 1984.

In-Situ Nondestructive Testing of Concrete, American Concrete Institute SP-82 Publication, ed. by V.M. Malhotra, 1984.

Malhotra, V.M., "Testing Hardened Concrete: Nondestructive Methods," ACI Monograph No. 9, American Concrete Institute/Iowa State University Press, Detroit, 1976.

Olson, L.D., and Thompson, R.W., "Case Histories Evaluation of Drilled Pier Integrity by the Stress Wave Propagation Method," Session Proceedings Publication Drilled Piers and Caissons II, ASCE National Spring Convention, Denver, Colorado, May, 1985.

Pederson, C. M. "Swede," and Senkowski, Lawrence J., "Slab Stabilization of PCC Pavements," a paper presented at the Transportation Research Board Meeting in Washington, D.C., by the Research and Development Division of the Oklahoma Department of Transportation, January, 1986.

Robertson, P.K., Campanella, R.G., et al, "Seismic CPT to Measure In situ Shear Wave Velocity," ASCE Journal of Geotechnical Engineering, Vol. 112, No. 8, August, 1986.

Stain, R.T., "Integrity Testing of Drilled Shafts", Foundation Drilling Magazine, ADSC, Part I-Vol. XVIII, No. 12, February, 1984, Part II-Vol. XVIII, No. 13, March/April, 1984.

Stewart, A.H., Brunette, T.L., and Goodman, J.R., "Use of Nondestructive Testing in Rehabilitation of Wood Cooling Towers," a paper to be presented at the ASCE Structures Congress '86 Meeting in New Orleans, September, 1986.

Stokoe, K.H., and Hoar, R.J., "Variables Affecting In situ Seismic Measurements," Proceedings of the Conference on Earthquake Engineering and Soil Dynamics, ASCE Geotechnical Engineering Division Specialty Conference, Pasadena, CA, Vol. II., 1978.

Stokoe, K.H., and Nazarian, S., "Nondestructive Testing of Pavements Using Surface Waves", Transportation Research Record, Washington D.C., 1984.

Stokoe, K.H., and Nazarian, S., "Use of Rayleigh Waves in Liquefaction Studies", Measurement and Use of Shear Wave Velocity for Evaluating Dynamic Soil Properities, ed. by Richard D. Woods, ASCE National Spring Convention, Denver, Colorado, May, 1985.

Woods, R.D., and Stokoe, K.H., "Shallow Seismic Exploration in Soil Dynamics," Richart Commemorative Lectures, ed. by Richard D. Woods, ASCE National Fall Convention, Detroit, Michigan, October, 1985.

EVALUATION OF THE NONLINEAR STABILIZED ROTATIONAL STIFFNESS OF PILE GROUPS

by Gary M. Norris*

Introduction

Objective: The purpose in this presentation is to provide and test a methodology for assessing the nonlinear variation in rotational stiffness (i.e., the spring constant K_θ, the ratio of the applied moment M to the associated rotation θ) of a highway bridge pile group.

Relevance: A knowledge of the rotational (and lateral) stiffness of a pile group is required for modeling the response of a pile founded structure (e.g., a highway bridge) subject to lateral loading. Lateral and rotational boundary element springs are employed, for example, in the seismic analysis of a highway bridge to simulate the soil-structure interaction response (i.e., the stiffness, not the damping) of the foundation moving relative to the "far" or "free" field soil. While earlier work (1) considered a method for assessing the equivalent combined lateral stiffness of a pile group, it has been found (2) that the pile group's rotational stiffness may, in many cases, be more dominant than its lateral stiffness in terms of its effect upon highway bridge response. Consequently, separate procedures are currently proposed for assessing the lateral stiffness (3,4) and the stabilized rotational stiffness (described here) of a highway bridge pile group under conditions of nonfailing soil-pile response.

Assumptions/Simplifications Relative to Proposed Procedure

It is assumed here that the rotational response of a pile group can be uncoupled from its lateral response (not appropriate for pile groups with batter piles) and that the rotational resistance derives from the axial (i.e., vertical) response of the piles about the corresponding axis of rotation.** It is further assumed that none of the piles reach their ultimate capacity (compression or tension) under rotational excitation. (A method for assessing such nonstable rotational response is demonstrated elsewhere [5].) While the lateral resistance of a pile group develops from near surface soils, it is the soils at depth that provide the greater part of the axial and, hence, the rotational resistance of the group. In turn, while pile group interference effects and pile cap contribution are important relative to lateral resistance (3,4), it is assumed that they can be ignored

---

* Associate Professor of Civil Engineering, University of Nevada, Reno, Nevada 89557.

** The piles are taken to be pin ended in a rigid cap relative to rotational response. Alternatively, the fixity of the piles in the cap relative to purely lateral response (3,4) is taken to vary between a cantilevered (i.e., fixed) and pinned (free) end condition depending upon design details.

relative to rotational response.*

Important Considerations in the Proposed Analysis

It is felt that a realistic analysis of the rotational response of a pile group should deal with several very important factors. First of all, there is an initial vertical load (i.e., a dead load) on the piles such that there are unequal axial pile stiffnesses in load versus unload conditions in association with subsequent rotational excitement. In turn, the axis of rotation of a regular arrangement of piles is not symmetrically located; and it shifts based upon changes in stiffness that ensue. Consequently, under uniform rotational excitation, a transient response occurs. However, after only two or three cycles, a stabilized response develops corresponding to equal unload-reload axial pile stiffnesses and a centrally located axis of rotation. Proper evaluation of this stabilized rotational stiffness requires an understanding of the transient response.

Since soil exhibits nonlinear stress-strain behavior, the value of stabilized rotational stiffness will depend upon the amplitude of rotation or, more appropriately, upon the nonlinear variation in unload-reload axial pile stiffness. To appropriately account for such nonlinear variation, one should model the unload-reload axial pile response (as assessed based upon unload-reload shear stress transfer and pile point load-displacement responses) in terms of nonlinear soil (unload-reload) stress-strain behavior.

To deal with variations in the shear stress transfer ("t-z") and point load ("q-z") responses with depth (or in a layered soil) as well as pile compressibility, a Coyle-Reese (6) type of analysis is needed. However, in using the unload-reload t-z and q-z relationships, one assesses the unload-reload ($\Delta Q-\Delta z$) axial pile response (and, hence, the unload-reload stiffness $k_{u/r} = \Delta Q/\Delta z$) instead of the backbone load-settlement (Q-z) curve.

To be appropriate, the shear stress transfer formulation should, of course, take account of interfacial (rather than purely soil stress-strain) behavior and pile installation effects. The installation of piles in clay, for instance, causes a disturbance of the clay along the pile shaft followed by a thixotropic strength gain.

---

* The cylindrical zone of soil affected in axial pile response does not significantly interfere with those of its neighbors unlike the large passive wedge that forms relative to lateral response. Therefore, the group effect is ignored. Secondly, separation occurs between the pile cap and the surrounding soil due to settlement of the soil away from the base of the pile cap and gapping along the vertical sides accompanying simultaneous lateral excitation. Hence, the contribution of the pile cap to rotational restraint is ignored.

Approach to the Problem

The procedure employed to assess rotational stiffness herein relies on existing methodologies from foundation engineering (the Coyle-Reese so-called "t-z" analysis for axial pile response) and soil dynamics (the Ramberg-Osgood formulation [see, e.g., 7] of small strain t-z and q-z response) that have been modified and integrated as required. Because the analysis is based upon recognized procedures, it is felt that it will be more acceptable to the practicing engineer. Consequently, it is more likely that the analysis will receive appropriate consideration. Of course, its adoption by any one group will depend upon its perceived capability to predict observed behavior. For that reason, a case study is included, one in which the predicted variations in rotational stiffness of four pile groups are compared with the back calculated values (independently obtained) from push back quick release full-scale field tests of the Rose Creek Bridge (8).

Overview of the Evaluation of Rotational Stiffness

The rotational stiffness K_θ of a pile group is

$$K_\theta = M/\theta \tag{1}$$

where M, the applied moment, is equal to the product of the axial force change, ΔQ_L or $\Delta Q_{u/r}$ (L for load, u/r for unload-reload), in the pile times its normal distance, r_L or $r_{u/r}$, from the axis of rotation, summed over all the piles in the group, i.e.,

$$K_\theta = \Sigma\Delta Q_L r_L + \Sigma\Delta Q_{u/r} r_{u/r} \tag{2}$$

In turn, the axial force change can be taken as the axial stiffness of the pile, k_L or $k_{u/r}$, times its displacement, Δz (L or u/r understood), i.e.,

$$\Delta Q = k\Delta z \tag{3}$$

where displacement Δz is given by

$$\Delta z = r\theta \tag{4}$$

where θ is the uniform rotation of the pile group expressed in radians. See Fig. 1. Consequently, moment M is equal to

$$M = \Sigma\Delta Qr = \Sigma k\Delta zr\theta = \Sigma kr^2\theta \tag{5}$$

and rotational stiffness K_θ is

$$K_\theta = kr^2\theta \tag{6}$$

where the nonlinear axial pile stiffnesses k are compatible with their associated values of displacement Δz (Equation 4).

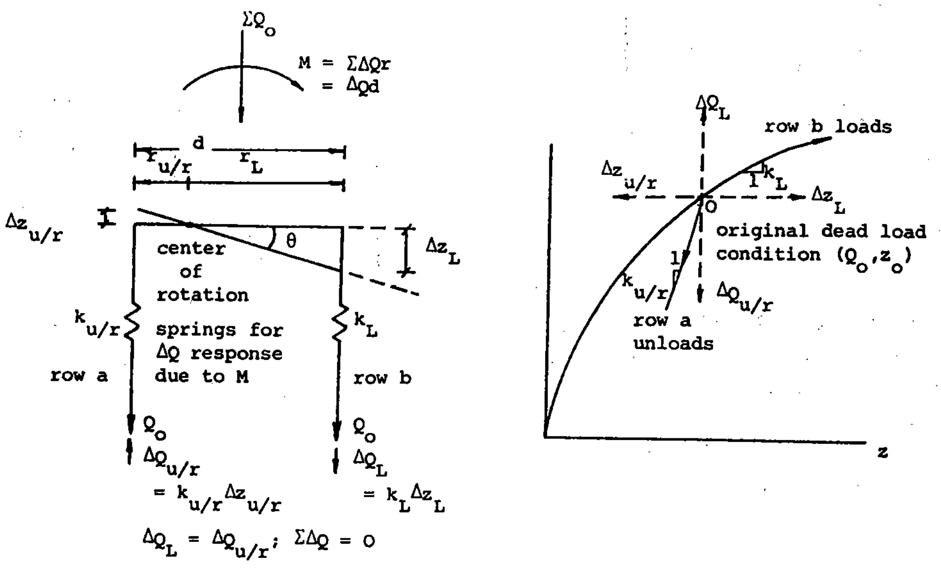

ΣQ_o
$M = \Sigma \Delta Q r$
$= \Delta Q d$
d
$r_{u/r}$
r_L
$\Delta z_{u/r}$
θ
Δz_L
center of rotation
$k_{u/r}$
springs for ΔQ response due to M
k_L
row a
row b
Q_o
$\Delta Q_{u/r}$
$= k_{u/r} \Delta z_{u/r}$
Q_o
ΔQ_L
$= k_L \Delta z_L$
$\Delta Q_L = \Delta Q_{u/r}$; $\Sigma \Delta Q = 0$
ΔQ_L
row b loads
$\Delta z_{u/r}$
k_L
1
Δz_L
o
original dead load condition (Q_o, z_o)
1
$k_{u/r}$
$\Delta Q_{u/r}$
row a unloads
z

Fig. 1 Initial response of a two row pile group to applied moment M.

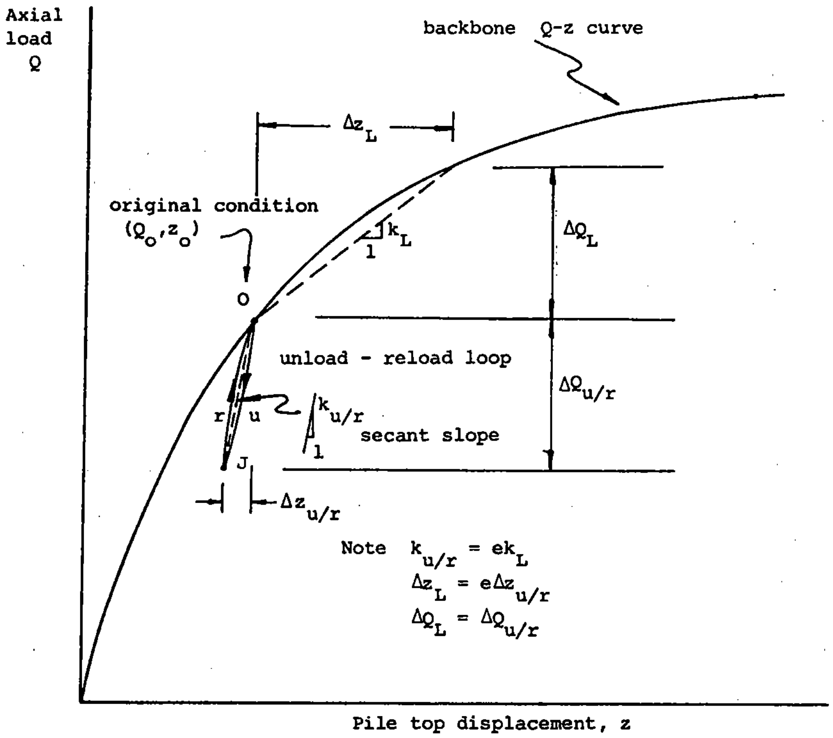

Fig. 2 Pile top load-settlement curve and the associated load or unload-reload response relative to an initial dead load condition.

In succeeding sections, the procedure for evaluating the nonlinear variation in axial pile stiffness k as a function of displacement amplitude Δz will be explained in full. This involves reviewing the Coyle-Reese "t-z" analysis for establishing the load-settlement (Q-z) backbone curve for axial pile response. See Fig. 2. Based on providing Ramberg-Osgood formulations for the backbone t-z and q-z curves (extended to include small strain response), one can, by assuming Masing rules, formulate the corresponding unload-reload responses. With a knowledge of such unload-reload shear stress transfer and end bearing behavior, the Coyle-Reese analysis can be used to assess unload-reload axial pile response (e.g., path OuJr Fig. 2). Given the initial condition of the piles associated with gravity loading (e.g., point O in Fig. 2), a shakedown analysis of the rotational response of the group is undertaken in order to demonstrate the transition from transient to stabilized M-θ behavior. This includes a corresponding consideration of the load/unload-reload Q-z travel paths of the piles. Finally, a procedure for evaluating just the stabilized unload-reload response $k_{u/r}$ of the piles and, hence, K_θ (Equation 6) of the group is presented and then demonstrated (the Rose Creek case study). Providing certain conditions are satisfied, this can be undertaken independently of the shakedown analysis of transient response.

Review of Coyle-Reese "t-z" Analysis

If one can put Ramberg-Osgood formulations to the t-z and q-z responses used to construct the backbone load-settlement curve of a pile, then the unload-reload responses become known and the same procedure that was used to establish the backbone curve can then be used to evaluate the unload-reload axial pile response. It is with this in mind that a review of the Coyle-Reese t-z analysis is presented.

Consider a compressible pile driven in layered clay and divided into segments (Fig. 3a). Each segment (Fig. 3b) of a given length L has, acting upon it, an axial force at the bottom Q_b,* an axial force at the top Q_t, and a shear force S over its lateral surface where S is

$$S = \tau dA_s \tag{7}$$

where

τ = mobilized shear stress due to movement z of the midpoint of the segment downward relative to the surrounding soil; and

dA_s = lateral surface area of the segment.

The average shear stress τ is assessed based upon conditions midheight

---

* For the element at the pile tip, this becomes the point load Q_p.

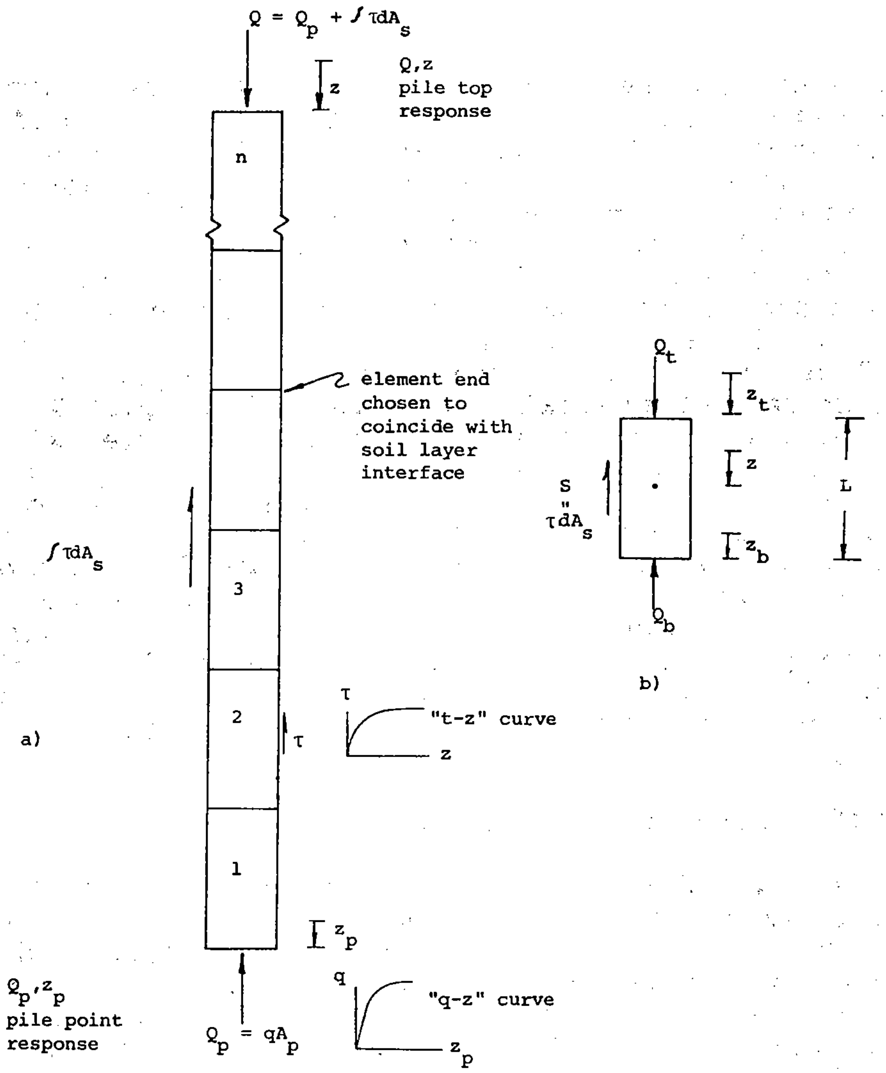
$Q = Q_p + \int \tau dA_s$
Q, z
pile top
response
z
n
element end
chosen to
coincide with
soil layer
interface
$\int \tau dA_s$
3
2
1
a)
τ
τ
"t-z" curve
z
z_p
Q_p, z_p
pile point
response
$Q_p = qA_p$
q
"q-z" curve
z_p
Q_t
z_t
z
L
$S = \tau dA_s$
z_b
Q_b
b)

Fig. 3 Idealization for a Coyle-Reese "t-z" analysis: a) pile and b) element.

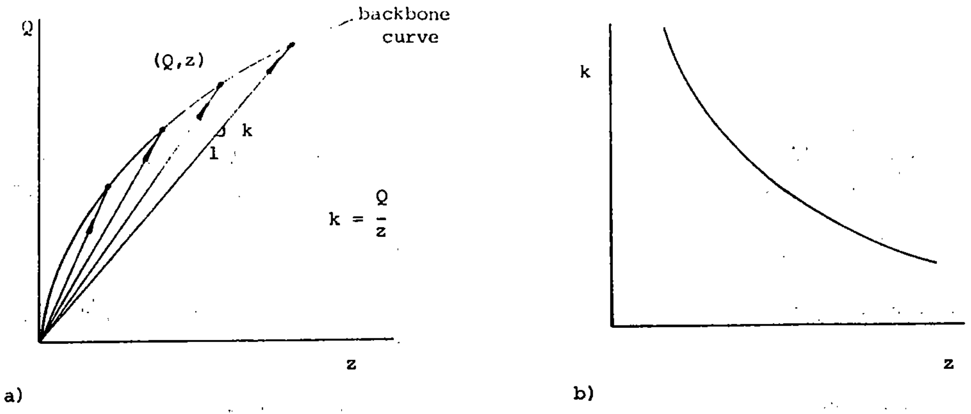

Fig. 4 Nonlinear a) Q-z and b) k vs. z axial pile response.

in the element from a shear stress transfer (t-z) curve representative of the soil over the length of the element. Movement z, midheight in the element, is a combination of the downward movement of the bottom of the element z_b (due to the pile tip movement and the cumulative compression of all the elements above) plus elastic compression z' of the lower half of the element, i.e.,

$$z = z_b + z' \tag{8}$$

where z' is evaluated based upon the average axial force Q' over the lower half of the element, i.e.,

$$z' = \frac{Q'(L/2)}{AE} \tag{9}$$

where A is the cross sectional area and E is the Young's modulus of the pile. Given that Q' is the average of the middle Q_m and bottom Q_b axial forces and that Q_m is itself $(Q_b + Q_t)/2$, then Q' is equal to $(3Q_b + Q_t)/4$ and z' becomes

$$z' = \frac{(3Q_b + Q_t)L}{8AE} \tag{10}$$

Note that Q_t is

$$Q_t = Q_b + S \tag{11}$$

The bottom force of the lowest element (Element 1 in Fig. 3a) is the point load on the pile Q_p. Note that Q_p is equal to the area of the point A_p times the bearing pressure q at the tip,

$$Q_p = qA_p \tag{12}$$

and q is assessed from movement z_p of the pile point from a point load-point displacement or q-z relationship.

Knowing the properties of the pile (A, E, A_s), the point load-point displacement relationship (q-z), and the shear transfer (t-z) curves for the different pile segments delineating the various soil layers (or the changes with depth in a uniform soil deposit), the Coyle-Reese procedure for evaluating the pile top load-deflection (the backbone Q-z) response of a single pile is as follows.*

1. Assume a value of displacement of the pile point z_p. From the q-z relationship corresponding to the soil within one pile diameter B below the pile tip, establish the net bearing pressure q and the point load Q_p (Equation 12) at the pile tip.

---

* A discussion of the evaluation of the q-z (hence, the Q_p-z_p) and t-z relationships is presented in the next section.

2. Start with the bottom segment of the pile (Element 1 of Fig. 3a). Take the bottom force and displacement to be $Q_b = Q_p$ and $z_b = z_p$ respectively.

3. For the segment under consideration, proceed as follows.

   a. Assume a value of elastic compression z' of the lower half of the segment. (As a first estimate, assess z' based on $Q_t = Q_b$ in Equation 10.)

   b. Evaluate the downward movement z of the middle of the segment from Equation 8.

   c. With z, establish the mobilized shear stress τ from the t-z relationship for the segment.

   d. Evaluate the shear force S based on Equation 7.

   e. Evaluate the axial load at the top of the segment Q_t based on Equation 11.

   f. Calculate a new value of z' based on Equation 10.

   g. Take z' in step a to be equal to z' from step f, and iterate until sufficient convergence is obtained.

4. Based on the value of Q_t obtained in the last iteration in step 2, calculate the elastic shortening z" of the entire segment where

$$z'' = \frac{(Q_b + Q_t)}{2} \frac{L}{AE} \tag{13}$$

   Establish the downward movement z_t of the top of the pile segment as

$$z_t = z_b + z'' \tag{14}$$

5. Move up one segment and take Q_b of the new segment to be equal to Q_t of the previous one; likewise, z_b to be equal to z_t.

6. Repeat steps 3 through 5 in turn, for each segment going up the length of the pile. The axial force Q and the corresponding displacement z at the pile top are equal to Q_t and z_t of the uppermost (i.e., the last) element. Plot the Q,z coordinate pair so established as a single point on the backbone load-settlement curve of Fig. 2.

7. Repeat steps 1 through 6 to obtain additional points as needed to complete the load-settlement curve. For each new value of assumed pile tip displacement z_p a different (Q,z) coordinate results.

In effect, the procedure outlined above for establishing the backbone load-settlement Q-z response at the pile top operates by means of secant lines as shown schematically in Fig. 4. The slope of these lines is the corresponding value of axial pile or spring stiffness k (= Q/z) under first loading conditions. When k is plotted separately as a function of displacement amplitude z, its nonlinear form appears as shown in Fig. 4b.

The same procedure can be used to consider the nonlinear variation in secant slope unload-reload response as shown in Fig. 5a. This is achieved by substituting unload-reload t-z and q-z relationships for the backbone t-z and q-z curves. Thereafter, one can consider that, in using the aforementioned procedure, ΔQ_p-Δz_p (pile tip) and ΔQ-Δz (pile top) responses are obtained instead of the corresponding Q_p-z_p and Q-z responses. The unload-reload stiffness at pile top $k_{u/r}$ is then $\Delta Q/\Delta z$ which varies nonlinearly with unload-reload displacement amplitude Δz as shown in Fig. 5b.

A computer program can easily be written for the foregoing procedure provided one is able to formulate expressions for the t-z and q-z relationships. (A very simple interactive BASIC program tailored specifically for the case study considered herein is provided in the Appendix.) Therefore, what remains is to discuss how such shear stress transfer and end bearing relationships are assessed and how one can formulate equations to fit them.

t-z and q-z Curves

Coyle and Reese (6) provide normalized shear stress transfer ($\tau/\alpha c$ versus z) curves for all clays for different depths over the pile length (0-10 ft., curve A; 10-20 ft., curve B; > 20 ft., curve C) as shown in Fig. 6a. The shear stress τ (or "t" in t-z terminology) in these curves is normalized by the value of undrained shear strength αc that can develop in the clay adjacent to the pile after pile installation (i.e., disturbance of the clay followed by thixotropic strength gain). One will note that the peak ordinate in curves C and B is not equal to one. This indicates that the maximum average stress τ that develops is less than the soil strength αc. This is attributed to some loss in contact between the pile and the soil (arising from wobble during pile driving or the shrinkage of concrete for cast-in-place piles) due to the reduced lateral earth pressure near the ground surface. The ratio $\zeta = \tau_{ult}/\alpha c$ is equal to 0.53 for curve C for a depth of 0-10 ft., 0.85 for curve B for a depth of 10-20 ft., and 1.0 for curve A for a depth greater than 20 ft. If one normalizes the Coyle-Reese curves by ζ, i.e., $\tau/\zeta\alpha c = \tau/\tau_{ult}$, then they appear as shown in Fig. 6b. (Note that curves B and C become a single curve.) Using either set of curves (Fig. 6a or 6b), the shear stress τ that develops in a given clay at a specified depth due to

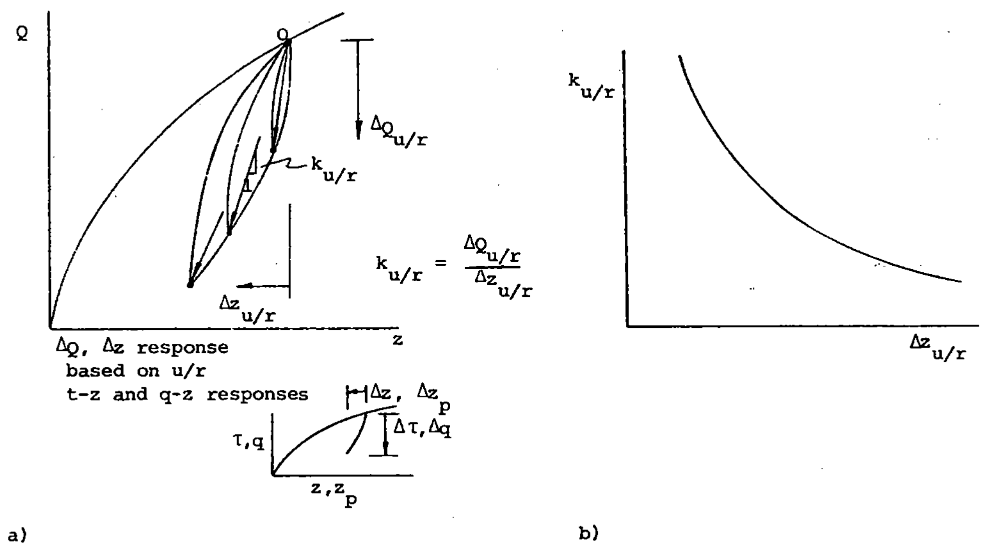
Q
Q
ΔQu/r
ku/r
ku/r = ΔQu/r / Δzu/r
Δzu/r
z
ΔQ, Δz response
based on u/r
t-z and q-z responses
Δz, Δzp
Δτ,Δq
τ,q
z,zp
a)
ku/r
Δzu/r
b)

Fig. 5 Nonlinear a) $\Delta Q_{u/r}$ - $\Delta z_{u/r}$ and b) $k_{u/r}$ vs. $\Delta z_{u/r}$ unload-reload response.

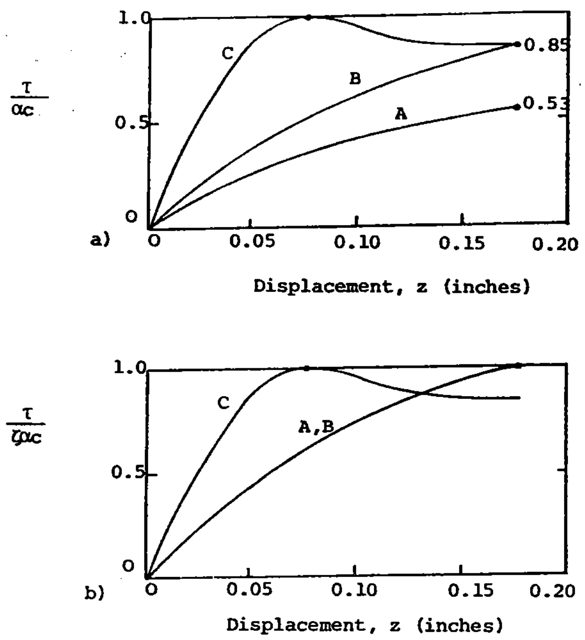

Fig. 6 Normalized t-z curves a) after Coyle and Reese (6) and b) as modified.

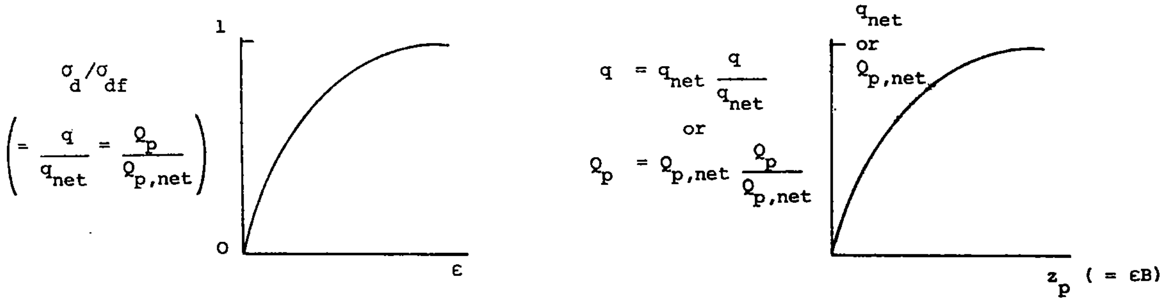
σd/σdf
(= q/qnet = Qp/Qp,net)
1
0
ε
q = qnet q/qnet
or
Qp = Qp,net Qp/Qp,net
qnet
or
Qp,net
zp (= εB)

Fig. 7 Point response q-z or Q_p-z_p curve from the soil stress-strain curve.

displacement z is

$$\tau = \left(\frac{\tau}{\alpha c}\right)_{A,B,\text{or } C} \alpha c \quad \text{or} \quad = \left(\frac{\tau}{\zeta\alpha c}\right)_{A \text{ or } B \text{ and } C} \zeta\alpha c \tag{15}$$

where αc corresponds to the clay in question and $(\tau/\alpha c)$ or $(\tau/\zeta\alpha c)$ to displacement z from curve A, B, or C from Fig. 6a or 6b for the given depth.

While Coyle and Reese do not provide shear stress transfer curves for sand, such curves can be assessed based on information provided by Kraft (9).

The nonlinear nature of the bearing pressure-displacement or q-z relationship (and, hence, the point load-point displacement or Q_p-z_p response) can be modeled directly from the soil's stress-strain curve for the case of a pile with its tip in clay (provided the clay extends to a depth B below and 2B above the pile point). This is demonstrated in the Appendix. With a knowledge of the deviator stress-axial strain curve from an actual or postulated unconsolidated undrained triaxial test of the clay at the pile tip, the q-z and Q_p-z_p curves can be obtained as demonstrated in Fig. 7 given that 1) the normalized value of pressure q/q_{net} and point load $Q_p/Q_{p,net}$ are identical to the stress level σ_d/σ_{df} in the clay (see Appendix A) and 2) the displacement z_p at the pile tip divided by the pile diameter B is equal to the strain in the clay in the mobilized region (see Appendix B), i.e.,

$$\varepsilon = z_p/B \tag{16}$$

and

$$Q_p/Q_{p,net} = q/q_{net} = \sigma_d/\sigma_{df} \tag{17}$$

where

$Q_{p,net}$, the net ultimate point load, is $q_{net}A_p$,

q_{net}, the net ultimate bearing capacity, is 9c, and

σ_{df}, the maximum deviator stress, is 2c.

For a pile point embedded in sand, Equation 16 may again be used but Equation 17 should not be. Appropriate formulation is presented in Appendix C.

Given the aforementioned process for constructing the t-z and q-z (or Q_p-z_p) curves, the next step is to formulate the expressions that fit these curves.

Ramberg-Osgood Formulation

Given the nonlinear form of the soil stress-strain (i.e., σ-ε or τ-γ) response, the Ramberg-Osgood equation for fit of the backbone curve as given by Richart (7) is

$$\text{(for } \sigma\text{-}\varepsilon)\qquad \frac{\varepsilon}{\varepsilon_r} = \frac{\sigma_d}{\sigma_{d,ult}}\left[1 + \beta\left(\frac{\sigma_d}{\sigma_{d,ult}}\right)^{R-1}\right]$$

$$\text{(for } \tau\text{-}\gamma)\qquad \frac{\gamma}{\gamma_r} = \frac{\tau}{\tau_{ult}}\left[1 + \beta\left(\frac{\tau}{\tau_{ult}}\right)^{R-1}\right] \tag{18}$$

The relationship between reference strain, ε_r or γ_r, initial tangent modulus, E_i or G_o, and ultimate stress, $\sigma_{d,ult}$ or τ_{ult}, i.e.,

$$\varepsilon_r = \frac{\sigma_{d,ult}}{E_i} \quad ; \quad \gamma_r = \frac{\tau_{ult}}{G_o} \tag{19}$$

is shown in Fig. 8. In turn, unload-reload response based on Masing rules (see Richart [7]) is expressed in the following fashion.

$$\frac{\Delta\varepsilon}{\varepsilon_r} = \frac{\Delta\sigma_d}{\sigma_{d,ult}}\left[1 + \beta_{u/r}\left(\frac{\Delta\sigma_d}{\sigma_{d,ult}}\right)^{R-1}\right]$$

$$\frac{\Delta\gamma}{\gamma_r} = \frac{\Delta\tau}{\tau_{ult}}\left[1 + \beta_{u/r}\left(\frac{\Delta\tau}{\tau_{ult}}\right)^{R-1}\right] \tag{20}$$

where

$$\beta_{u/r} = \frac{\beta}{2^{R-1}} \tag{21}$$

If one now considers the normalized t-z curves of Fig. 6b and lets the nominal reduced strength $\zeta\alpha c$ be τ_{ult}, then equations 18-21 apply, provided one can convert the abcissa from displacement z to shear strain γ.

Based on a study by Robinsky and Morrison (10) of the soil displacement pattern adjacent to a vertically loaded pile, it is surmised that the average shear strain γ within a zone B/2 wide adjacent to the pile, accounts for seventy-five percent of the shear displacement z as shown in Fig. 9. Assuming that the vertical pile response is domina-

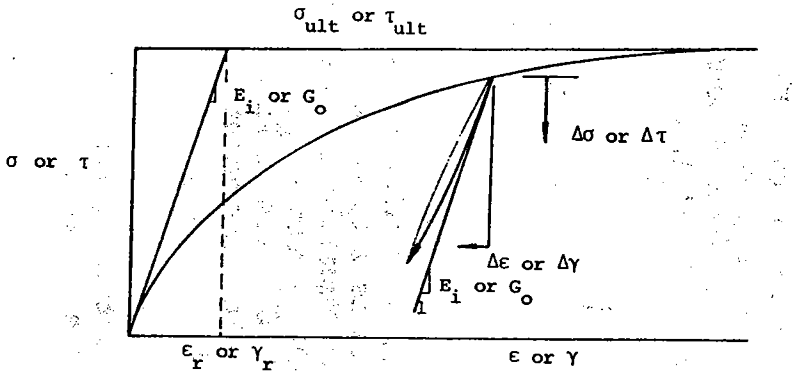

Fig. 8 Basic stress-strain curve with unload-reload loop.

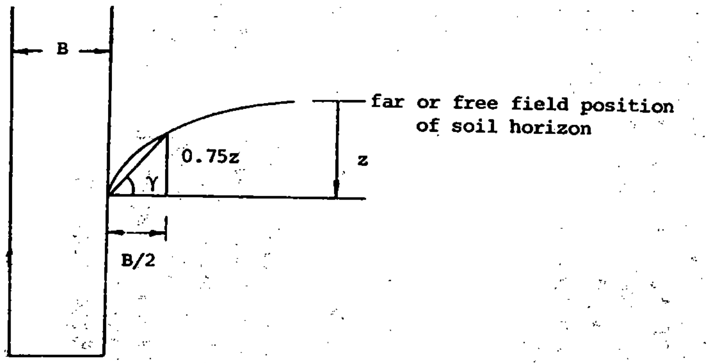
B
far or free field position of soil horizon
0.75z
γ
z
B/2

Fig. 9 Idealized relationship between shear strain γ of the soil and displacement z of the pile.

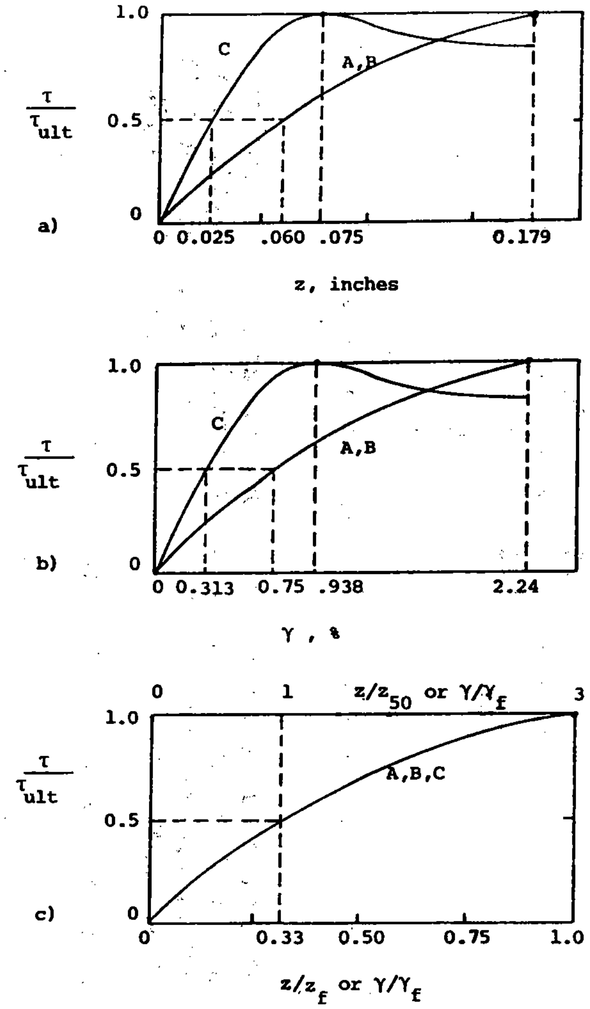

Fig. 10 Curves of τ/τ_{ult} a) vs. z, b) vs. γ and c) vs. z/z_{50} or f or γ/γ_{50} or f.

ted by this zone of soil, one has that

$$\gamma\ (= \tan\gamma) = \frac{0.75z}{B/2} = \frac{1.5z}{B}$$

or

$$\gamma = 0.125\ \frac{z}{B}\ \text{(for z in inches and B in feet)} \qquad (22)$$

While not stated, it is assumed here that displacement z relative to curves A, B, and C of Fig. 6 represents the typical size pile (B = 1 ft.). Therefore, one has the correspondence between z and γ at fifty and one hundred percent stress levels as shown in Figs. 10a and 10b.

From an inspection of Fig. 10, note that

$$\frac{z_{50}}{z_f} = \frac{\gamma_{50}}{\gamma_f} = P \qquad (23)$$

where P is equal to 1/3 for all curves; and, secondly, if the γ (or z) axis of Fig. 10b (or a) were normalized by either γ_f or γ_{50} (or z_f or z_{50}), all curves would become one and the same (Fig. 10c).

With the above mentioned transformation of the t-z curves to τ -γ curves, Equation 18 can then be used to assess backbone and Equation 20 to assess unload-reload response as discussed below. The associated evaluation of fitting parameters β, R-1, and $\beta_{u/r}$ (equal to 9, 0.6674, and 5.67, respectively - the same for all curves A, B, and C) is presented in detail in Appendix D.* In Appendix D, it is also shown that

$$z_r = \frac{z_f}{10} \quad ; \quad \gamma_r = \frac{\gamma_f}{10} \qquad (24)$$

where z_f and γ_f values are given in Fig. 10.

With a knowledge of β, R-1, $\beta_{u/r}$, and z_r, one can evaluate the shear stress τ due to displacement z as follows: assess z/z_r where z_r is given by Equation 24; evaluate τ/τ_{ult} based on Equation 18 as a function of γ/γ_r (= z/z_r); and assess $\tau = (\tau/\tau_{ult})\tau_{ult}$ where $\tau_{ult} = \zeta\alpha c$ of the clay layer in question. The same procedure is also used to assess stress change $\Delta\tau$ associated with unload-reload movement Δz provided Equation 20 is substituted for Equation 18.

---

* Note that emphasis is placed on establishing fitting parameters that are appropriate over the small strain range as required for analysis of seismic response.

Given the proportionality between point displacement z_p and soil strain ε (Equation 16) and between load level $Q_p/Q_{p,net}$ (where $Q_{p,net} = 9cA_p$) and stress level in the soil σ_d/σ_{df} (Equation 17), Equations 18 and 20 can likewise be expressed as

$$\frac{z_p}{z_{pr}} = \frac{Q_p}{Q_{p,net}} \left[1 + \beta \left(\frac{Q_p}{Q_{p,net}} \right)^{R-1} \right] \qquad (25)$$

$$\frac{\Delta z_p}{z_{pr}} = \frac{\Delta Q_p}{Q_{p,net}} \left[1 + \beta_{u/r} \left(\frac{\Delta Q_p}{Q_{p,net}} \right)^{R-1} \right] \qquad (26)$$

Since the point load of a pile with its tip in clay is relatively small (and, therefore, of lesser importance), it is deemed sufficiently accurate to take z_{pr} to be equal to z_{p50}* or

$$z_{pr} = z_{p50} = \varepsilon_{50}B = P'\varepsilon_f B \qquad (27)$$

where ε_{50} is the value of strain in the clay at the pile tip at a stress level of fifty percent and where ε_{50} may be expressed as some fraction P' of its failure strain ε_f. Applying the condition that $z_p = z_{pf} = \varepsilon_f B$ for $Q_p = Q_{p,net}$ (i.e., in Equation. 25) one obtains the relationship

$$\beta = \frac{1}{P'} - 1 \qquad (28)$$

Likewise, applying the condition that $z_p = z_{p50} = P'\varepsilon_f B$ at $Q_p = Q_{p50} = 0.5Q_{p,net}$ leads to the result that

$$R-1 = \log(1/\beta)/\log(0.5) \qquad (29)$$

In turn, $\beta_{u/r}$ can be evaluated using Equation. 21. Therefore, based on an estimate of the failure strain ε_f and the ratio P' ($= \varepsilon_{50}/\varepsilon_f$) of the clay at the pile point, one can evaluate the parameters β, R-1, $\beta_{u/r}$ and z_{pr} for use relative to the assessment of point load displacement response (Equation 25 or 26).

Typically what is done is specify a pressure or load level PL ($= Q_p/Q_{p,net}$) for load conditions or a change ΔPL ($= \Delta Q_p/Q_{p,net}$) for unload-reload response and then using either Equation 25 or 26, calculate z_p/z_{pr} or $\Delta z_p/z_{pr}$. Thereafter $z_p = (z_p/z_{pr})\, z_{pr}$ and $Q_p = \text{PL}\, Q_{p,net}$ for load conditions or $z_p = (\Delta z_p/z_{pr})\, z_{pr}$ and $\Delta Q_p = \Delta\text{PL}\, Q_{p,net}$ for unload-reload response.

---

* The effect of this simplification is to make the Ramberg-Osgood backbone curve more of a straight line up to a level of strain equal to ε_{50}.

Given the difference between the stress and the pressure (or load) level in sand, a different procedure is required for point load-point displacement response for a pile with its tip resting in sand.

Analysis Using the Computer Program Provided

The computer program ROSE CREEK appearing in Appendix E is a very simple interactive BASIC program that employs the foregoing Ramberg-Osgood formulation. It was written specifically to assess both axial pile backbone curve (Q,z) coordinates and unload-reload ($\Delta Q, \Delta z$) values (and stiffness $k_{u/r} = \Delta Q/\Delta z$) based on the Coyle-Reese procedure outlined earlier. Corresponding to the conditions at Rose Creek, it is limited to the analysis of a "floating or "friction" pile in layered clay.

To use the program one must first input the diameter B and AE values of the pile. Corresponding to conditions at the pile point, the program then prompts the user for the value of $Q_{p,net}$ (= $9cA_p$) and, for unload-reload response, the value of the point load Q_p from dead load conditions.* (Q_p is then taken as the maximum point unload ΔQ_p that can occur.**) The reference displacement for point response z_{pr} (Equation 27) is evaluated and entered, along with values of $\beta_{u/r}$ and R-1 for both point and shaft responses. The evaluation of values, z_{pr} and $\beta_{u/r}$ (Equation 21) and R-1 (Equation 29) associated with pile point response, requires knowledge of β (Equation 28) and hence, an estimate of the failure strain ε_f and the ratio P (= $\varepsilon_{50}/\varepsilon_f$) of the (undisturbed) clay located just beneath the pile tip. On the other hand, values of $\beta_{u/r} = 5.67$ ($\beta = 9$) and R-1 = 0.6674 are used for the Coyle-Reese shear stress transfer curves A,B, and C for shaft response as discussed earlier.

The program prompts the user for the number of pile segments and values of τ_{ult}, m^+ and L for each element starting at the pile point and proceeding, in order, up the pile. Thereafter it asks for input of the change in pressure level $\Delta PL = \Delta Q_p/Q_{p,net}$ at the point for which the analysis is to be considered.++ With knowledge of ΔPL the program computes the point unload ΔQ_p (=$\Delta PL\ Q_{p,net}$) and Δz_p (Equation 26) and proceeds up through the elements based on the Coyle-Reese procedure outlined earlier to establish the pile top unload-reload displacment Δz (Δz_t of the last element), the force ΔQ (ΔQ_t of the last element) and the axial pile stiffness $k_{u/r} = \Delta Q/\Delta z$. (Corresponding pile point Δz_p and ΔQ_p values are also printed at this time.)

---

* Q_p can be assessed based on an analysis of backbone curve response using the same program. This is discussed further on in this section.

** Once ΔQ_p reaches the original value of Q_p, the pile tip is completely unloaded. Thereafter ΔQ_p cannot increase further as Δz_p increases because the point separates from the soil beneath it.

+ m is either 1070 for curve C or 447 for curves A and B.

++ Note that while one may increase ΔPL indefinitely, the maximum point unload ΔQ_p is limited to Q_p from dead load conditions. Therefore, increasing ΔPL beyond the value associated with Q_p is only a mechanism for considering greater displacements Δz_p at a constant value of ΔQ_p (= Q_p).

In the process of making one run, the program prints values of ΔQ_t and Δz_t for each element along with the change in stress level in the adjacent soil ($\Delta SL = \Delta\tau/\tau_{ult}$ from Equation 20). Note that this change in stress level in unload-reload response can exceed a value of one corresponding to the shear stress unloading to zero and then reversing in direction.*

With one run of the program complete and values of ΔQ, Δz, $k_{u/r}$ and Δz_p, ΔQ_p printed, the program prompts the user for a new value of change in pressure level from which a new set of values is to be determined. (If, however, one wishes to stop, then 999 is entered.) Such use of the program is demonstrated in a subsequent section relative to the Rose Creek study.

It should be noted that program ROSE CREEK can also be used to assess (Q,z) points along the backbone curve. To do so one needs to input values of β for pile point and shaft response (instead of $\beta_{u/r}$ values). Likewise, the value of $Q_{p,net}$ should be entered when the value of the maximum point "unload" is requested. Finally an additional statement (see LINE 245 in Appendix E) should be entered limiting the value of stress level $SL = \tau/\tau_{ult}$ in shear stress transfer response to one.

When evaluating backbone response, the value of the point load Q_p corresponding to the dead load condition can be obtained by trial and error by inputting different PL values until the pile top load Q equals the dead load. The corresponding point load Q_p is the value of interest. Likewise, the ultimate capacity of the pile Q_{ult} can be assessed by inputing a value of PL at the point equal to one (i.e., $Q_p = Q_{p,net}$) and checking that SL in each element up through the last one reaches a value of unity. The value of Q at the pile top in that instance is Q_{ult}. If, however, for some unusual soil condition the SL in one or more elements does not reach unity (e.g., ε_f of the soil at the point is very large), then one can increase the value of PL above one until all SL's reach a value of unity. (While PL is fictitiously increased beyond one, the program limits Q_p to $Q_{p,net}$.) Once this occurs the pile top load ceases to grow and its value is equal to Q_{ult}.*

---

* If the magnitude of unloading is great or the original shear stress under dead load conditions is small, it may be necessary to assess when the unload response reaches the backbone curve on the unload side. This is ignored herein.

While program ROSE CREEK was developed primarily for use in the evaluation of unload-reload axial pile stiffness ($k_{u/r}$ vs. Δz), knowledge of the point load Q_p for dead load conditions and the capacity, Q_{ult} are required for consideration of changes in the stabilized rotational stiffness K_θ of the pile group. More on this later.

Variation in Rotational Response of the Pile Group

Given the capability of assessing the backbone Q-z curve (and, hence, the stiffness k_L in load due to the difference between points on the curve**) as well as the variation in the unload-reload stiffness $k_{u/r}$ (= $\Delta Q/\Delta z$) as a function of displacement amplitude Δz (see Fig. 5), a question arises as to the dependence of the rotational response of the pile group on the various axial pile response travel paths. In particular, there may be some transient rotational response even with constant moment or rotational excitation prior to the onset of stabilized behavior. While it is the stabilized stiffness K_θ of the group that is of interest herein, it is still important that one comprehend the transient response in order to have an appreciation of the conditions necessary for the development of stabilized behavior.

To study the development of such stabilized behavior, imagine a two row pile group (see Fig. 1) under uniform rotational excitation θ_{max}. Rather than deal with the curvilinear axial pile travel paths, consider the paths as delineated by the secant slopes k_L and $k_{u/r}$ (see Fig. 2) where values of k_L and $k_{u/r}$ employed correspond to the peak displacements. Let $e = k_{u/r}/k_L$ where e corresponds to the value of θ_{max} and the initial point considered.

At this point, consider rotation θ and moment M corresponding to change 0-1 as featured in Figs. 11 and 12. Applied moment M causes axial force changes ΔQ_L and $\Delta Q_{u/r}$ which are equal and opposite (Fig. 2) if there is to be no change in vertical force equilibrium. Note, however, that, due to the differences in spring stiffnesses ($k_{u/r} > k_L$), the vertical displacement at the pile heads of the two rows is different, i.e.,

---

* The backbone Q-z curve in tension can likewise be assessed by setting the program for load conditions and inputting a value of $Q_{p,net} = 0$. Accordingly, the pile top response becomes a function of just pile shaft behavior and Q_{ult} in tension (i.e., T_{ult}) is just the shaft capacity Q_s, which is equal to the integration of τ_{ult} over the lateral surface of the shaft.

** Note that k_L is not the k of Fig. 4b. Stiffness k_L is the secant slope associated with the initial point (not the origin).

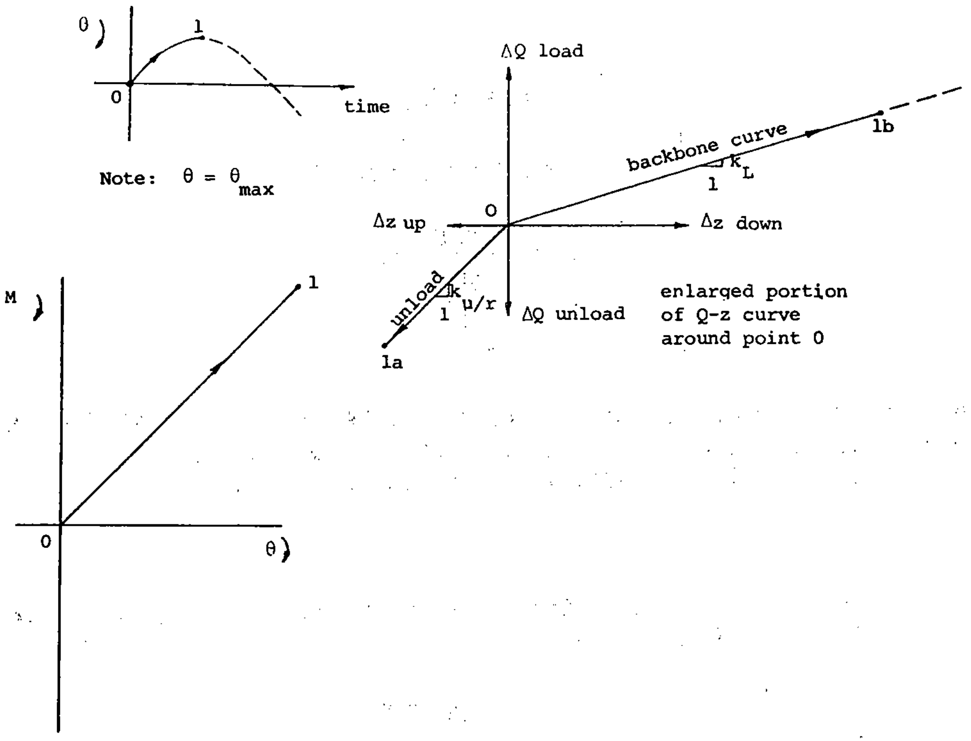
θ
1
0
time
Note: θ = θmax
ΔQ load
backbone curve
kL
1
1b
0
Δz up
Δz down
unload
ku/r
1
1a
ΔQ unload
enlarged portion of Q-z curve around point 0
M
1
0
θ

Fig. 11 θ vs. time, Q-z and M-θ responses over interval 0-1.

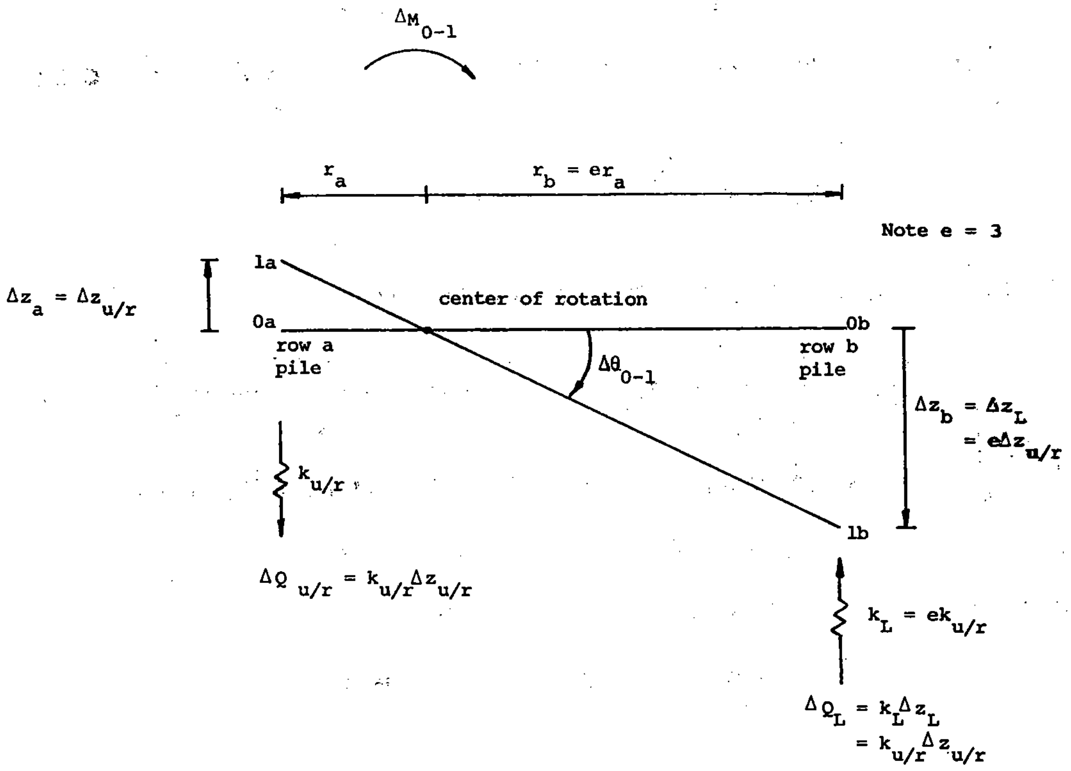
ΔM0-1
ra
rb = era
Note e = 3
Δza = Δzu/r
1a
center of rotation
0a
0b
row a pile
row b pile
Δθ0-1
Δzb = ΔzL = eΔzu/r
ku/r
1b
ΔQu/r = ku/rΔzu/r
kL = eku/r
ΔQL = kLΔzL = ku/rΔzu/r

Fig. 12 Rotational displacement during interval 0-1.

$$\Delta Q_L = \Delta Q_{u/r}$$

$$k_L \Delta z_L = k_{u/r} \Delta z_{u/r}$$

$$\Delta z_L = \frac{k_{u/r}}{k_L} \Delta z_{u/r} \qquad (30)$$

$$z_L = e\ z_{u/r}$$

Consequently, the center of rotation shifts toward the stiffer unload-reload piles, i.e., radii r, based on Equation 30 (where $\Delta z = r\theta$ [Equation 4]), are likewise related by ratio e; or

$$r_L = e\ r_{u/r} \qquad (31)$$

Given that the sum of the radii is equal to the distance d between the two pile rows (Fig. 12) or

$$r_L + r_{u/r} = d \qquad (32)$$

one has, from Equations 30 and 31, that

$$r_{u/r} = \frac{d}{(e + 1)} \quad ; \quad r_L = \frac{e\ d}{(e + 1)} \qquad (33)$$

The rotation associated with point 1 or θ_1 is equal to the change $\Delta\theta_{0-1}$ where

$$\Delta\theta_{0-1} = \frac{\Delta z_{u/r}}{r_{u/r}} \quad ; \quad \text{also} = \frac{\Delta z_L}{r_L}$$

or (substituting for r as given in Equation 33)

$$\Delta\theta_{0-1} = \frac{(e + 1)}{d} \Delta z_{u/r} \quad ; \quad \text{also} = \frac{(e + 1)}{e\ d} \Delta z_L \qquad (34)$$

Moment M_1 to cause rotation θ_1 is equal to the change ΔM_{0-1} where

$$\Delta M_{0-1} = \Delta Q_{u/r} d \quad ; \quad \text{also} = \Delta Q_L d$$

or (substituting for ΔQ as given in Equation 3)

$$\Delta M_{0-1} = k_{u/r} \Delta z_{u/r} d \quad ; \quad \text{also} = k_L \Delta z_L d \qquad (35)$$

Given values of d, e, $k_{u/r}$ (or k_L) and $\Delta z_{u/r}$ (or Δz_L), one can evaluate M_1 and θ_1 and plot the corresponding M-θ coordinate as shown in Fig. 11.* Note that this corresponds to the 0-1 Q-z travel paths for piles of rows a (unload) and b (load) of the group (Fig. 11).

If at this point the rotation θ is reversed (i.e., $\Delta\theta_{1-2}$ opposite in sense from $\theta_1 = \Delta\theta_{0-1}$), then the piles of row a will reload retracing the Q-z path 0-1a (now 1a-2a) while those of row b will unload corresponding to path 1b-2b also at slope $k_{u/r}$ (Fig. 13). Given the equal spring resistances $k_{u/r}$ for both rows a and b relative to the 1-2 change, the instantaneous center of rotation shifts to the middle of the group, i.e., $r_a = r_b = d/2$ (Fig. 14). As a result,

$$\Delta\theta_{1-2} = \frac{\Delta z_{1-2}}{d/2} = \frac{\Delta z_{u/r}}{d/2} \quad ; \quad \theta_2 = \theta_1 + \Delta\theta_{1-2}^{**} \qquad (36)$$

$$\Delta M_{1-2} = \Delta Q_{1-2}d = \Delta Q_{u/r}d \quad ; \quad M_2 = M_1 + \Delta M_{1-2} \qquad (37)$$

such that θ_2 falls between 0 and θ_1 while $M_2 = 0$. As shown in Fig. 13, the forces in the piles ($Q_2 = Q_0 + \Delta Q_{0-1} + \Delta Q_{1-2}$) of both rows are again equal to the initial value Q_0 while there is a residual displacement ($z_2 = z_0 + \Delta z_{0-1} + \Delta z_{1-2} \neq z_0$) to the piles of row b. This corresponds to the fact that θ_2 is not zero (Fig. 14) and that the M-θ line in Fig. 13 does not pass through the origin.

As θ decreases further and tends toward θ_{max} of the opposite sense (Fig. 15), there is a change in the orientation of the travel paths of the piles. Piles of row a displace according to stiffness k_L associated with path 2a-3a-4a along the backbone curve, while those of row b continue at slope $k_{u/r}$ (path 2b-3b-4b) in further unloading. Accordingly, the center of rotation shifts toward row b yielding the 2-3-4 line in the M-θ curve of Fig. 15. (An evaluation of the M and θ values for points 1-8 is demonstrated in Appendix F for the case where e = 3.) One will note that, corresponding to point 3 where θ is again zero, moment M is not. Corresponding to this condition of a level foundation, there are residual forces in the piles ($Q_3 \neq Q_0$) as shown in Fig. 15.

---

* If one were to consider, in addition, intermediate points between 0 and 1, then the resulting 0-1 M-θ line would be curved upward corresponding to higher values of k for the smaller displacements Δz (e.g., see Fig. 5) leading up to Point 1.

** Substituting $\Delta\theta_{0-1}$, as given in Equation 34, and taking account of the direction of rotational change, $\theta_2 = (e-1)\ \Delta z_{u/r}/d$.

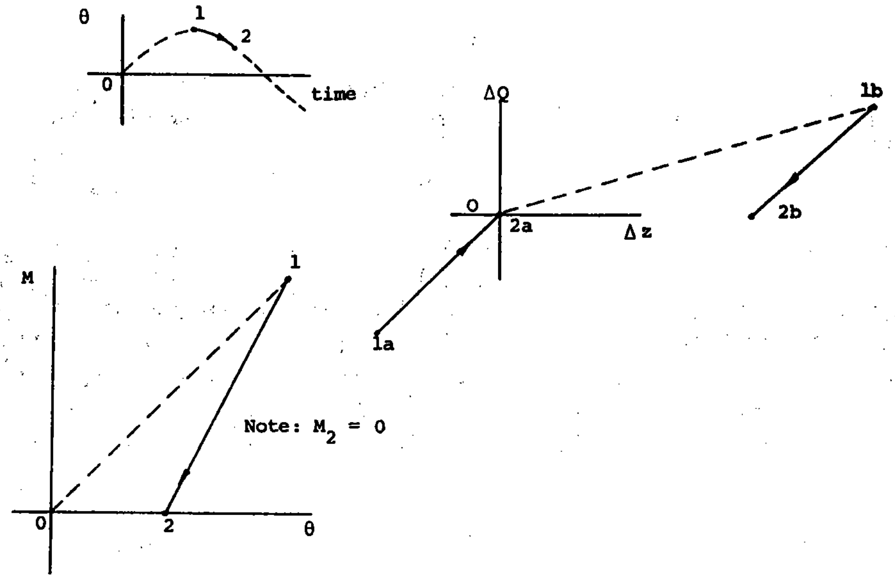

Fig. 13 θ vs. Q-z and M-θ responses over interval 1-2.

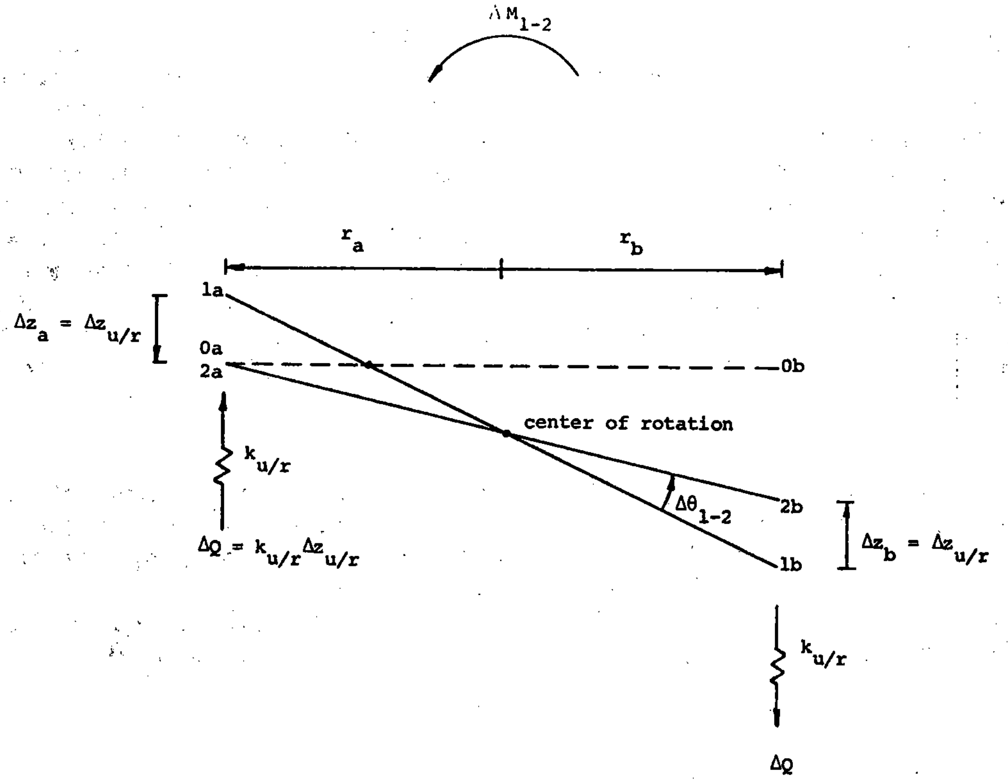
ΔM_{1-2}
r_a
r_b
1a
$\Delta z_a = \Delta z_{u/r}$
0a
2a
0b
center of rotation
$k_{u/r}$
$\Delta Q = k_{u/r} \Delta z_{u/r}$
$\Delta\theta_{1-2}$
2b
1b
$\Delta z_b = \Delta z_{u/r}$
$k_{u/r}$
ΔQ

Fig. 14 Rotational displacement during interval 1-2.

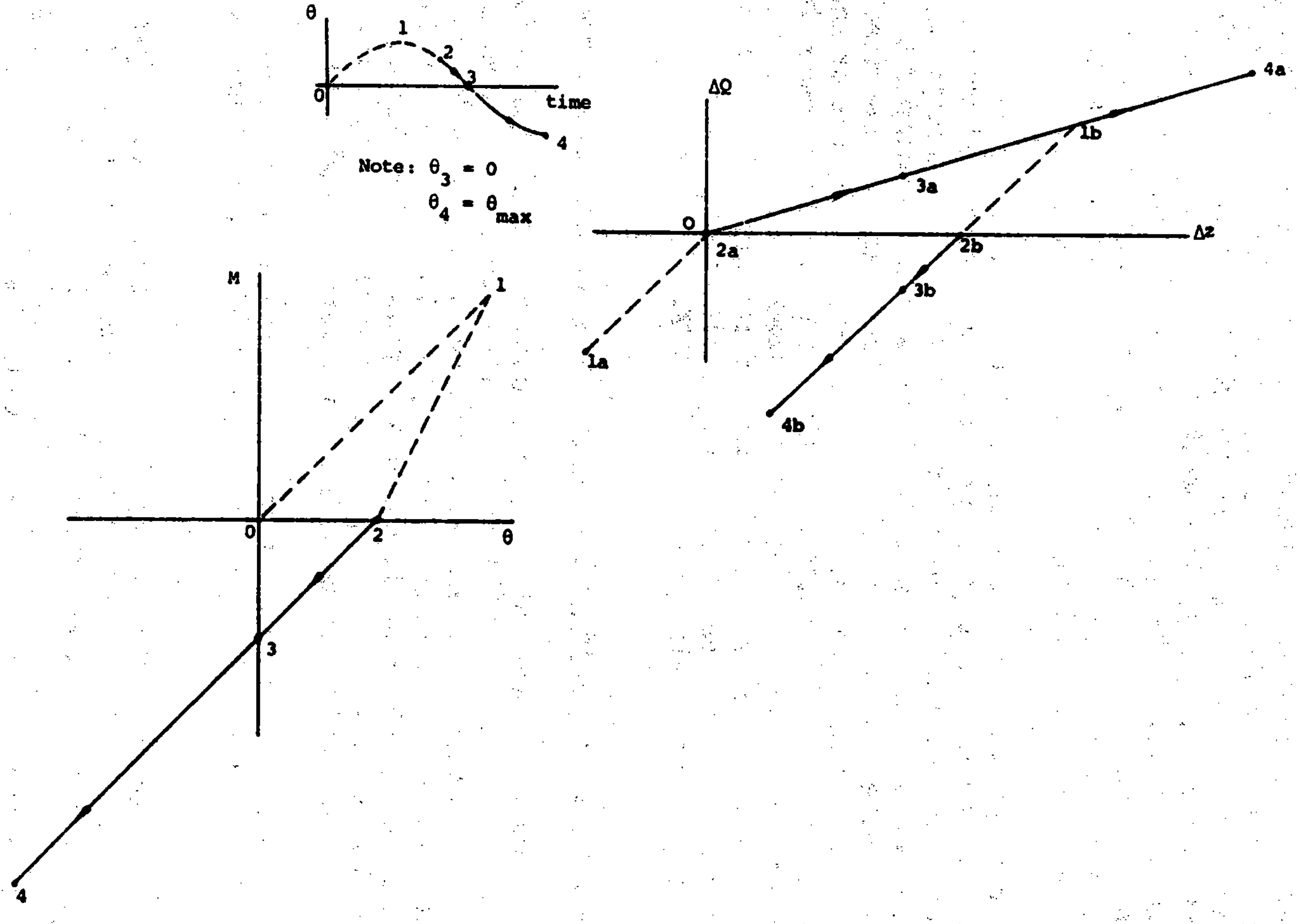
θ
1
2
3
0
time
4
M
1
0
2
θ
3
4
ΔΩ
O
2a
1a
3a
1b
4a
Δz
2b
3b
4b

Note: $\theta_3 = 0$
$\theta_4 = \theta_{max}$

Fig. 15 Response over interval 2-3-4.

Continued excitation of rotational amplitude θ_{max} leads to the Q-z and M-θ diagrams shown in Figs. 16 and 17.* Note that the M-θ curve of Fig. 16 stiffens as it tends toward the stabilized response (line X-Y) of slope K_θ associated with equal unload-reload pile reactions (line X-Y of Fig. 17 of slope $k_{u/r}$) acting about a centrally located axis of rotation. Corresponding to the two to three cycles of transient behavior, energy is absorbed due to the aforementioned mechanism of response. (The hysteresis losses associated with the M-θ loops is not due to material damping.) Furthermore, a permanent displacement develops as characterized by the difference in the z coordinates of points 0 and the X-Y line at $Q=Q_0$ of Fig. 17.

Given this understanding of the stiffening in rotational resistance, the development of a permanent rotationally induced settlement, and the existence of a pile group mechanism for energy absorption, all associated with transient behavior, one is better equipped to deal with the simpler stabilized behavior. Accordingly, one need not consider large amounts of permanently induced settlement or energy loss. Furthermore, the stabilized stiffness K_θ can be assessed based on Equation 6 in which k is the unload-reload value $k_{u/r}$ and r is in relation to a symmetrically located axis of rotation. For such work, one need only know the variation in $k_{u/r}$ with $\Delta z_{u/r}$ (see Fig. 5) as assessed, for example, with program ROSE CREEK.

Stabilized Rotational Stiffness of Pile Groups at Rose Creek Bridge

The procedure presented herein was used to assess the variation in stabilized rotational stiffness of pile groups of the Rose Creek Bridge near Winnemucca, Nevada for comparison with reported (i.e. back calculated) values as determined from system ID evaluation of bridge response data from full-scale push-back quick release bridge tests (8). The free vibration data obtained in such tests spanned from ambient level conditions up to design level lateral loading.**

Figs. 18 and 19 present the soil profiles established from boring logs for Groups 3 and 4 along with associated values of unconfined

---

* The M-θ loops correspond to lines of two distinct slopes. One slope (e.g., of line 2-3-4) corresponds to the piles of row a and b, all moving along an unload-reload Q-z line of slope $k_{u/r}$. The other slope (e.g., line 4-5-6) corresponds to one row of piles moving along the backbone Q-z curve at slope k_L, while the other moves along an unload-reload line of slope $k_{u/r}$.

** To obtain bridge test data, the bridge was laterally loaded to its release position approximately forty times at each load amplitude. Therefore, while free vibration response ensued, the effective stiffness of such free response data reflected the stabilized stiffness associated with the amplitude of deflection or rotation at the release position.

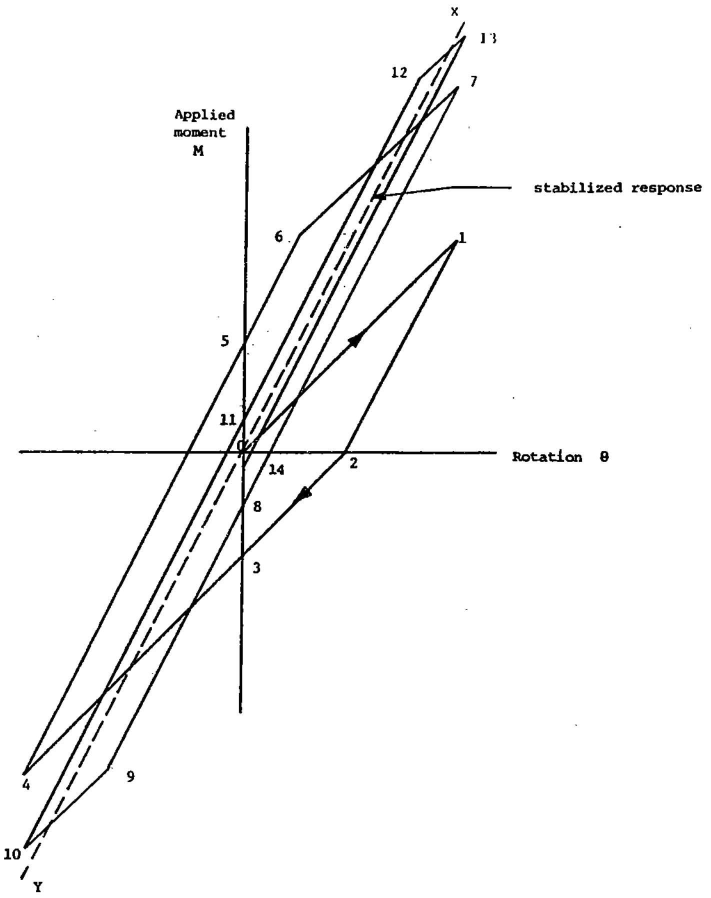

Fig. 16 M-θ response of a two row pile group under uniform rotational excitation.

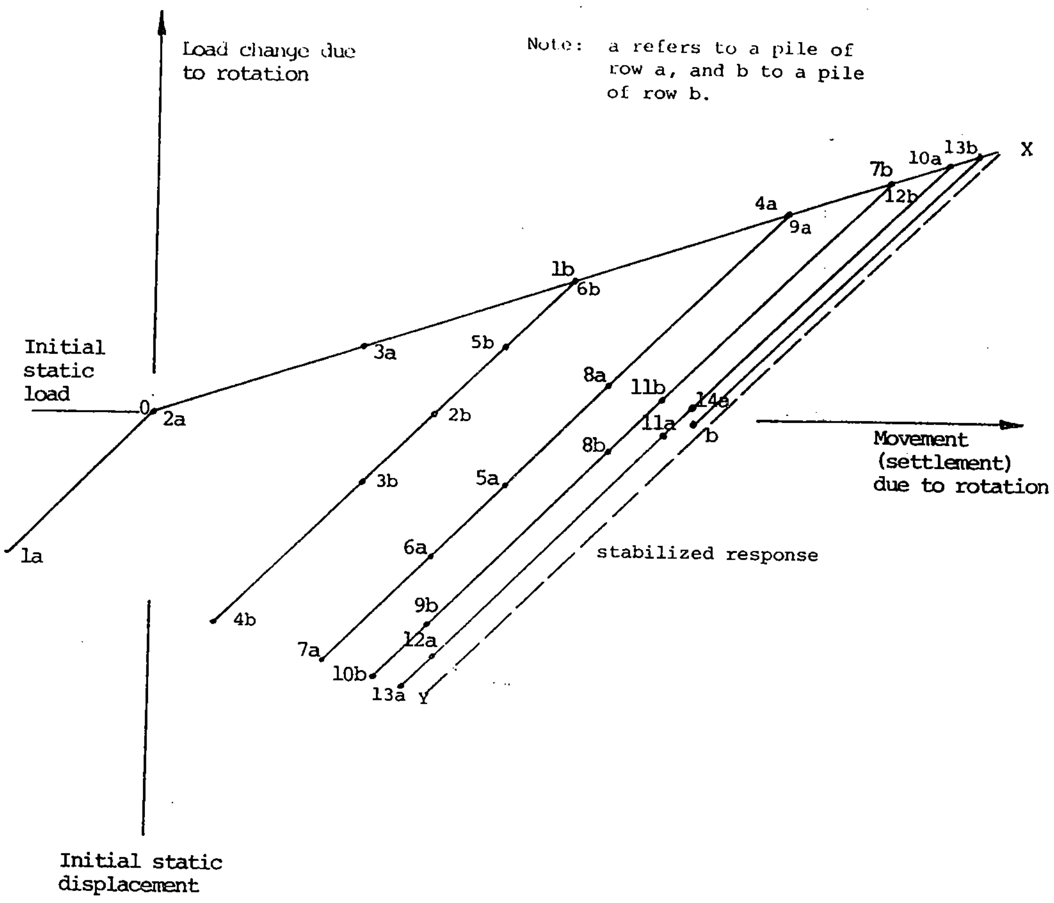

Note: a refers to a pile of row a, and b to a pile of row b.

Fig. 17 Q-z response of a two row pile group under uniform rotational excitation.

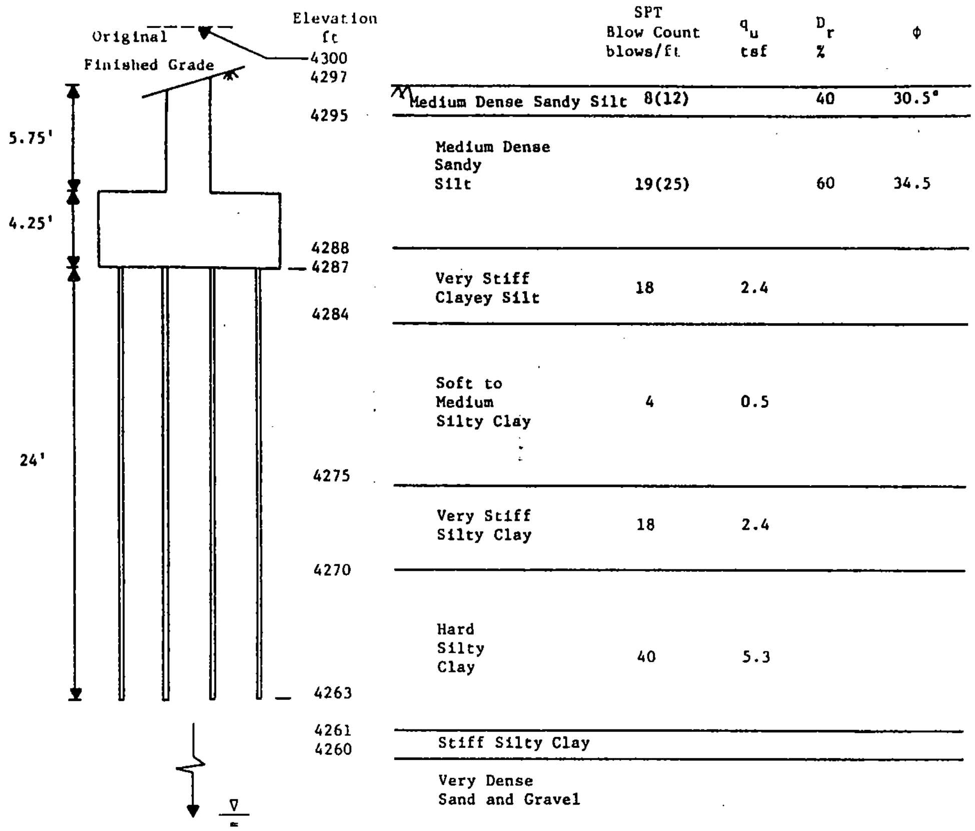

Original
Finished Grade
Elevation ft
4300
4297
4295
4288
4287
4284
4275
4270
4263
4261
4260
5.75'
4.25'
24'
SPT Blow Count blows/ft
q_u tsf
D_r %
ϕ
Medium Dense Sandy Silt 8(12) 40 30.5°
Medium Dense Sandy Silt 19(25) 60 34.5
Very Stiff Clayey Silt 18 2.4
Soft to Medium Silty Clay 4 0.5
Very Stiff Silty Clay 18 2.4
Hard Silty Clay 40 5.3
Stiff Silty Clay
Very Dense Sand and Gravel

Fig. 18 Soil profile for Pile Group 3.

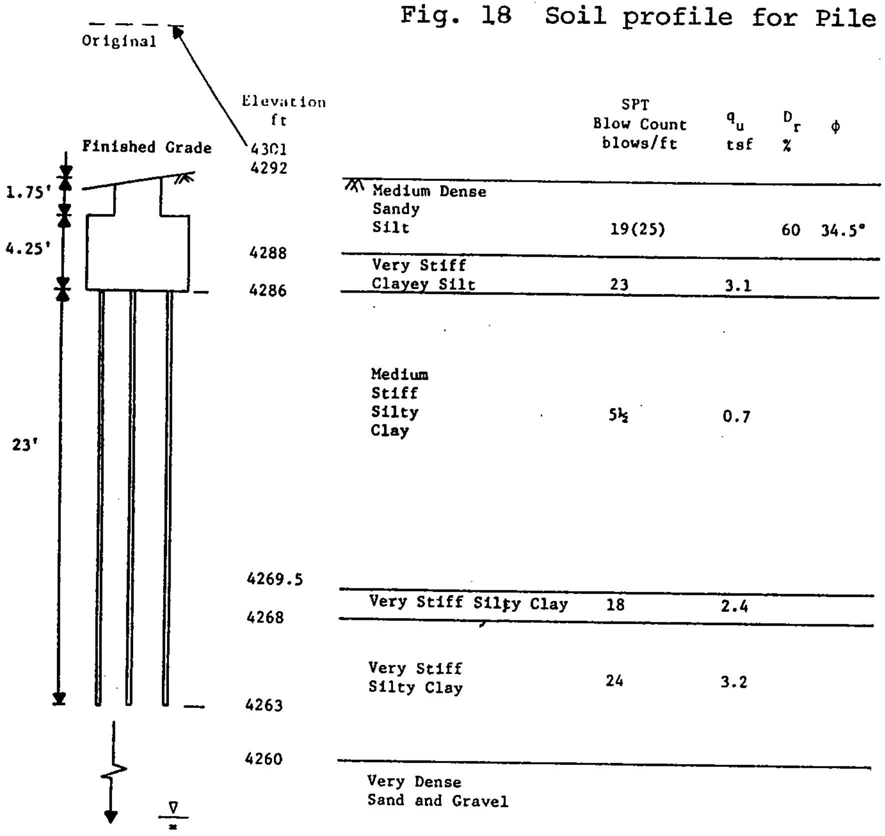

Original
Finished Grade
Elevation ft
4301
4292
4288
4286
4269.5
4268
4263
4260
1.75'
4.25'
23'
SPT Blow Count blows/ft
q_u tsf
D_r %
ϕ
Medium Dense Sandy Silt 19(25) 60 34.5°
Very Stiff Clayey Silt 23 3.1
Medium Stiff Silty Clay 5½ 0.7
Very Stiff Silty Clay 18 2.4
Very Stiff Silty Clay 24 3.2
Very Dense Sand and Gravel

Fig. 19 Soil profile for Pile Group 4.

compressive strength q_u (=2c) or relative D_r density of the soil.* (Soil profils for Groups 1 and 2 are given in Ref. 4.) Groups 1 and 4 are a rectangular pattern of 5 rows of 3 piles, while Groups 2 and 3 are 5 rows of 4 piles. All piles are spaced at 3 ft. on center. The stabilized axis of each group (for transverse excitation of the bridge) is taken through the middle row at the bottom of the pile cap. Note that the pile cap is embedded (6 ft. for Groups 1 and 4 and 10 ft. for Groups 2 and 3).

All piles are pipe piles 12.75 in. in diameter by 3/8 in. thick that have been driven with a closed end and backfilled with concrete. Based on a reported concrete compressive strength of 4032 psi, the AE value for the steel and concrete cross section is 8.322×10^5 kips. The dead load, on the other hand, is 58.6 kips per pile in Groups 1 and 4 and 55 kips in Groups 2 and 3.

Table 1 represents a tabulation of soil data relative to Pile Group 4 in preparation for the assessment of axial pile stiffness $k_{u/r}$ as a function of pile top displacement Δz using program ROSE CREEK. In reference to Table 1, note that there are 6 elements of various length chosen on the basis of the occurrence of soil boundaries or Coyle-Reese zones (i.e., A,B,C over depths 0-10, 10-20, and > 20 ft.) or the desire to keep to the segment length to a reasonable value (maximum of, say, 5 to 7 ft.). Note that segment 6 is taken to depth 10 ft. corresponding to the Coyle-Reese t-z curve A and segments 5 and 4, still of the same medium stiff silty clay coincide with the 10-20 ft. depth associated with curve B, while below 20 ft., segments 3, 2 and 1 reflect different soils. The elements are numbered 1 through 6 going up the pile in accordance with the sequence in which they are considered.

Corresponding to the very stiff silty clay at the pile point, ε_f for point resistance was taken as 4% and P' as 1/8 thus, yielding a value of z_{pr} (Equation 27) of 0.06375 in.** Point capacity $Q_{p,net}$ (= $9_c A_p$) is 25.54 kips while the maximum unload ΔQ_p (equal to Q_p for dead load conditions in Table 2) is 13.70 kips. Given that P' is 1/8, $\beta_{u/r}$ and R-1 for point response are 1 and 2.807 respectively based on Equations 21 and 29 (and $\beta = 7$ from Equation 28). Values of $\beta_{u/r}$ = 5.67 ($\beta = 9$) and R-1 = 0.6674 are applicable to all shear stress transfer curves (A,B, and C).

---

* q_u in tsf is taken equal to N/7.5 after Terzaghi and Peck. (See Fig. 4 on p. 7.1-87 of Ref 11.) Evaluation of ϕ based on N is after Peck Hanson and Thornburn (13).

** The same values of ε_f and P' for point resistance were adopted for piles of Groups 1-3.

Table 1

Soil Data for Pile Group 4

	Pile Segment	Elev. ft.	Depth ft.	L ft.	Curve	c ksf	α^{+}	ζ^{++}	τ_{ult} ksf	m^{+++}
Med. Stiff Silty Clay	6	4286-4282	6-10	4	A	0.7	0.9	0.53	0.33	477
	5	4282-4272	10-15	5	B	0.7	0.9	0.85	0.53	447
	4	4277-4272	15-20	5	B	0.7	0.9	0.85	0.53	447
	3	4272-4269.5	20-22.5	2.5	C	0.7	0.9	1.0	0.72	1070
V. Stiff	2	4269.5-4268	22.5-24	1.5	C	2.4	0.4	1.0	0.96	1070
V. Stiff	1	4268-4263	24-29	5	C	3.2	0.4	1.0	1.28	1070

+ From "Average Curve for Concrete Piles" in Fig. 2, p. 7.2-196 of Ref. 12

++ = 0.53, 0.85 and 1.0 for curve A, B or C for depths 0-10, 10-20, >20 ft.

+++ $m = 1/\gamma_r = 447$ for curves A or B and 1070 for curve C

Providing program ROSE CREEK with the above required data and layer information from Table 1, values of Δz_p, ΔQ_p and Δz, ΔQ and $k_{u/r}$ obtained for different specified values of P_{PL} are listed in Table 2. (Note also the Q_p and Q_{ult} values obtained for load conditions.) The unload-reload axial pile stiffness curve for a pile of Group 4 shown in Fig. 20 was obtained by plotting $k_{u/r}$ vs. Δz values from Table 2. (To better highlight small deflection response, the curve was plotted in semilogrithmic form rather than as shown in Fig. 5b.)

Table 2 indicates the level at which the pile point completely unloads. This condition is also noted by an upper hash mark on the curve of Fig. 20 which coincides with a slight change in form of the $k_{u/r}$ vs. Δz variation. A lower hash mark appearing on the same curve indicates the limit of stabilized response as dictated by one of two conditions as noted in Fig. 21. First, there can be no further expansion of the Q-z unload-reload loop once Q reaches Q_{ult}.* The value of ΔQ_{limit} at pile top associated with this condition (Fig. 21a) is

$$\Delta Q_{limit} = 2\ (Q_{ult} - DL) \tag{38}$$

where DL is the dead load on the pile. The other condition corresponds to the lower end of the unload-reload loop reaching the tensional capacity T_{ult} of the pile for which

$$\Delta Q_{limit} = 2\ (DL + T_{ult})$$

or

$$\Delta Q_{limit} = 2\ (DL + Q_{ult} - Q_{p,net}) \tag{39}$$

given that T_{ult} is equal to the full shaft capacity Q_s while Q_{ult} is the shaft capacity plus point resistance,

$$T_{ult} = Q_s \quad ; \quad Q_s = \int \tau_{ult} dA_s \tag{40}$$

$$Q_{ult} = Q_{p,net} + Q_s \tag{41}$$

The value of ΔQ_{limit} is the lower of the values assessed on the basis of Equations 38 and 39. The associated values of Δz and $k_{u/r}$ for Group 4 indicated in Table 2 mark the end of the corresponding stabilized $k_{u/r}$ vs. Δz curve of Fig. 20.**

---

* While the stabilized unload-reload response shown earlier was characterized by a straight line (XY of Fig. 16), this was the secant slope of the associated loop.

** Beyond the Δz value associated with ΔQ_{limit} the Q-z travel path becomes horizontal (along Q_{ult} in Fig. 21a or the dotted line associated with T_{ult} in Fig. 21b) until rotation is reversed and Δz decreases. An example of such nonstable response evaluation is presented elsewhere (5).

Table 2

Pile Group 4: Results from Program ROSE CREEK

Unload-reload response

	Δz_p in	ΔQ_p kips	Δz in	ΔQ kips	$k_{u/r}$ kips/in
$1x10^{-8}$	$6.375x10^{-10}$	$2.554x10^{-7}$	$1.637x10^{-9}$	$4.492x10^{-6}$	2744
$1x10^{-5}$	$6.375x10^{-7}$	$2.554x10^{-4}$	$1.626x10^{-6}$	$4.440x10^{-3}$	2730
$1x10^{-4}$	$6.375x10^{-6}$	$2.554x10^{-3}$	$1.590x10^{-5}$	$4.265x10^{-2}$	2682
$1x10^{-3}$	$6.375x10^{-5}$	$2.554x10^{-2}$	$1.468x10^{-4}$	0.3637	2505
$3x10^{-3}$	$1.913x10^{-4}$	$7.662x10^{-2}$	$4.089x10^{-4}$	0.9542	2334
$1x10^{-2}$	$6.375x10^{-4}$	0.2554	$1.226x10^{-3}$	2.542	2073
$3x10^{-2}$	$1.913x10^{-4}$	0.7662	$3.307x10^{-3}$	5.912	1787
0.10	$6.385x10^{-3}$	2.554	$9.875x10^{-3}$	14.41	1460
0.30	$1.978x10^{-2}$	$\underline{7.662}$ +	$2.791x10^{-2}$	$\underline{32.67}$ ++	1171
0.5364	$4.015x10^{-2}$	13.70	$5.350x10^{-2}$	53.00	991
0.70	$6.100x10^{-2}$	13.70	$7.700x10^{-2}$	64.57	829

Load response

0.5364	0.07589	13.70	0.09055	58.60 = DL
1	0.5100	25.54	0.5297	79.81 = Q_{ult}

+ Tip unloaded

++ End of stabilized response, ΔQ_{limit} reached where

$\Delta Q_{limit} = 2(Q_{ult}-DL) = 2(79.81-58.60) = 42.44$

vs

$\Delta Q_{limit} = 2(DL+Q_{ult}-Q_{p,net}) = 2(58.60+79.81-25.54) = 225.74$

Use 42.44 kips

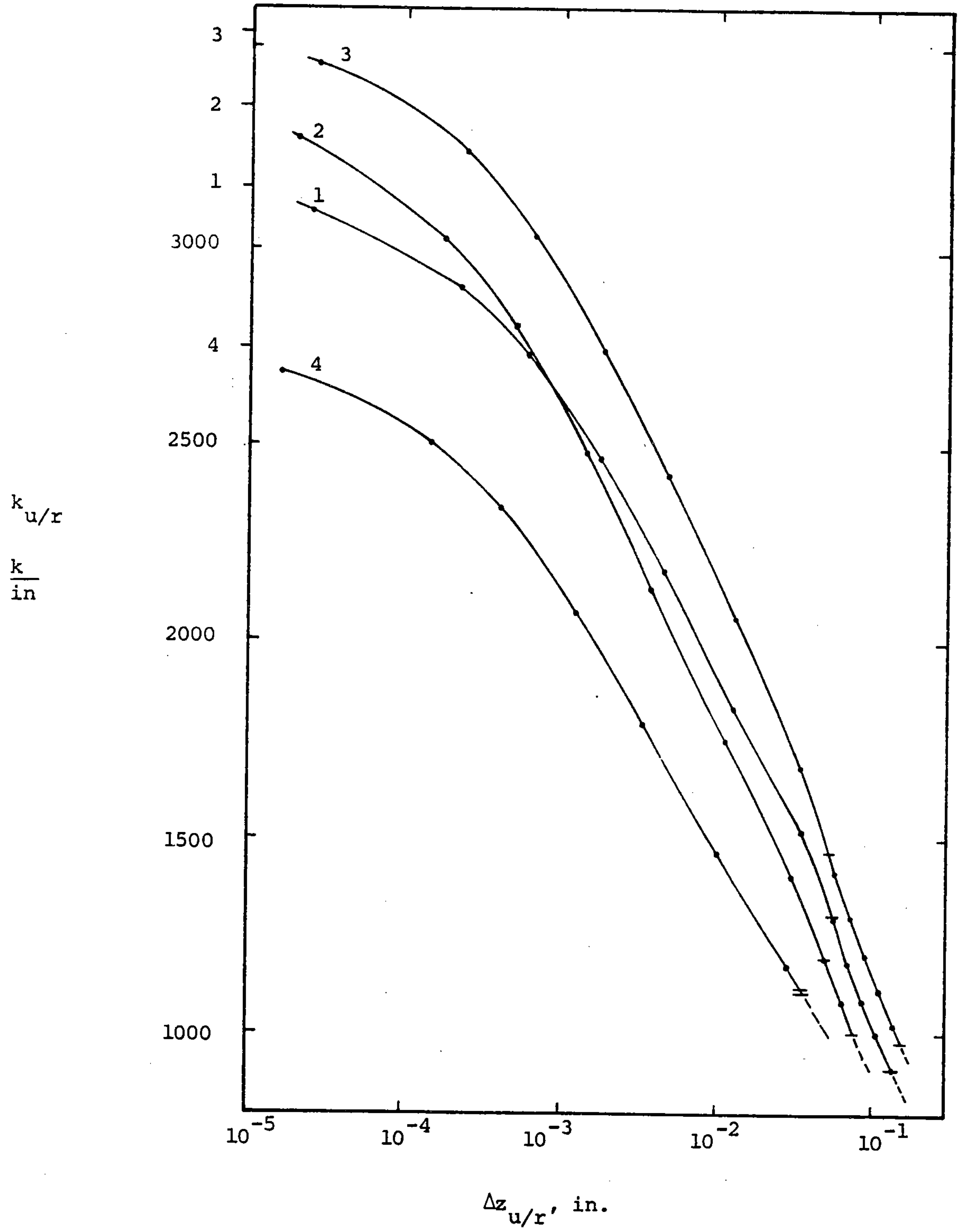

Fig. 20 Axial pile stiffness $k_{u/r}$ vs. $\Delta z_{u/r}$ curves for piles of Groups 1-4.

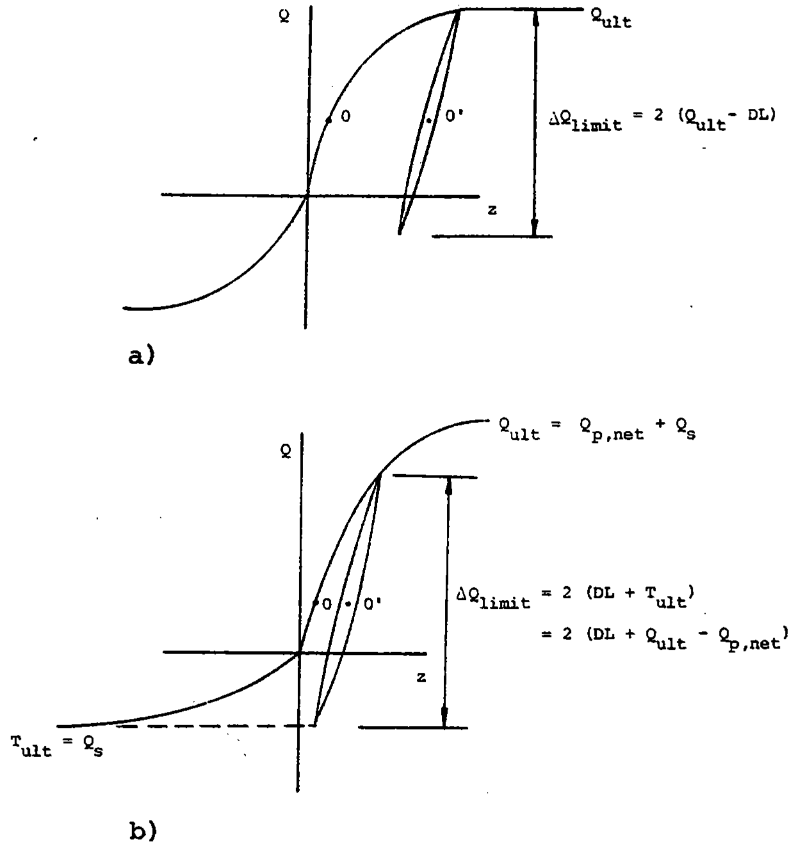
Q
Q_{ult}
O
O'
$\Delta Q_{limit} = 2\ (Q_{ult} - DL)$
z
a)
Q
$Q_{ult} = Q_{p,net} + Q_s$
O
O'
$\Delta Q_{limit} = 2\ (DL + T_{ult})$
$= 2\ (DL + Q_{ult} - Q_{p,net})$
z
$T_{ult} = Q_s$
b)

Fig. 21 Limit of stabilized response due to ΔQ_{limit} a) associated with Q_{ult} and b) T_{ult}.

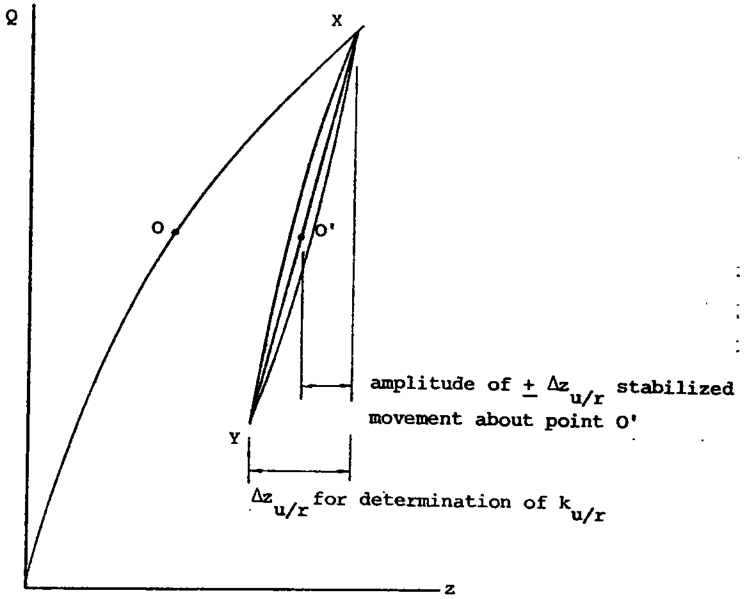
Q
X
O
O'
amplitude of $\pm \Delta z_{u/r}$ stabilized movement about point O'
Y
$\Delta z_{u/r}$ for determination of $k_{u/r}$
z

Fig. 22 Relationship between $\Delta z_{u/r}$ for evaluation of $k_{u/r}$ and amplitude of pile head movement $\pm \Delta z_{u/r}$.

Curves of the axial pile stiffness variation for piles of Groups 1,2, and 3 are also shown in Fig. 20. (A short horizontal line, one for each curve, located on the left hand axis indicates the initial tangent value of $k_{u/r}$ for so called "ambient" conditions.) All such curves reflect virgin response and should there be any past history of cyclic loading to a level of stabilized deflection Δz and stiffness $k_{u/r}$ then the pile's subsequent response would be as follows: upon subsequent cylic loading the $k_{u/r}$ vs. Δz path would be a horizontal straight line at the value of $k_{u/r}$ from previous loading all the way across to the virgin curve (at Δz from previous loading) and then down the virgin curve.

Given the nonlinear variation in unload-reload axial pile stiffness shown in Fig. 20, it is a simple matter to assess the variation in stabilized rotational stiffness K_θ of the group. For a specified value of rotation θ, one calculates the pile top displacements Δz of the various rows (Equation 4), and then establishes associatd values of $k_{u/r}$ based on Fig. 20. Thereafter K_θ is evaluated using Equation 6. This is repeated for several values of θ and the (K_θ, θ) values plotted.

A note of caution should be sounded regarding the relationship between the unload-reload amplitude of axial pile displacement $\pm \Delta z_{u/r}$ and the value of $\Delta z_{u/r}$ for the determination of the stiffness $k_{u/r}$. As shown in Fig. 22, $\Delta z_{u/r}$ for the assessment of the secant stiffness $k_{u/r}$ of the stabilized unload-reload loop is twice the value of the amplitude of pile head displacement $\pm \Delta z_{u/r}$ associated with rotation θ (Equation 4).

The aforementioned process is demonstrated in Appendix G relative to Group 4 calculations. The resulting curve is shown in Fig. 23 along with data points representing recorded (i.e., back calculated) field response. A curve and data points for Group 1 are also included. Fig. 24 presents a similar comparison of predicted versus observed response for Groups 2 and 3.* Note that the curves are shown to end abruptly at an upper limit of rotation θ corresponding to the outer pile row reaching its limit of stabilized deflection Δz (and stiffness $k_{u/r}$) associated with the lower hash mark of the $k_{u/r}$ curve of Fig. 20. Likewise horizontal lines are shown on the left-hand axis corresponding to rotational stiffnesses K_θ associated with the initial tangent stiffnesses $k_{u/r}$ of Fig. 20. Ambient level values from field response data are also shown and they are decidedly lower than the predicted values. This indicates that the pile groups have been loaded in the past such that the ambient level field results no longer represent virginal response.**

---

* Note that Groups 1 and 4 and, separately, 2 and 3 have similar soil conditions and the same number of piles in the group.

** This same bridge was tested in an earlier series to much smaller load amplitudes. See Ref. 2.

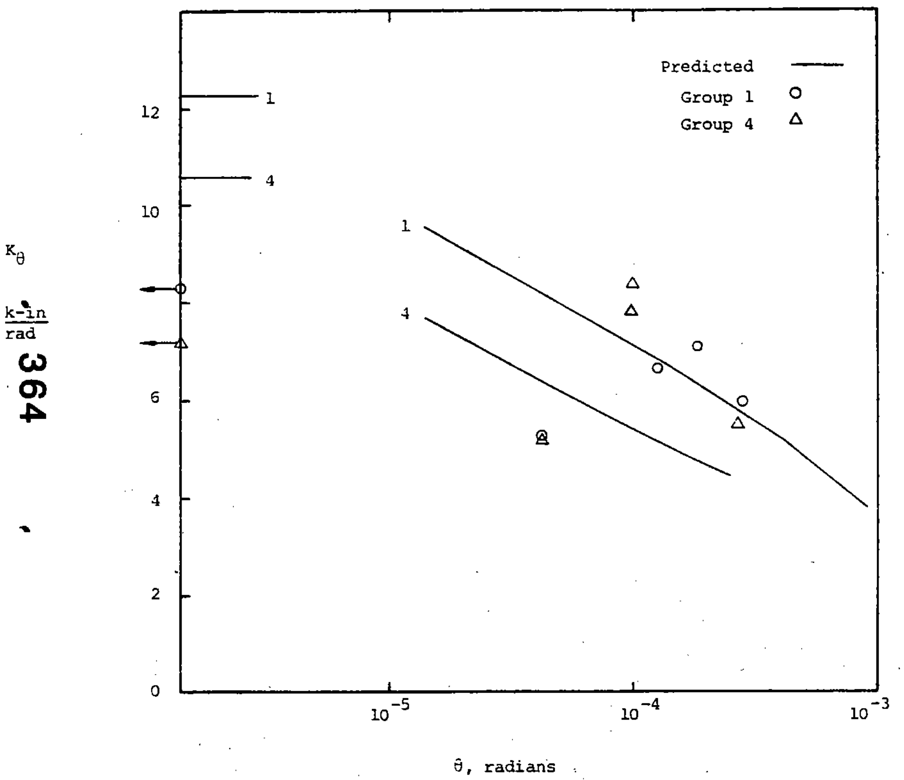

Fig. 23 Stabilized rotational stiffness K_θ vs. θ for Groups 1 and 4.

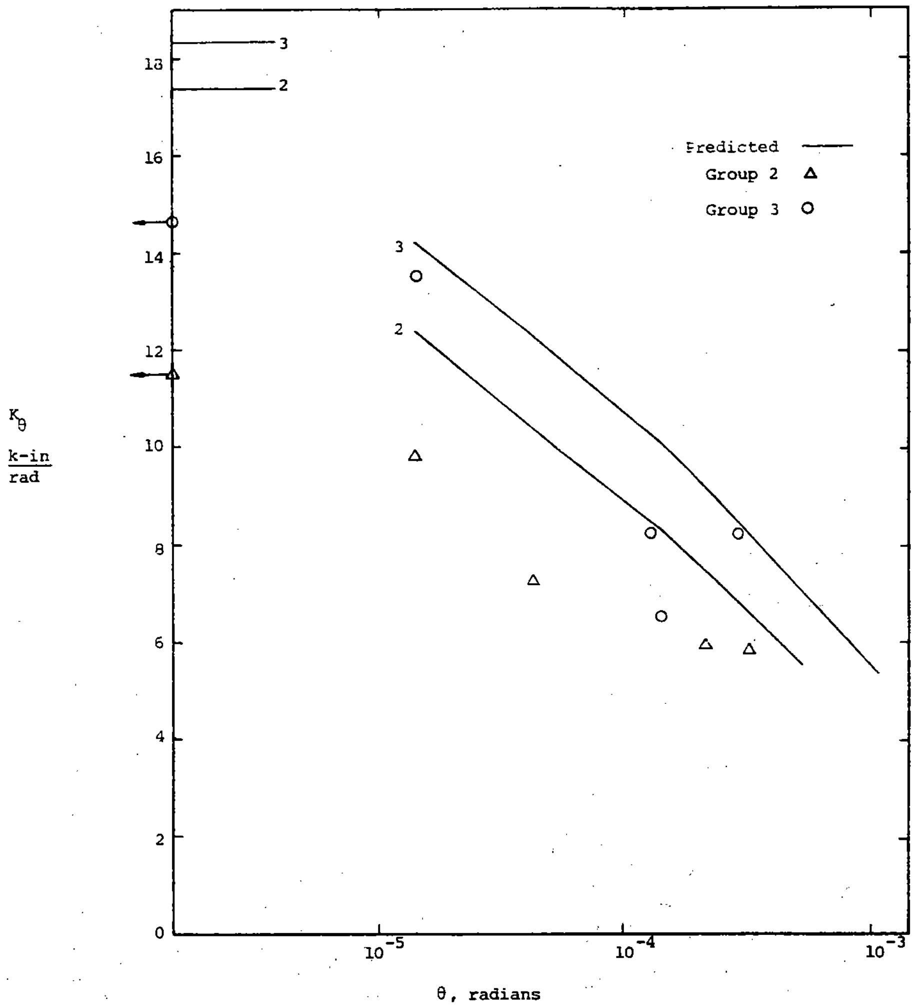

Fig. 24 Stabilized rotational stiffness K_θ vs. θ for Groups 2 and 3.

Given the uncertainty* and the scatter associated with the field data, the predicted response appears to be quite reasonable. Certainly, the predicted response yields a trend to the data that would be hard to distinguish otherwise. Ignoring the ambient level field data (because it no longer reflects virgin response), the predicted curves for Groups 1 and 4 in Fig. 23 seem to be approximately correct. Curves 2 and 3 in Fig. 24, on the other hand, seem to overpredict the variation in field related rotational stiffness by a constant value of approximately 1.8 x 10^7 k-in/rad. This amounts to a variation that is from 15 to 30% too high over the range in rotational amplitude considered. While there are a number of variables that might be changed to improve the foregoing comparison, it should be noted that the predicted results presented herein represent a first attempt using only commonly available soil boring data.

Summary and Conclusions

A method for the evaluation of the nonlinear variation in stabilized rotational stiffness of a pile group has been presented. Stabilized rotational stiffness develops under uniform excitation after two to three cycles of transient response, assuming nonfailing soil-pile conditions prevail. (Nonstable response is treated elsewhere [5].) The transient response is characterized by a stiffening in rotational resistance, a decrease in damping associated with system (not material) behavior and a permanent rotationally induced settlement of the group. The stabilized response corresponds to equal unload-reload axial pile responses about a centrally located axis of rotation of a symmetric or regular arangement of piles. Knowing the variation in unload-reload axial pile stiffness $k_{u/r}$ as a function of displacement $\Delta z_{u/r}$ the variation in the rotational stiffness K_θ of the group with θ, the amplitude of rotation, is easily assessed.

To assess unload-reload axial pile stiffness, one relies on existing techniques from both foundation engineering (t-z analysis) and soil dynamics (Ramberg-Osgood formulation) that have been modified and integrated as required. The actual evaluation requires only a few formulas and a very simple interactive program. Furthermore, the required input can be assessed based on standard subsurface investigation data (e.g., soil borings with blow counts).

The method has been used to assess the variation in rotational stiffness of pile groups of the Rose Creek Bridge and this variation compared with values back calculated from system ID analysis of full scale bridge test results. Given the scatter and uncertainty associated with the experimental (i.e., the back calculated) results, the method appears to be quite suitable in light of its simplicity and intended use (i.e., by the bridge designer for the seismic analysis of highway bridge response).

---

* Reevaluation using more refined system ID techniques have resulted in many K_θ values for Groups 2 and 3 that are approximately one-half of earlier reported values. At the same time, values for Groups 1 and 4 have changed moderately. It is unclear at this time whether system ID techniques can be further refined and what such changes will cause.

At present the method has been formulated and demonstrated for piles in layered clay. Additional work will be required before the t-z and q-z responses of sand are incorporated. Note however, that for a pile with its point in a bearing stratum (e.g., dense sand, gravel or rock), it may be sufficient to treat only the point load-point displacement behavior and the compressibility of the pile ignoring all t-z response along the shaft (i.e., $Q = Q_p$, $z = z_p + z'$, $z' = QL/AE$). In that instance, the simple point load-point displacement formulation given herein (for relatively insignificant tip response, as occurs in clay) is both inappropriate and inaccurate.

Acknowledgements

This work was undertaken as part of a larger study entitled "The Lateral and Rotational Stiffness of Pile Foundations for the Seismic Analysis of Highway Bridges" funded under NSF contract No. CEE8206224. Such support is gratefully acknowledged.

References

1. Douglas, B.M. and G.M. Norris, "Bridge Dynamic Tests: Implications for Seismic Design," *Journal of Technical Topics in Civil Engineering*, ASCE, Vol. 109, No. 1, April 1983, pp. 1-22.

2. Douglas, B.M. and W.H. Reid, "Dynamic Tests and System Identification of Bridges," *Journal of the Structural Division*, ASCE, Vol. 108, No. ST10, October 1982, pp. 2295-2312.

3. Norris, G.M., and R.L. Sack, "Evaluation of the Lateral Stiffness of Pile Groups for Seismic Analysis of Highway Bridges: Part A," *Proceedings of the 22nd Symposium on Engineering Geology and Soils Engineering*, 1986, pp. 323-343.

4. Norris, G.M. and R.L. Sack, "Evaluation of the Lateral Stiffness of Pile Groups for Seismic Analysis of Highway Bridges: Part B," *Proceedings of the 22nd Symposium on Engineering Geology and Soils Engineering*, 1986, pp. 344-363.

5. Norris, G.M. "Nonstable Rotational Stiffness of a Pile Group," *Proceedings of the Third U.S. National Conference on Earthquake Engineering*, EERI, 1986 (to be held August 1986).

6. Coyle, H.M. and L.C. Reese, "Load Transfer of Axially Loaded Piles in Clay," *Journal of the Soil Mechanics and Foundations Division*, ASCE, Vol. 92, No. SM2, March 1966, pp. 1-26.

7. Richart, F.E., "Nonlinear Soil Models for Irregular Cyclic Loadings," *Journal of the Geotechnical Engineering Division*, ASCE, Vol. 105, No. GT6, June 1979, pp. 715-726.

8. Douglas, B.M. and J.A. Richardson, "Maximum Amplitude Dynamic Tests of a Highway Bridge," Proceedings of the Eighth World Conference on Earthquake Engineering," 1984, Vol. VI, pp 889-896. (Now with revised values available from The Center for Civil Engineering Earthquake Research, University of Nevada, Reno, Nevada 89557.)

9. Kraft, LM., R.P. Ray and T. Kagawa, "Theoretical t-z Curves," *Journal of the Geotechnical Engineering Division*, ASCE, Vol. 197, No. GT11, November 1981, pp. 1543-1561.

10. Poulas, H.G. and E.H. Davis, *Pile Foundation Analysis and Design*, John Wiley and Sons, New York, 1980 (see Fig. 2.8 on p. 13 after Robinsky and Morrison).

11. U.S. Navy, NAVFAC DM-7.1, *Design Manual: Soil Mechanics*, U.S. Government Printing Office, Washington D.C., 1982.

12. U.S. Navy, NAVFAC DM-7.2, *Design Manual: Foundations and Earth Structures*, U.S. Government Printing Office, Washington D.C., 1982.

13. Peck, R.B., W.E. Hanson and T.H. Thornburn, Foundation Engineering, Second Edition, John Wiley and Sons, New York, 1974.

14. Duncan, J.M. and A.L. Buchignani, "An Engineering Manual for Settlement Studies," ITTE Report, University of California, Berkeley, 1976.

15. Seed, H.B. and I.M. Idriss, "Soil Moduli and Damping Factors for Dynamic Response Analyses," EERC Report No. 70-10, University of California, Berkeley, 1970.

APPENDIX A

RELATIONSHIP BETWEEN STRESS, PRESSURE, AND LOAD LEVELS FOR UNDRAINED LOADING OF SATURATED CLAY

The pressure-settlement q-z relationship for a loaded area of clay is nonlinear as shown, for example, in Fig. A.1. Depending on the depth of the embedment D of the loaded area, the net ultimate bearing capacity q_{net} of a circular or square foundation of width B ranges from 1.2 (5.14c) = 6.2c for shallow or surface conditions to 9c for a deep foundation ($D \geq 4B$). Note that q_{net} is independent of the width B of the foundation.

As demonstrated in Fig. A.2 relative to the simple yet conservative treatment of the bearing capacity of a shallow strip foundation ($q_{net} = 4c < 5.14c$), the pressure level q/q_{net} at the base of the foundation is equal to the stress level σ_d/σ_{df}, in the clay in undrained loading. Given that the load on the foundation Q is equal to qA, one has that the load level, Q/Q_{net}, is also the same, i.e.,

$$Q/Q_{net} = q/q_{net} = \sigma_d/\sigma_{df} \tag{A.1}$$

This same argument applies equally to a deep foundation. Hence, Equation A.1 gives rise to Equation 17.

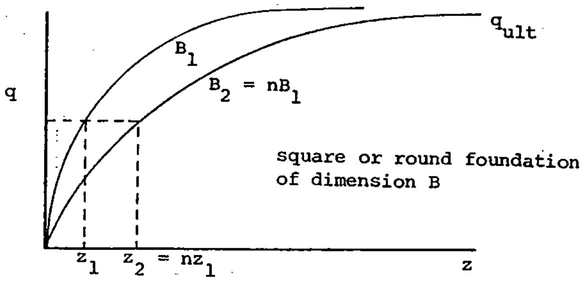

Fig. A.1 Pressure-settlement curve for undrained loading of saturated clay.

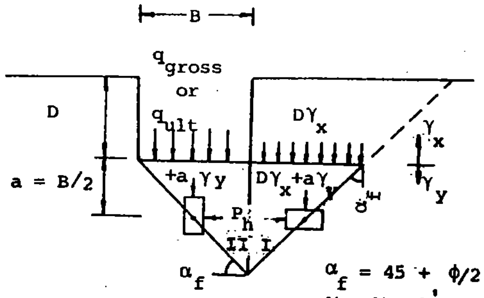
B
q_{gross} or q_{ult}
D
$D\gamma_x$
γ_x
γ_y
$a = B/2$
$+a\gamma_y$
$D\gamma_x + a\gamma_y$
P_h
II
I
σ_h
α_f

strip footing

$D\gamma_x$ = overburden pressure at foundation level

$\alpha_f = 45 + \phi/2 = 45^\circ$

γ_x, $\gamma_y = \gamma'$ or γ depending of location of water table

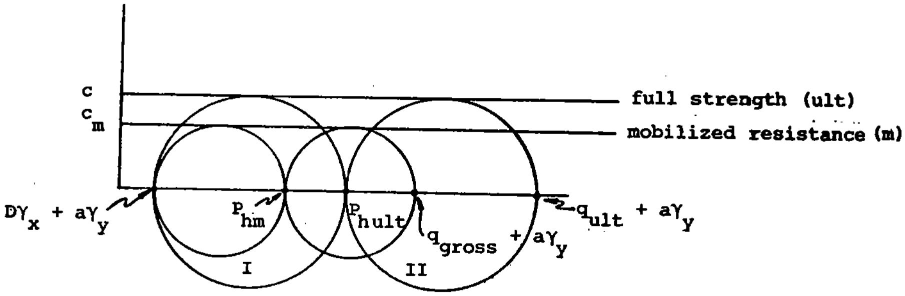
c
c_m
full strength (ult)
mobilized resistance (m)
$D\gamma_x + a\gamma_y$
P_{hm}
P_{hult}
$q_{gross} + a\gamma_y$
$q_{ult} + a\gamma_y$
I
II

ultimate condition - strength c

$$(q_{ult} + a\gamma_y) = (D\gamma_x + a\gamma_y) + 4c$$
$$q_{ult} = D\gamma_x + 4c$$
$$q_{net} = q_{ult} - D\gamma_x$$
$$q_{net} = 4c$$

design level condition - mobilized resistance c_m

$$(q_{gross} + a\gamma_y) = (D\gamma_x + a\gamma_y) + 4c_m$$
$$q_{gross} = D\gamma_x + 4c_m$$
$$q = q_{gross} - D\gamma_x$$
$$q = 4c_m$$

pressure level

stress level

$$\frac{q}{q_{net}} = \frac{4c_m}{4c} = \frac{c_m}{c} = \frac{\sigma_d/2}{\sigma_{df}/2} = \frac{\sigma_d}{\sigma_{df}}$$

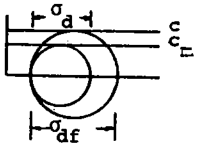
σ_d
c
c_m
σ_{df}

Fig. A.2 Relationship between undrained stress and pressure level for a strip footing in clay.

APPENDIX B

RELATIONSHIP BETWEEN SOIL STRAIN AND DISPLACEMENT

A commonly used expression for the undrained settlement z beneath a loaded area on (or in) saturated clay is

$$z = \frac{q\,B}{E}(1 - \nu^2)I \qquad \text{(B.1)}$$

where the Poisson's ratio ν is equal to one-half, E is the equivalent linear Yong's modulus corresponding to the stress (or pressure) level in the clay, and I is the so-called influence factor (reflecting the foundation shape and rigidity, its relative embedment, and the point on the foundation [center edge, corner, etc.] of interest) as assessed from the theory of elasticity. Equation B.1 can be used to assess nonlinear response provided E is chosen accordingly (i.e., based on the stress or pressure level in the clay). One will note from Equation B.1 that z is proportional to B provided, of course, that one compares the nonlinear displacements of different size footings at the same pressure or stress level in the clay so that E remains the same. This is shown, for example, in Fig. A.1 where z is proportional to B at the same pressure q and, hence, pressure level q/q_{net} (since q_{net} is independent of B). If, on the other hand, one normalizes the displacement z by width B of the foundation, then a single curve results. See Fig. B.1. That z/B is equal to the soil strain ε at stress level σ_d/σ_{df} or at pressure level q/q_{net} relative to undrained point load-point displacement response in clay is shown below.

Rearranging Equation B.1 and introducing q_{net}/c, where q_{net} is equal to 9c, yields

$$\frac{z}{B} = \frac{q_{net}}{c}\,\frac{c}{q_{net}}\,\frac{q}{E}(1 - \nu^2)I = \frac{9c}{c}\,\frac{c}{E}\,\frac{q}{q_{net}}\,(1 - \nu^2)I$$

or

$$\frac{z}{B} = \frac{q}{q_{net}}\,\frac{9x}{E/c} \quad ; \quad x = (1 - \nu^2)\,I \qquad \text{(B.2)}$$

Given that $I = I_0 I_1 = 0.50\,(0.60) = 0.30$ for a deep foundation (see, e.g., the chart by Janbu et al. on page 23 of Ref. 14) and $(1 - \nu^2) = (1 - 0.5^2) = 0.75$, x is equal to 0.225. If one takes the vertical axis of Fig. B.1 to be normalized by q_{net}, then Equation B.2 represents the form of such a curve where secant slope (E/c)/9x varies with E as a function of the stress level or strain in the soil. See Fig. B.2.

Consider now the stress-strain relationship of the soil, i.e.,

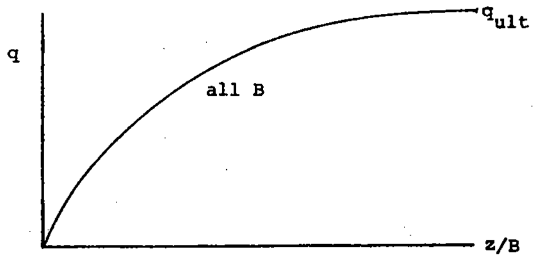

Fig. B.1 Pressure-normalized displacement response for undrained loading of saturated clay.

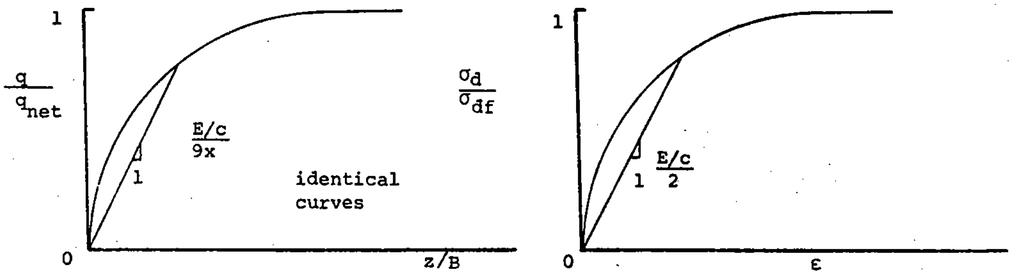

Fig. B.2 Relationship between the pressure level-normalized displacement curve and the stress level-strain curve.

$$\varepsilon = \frac{\sigma_d}{E} = \frac{\sigma_{df}}{c}\,\frac{c}{\sigma_{df}}\,\frac{\sigma_d}{E} = \frac{2c}{c}\,\frac{c}{E}\,\frac{\sigma_d}{\sigma_{df}}$$

$$\varepsilon = \frac{\sigma_d}{\sigma_{df}}\,\frac{2}{E/c} \qquad \text{(B.3)}$$

Note that Equation B.3 represents the nonlinear form of the normalized stress-strain curve having a variable secant slope of (E/c)/2. Equating stress and pressure levels (see Equation A.1) from Equations B.2 and B.3 yields

$$\frac{q}{q_{net}} = \frac{\sigma_d}{\sigma_{df}}$$

$$\frac{E/c}{9x}\,\frac{z}{B} = \frac{E/c}{2}\,\varepsilon$$

$$\frac{z}{B} = 4.5 \times \varepsilon$$

or

$$\frac{z}{B} = \varepsilon \qquad \text{(B.4)}$$

for x = 0.225. Equation B.4 is Equation 16 of the main text.

APPENDIX C

RELATIONSHIP BETWEEN STRESS, PRESSURE, AND LOAD LEVELS FOR SAND

For the pile point embedded in sand, Equation 16 may be used but Equation 17 should not. Instead, the load level ($Q_p/Q_{p,net}$) and the pressure level (q/q_{net}) are equal to the ratio of bearing capacity factors N_q/N_{qm}, i.e.,

$$Q_p/Q_{p,net} = q/q_{net} = N_q/N_{qm} \qquad (C.1)$$

where N_q and N_{qm} are the same expression for bearing capacity of a deep foundation evaluated for the full and mobilized friction angles of the sand (ϕ and ϕ_m) respectively. In turn, the mobilized friction angle ϕ_m expressed as a function of the stress level σ_d/σ_{df} and the full friction angle ϕ, as given in Fig. C.1, is

$$\tan^2(45 + \phi_m/2) = \frac{\sigma_d}{\sigma_{df}}[\tan^2(45 + \phi/2) - 1] + 1 \qquad (C.2)$$

Therefore, with a knowledge of the stress-strain curve of the sand at a confining pressure equal to the vertical effective stress $\bar{\sigma}_{vo}$ at the pile tip, one can assess corresponding points on the q-z and Q_p-z_p curves based on Equation 16 (z_p from ε), C.2 (ϕ_m from σ_d/σ_{df} and ϕ), and C.1 ($Q_p/Q_{p,net} = q/q_{net}$ from ϕ_m and ϕ). In addition, note that q_{net} in sand is equal to $\bar{\sigma}_{vo}N_q$; while $Q_{p,net}$ is given by Equation 12.

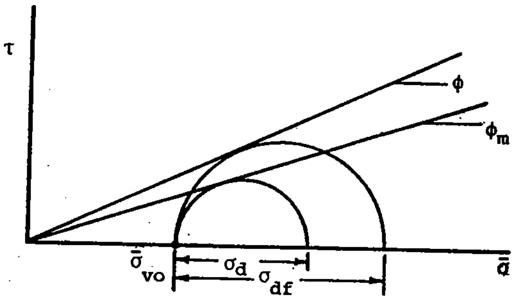

$$SL = \frac{\sigma_d}{\sigma_{df}} = \frac{\tan^2(45+\phi_m/2)-1}{\tan^2(45+\phi/2)-1}$$

C. 1 Relationship between mobilized friction and stress level for sand.

APPENDIX D

SMALL STRAIN t-z RESPONSE AND CORRESPONDING RAMBERG-OSGOOD FITTING PARAMETERS

Given that the t-z curves are to be used to consider small strain (i.e., seismic) response, it becomes important to appropriately assess their variation over this range. Unfortunately, data provided by Coyle and Reese for curves A, B, and C start well above this level of excitation making it necessary to reconstruct this range of the curves based upon reasoning. In doing so, one must realize that the curves represent an interface response and not purely soil behavior.

Consider the secant modulus of the τ-γ curve at a fifty percent stress level, i.e.,

$$G_{50} = \frac{\tau_{50}}{\gamma_{50}} = \frac{0.5\tau_{ult}}{\gamma_{50}} \quad ; \quad \gamma_{50} = P\gamma_f$$

$$G_{50} = \frac{0.5\tau_{ult}}{P\gamma_f} \tag{D.1}$$

such that

$$G_{50} = 160\ \tau_{ult} \text{ for } \gamma_f = 0.938\% \ (\gamma_{50} = 0.31\%) \text{ for curve C}$$

$$G_{50} = 67\ \tau_{ult} \text{ for } \gamma_f = 2.24\% \ (\gamma_{50} = 0.75\%) \text{ for curves A and B}$$

If one takes the ratio of G_{50}/G_o to be 0.15, corresponding to the G/G_o value for γ between 0.31 to 0.75% from the Seed and Idriss (15), shear modulus reduction curve, then the initial tangent modulus G_o is

$$G_o = G_{50}/(G_{50}/G_o) = \frac{0.5\ \tau_{ult}}{P\gamma_f(G_{50}/G_o)}$$

or

$$G_o \ (= \frac{160}{0.15}\ \tau_{ult}) = 1070\ \tau_{ult} \text{ for curve C}$$

$$G_o \ (= \frac{67}{0.15}\ \tau_{ult}) = 447\ \tau_{ult} \text{ for curves A and B}$$

Alternatively,

$$G_o = m\ \tau_{ult} \quad ; \quad m = \frac{0.5}{P\gamma_f(G_{50}/G_o)} \tag{D.2}$$

where m = 1070 for curve C and m = 447 for curves A and B.* Consequently, γ_r, as given by Equation 19, becomes

$$\gamma_r = \frac{\tau_{ult}}{G_o} = \frac{\tau_{ult}}{m\,\tau_{ult}}$$

or

$$\gamma_r = \frac{1}{m} \qquad \text{(D.3)}$$

Based on Equations D.2 and D.3, note that

$$\frac{\gamma_f}{\gamma_r}\ (= \gamma_f m) = \frac{0.5}{P(G_{50}/G_o)} \qquad \text{(D.4)}$$

and

$$\frac{\gamma_{50}}{\gamma_r}\ \left(= \frac{P\gamma_f}{\gamma_r}\right) = \frac{0.5}{(G_{50}/G_o)} \qquad \text{(D.5)}$$

or

$$\frac{\gamma_f}{\gamma_r} = 10 \quad ; \quad \frac{\gamma_{50}}{\gamma_r} = 3.33 \text{ for curves A, B, and C}$$

Based on Equation 22, a similar relationship holds relative to displacements, i.e.,

$$\frac{z_f}{z_r} = \frac{\gamma_f}{\gamma_r} \qquad \text{(D.6)}$$

$$\frac{z_{50}}{z_r} = \frac{\gamma_{50}}{\gamma_r} \qquad \text{(D.7)}$$

---

* The range in m is reasonable given that G_o = 1000 to 2300 c for undisturbed clay. Note also that m is less at shallow depths (curves A and B) corresponding to the greater amount of disturbance due to pile driving occurring there.

If, at this point, one lets $\gamma = \gamma_f$ in Equation 18, corresponding to stress level $\tau/\tau_{ult} = 1$, then

$$\beta = \frac{\gamma_f}{\gamma_r} - 1 \qquad \text{(D.8)}$$

where γ_f/γ_r is given by Equation D.4. Accordingly, $\beta = 9$ for curves A, B, and C.

Setting $\gamma = \gamma_{50}$ or $P\gamma_f$ (Equation 23) in Equation 18, corresponding to $\tau/\tau_{ult} = 0.50$, leads to an expression for R-1 of

$$R\text{-}1 = \log \left[\frac{2P\beta + 2P - 1}{\beta} \right] \Big/ \log(0.50) \qquad \text{(D.9)}$$

where R-1 is equal to 0.6674 for curves A, B, and C for the aforementioned values of P and γ_f. Knowing β and R-1, $\beta_{u/r}$ can then be evaluated based on Equation 21. As a result, $\beta_{u/r}$ is equal to 5.67 for curves A, B, and C.

While values of $\beta = 9$, R-1 = 0.6674, $\beta_{u/r} = 5.67$, and $\gamma_r = \gamma_f/10$ (also $z_r = z_f/10$) are appropriate for the Coyle-Reese curves A, B, C considered heretofore, the values of β, R-1, $\beta_{u/r}$ and γ_f/γ_r for other t-z curves in clay may be assessed using the equations given above if the values of P and G_{50}/G_o are provided.

Since G_o in sands is proportional to $(\bar{\sigma}_{vo})^{0.5}$ rather than τ_{ult}, a somewhat different formulation is required for t-z curves in sand.

APPENDIX E

PROGRAM ROSE CREEK

The following interactive program can be used to assess either unload-reload or backbone curve axial pile response. The user is prompted for various information as discussed in the text of the paper. Note that the units required are specified. Values of β for both point and side shear response should reflect unload-reload or load values depending on whether stabilized or backbone curve response is desired. Take the maximum point unload (MP in the listing) to be Q_p from dead load conditions when analyzing unload-reload behavior and $Q_{p,net}$ when analyzing backbone curve response. When analyzing backbone curve response add the following line to the program

```
245 IF SL>1 THEN SL=1
```

After inputting the basic soil and pile information, the user is prompted for the pressure level (or change in pressure level) for which the analysis is to be carried out. The program then runs through the pile elements and at the end reports the displacement and load values at the top of the last element (the pile top) and the associated point displacement and load values. Thereafter it prompts the user for another pressure level to begin a new run. If after several runs, one wishes to stop, just type 999 for the value of pressure level.

```
 10 INPUT "DIAMETER(FT)=";B
 20 INPUT "AE(KIPS)=";AE
 30 INPUT "Q/P,NET(KIPS)=";QN
 35 INPUT "MAX POINT UNLOAD(KIPS)=";MP
 40 INPUT "Z,PR(INCHES)=";ZR
 50 INPUT "BETA FOR POINT=";BP
 60 INPUT "R-1 FOR POINT=";RP
 70 INPUT "BETA FOR SIDE=";BS
 80 INPUT "R-1 FOR SIDE=";RS
 85 PRINT
 90 INPUT "NUMBER OF PILE ELEMENTS=";N
 100 FOR I=1 TO N
 110 PRINT "SEGMENT ";I
 120 INPUT "TULT(KSF),M,L(FT)=";TU(I),M(I),L(I)
 130 NEXT
 135 PRINT
 140 INPUT "PRESS/STRESS LEVEL AT POINT=";PL
 145 IF PL=999 THEN GOTO 470
 150 QP=PL*QN
 160 IF QP>MP THEN QP=MP
 170 QB=QP
 180 ZP=ZR*PL*(1+BP*PL↑(RP))
 190 ZB=ZP
 200 FOR I=1 TO N
 210 Z1=12*(QB*L)/(2*AE)
 220 ZM=ZB+Z1
 230 OZ=Z1
 240 GOSUB 500
 250 T=SL*TU(I)
 260 S=3.14159*B*L(I)*T
 270 QT=QB+S
 280 Z1=12*(QT+3*QB)*L(I)/(8*AE)
 290 Z2=12*(QT+QB)/2*L(I)/AE
 300 ZT=ZB+Z2
 310 Y=(Z1-OZ)/Z1
 320 IF ABS(Y)<1.0E-05 THEN GO TO 340
 330 GO TO 220
 335 PRINT
 340 PRINT "SEGMENT ";I
 350 PRINT "STRESS LEVEL IN SOIL=";SL
 360 PRINT "TOP DISP(IN)=";ZT
 370 PRINT "TOP LOAD(KIPS)=";QT
 380 IF I<N GOTO 440
 390 K=QT/ZT
 400 PRINT "STIFFNESS,K(KIPS/IN)=";K
 405 PRINT
 410 PRINT "POINT DISP(IN)=";ZP
 420 PRINT "POINT LOAD(KIPS)=";QP
 425 PRINT
 430 GOTO 140
 440 QB=QT
 450 ZB=ZT
 455 PRINT
 460 NEXT
 470 STOP
 500 SL=.2
 510 OS=SL
 520 SL=(.125*ZM/B*M(I))/(1+BS*SL↑(RS))
 530 X=(OS-SL)/SL
 540 IF ABS(X)>1E-05 THEN GOTO 510
 550 RETURN
```

APPENDIX F

EVALUATION OF THE ROTATIONAL RESPONSE OF A TWO-ROW PILE GROUP

Consider a pile group composed of two pile rows, rows a and b (see Fig. 1) spaced distance d apart. Take $e = k_{u/r}/k_L = 3$ for the analysis considered below. For points 1-8 of Figs. 16 and 17 (see also Figs. 11-15),

$$\theta = \Sigma\Delta\theta \quad ; \quad M = \Sigma\Delta M$$

$$z - z_o = \Sigma\Delta z \quad ; \quad Q - Q_o = \Sigma\Delta Q \tag{F.1}$$

where

$$\begin{aligned} \Delta z &= r\Delta\theta \quad ; \quad \Sigma r = d \\ \Delta z_L &= e\Delta z_{u/r} \quad ; \quad r_L = e\Delta r_{u/r} \\ \Delta Q &= k\Delta z \quad ; \quad \Delta Q_L = \Delta Q_{u/r} = \Delta Q \\ \Delta M &= \Delta Q d \end{aligned} \tag{F.2}$$

Equations F.1 can also be expressed in the form

new value = old value + change over interval (F.3)

Let the amplitude of unload-reload displacement $\Delta z_{u/r}$, the axial stiffness $k_{u/r}$ and the distance d be known values for purposes of the relative evaluation of (M,θ) and (Q,z) coordinates of Figs. 16 and 17. Consider in sequence, responses 0-1, 1-2, 2-3, etc. as evaluated on Plates F.1 through F.8.

CALCULATIONS

PLATE NO. F.1

$\underline{0\text{-}1}$: Row a unloads while row b loads as θ increases from 0 to θ_{max} (Figs. 11 and 12).*

$$\left.\begin{aligned} r_L &= 3\,r_{u/r} \\ r_L + r_{u/r} &= d \end{aligned}\right\} \quad r_{u/r} = \frac{d}{4} \quad ; \quad r_L = \frac{3}{4}d$$

$$r_a = r_{u/r} = \frac{d}{4} \qquad\qquad r_b = r_L = \frac{3}{4}d$$

$$\begin{aligned} \Delta z_a &= \Delta z_{u/r} \uparrow \\ z_a - z_0 &= 0 + \Delta z_a \\ &= \Delta z_{u/r} \uparrow \end{aligned} \qquad\qquad \begin{aligned} \Delta z_b &= \Delta z_L = \frac{3}{4}\Delta z_{u/r} \downarrow \\ z_b - z_0 &= 0 + \Delta z_b \\ &= 3\Delta z_{u/r} \downarrow \end{aligned}$$

$$\begin{aligned} \Delta Q &= k\Delta z = k_{u/r}\,\Delta z_{u/r} \quad \uparrow a \quad \downarrow b \\ Q - Q_0 &= 0 + \Delta Q \\ &= k_{u/r}\,\Delta z_{u/r} \quad \uparrow a \quad \downarrow b \end{aligned}$$

$$\begin{aligned} \Delta M_{0\text{-}1} &= \Delta Q\,d = k_{u/r}\,\Delta z_{u/r}\,d \circlearrowright \\ M_1 &= 0 + \Delta M_{0\text{-}1} = k_{u/r}\,\Delta z_{u/r}\,d \circlearrowright \end{aligned}$$

$$\begin{aligned} \Delta\theta_{0\text{-}1} &= \Delta z/r = \Delta z_{u/r}/(d/4) = 4\,\Delta z_{u/r}/d \circlearrowright \\ \theta_1 &= 0 + \Delta\theta_{0\text{-}1} \\ &= 4\,\Delta z_{u/r}/d \circlearrowright = \theta_{max} \end{aligned}$$

---

* It is understood that $r_a, r_b, \Delta z_a, \Delta z_b$ and ΔQ correspond to the 0-1 change while z_a, z_b and Q are values at the end of the change, i.e., at 1. Subscripts 0-1 and 1 have been omitted relative to these quantities for purposes of simplification, but not for M and θ values.

CALCULATIONS

PLATE NO. F.2

$\underline{1\text{-}2}$: Row a reloads along its unload path to its original condition as row b unloads to its original loads and M decreases to 0 as θ is reversed (Figs. 13 and 14).

$$r_a = r_b = \frac{d}{2}$$

$$\Delta z_a = \Delta z_b = \Delta z_{u/r} \quad \downarrow a \quad \uparrow b$$

$$\begin{aligned} z_a - z_0 &= (z_a - z_0)_{old} + \Delta z_a \\ &= 0 \end{aligned} \qquad\qquad \begin{aligned} z_b - z_0 &= (z_b - z_0)_{old} + \Delta z_b \\ &= 2\,\Delta z_{u/r} \downarrow \end{aligned}$$

$$\begin{aligned} \Delta Q &= k\Delta z = k_{u/r}\,\Delta z_{u/r} \quad \downarrow a \quad \uparrow b \\ Q - Q_0 &= (Q - Q_0)_{old} + \Delta Q \\ &= 0 \end{aligned}$$

$$\begin{aligned} \Delta M_{1\text{-}2} &= \Delta Q\,d = k_{u/r}\,\Delta z_{u/r}\,d \circlearrowleft \\ M_2 &= M_1 + \Delta M_{1\text{-}2} \\ &= 0 \end{aligned}$$

$$\begin{aligned} \Delta\theta_{1\text{-}2} &= \Delta z/r = \Delta z_{u/r}/(d/2) = 2\,\Delta z_{u/r}/d \circlearrowleft \\ \theta_2 &= \theta_1 + \Delta\theta_{1\text{-}2} \\ &= 2\,\Delta z_{u/r}/d \circlearrowright \end{aligned}$$

Check :

$$\begin{aligned} \theta_2 &= (z_b - z_a)/d = [(z_b - z_0) - (z_a - z_0)]/d \\ &= [2\,\Delta z_{u/r} \downarrow - 0]/d \\ &= 2\,\Delta z_{u/r}/d \circlearrowright \end{aligned} \qquad \text{OK}$$

CALCULATIONS
PLATE NO. F.3

2-3 : Row a continues to load but now along the backbone Q-z curve while row b continues to unload as θ decreases to 0 (Fig. 15).

$r_b = r_{u/r} = \frac{d}{4}$ $\qquad$ $r_a = r_L = \frac{3}{4}d$

$\Delta z_b = \Delta z_{u/r}/2 \uparrow$ $\qquad$ $\Delta z_a = 3\Delta z_b = 1\tfrac{1}{2}\,\Delta z_{u/r} \downarrow$

$z_b - z_o = (z_b - z_o)_{old} + \Delta z_b$ $\qquad$ $z_a - z_o = (z_a - z_o)_{old} + \Delta z_a$

$\quad = 1\tfrac{1}{2}\,\Delta z_{u/r} \downarrow$ $\qquad$ $= 1\tfrac{1}{2}\,\Delta z_{u/r} \downarrow$

$\Delta Q = k\Delta z = k_{u/r}\Delta z_{u/r}/2 \quad \downarrow a \quad \uparrow b$

$Q - Q_o = (Q - Q_o)_{old} + \Delta Q$

$\quad = \tfrac{1}{2}\,k_{u/r}\,\Delta z_{u/r} \quad \downarrow a \quad \uparrow b$

$\Delta M_{2\text{-}3} = \Delta Q d = \tfrac{1}{2}\,k_{u/r}\,\Delta z_{u/r}\,d$ ↻

$M_3 = M_2 + \Delta M_{2\text{-}3}$

$\quad = \tfrac{1}{2}\,k_{u/r}\,\Delta z_{u/r}\,d$ ↻

$\Delta\theta_{2\text{-}3} = \Delta z/r = (\Delta z_{u/r}/2)/(d/4)$ ↻

$\theta_3 = \theta_2 + \Delta\theta_{2\text{-}3}$

$\quad = 0$

Check :

$\theta_3 = (z_b - z_a)/d = [(z_b - z_o) - (z_a - z_o)]/d$

$\quad = [1\tfrac{1}{2}\,\Delta z_{u/r} \downarrow - 1\tfrac{1}{2}\,\Delta z_{u/r} \downarrow]/d$

$\quad = 0$ $\qquad$ OK

CALCULATIONS
PLATE NO. F.4

3-4: Rows a and b continue as in 2-3 as θ goes from 0 to θ_{max} of the opposite sense (Fig. 15). $|\Delta\theta|_{3\text{-}4} = |\Delta\theta|_{0\text{-}1}$

$r_b = \frac{d}{4}$ $\qquad$ $r_a = \frac{3}{4}d$

$\Delta z_b = \Delta z_{u/r} \uparrow$ $\qquad$ $\Delta z_a = \frac{3}{4}\,\Delta z_{u/r} \downarrow$

$z_b - z_o = (z_b - z_o)_{old} + \Delta z_b$ $\qquad$ $z_a - z_o = (z_a - z_o)_{old} + \Delta z_a$

$\quad = \tfrac{1}{2}\,\Delta z_{u/r} \downarrow$ $\qquad$ $= 4\tfrac{1}{2}\,\Delta z_{u/r} \downarrow$

$\Delta Q = k\Delta z = k_{u/r}\,\Delta z_{u/r} \quad \downarrow a \quad \uparrow b$

$Q - Q_o = (Q - Q_o)_{old} + \Delta Q$

$\quad = 1\tfrac{1}{2}\,k_{u/r}\,\Delta z_{u/r} \quad \downarrow a \quad \uparrow b$

$\Delta M_{3\text{-}4} = \Delta Q d = k_{u/r}\,\Delta z_{u/r}\,d$ ↻

$M_4 = M_3 + \Delta M_{3\text{-}4}$

$\quad = 1\tfrac{1}{2}\,k_{u/r}\,\Delta z_{u/r}\,d$ ↻

$\Delta\theta_{3\text{-}4} = \Delta z/r = \Delta z_{u/r}/(d/4) = 4\Delta z_{u/r}/d$ ↻

$\theta_4 = \theta_3 + \Delta\theta_{3\text{-}4}$

$\quad = 4\,\Delta z_{u/r}/d$ ↻ $= \theta_{max}$

Check :

$\theta_4 = (z_b - z_a)/d = [(z_b - z_o) - (z_a - z_o)]/d$

$\quad = [\tfrac{1}{2}\,\Delta z_{u/r} \downarrow - 4\tfrac{1}{2}\,\Delta z_{u/r} \downarrow]/d$

$\quad = 4\Delta z_{u/r}/d$ ↺ $\qquad$ OK

CALCULATIONS
PLATE NO. F.5

4-5: Row a now starts to unload and row b to reload as θ reverses and increases to 0 (Figs. 16 and 17).

$$r_a = r_b = \frac{d}{2}$$

$$\Delta z_a = \Delta z_b = 2\Delta z_{u/r} \quad \uparrow a \quad \downarrow b$$

$$z_a - z_o = (z_a - z_o)_{old} + \Delta z_a \qquad z_b - z_o = (z_b - z_o)_{old} + \Delta z_b$$
$$= 2\tfrac{1}{2}\,\Delta z_{u/r} \downarrow \qquad\qquad = 2\tfrac{1}{2}\,\Delta z_{u/r} \downarrow$$

$$\Delta Q = k\Delta z = k_{u/r}\,(2\Delta z_{u/r}) = 2k_{u/r}\Delta z_{u/r} \quad \uparrow a \quad \downarrow b$$
$$Q - Q_o = (Q - Q_o)_{old} + \Delta Q$$
$$= \tfrac{1}{2}\,k_{u/r}\,\Delta z_{u/r} \quad \uparrow a \quad \downarrow b$$

$$\Delta M_{4\text{-}5} = \Delta Q d = 2k_{u/r}\,\Delta z_{u/r}\,d \circlearrowright$$
$$M_5 = M_4 + \Delta M_{4\text{-}5}$$
$$= \tfrac{1}{2}\,k_{u/r}\,\Delta z_{u/r}\,d \circlearrowright$$

$$\Delta\theta_{4\text{-}5} = \Delta z/r = 2\Delta z_{u/r}/(d/2) = 4\Delta z_{u/r}/d \circlearrowright$$
$$\theta_5 = \theta_4 + \Delta\theta_{4\text{-}5}$$
$$= 0$$

Check:

$$\theta_5 = (z_b - z_a)/d = [(z_a - z_o) - (z_b - z_o)]/d$$
$$= [2\tfrac{1}{2}\Delta z_{u/r} \downarrow - 2\tfrac{1}{2}\,\Delta z_{u/r} \downarrow]/d$$
$$= 0 \qquad \text{OK}$$

CALCULATIONS
PLATE NO. F.6

5-6: Rows a and b continue as in 4-5 until at 6 row b once again reaches the backbone curve (Figs. 16 & 17).

$$r_a = r_b = \frac{d}{2}$$

$$\Delta z_a = \Delta z_b = \Delta z_{u/r}/2 \quad \uparrow a \quad \downarrow b$$

$$z_a - z_o = (z_a - z_o)_{old} + \Delta z_a \qquad z_b - z_o = (z_b - z_o)_{old} + \Delta z_b$$
$$= 2\,\Delta z_{u/r} \downarrow \qquad\qquad = 3\,\Delta z_{u/r} \downarrow$$

$$\Delta Q = k\Delta z = k_{u/r}\,\Delta z_{u/r}/2 \quad \uparrow a \quad \downarrow b$$
$$Q - Q_o = (Q - Q_o)_{old} + \Delta Q$$
$$= k_{u/r}\,\Delta z_{u/r} \quad \uparrow a \quad \downarrow b$$

$$\Delta M_{5\text{-}6} = \Delta Q d = \tfrac{1}{2}\,k_{u/r}\,\Delta z_{u/r}\,d \circlearrowright$$
$$M_6 = M_5 + \Delta M_{5\text{-}6}$$
$$= k_{u/r}\,\Delta z_{u/r}\,d \circlearrowright$$

$$\Delta\theta_{5\text{-}6} = \Delta z/r = (\Delta z_{u/r}/2)/(d/2) = \Delta z_{u/r}/d \circlearrowright$$
$$\theta_6 = \theta_5 + \Delta\theta_{5\text{-}6}$$
$$= \Delta z_{u/r}/d \circlearrowright$$

Check:

$$\theta_6 = (z_b - z_a)/d = [(z_b - z_o) - (z_a - z_o)]/d$$
$$= [3\Delta z_{u/r} \downarrow - 2\,\Delta z_{u/r} \downarrow]/d$$
$$= \Delta z_{u/r}/d \circlearrowright \qquad \text{OK}$$

CALCULATIONS

PLATE NO. F.7

$\underline{6\text{-}7}$: Row a and b continue as in 5-6 except row b now moves along the backbone curve as θ increases to θ_{max} (Figs 16 & 17)

$r_a = \frac{d}{4}$ $\qquad$ $r_b = \frac{3}{4}d$

$\Delta z_a = \frac{3}{4}\Delta z_{u/r} \uparrow$ $\qquad$ $\Delta z_b = 2\,1/4\,\Delta z_{u/r} \downarrow$

$z_a - z_o = (z_a - z_o)_{old} + \Delta z_a$ $\qquad$ $z_b - z_o = (z_b - z_o)_{old} + \Delta z_b$

$= 1\,1/4\,\Delta z_{u/r} \downarrow$ $\qquad$ $= 5\,1/4\,\Delta z_{u/r} \downarrow$

$\Delta Q = k\,\Delta z = k_{u/r}\,\frac{3}{4}\Delta z_{u/r} = \frac{3}{4}\,\Delta z_{u/r} \quad \uparrow a \quad \downarrow b$

$Q - Q_o = (Q - Q_o)_{old} + \Delta Q$

$= 1\,3/4\,k_{u/r}\,\Delta z_{u/r} \quad \uparrow a \quad \downarrow b$

$\Delta M_{6\text{-}7} = \Delta Q\,d = 3/4\,k_{u/r}\,\Delta z_{u/r}\,d \;\circlearrowright$

$M_7 = M_6 + \Delta M_{6\text{-}7}$

$= 1\,3/4\,k_{u/r}\,\Delta z_{u/r}\,d \;\circlearrowright$

$\Delta\theta_{6\text{-}7} = \Delta z/r = (\frac{3}{4}\Delta z_{u/r})/(d/4) = 3\Delta z_{u/r}/d \;\circlearrowright$

$\theta_7 = \theta_6 + \Delta\theta_{6\text{-}7}$

$= 4\,\Delta z_{u/r}/d \;\circlearrowright\; = \theta_{max}$

Check:

$\theta_7 = (z_b - z_a)/d = [(z_b - z_o) - (z_a - z_o)]/d$

$= [5\,1/4\,\Delta z_{u/r} \downarrow - 1\,1/4\,\Delta z_{u/r} \downarrow]/d$

$= 4\,\Delta z_{u/r}/d \;\circlearrowright$ $\quad$ OK

CALCULATIONS

PLATE NO. F.8

$\underline{7\text{-}8}$: Row a reloads and row b unloads as θ reverses and decreases from θ_{max} to 0 (Figs. 16 and 17). $|\Delta\theta_{7\text{-}8}| = |\Delta\theta_{4\text{-}5}|$

$r_a = r_b = \frac{d}{2}$

$\Delta z_a = \Delta z_b = 2\Delta z_{u/r} \quad \downarrow a \quad \uparrow b$

$z_a - z_o = (z_a - z_o)_{old} + \Delta z_a$ $\qquad$ $z_b - z_o = (z_b - z_o)_{old} + \Delta z_b$

$= 3\,1/4\,\Delta z_{u/r} \downarrow$ $\qquad$ $= 3\,1/4\,\Delta z_{u/r}$

$\Delta Q = k\,\Delta z = k_{u/r}(2\Delta z_{u/r}) = 2k_{u/r}\,\Delta z_{u/r} \quad \downarrow a \quad \uparrow b$

$Q - Q_o = (Q - Q_o)_{old} + \Delta Q$

$= 1/4\,k_{u/r}\,\Delta z_{u/r} \quad \downarrow a \quad \uparrow b$

$\Delta M_{7\text{-}8} = \Delta Q\,d = 2k_{u/r}\,\Delta z_{u/r}\,d \;\circlearrowleft$

$M_8 = M_7 + \Delta M_{7\text{-}8}$

$= 1/4\,k_{u/r}\,\Delta z_{u/r}/d \;\circlearrowright$

$\Delta\theta_{7\text{-}8} = \Delta z/r = 2\Delta z_{u/r}/(d/2) = 4\,\Delta z_{u/r}/d \;\circlearrowleft$

$\theta_8 = \theta_7 + \Delta\theta_{7\text{-}8}$

$= 0$

Check:

$\theta_8 = (z_b - z_a)/d = [(z_b - z_o) - (z_a - z_o)]/d$

$= [3\,1/4\,\Delta z_{u/r} \downarrow - 3\,1/4\,\Delta z_{u/r}]$

$= 0$ $\quad$ OK

APPENDIX G

EVALUATION OF K_θ GIVEN THE $k_{u/r}$ VS. $\Delta z_{u/r}$ CURVE

If one knows the axial pile $k_{u/r}$ vs. $\Delta z_{u/r}$ variation then the stabilized rotational stiffness of the group is given by Equation 6. The $k_{u/r}$ values in Equation 6 are chosen in accordance with the $\Delta z_{u/r}$ displacements due to rotation θ. Recall, however, that $k_{u/r}$ is based on the value of $\Delta z_{u/r}$ that is twice the amplitude of pile movement $\pm \Delta z_{u/r}$ as indicated in Fig. 21.

Given the $k_{u/r}$ vs. $\Delta z_{u/r}$ variation for Pile Group 4 as shown in Fig. 20, the tabulation of K_θ, θ values used to establish the K_θ vs. θ curve of Fig. 23 is demonstrated in Plates G.1-G.2. One will note from the calculations that rather than set the value of θ, the displacement of the outer pile row is chosen and θ calculated. This is solely a matter of preference.

CALCULATIONS
PLATE NO. G.1
PILE GROUP 4

$K_\theta = \Sigma k_{u/r} r^2$

$\theta = \frac{\Delta z}{r}$

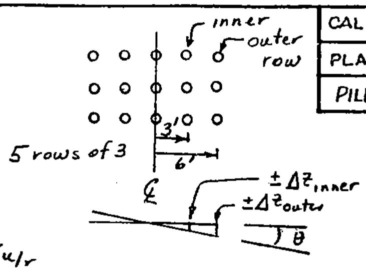

$\pm\Delta z_{u/r}$ for θ

$\Delta z_{u/r} = 2(\pm\Delta z_{u/r})$ for $k_{u/r}$

$\underline{\pm\Delta z_{outer\ row} = 0.001\ in.}$

Fig. 20

$\pm\Delta z_{outer} = 0.001$ in. or $\Delta z_{u/r} = 0.002$ in. $\rightarrow k_{u/r} = 1945$ k/in

$\pm\Delta z_{inner} = 0.0005$ $\quad = 0.001 \quad = 2120$

$K_\theta = \underset{\substack{whole\\group}}{\Sigma k_{u/r} r^2} = 2\underset{\substack{half\\group}}{\Sigma k_{u/r} r^2}$

$= 2\left[3(1945\tfrac{k}{in})(6ft)^2 + 3(2120\tfrac{k}{in})(3ft)^2\right] 144\tfrac{in^2}{ft^2}$

$= 6\left[(1945)(36) + (2120)(9)\right] 144$

$= 7.70 \times 10^7 \frac{k\text{-}in}{rad}$

$\theta = \Delta z/r = \frac{0.001\ in}{6(12)\ in} = 1.39 \times 10^{-5}\ rad$

$\underline{\pm\Delta z_{outer\ row} = 0.003\ in}$

$\pm\Delta z_{outer} = 0.003$ in. or $\Delta z_{u/r} = 0.006$ in $\rightarrow k_{u/r} = 1600$ k/in

$\pm\Delta z_{inner} = 0.0015$ $\quad = 0.003 \quad = 1820$

$K_\theta = 6\left[(1600)(36) + (1820)(9)\right] 144$

$= 6.39 \times 10^7 \frac{k\text{-}in}{rad}$

CALCULATIONS
PLATE NO. G.2
PILE GROUP 4

$\theta = \Delta z/r = \frac{0.003}{6(12)} = 4.17 \times 10^{-5}\ rad$

$\underline{\pm\Delta z_{outer\ row} = 0.010\ in}$

$\pm\Delta z_{outer} = 0.010$ in or $\Delta z_{u/r} = 0.020 \rightarrow k_{u/r} = 1260$ k/in

$\pm\Delta z_{inner} = 0.005$ $\quad = 0.010 \quad = 1455$

$K_\theta = 6\left[(1260)(36) + (1455)(9)\right] 144$

$= 5.05 \times 10^7 \frac{k\text{-}in}{rad}$

$\theta = \Delta z/r = \frac{0.010}{6(12)} = 1.39 \times 10^{-4}\ rad$

$\underline{\pm\Delta z_{outer\ row} = 0.0175\ in.}$ end of stabilized response associated with outer row

$\pm\Delta z_{outer} = 0.0175$ in or $\Delta z_{u/r} = 0.035$ in. $\rightarrow k_{u/r} = 1100$ k/in

$\pm\Delta z_{inner} = 0.008375$ $\quad = 0.0175 \quad = 1295$

$K_\theta = 6\left[(1100)(36) + (1295)(9)\right] 144$

$= 4.46 \times 10^7 \frac{k\text{-}in}{rad}$

$\theta = \Delta z/r = \frac{0.0175}{6(12)} = 2.43 \times 10^{-4}\ rad$

Ambient, $k_{u/r} = 2740 \frac{k}{in}$

$K_\theta = 6\left[(2740)(36) + (2740)(9)\right] 144$

$= 10.65 \times 10^7 \frac{k\text{-}in}{rad}$

REFRACTION SEISMIC STUDY TO EXPLORE A BORROW SOURCE IN A REMOTE AREA

by

Harry Ludowise, Federal Highway Administration

ABSTRACT

The 81 Km. Darien Gap is the only remaining break in the Pan American Highway. The 22 Km. Atrato Swamp crossing is the major physical barrier to cross in closing the gap. Locating a borrow source for a rock fill in this isolated area is one of the key tasks in designing the swamp crossing. In 1981, a refraction seismic survey was made to supplement the limited boring information available on a possible borrow site. The decision to use geophysical methods was made because the area is very remote and drilling equipment was difficult to mobilize. The refraction seismograph proved to be very successful in determining the depth of soil over solid rock. The topography is extremely irregular and a computer program that allows for both vertical and horizontal corrections was used to analyze the data. This program made possible a rapid analysis of the data and eliminated many tedious hours of hand calculations.

This paper presents a case history of the exploration of a proposed borrow source in a remote area using a seismograph. It also discusses the capabilities of the computer program SIPB.

INTRODUCTION

The 81 Km. Darien Gap in southern Panama and northern Colombia is the only incomplete section of the Pan American Highway and all that prevents one from driving from Alaska to South America (Figure 1). During early reconnaissance studies, the Atrato Swamp section of the Gap was considered to be a major barrier to highway construction and the recommended route was shifted to the west along the chain of mountains which form the backbone of South America (Figure 2). The western, or Choco route, had a number of serious disadvantages. Being in the mountains, it would require tighter curves resulting in a 30 mph design, while the remainder of the route was 60 mph. The mountains were known to be subject to landsliding, resulting in high maintenance costs, and also, the route was longer.

These disadvantages caused the Interamerican Highway Committee to request an additional study of the Atrato route, which had a number of advantages. It was a shorter distance (81 Km. versus 431 Km.) to a connection with an existing road. Only 22 Km. would be difficult swamp construction. In addition, it would open up a populated area to commerce, whereas the Choco route went through sparsely populated mountains (Figure 3). The study made in 1968-69 showed that not only was the Atrato route practical to construct, but the estimated cost would be only $60 million as opposed to $176 million for the Choco route (1969 dollars).

The construction method recommended for the swamp crossing was to place a shot rock fill directly on top of the organic mat of the swamp surface. The load imposed by the fill would consolidate the underlying soft layers so the increased bearing capacity of these layers would support the load of the final embankment. It was estimated that 25 feet of fill placed in five lifts would result in a final height of 12 feet above the swamp surface, requiring an estimated 11 million cubic yards of shot rock. Half of the rock would come from the hills on the west side of the swamp and the remainder from a series of hills, known as the Lomas Las Aisladas, on the edge of the swamp.

EXPLORATION OF THE LOMAS

The Lomas Las Aisladas, three elongated hills that rise above the low ground at the edge of the swamp, appear to be the weathered remnants of an igneous intrusion. They are isolated and accessible only by foot or by helicopter. During the 1969 study, a core drill was flown in and one hole drilled in the large loma. This boring proved that although they were deeply weathered, the lomas were underlain by rock and were a possible source of borrow. A few resistivity and seismic tests were run at the same time to extend the boring information. Since the proposed road ran between the small and middle loma, it was decided to start a detailed exploration on these two, followed by exploration on the large loma, if the small and middle lomas did not contain enough rock. In 1974, a Colombian firm was engaged to do the additional exploration work which proved that there was not enough rock in the small loma to make an economical borrow source. They also drilled eight holes along the crest of the middle loma finding rock within a few meters of the surface. Unfortunately, these borings showed only what was under the crest of the loma where less soil cover might be expected due to erosion. If a quarry were opened, it would be located on the lower flanks of the loma, not on the crest where the borings were taken. In addition, if the rock formation under the loma were similar to a dike, the rock deposit might be only a few meters wide and centered under the crest.

A refraction seismic study was organized in 1981 to explore the middle loma. The object of the study was to estimate the quantity of rock under the loma and to anticipate amount of soil cover. A second objective of the seismic study was the selection of the most favorable area for a quarry site. Between the study in 1969 and that in 1981, a logging company had dredged a canal to the vicinity of the small loma to facilitate operations. This made the proposed study more economical as the area was now accessible by boat. The Colombian government had also built a survey camp, where the crew could stay, between the canal and the small loma. This camp was 8 hours by motor boat from the nearest village, but only a half-hour by foot to the middle loma. A Colombian consulting engineering firm (La Vialidad Ltda.), engaged to make a topographic map of the middle loma at the time of the seismic work, furnished the ground control to reference the seismic lines, and also ran the camp.

SEISMIC WORK

Preliminary plans were to run the seismic lines across the loma developing cross sections. Unforeseen problems, discovered after arrival at the site, revealed that the work would take longer than anticipated. Much of the clearing that was to be done in advance of the seismic crew had not been completed. The explosives, which were to be picked up on the way out to the camp, were not available for over a week and a special trip was necessary to get them. The loma proved to be more rugged than the contour map indicated, and in many places the topography was too irregular for reliable seismic work. The extra clearing work, delay in obtaining the explosives, plus the discovery that some of the loma was not suitable for seismic work, made it necessary to revise the work plan by eliminating several of the proposed seismic lines.

Figure 4 shows the relationship of the camp, the proposed alignment, and the lomas. It also shows the placement and length of all 16 seismic lines. Three shot points were used on all the lines. All the work was done using the 15.2 meter cable, although the geophones were irregularly spaced to adjust the line length to best fit the topography.

The equipment used was a 12 channel Oyo PS-10 seismograph with two cables. One cable had a 10.6 meter spacing and the other, a 15.2 meter spacing. The explosive used was 40 percent dynamite manufactured in Colombia. Electric blasting caps marked "Delay 30 Seconds, the only type available, were used in lieu of instantaneous special seismic caps normally used for seismic work. Delay blasting caps are manufactured for rock blasting and the delay time is too variable for seismic work. These caps proved to be even more inconsistent than expected and delays measured during this investigation varied from 0 milliseconds to over 140 milliseconds. The exact shot instant needed to determine seismic velocities at shallow depths was calculated using the soil velocity found from the first geophones on the seismic line and the measured distance between the shot point and the first geophone. This procedure could result in small errors in calculating velocity of the surface layer (V_1), but since the soil was relatively deep with three or more geophones being used to calculate V_1 point, these errors were considered to be within acceptable limits.

The seismic information was analyzed by a computer program entitled, "Computer Analysis of Refraction Data," SIPB by the U.S. Department of Interior, Bureau of Mines. This computer program is capable of handling vertical and horizontal deviations from a straight level geophone line. The results are plotted in a profile format which shows the ground surface and the various velocity layers below the surface. Figure 5 is an example of a typical page of computer output. The program prints out up to nine pages of information including the input data, a time distance graph, and a summary of the calculations. It permits the use of up to 12 geophones and seven shot points, and will handle up to five subsurface layers. This program has a number of other options available to the user, making it a most versatile program.

When evaluating the quality of rock based on seismic velocities, the general rule is: the higher the velocity, the harder and more dense the rock. Caution should be used with this procedure as the velocities measured are bulk velocities which include the joints and voids in the rock. Therefore, sound, hard rock with large soil-filled joints may exhibit an unusually low velocity. The velocity of sound in water is approximately 1,525 meters per second. Soils, sand, gravels, and weathered rock can have similar velocities depending on the degree of water saturation. When the velocity is 1,825 meters per second or higher, it is doubtful if a rock can be ripped economically with a crawler tractor.

When no rock velocity was found on a seismic line, a minimum depth procedure was used. This procedure uses the length of the line, the measured velocities, and an assumed velocity for rock. The calculation indicated the shallowest possible depth that a rock layer with the assumed velocity could occur.

The seismic results corroborated previous investigations which showed a deeply weathered soil mantle over the entire loma. Measured velocities of the soil were around 800 meters per second and the rock about 2,500 meters per second. The depth of weathering varied, but was in the range of 20 to 30 meters. Drill hole and resistivity data, as well as observations made in test pits and scarps left by small landslides, confirmed the seismic results. There were several outcrops of broken rock exposed at scattered points on the loma. Seismic lines run in the vicinity of the outcrops indicated unweathered rock no closer to the surface there than elsewhere. This led to the conclusion that these outcrops were pinnacles of rock more resistant to weathering and not representative of the general rock quality.

The study indicated that the soil cover is thinnest on the northeast end of the loma and it was recommended that any additional exploration drilling be concentrated in the area of seismic lines 12 through 16. The recommended additional exploration has not been made as of 1986. Since this study was completed, the Colombian government has extended the road as far as the lomas, and if Interamerican Highway funding is not available, they intend to continue to extend the road by digging a canal through the swamp and using a ferry system. Should this happen, the rock will not be needed and the follow-up exploration will not take place. Nevertheless, this study did show the value of a preliminary geophysical survey used to evaluate a materials source in an isolated area, so expensive drilling can be concentrated in the most favorable locations to provide necessary information with minimum cost.

REFERENCES

Mooney, Harold M. (1973). "Handbook of Engineering Geophysics," Bison Instruments, Minneapolis, MN.

Report of the Darien Subcommittee, "Final Conclusions and Recommendations Regarding Location, Design, and Construction of the Pan American Highway Through the DARIEN GAP in the Republics of Panama and Colombia," Pan American Highway Congresses, Lima, Peru, February 3-6, 1969.

Redpath, Bruce B. (1973). "Seismic Refraction Exploration for Engineering Site Investigations," Report TR E-73-4, U.S. Army Engineer Waterways Experiment Station Explosive Excavation Research Laboratory, Livermore, CA.

Scott, James H., Tibbetts, Benton L., and Burdick, Richard G. (1972). "Computer Analysis of Seismic Refraction Data," Bureau of Mines Report of Investigations 7595, U.S. Department of Interior, Bureau of Mines.

Pan American Highway System

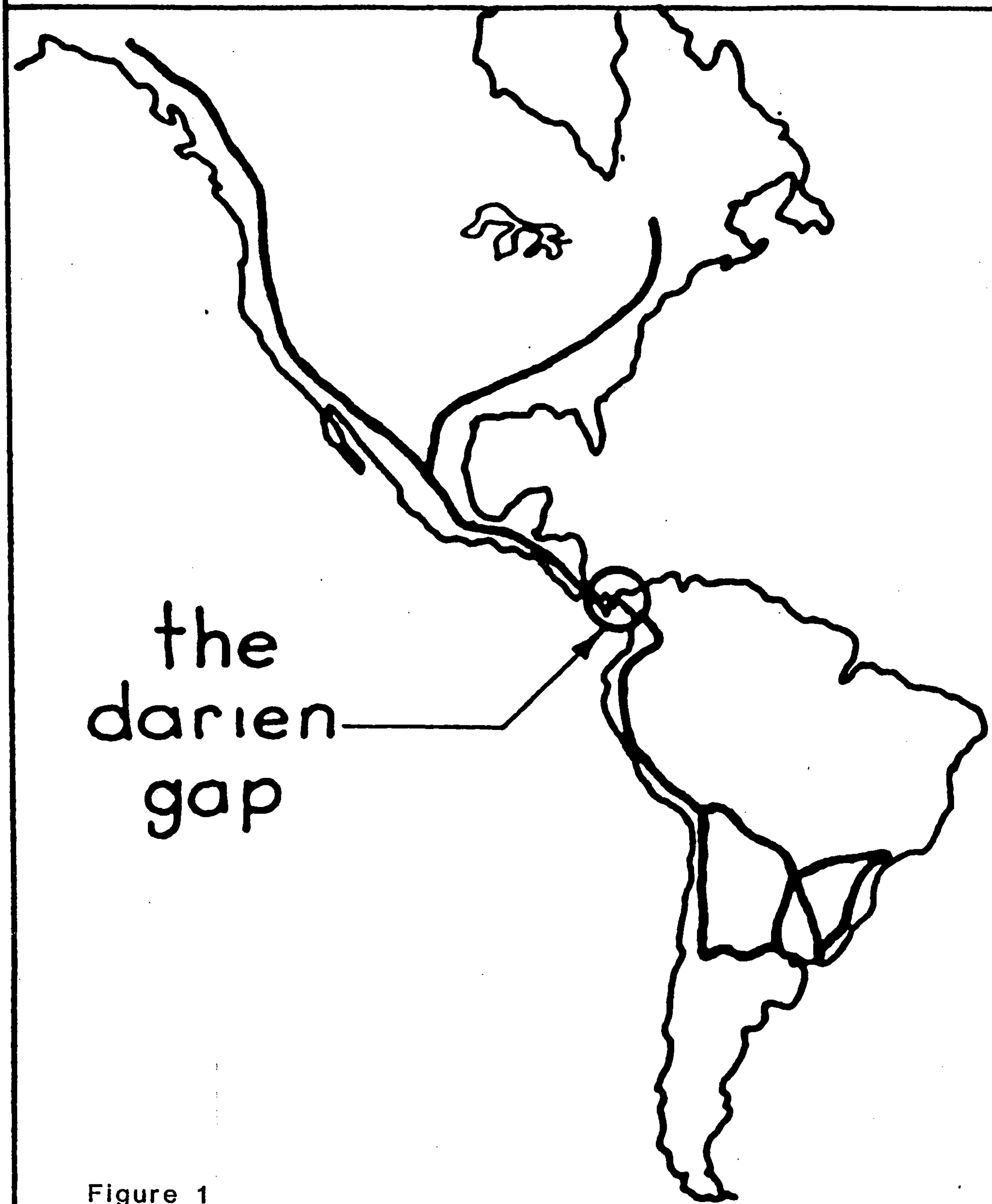
the darien gap

Figure 1

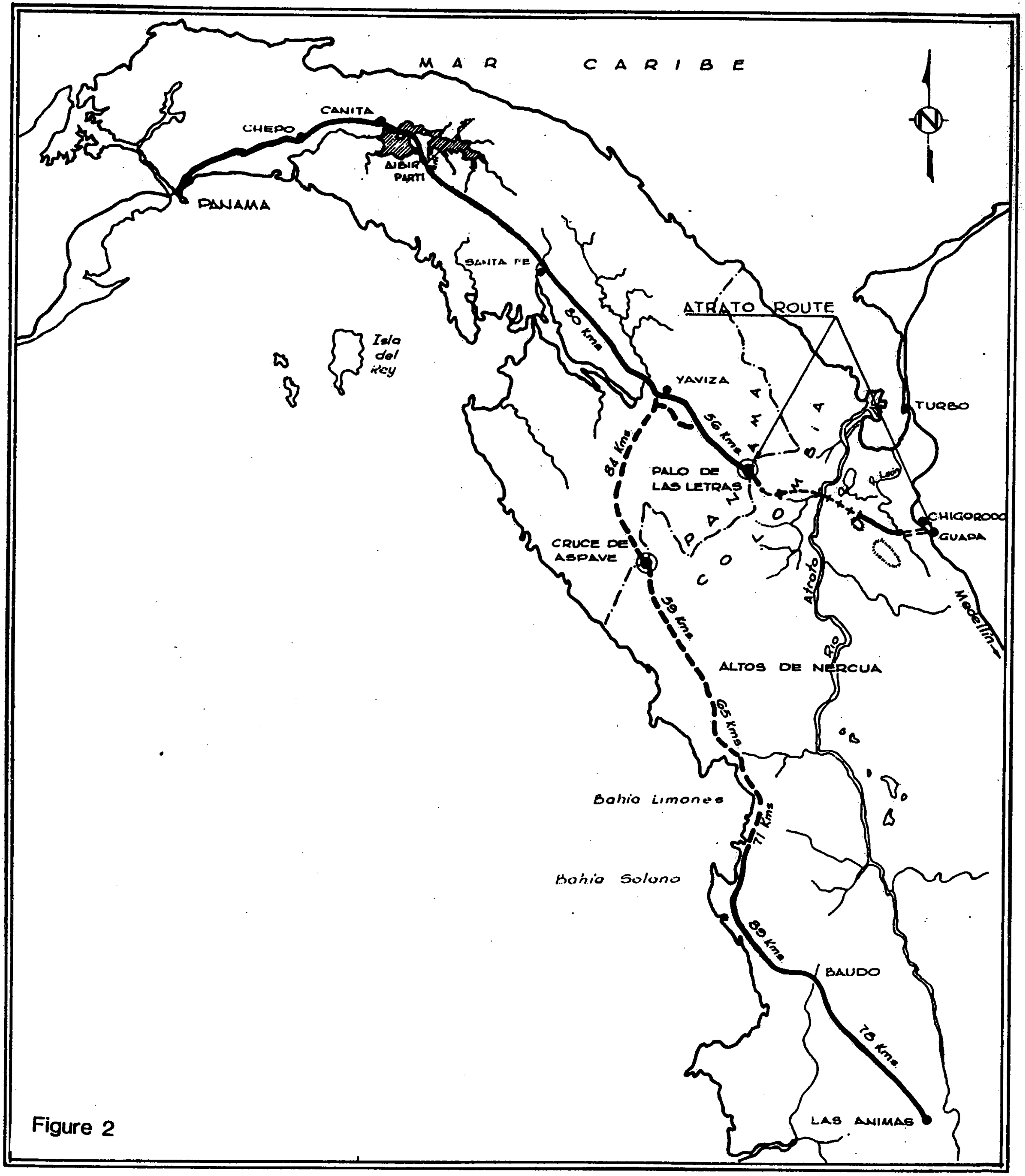
MAR CARIBE
N
CANITA
CHEPO
PANAMA
AIBIR PARTI
SANTA FE
80 Kms
ATRATO ROUTE
Isla del Rey
YAVIZA
56 Kms
84 Kms
PANAMA
COLOMBIA
TURBO
PALO DE LAS LETRAS
CHIGORODO
GUAPA
CRUCE DE ASPAVE
Atrato
Medellín
39 Kms
ALTOS DE NERCUA
Rio
65 Kms
Bahia Limones
71 Kms
Bahia Solano
89 Kms
BAUDO
76 Kms
LAS ANIMAS

Figure 2

VICINITY MAP OF ATRATO ROUTE
Republic of Colombia

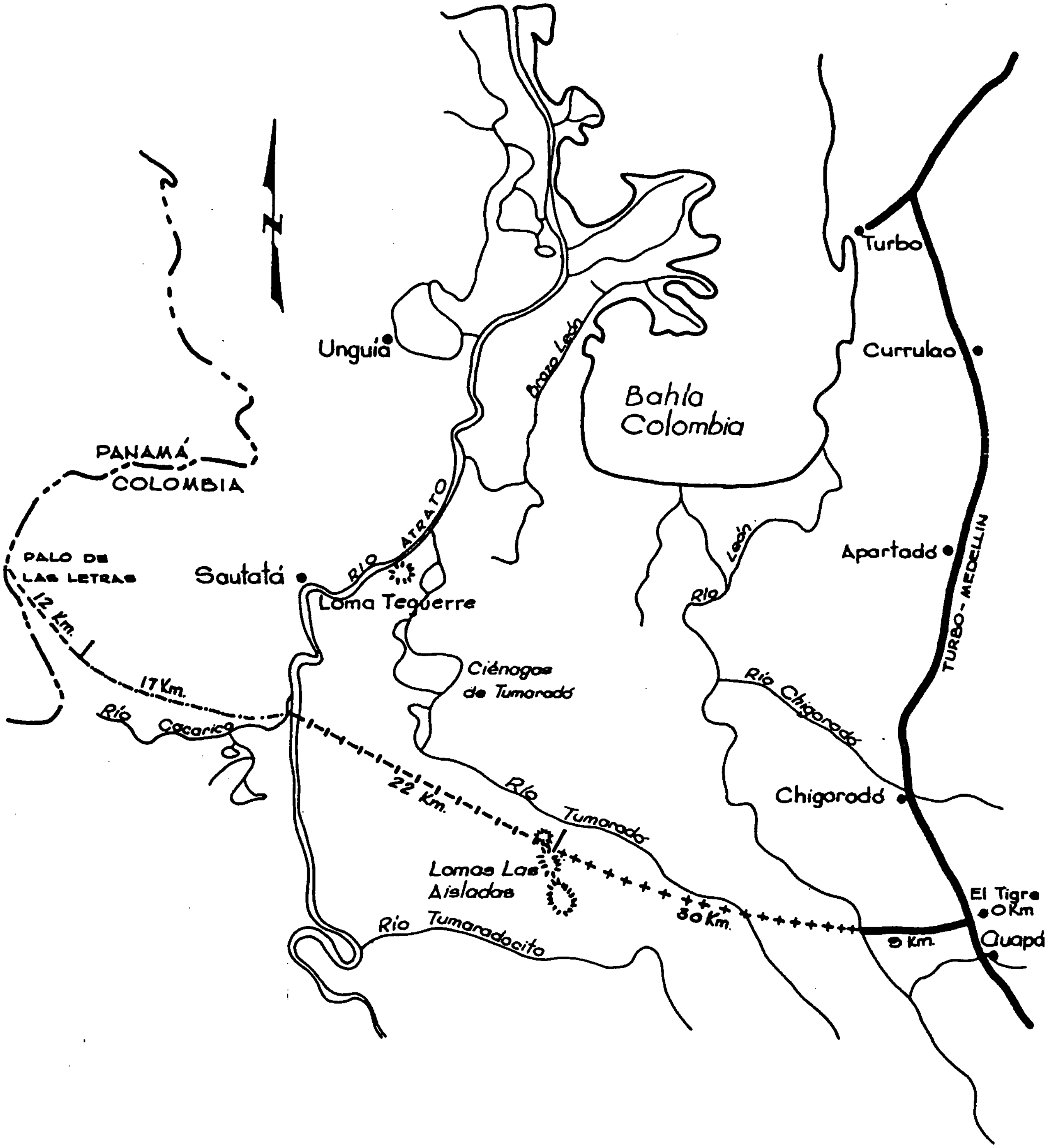
N
Unguia
Turbo
Currulao
Bahla Colombia
Brazo León
PANAMA
COLOMBIA
PALO DE LAS LETRAS
Sautatá
Rio ATRATO
Loma Tequerre
Ciénagas de Tumaradó
Rio León
Apartadó
TURBO - MEDELLIN
Rio Chigorodó
12 Km.
17 Km.
Rio Cacarica
22 Km.
Rio Tumaradó
Chigorodó
Lomas Las Aisladas
30 Km.
El Tigre
0 Km
5 Km.
Guapá
Rio Tumaradocito
Scale in Kilometers
0K
5K
10K
20K
1: 447,500

Figure 3

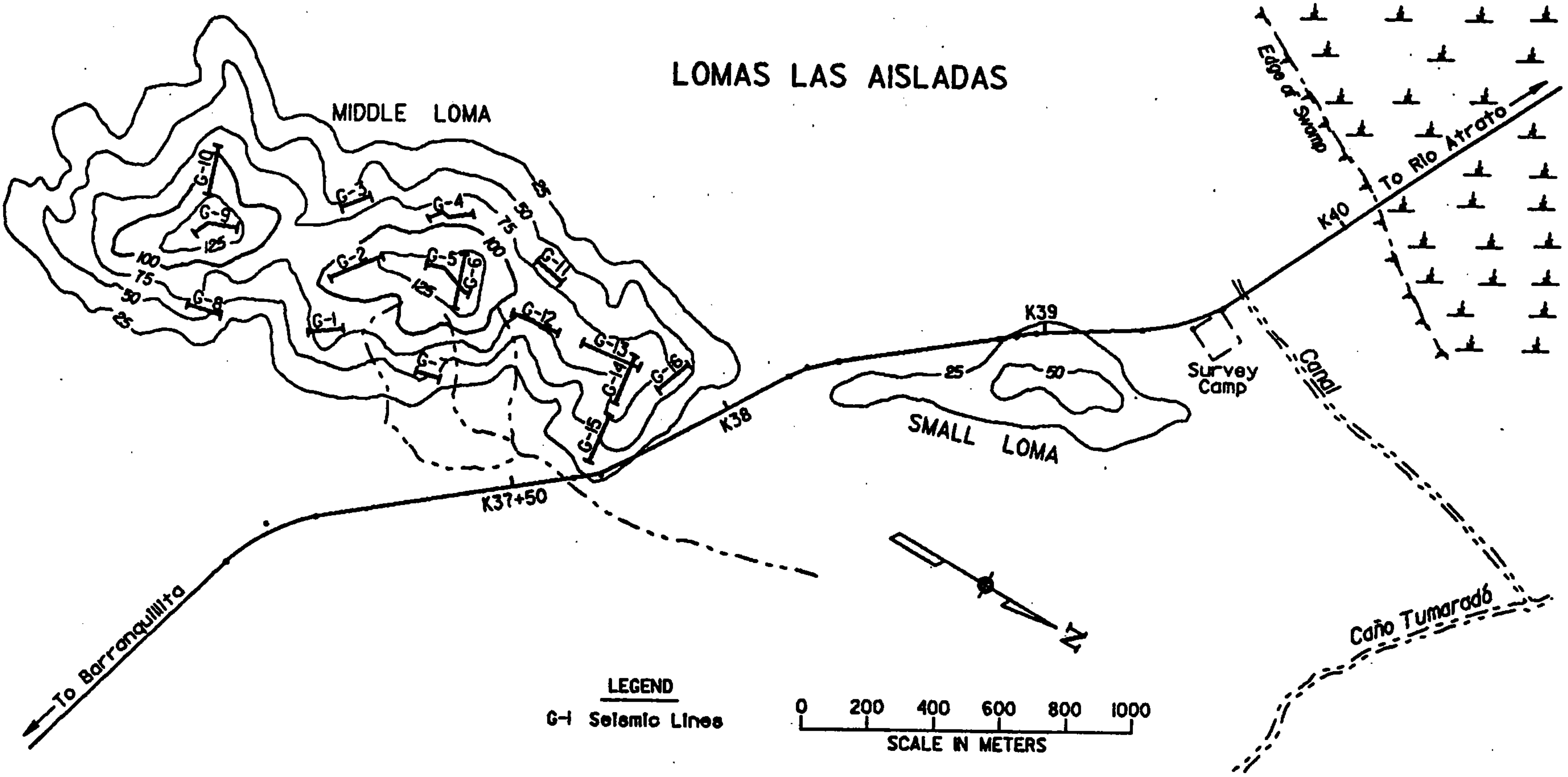
LOMAS LAS AISLADAS
MIDDLE LOMA
SMALL LOMA
G-1
G-2
G-3
G-4
G-5
G-6
G-7
G-8
G-9
G-10
G-11
G-12
G-13
G-14
G-15
G-16
25
50
75
100
125
To Barranquillita
K37+50
K38
K39
K40
To Rio Atrato
Edge of Swamp
Survey Camp
Canal
Caño Tumaradó
N
LEGEND
G-1 Seismic Lines
0
200
400
600
800
1000
SCALE IN METERS

Figure 4

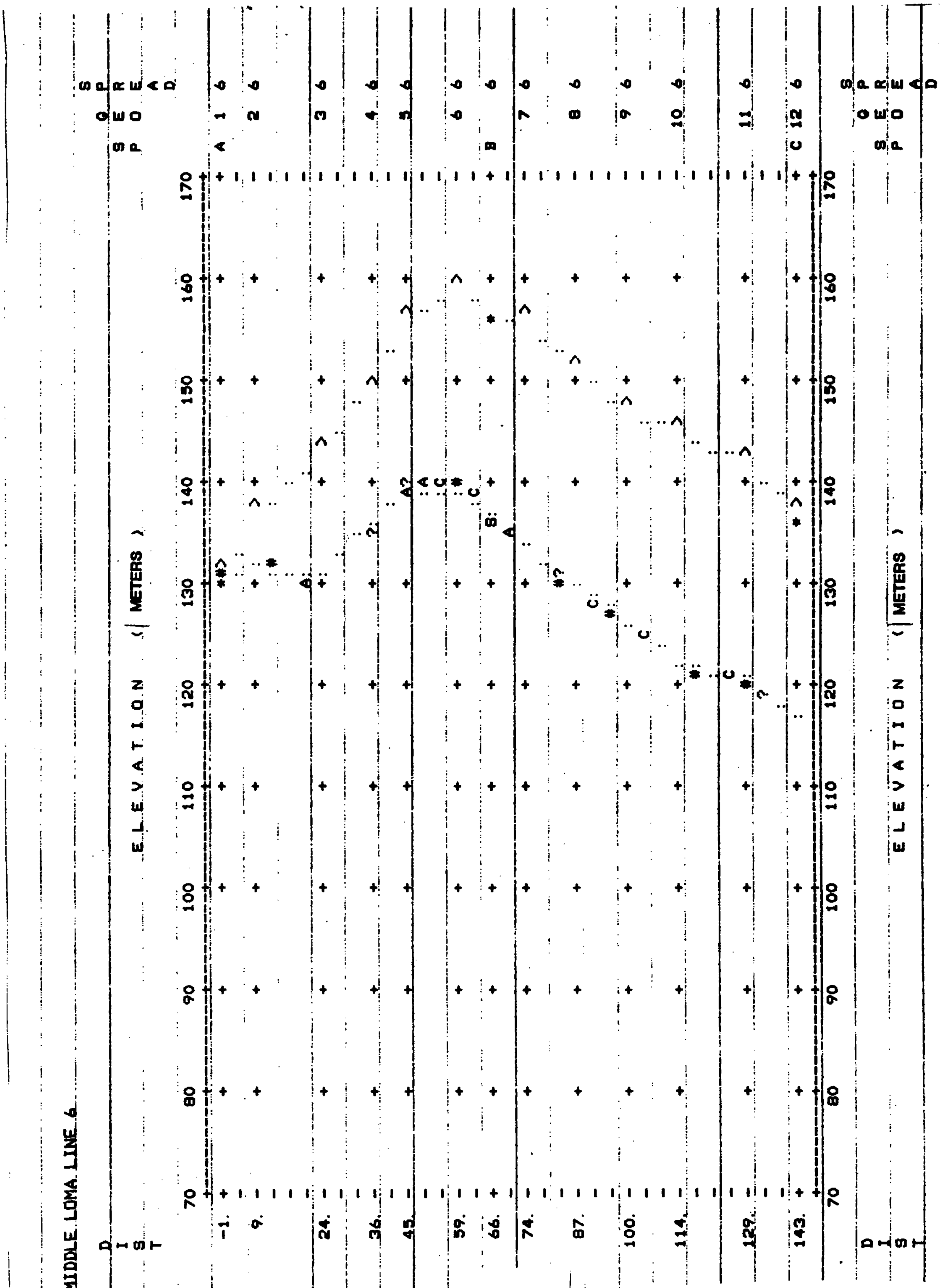
MIDDLE LOMA LINE 6
D I S T
E L E V A T I O N (METERS)
70
80
90
100
110
120
130
140
150
160
170
-1.
9.
24.
36.
45.
59.
66.
74.
87.
100.
114.
129.
143.
S P
G E O
S P R E A D
A 1 6
2 6
3 6
4 6
5 6
6 6
B 6
7 6
8 6
9 6
10 6
11 6
C 12 6

Figure 5

COMPUTER SPREADSHEETS IN GEOTECHNICAL DESIGN

by

Michael D. Remboldt
U.S.D.A. Forest Service
Intermountain Region
Ogden, Utah

ABSTRACT

The increasing availability of low-cost personal computers and software offers powerful and efficient new items for the engineers toolkit.

Spreadsheet software is especially useful for the geotechnical engineer in that it offers relief from time consuming iterative calculations; provides clear, easy-to-read reports automatically; virtually eliminates the need for time consuming programming for sensitivity studies; and can be integrated with government agency analysis standards documentation to provide quick design review for contract design work.

A few examples of spreadsheet application are bearing capacity analysis for spread footings and piles, retaining wall design, and economic analysis. Examples of spreadsheets for these applications are detailed and discussed.

Minimum required time to become skilled in spreadsheet use and the low initial investment make the personal computer based spreadsheet an attractive tool for the geotechnical engineer.

INTRODUCTION

What is a SPREADSHEET?

Those traditionally familiar with spreadsheets as most of us know them are accountants and bookeepers. Spreadsheets are groups of information (usually numbers) arranged in a matrix of rows and columns. We have all seen balance sheets and financial statements arranged in spreadsheet fashion.

With the advent of the personal computer in the last decade software was written which transferred the spreadsheet from paper to the computer screen and mass storage. Here any similarity with paper and computers ends. Computer spreadsheets open new horizons because they don't merely display numbers but do the calculating, too.

What is in it for ME?

Spreadsheets offer the engineer tools for complex calculations, sensitivity analysis, performing repetitive calculations, and providing professional looking reports. Learning to use a computer spreadsheet is easy and their application is time saving and cost effective. spreadsheets provide an opportunity to do many of those things that we couldn't do before because of lack of time and programming skills.

Figures 1 and 2 are included to help familiarize the reader with the basic structure of a computer spreadsheet. Fig. 1 is printout of a spreadsheet designed to aid in determining specification limits for a statistically based pay factor/percent within limits type of aggregate specification. Note the division of the worksheet into "cells" delimited by numbered rows and lettered columns. Each cell may contain text (which in some cases extends to an adjacent cell or cells), numbers, or formulas. Fig. 2 is a printout of the actual contents of each cell as inputted into the computer. Note cell C3 (column C row 3) contains a formula which references other cells to calculate the contents of C3. While the actual contents of C3 is a formula the calculated result is displayed (and/or printed). Cells may also contain logical expressions such as contained in cells C30 or C35. formulas may contain any trigonometric or mathematical function commonly used in scientific and engineering calculations. Entries, whether they be numbers, text, or formulas are entered directly onto the screen by moving the cursor (using arrow keys) to the cells into which the information is desired to be placed.

Cell contents may be easily duplicated to other cells, including formulas. When duplicating a formula to be an absolute reference (i.e. the cell referred to is always the same) or a relative reference. The contents of cell D30 was copied into cells D31, D32, D33, D34, and D35 with one command. Note that the formula reference to B16, B15, and B19 were specified as absolute whereas the reference to cell C30 is relative and changed in the copy relative to the location of the formula.

Entire blocks of cells may be moved at will to other locations for whatever reason. In such a move cells referenced of the spreadsheet change with respect to the relative movement of the block.

Spreadsheets automatically recalculate when the contents of a cell is changed. A change in the contents of input variable cell B7 in our example ("high" of specification range in example) and the spreadsheet recalculates automatically everything to reflect this change. This automatic feature can be turned off and recalculation forced manually. Order of recalculation can be specified across rows, down columns, or to search for the basic level of calculation and work up through the established hierarchy.

Many spreadsheet software packages include graphics capability and are designed to access data to/from other software such as database and word processing programs.

Thus, briefly, we have touched on the great power of the computer spreadsheet which include these factors:

1. Ease of use. Inputting data, text, formulas, and logical expressions are easy because the user places them into their final position exactly as she sees them.

2. Flexibility. The user can change input data and/or formulas at will without frustrating "de-bugging" required in more conventional programming.

3. Power. The spreadsheet incorporates mathematical, tri gonometric, and logical functions which can be duplicated and recalculated with one stroke. This makes spreadsheets ideal for sensitivity studies ("what-if" type questions).

4. Cost effective. Application of spreadsheets to repetitive calculations results in work that can be done in a fraction of the time required to perform identical calculations by hand. Initial setup of spreadsheet

templates takes much less time than conventional programming and debugging. A bonus of the spreadsheet is that with minimal effort the output can be structured into an attractive and organized report. The spreadsheet (and its contents) are ready to be filed in compact form (digital mass storage) for future documentation and/or re-use.

5. Users of identical spreadsheet software can exchange "templates" (spreadsheets structured for specific purposes) to avoid duplicity in effort and achieve consistency in technology application.

SPREADSHEET USE IN GEOTECHNICAL ENGINEERING

Applications

The variety of potential applications for use of the spreadsheet by a geotechnical engineer great. Below is a short list of suggested applications just to get the creative juices flowing:

1. Foundation design.
2. Slope stability sensitivity analysis.
3. Seepage analysis (Kleiner 1985).
4. Bearing capacity analysis.
5. Retaining wall design.
6. Project management.
7. Economic projections and cost analysis.
8. Earthwork quantity calculations.
9. Statistical analysis including regression.
10. Refraction seismograph calculations.
11. Pile capacity calculations.
12. Pavement design.

Following is a brief discussion of four spreadsheets designed by the author which will hopefully illustrate some of the possibilities for geotechnical design and analysis.

Economic Analysis

Figure 3 is a spreadsheet used to calculate the cost of several alternatives for surface stabilization of a remote native surfaced airfield. The geometry of stabilizer application on the runway was calculated and inputted in column 2. The remaining cell contents were automatically calculated. Room was made for 5 alternatives to be calculated and displayed at the same time by merely inputting the formulas for the first row and then duplicating this row 4 times. The maintenance section was copied from the first two sections and then modified by the addition of a column for calculation of present worth of 10 years annual disbursement for maintenance application. construction of this spreadsheet took 20 minutes and was used to evaluate 20 different alternatives in 40 minutes. This represents 720 separate calculations including a printed report completed in 45 minutes. Estimated time for hand calculation is about 4 hours with no printed report.

Retaining Wall Design

Figure 4 is a sketch of a mechanically stabilized embankment (in this case a retaining wall underneath a road) using welded wire fabric. Figures 5a. and 5b. are the completed templates for calculation of external and internal stability. Figures 6a. and 6b. are examples of analysis of a specific wall geometry. Note that cells into which data must be placed prior to calculation contain "???" on the initial template. Thus there is no confusion as to what and where information is required. The template indicates zeros or an "ERR" (error) label in other cells because the initial template contains only zeros (the text "???"'s are considered zero). Recalculation of the spreadsheet with the "???" cells replaced with appropriate numerical values will result in meaningful contents of the remaining cells.

This spreadsheet was design in response to an obligation to review retaining wall designs submitted for a large project which included over 2000 lineal feet of welded wire wall for a total of almost 40,000 face square feet in various native materials with eight different wall geometries.

The first section of the spreadsheet is for inputting basic data such as gross geometry, soil parameters, loading geometry, and corrosion reduction requirements. The second section calculates external stability by first calculating vertical and horizontal loads and moments, calculating factors of safety against sliding and overturning, and finally calculating location of vertical resultant at the toe and toe pressure.

The third unit calculates internal stability. The user must input the mat spacing and corresponding depths for each mat and wire sizes and wire spacing. The spreadsheet then calculates reduced wire area (for corrosion), longitudinal wire stress, length of wire embedment (behind assumed failure plane)(this is a displayed intermediate calculation), and finally factors of safety against pullout for each mat for three different soil types. Formulas used for pullout resistance are after Nielson and Anderson

(1984).

The time required for an experienced wall designer to design a spreadsheet like this would be approximately 12 hours. Setting up and recalculating the spreadsheet template to accommodate different conditions takes about 10 minutes. Calculating and printing the results thereof for eight different conditions takes less than 2 hours and includes 39 calculations per layer or 3120 calculations for the whole job. This compares to an estimated 32 hours of hand calculation with no printed report.

Sensitivity Analysis -- Bearing Capacity of Footing on Slopes

The analysis of required for the retaining wall project mentioned above also required an extensive analysis of bearing capacity and slope stability of the slopes upon which the walls were proposed to be constructed. A spreadsheet was designed to calculate bearing capacity after Winterkorn and Fang (1975). (See figure 7). No printout is included in this paper because the spreadsheet was rather large with numerous intermediate calculations. Essentially the method involves a crude method of slices type series of calculations. Once set up the spreadsheet allowed analysis of sensitivity of bearing capacity to slope angle, friction angle, wall geometry, and loading. Slope stability was evaluated using a commercially available software package designed specifically for slope stability analysis. The results were used to specify required base width -- wall height ratios corresponding to preferred factors of safety. The analysis involved thousands of calculations which otherwise could not have been done considering time. Convergence on a solution was relatively simple and fast. Time to complete the template was about 2 days.

Static Bearing capacity Analysis of Piles

A spreadsheet template developed to evaluate static bearing capacity of single piles in cohesionless material is shown in Figure 9. Figure 8 sketches the geometric assumptions and outlines the general equation. This method is discussed in the FHWA's "Manual on Design and Construction Driven Pile Foundations" (FHWA DP-66-1, 1985) and by Bowles (1977).

Manual calculation of bearing capacity using the Nordlund (1963) method can be rather tedious because of the need to refer to the many charts and the required interpolation. This spreadsheet uses a powerful feature called the Lookup function. This is essentially a command for the computer to return a "y" value for a given "x" from a specified table of "x-y" values residing in the spreadsheet. Several lookup tables were easily constructed by reading the charts and inputting the values in the template. The tables were then expanded (using the spreadsheet to do the work, of course) by insertion of blank rows and columns and filling them with interpolated numbers. Figures 10-12 are some of the charts which were included in the lookup tables for this spreadsheet.

Figure 13 is a printout of a sample problem (from the FHWA manual pp. 177-185). The lookup table were not printed because of their large size. The results agree with those in the FHWA manual.

The first part of the template is for input of basic data such as pile geometry and location. Then in the second part of the template the first column is for data input of depth (of layer interfaces). Columns 3 through 5 are for input of soil friction angle, effective soil mass density, and pile type (from table above including a "no-pile" option for piles below ground). The spreadsheet then calculates skin and tip ultimate static capacity showing intermediate calculation and parameters.

*****

These four spreadsheets discussed are not technically complex and do not involve new technical concepts but hopefully serve as an introduction to the potential uses of the computer spreadsheet.

The use of spreadsheets is, of course, not limited to design for the geotechnical engineer. It has bee, for example, of great value to the soils laboratory. It is ideal for such applications because of the report-like format and ability to "program" it to do any required calculations. Also the spreadsheet software (if so designed) can also illustrate results in graphical form (such as moisture-density relationships).

COST

The state of the micro-computer industry is such that now virtually anyone can afford to be using a computer and spreadsheet package. The problem in obtaining such is usually either inertia to change or reluctance on the part of some to spend money on something unproven for cost efficiency. Below are costs (August 1986) which can be used to build a justification for such an acquisition.

Hardware

The hardware should be completely IBM compatible as this is by far the most popular system (thought not necessarily the best). Included in the package should be 640 k RAM (allows enough room for the "biggies" that engineering computations will require), two double-density/double sided floppy disk drives, a monochrome monitor (color monitors, unless you spend lots of money, generally have terrible resolution and are hard on the eyes), a "math-coprocessor" chip (actually a second computer that handles all the math functions--speeds things up as much as 6 to 10 times), and a good dot-matrix printer.

The best values are IBM-compatible "clones". There are a multitude out there and the deciding factors must be cost, warranty (get at least 90 days, some have 1 year), dealer reliability, and compatibility (some are really not fully compatible-best to buy software first and then try it out on the computer before you buy). The best choice for the dollar in printers is an Epson compatible model. Get one that is fairly fast and can print in "near-letter-quality".

Below are current prices for these items:

ITEM	COST
1. IBM-XT compatible clone -256 k RAM -single disk drive -8 expansion slots - monochrome monitor	$ 750.00
2. 640 k RAM upgrade	$ 75.00
3. 2nd floppy disk drive	$ 115.00
4. Epson compatible printer	$ 370.00
5. 8087 math co-processor	$ 180.00
TOTAL	$1,490.00

Software

The most widely used and one of the best spreadsheet software packages available for the MS-DOS (IBM) operating system is LOTUS 1-2-3. Release 2 (the latest) includes graphics and a database program and sells retail for $495.

Again, in addition to function, one must consider what is most popular and widely used. LOTUS 1-2-3 almost a "household" word. Another excellent spreadsheet program is SuperCalc3 or SuperCalc4.

Most users have discovered that it is best to buy separate software packages rather than combined. That is, get a separate spreadsheet, separate word processor, etc. The actual convenience of having a 3-in-1 spreadsheet-wordprocessor-database package have been exaggerated. Chances are that there is a weak portion of the software and then one also loses the capability of sharing spreadsheet templates since most other users are using 1-2-3.

Cost/Benefit

The actual cost/benefit ratio will depend on how much use the system has. The author's experience seems to indicate that the use of the spreadsheet saves probably about 75% in time compared to performing the same analysis/calculations by hand. Also it seems that the spreadsheet is being used approximately 5% to 10% of working hours. The following analysis is based on an 8 hour day.

PERCENT USE	TIME SAVED hr/day	WAGE PLUS BENEFITS $/hour	TIME REQUIRED TO RECOVER $1,985 COST days
5	1.2	$20	83
10	2.4	$20	41
15	3.6	$20	28
25	6.0	$20	17
5	1.2	$25	66
10	2.4	$25	33
15	3.6	$25	22
25	6.0	$25	13

The capitol recovery time decreases very quickly when percentage of use increases just a small amount and also when upper level designers/managers use the system (higher salary).

Another way to look at cost savings to consider a single large design/review project. Using the welded wire retaining wall template discussed above, time of development plus use of the spreadsheet was estimated at 12+2=14 hours. Time required to do the same amount of calculation by hand is (at very best!) 32 hours. Total savings in time is 56% and savings in dollars probably around $300 to $350. The next time the template is used the savings will be on the order of 88% and $700! It doesn't take too many projects like these to recover the initial investment.

SUMMARY

Geotechnical engineers can greatly improve their efficiency and reduce design costs by using computer spreadsheets. The average office with an average workload should be able to recover the costs of the required hardware and software in 4 to 16 weeks.

In addition to cost savings spreadsheets offer freedom to explore variations in design and encourage creativity while giving an added element of neatness and organization. Finished projects can be printed into a report instantly. Also spreadsheets often avoid the need for costly programming by conventional means or purchase of specialty software.

Computer spreadsheets should soon become an everyday tool for the geotechnical engineer.

```
   ! A !! B !!           C            !!           D           !!   E   !!  F  !
  1!CALCULATION OF TOLERANCES AND PAY FACTORS FOR
  2!GRAD. "D" SP*** #200 SIEVE *** n = 5 ***
  3!
  4!specification range:
  5!   low  high                   sigma (based on 90.00% CONFIDENCE)
  6!----------------------------------------------------------------------------
  7!     6    15                   3.510
  8!----------------------------------------------------------------------------
  9!
 10!
 11!
 12!alpha    .01                      Z(.995) =                 2.575
 13!beta =    .1                      Z(.950) =                 1.645
 14!AQL =   10.5
 15!n =        5
 16!sigma  3.510
 17!
 18!
 19!Kl =      6.5
 20!Kh =     14.5
 21!
 22!RQLl =    3.9
 23!RQLh =   17.1
 24!
 25!
 26!*** #200 SIEVE *** n = 5 ***
 27!%
 28!WITH-       Z
 29!IN       FROM                ACTUAL                   % PASS.     MEAN
 30!LIMITS TABLE                     Z                   (SIEVE)DEVIATION
 31!----------------------------------------------------------------------------
 32!     98 2.054                 2.054                      9.7          .8
 33!     78 .7721                 .7721                      7.7         2.8
 34!     68  .465                  .465                      7.2         3.3
 35!     60 .2533                 .2533                      6.9         3.6
 36!     47 .0753                -.0753                      6.3         4.2
```

Figure 1

```
  ¦ A ¦¦ B ¦¦         C          ¦¦         D          ¦¦  E  ¦¦  F  ¦
 1¦CALCULATION OF TOLERANCES AND PAY FACTORS FOR
 2¦GRAD. "D" SP*** #200 SIEVE *** n = 5 ***
 3¦
 4¦specification range:
 5¦low   high  sigma                        (based on 90.00% CONFIDENCE)
 6¦--------------------------------------------------------------------------------
 7¦ 6     15    ((B7-A7)/2)/1.282
 8¦--------------------------------------------------------------------------------
 9¦
10¦
11¦
12¦alpha  .01                          Z(.995) =              2.575
13¦beta = .1                           Z(.950) =              1.645
14¦AQL =  (B7-A7)/2+A7
15¦n =     5
16¦sigma  C7
17¦
18¦
19¦Kl =   B14-E12*B16/SQRT(B15)
20¦Kh =   B14+E12*B16/SQRT(B15)
21¦
22¦RQLl = B19-E13*B16/SQRT(B15)
23¦RQLh = B20+E13*B16/SQRT(B15)
24¦
25¦
26¦*** #200 SIEVE *** n = 5 ***
27¦%
28¦WITH-      Z
29¦IN      FROM       ACTUAL                       % PASS.            MEAN
30¦LIMITS TABLE       Z                            (SIEVE)         DEVIATION
31¦--------------------------------------------------------------------------------
32¦ 98    2.054 IF(A32>=50,B32,(-1)*B32) C32*(B16/SQRT(B15))+B19  (B14-D32)
33¦ 78    .7721 IF(A33>=50,333,(-1)*B33) C33*(B16/SQRT(B15))+B19  (B14-D33)
34¦ 68    .465  IF(A34>=50,B34,(-1)*B34) C34*(B16/SQRT(B15))+B19  (B14-D34)
35¦ 60    .2533 IF(A35>=50,B35,(-1)*B35) C35*(B16/SQRT(B15))+B19  (B14-D35)
36¦ 47    .0753 IF(A36>=50,B36,(-1)*B36) C36*(B16/SQRT(B15))+B19  (B14-D36)
```

Figure 2

INDIAN CREEK AIRFIELD
SURFACE STABILIZATION ALTERNATIVES

MgCl:

ALTER. #	AREA SQ.YD.	NO. GALLONS	LIQUID WIEGHT LB.	SOLIDS LB.	HEXA-HYDRATE WEIGHT TONS	HEXA-HYDRATE (DRY FLAKES) COSTS MATERIAL COST	TRANSP. COST	TOTAL	PRE-MIX WEIGHT TONS	PRE-MIX SOLN. (WET) COSTS MATERIAL COST	TRANSP. COST	TOTAL
1	13333	6667	73333	22733	24.2	$7,255.32	$5,103.19	$12,358.51	36.7	$6,666.67	$7,350.00	$14,016.67
2	26667	13333	146667	45467	48.4	$14,510.64	$9,456.38	$23,967.02	73.3	$13,333.33	$13,950.00	$27,283.33
3	40000	20000	220000	68200	72,6	$21,765.96	$13,809.57	$35,575.53	110.0	$20,000.00	$20,550.00	$40,550.00
4	36667	18333	201667	62517	66.5	$19,952.13	$12,721.28	$32,673.40	100.0	$18,333.33	$18,900.00	$37,233.33
5	20000	10000	110000	34100	36.3	$10,882.98	$7,279.79	$18,162.77	55.0	$10,000.00	$10,650.00	$20,650.00

LignoSulfonate:

ALTER. #	AREA SQ.YD.	NO. GALLONS	LIQUID WIEGHT LB.	--SOLIDS WEIGHT-- LB.	TONS	----COSTS (DRY MATERIAL)---- MATERIAL COST	TRANSP. COST	TOTAL
1	13333	6667	70000	35000	17.5	$3,920.00	$4,125.00	$8,045.00
2	26667	13333	140000	70000	35.0	$7,840.00	$7,250.00	$15,090.00
3	40000	20000	210000	105000	52.5	$11,760.00	$10,375.00	$22,135.00
4	36667	18333	192500	96250	48.1	$10,780.00	$9,593.75	$20,373.75
5	20000	10000	105000	52500	26.3	$5,880.00	$5,687.50	$11,567.50

MAINTENANCE APPLICATIONS

MgCl:

ALTER. #	AREA SQ.YD.	NO. GALLONS	LIQUID WIEGHT LB.	SOLIDS LB.	HEXA-HYDRATE WEIGHT TONS	HEXA-HYDRATE (DRY FLAKES) COSTS MATERIAL COST	TRANSP. COST	TOTAL	P.W. COST n=10 YR. i=4%	PRE-MIX WEIGHT TONS	PRE-MIX SOLN. (WET) COSTS MATERIAL COST	TRANSP. COST	TOTAL	P.W. COST n=10 YR. i=4%
1	13333	3333	36667	11367	12.1	$3,627.66	$2,926.60	$6,554.26	$53,160.00	18.3	$3,333.33	$4,050.00	$7,383.33	$59,885.45
2	26667	6667	73333	22733	24.2	$7,255.32	$5,103.19	$12,358.51	$100,238.59	36.7	$6,666.67	$7,350.00	$14,016.67	$113,687.72
3	26667	6667	73333	22733	24.2	$7,255.32	$5,103.19	$12,358.51	$100,238.59	36.7	$6,666.67	$7,350.00	$14,016.67	$113,687.72
4	23333	5833	64167	19892	21.2	$6,348.40	$4,559.04	$10,907.45	$88,469.16	32.1	$5,833.33	$6,525.00	$12,358.33	$100,237.15
5	13333	3333	36667	11367	12.1	$3,627.66	$2,926.60	$6,554.26	$53,160.00	18.3	$3,333.33	$4,050.00	$7,383.33	$59,885.45

LignoSulfonate:

ALTER. #	AREA SQ.YD.	NO. GALLONS	LIQUID WIEGHT LB.	--SOLIDS WEIGHT-- LB.	TONS	----COSTS (DRY MATERIAL)---- MATERIAL COST	TRANSP. COST	TOTAL	P.W. COST n=10 YR. i=4%
1	13333	3333	35000	17500	8.8	$1,960.00	$2,562.50	$4,522.50	$36,681.53
2	26667	6667	70000	35000	17.5	$3,920.00	$4,125.00	$8,045.00	$65,252.16
3	26667	6667	70000	35000	17.5	$3,920.00	$4,125.00	$8,045.00	$65,252.16
4	23333	5833	61250	30625	15.3	$3,430.00	$3,734.38	$7,164.38	$58,109.50
5	13333	3333	35000	17500	8.8	$1,960.00	$2,562.50	$4,522.50	$36,681.53

Figure 3

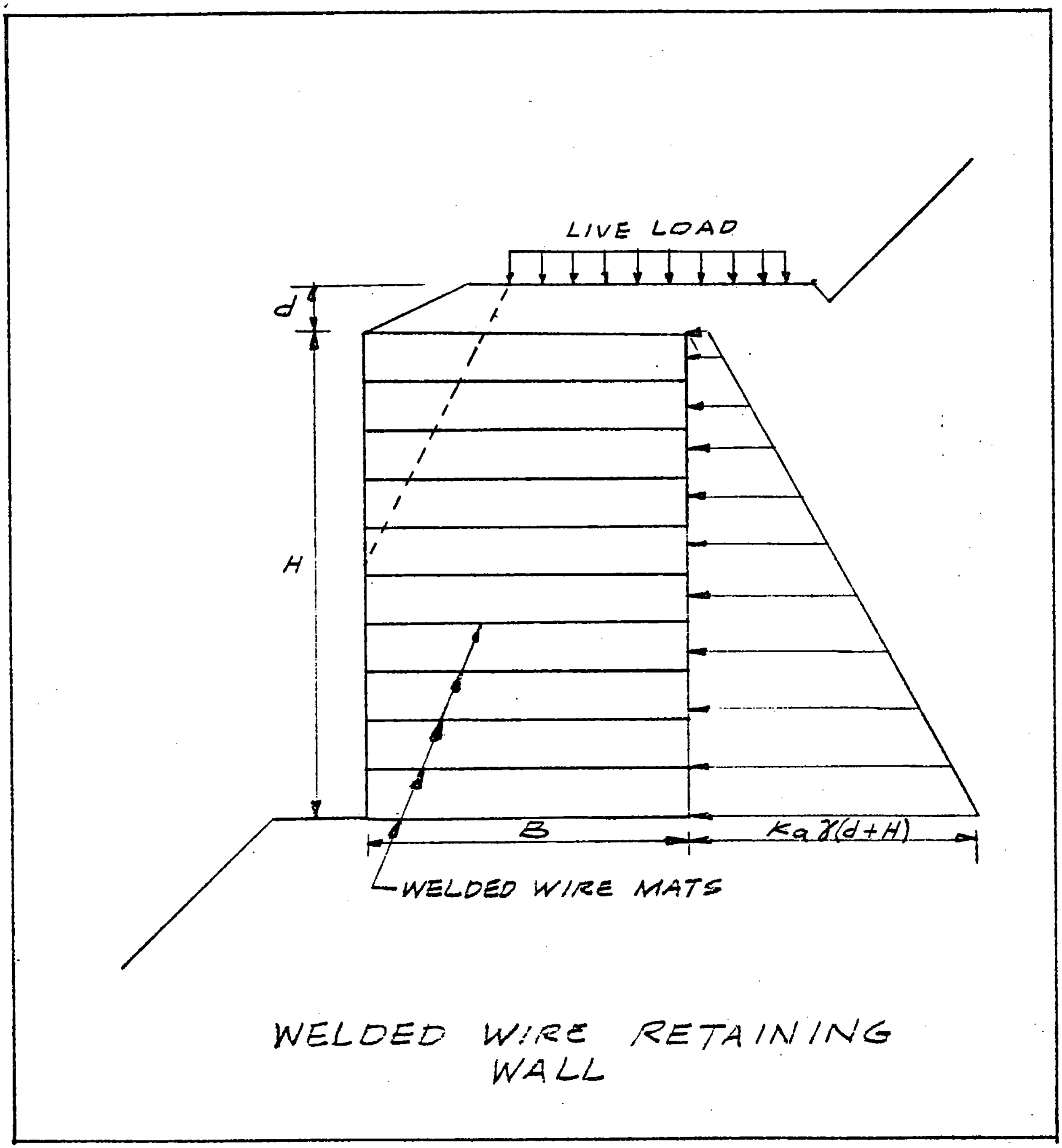
LIVE LOAD
d
H
B
$K_a \gamma (d+H)$
WELDED WIRE MATS
WELDED WIRE RETAINING WALL

Figure 4

```
***WELDED WIRE RETAINING WALL DESIGN***


B A S I C   I N P U T   D A T A :

Soil and Geometry

==========================================================================================================
Wall Height,                 !     PHI Soil             !     DENSITY soil                  !    Ka Coefficient
Feet.            ???         !     Wall, deg.     ???   !     Wall, k/cu.ft.      ???       !    Behind Wall    ???
                             !                          !                                   !
Base Width,                  !     PHI Soil             !     DENSITY soil                  !
Feet.            ???         !     Native, deg.   ???   !     Native, k/cu.ft.    ???       !
==========================================================================================================


==========================================================================================================
* LOADING *                      Soil      Offset      Width          !    * WIRE *
                                Depth    From Wall     Above          !    Soil/Wire Friction Angle, deg. =          ???
                               (Equiv.)      Edge       Wall          !    Dia. Reduction for Corrosion, in.=        ???
                                  ft.         ft.        ft.          !
***LIVE LOAD:                    ???         ???           0          !
                                                                      !
***DEAD LOAD:                    ???         ???           0          !
==========================================================================================================






***EXTERNAL STABILITY WORKSHEET***

**********************************************************************
*                                                                    *
*        Vertical Loading:                                           *
*                                                                    *
*                                     MOMENT                         *
*                             LOAD       ARM    MOMENT               *
*        DESCRIPTION          K/FT     FT/FT   K-FT/FT               *
*        ----------------------------------------------              *
*        WALL DEADLOAD        0.00      0.00      0.00               *
*        DEADLOAD SURCHARGE   0.00      0.00      0.00               *
*        LIVELOAD SURCHARGE   0.00      0.00      0.00               *
*        ----------------------------------------------              *
*        TOTALS               0.00      0.00      0.00               *
*                                                                    *
*                                                                    *
*                                                                    *
*        Horizontal Loading:                                         *
*                                                                    *
*                                     MOMENT                         *
*                             LOAD       ARM    MOMENT               *
*        DESCRIPTION          K/FT     FT/FT   K-FT/FT               *
*        ----------------------------------------------              *
*        LAT. SOIL PRESS.                                            *
*           BEHIND WALL       0.00      0.00      0.00               *
*                                                                    *
*        LIVELOAD INDUCED     0.00      0.00      0.00               *
*           LAT. PRESS.                                              *
*        ----------------------------------------------              *
*        TOTALS               0.00      0.00      0.00               *
*                                                                    *
*                                                                    *
*        ***MIN. OVERTURNING F.S. =     ERR <------                  *
*                                                                    *
*        ***MIN. SLIDING F.S. =         ERR <------                  *
*                                                                    *
*                                                                    *
*        MAX. DISTANCE OF VERT. RESULTANT FROM TOE =     ERR FT.     *
*        ECCENTRICITY =                                  ERR FT.     *
*        MAXIMUM ALLOWABLE ECCENTRICITY =               0.00 FT.     *
*                                                                    *
*        MAXIMUM TOE PRESSURE =                          ERR KSF     *
*                                                                    *
**********************************************************************
```

Figure 5a.

```
***INTERNAL STABILITY WORKSHEET***
**************************************************************************************************************************************************************************************************
*
*  ---------------------------------------------------------------------------------------------------------------------------------------------------------------------------------------   *
*        MAT DEPTH   --LOADING--      --WIRE SIZE-- --CORRODED WIRE SECTION PROPERTIES--                      NO.      NO.    LONG.             S. SAND  S. SAND  W. SAND  W. SAND PEA GRAV.PEA GRAV.   *
*        FROM TOP   VERT.  HORIZ.   LONG.   TRANS. --LONGITUDINAL--  --TRANSVERSE--    LONG.    TRANS.   LONG.    TRANS.   WIRE           PULLOUT  PULLOUT  PULLOUT  PULLOUT  PULLOUT  PULLOUT   *
*        OF WALL                                    AREA     DIA.     AREA     DIA.  SPACING  SPACING WIRES /   WIRES   STFESS    Le   RESIST.    F.S.   RESIST.    F.S.   RESIST.    F.S.    *
*  MAT #     FT.  KSF/FT. KSF/FT. (Wxx.x) (Wxx.x) SQ. IN.    FT.  SQ. IN.     FT.     IN.      IN.    FOOT    / FOOT    KSI    FT. KIPS/FT.          KIPS/FT.          KIPS/FT.            *
*  ---------------------------------------------------------------------------------------------------------------------------------------------------------------------------------------   *
*   ???      ???     ERR     ERR    ???     ???    0.000    0.000    0.000    0.000    ???      ???      ERR      ERR      ERR    0.00   ERR      ERR      ERR      ERR      ERR      ERR     *
*   ???      ???     ERR     ERR    ???     ???    0.000    0.000    0.000    0.000    ???      ???      ERR      ERR      ERR    0.00   ERR      ERR      ERR      ERR      ERR      ERR     *
*   ???      ???     ERR     ERR    ???     ???    0.000    0.000    0.000    0.000    ???      ???      ERR      ERR      ERR    0.00   ERR      ERR      ERR      ERR      ERR      ERR     *
*   ???      ???     ERR     ERR    ???     ???    0.000    0.000    0.000    0.000    ???      ???      ERR      ERR      ERR    0.00   ERR      ERR      ERR      ERR      ERR      ERR     *
*   ???      ???     ERR     ERR    ???     ???    0.000    0.000    0.000    0.000    ???      ???      ERR      ERR      ERR    0.00   ERR      ERR      ERR      ERR      ERR      ERR     *
*   ???      ???     ERR     ERR    ???     ???    0.000    0.000    0.000    0.000    ???      ???      ERR      ERR      ERR    0.00   ERR      ERR      ERR      ERR      ERR      ERR     *
*   ???      ???     ERR     ERR    ???     ???    0.000    0.000    0.000    0.000    ???      ???      ERR      ERR      ERR    0.00   ERR      ERR      ERR      ERR      ERR      ERR     *
*   ???      ???     ERR     ERR    ???     ???    0.000    0.000    0.000    0.000    ???      ???      ERR      ERR      ERR    0.00   ERR      ERR      ERR      ERR      ERR      ERR     *
*   ???      ???     ERR     ERR    ???     ???    0.000    0.000    0.000    0.000    ???      ???      ERR      ERR      ERR    0.00   ERR      ERR      ERR      ERR      ERR      ERR     *
*   ???      ???     ERR     ERR    ???     ???    0.000    0.000    0.000    0.000    ???      ???      ERR      ERR      ERR    0.00   ERR      ERR      ERR      ERR      ERR      ERR     *
*   ???      ???     ERR     ERR    ???     ???    0.000    0.000    0.000    0.000    ???      ???      ERR      ERR      ERR    0.00   ERR      ERR      ERR      ERR      ERR      ERR     *
*   ???      ???     ERR     ERR    ???     ???    0.000    0.000    0.000    0.000    ???      ???      ERR      ERR      ERR    0.00   ERR      ERR      ERR      ERR      ERR      ERR     *
*   ???      ???     ERR     ERR    ???     ???    0.000    0.000    0.000    0.000    ???      ???      ERR      ERR      ERR    0.00   ERR      ERR      ERR      ERR      ERR      ERR     *
*   ???      ???     ERR     ERR    ???     ???    0.000    0.000    0.000    0.000    ???      ???      ERR      ERR      ERR    0.00   ERR      ERR      ERR      ERR      ERR      ERR     *
*   ???      ???     ERR     ERR    ???     ???    0.000    0.000    0.000    0.000    ???      ???      ERR      ERR      ERR    0.00   ERR      ERR      ERR      ERR      ERR      ERR     *
*   ???      ???     ERR     ERR    ???     ???    0.000    0.000    0.000    0.000    ???      ???      ERR      ERR      ERR    0.00   ERR      ERR      ERR      ERR      ERR      ERR     *
*   ???      ???     ERR     ERR    ???     ???    0.000    0.000    0.000    0.000    ???      ???      ERR      ERR      ERR    0.00   ERR      ERR      ERR      ERR      ERR      ERR     *
*   ???      ???     ERR     ERR    ???     ???    0.000    0.000    0.000    0.000    ???      ???      ERR      ERR      ERR    0.00   ERR      ERR      ERR      ERR      ERR      ERR     *
*   ???      ???     ERR     ERR    ???     ???    0.000    0.000    0.000    0.000    ???      ???      ERR      ERR      ERR    0.00   ERR      ERR      ERR      ERR      ERR      ERR     *
*   ???      ???     ERR     ERR    ???     ???    0.000    0.000    0.000    0.000    ???      ???      ERR      ERR      ERR    0.00   ERR      ERR      ERR      ERR      ERR      ERR     *
*   ???      ???     ERR     ERR    ???     ???    0.000    0.000    0.000    0.000    ???      ???      ERR      ERR      ERR    0.00   ERR      ERR      ERR      ERR      ERR      ERR     *
*   ???      ???     ERR     ERR    ???     ???    0.000    0.000    0.000    0.000    ???      ???      ERR      ERR      ERR    0.00   ERR      ERR      ERR      ERR      ERR      ERR     *
*   ???      ???     ERR     ERR    ???     ???    0.000    0.000    0.000    0.000    ???      ???      ERR      ERR      ERR    0.00   ERR      ERR      ERR      ERR      ERR      ERR     *
*   ???      ???     ERR     ERR    ???     ???    0.000    0.000    0.000    0.000    ???      ???      ERR      ERR      ERR    0.00   ERR      ERR      ERR      ERR      ERR      ERR     *
*   ???      ???     ERR     ERR    ???     ???    0.000    0.000    0.000    0.000    ???      ???      ERR      ERR      ERR    0.00   ERR      ERR      ERR      ERR      ERR      ERR     *
*   ???      ???     ERR     ERR    ???     ???    0.000    0.000    0.000    0.000    ???      ???      ERR      ERR      ERR    0.00   ERR      ERR      ERR      ERR      ERR      ERR     *
*   ???      ???     ERR     ERR    ???     ???    0.000    0.000    0.000    0.000    ???      ???      ERR      ERR      ERR    0.00   ERR      ERR      ERR      ERR      ERR      ERR     *
*   ???      ???     ERR     ERR    ???     ???    0.000    0.000    0.000    0.000    ???      ???      ERR      ERR      ERR    0.00   ERR      ERR      ERR      ERR      ERR      ERR     *
*   ???      ???     ERR     ERR    ???     ???    0.000    0.000    0.000    0.000    ???      ???      ERR      ERR      ERR    0.00   ERR      ERR      ERR      ERR      ERR      ERR     *
*   ???      ???     ERR     ERR    ???     ???    0.000    0.000    0.000    0.000    ???      ???      ERR      ERR      ERR    0.00   ERR      ERR      ERR      ERR      ERR      ERR     *
*   ???      ???     ERR     ERR    ???     ???    0.000    0.000    0.000    0.000    ???      ???      ERR      ERR      ERR    0.00   ERR      ERR      ERR      ERR      ERR      ERR     *
*   ???      ???     ERR     ERR    ???     ???    0.000    0.000    0.000    0.000    ???      ???      ERR      ERR      ERR    0.00   ERR      ERR      ERR      ERR      ERR      ERR     *
*   ???      ???     ERR     ERR    ???     ???    0.000    0.000    0.000    0.000    ???      ???      ERR      ERR      ERR    0.00   ERR      ERR      ERR      ERR      ERR      ERR     *
*   ???      ???     ERR     ERR    ???     ???    0.000    0.000    0.000    0.000    ???      ???      ERR      ERR      ERR    0.00   ERR      ERR      ERR      ERR      ERR      ERR     *
*
**************************************************************************************************************************************************************************************************
```

Figure 5b.

```
         ***WELDED WIRE RETAINING WALL DESIGN***
            CHALK CREEK, FISHLAKE N.F.


  B A S I C   I N P U T   D A T A :

  Soil and Geometry

=========================================================================================================
Wall Height,                   !     PHI Soil               !  DENSITY soil                   !   Ka Coefficient
Feet.             25.5         !     Wall, deg.          34 !  Wall, k/cu.ft.        0.125    !   Behind Wall      0.33
                               !                            !                                 !
Base Width,                    !     PHI Soil               !  DENSITY soil                   !
Feet.               18         !     Native, deg.        30 !  Native, k/cu.ft.      0.125    !
=========================================================================================================

=========================================================================================================
* LOADING *                 Soil        Offset      Width       !   * WIRE *
                           Depth     From Wall      Above       !   Soil/Wire Friction Angle, deg. =          20
                         (Equiv.)         Edge       Wall       !   Dia. Reduction for Corrosion, in.=     0.026
                             ft.           ft.        ft.       !
***LIVE LOAD:                  2             4         14       !
                                                                !
***DEAD LOAD:           2.666666             4         14       !
=========================================================================================================
```

```
***EXTERNAL STABILITY WORKSHEET***

*************************************************************************
*                                                                       *
*       Vertical Loading:                                               *
*                                                                       *
*                                        MOMENT                         *
*                               LOAD        ARM     MOMENT              *
*       DESCRIPTION             K/FT      FT/FT   K-FT/FT               *
*       -------------------------------------------------               *
*       WALL DEADLOAD          57.38       9.00    516.38               *
*       DEADLOAD SURCHARGE      4.67      11.00     51.33               *
*       LIVELOAD SURCHARGE      3.50      11.00     38.50               *
*       -------------------------------------------------               *
*       TOTALS                 65.54      31.00    606.21               *
*                                                                       *
*                                                                       *
*                                                                       *
*       Horizontal Loading:                                             *
*                                                                       *
*                                        MOMENT                         *
*                               LOAD        ARM     MOMENT              *
*       DESCRIPTION             K/FT      FT/FT   K-FT/FT               *
*       -------------------------------------------------               *
*       LAT. SOIL PRESS.                                                *
*          BEHIND WALL         16.36       9.39    153.63               *
*                                                                       *
*       LIVELOAD INDUCED        2.32      14.08     32.73               *
*          LAT. PRESS.                                                  *
*       -------------------------------------------------               *
*       TOTALS                 18.69      23.47    186.36               *
*                                                                       *
*                                                                       *
*                                                                       *
*       ***MIN. OVERTURNING F.S. =     3.05 <------                     *
*                                                                       *
*       ***MIN. SLIDING F.S. =         1.92 <------                     *
*                                                                       *
*                                                                       *
*       MAX. DISTANCE OF VERT. RESULTANT FROM TOE =      6.15 FT.       *
*       ECCENTRICITY =                                   2.85 FT.       *
*       MAXIMUM ALLOWABLE ECCENTRICITY =                 3.00 FT.       *
*                                                                       *
*       MAXIMUM TOE PRESSURE =                          11.42 KSF       *
*                                                                       *
*                                                                       *
*************************************************************************
```

Figure 6a.

```
***INTERNAL STABILITY WORKSHEET***
*******************************************************************************************************************************************************************************
-----------------------------------------------------------------------------------------------------------------------------------------------------------------------------
                                                                                                                                      S. SAND  S. SAND  W. SAND  W. SAND PEA GRAV.PEA GRAV.
                  --LOADING--        --WIRE SIZE-- --CORRODED WIRE SECTION PROPERTIES--                    NO.      NO.     LONG.           PULLOUT  PULLOUT  PULLOUT  PULLOUT  PULLOUT  PULLOUT
         MAT     VERT.    HORIZ.     LONG.   TRANS. --LONGITUDINAL--  --TRANSVERSE--     LONG.    TRANS.   LONG.    TRANS.    WIRE         Le  RESIST.     F.S.  RESIST.     F.S.  RESIST.     F.S.
        DEPTH                                       AREA      DIA.     AREA      DIA.  SPACING  SPACING  WIRES /   WIRES    STRESS        FT. KIPS/FT.           KIPS/FT.          KIPS/FT.
MAT #    FT.   KSF/FT.  KSF/FT.   (Wxx.x)  (Wxx.x) SQ. IN.     FT.  SQ. IN.      FT.      IN.      IN.    FOOT   / FOOT     KSI
-----------------------------------------------------------------------------------------------------------------------------------------------------------------------------
  1      0.0     0.52     0.34      4.5      3.5    0.036    0.018    0.027    0.015      6.0      9.0     2.00     1.33     7.07    4.44    1.790     3.56    2.447     4.84    2.597     5.12
  2      1.5     0.68     0.44      4.5      3.5    0.036    0.018    0.027    0.015      6.0      9.0     2.00     1.33     9.31    5.24    2.791     4.19    3.448     5.18    3.623     5.44
  3      3.0     0.85     0.55      4.5      3.5    0.036    0.018    0.027    0.015      6.0      9.0     2.00     1.33    11.57    6.04    3.998     4.03    4.666     5.64    4.002     5.90
  4      4.5     1.02     0.66      4.5      3.5    0.036    0.018    0.027    0.015      6.0      9.0     2.00     1.33    13.86    6.83    4.870     4.92    6.101     6.16    6.366     6.42
  5      6.0     1.20     0.78      4.5      3.5    0.036    0.018    0.027    0.015      6.0      9.0     2.00     1.33    16.41    7.63    5.750     4.99    7.066     6.70    8.190     6.98
  6      7.5     1.39     0.90      4.5      3.5    0.036    0.018    0.027    0.015      6.0      9.0     2.00     1.33    18.97    8.43    6.748     4.97    9.866     7.27   10.259     7.56
  7      9.0     1.58     1.03      4.5      3.5    0.036    0.018    0.027    0.015      6.0      9.0     2.00     1.33    21.52    9.23    7.863     5.11   12.102     7.86   12.570     8.17
  8     10.5     1.77     1.15      4.5      3.5    0.036    0.018    0.027    0.015      6.0      9.0     2.00     1.33    24.08   10.02    9.025     5.28   14.573     8.46   15.125     8.78
  9     12.0     1.95     1.27      4.5      3.5    0.036    0.018    0.027    0.015      6.0      9.0     2.00     1.33    26.64   10.82   10.445     5.48   17.200     9.07   17.924     9.41
 10     13.5     2.14     1.39      4.5      3.5    0.036    0.018    0.027    0.015      6.0      9.0     2.00     1.33    29.19   11.62   11.913     5.71   20.222     9.69   20.966    10.04
 11     15.0     2.33     1.51      4.5      3.5    0.036    0.018    0.027    0.015      6.0      9.0     2.00     1.33    31.75   12.42   13.497     5.94   23.490    10.31   24.252    10.68
 12     16.5     2.52     1.64      4.5      3.5    0.036    0.018    0.027    0.015      6.0      9.0     2.00     1.33    34.31   13.21   15.200     6.20   26.013    10.93   27.781    11.32
 13     18.0     2.70     1.76      7.0      3.5    0.058    0.023    0.027    0.015      6.0      9.0     2.00     1.33    22.59   14.01   17.340     6.50   30.782    11.68   31.074    12.09
 14     19.5     2.89     1.88      7.0      3.5    0.058    0.023    0.027    0.015      6.0      9.0     2.00     1.33    24.16   14.81   19.319     6.85   34.708    12.31   35.952    12.75
 15     21.0     3.08     2.00      7.0      3.5    0.058    0.023    0.027    0.015      6.0      9.0     2.00     1.33    25.73   15.61   21.418     7.14   38.072    12.95   40.236    13.40
 16     22.5     3.27     2.12      7.0      3.5    0.058    0.023    0.027    0.015      6.0      9.0     2.00     1.33    27.29   16.40   23.636     7.42   43.274    13.59   44.705    14.06
 17     24.0     3.45     2.24      7.0      3.5    0.058    0.023    0.027    0.015      6.0      9.0     2.00     1.33    28.86   17.20   25.975     7.71   47.914    14.23   49.581    14.72
 18     25.5     3.64     2.37      4.5      3.5    0.036    0.018    0.027    0.015      6.0      9.0     2.00     1.33    24.82   18.00   27.800    15.71   52.237    29.43   54.069    30.46
*******************************************************************************************************************************************************************************
```

Michael Remboldt
Computer
Spreadsheets
page 18

Figure 6b.

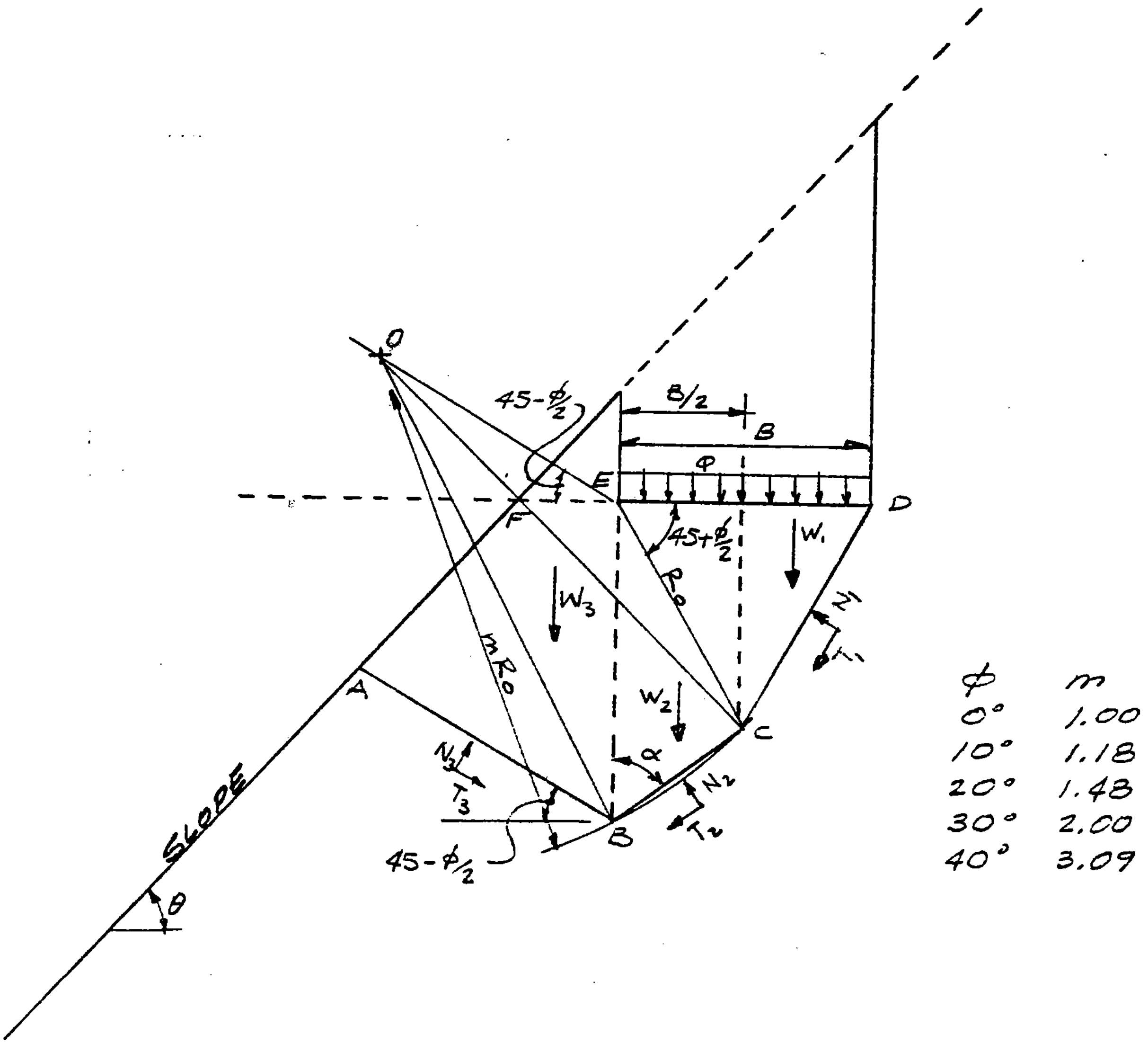
O
45-φ/2
B/2
B
E
q
D
F
W1
W3
45+φ/2
R0
N1
T1
mR0
W2
A
C
N3
T3
α
N2
T2
B
45-φ/2
SLOPE
θ

φ	m
0°	1.00
10°	1.18
20°	1.48
30°	2.00
40°	3.09

FOOTINGS ON SLOPES

AFTER WINTERKORN & FANG, 1975

Figure 7

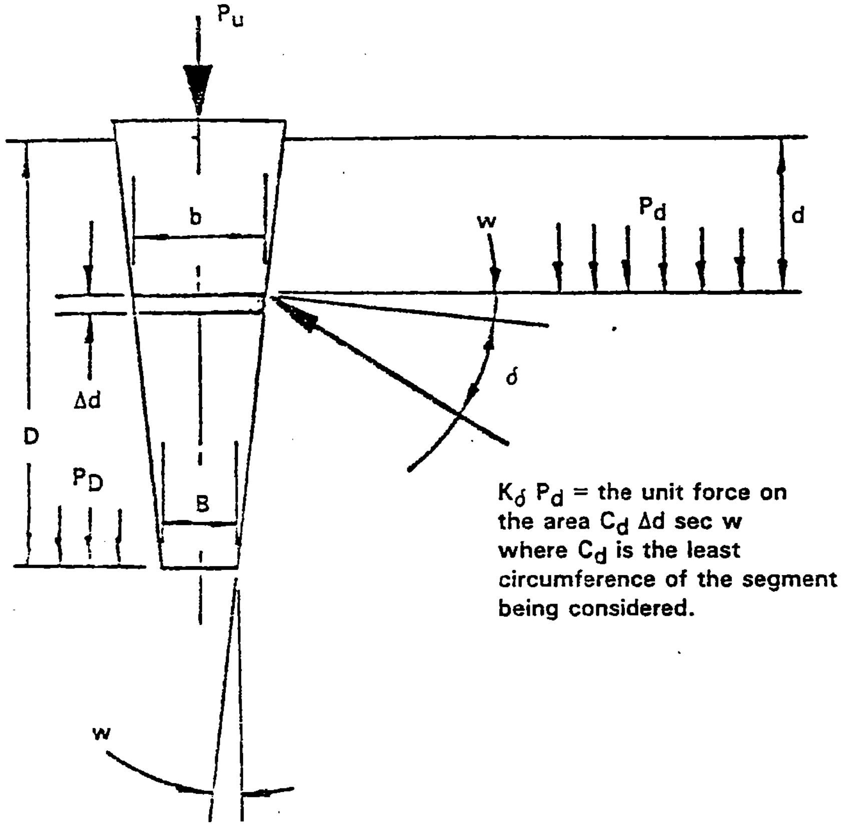

K_δ P_d = the unit force on the area C_d Δd sec w where C_d is the least circumference of the segment being considered.

$$Q_u = \alpha N'_q \times A_p \times P_D + \sum_{d=0}^{d=D} K_\delta \times C_F \times P_d \frac{\sin(\delta + W)}{\cos W} \times C_d \times \Delta d$$

FIGURE 9-9 NORDLUND'S GENERAL EQUATION FOR ULTIMATE PILE CAPACITY

Figure 8

```
STATIC ULTIMATE PILE CAPACITY FOR COHESIONLESS SOILS
NORDLAND METHOD

   B A S I C   I N P U T   D A T A

=====================================================================!   !==================================================!
Pile Length                          !    Pile Taper                    !   !   ###PILE TYPES###                                 !
Feet =                        ???    !    in. dia./in. length  =   ??? !   !   (0) No Pile                                      !
                                     !                                  !   !   (1) Pipe piles, non-tapered portion of monotube piles
Pile Perimeter at                    !                                  !   !   (2) Timber piles                                 !
Point, in. =                  ???    !                                  !   !   (3) Precast concrete piles                       !
                                     !                                  !   !   (4) Raymond step-taper piles                     !
Effective Pile Point                 !    Depth of Pile Tip             !   !   (5) Raymond uniform taper piles                  !
Diameter, in. =               ???    !    From Surface, ft.  =     ??? !   !   (6) H-piles and augercast piles                  !
=====================================================================!   !   (7) Tapered portion of monotube piles            !
                                                                            !                                                  !
Pile Tip Area =              0.00 sq.ft.                                    !==================================================!
Pile Taper Angle =           0.00 radians
Pile Taper Angle =           0.00 degrees

   P I L E   C A P I C I T Y   W O R K S H E E T
---------------------------------------------------------------------------------------------------------------------------------------
                                                       Average                             Effective Ave. Segment                                                      Ultimate
                         Soil    Effective             Specific  Soil/Pile     Lateral    Overburden   Effective              Ultimate      Ultimate                   Pile
         Segment     Friction         Soil        Pile Pile Volume  Friction Earth Press.   Press. at  Overburden               Segment  Cummulative Ultimate  Capicity
  Depth  Thickness      Angle      Density        Type        V     Angle Coefficient  Pile Point    Pressure     Alpha          Qs           Qs       Qp   Qs + Qp
    Ft.        Ft.       deg.          pcf (See Above)  cu.ft./ft.      deg.         K          psf         psf    Coeff.        tons         tons     tons      tons
---------------------------------------------------------------------------------------------------------------------------------------
    ???
               ???        ???          ???         ???       0.00       0.0      0.00                                                                    ERR       ERR
    ???
               ???        ???          ???         ???       0.00       0.0      0.00         0           0       ERR         ERR          ERR      ERR       ERR
    ???
               ???        ???          ???         ???       0.00       0.0      0.00         0           0       ERR         ERR          ERR      ERR       ERR
    ???
               ???        ???          ???         ???       0.00       0.0      0.00         0           0       ERR         ERR          ERR      ERR       ERR
    ???
               ???        ???          ???         ???       0.00       0.0      0.00         0           0       ERR         ERR          ERR      ERR       ERR
    ???
               ???        ???          ???         ???       0.00       0.0      0.00         0           0       ERR         ERR          ERR      ERR       ERR
    ???
               ???        ???          ???         ???       0.00       0.0      0.00         0           0       ERR         ERR          ERR      ERR       ERR
    ???
               ???        ???          ???         ???       0.00       0.0      0.00         0           0       ERR         ERR          ERR      ERR       ERR
    ???
               ???        ???          ???         ???       0.00       0.0      0.00         0           0       ERR         ERR          ERR      ERR       ERR
    ???
               ???        ???          ???         ???       0.00       0.0      0.00         0           0       ERR         ERR          ERR      ERR       ERR
    ???
               ???        ???          ???         ???       0.00       0.0      0.00         0           0       ERR         ERR          ERR      ERR       ERR
    ???
               ???        ???          ???         ???       0.00       0.0      0.00         0           0       ERR         ERR          ERR      ERR       ERR
    ???
                                                                                              0           0       ERR         ERR          ERR      ERR       ERR
```

Figure 9

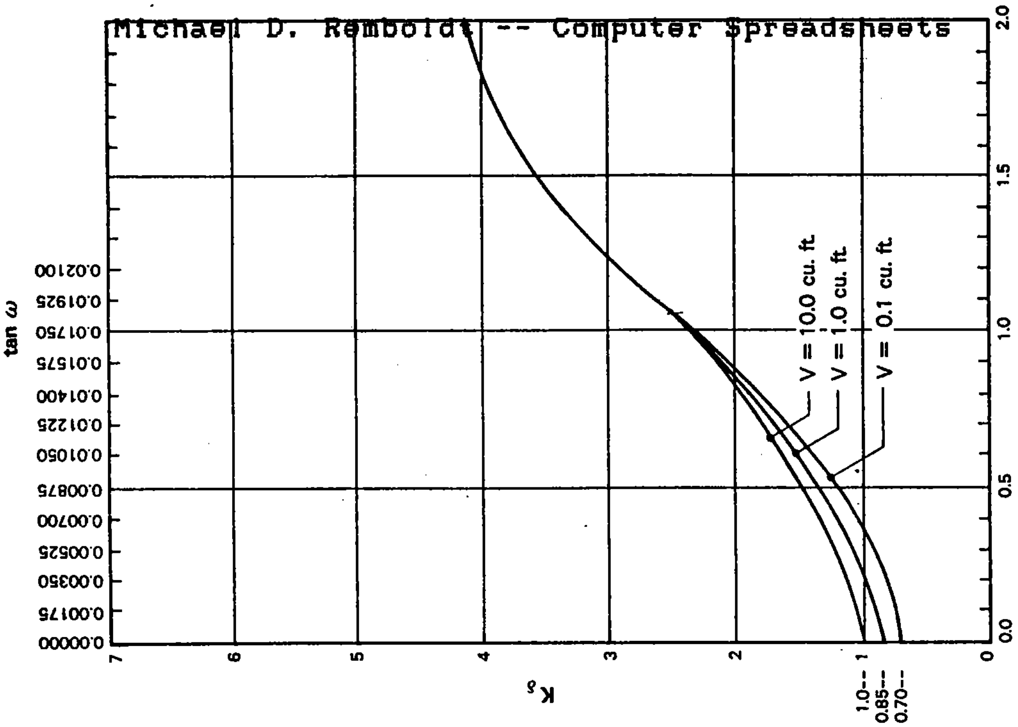

FIGURE 9-10 DESIGN CURVES FOR EVALUATING K_δ FOR PILES WHEN Φ = 25° (After Nordlund, 1979)

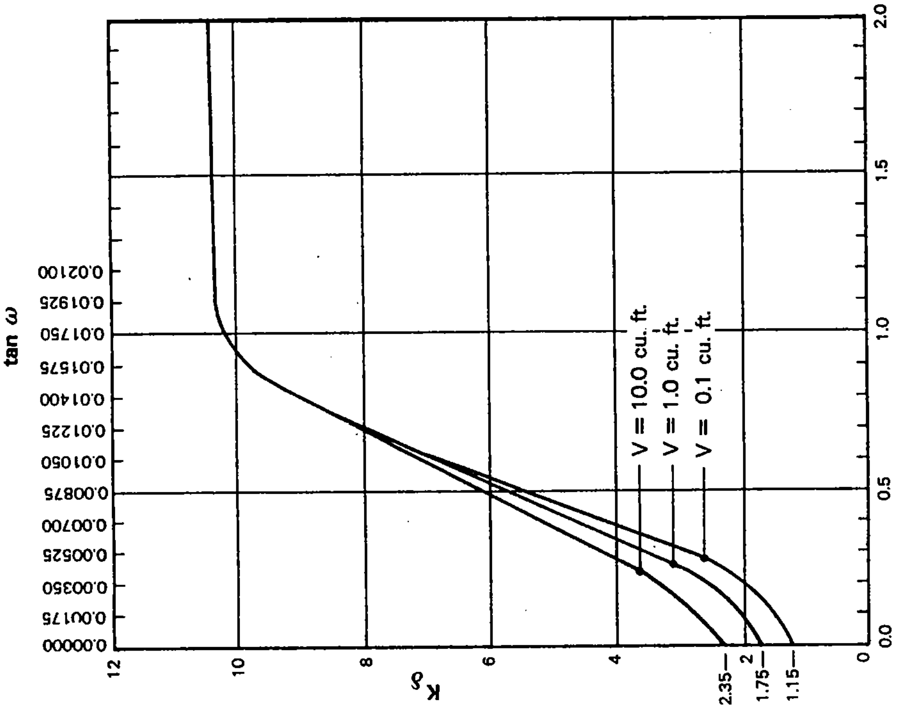

FIGURE 9-12 DESIGN CURVES FOR EVALUATING K_δ FOR PILES WHEN Φ = 35° (AFTER NORDLUND, 1979)

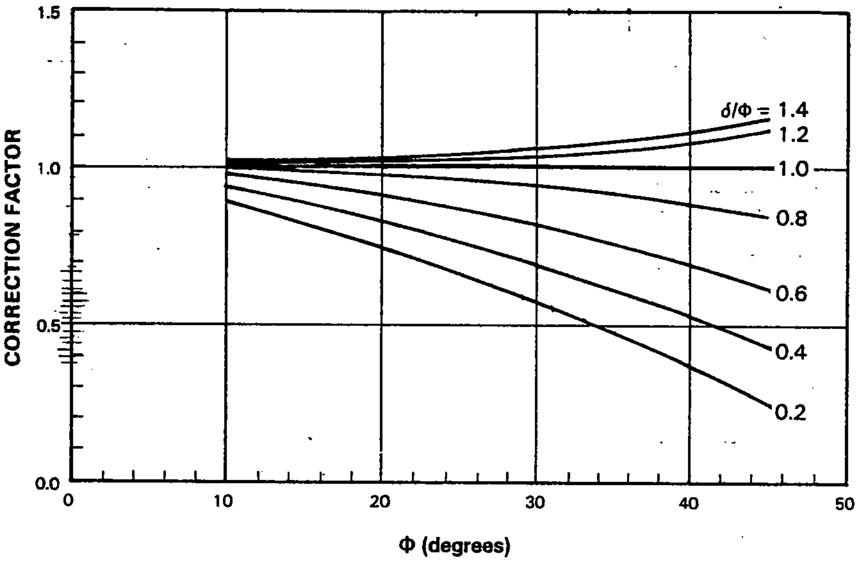

FIGURE 9-15 CORRECTION FACTOR FOR Kδ WHEN δ ≠ Φ
(After Nordlund, 1979)

Figure 11

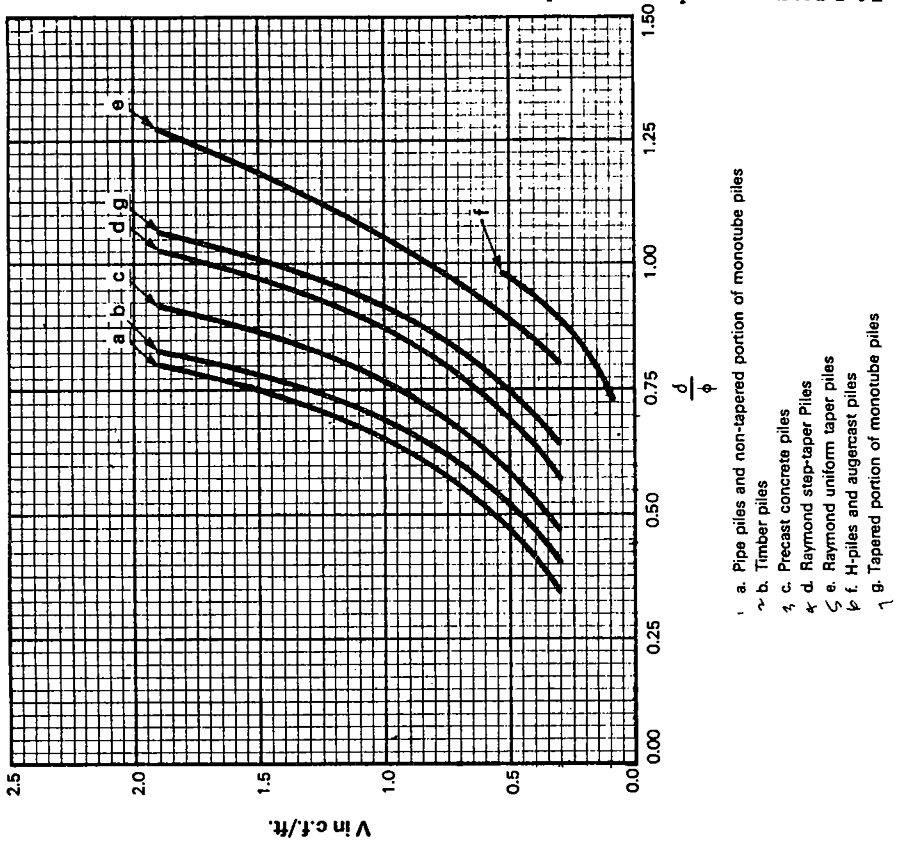

FIGURE 9-14 RELATION OF δ/φ AND PILE DISPLACEMENT, V, FOR VARIOUS TYPES OF PILES
(After Nordlund, 1979)

151

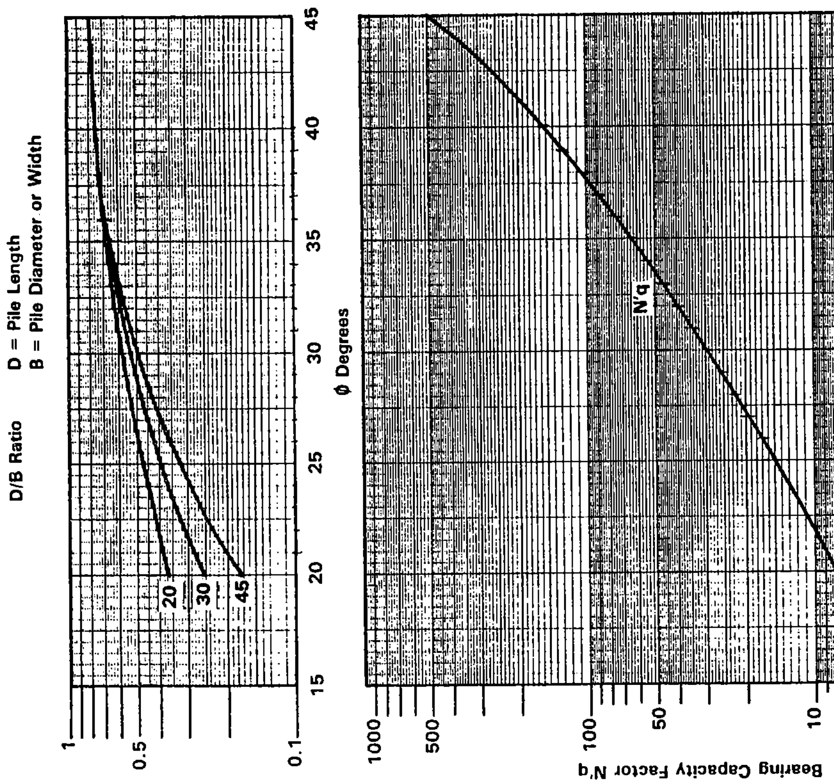

FIGURE 9-16 CHART FOR ESTIMATING α COEFFICIENT AND BEARING CAPACITY FACTOR N'q
(Chart Modified from Bowles, 1977)

153

422

Figure 12

```
STATIC ULTIMATE PILE CAPACITY FOR COHESIONLESS SOILS
NORDLAND METHOD

   B A S I C   I N P U T   D A T A

========================================================================|      |=========================================================|
Pile Length                           !      Pile Taper                 !      !  ###PILE TYPES###                                       !
Feet =                          30    !      in. dia./in. length  =   0 !      !  (0) No Pile                                            !
                                      !                                 !      !  (1) Pipe piles, non-tapered portion of monotube piles  !
Pile Perimeter at                     !                                 !      !  (2) Timber piles                                       !
Point, in. =                    48    !                                 !      !  (3) Precast concrete piles                             !
                                      !                                 !      !  (4) Raymond step-taper piles                           !
Effective Pile Point                  !      Depth of Pile Tip          !      !  (5) Raymond uniform taper piles                        !
Diameter, in. =              13.54    !      From Surface, ft.  =    38 !      !  (6) H-piles and augercast piles                        !
========================================================================|      !  (7) Tapered portion of monotube piles                  !
                                                                               !                                                         !
Pile Tip Area =               1.00 sq.ft.                                      |=========================================================|
Pile Taper Angle =            0.00 radians
Pile Taper Angle =            0.00 degrees

    P I L E   C A P I C I T Y   W O R K S H E E T

------------------------------------------------------------------------------------------------------------------------------------------------------------
                                                          Average.                               Effective Ave. Segment                                                     Ultimate
                           Soil  Effective                Specific  Soil/Pile      Lateral      Overburden   Effective              Ultimate     Ultimate                 Pile
            Segment    Friction       Soil       Pile Pile Volume   Friction  Earth Press.       Press. at   Overburden              Segment   Cummulative   Ultimate   Capicity
   Depth  Thickness      Angle    Density        Type        V       Angle  Coefficient       Pile Point     Pressure      Alpha        Qs            Qs         Qp    Qs + Qp
     Ft.        Ft.       deg.        pcf (See Above)  cu.ft./ft.     deg.       K                 psf          psf     Coeff.       tons          tons       tons      tons
------------------------------------------------------------------------------------------------------------------------------------------------------------
       0
                  6         34        105           0       0.00       0.0        0.00                                                                       0        NA
       6
                  2         34       42.6           0       0.00       0.0        0.00             630          315       0.66        0.0           0.0      11.2        NA
       8
                 18         34       42.6           3       1.00      25.5        1.55             715          673       0.66        0.0           0.0      12.7        NA
      26
                 12         40       60.6           3       1.00      30.0        2.70            1482         1099       0.66       26.3          26.3      86.1        NA
      38
                  0          0   ???         ???            0.00       0.0        0.00            2209         1846       0.75       59.8          86.1     120.4     214.5
```

Figure 13

REFERENCES

Bowles, Joseph E., 1977, Foundation Analysis and Design: McGraw-Hill, San Francisco.

Kleiner, David E., 1985, Engineering With Spreadsheets: Civil Engineering Magazine, Oct. 1985, pp. 55-57

Nieslon, Mark R. and Loren Anderson (Dept. of Civil Engineering Utah State University, Logan, Utah), 1984, Pullout Resistance of Wire Mats Embedded in Soil: Research report for Hilfiker Company, April, 1984.

Nordlund, R. L., 1963, Bearing Capacity of Piles in Cohesionless Soils, JSMFD, ASCE, vol. 89, SM 3, May, pp 1-36 (see also closure July 1964 with errata).

Federal Highway Administration Manual on Design and Construction of Driven Pile Foundations, 1985, FHWA publication DP-66-1.

Winterkorn, Hans f. and Hsai-Yang Fang, 1975, Foundation Engineering Handbook, Van Nostrand Reinhold Company, Cincinnati.

COMPUTER SYSTEMS COMPANIES

Burgoyne computers, Inc.
555 East 400 South
Salt Lake City, UT 84102
(801) 531-1389

WestWind Computer
1690 65th Street
Emeryville, CA 94608
(415) 652-3222

SOFTWARE COMPANIES (SPREADSHEETS)

LOTUS 1-2-3:

Lotus Development Corp.
55 Cambridge Parkway
Cambridge, MA 02142

SuperCalc:

Computer Associates
2195 Fortune Dr.
San Jose, CA 95121
(408) 942-1727

ATTENDANCE LIST
37th Annual Highway Geology Symposium
Helena, Montana

Lee Abramson
Parsons Brinckerhoff
One Penn Plaza
New York, NY 10119
(212) 613-5247

Ron Anderson
The Tensar Corporation
390 Union Blvd., Suite 260
Lakewood, CO 80228
(303) 986-6742

John L. Anton
Materials & Soils
South Dakota DOT
Pierre, SD 57501
(605) 773-3401

Joe Armstrong
Montana DOH
2701 Prospect Ave.
Helena, MT 59620
(406) 444-6280

Tom Bass
ARMCO, Inc.
3211 Energy Lane
Casper, WY 82604
(307) 235-0410

Joe Barcomb
US Forest Service
506 Hwy 2 West
Libby, MT 59923
(406) 293-6211

R. Scott Barnes
Montana DOH
2701 Prospect Ave.
Helena, MT 59620
(406) 444-6275

Ed Belknap
Colorado DOH
4340 E. Louisiana Ave.
Denver, CO 80222
(303) 757-9424

Dick Berg
Montana Bureau of Mines & Geology
Montana Tech
Butte, MT 59701
(406) 496-4172

William D. Bingham
North Carolina DOT
P.O. Box 25201
Raleigh, NC 27611
(919) 733-6911

John Bloomingdale
US Forest Service
Westside Engineering Zone
Gold Beach, OR 97444
(503) 247-7026

Tim Bowen
Colorado DOH
Box 1430
Glenwood Springs, CO 81602
(303) 945-8080

Scott C. Branson
P.O. Box 8329
Missoula, MT 59807
(800) 348-7098

F.C. (Bud) Budinger
Budinger & Associates
North 920 Lake
Spokane, WA 99212
(509) 535-8841

Michal Bukovansky
Golder Associates
17301 West Colfax Ave. #275
Golden, CO 80401
(303) 278-8662

Vernon L. Bump
South Dakota DOT
700 E. Broadway
Pierre, SD 57501
(605) 773-3401

Josh Burrows
Diamond Drill Contracting Company
P.O. Box 11307
Spokane, WA 99211
(800) 325-1563

William Capaul
Idaho Transportation Department
P.O. Box D
Coeur D'Alene, ID 83814
(208) 664-8181

Hank Carlson
Evergreen Systems, Inc.
P.O. Box 345
King's Park, NY 11754
(516) 368-4000

Chien-Tan Chang
Federal Highway Administration
6300 Georgetown Pike
Mclean, VA 22101
(703) 285-2357

Ron Chassie
Federal Highway Administration
708 S.W. 3rd St.
Portland, OR 97068
(503) 221-2095

Massimo Ciarla
Terra Aqua Inc.
5 Thomas Mellon Circle #248
San Francisco, CA 94134
(415) 468-5980

John D. Coffee
Federal Highway Administration
711 S. Capitol Way, Suite 501
Olympia, WA 98501
(206) 753-2119

Jim Coffin
Wyoming Highway Department
P.O. Box 1708
Cheyenne, WY 82001
(307) 777-7450

Jeffery Collins
Montana Division of Forestry
2505 Spurgin Road
Missoula, MT 59801
(406) 728-4300

Debra Corcoran
South Dakota DOT
700 Broadway Ave. E.
Pierre, SD 57501
(605) 773-3871

Dave Cough
Federal Highway Administration
301 S. Park
Helena, MT 59626
(404) 449-5308

John Jay Crawford
GMT Consultants, Inc.
P.O. Box 3418
Missoula, MT 59806
(406) 721-2182

H.E. (Hank) Davis
Mobile Drilling Company
P.O. Box 610
Aptos, CA 95001
(408) 688-6387

Dennis Debus
Maryland State Highway
Administration
2323 West Joppa Road
Brooklandville, MD 21022
(301) 321-3437

Gary Dees
Montana Department of Highways
2701 Prospect Avenue
Helena, MT 59620
(406) 444-6014

Craig S. Dewey
Flathead National Forest
P.O. Box 147
Kalispell, MT 59901
(406) 755-5401

Bill Dunbar
Federal Highway Administration
301 S. Park
Helena, MT 59626
(406) 449-5310

Howard Dutro
Slope Indicator Company
3668 Albion Place North
Seattle, WA 98103

Mary Jean Edgar
530 Wm. Penn Pl.
Pittsburgh, PA 15219
(412) 261-0710

R.P. (Bob) Elliott
University of Arkansas
340 Engineering Building
Fayetteville, AR 72701
(501) 575-6028

Jeffrey I. Enyart
The Reinforced Earth Company
3333 Quebec St., Suite G
Denver, CO 80207
(303) 399-5500

Don Fenton
Federal Highway Administration
301 South Park
Helena, MT 59626
(406) 449-5310

John A. Franceski
Schnabel Foundation Company
8000 East Girard #317
Denver, CO 80231
(303) 696-7268

Leroy Foster
South Dakota DOT
700 E. Broadway
Pierre, SD 57501
(605) 773-3870

John B. Gilmore
Colorado DOH
4340 E. Louisiana
Denver, CO 80222
(303) 757-9275

Joseph A. Gutierrez
P.O. Box 4195
Winston Salem, NC 27105
(919) 767-4600 Ext. 246

Mike Hager
Wyoming Highway Department
P.O. Box 1708
Cheyenne, WY 82001
(307) 777-4202

Richard L. Hall
Schnabel Foundation Company
4720 Montgomery Lane
Bethesda, MD 20814
(301) 657-3063

Jim D. Hammell
South Dakota DOT
700 Broadway Ave. E.
Pierre, SD 57501
(605) 773-3401

Carol Hammond
USDA Forest Service
1221 S. Main
Moscow, ID 83843
(208) 882-3557

Neil F. Hawks
Transportation Research Borad
2101 Constitution Ave. NW
Washington, DC 20013
(202) 334-2957

Bill Hilfiker
Hilfiker Retaining Walls
P.O. Drawer L
Eureka, CA 95501

Bob Hinshaw
US Forest Service
P.O. Box 7669
Missoula, MT 59803
(406) 329-3330

Sam Holder
Federal Highway Administration
(CDFP)
P.O. Box 25246
Denver, CO 80225
(303) 236-4394

Kim Hooper
Nezperce National Forest
Route 2
Grangeville, ID 83530
(208) 983-1950

Jeffrey L. Hynes
Colorado Geological Survey
1313 Sherman Street, Room 715
Denver, CO 80203
(303) 866-3520

Hal L. James
Montana Bureau of Mines & Geology
Montana Tech
Butte, MT 59701
(406) 496-4175

Charles T. Janik
Pennsylvania DOT
1118 State Street
Harrisburg, PA 17120
(717) 787-4209

Jerry Jensen
Jensen Drilling Company
1775 Henderson Avenue
Eugene, OR 97403
(503) 726-7435

John Jensen
1775 Henderson Company
Eugene, OR 97403
(503) 726-7435

Gary D. Johnson
Idaho Transportation Dept.
P.O. Box 97
Rigby, ID 83442
(208) 745-7781/Ext. 47

Walter V. Jones
Northern Engineering & Testing
P.O. Box 281
North Salt Lake, UT 84054
(801) 298-9314

Stephen C. Joppa
1420 E. 6th
Helena, MT 59620
(406) 444-3755

Dennis G. Keaster
Montana DOH
2701 Prospect Ave.
Helena, MT 59620
(406) 444-6278

Richard Kennedy
US Forest Service
Nezperce National Forest
Grangeville, ID 83530
(208) 983-1950

Wayne Kinzer
Idaho Transportation Department
26th & N & S Highway
Lewiston, ID 83501
(208) 746-1345

David Kirk
Sprague & Henwood, Inc.
P.O. Box 170
Couer D'Alene, ID 83814
(208) 765-0211

Erik Kleschen
Montana DOH
2701 Prospect Avenue
Helena, MT 59620
(406) 444-6396

Hank Knoble
Central Mine Equipment Company
6200 North Broadway
St. Louis, MO 63147
(314) 381-5900

Dr. William N. Laval
Lewis Clark State College
Lewiston, ID 83501
(208) 799-2342

Leo A. Legatski
Elastizell Corporation of America
P.O. Box 1462
Ann Arbor, MI 48106
(313) 761-6900

Tony Leonard
American Excelsior Company
609 South Front Street
Yakima, WA 98901
(509) 575-5794

Jack R. Liedle
Montana DOH
2701 Prospect Ave.
Helena, MT 59620
(406) 444-6276

Michael T. Long
Oregon DOT
9002 SE McLoughlin Blvd.
Milwaukie, OR 97222
(503) 653-3080

Horst Lossman
Oman Construction Company
P.O. Box 146
Nashville, TN 37202
(615) 385-2500

Bill Lovell
School of Civil Engineering
Purdue University
W. Lafayette, IN 47907
(317) 494-5034

Douglas W. Lovell
Stiller & Associates
P.O. Box 470
Helena, MT 59624
(406) 443-5210

Steve M. Lowell
Washington DOT
Box 167
Olympia, WA 98501
(206) 753-4660

Harry Ludowize
Federal Highway Administration
610 E. 5th St.
Vancouver, WA 98661
(206) 696-7738

Dick Lueck
New Mexico Highway Department
P.O. Box 1149
Santa Fa, NM 87504
(505) 982-0955

Blair Lunde
South Dakota DOT
700 E. Broadway
Pierre, SD 57501
(605) 773-3544

Leonard C. Mahlum
Montana DOH
2701 Prospect Ave.
Helena, MT 59620
(406) 444-6397

Henry Mathis
Kentucky Dept. of Highways
Wilkerson Blvd.
Frankfort, KY 40622
(502) 564-3160

Earle W. Mayberry
Montana DOH
2701 Prospect Ave.
Helena, MT 59620
(406) 444-6277

Willard McCasland
Oklahoma DOT
321 Sahoma Terrace
Edmond, OK 73013
(405) 521-2677

Doug McClelland
U.S. Forest Service
P.O. Box 7669
Missoula, MT 59807
(406) 329-3351

Richard L. McKillip
Dougherty Foundation Products, Inc.
P. O. Box 636, Route 2
Cadiz, KY 42211
(502) 522-6935

Gary McWhorter
Montana Power Company
40 East Broadway
Butte, MT 59701
(406)723-5421

Stanley M. Miller
Dept. of Geology & Geology Engr.
University of Idaho
Moscow, ID 83843
(208) 885-7977

Steve Mills
Lewis Clark State College
Lewiston, ID 83501
(208) 743-0219

Michael Mitchell
Lolo National Forest
Ft. Missoula, Bldg. #24
Missoula, MT 59801
(406) 329-3964

Harry L. Moore
Tennessee DOT
P. O. Box 58
Knoxville, TN 37901
(615) 673-6219

Gary Norris
Department of Civil Engineering
University of Nevada Reno
Reno, Nevada 89557
(702) 784-6835

Norm Norrish
Golder Associates
4104 - 148th Avenue N.E.
Redmond, WA 98052
(206) 883-0777

Larry D. Olson
Olson - Church, Inc.
925 East 17th Avenue
Denver, CO 80218
(303) 830-7066

Frank A. Oneida
Idaho Transportation Department
P.O. Box 8028
Boise, ID 83707
(208) 334-3947

Les Peterson
Montana Dept. of Highways
2701 Prospect Avenue
Helena, MT 59620
(406) 444-6013

Lawrence A. Pierson
Oregon DOT
1178 Chemeketa St., Rm. 104
Salem, OR 97310
(503) 373-7994

Donald Porior
U.S. Forest Service
Westside Engineering Zone
Gold Beach, OR 97415
(503) 247-7026

Ron Pozun
Wyoming Highway Department
P.O. Box 1708
Cheyenne, WY 82001
(307) 777-4207

Gary Quinn
Northern Engineering & Testing
P. O. Box 951
Great Falls, MT 59403
(406) 453-1641

Rodney W. Prellwitz
U.S. Forest Service
P.O. Box 8089
Missoula, MT 59807
(406) 721-5694

Loren Rausher
Utah Dept. of Transportation
4501 So. 2700 West
Salt Lake City, UT 84119
(801) 965-4326

R. Bruce Reeves
(Lang Tendons, Inc.)
3623 Chain Bridge Rd.
Fairfax, VA 22030
(703) 591-3453

Michael Remboldt
USDA Forest Service
325 - 24th St.
Ogden, UT 84404
(801) 625-5238

Clyde Robbe
Montana Power Company
40 East Broadway
Butte, MT 59701
(406) 723-5421

Lawrence A. Rockers
Kansas Dept. of Transportation
2300 Van Buren
Topeka, KS 66611
(913) 296-3008

Helen Rueda
U.S. Forest Service
97976 Ocean Way
Gold Beach, OR 97444
(503) 247-7026

Patrick T. Ryan
University of Tennessee
Dept. of Geological Sciences
Knoxville, TN 37996-1410
(615) 974-2366

Kevin Sauve
American Excelsior Company
609 South Front Street
Yakima, WA 98901
(509) 575-5794

Milbert Schaffer
South Dakota DOT
Pierre, SD 57501
(605) 773-3870

Mike Schulte
Wyoming Highway Department
P.O. Box 1708
Cheyenne, WY 82001
(307) 777-7450

Bill Schultz
Montana Division of Forestry
2705 Spurgin Road
Missoula, MT 59801
(406) 728-4300

William F. Sherman
Wyoming Highway Department
P.O. Box 1708
Cheyenne, WY 82001
(307) 777-7450

Brian L. Smith
Idaho DOT
P.O. Box 97
Rigby, ID 83442
(208) 745-7781

Ernest L. Smith
Western Area Power Administration
P. O. Box 3402
Golden, CO 80401
(303) 231-7423

Robert M. Smith
Idaho DOT
P.O. Box 7129
Boise, ID 83707
(208) 334-5253

Dan Sowle
New Mexico Highway Department
2816 Camino Principe
Santa Fe, NM 87505
(505) 982-0955 x356

John Steward
USDA Forest Service
P.O. Box 3623
Portland, OR 97208
(503) 221-2413

Harry Strong
Montana Dept. of Highways
104 18th Ave. NE, Box 1359
Great Falls, MT 59401
(406) 727-4350

Warren Sulzle
South Dakota DOT
Pierre, SD 57501
(605) 773-3401

Ernie Taylor
International Constr. Equip. Inc.
301 Warehouse Drive
Matthews, NC 28105

Glen R. Thommen
Oregon DOT
329 Transportation Bldg.
Salem, OR 97310
(503) 378-6551

Sam I. Thornton
Department of Civil Engineering
University of Arkansas
Fayetteville, AR 72701
(501) 575-6024

C. Allen Torbett
Dept. of Geological Sciences
University of Tennessee
Knoxville, TN 37996-1410
(615) 974-2366

A. Keith Turner
Department of Geology
Colorado School of Mines
Golden, CO 80401
(303) 273-3802

Don Turner
Oregon DOT
Milwaukie, OR 97222
(503) 653-3080

Richard L. Van Dyke
U.S. Forest Service
93976 Ocean Way
Gold Beach, OR 97444
(503) 247-7026

Suneel N. Vanikar
Federal Highway Administration
(HNG-31)
400, 7th St. S.W.
Washington, DC 20013
(202) 366-1572

William S. Warfield V
Montana DOH
2701 Prospect Avenue
Helena, MT 59632
(406) 444-6276

Robert H. West
Oregon DOT
2960 State St.
Salem, OR 97310
(503) 373-7801

Mike Whaley
Advanced Drainage Systems
San Francisco, CA

Burrell Whitlow
Geotechnics, Inc.
P. O. Box 217
Vinton, VA 24179

Edith M. Wilde
Montana Bureau of Mines & Geology
Montana Tech
Butte, MT 59701
(406) 496-4330

William Thomas Wills, Jr.
Maryland State Highway
Administration
2323 West Joppa Road
Brooklandville, MD 21022
(301) 321-3436

Myron L. Wilson
Montana DOH
2701 Prospect Avenue
Helena, MT 59620
(406) 444-6395

William A. Wisner
Florida Dept. of Transportation
P. O. Box 1029
Gainsville, FL 32602
(904) 373-5304

Michael Wood
Wyoming Highway Department
P.O. Box 1708
Cheyenne, WY 82001
(307) 777-4207

Bill Woodcock
Construction Materials Company, Inc.
3938 - 150th Avenue N.E.
Redmond, WA 98052
(206) 881-8806

Terry L. Yarger
Montana DOH
2701 Prospect Avenue
Helena, MT 59620
(406) 444-6282

T. Leslie Youd
368 Clyde Building
Bringham Young University
Orem, UT 84057
(801) 378-56327

Edward J. Zeigler
Rummel, Klepper & Kahl
9580 Frederick Road
Ellicott City, MD 21043
(301) 247-2260

Mark Zitzka
Federal Highway Administration
301 S. Park Ave.
Helena, MT 59626
(406) 449-5310